

UC Berkeley

UC Berkeley Electronic Theses and Dissertations

Title

Development of Transition-Metal Catalysts for Selective Hydrofunctionalization of Unactivated Alkenes

Permalink

<https://escholarship.org/uc/item/7ts209c9>

Author

Xi, Yumeng

Publication Date

2019

Peer reviewed|Thesis/dissertation

Development of Transition-Metal Catalysts for Selective Hydrofunctionalization of
Unactivated Alkenes

By

Yumeng Xi

A dissertation submitted in partial satisfaction of the

requirements for the degree of

Doctor of Philosophy

in

Chemistry

in the

Graduate Division

of the

University of California, Berkeley

Committee in charge:

Professor John F. Hartwig, Chair

Professor Richmond Sarpong

Professor K. Peter C. Vollhardt

Professor Alexis T. Bell

Fall 2019

Abstract

Development of Transition-Metal Catalysts for Selective Hydrofunctionalization of Unactivated Alkenes

by

Yumeng Xi

Doctor of Philosophy in Chemistry

University of California, Berkeley

Professor John F. Hartwig, Chair

The following dissertation discusses the development of transition-metal catalysts for selective hydroboration and hydroamination of unconjugated and unstrained alkenes, termed “unactivated alkenes.” These reactions proceed with high levels of enantioselectivity and, for reactions of unsymmetrical internal alkenes, with high regioselectivity.

Chapter 1 is an overview of transition-metal-catalyzed hydrofunctionalization of unactivated alkenes. This review focuses on the challenges and strategies for achieving asymmetric hydroamination and hydroboration of unactivated alkenes, particularly unactivated internal alkenes. Mechanistic aspects of these reactions are also discussed. The summary of previous literature precedents highlights how the work described in this dissertation fills knowledge gaps in this field.

Chapter 2 describes the development of copper-catalyzed regioselective and enantioselective hydroboration of unsymmetrical internal alkenes. This process, coupled with a series of subsequent stereospecific transformations of the enantioenriched hydroboration products, constitutes a formal hydrofunctionalization that efficiently converts internal alkenes to a diverse set of enantioenriched compounds with distinct functional groups.

Chapter 3 describes the mechanistic study of the copper-catalyzed asymmetric hydroboration of alkenes. A comprehensive study by both experiment and computation reveals the fundamental principles that govern the efficiency of the copper catalysts for reactions with alkenes and selectivity observed for the alkene hydroboration.

Chapter 4 describes the development of new bisphosphine ligands for asymmetric hydroboration of 1,1-disubstituted alkenes. Trimethylgermyl groups on the bisphosphine ligand significantly increase enantioselectivity of the hydroboration of 1,1-disubstituted alkenes. In addition, this new set of ligands forms a catalyst that is highly active toward the hydroboration of unactivated 1,2-disubstituted alkenes.

Chapter 5 describes the development of copper-catalyzed formal hydroamination of unsymmetrical internal alkenes. Similar to the hydroboration discussed in Chapter 2, the hydroamination

occurs with high enantioselectivity and regioselectivity. This work revealed that the polar functional groups proximal to the alkene controlled the regioselectivity through inductive effects.

Chapter 6 describes the development of iridium-catalyzed asymmetric hydroamination of unactivated internal alkenes. A combination of a cationic iridium complex and 2-amino-6-methylpyridine, was essential to the development of the hydroamination. This is the first example of a direct, highly enantioselective addition of an N-H bond to an unactivated internal alkene.

Table of Contents

Chapter 1. Overview of Transition-Metal-Catalyzed Hydrofunctionalization of Unactivated Alkenes	1
1.1 Overview of Hydrofunctionalization of Alkenes	2
1.2 Hydroboration of Alkenes	8
1.3 Hydroamination of Alkenes	15
1.4 Summary	23
1.5 References	23
Chapter 2. Copper-Catalyzed Hydroboration of Unsymmetrical Internal Alkenes for Diverse Formal Functionalization	28
2.1 Introduction	29
2.2 Results and Discussion	30
2.3 Conclusions	37
2.4 Experimental	37
2.5 References	67
Chapter 3. Mechanistic Study of the Copper-Catalyzed Asymmetric Hydroboration of Alkenes	70
3.1 Introduction	71
3.2 Results and Discussion	72
3.3 Conclusions	96
3.4 Experimental	98
3.5 References	132
Chapter 4. Development of Ligands Containing Trimethylgermyl Groups for Asymmetric Hydroboration of 1,1-Disubstituted Alkenes and Hydroboration of Unactivated 1,2-Disubstituted Alkenes	136
4.1 Introduction	137
4.2 Results and Discussion	138
4.3 Conclusions	146
4.4 Experimental	147
4.5 References	163
Chapter 5. Copper-Catalyzed Formal Hydroamination of Unsymmetrical Internal Alkenes	165
5.1 Introduction	166
5.2 Results and Discussion	167
5.3 Conclusions	173
5.4 Experimental	173
5.5 References	198

Chapter 6. Iridium-Catalyzed Asymmetric Hydroamination of Unactivated Internal Alkenes	201
6.1 Introduction	202
6.2 Results and Discussion	202
6.3 Conclusions	208
6.4 Experimental	208
6.5 References	231

Acknowledgements

I can't believe it has been five years since I moved to California for graduate school and that I will finally be receiving a Ph.D. degree from UC Berkeley. The past few years have been unique five years with excitement and frustration, which include countless nights at the bench and in the glovebox. It could be never an easy task to complete a PhD degree. Without the support, encourage, and help from my coworkers, friends, and family, I could never have come this far. For this reason, I have a lot to be grateful to.

First, I would like to thank my advisor, Prof. John F. Hartwig. I still remember the first time I met John during an ACS meeting. He spent some time out of his busy schedule to sit down with me and learn about my research. Without his help, I could never have imagined that I would be joining his group a year after. Life in the Hartwig group was never easy. John has very high standards, and it takes a huge amount of effort on a daily basis to meet his expectation. I appreciate this pressure from him, and it keeps pushing me forward. John has been the role model of a scientist, scholar, and mentor. I am always impressed by his dedication, diligence, and enthusiasm for chemistry as well as his broad knowledge of every aspect of organometallic chemistry. I benefited tremendously from discussions with him as well as from his advice on scientific writing and presentation skills.

Over the past few years, I had the pleasure to work with a number of talented scientists in the group. I would like to thank some "senior" graduate students, Allie Strom, Rebecca Green, Mike Mormino, Matt Peacock, and Sophie Arlow, my fellow graduate student, Xingyu Jiang, and a few postdocs, York Schramm, Bijie Li, and Qian Li, who lent me their hands when I struggled to survive my early years. And a thank you to Trevor Butcher, who was a summer undergraduate student at the time, and Jing Zhang for their tremendous help with my first project, when I was rushing to beat the clock. After York Schramm left for job during my third year, I took over the responsibility from him to train Shay Pedram, a wonderful undergraduate student in the group. Shay's experimental skills never ceased to amaze me, and he helped me a lot with ligand synthesis and substrate preparation. Bo Su is the person I talked to when I faced any problems with research. I always found a solution after our insightful discussions. I enjoyed every conversation with him about chemistry or other topics and will always remember the numerous nights that we walked out of Latimer hall after midnight together. I wish him success with his independent career at Nankai University. Taegyo Lee is my favorite person in 702 Latimer as well as my "hood mate". I still remember us working hard at every night side by side in our early years, as well as our many discussions. I was always impressed by his diligence and passion for chemistry. I also enjoyed discussions with Trevor Butcher, who later came back for graduate school in the group, Eric Kalkman, Noam Saper, and Jason Ma. I would also like to thank the past and current mates in 702 Latimer, Taegyo Lee, Matt Peacock, Chris Hill, Eric Kalkman, Alex Fawcett, and Jason Ma for a great working environment. Finally, my special thank goes to Anneke Runtupalit, our administrative assistant.

I must thank my dissertation committee members, who were also on my qualifying exam committee, Profs. Richmond Sarpong, Peter Vollhardt, and Alex Bell for their time. Prof. Bob Bergman, who was the chair of my qualifying exam committee, was unfortunately not available to read my thesis due to his busy teaching schedule. I am grateful to him for his advice while serving as the chair, but more importantly, for his offer of his GSI position in Chem 200/260 class. I learned tremendously from working closely with him in this class. From his lectures and many discussions on problem sets and exams, I have consolidated my understanding of physical organic

chemistry. His passion for teaching has also helped shaped my philosophy of education in my future career. My GSI experience with Bob was definitely a highlight of my time here.

I would also like to thank my previous mentors, Profs. Xiaodong Shi, Aiwen Lei, Zhen Yang, and Jiahua Chen. It is because of their encouragement and support over the years that I have come this far.

Last but not least, I would like to express my gratitude to my parents for their caring and encouragement throughout the ups and the downs. Without them, it would have been impossible for me to be here today. Life would be nothing special without my friends. Sneaking out of my busy schedule and spending the time with them exploring the Bay area and many parts of the country made my years at Berkeley more enjoyable.

CHAPTER 1

Overview of Transition-Metal-Catalyzed Hydrofunctionalization of Unactivated Alkenes

1.1 Overview of Hydrofunctionalization of Alkenes

1.1.1 Introduction

The hydrofunctionalization of alkenes,¹ which adds a hydrogen atom and a functional group across an olefin concomitantly, is one of the most direct approaches to introduce a functional group into an organic molecule. This reaction produces value-added products utilizing alkenes as the starting material, which are commercially available on the large scale and/or are readily accessible through chemical synthesis. Because hydrofunctionalization is an addition reaction, it proceeds with complete atom-economy, thereby forming no co-products for which separation and disposal are required. In light of these attributes, extensive efforts have been devoted to developing efficient catalysts to promote these processes.

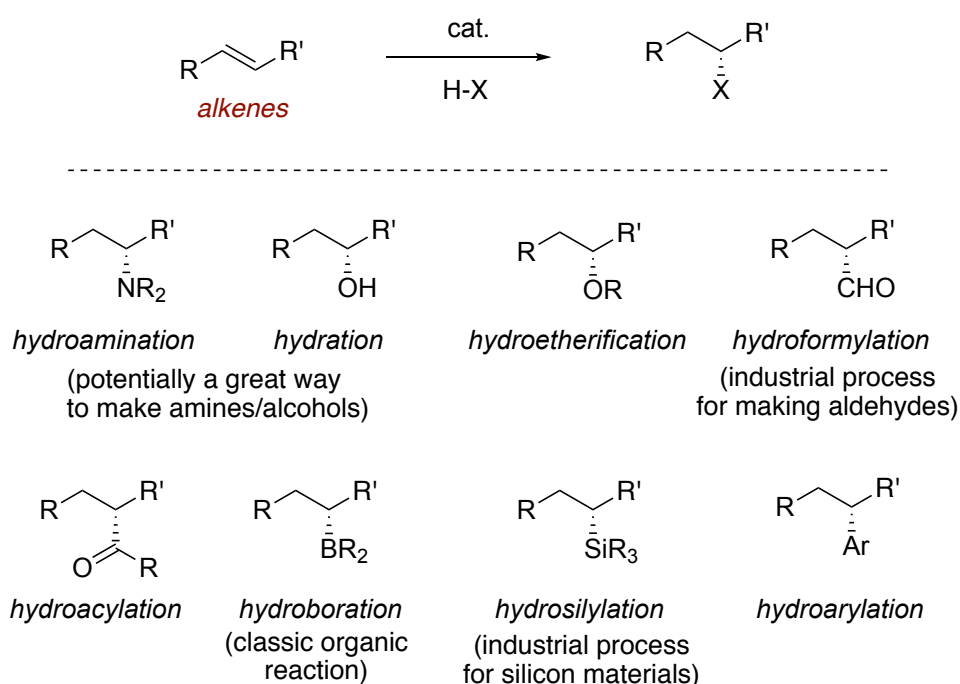
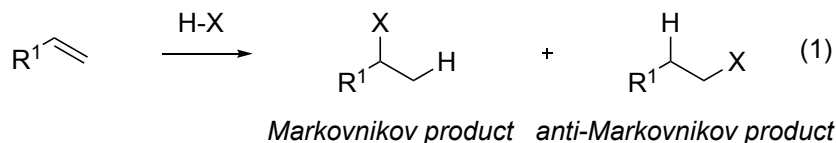


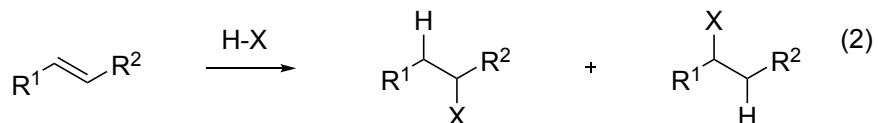
Figure 1.1 Several types of hydrofunctionalizations of alkenes

There are many types of hydrofunctionalization reactions, including hydroamination, hydroboration, hydroformylation, hydrosilylation, and hydroarylation (Figure 1.1). Each reaction introduces one distinct type of functional group. Often distinct catalysts are used for different types of reactions. Many metal catalysts were reported to catalyze hydroamination of alkenes, ranging from catalysts of early transition-metals, such as yttrium,² lanthanum,³ and zirconium,⁴ to late transition-metals, such as palladium,⁵ rhodium,⁶ and iridium.⁷ A large body of catalysts that promote hydroboration is based on rhodium,⁸ but recently base metal complexes also show great promise to be efficient catalysts.⁹ Traditional catalysts developed for hydroarylation of gaseous alkenes with simple arenes include iridium catalysts¹⁰ and ruthenium catalysts,¹¹ but catalysts based on nickel and NHC ligands were recently demonstrated by our group to be exceptionally selective for formation of the product from formal *anti*-Markovnikov addition.¹²

terminal alkenes



internal alkenes



Hydrofunctionalization of alkenes that are unsymmetrical leads to formation of two constitutional isomers. The regioselectivity for formation of one constitutional isomer over the other arises when one direction of the alkene addition with respect to the reagent is preferred over the other. For example, reactions of terminal alkenes form two products, the branched and linear products. The branched product is also called Markovnikov product, which is based on the Markovnikov's rule for the additions of acids to alkenes, and the linear product is called *anti*-Markovnikov product. Hydrofunctionalization of internal alkenes forms two products, the ratio of which is often difficult to control. As discussed in section 1.1.2, the regioselectivity can be sensitive to steric and electronic effects, and is often achieved by the use of directing groups. In addition, the control of regioselectivity can be complicated by competing isomerization of the internal alkenes.

The scope of the alkenes that undergo catalytic hydrofunctionalization reactions varies significantly by the type of reactions. In general, activated alkenes, including those that are conjugated, such as vinylarenes, dienes, and α,β -unsaturated compounds, and those are strained, such as norbornene, are more reactive towards hydrofunctionalization than are simple alkenes. Alkenes, including conjugated alkenes, terminal alkenes, and internal alkenes, were demonstrated to undergo hydroformylation. Internal alkenes generally undergo isomerizing hydroformylation to afford terminal aldehyde products. Hydroboration of conjugated alkenes and terminal alkenes constitutes a majority of the literature examples on this topic. Again, unactivated internal alkenes generally undergo hydroboration to generate products with the boron-containing group at the terminal position. The scope of alkenes that undergo hydroamination is the most limited among the three reactions. There are many challenges associated with this reaction, which will be discussed later in the chapter.

1.1.2 Hydrofunctionalization of Unactivated Internal Alkenes

As discussed in section 1.1.1, examples of hydrofunctionalization of unactivated internal alkenes are more limited than those of activated alkenes and terminal alkenes. The alkene in vinylarenes, dienes, and α,β -unsaturated compounds is polarized and electron-deficient, thus, activated towards hydrofunctionalization in most cases. The hydrofunctionalization of strained alkenes is thermodynamically driven by the release of ring strain. In general, unactivated internal alkenes are less reactive than unactivated terminal alkenes for metal-catalyzed hydrofunctionalization. This difference in reactivity is most likely due to the greater steric hinderance of internal

alkenes than of terminal alkenes. Hydrofunctionalization of internal alkenes is also thermodynamically less favorable than that of terminal alkenes.

Aside from the thermodynamic and kinetic aspects of the reaction, hydrofunctionalization of unactivated internal alkenes is challenging to achieve because it faces many other problems (Figure 1.2). As mentioned in section 1.1.1, many hydrofunctionalizations of unactivated internal alkenes produce products in which the functional group is installed at the terminal position. This result is due to a chain-walking process in which the initially formed secondary alkylmetal species by alkene insertion undergoes an iterative sequence comprising β -H elimination and olefin re-insertion to form the corresponding primary alkylmetal species, which is more thermodynamically stable than the secondary alkylmetal species. In other cases, the β -H elimination of the initial secondary alkylmetal species directly leads to the formation of functionalized alkene products. This process is a net oxidation. Furthermore, many catalysts for hydrofunctionalization catalyze competent alkene isomerization. Thus, sometimes hydrofunctionalization of internal alkenes affords a mixture of products.

A few systems were developed to catalyze hydrofunctionalization of internal alkenes (Figure 1.3). For example, hydroboration¹³ and formal hydroamination^{14, 15} of unactivated internal alkenes occur without alkene isomerization when catalyzed by a copper hydride complex. The origin of the lack of alkene isomerization in this copper system was studied in detail in Chapter 3. Hydroboration of unactivated internal alkenes with catecholborane catalyzed by rhodium complexes afforded exclusive branched products.¹⁶ Hydrosilylation of unactivated internal alkenes catalyzed by Speier's catalyst also proceeded without alkene isomerization.¹⁷ Finally, recent development of (formal) hydrofunctionalizations based on radical intermediates also enabled the use of internal alkenes for many transformations.¹⁸⁻²³

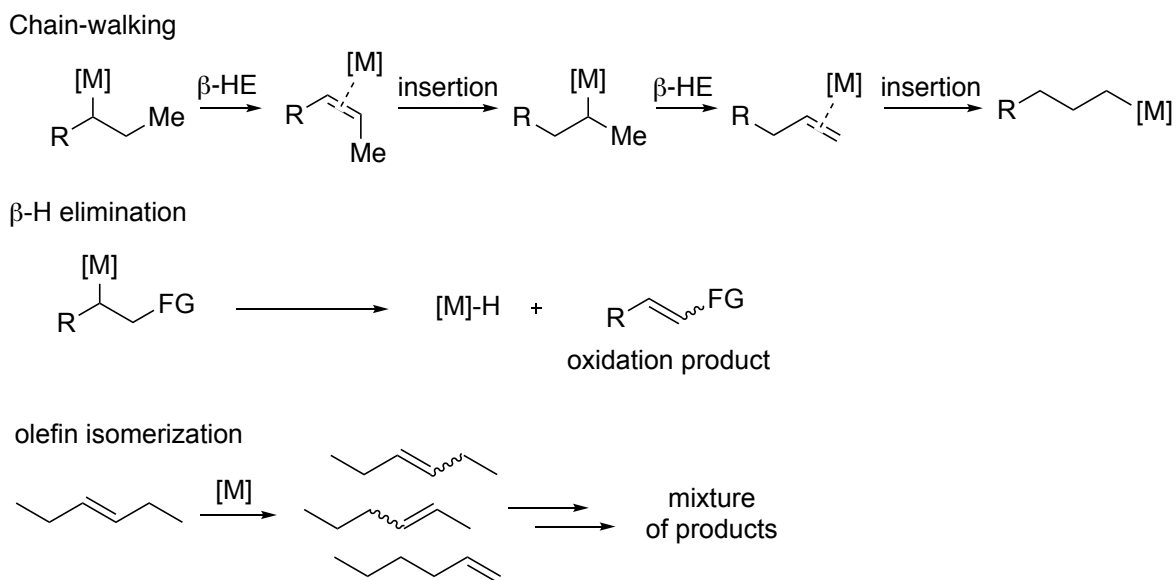


Figure 1.2 Common pitfalls in hydrofunctionalization of internal alkenes

The use of directing groups^{24, 25} is an alternative approach to achieve hydrofunctionalization of internal alkenes. Directing groups impart several beneficial effects on the reaction. First, incorporation of directing groups usually accelerates the reaction rate by increasing the effective

molarity of the reactants. Second, reactions with substrates containing directing groups occur by the formation of a metallacycle intermediate, which is formed after alkene insertion in the case of hydrofunctionalization. Because of the rigidity of the metallacycle, access of the metal to β -hydrogens, which is a prerequisite for β -H elimination to occur, is largely suppressed. Finally, the reactions of substrates containing directing groups usually proceed with control of regioselectivity, as discussed in the next paragraph.

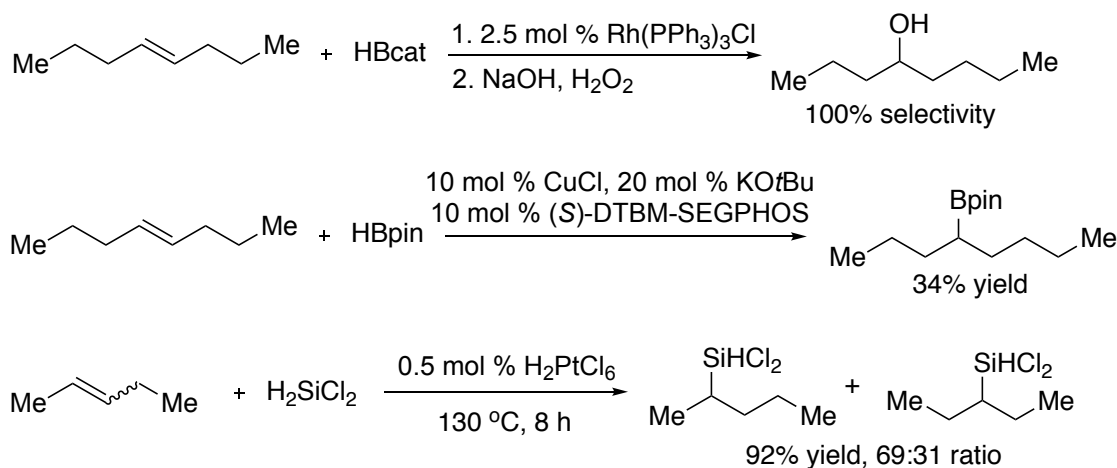
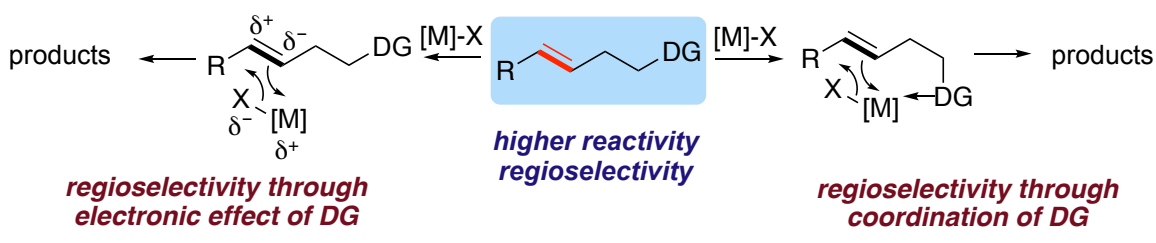


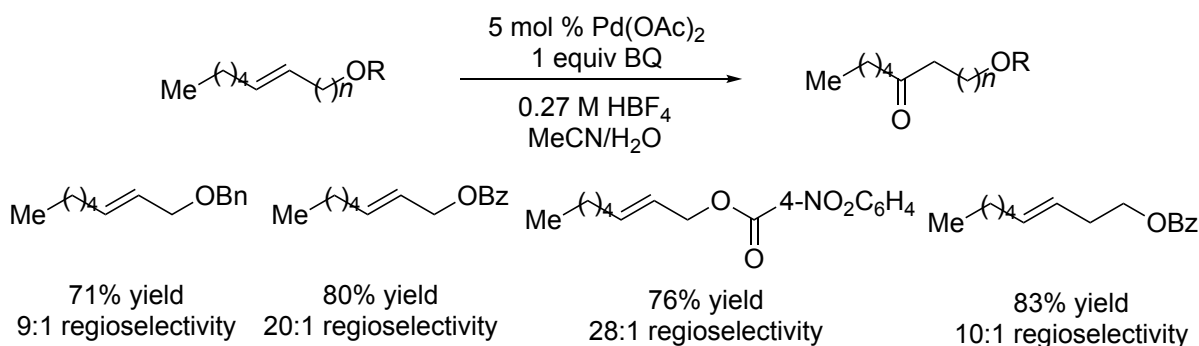
Figure 1.3 Examples of hydrofunctionalization of unactivated internal alkenes without alkene isomerization

The control of regioselectivity is a challenge for the hydrofunctionalization of internal alkenes, but is an important aspect of the hydrofunctionalization. High levels of regioselectivities demonstrate exquisite control of catalysts. For practical reasons, achieving high regioselectivity is often necessary because separation of isomeric products could be difficult.

There are three major ways to achieve regioselectivity in the hydrofunctionalization reactions (Figure 1.4). First, the regioselectivity can be determined by steric effects. Unsymmetrical internal alkenes bearing substituents different by size undergo hydrofunctionalization that could favor the formation of one product over the other. Second, the regioselectivity can be dictated by electronic effects.²⁶⁻²⁸ For example, Grubbs showed that the Wacker oxidation of allylic and homoallylic compounds occurred with high regioselectivity.²⁷ In this case, electron-deficient groups proximal to the alkene polarize the alkene through inductive effects, eventually leading to the observed regioselectivity. This polarization is also the origin of the regioselectivity observed in the reactions discussed in Chapters 2 and 5. Because this approach relies on the inductive effects of the polar groups, the regiocontrol is very sensitive to the position of these groups. Third, as discussed earlier, high regioselectivity of reactions with unsymmetrical alkenes can be achieved by the use of directing groups. This regioselectivity is generally controlled by the ring size of the metallacycle intermediate formed during the reaction. For example, Evans showed that the hydroboration of a β,γ -unsaturated amide occurred with exclusive formation of the carbon-boron bond at the β -position.²⁹



A. Regioselectivity controlled by electronic effects



B. Regioselectivity achieved by directing groups

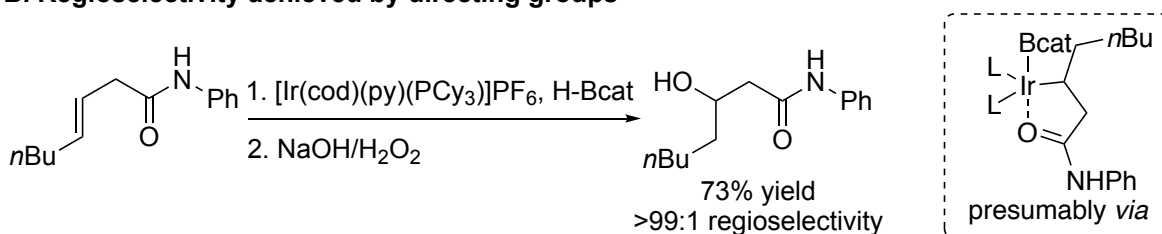


Figure 1.4 Strategies to control regioselectivity in functionalization of internal alkenes

1.1.3 Examples of Asymmetric Hydrofunctionalization of Unactivated Internal Alkenes

Asymmetric hydrofunctionalization of alkenes creates at least one stereogenic center at an alkene carbon. Because hydrofunctionalization could introduce many different functional groups based on the choice of the reagent, it would be an attractive approach for setting stereocenters that are remote to other functional groups in aliphatic systems.

The majority of asymmetric hydrofunctionalizations is focused on vinylarenes and terminal alkenes. Many catalysts were reported to promote a range of different hydrofunctionalization reactions with high enantioselectivity (>90% ee). However, examples of asymmetric hydrofunctionalization of unactivated internal alkenes are rare. In this section, a few representative examples will be discussed. Examples related to hydroboration and hydroamination will be covered in their respective section.

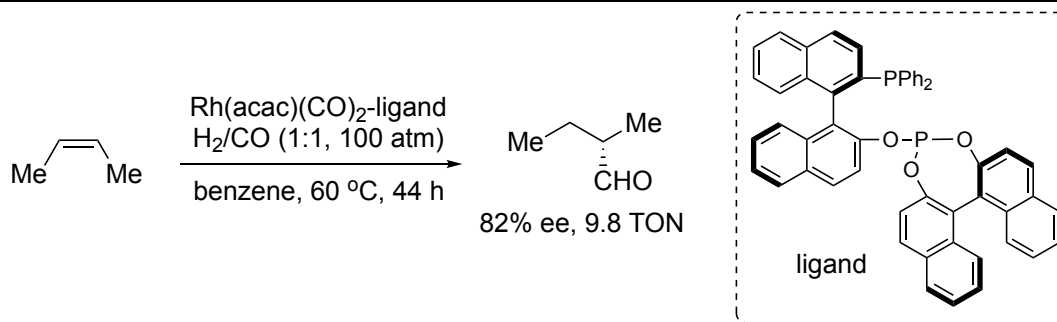


Figure 1.5 Asymmetric hydroformylation of *cis*-2-butene catalyzed by rhodium-phosphinephosphite complexes

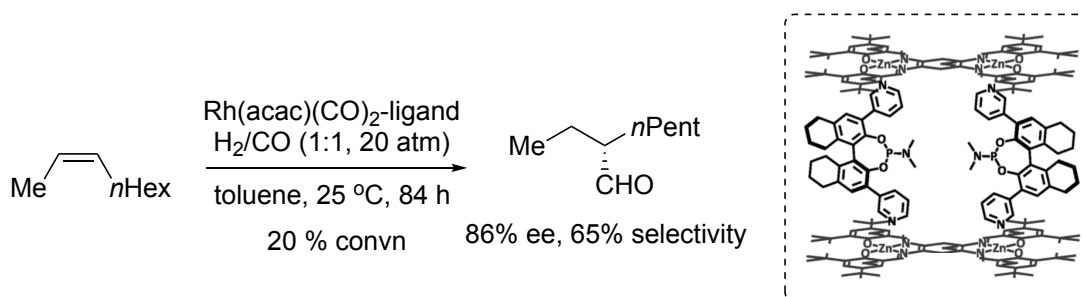


Figure 1.6 Asymmetric hydroformylation of *cis*-2-octene catalyzed by a chiral supramolecular assembly containing a rhodium center

A few examples of asymmetric hydroformylation of unactivated internal alkenes have been published. In 1994, Takaya and Nozaki reported that rhodium catalysts ligated by a chiral phosphine-phosphite hybrid ligand catalyzed hydroformylation of *cis*-2-butene in higher than 80% enantioselectivity (Figure 1.5).³⁰ This catalyst is one of the earliest examples to show that hydrofunctionalization of aliphatic internal alkenes can occur with high enantioselectivity. Reek reported a supramolecular assembly of a rhodium catalyst for hydroformylation (Figure 1.6).³¹ Although the catalyst was not particularly active, the enantioselectivity of the hydroformylation was measured to be 86% ee. This high ee resulted from the spatial confinement around metal center in a chiral pocket.

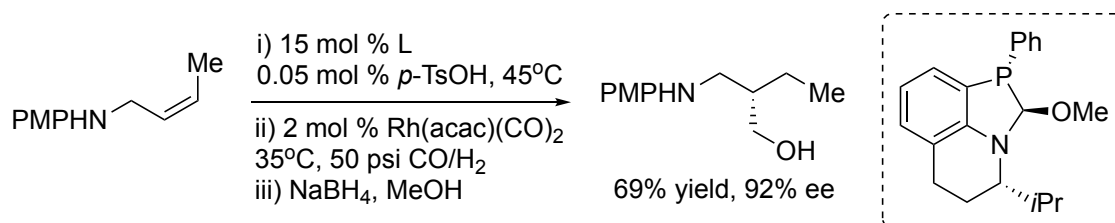


Figure 1.7 Asymmetric hydroformylation of allylamines using a chiral scaffolding ligand

Directed hydrofunctionalization of internal alkenes could also proceed with high enantioselectivity. A unique example reported by Tan showed that a rhodium complex containing a chiral phosphine ligand that reversibly binds to the substrate by covalent bonds, catalyzed the hydroformylation of homoallylic amine with high enantioselectivity and regioselectivity (Figure 1.7).³² The alkene substrate was incorporated into the ligand that is on the rhodium center during the

reaction, in which the ligand induced the stereoselectivity as a common auxiliary would. More recently, a directed hydroalkynylation of β,γ -unsaturated amides was reported by Li (Figure 1.8).³³ This reaction proceeded with high enantioselectivity and regioselectivity. In this case, the oxygen atom of the amide coordinates to the iridium center to control the regioselectivity of this reaction.

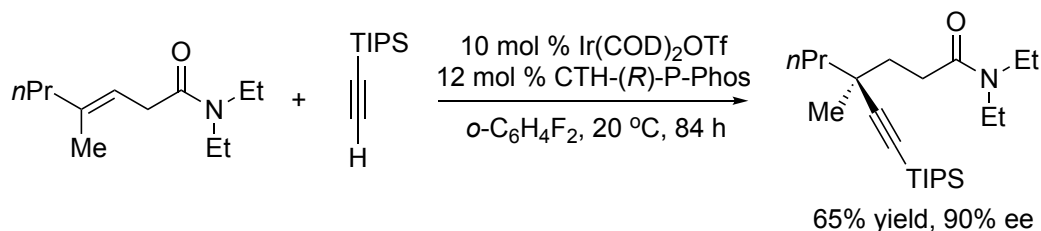


Figure 1.8 Asymmetric hydroalkynylation of β,γ -unsaturated amides

1.2 Hydroboration of Alkenes

1.2.1 Introduction

The hydroboration of alkenes is a classic and important transformation in organic synthesis.³⁴ Organoboron compounds, usually prepared by hydroboration, are versatile synthetic intermediates that participate in many carbon-carbon, and carbon-heteroatom bond-forming reactions.³⁵ Many of these bond-forming reactions are stereospecific.³⁶ Thus, utilizing enantioenriched organoboron compounds as starting materials would lead to a wide range of chiral functionalized molecules.

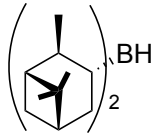
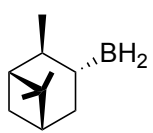
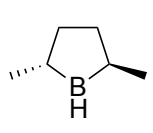
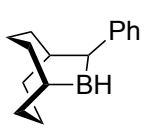
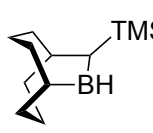
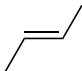
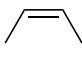
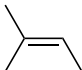
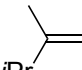
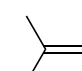
alkene					
	14	73	99.5	96	95
	99	24	98	32	84
	15	53	98	74	-
	32	-	2	38	52
	-	5	-	78	66

Figure 1.9 Asymmetric hydroboration of different classes of alkenes using chiral borane reagents

Many chiral boron reagents have been devised to control the stereoselectivity of the reaction.³⁷ The seminal work by H. C. Brown,³⁸ Masamune,³⁹ and Soderquist⁴⁰ showed that these chiral

reagents hydroborate a wide range of unactivated alkenes, including disubstituted alkenes and trisubstituted alkenes, with high diastereoselectivity (Figure 1.9). However, the need for stoichiometric amounts of chiral reagents largely limits their application in practical synthesis.

Catalytic asymmetric hydroboration is a better approach to access enantioenriched organoboron compounds.⁴¹ Extensive efforts have been dedicated to developing catalysts for such a reaction. The catalysts for asymmetric hydroboration have been dominated by rhodium complexes. The scope of the asymmetric hydroboration catalyzed by rhodium encompasses vinylarenes,⁴² strained alkenes,⁴³ and internal alkenes bearing directing groups.⁴⁴ Representative examples are discussed in section 1.2.2.

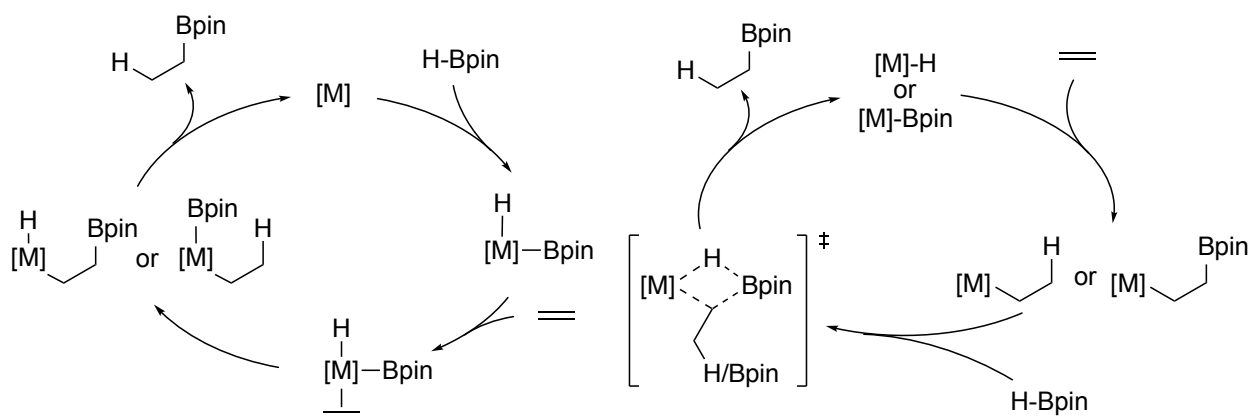


Figure 1.10 Two general types of mechanisms for catalytic hydroboration

Figure 1.10 depicts two general types of mechanisms for metal-catalyzed hydroboration. The first type of the mechanism involves oxidative addition of B-H bond to form a hydrido boryl complex, migratory insertion of an alkene into either a metal-hydride bond or a metal-boryl bond, and reductive elimination. The second mechanism involves migratory insertion of an alkene into a metal hydride or a metal boryl complex, and σ -bond metathesis. The mechanism by which the hydroboration occurs depends on the identity of the metal, the ancillary ligands, the alkene, and boron reagents.

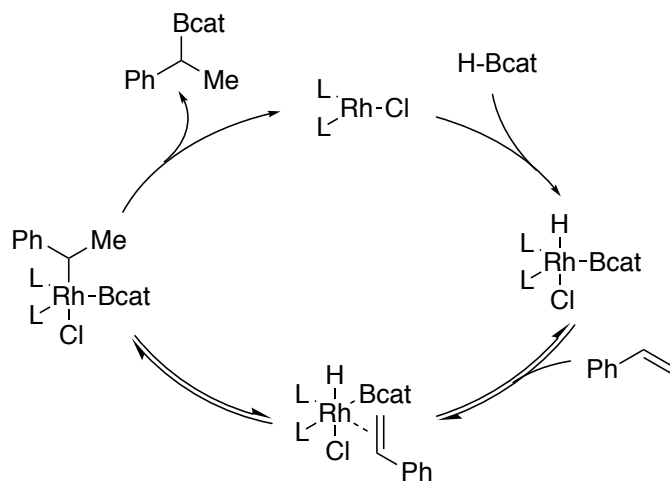
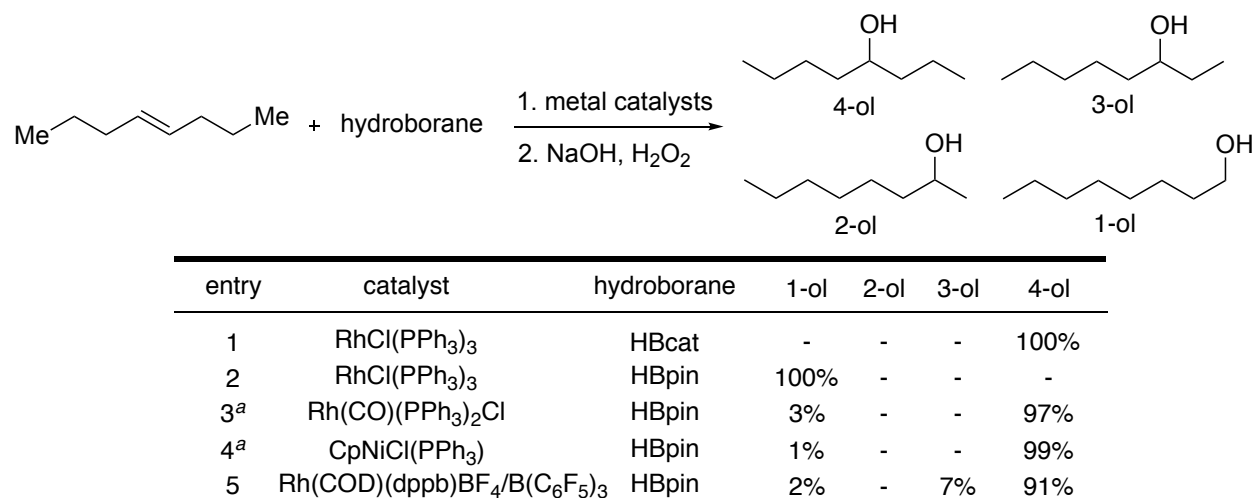


Figure 1.11 Proposed catalytic cycle for hydroboration

The mechanism of rhodium-catalyzed hydroboration of vinylarenes with catecholborane was studied extensively (Figure 1.11).^{16, 45} Despite complication in the system, it is generally believed that the catalytic reaction occurs by oxidative addition of B-H bond to a rhodium(I) species, followed by olefin insertion into the rhodium-hydride bond and reductive elimination of the rhodium-boryl bond.



^awere not reproducible

Figure 1.12 Hydroboration of *trans*-4-octene

A limited number of examples on hydroboration of unactivated internal alkenes was reported. The product selectivity depends on the identity of the metal, the borane reagent, and the additive used (Figure 1.12). For example, hydroboration of *trans*-4-octene using catecholborane catalyzed by Wilkinson's catalyst afforded exclusively the branched product with the boryl group at C4 position,¹⁶ but hydroboration of *trans*-4-octene using pinacolborane catalyzed by the same catalyst afforded exclusively the linear product.⁴⁶ It is likely because the C-B reduction elimination in the former case is faster than in the latter case due to the different Lewis acidity of the boron in these two borane reagents. Srebnik reported that hydroboration of *trans*-4-octene using pinacolborane catalyzed by Rh(CO)(PPh₃)₂Cl or CpNiCl(PPh₃) afforded the product with the boryl group attached at C4 position.⁴⁷ However, we were not able to reproduce these results. Crudden reported that the combination of a cationic rhodium complex and a Lewis acid also catalyzed hydroboration of *trans*-4-octene with 91% selectivity toward the product with the boryl group attached at C4 position.⁴⁸

Cases in which enantioselective hydroboration of unactivated internal alkenes was achieved are extremely limited. Only rhodium and copper complexes have been shown to catalyze asymmetric hydroboration of internal alkenes without alkene isomerization. These reactions will be discussed in detail in sections 1.2.2 and 1.2.3. Recently, Lu reported an enantioselective synthesis of benzylic boronates by isomerizing hydroboration using a cobalt catalyst (Figure 1.13).⁴⁹ It was demonstrated that a mixture of internal alkenes bearing phenyl groups at least two carbons away from the alkene underwent rapid isomerization and selective hydroboration to afford a single product in high enantioselectivity.

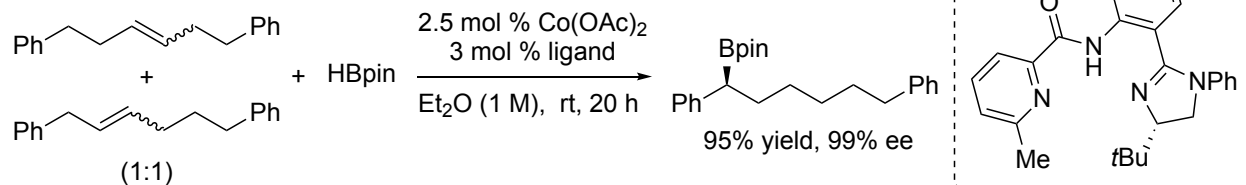


Figure 1.13 Asymmetric isomerizing hydroboration of internal alkenes

1.2.2 Asymmetric Hydroboration Catalyzed by Rhodium Complexes

Rhodium-catalyzed hydroboration constitutes the majority of examples of catalytic asymmetric hydroboration. The first examples of catalytic asymmetric hydroboration were reported by Burgess⁵⁰ and Hayashi,⁵¹ respectively, in which rhodium complexes of chiral bisphosphines were shown to induce enantioselectivity in hydroboration of vinylarenes. In particular, high enantioselectivity was achieved with complexes of axially chiral biaryl bisphosphines, such as BINAP, (Figure 1.14). Subsequently, P,N-ligands based on biaryl backbone, such as QUINAP⁵² and Pyphos,⁵³ were reported; the reactions catalyzed by rhodium complexes formed by these P,N-ligands occurred under mild conditions with broad scope of alkenes. The origin of the high enantioselectivity has been the subject of numerous studies, but such understanding is still lacking.

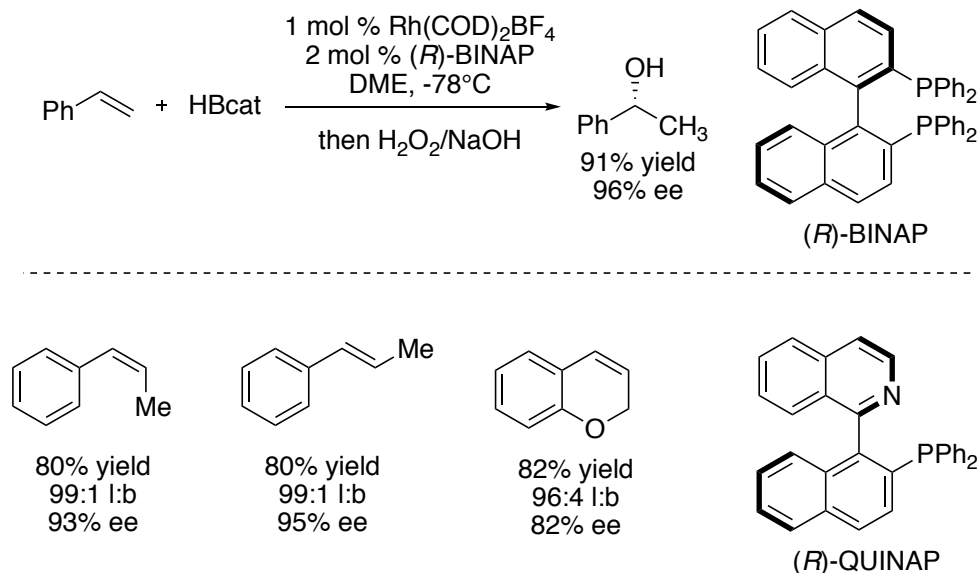


Figure 1.14 Asymmetric hydroboration of vinylarene derivatives

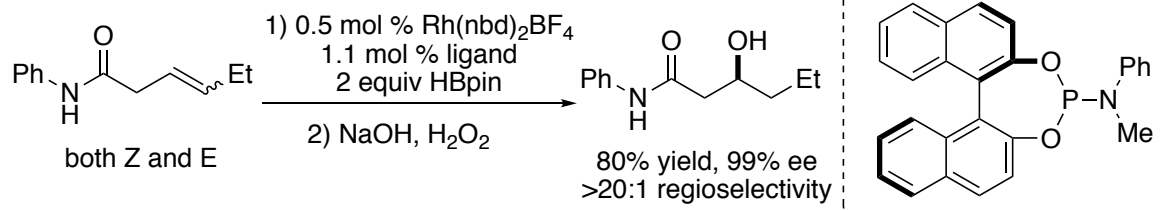
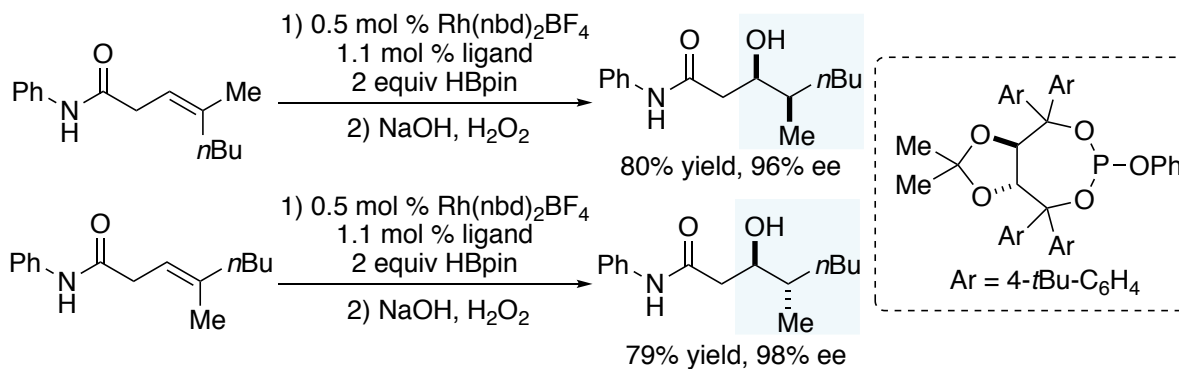
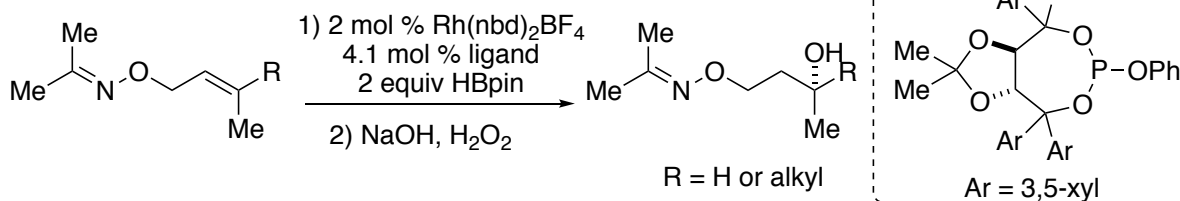
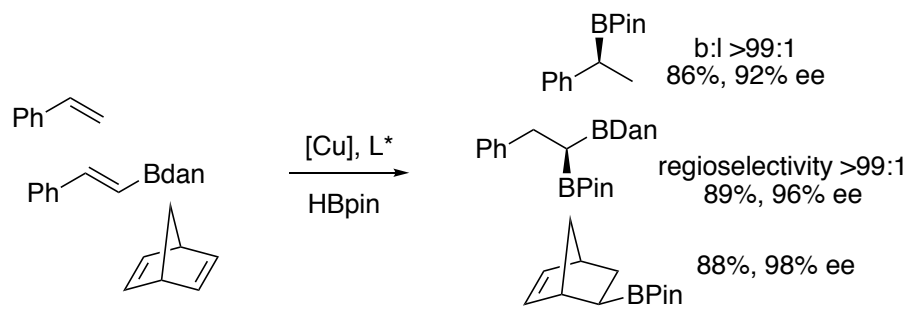
1,2-disubstituted alkenes**trisubstituted alkenes bearing amides as directing groups****trisubstituted alkenes bearing oximes as directing groups**

Figure 1.15 Directed asymmetric hydroboration of internal alkenes

1.2.2.1 Examples of Asymmetric Hydroboration of Internal Alkenes Catalyzed by Rhodium Complexes

Significant progress towards development of catalysts for directed hydroboration of alkenes has been made during the past decade. Among all reported catalysts, the rhodium complexes of monodentate phosphite and phosphoramidite ligands derived from TADDOL and BINOL reported by Takacs, are particularly active as catalysts for hydroboration of internal alkenes that bear a proximal directing group (Figure 1.15).⁴⁴ For example, Takacs showed that trisubstituted alkenes underwent hydroboration directed by an adjacent amide to afford secondary boronates with a vinal stereogenic center in high enantioselectivity.⁵⁴ Because the B-H addition is *syn*, the relative configuration of the newly formed stereocenters is set by the geometry of the starting alkene. The absolute configuration of the stereocenters is dictated by the rhodium complex. Reactions starting from both (*E*)- and (*Z*)-alkenes occurred with high enantioselectivity. The precise control of the stereoselectivity and the creation of two vicinal stereocenters render this system unique in the field of hydrofunctionalization. Later, this catalyst system was extended to trisubstituted alkenes bearing an oxime⁵⁵ and a phosphonate⁵⁶ as directing groups. In this case, tertiary boronates were obtained in high enantioselectivity.

The mechanism of the directed hydroboration was investigated by DFT calculations.⁵⁷ The results supported a mechanism similar to that of the rhodium-catalyzed hydroboration of vinylarenes, which includes B-H oxidative addition, alkene insertion into a rhodium-hydride bond, and C-B reductive elimination. However, studies with detailed experimental evidences were not reported.



Proposed mechanism:

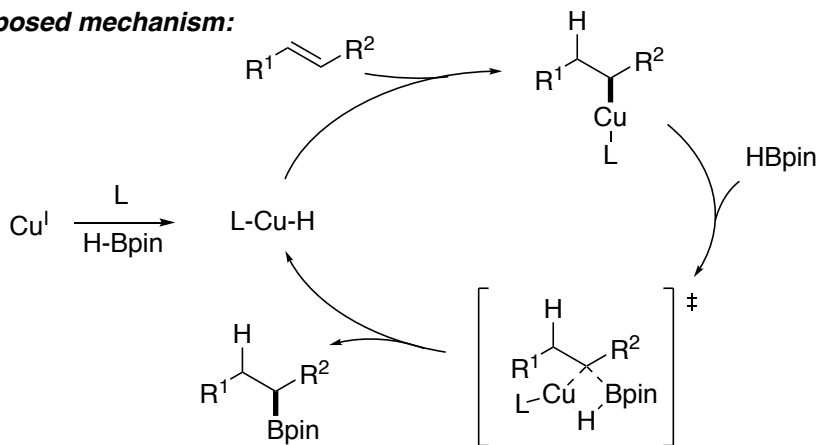


Figure 1.16 Copper-catalyzed asymmetric hydroboration

1.2.3 Asymmetric Hydroboration Catalyzed by Copper Complexes

Copper complexes catalyze hydroboration of alkenes with high enantioselectivity (Figure 1.16). The first report on this topic appeared in 2009 by Yun.⁵⁸ A combination of CuCl, a base, and a chiral bisphosphine ligand catalyzed hydroboration of vinylarenes. Later, this reaction was extended to β -substituted vinylarenes,⁵⁹ strained alkenes,⁶⁰ and vinylboronates.⁶¹

The mechanism of the hydroboration was proposed by Yun based on DFT calculations⁶² and literature precedents.⁶³ The reaction was believed to occur by the intermediacy of a copper hydride, which inserts an alkene to form an alkylcopper intermediate. Sigma-bond metathesis of the alkylcopper and pinacolborane releases the product and regenerates the copper hydride. However, no detailed experimental evidence was provided until our work described in Chapter 3.⁶⁴ We have isolated and characterized a series of relevant copper intermediates, and studies these complexes in stoichiometric reactions to gain information on each step of the catalytic cycle. We also revealed how the identity of the ligand and the alkene determined the catalyst resting state and ultimately controlled the efficiency of the catalysis.

1.2.3.1 Examples of Asymmetric Hydroboration of Unactivated Internal Alkenes Catalyzed by Copper Complexes

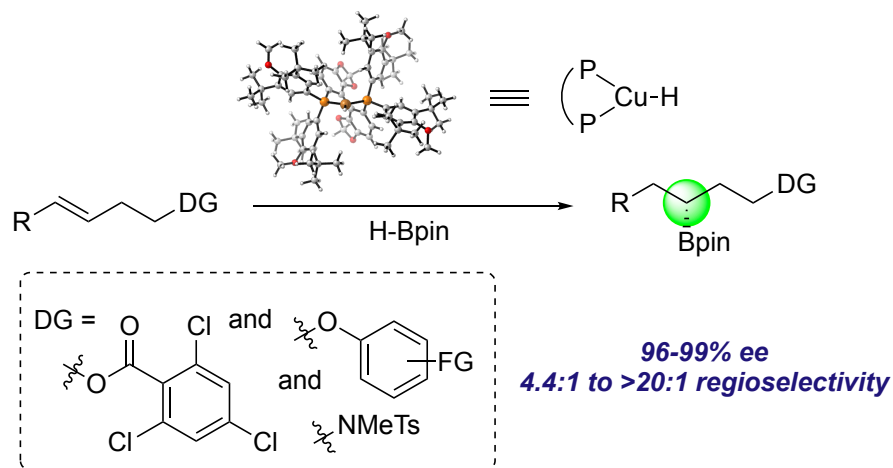


Figure 1.17 Copper-catalyzed asymmetric hydroboration of unsymmetrical internal alkenes

We were the first to show that the copper system catalyzed hydroboration of unactivated internal alkenes (Figure 1.17).¹³ Details were discussed in Chapter 2. Internal alkenes bearing electron-withdrawing groups at the β -position, such as alkoxy carbonyl, aryloxy and sulfonamido groups, underwent hydroboration in high yields, and with high regioselectivity and enantioselectivity. DFT calculations implied that the regioselectivity was controlled by inductive effects of these polar groups, like that in Grubbs' Wacker oxidation (Figure 1.4).⁶⁵ These electron-withdrawing groups also activated the alkene towards hydroboration; unactivated internal alkenes without or with these groups at least three carbons away from the alkene underwent hydroboration in low yields. In all cases, alkene isomerization that would lead to the formation of terminal products was not observed. The origin of this unique selectivity was revealed by our mechanistic study.⁶⁴ We showed that the reaction of the secondary alkylcopper intermediate with pinacolborane is much faster than the β -H elimination.

Our mechanistic understanding prompted us to devise new ligands to enhance the activity of the copper catalysts towards hydroboration of unactivated internal alkenes. As described in Chapter 4, we identified a catalyst that promotes the hydroboration of *trans*-4-octene with much higher yield under milder conditions than those previously reported.

1.2.4 Asymmetric Protoboration

Finally, an alternative strategy to achieve the “formal” hydroboration of alkenes has become attractive in the past decade. This method, termed protoboration, utilizes a combination of a diboron reagent and an alcohol to deliver a boryl group and a hydrogen atom to the alkene (Figure 1.18).⁶⁶ Hoveyda reported that copper complexes of NHC ligands catalyzed protoboration of vinylarenes⁶⁷ and 1,1-disubstituted alkenes⁶⁸ in high enantioselectivity. The key step in this reaction was believed to be the migratory insertion of an alkene into a copper-boryl bond,⁶⁶ based on early studies by Sadighi.⁶⁹ Later, Ito⁷⁰ and Shi⁷¹ independently extended this strategy to the

protoboration of terminal alkenes with high enantioselectivity. Parallel to this reaction, Aggarwal reported a rhodium variant that also achieved high enantioselectivity.⁷²

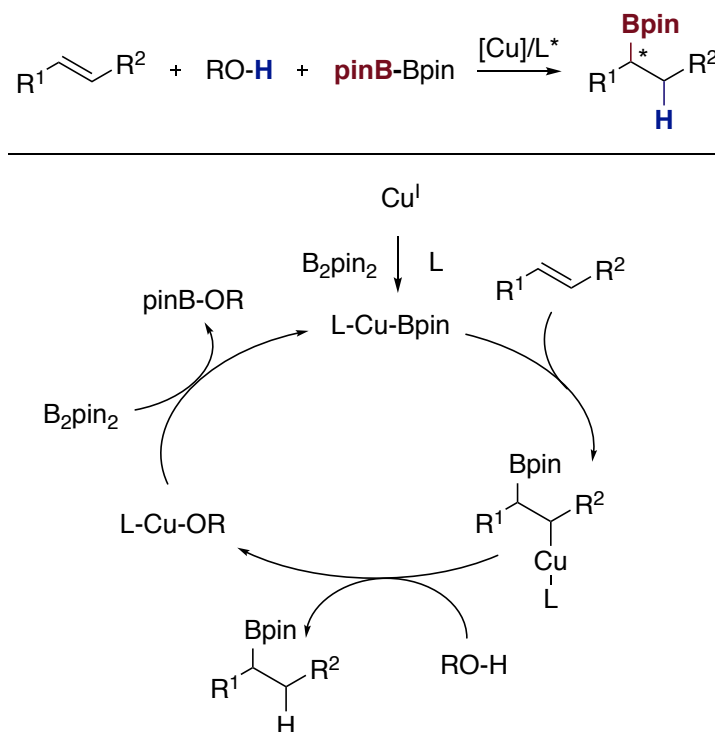


Figure 1.18 Copper-catalyzed formal hydroboration of unactivated alkenes

1.3 Hydroamination of Alkenes

1.3.1 The Fundamental of Hydroamination

The hydroamination of alkenes converts an alkene and an amine to functionalized amines, which are of particular importance in pharmaceutical industry.⁷³⁻⁷⁷ Over 50% of the drugs on the market contain at least one amine. Hydroamination is a direct approach to create amines because it is an addition reaction, which generates no waste, and it also uses alkenes as the starting materials, which are abundant feedstock chemicals. Although many catalysts were developed to promote hydroamination, the current reaction is still far from a general and efficient methodology that can be directly adopted by the pharmaceutical industry for practical synthesis of chiral amines.

1.3.1.1 Thermodynamics of Hydroamination

Many challenges hinder the development of the hydroamination. The most important and understood aspect of the hydroamination is that the reaction is close to thermoneutral in many cases. Although the enthalpy of the reaction is negative, it is counterbalanced by a negative entropy because the reaction is an addition. Because intramolecular hydroamination has a less negative entropy than the intermolecular variant, the former is thermodynamically more favorable than the latter, which has been extensively studied.

In 2006, our group reported direct measurement of the thermodynamics of a series hydroaminations of vinylarenes with aniline derivatives (Figure 1.19).⁷⁸ The enthalpy of the addition of N-methylaniline to styrene was determined to be -10 kcal/mol and the entropy was -27 eu. The overall free energy was -0.28 kcal/mol at 80 °C. This result indicates that the reaction conducted at a higher temperature would be less favorable than that at a lower temperature. Substituents on the reactants have a substantial effect on the equilibrium constant of the reaction. The reaction of a disubstituted vinylarene is thermodynamically uphill by 1.3 kcal/mol. DFT calculations showed that the hydromination of a tetrasubstituted alkene is uphill by 4.9 kcal/mol.²²

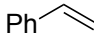
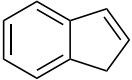
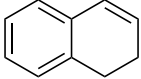
olefin	+	amine	$\xrightleftharpoons[\text{toluene-}d_8, 80\text{ }^\circ\text{C}]{\text{catalyst}}$	addition product
olefin		amine		ΔG (kcal/mol)
		<i>m</i> -anisidine		-3.54
		<i>m</i> -anisidine		0.26
		<i>m</i> -anisidine		1.31

Figure 1.19 Direct measurement of thermodynamics of hydroamination

The thermodynamics of the hydroamination poses a significant challenge. The reaction of unactivated internal alkenes, which have a smaller thermodynamic driving force than that of terminal alkenes, would be particularly difficult to achieve. The potential reversibility of the reaction would likely preclude the development of an asymmetric variant because of racemization of the product.^{79, 80} Substituent effects on the hydroamination could lead to a system that is thermodynamically favorable enough to suppress the reverse of hydroamination.

1.3.1.2 Mechanisms of Hydroamination

There are three major mechanistic pathways for hydroamination, which are illustrated in Figure 1.20. The mechanism primarily depends on the metal. The first mechanism involves migratory insertion of an alkene into a metal-amido bond.⁸¹ The amido intermediate was formed initially by ligand exchange of the precatalyst and an amine. Alkene insertion into this species forms an alkylmetal intermediate, which undergoes protonolysis with another amine molecule to release the product and regenerate the amido species. This mechanism is common for catalysts of early transition metals, main-group metals, and lanthanides. Because the mechanism involves amido complexes of early transition metals, the hydroamination is usually not compatible with air, moisture, and functional groups.

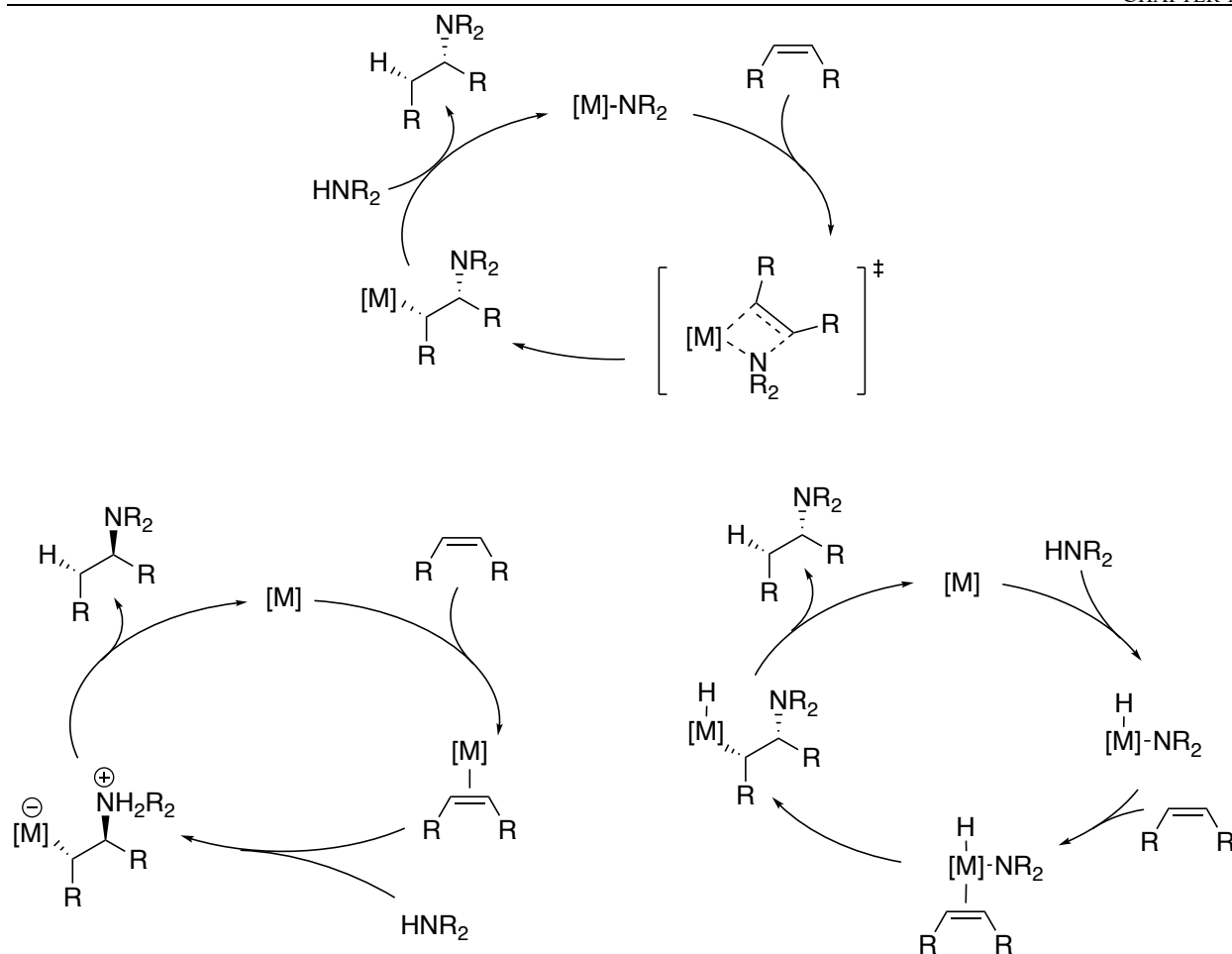


Figure 1.20 General mechanisms of hydroamination

The second mechanism involves an outer-sphere nucleophilic addition of a metal-bound olefin complex by an amine.⁸²⁻⁸⁶ The addition forms a zwitterionic intermediate, an alkylmetal species with a protonated amine at the β -position. Finally, protonolysis of the metal-carbon bond by the protonated amine forms the product. The protonolysis step can be concerted or through a sequence consisted of oxidative addition and reductive elimination. This mechanism is common for most of the late transition-metal catalysts. Because productive catalysis occurs only after the formation of metal-olefin complexes, the competition between amines and alkenes towards metal binding is important in determining the reaction efficiency. In general, the equilibrium favors the amine binding because basic amines are better σ -donors than alkenes. The use of an electron-deficient metal catalyst would lead to a lower barrier for the outer-sphere nucleophilic addition (versus the olefin complex) than the use of an electron-rich one, but the amine binding would be stronger in the former case than in the latter and *vice versa*. The balance between the electronic properties of the catalyst and the basicity and nucleophilicity of the amine determines the efficiency of the hydroamination. Finally, the rate-limiting step of many reactions that occur by this mechanism is protonolysis of the zwitterionic intermediate. However, the effect of the ligands on this step have not been fully understood.

The third mechanism involves an oxidative addition of N-H bond of an amine.⁸⁷ The hydrido amido metal species formed by oxidative addition undergoes olefin migratory insertion to generate an alkyl hydrido metal intermediate, which reductively eliminates to form the product. This mechanism almost exclusively belongs to iridium catalysts.^{7, 88, 89}

Several other pathways usually observed in the hydroamination complicate the reaction. As discussed in section 1.1.2, many catalysts form hydroamination also catalyze competing isomerization. For the reactions of terminal alkenes, the isomerization will form internal alkenes, which are much less reactive than terminal alkenes, leading to hydroamination products in low yields; for the reactions of internal alkenes, the isomerization will form terminal alkenes, which react much faster than internal alkenes, leading to a mixture of hydroamination products. In addition, many reactions form a mixture of hydroamination and oxidative amination products, which are resulted from β -H elimination. This leads to products in low yields.

1.3.2 Asymmetric Intramolecular Hydroamination

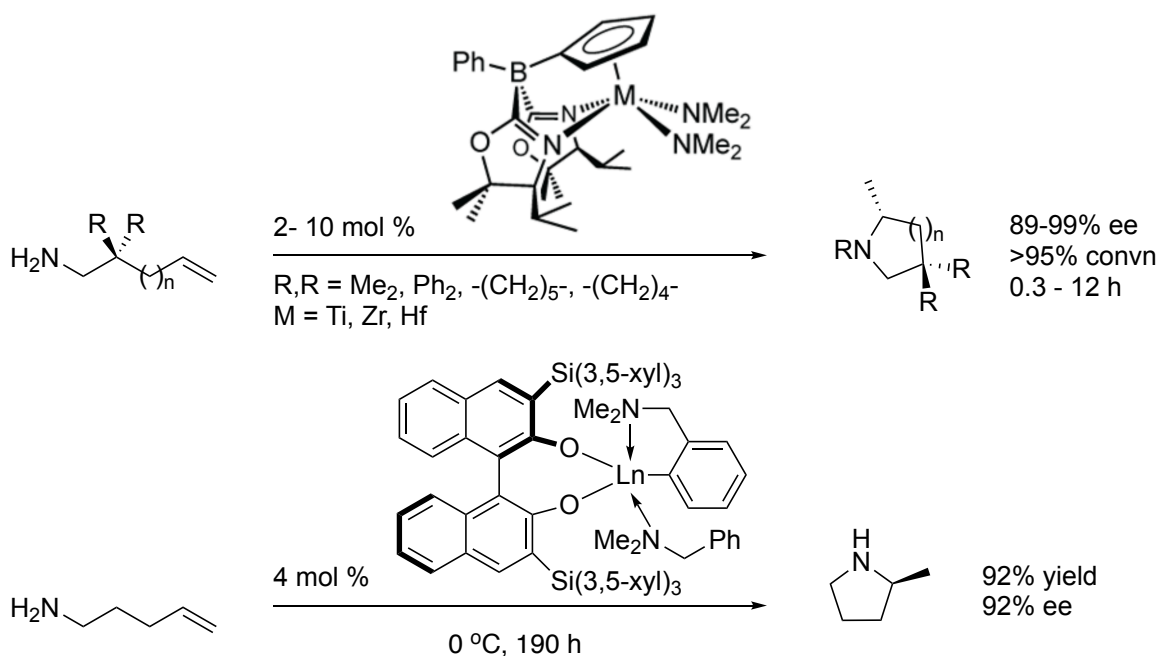


Figure 1.21 Asymmetric intramolecular hydroamination catalyzed by early transition-metal catalysts

Catalysts for asymmetric intramolecular hydroamination have been extensively developed.⁹⁰⁻⁹² Many transition-metal complexes catalyze hydroamination of aminoalkenes with high enantioselectivity. The first asymmetric hydroamination was reported by Marks using chiral lanthanocene catalysts.⁹³ Later, rare earth metal catalysts based on non-metallocene ligands were reported by Scott⁹⁴ and Hultsch.⁹⁴ These catalysts are derived from axially chiral bisarylamido or binaphtholate ligands. Catalysts of alkali metals,⁹⁵ alkaline earth metals,⁹⁶ and group 12 metals^{97, 98} have also been shown to promote asymmetric hydroamination. High levels of enantioselectivity was achieved with zirconium catalysts supported by chiral cyclopentadienylbis(oxazolinyl)borate ligand developed by Sadow (Figure 1.21).^{99, 100} Aminoalkenes bearing geminal groups underwent hydroamination with high enantioselectivity to form products containing five-, six-, and seven-

membered rings. Mechanistic investigation indicated that the reaction occurred by a concerted transition state involving six atoms for simultaneous C–N and C–H bond formation and N–H bond cleavage from two aminoalkene units. Hultsch reported a lutetium binaphtholate catalyst that promoted the hydroamination of 5-amino-1-pentene with 92% ee.²

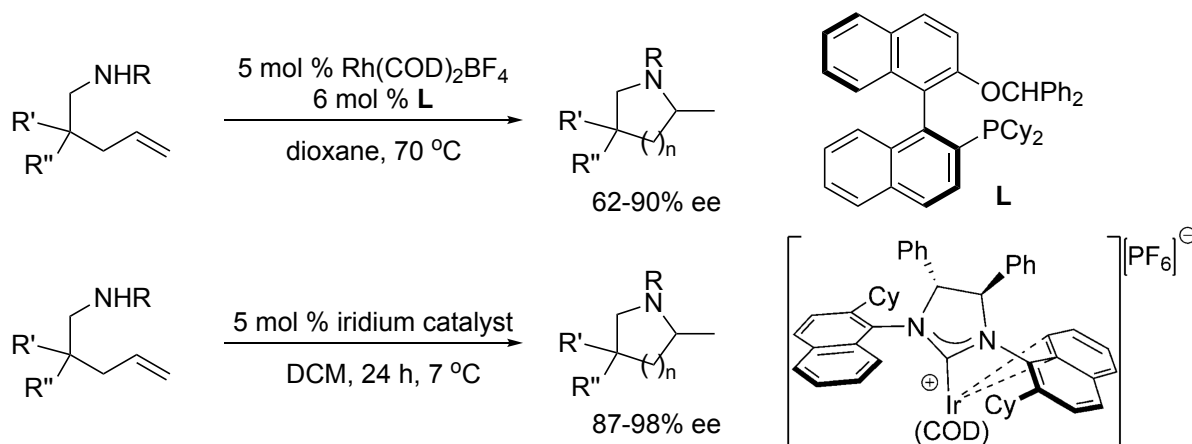


Figure 1.22 Asymmetric intramolecular hydroamination catalyzed by late transition-metal catalysts

Catalysts based on late transition-metals have been demonstrated to be compatible with a range of functional groups, including hydroxy, silyloxy, alkoxy carbonyl, acyl, cyano groups, and a chlorine atom. Platinum catalysts reported by Widenhoefer,¹⁰¹ rhodium catalysts reported by Hartwig,^{84, 85, 102, 103} palladium catalysts reported by Michael,¹⁰⁴ and iridium catalysts^{83, 105, 106} were investigated extensively. However, only a few catalyzed hydroamination in high enantioselectivity (Figure 1.22). Built upon the work of Hartwig,^{102, 103} Buchwald reported an asymmetric variant of the rhodium-catalyzed hydroamination. The reaction afforded products in enantioselectivity typically ranging from 80-90%.¹⁰⁷ However, this rhodium catalytic system was not active towards primary aminoalkenes that do not contain geminal groups, such as 5-amino-1-pentene. In 2016, Dorta reported that high enantioselectivity of hydroamination unactivated aminoalkenes was achieved by an iridium catalyst ligated by a chiral NHC. This enantioselectivity is the highest among all reported for this type of hydroamination using late transition-metal catalysts.¹⁰⁶

1.3.3 Asymmetric Intermolecular Hydroamination of Unactivated Alkenes

Examples of asymmetric intermolecular hydroamination of unactivated alkenes are extremely rare (Figure 1.23). Hultsch reported an yttrium binaphtholate complex that catalyzed hydroamination of unactivated terminal alkenes with primary amines with modest enantioselectivity (up to 61% ee).¹⁰⁸ Widenhoefer reported a cationic gold system that catalyzed hydroamination of unactivated terminal alkenes with cyclic ureas with up to 78% ee.¹⁰⁹ Early this year, Hull reported a directed hydroamination of allylamines with secondary amines with high enantioselectivity.¹¹⁰ Finally, Beauchemin reported that a chiral aldehyde catalyzed a Cope-type hydroamination of allylamines with hydroxylamine derivatives with high enantioselectivity.¹¹¹

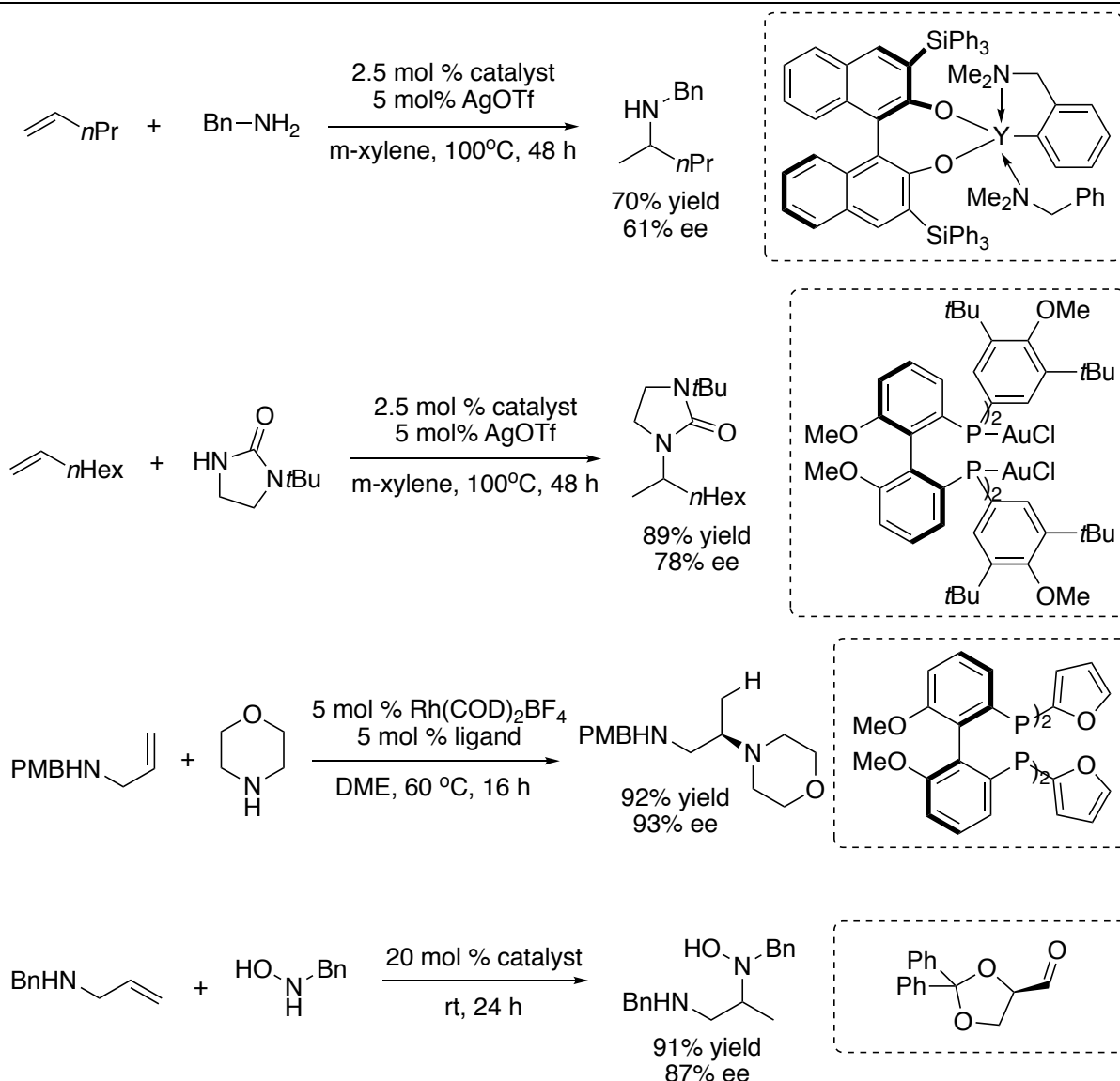


Figure 1.23 Asymmetric intermolecular hydroamination of unactivated terminal alkenes

Prior to the work described in Chapter 6, direct, asymmetric hydroamination of unactivated internal alkenes is unknown.

1.3.4 Intermolecular Hydroamination of Unactivated Internal Alkenes

Racemic versions of catalytic hydroamination unactivated internal alkenes were developed recently.²¹⁻²³ As discussed in section 1.3.1.2, direct hydroamination of unactivated internal alkenes, especially those that are tri- and tetra-substituted can be thermodynamically uphill. To overcome this challenge, a photocatalytic hydroamination was developed.²² Knowles reported that unactivated alkenes, including tri- and tetra-substituted ones, undergo hydroamination with secondary

aliphatic amines to afford the products in good yields. Here, the light absorption provides a viable thermodynamic driving force.

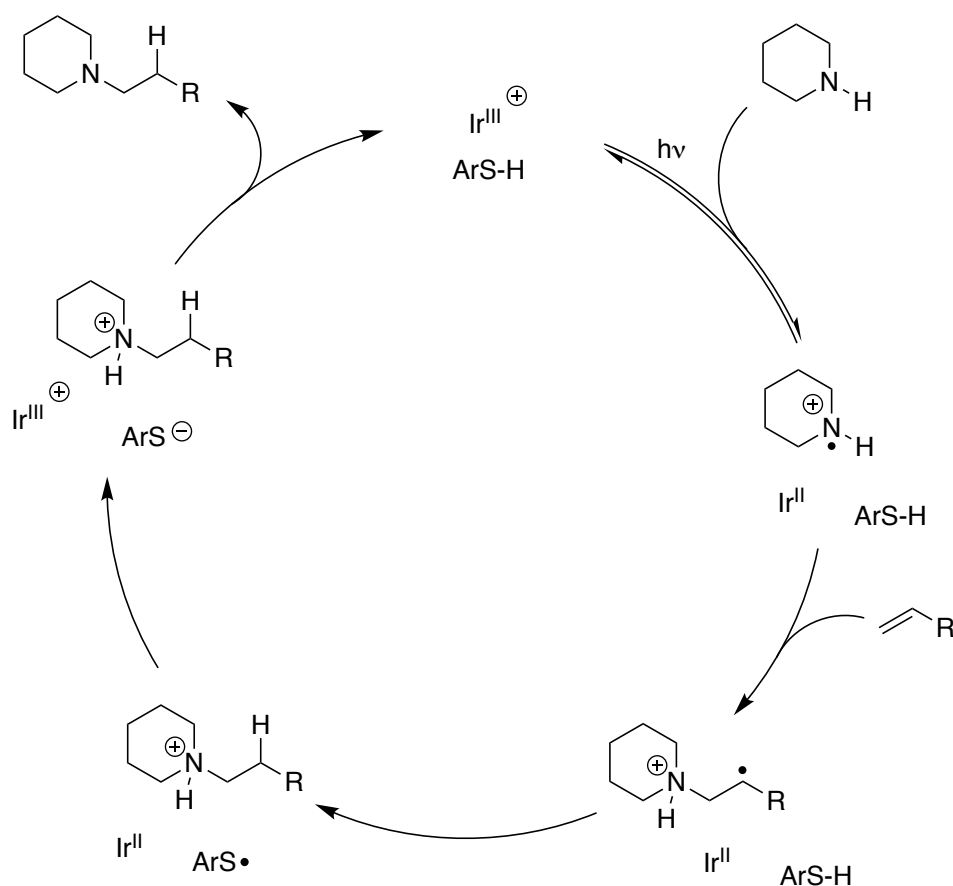
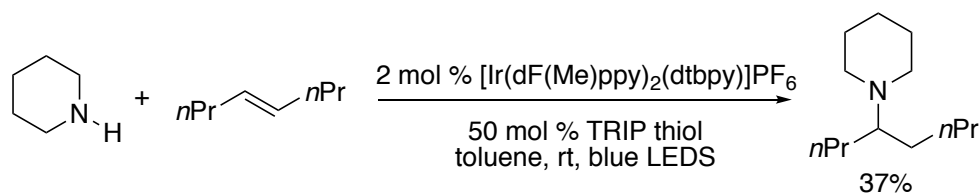


Figure 1.24 Photocatalytic intermolecular hydroamination of unactivated internal alkenes

The mechanism of the reaction is shown in Figure 1.24. The catalytic cycle starts with photoexciting of catalyst $[\text{Ir}(\text{dF}(\text{CF}_3)\text{ppy})_2(\text{bpy})]\text{PF}_6$ to its excited state, which undergoes a single-electron oxidation of an amine to afford the corresponding aminium radical cation and an iridium(II) species, the reduced form of the catalyst. The electrophilic aminium radical cation undergoes a rapid addition to a nucleophilic alkene to form a carbon-centered radical which is more stable than the nitrogen-centered radical. Trapping of the carbon-centered radical with a thiol reagent through hydrogen atom transfer affords the hydroamination product in protonated form and a sulfur-centered radical. Finally, oxidation of the radical by the iridium(II) forms the corresponding

thiolate, which reacts with the ammonium product to release the hydroamination product and the thiol.

Hydroamination of internal alkenes bearing directing groups was reported by Engle.¹¹² Similar to the rhodium-catalyzed directed hydroboration, the palladium-catalyzed hydroamination occurred with high regioselectivity. The regioselectivity is likely dictated by the size of the pallacycle intermediate formed by outer-sphere nucleophilic addition of the amine reagent, phthalimide.

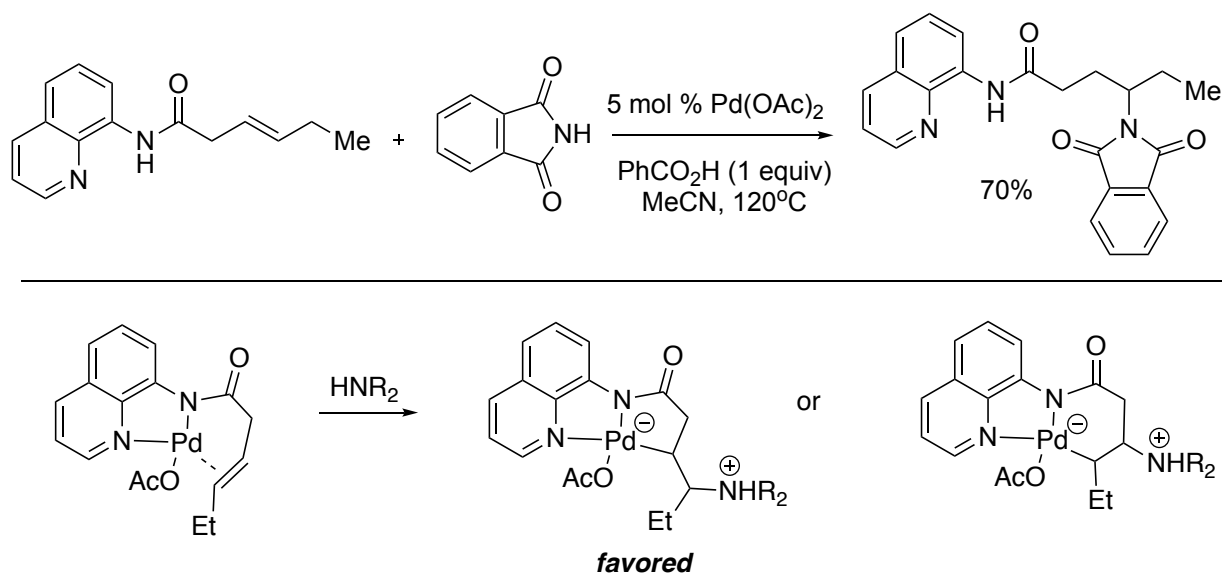


Figure 1.25 Directed intermolecular hydroamination of internal alkenes

1.3.5 Asymmetric Formal Hydroamination

The unfavorable thermodynamics of the hydroamination of internal alkenes is the major challenge that hinders the development of effective catalysts. Other strategies were also explored to achieve a formal hydroamination. Similar to the concept of protoboration discussed in the end of section 1.2.3, formal hydroamination was achieved using a combination of a reducing reagent, usually hydrosilanes, and an electrophilic aminating reagent, which was first reported by Johnson.¹¹³ Because the overall reaction is from an alkene, a silane, and an electrophilic aminating reagent to an amine and an aryloxy silane, the net reaction is much more thermodynamically favored than the corresponding hydroamination reaction. In this reaction, a weak silicon-hydrogen bond, a weak nitrogen-oxygen bond, and a π -bond are broken, and a strong silicon-oxygen bond, a strong carbon-hydrogen bond, and a carbon-nitrogen bond are formed.

In 2013, Buchwald¹¹⁴ and Miura¹¹⁵ independently developed a copper catalytic system for the formal hydroamination (Figure 1.26). Derived from chiral bisphosphine ligands, especially those of axially chiral biaryl backbones, the catalysts were highly active for enantioselective hydroamination of several classes of alkenes. The mechanism of the reaction¹¹⁶ involves a copper hydride intermediate, similar to that of the copper-catalyzed hydroboration.

The copper-catalyzed formal hydroamination enabled access to highly enantioenriched aliphatic amines from internal alkenes.¹⁴ Buchwald reported formal hydroamination of unactivated internal alkenes, mostly *trans*-2-butene, with a range of modified electrophilic aminating reagents.

Concurrent with this work, we developed the hydroamination of internal alkenes bearing electron-withdrawing groups, which proceeded in high enantioselectivity and good regioselectivity.¹⁵ This work is described in Chapter 5.

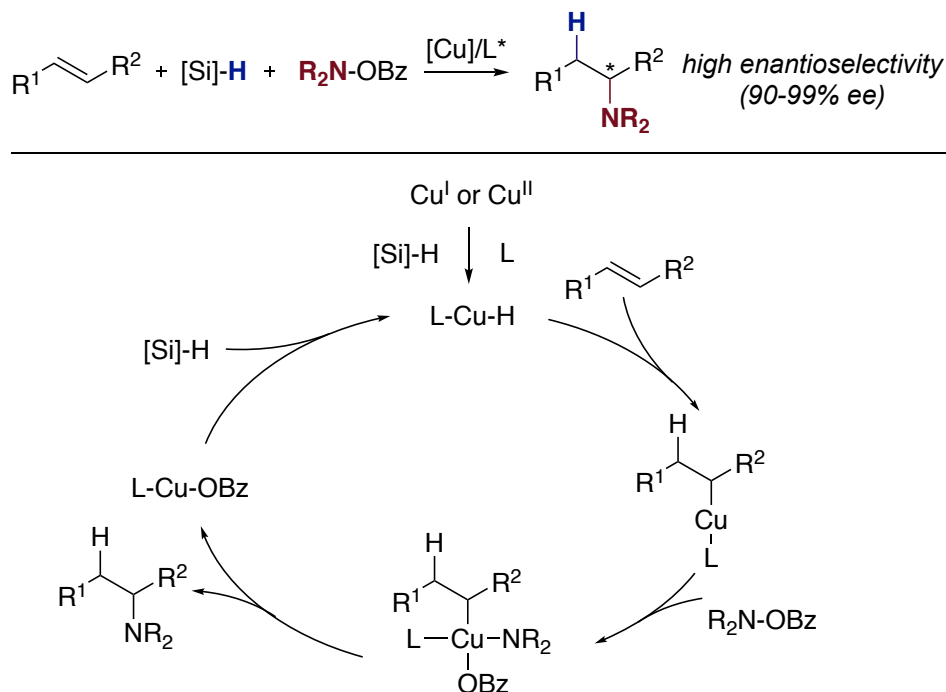


Figure 1.26 Asymmetric formal hydroamination of alkenes

1.4 Summary

For decades, many catalysts have been developed for hydrofunctionalization of unactivated alkenes. These catalysts have been demonstrated to catalyze hydrofunctionalization of several classes of alkenes with promising control of stereoselectivity. However, these methods are still far from a general, efficient, and robust synthetic methodology. Examples of hydrofunctionalization of unactivated alkenes that bear more than one substituent are limited, and examples of hydrofunctionalization of unactivated alkenes that bear more than two substituents are still rare. As recent reports of asymmetric hydrofunctionalizations of unactivated internal alkenes begin to emerge, these reports will deepen our understanding of these transformations and inspire future developments on this topic.

1.5 References

- [1] Ananikov, V. P.; Tanaka, M., *Hydrofunctionalization*. Springer: Berlin Heidelberg, 2013.
- [2] Gribkov, D. V.; Hultsch, K. C.; Hampel, F., *J. Am. Chem. Soc.* **2006**, *128*, 3748.
- [3] Gagne, M. R.; Marks, T. J., *J. Am. Chem. Soc.* **1989**, *111*, 4108.
- [4] Gribkov, D. V.; Hultsch, K. C., *Angew. Chem. Int. Ed.* **2004**, *43*, 5542.
- [5] Kawatsura, M.; Hartwig, J. F., *J. Am. Chem. Soc.* **2000**, *122*, 9546.

- [6] Utsunomiya, M.; Kuwano, R.; Kawatsura, M.; Hartwig, J. F., *J. Am. Chem. Soc.* **2003**, *125*, 5608.
- [7] Dorta, R.; Egli, P.; Zürcher, F.; Togni, A., *J. Am. Chem. Soc.* **1997**, *119*, 10857.
- [8] Männig, D.; Nöth, H., *Angew. Chem. Int. Ed.* **1985**, *24*, 878.
- [9] Obligacion, J. V.; Chirik, P. J., *Nat. Rev. Chem.* **2018**, *2*, 15.
- [10] Matsumoto, T.; Taube, D. J.; Periana, R. A.; Taube, H.; Yoshida, H., *J. Am. Chem. Soc.* **2000**, *122*, 7414.
- [11] Lail, M.; Arrowood, B. N.; Gunnoe, T. B., *J. Am. Chem. Soc.* **2003**, *125*, 7506.
- [12] Bair, J. S.; Schramm, Y.; Sergeev, A. G.; Clot, E.; Eisenstein, O.; Hartwig, J. F., *J. Am. Chem. Soc.* **2014**, *136*, 13098.
- [13] Xi, Y.; Hartwig, J. F., *J. Am. Chem. Soc.* **2016**, *138*, 6703.
- [14] Yang, Y.; Shi, S.-L.; Niu, D.; Liu, P.; Buchwald, S. L., *Science* **2015**, *349*, 62.
- [15] Xi, Y.; Butcher, T. W.; Zhang, J.; Hartwig, J. F., *Angew. Chem. Int. Ed.* **2016**, *55*, 776.
- [16] Evans, D. A.; Fu, G. C.; Anderson, B. A., *J. Am. Chem. Soc.* **1992**, *114*, 6679.
- [17] Benkeser, R. A.; Muench, W. C., *J. Am. Chem. Soc.* **1973**, *95*, 285.
- [18] Gui, J.; Pan, C.-M.; Jin, Y.; Qin, T.; Lo, J. C.; Lee, B. J.; Spengel, S. H.; Mertzman, M. E.; Pitts, W. J.; La Cruz, T. E.; Schmidt, M. A.; Darvatkar, N.; Natarajan, S. R.; Baran, P. S., *Science* **2015**, *348*, 886.
- [19] Crossley, S. W. M.; Obradors, C.; Martinez, R. M.; Shenvi, R. A., *Chem. Rev.* **2016**, *116*, 8912.
- [20] Green, S. A.; Huffman, T. R.; McCourt, R. O.; van der Puyl, V.; Shenvi, R. A., *J. Am. Chem. Soc.* **2019**, *141*, 7709.
- [21] Nguyen, T. M.; Manohar, N.; Nicewicz, D. A., *Angew. Chem. Int. Ed.* **2014**, *53*, 6198.
- [22] Musacchio, A. J.; Lainhart, B. C.; Zhang, X.; Naguib, S. G.; Sherwood, T. C.; Knowles, R. R., *Science* **2017**, *355*, 727.
- [23] Zhu, Q.; Graff, D. E.; Knowles, R. R., *J. Am. Chem. Soc.* **2018**, *140*, 741.
- [24] Rousseau, G.; Breit, B., *Angew. Chem. Int. Ed.* **2011**, *50*, 2450.
- [25] Hoveyda, A. H.; Evans, D. A.; Fu, G. C., *Chem. Rev.* **1993**, *93*, 1307.
- [26] Mei, T.-S.; Werner, E. W.; Burckle, A. J.; Sigman, M. S., *J. Am. Chem. Soc.* **2013**, *135*, 6830.
- [27] Morandi, B.; Wickens, Z. K.; Grubbs, R. H., *Angew. Chem. Int. Ed.* **2013**, *52*, 9751.
- [28] Lerch, M. M.; Morandi, B.; Wickens, Z. K.; Grubbs, R. H., *Angew. Chem. Int. Ed.* **2014**, *53*, 8654.
- [29] Evans, D. A.; Fu, G. C., *J. Am. Chem. Soc.* **1991**, *113*, 4042.
- [30] Sakai, N.; Nozaki, K.; Takaya, H., *J. Chem. Soc., Chem. Commun.* **1994**, 395.
- [31] Gadzikwa, T.; Bellini, R.; Dekker, H. L.; Reek, J. N. H., *J. Am. Chem. Soc.* **2012**, *134*, 2860.
- [32] Worthy, A. D.; Joe, C. L.; Lightburn, T. E.; Tan, K. L., *J. Am. Chem. Soc.* **2010**, *132*, 14757.
- [33] Wang, Z.-X.; Li, B.-J., *J. Am. Chem. Soc.* **2019**, *141*, 9312.
- [34] Zaidlewicz, M., *Hydroboration*. John Wiley & Sons, Inc.: 2000.
- [35] Hall, D. G., *Boronic Acids: Preparation and Applications in Organic Synthesis and Medicine*. Wiley-VCH: Weinheim, 2005.
- [36] Leonori, D.; Aggarwal, V. K., *Angew. Chem. Int. Ed.* **2015**, *54*, 1082.
- [37] Thomas, S. P.; Aggarwal, V. K., *Angew. Chem. Int. Ed.* **2009**, *48*, 1896.
- [38] Brown, H. C.; Singaram, B., *Acc. Chem. Res.* **1988**, *21*, 287.

- [39] Masamune, S.; Kim, B. M.; Petersen, J. S.; Sato, T.; Veenstra, S. J.; Imai, T., *J. Am. Chem. Soc.* **1985**, *107*, 4549.
- [40] Gonzalez, A. Z.; Román, J. G.; Gonzalez, E.; Martinez, J.; Medina, J. R.; Matos, K.; Soderquist, J. A., *J. Am. Chem. Soc.* **2008**, *130*, 9218.
- [41] Crudden, Cathleen M.; Edwards, D., *Eur. J. Org. Chem.* **2003**, *2003*, 4695.
- [42] Carroll, A.-M.; O'Sullivan, T. P.; Guiry, P. J., *Adv. Synth. Catal.* **2005**, *347*, 609.
- [43] Rubina, M.; Rubin, M.; Gevorgyan, V., *J. Am. Chem. Soc.* **2003**, *125*, 7198.
- [44] Smith, S. M.; Thacker, N. C.; Takacs, J. M., *J. Am. Chem. Soc.* **2008**, *130*, 3734.
- [45] Burgess, K.; Van der Donk, W. A.; Westcott, S. A.; Marder, T. B.; Baker, R. T.; Calabrese, J. C., *J. Am. Chem. Soc.* **1992**, *114*, 9350.
- [46] Pereira, S.; Srebniak, M., *J. Am. Chem. Soc.* **1996**, *118*, 909.
- [47] Pereira, S.; Srebniak, M., *Tetrahedron Lett.* **1996**, *37*, 3283.
- [48] Lata, C. J.; Crudden, C. M., *J. Am. Chem. Soc.* **2010**, *132*, 131.
- [49] Chen, X.; Cheng, Z.; Guo, J.; Lu, Z., *Nat. Commun.* **2018**, *9*, 3939.
- [50] Burgess, K.; Ohlmeyer, M. J., *J. Org. Chem.* **1988**, *53*, 5178.
- [51] Hayashi, T.; Matsumoto, Y.; Ito, Y., *J. Am. Chem. Soc.* **1989**, *111*, 3426.
- [52] Brown, J. M.; Hulmes, D. I.; Layzell, T. P., *J. Chem. Soc., Chem. Commun.* **1993**, 1673.
- [53] Kwong, F. Y.; Yang, Q.; Mak, T. C. W.; Chan, A. S. C.; Chan, K. S., *J. Org. Chem.* **2002**, *67*, 2769.
- [54] Smith, S. M.; Takacs, J. M., *J. Am. Chem. Soc.* **2010**, *132*, 1740.
- [55] Shoba, V. M.; Thacker, N. C.; Bochat, A. J.; Takacs, J. M., *Angew. Chem. Int. Ed.* **2016**, *55*, 1465.
- [56] Chakrabarty, S.; Takacs, J. M., *J. Am. Chem. Soc.* **2017**, *139*, 6066.
- [57] Yang, Z.-D.; Pal, R.; Hoang, G. L.; Zeng, X. C.; Takacs, J. M., *ACS Catal.* **2014**, *4*, 763.
- [58] Noh, D.; Chea, H.; Ju, J.; Yun, J., *Angew. Chem. Int. Ed.* **2009**, *48*, 6062.
- [59] Noh, D.; Yoon, S. K.; Won, J.; Lee, J. Y.; Yun, J., *Chem. Asian J.* **2011**, *6*, 1967.
- [60] Lee, H.; Lee, B. Y.; Yun, J., *Org. Lett.* **2015**, *17*, 764.
- [61] Feng, X.; Jeon, H.; Yun, J., *Angew. Chem. Int. Ed.* **2013**, *52*, 3989.
- [62] Won, J.; Noh, D.; Yun, J.; Lee, J. Y., *J. Phys. Chem. A* **2010**, *114*, 12112.
- [63] Deutsch, C.; Krause, N.; Lipshutz, B. H., *Chem. Rev.* **2008**, *108*, 2916.
- [64] Xi, Y.; Hartwig, J. F., *J. Am. Chem. Soc.* **2017**, *139*, 12758.
- [65] Obligacion, J. V.; Chirik, P. J., *J. Am. Chem. Soc.* **2013**, *135*, 19107.
- [66] Semba, K.; Fujihara, T.; Terao, J.; Tsuji, Y., *Tetrahedron* **2015**, *71*, 2183.
- [67] Lee, Y.; Hoveyda, A. H., *J. Am. Chem. Soc.* **2009**, *131*, 3160.
- [68] Corberán, R.; Mszar, N. W.; Hoveyda, A. H., *Angewandte Chemie* **2011**, *123*, 7217.
- [69] Laitar, D. S.; Tsui, E. Y.; Sadighi, J. P., *Organometallics* **2006**, *25*, 2405.
- [70] Iwamoto, H.; Imamoto, T.; Ito, H., *Nat. Commun.* **2018**, *9*, 2290.
- [71] Cai, Y.; Yang, X.-T.; Zhang, S.-Q.; Li, F.; Li, Y.-Q.; Ruan, L.-X.; Hong, X.; Shi, S.-L., *Angew. Chem. Int. Ed.* **2018**, *57*, 1376.
- [72] Smith, J. R.; Collins, B. S. L.; Hesse, M. J.; Graham, M. A.; Myers, E. L.; Aggarwal, V. K., *J. Am. Chem. Soc.* **2017**, *139*, 9148.
- [73] Brunet, J.-J.; Neibecker, D.; Niedercorn, F., *J. Mol. Catal.* **1989**, *49*, 235.
- [74] Müller, T. E.; Beller, M., *Chem. Rev.* **1998**, *98*, 675.
- [75] Müller, T. E.; Hultsch, K. C.; Yus, M.; Foubelo, F.; Tada, M., *Chem. Rev.* **2008**, *108*, 3795.
- [76] Huang, L.; Arndt, M.; Gooßen, K.; Heydt, H.; Gooßen, L. J., *Chem. Rev.* **2015**, *115*, 2596.

- [77] Reznichenko, A. L.; Hultzs, K. C., In *Hydroamination of Alkenes. In Organic Reactions*, 2015; pp 1.
- [78] Johns, A. M.; Sakai, N.; Ridder, A.; Hartwig, J. F., *J. Am. Chem. Soc.* **2006**, *128*, 9306.
- [79] Pawlas, J.; Nakao, Y.; Kawatsura, M.; Hartwig, J. F., *J. Am. Chem. Soc.* **2002**, *124*, 3669.
- [80] Adamson, N. J.; Jeddi, H.; Malcolmson, S. J., *J. Am. Chem. Soc.* **2019**, *141*, 8574.
- [81] Hong, S.; Marks, T. J., *Acc. Chem. Res.* **2004**, *37*, 673.
- [82] Cochran, B. M.; Michael, F. E., *J. Am. Chem. Soc.* **2008**, *130*, 2786.
- [83] Hesp, K. D.; Tobisch, S.; Stradiotto, M., *J. Am. Chem. Soc.* **2010**, *132*, 413.
- [84] Julian, L. D.; Hartwig, J. F., *J. Am. Chem. Soc.* **2010**, *132*, 13813.
- [85] Liu, Z.; Yamamichi, H.; Madrahimov, S. T.; Hartwig, J. F., *J. Am. Chem. Soc.* **2011**, *133*, 2772.
- [86] Bender, C. F.; Brown, T. J.; Widenhoefer, R. A., *Organometallics* **2016**, *35*, 113.
- [87] Casalnuovo, A. L.; Calabrese, J. C.; Milstein, D., *J. Am. Chem. Soc.* **1988**, *110*, 6738.
- [88] Zhou, J.; Hartwig, J. F., *J. Am. Chem. Soc.* **2008**, *130*, 12220.
- [89] Sevov, C. S.; Zhou, J.; Hartwig, J. F., *J. Am. Chem. Soc.* **2012**, *134*, 11960.
- [90] Hultzs, K. C., *Org. Biomol. Chem.* **2005**, *3*, 1819.
- [91] Hultzs, K. C., *Adv. Synth. Catal.* **2005**, *347*, 367.
- [92] Hannedouche, J.; Schulz, E., *Chem. Eur. J.* **2013**, *19*, 4972.
- [93] Gagne, M. R.; Brard, L.; Conticello, V. P.; Giardello, M. A.; Stern, C. L.; Marks, T. J., *Organometallics* **1992**, *11*, 2003.
- [94] O'Shaughnessy, P. N.; Scott, P., *Tetrahedron Asym.* **2003**, *14*, 1979.
- [95] Martínez, P. H.; Hultzs, K. C.; Hampel, F., *Chem. Commun.* **2006**, 2221.
- [96] Zhang, X.; Emge, T. J.; Hultzs, K. C., *Angew. Chem. Int. Ed.* **2012**, *51*, 394.
- [97] Wood, M. C.; Leitch, D. C.; Yeung, C. S.; Kozak, J. A.; Schafer, L. L., *Angew. Chem. Int. Ed.* **2007**, *46*, 354.
- [98] Knight, P. D.; Munslow, I.; O'Shaughnessy, P. N.; Scott, P., *Chem. Commun.* **2004**, 894.
- [99] Manna, K.; Everett, W. C.; Schoendorff, G.; Ellern, A.; Windus, T. L.; Sadow, A. D., *J. Am. Chem. Soc.* **2013**, *135*, 7235.
- [100] Manna, K.; Xu, S.; Sadow, A. D., *Angew. Chem. Int. Ed.* **2011**, *50*, 1865.
- [101] Bender, C. F.; Widenhoefer, R. A., *J. Am. Chem. Soc.* **2005**, *127*, 1070.
- [102] Takemiya, A.; Hartwig, J. F., *J. Am. Chem. Soc.* **2006**, *128*, 6042.
- [103] Liu, Z.; Hartwig, J. F., *J. Am. Chem. Soc.* **2008**, *130*, 1570.
- [104] Michael, F. E.; Cochran, B. M., *J. Am. Chem. Soc.* **2006**, *128*, 4246.
- [105] Kashiwame, Y.; Kuwata, S.; Ikariya, T., *Chem. Eur. J.* **2010**, *16*, 766.
- [106] Sipos, G.; Ou, A.; Skelton, B. W.; Falivene, L.; Cavallo, L.; Dorta, R., *Chem. Eur. J.* **2016**, *22*, 6939.
- [107] Shen, X.; Buchwald, S. L., *Angew. Chem. Int. Ed.* **2010**, *49*, 564.
- [108] Reznichenko, A. L.; Nguyen, H. N.; Hultzs, K. C., *Angew. Chem. Int. Ed.* **2010**, *49*, 8984.
- [109] Zhang, Z.; Lee, S. D.; Widenhoefer, R. A., *J. Am. Chem. Soc.* **2009**, *131*, 5372.
- [110] Vanable, E. P.; Kennemur, J. L.; Joyce, L. A.; Ruck, R. T.; Schultz, D. M.; Hull, K. L., *J. Am. Chem. Soc.* **2019**, *141*, 739.
- [111] MacDonald, M. J.; Schipper, D. J.; Ng, P. J.; Moran, J.; Beauchemin, A. M., *J. Am. Chem. Soc.* **2011**, *133*, 20100.
- [112] Gurak, J. A.; Yang, K. S.; Liu, Z.; Engle, K. M., *J. Am. Chem. Soc.* **2016**, *138*, 5805.
- [113] Campbell, M. J.; Johnson, J. S., *Org. Lett.* **2007**, *9*, 1521.
- [114] Zhu, S.; Niljianskul, N.; Buchwald, S. L., *J. Am. Chem. Soc.* **2013**, *135*, 15746.

-
- [115] Miki, Y.; Hirano, K.; Satoh, T.; Miura, M., *Angew. Chem. Int. Ed.* **2013**, *52*, 10830.
[116] Bandar, J. S.; Pirnot, M. T.; Buchwald, S. L., *J. Am. Chem. Soc.* **2015**, *137*, 14812.

CHAPTER 2

Copper-Catalyzed Hydroboration of Unsymmetrical Internal Alkenes for Diverse Formal Functionalization

2.1 Introduction

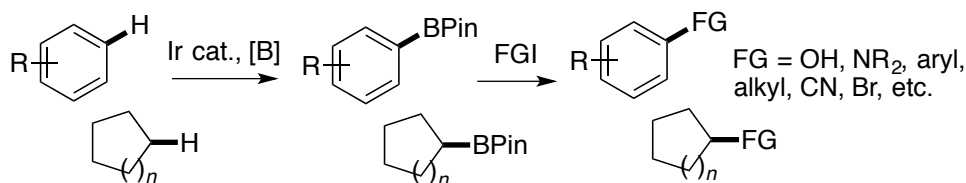
Alkenes are versatile starting materials that are available on a large scale from commercial sources or through chemical synthesis.¹ Many functionalizations of terminal alkenes have been reported, including functionalizations that occur enantioselectively.² However, functionalizations of internal alkenes are more limited, and enantioselective reactions of internal alkenes are particularly rare. Yet, asymmetric hydrofunctionalization³ of internal alkenes, if they could be conducted with high regioselectivity and enantioselectivity, would generate functionalized alkyl groups efficiently with control of absolute and relative configuration by formation of C-C or C-X (X = O, N, S, or P, etc.) bonds.

Over the past two decades, we have developed first-row catalysts for the hydroboration of vinylarenes⁴ and catalysts for the borylation⁵ of aromatic and aliphatic C-H bonds that enable the preparation of a wide range of functionalized compounds after subsequent transformations of organoboronates.⁶ The synthetic versatility of a Bpin (pin = pinacolate) group makes organoboronates valuable intermediates for the formation of a range of products. We envisioned that an asymmetric hydroboration of internal alkenes, followed by stereospecific transformations⁷ of the resulting secondary boronates, would provide an array of enantioenriched compounds containing a diverse range of functional groups (Scheme 2.1).

Transition metal-catalyzed hydroborations^{7b,8} of alkenes have the potential to occur with chemo- and stereoselectivity that complements those of uncatalyzed hydroborations. However, catalytic enantioselective hydroboration of alkenes is mostly limited to styrene derivatives and strained alkenes.⁹ The few examples of hydroboration of internal alkenes include rhodium-catalyzed asymmetric hydroboration of disubstituted and trisubstituted alkenes reported by Takacs.¹⁰ In these cases, the regioselectivity was dictated by coordination of an amide or an oxime group to the rhodium catalyst.

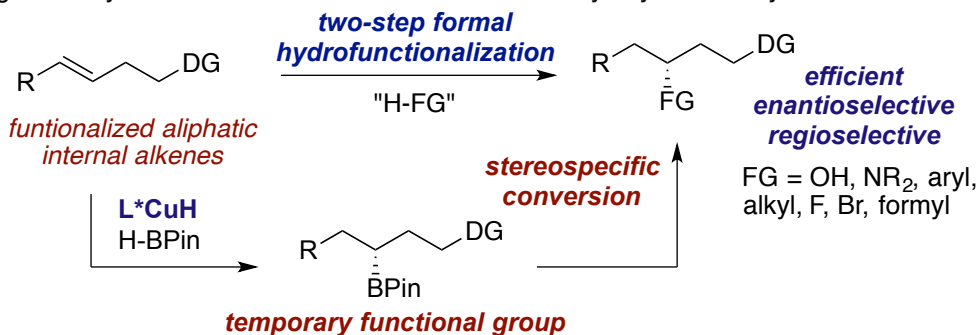
Scheme 2.1 Strategy for regio- and enantioselective hydrofunctionalization of internal alkenes

Previous work: general functionalization of C-H bonds by C-H borylation



This work:

general hydrofunctionalization of internal alkenes by asymmetric hydroboration



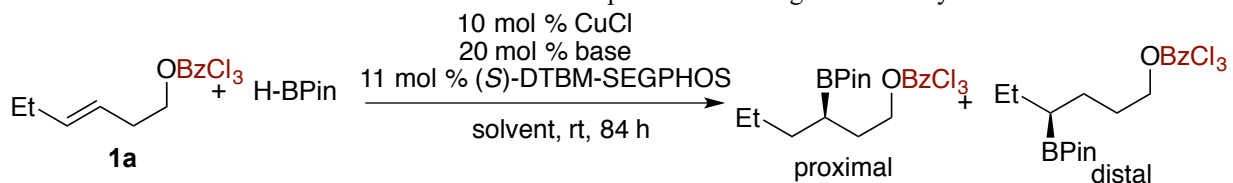
Recently, we reported that hydroaminations of internal alkenes containing polar groups at the homoallylic position occur with high regioselectivity that results from the inductive effects of electronegative groups proximal to the alkene.¹¹ This formal hydroamination was proposed to proceed via a chiral, non-racemic copper hydride¹² intermediate. Based on recent observations that the insertion of an internal alkene into a Cu-H bond is highly enantioselective and irreversible under the catalytic conditions,^{11,13} we envisioned that an asymmetric hydroboration of related alkenes would create a platform for diverse hydrofunctionalizations that form products containing new carbon-oxygen, carbon-halogen, and carbon-carbon bonds, if the intermediate alkylcopper complex would react with the borane to form a new B-C bond and regenerate the copper hydride.¹⁴

Herein, we report a two-step strategy for diverse hydrofunctionalizations of internal alkenes via regioselective and enantioselective copper-catalyzed hydroboration. This hydroboration occurs with a high regioselectivity that complements that of rhodium- and iridium-catalyzed hydroborations^{9a,15} and constitutes the first copper-catalyzed hydroboration of unconjugated internal alkenes.^{9d,16} We show that a wide range of functional groups can be incorporated in an acyclic aliphatic chain in a regio- and enantioselective manner by the combination of this hydroboration and a diverse set of reactions at the C-B bond.

2.2 Results and Discussion

To establish a system for regioselective hydroboration of internal alkenes, we investigated the reaction of pinacolborane and *trans*-3-hexenyl 2,4,6-trichlorobenzoate (**1a**), which we showed previously to undergo regioselective hydroamination,¹¹ in the presence of a copper catalyst CuCl and (*S*)-DTBM-SEGPHOS, a base additive. Table 2.1 summarizes our studies on the identification of reaction conditions. These studies showed that reactions conducted with stronger bases, such as KO*t*Bu and KHMDS (entries 3, 5), occurred with much higher yields than did reactions with weaker bases such as LiO*t*Bu and KOPh (entries 2, 4). Reactions conducted in cyclohexane were faster than those conducted in toluene (entry 6), whereas those in THF led to no products (entry 7).

Table 2.1 Evaluation of effect of reaction parameters for regioselective hydroboration^a



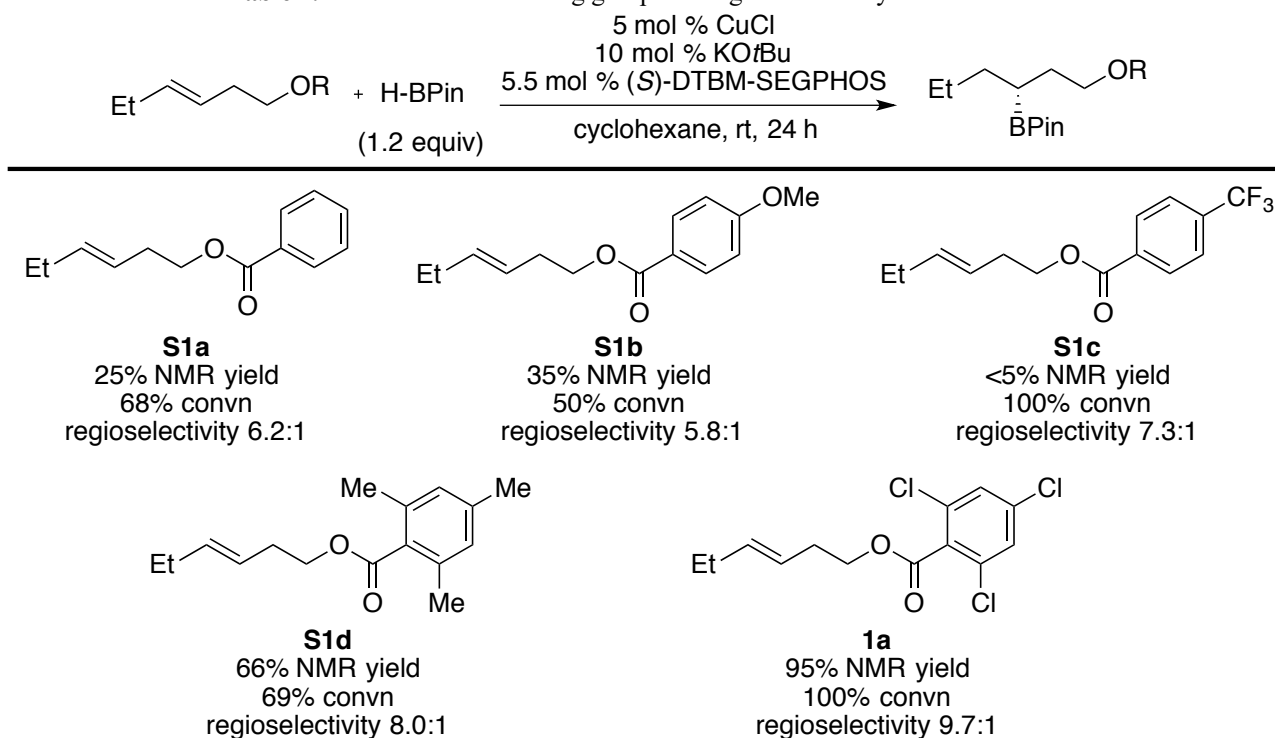
entry	base	solvent	yield ^b (%)	p:d ^b	ee ^c (%)
1	NaO <i>t</i> Bu	toluene	21	8.9:1	-
2	LiO <i>t</i> Bu	toluene	0	-	-
3	KO <i>t</i> Bu	toluene	94	9.0:1	97
4	KOPh	toluene	14	8.8:1	-
5	KHMDS	toluene	91	9.1:1	96
6	KHMDS	cyclohexane	92	10:1	97
7	KHMDS	THF	0	-	-

8 ^d	KOtBu	cyclohexane	95	10:1	97
9 ^e	KOtBu	cyclohexane	88	9.6:1	97

^aReaction conditions: **1a** (0.1 mmol), HBPin (2 equiv), CuCl (10 mol %) and (*S*)-DTBM-SEGPHOS (11 mol %), base (20 mol %) in solvent (0.2 mL), rt, 84 h; ^bDetermined by GC analysis; ^cDetermined by SFC for the major isomer; ^d12 h; ^eReaction conditions: **1a** (0.1 mmol), HBPin (1.2 equiv), CuCl (2.5 mol %), (*S*)-DTBM-SEGPHOS (3 mol %), base (5 mol %), rt, 36 h.

In addition, we investigated the effect of substituents of the homoallylic benzoates on the regioselectivity and yield of the hydroboration (Table 2.2). The studies showed that the regioselectivity was higher for substrates containing more electron-withdrawing groups on the phenyl ring of the benzoate than for substrates containing less electron-withdrawing groups on the phenyl ring of the benzoate (**S1a–S1c**). These data suggest that the regioselectivity is sensitive to electronic properties of the alkenes. However, the yield decreased with this change to the substrate because reduction of the ester moiety occurred by the copper hydride. The competing reduction was not observed for substrates containing substituents at both the 2- and 6-positions of the aryl ring.

Table 2.2 Evaluation of directing groups for regioselective hydroboration^a

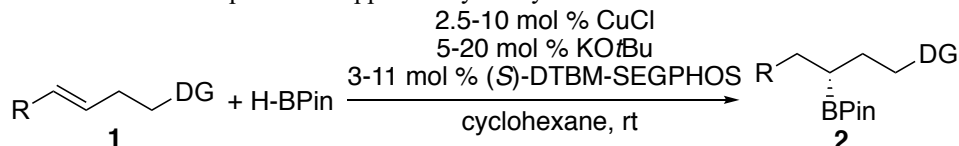


^aRegioselectivity was determined by GC analysis; yields and conversions were determined by ¹H NMR spectroscopy.

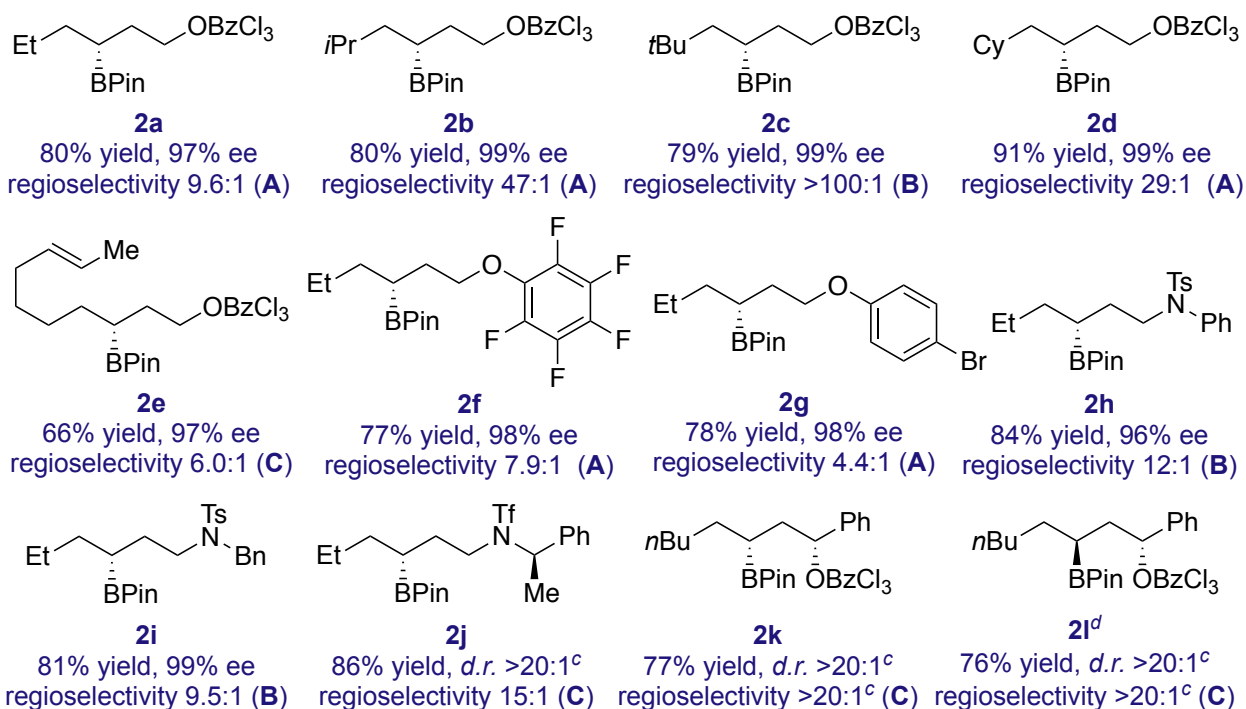
After identifying suitable conditions for copper-catalyzed hydroboration, we evaluated the scope of the reactions with homoallylic esters, ethers, and sulfonamides (Table 2.3). Homoallylic trichlorobenzoates containing ethyl-, isopropyl-, *tert*-butyl-, and cyclohexyl substituents (**1a–1d**) underwent hydroboration in good yields with high regioselectivity and excellent enantioselectivity. The reactions of alkenes with branching α to the alkene afforded a single constitutional isomer, suggesting that steric factors strongly influence the regioselectivity. Site-selective hydroboration

of a non-conjugated diene (**1e**) occurred at the alkene proximal to the ester over the alkene distal to the ester.

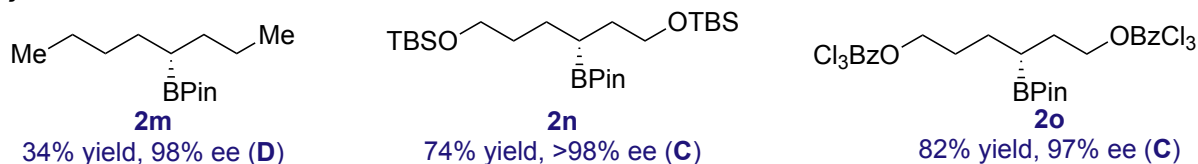
Table 2.3 Scope of the copper-catalyzed hydroboration of internal alkenes^{a,b}



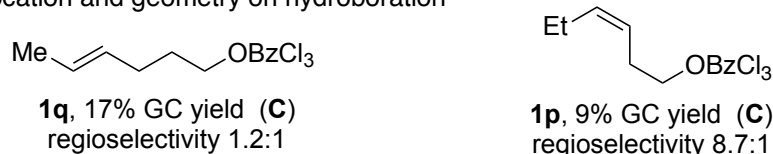
Unsymmetrical internal alkenes



Symmetrical internal alkenes



Effect of olefin location and geometry on hydroboration



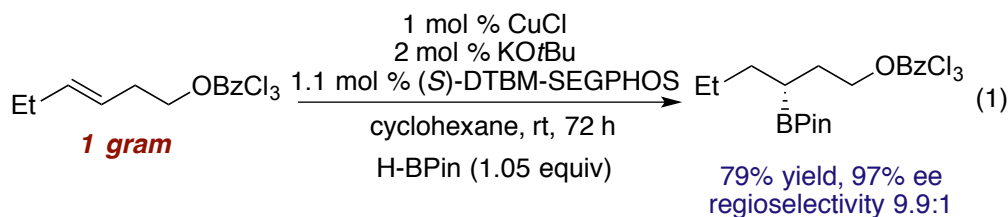
^aConditions: **A** (2.5 mol % Cu loading), **B** (5 mol % Cu loading), **C** (10 mol % Cu loading), **D** (10 mol % Cu loading). See section 2.4.2 for details on conditions **A-D**; ^bRegioselectivity determined by GC; ^cDetermined by ¹H NMR analysis; ^d(*R*)-DTBM-SEGPHOS used as the ligand. BzCl₃, 2,4,6-trichlorobenzoyl group.

To assess further the effect of the electronic properties of the substituent on the regioselectivity, we conducted hydroboration with alkenes bearing phenoxy groups at the homoallylic position. Electron-poor, halogen-substituted homoallylic phenyl ethers underwent hydroboration to form boronates **2f** and **2g** in good yields. The regioselectivity of the hydroboration of the more electron-poor phenyl ether (**2f**, 7.9:1) was higher than that of the hydroboration of the less electron-poor phenyl ether (**2g**, 4.4:1).

To expand the potential synthetic applications of the hydroboration, we examined the hydroboration of aryl- and alkyl-substituted homoallylic tosylamides (**1h**, **1i**). The corresponding boronates **2h** and **2i** were formed in good yields and with high regioselectivity when the reaction was conducted with 5 mol% catalyst.

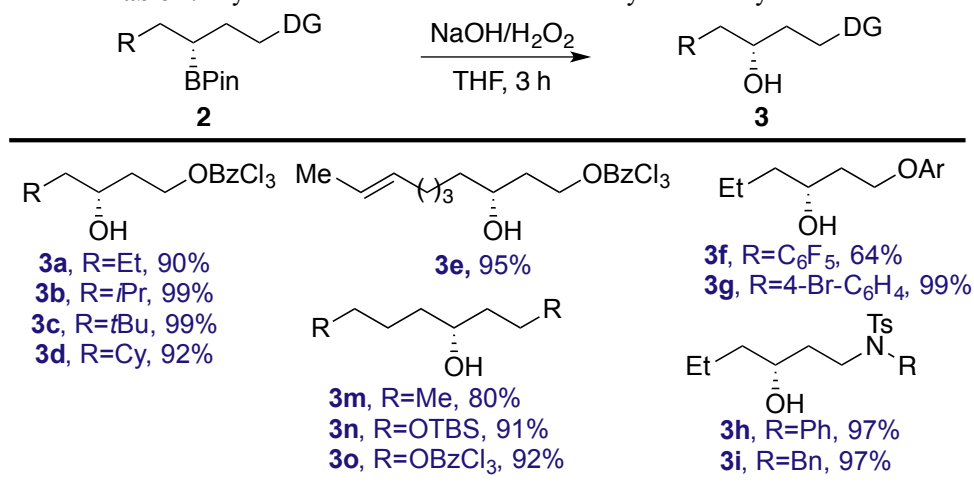
Reactions of chiral non-racemic alkenes occurred with diastereoselectivity controlled by the catalyst. Enantiopure trifluoromethylsulfonamide **1j** containing a remote stereocenter underwent hydroboration to form **2j** in high yield with high regioselectivity and excellent diastereoselectivity. Moreover, the reactions of enantioenriched alkenes in which the stereogenic center is proximal to the alkene occurred with diastereoselectivity controlled by the catalyst. The hydroboration of (*R*)-**1k** catalyzed by the (*S*)-DTBM-SEGPHOS-copper complex formed the addition product **2k** in 77% yield. The same reaction catalyzed by the (*R*)-DTBM-SEGPHOS-copper complex formed the corresponding diastereomer **2l** in a comparable yield (76%). Both reactions occurred with excellent diastereoselectivity (>20:1) and regioselectivity (>20:1).

In addition, symmetrical internal alkenes underwent hydroboration. Alkenes **1n** and **1o** bearing siloxy and alkoxy carbonyl groups reacted in good yields to form boronates **2n** and **2o**. However, the unfunctionalized internal alkene *trans*-4-octene reacted in less than 5% yield under conditions **C**. Reactions conducted with three equivalents of alkene and limiting HBPIn (conditions **D**) did lead to the corresponding boronate **2m** in 34% yield, but the difference in reactivity of 1-octene and the symmetrical ethers suggests that polar groups proximal to the alkene enhance the reactivity of the alkene, even if the C=C bond lacks a dipole because it is symmetric.

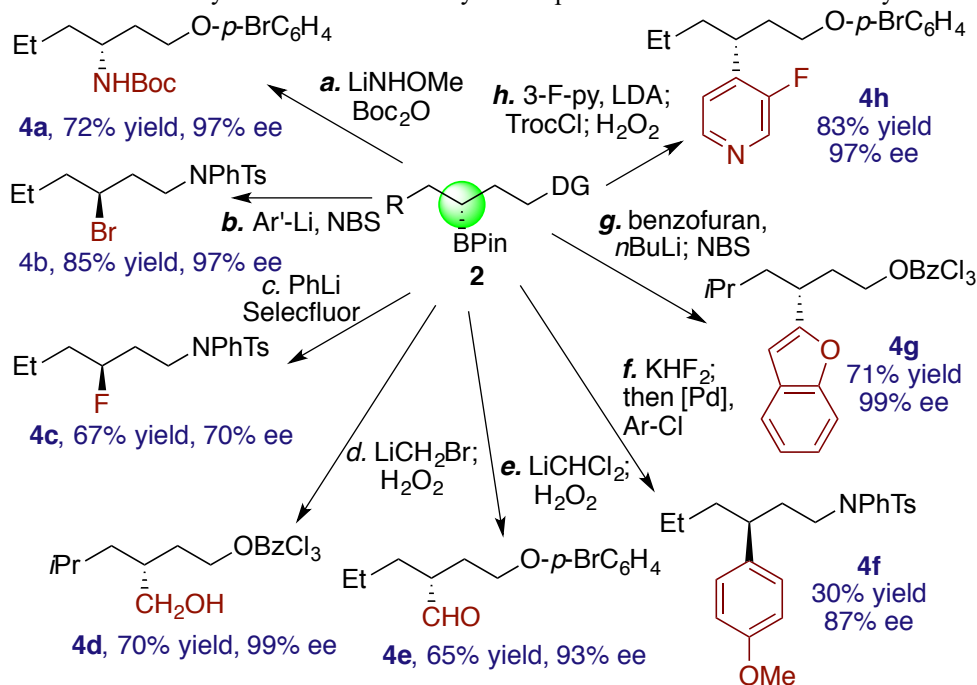


Both the reactivity and regioselectivity of this hydroboration are sensitive to the structure of the substrate (Table 2.3, bottom). *cis*-Alkene **1p**, which is analogous to the *trans*-alkene **1a**, underwent hydroboration in low yield (9% by GC) and with regioselectivity that is slightly lower than that of its *trans*-counterpart. The homoallylic trichlorobenzoate **1q** underwent hydroboration with poor regioselectivity (1.2:1) and low yield (17% by GC).

To demonstrate the practicality of this method, we conducted the hydroboration of **1a** on a gram-scale with 1 mol % catalyst loading (eq 1). The corresponding boronates were obtained with high regioselectivity and excellent enantioselectivity, and they formed in yields comparable to those of the small-scale reactions.

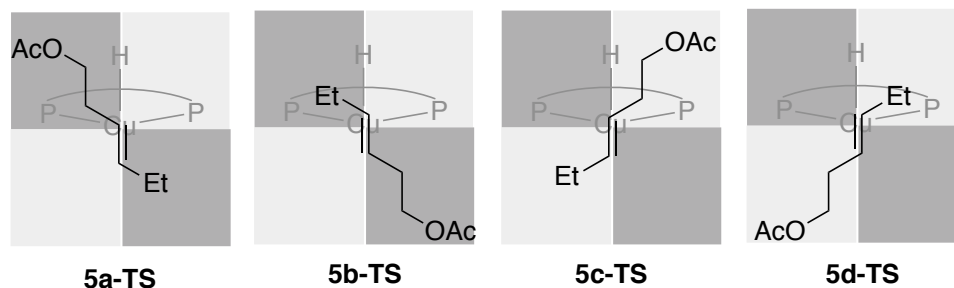
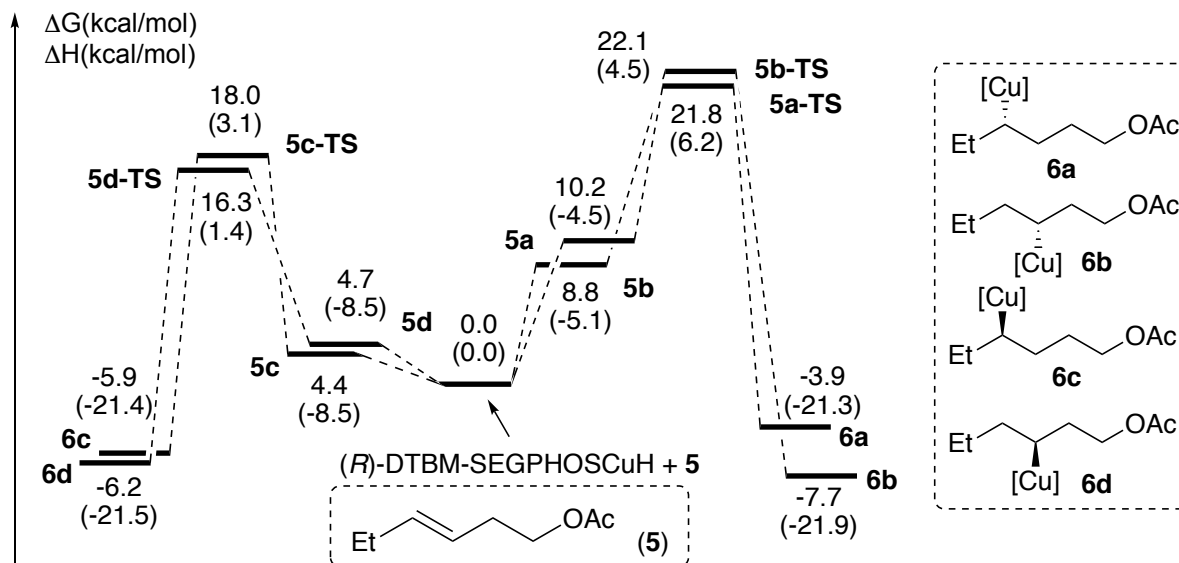
Table 2.4 Synthesis of enantioenriched secondary alcohols by oxidation

To assess the potential of the asymmetric hydroboration of internal alkenes with pinacolborane to enable a diverse set of regio- and enantioselective hydrofunctionalizations, we conducted transformations that convert C-B bonds to various C-C and C-X bonds (X = F, Br, N, O) stereospecifically. Analogous to the classic combination of hydroboration and oxidation of terminal alkenes to afford linear alcohols, the combination of the asymmetric hydroboration and oxidation of the resulting secondary boronates afforded enantioenriched secondary alcohols in excellent yields (Table 2.4). This sequence of hydroboration and oxidation constitutes a formal regio- and enantioselective hydration of internal alkenes.

Scheme 2.2 Diverse hydrofunctionalization by stereospecific conversion of secondary boronates^a

^aSee experimental section for detailed conditions.

Scheme 2.3 DFT calculations of alkene insertions to form the four isomeric alkylcopper intermediates with (*R*)-DTBM-SEGPHOS^a



^aGeometry optimizations were performed at the B3LYP/SDD-6-31G(d) level. Single-point energies were calculated at M06/SDD-6-311+G(d,p) level with solvent correction (SMD, cyclohexane).

The chiral boronates also form a range of compounds containing new C-C and C-X bonds stereospecifically.^{7c} Compound **2g** underwent amination¹⁷ to form Boc-protected amine **4a**, and compound **2h** underwent stereo-invertive bromination¹⁸ and fluorination¹⁹ to afford the corresponding alkyl bromide **4b** and fluoride **4c**. In addition, **2b** and **2g** underwent homologation²⁰ with LiCH₂Br and LiCHCl₂ to yield primary alcohol **4d** and aldehyde **4e**, respectively. Finally, boronates **2b**, **2i** and **2g** underwent stereospecific arylations and heteroarylations²¹ to produce the collection of aryl and heteroaryl derivatives **4f-4h**. With the exception of the arylation with 4-chloroanisole to form the anisyl derivative, each of the reactions occurred in high yield and with complete or predominant conservation of the enantiomeric excess of the products from the hydroboration (Scheme 2.2).

Previous data on the regioselectivity of the hydroamination of **1a**,¹¹ and the current data on the hydroboration of the same alkene, show that the regioselectivity is higher for reaction of the alkene bearing the more electron-withdrawing substituents than for reactions of the alkene bearing the less electron-withdrawing substituents at this position.

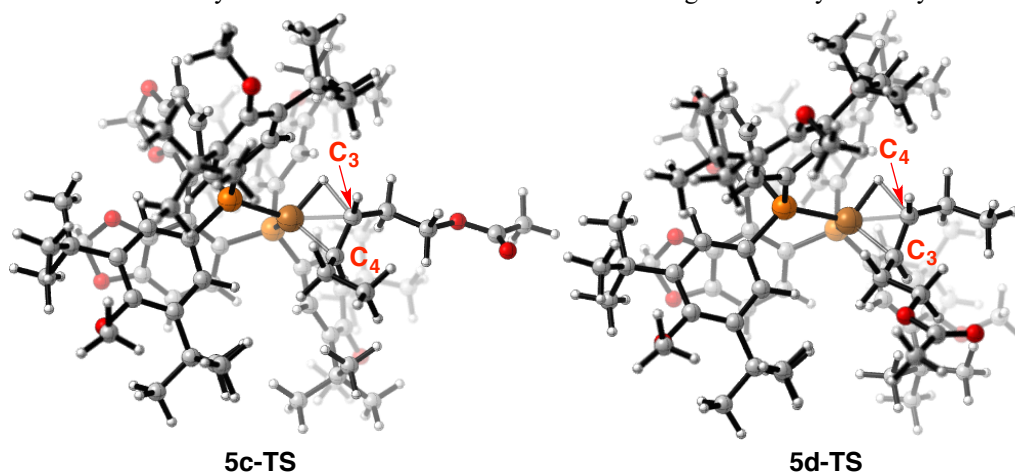
To gain insight into the origin of regioselectivity and enantioselectivity, we calculated possible transition states for the insertion of the alkene (**5**) into the Cu-H bond of (*R*)-DTBM-

SEGP_{HOS}CuH.²² Scheme 2.3 (bottom) shows four isomeric transition states for alkene insertions (**5a-TS** – **5d-TS**) leading to either of the two constitutional isomers of the alkylboronate and the two enantiomers of each constitutional isomer.²³ These calculations were conducted on the smaller homoallylic acetate because reactions of the trichlorobenzoate, pivalate, and acetate all occur with similar regioselectivity.²⁴ The energy of transition state **5d-TS**, leading to the major constitutional isomer **6d**, is 1.7 kcal/mol lower than that of the second lowest-energy transition state, **5c-TS**, leading to the minor constitutional isomer **6c**. This difference in energy agrees well with the regioselectivity (5.4:1) observed for reaction of trans-3-hexenyl acetate **5**.

The results of these calculations also mirrored the observed enantioselectivity. The energies of transition states **5c-TS** and **5d-TS** forming the major enantiomers (**6c**, **6d**) were computed to be lower than those of transition states **5a-TS** and **5b-TS** leading to the minor enantiomers (**6a**, **6b**) by approximately 5 kcal/mol. This difference in energy appears to result from steric repulsion between substituents on the alkene and equatorial phosphorus-bound substituents of the ligand (dark gray areas in the quadrant diagrams).

To understand the factors that contribute to the observed regioselectivity, we performed an NBO analysis of the alkene reactant and the two transition states (**5c-TS** and **5d-TS**) that form the two constitutional isomers. The regioselectivity appears to be determined by the differences between the charges on the olefinic carbons in the ground state and transition state. As shown in Scheme 2.4, a significant negative charge accumulates in the transition state at the carbon forming the Cu-C bond. This negative charge is stabilized by the positive charge on the nearby *O*-bound carbon due to the inductive effect of the acetoxy group (i.e. the C–O bond dipole).²⁴ This proposed inductive effect is consistent with the observation that the regioselectivity decreases when the alkene is located further from the benzoyloxy group.

Scheme 2.4 NBO analysis of transition states that determine the regioselectivity of the hydroboration.



	5c-TS	5d-TS	5	LCuH^a
NBO charge on C3	-0.264	-0.510	-0.194	-
NBO charge on C4	-0.498	-0.244	-0.166	-
NBO charge on Cu	-0.053	-0.051	-	0.087
NBO charge on H	-0.060	-0.072	-	-0.449

^aL = (*R*)-DTBM-SEGP_{HOS}

2.3 Conclusions

In summary, we report a strategy for diverse hydrofunctionalization of aliphatic internal alkenes with high regioselectivity and enantioselectivity comprising a copper-catalyzed asymmetric hydroboration and stereospecific derivatizations of the secondary boronate product of the hydroboration. By this strategy, we have generated, with high enantioselectivity, an array of products bearing distinct functional groups bound to one of the two carbon atoms of the alkene by a carbon-carbon or carbon-heteroatom bond. DFT calculations strongly suggest that the regioselectivity is controlled by the stabilization of the accumulating negative charge on the copper-bound carbon atom by the proximal polar group during formation of the transition states. Efforts to expand the scope of the hydroboration are currently underway in our laboratory.

2.4 Experimental

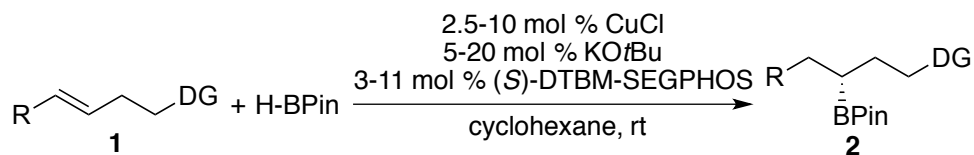
2.4.1 General Methods and Materials

All reagents were purchased from commercial suppliers, stored in the glove box and used as received. Glassware was dried at 130 °C for at least 4 hours before use. Anhydrous cyclohexane was purchased from Aldrich, stored in a dry box, and used as received without further purification. CuCl was purchased from Aldrich. (*S*)-DTBM-SEGPHOS was used as received from Takasago. (*R*)-DTBM-SEGPHOS was purchased from Strem. Pinacolborane (HBPin) was purchased from Aldrich and stored in a dry box. All catalytic reactions were set up in an argon-filled dry box with oven-dried glassware and were stirred with Teflon-coated magnetic stirring bars. All products for hydroboration, oxidation and derivatization were purified by flash column chromatography with a Teledyne Isco CombiFlash® R_f system using RediSep R_f Gold™ columns.

¹H NMR spectra were recorded on Bruker AVB-400, AVQ-400, AV-500 and AV-600 instruments with 400, 400, 500, and 600 MHz frequencies, and ¹³C were recorded on a Bruker AV-600 instrument with a ¹³C operating frequency of 150 MHz. ¹⁹F NMR spectra were recorded on a Bruker AVQ-400 spectrometer with a ¹⁹F operating frequency of 376 MHz. Chemical shifts (δ) are reported in ppm relative to the residual solvent signal (CDCl₃ δ = 7.26 for ¹H NMR and δ = 77.0 for ¹³C NMR = 7.26 ppm; acetone-*d*₆ = 2.05 ppm for ¹H and 29.9 ppm for ¹³C). Crude reaction mixtures were analyzed by ¹H NMR spectroscopy recorded on the Bruker AV-500. Quantitative analysis by GC was performed with dodecane as an internal standard. High-resolution mass spectral data were obtained with a Thermo Finnigan LTQ FT Instrument in the QB3/Chemistry Mass Spectrometry Facility, University of California, Berkeley. GC analysis was performed on an Agilent 7890 GC equipped with an HP-5 column (25 m x 0.20 mm x 0.33 μm film) and an FID detector. Chiral SFC analysis was conducted on a JASCO SFC system. Chiral HPLC analysis was conducted on Waters chromatography system. Racemic samples were obtained using racemic DTBM-SEGPHOS as the ligand, which was prepared by mixing equal amounts of (*S*)-DTBM-SEGPHOS and (*R*)-DTBM-SEGPHOS.

2.4.2 General Procedure for Catalytic Hydroboration

Representative procedure for the catalytic hydroboration on a 0.4 mmol scale using Condition A (General Procedure)



In an argon-filled dry box, a 1-dram vial was charged with CuCl (1.0 mg, 2.5 mol %), KOtBu (2.2 mg, 5 mol %), (S)-DTBM-SEGPBOS (14.2 mg, 3 mol %) and cyclohexane (400 μL). The mixture was allowed to stir at ambient temperature for 3 minutes before the addition of pinacolborane (71 μL , 0.48 mmol, 1.2 equiv). After brief stirring (30 – 60 seconds), the solution was added the alkene (0.4 mmol, 1 equiv), which was pre-weighed in another vial. The second vial was then washed four times with 100 μL cyclohexane each time. If the alkene is a solid, it was added in one portion, followed by cyclohexane (400 μL). The vial was then capped, sealed with electrical tape, and removed from the box. After 36 h of stirring at rt, an aliquot of 20 μL was removed and analyzed by GC. The reaction vial was diluted with 2 mL of ethyl acetate and the resulting solution was filtered through Celite. The crude material was concentrated *in vacuo* and purified by flash column chromatography (CombiFlash) to afford the pure product.

Summary of Conditions **A-D** in Table 2.3:

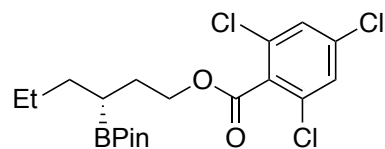
Condition A: Alkene (1 equiv), pinacolborane (1.2 equiv), CuCl (2.5 mol %), KOtBu (5 mol %), (S)-DTBM-SEGPBOS (3 mol %), 36 h, rt.

Condition B: Alkene (1 equiv), pinacolborane (1.2 equiv), CuCl (5 mol %), KOtBu (10 mol %), (S)-DTBM-SEGPBOS (5.5 mol %), 36 h, rt.

Condition C: Alkene (1 equiv), pinacolborane (2 equiv), CuCl (10 mol %), KOtBu (20 mol %), (S)-DTBM-SEGPBOS (11 mol %), 84 h, rt.

Condition D: Alkene (3 equiv), pinacolborane (1 equiv), CuCl (10 mol %), KOtBu (20 mol %), (S)-DTBM-SEGPBOS (11 mol %), 84 h, rt.

2.4.3. Compound Characterization



Compound 2a was synthesized according to the **General Procedure Condition A** with **1a** (123 mg, 0.400 mmol), HBPIn (71 μL , 0.48 mmol, 1.2 equiv), CuCl (1.0 mg, 2.5 mol %), KOtBu (2.2 mg, 5 mol %), and (S)-DTBM-SEGPBOS (14.2 mg, 3 mol %). Compound **2a** was purified by flash column chromatography (5% ethyl acetate in hexane) and obtained as a colorless oil in 80% yield.

^1H NMR (500 MHz, CDCl_3) δ 7.32 (s, 2H), 4.46 – 4.31 (m, 2H), 1.91 – 1.74 (m, 2H), 1.50 – 1.21 (m, 5H), 1.21 (s, 12H), 0.88 (t, $J = 7.0$ Hz, 3H).

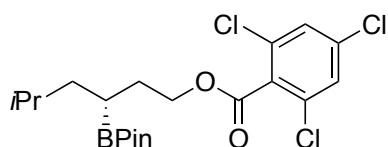
^{13}C NMR (151 MHz, CDCl_3) δ 163.96, 135.81, 132.55, 132.43, 127.82, 82.98, 66.21, 33.12, 29.57, 24.71, 24.60, 21.99, 19.68, 14.29.

^{11}B NMR (192 MHz, CDCl_3) δ 33.2.

HRMS (EI+) Calculated for $\text{C}_{19}\text{H}_{26}\text{B}^{35}\text{Cl}_3\text{O}_4$ $[\text{M}]^+$: 434.0990, Found: 434.0989.

$[\alpha]_{\text{D}}^{23} = -8.2$ ($c = 1.0$, DCM).

SFC analysis indicated 97% ee (compound **3a**) after oxidation.



Compound 2b was synthesized according to the **General Procedure Condition A** with **1b** (129 mg, 0.401 mmol), HBPIn (71 μL , 0.48 mmol, 1.2 equiv), CuCl (1.0 mg, 2.5 mol %), KO t Bu (2.2 mg, 5 mol %), and (*S*)-DTBM-SEGPHOS (14.2 mg, 3 mol %). Compound **2b** was purified by flash column chromatography (5% ethyl acetate in hexane) and obtained as colorless oil in 80% yield.

^1H NMR (500 MHz, CDCl_3) δ 7.33 (s, 2H), 4.44 – 4.35 (m, 2H), 1.88 – 1.76 (m, 2H), 1.59 (septet, $J = 6.8$ Hz, 1H), 1.44 – 1.31 (m, 1H), 1.27 – 1.18 (m, 2H), 1.22 (s, 12H), 0.87 (d, $J = 6.6$ Hz, 6H).

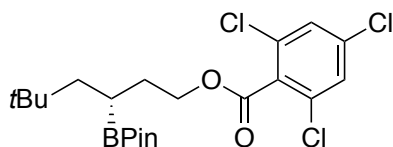
^{13}C NMR (151 MHz, CDCl_3) δ 164.01, 135.84, 132.58, 132.44, 127.85, 83.01, 66.20, 40.18, 29.94, 27.04, 24.72, 24.63, 22.97, 22.41, 17.69.

^{11}B NMR (192 MHz, CDCl_3) δ 33.7.

HRMS (EI+) Calculated for $\text{C}_{20}\text{H}_{28}\text{B}^{35}\text{Cl}_3\text{O}_4$ $[\text{M}]^+$: 448.1146, Found: 448.1141.

$[\alpha]_{\text{D}}^{23} = -7.5$ ($c = 1.0$, DCM).

SFC analysis indicated 99% ee (compound **3b**) after oxidation.



Compound 2c was synthesized according to the **General Procedure Condition B** with **1c** (134 mg, 0.399 mmol), HBPIn (71 μL , 0.48 mmol, 1.2 equiv), CuCl (2.0 mg, 5 mol %), KO t Bu (4.4 mg, 5 mol %), and (*S*)-DTBM-SEGPHOS (25.9 mg, 5.5 mol %). Compound **2c** was purified by flash column chromatography (5% ethyl acetate in hexane) and obtained as white solid in 79% yield.

^1H NMR (500 MHz, CDCl_3) δ 7.30 (s, 2H), 4.37 (t, $J = 7.1$ Hz, 2H), 1.84 (dq, $J = 14.5, 7.3$ Hz, 1H), 1.73 (dt, $J = 13.7, 7.0$ Hz, 1H), 1.57 (dd, $J = 13.4, 10.2$ Hz, 1H), 1.21 (s, 6H), 1.20 (s, 6H), 1.17 – 1.05 (m, 2H), 0.85 (s, 9H).

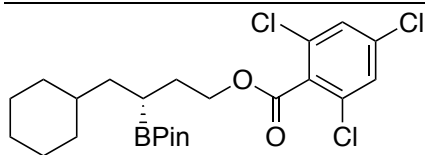
^{13}C NMR (151 MHz, CDCl_3) δ 163.93, 135.83, 132.56, 132.38, 127.84, 83.03, 65.81, 45.16, 31.68, 30.96, 29.57, 24.75, 24.72, 15.52.

^{11}B NMR (192 MHz, CDCl_3) δ 33.8.

HRMS (ESI+) Calculated for $\text{C}_{21}\text{H}_{30}\text{B}^{35}\text{Cl}_3\text{O}_4\text{Na}$ $[\text{M}+\text{Na}]^+$: 485.1195, Found: 485.1191.

$[\alpha]_{\text{D}}^{23} = -10.9$ ($c = 1.0$, DCM).

SFC analysis indicated 99% ee (compound **3c**) after oxidation.



Compound 2d was synthesized according to the **General Procedure Condition A** with **1d** (145 mg, 0.401 mmol), HBPIn (71 μ L, 0.48 mmol, 1.2 equiv), CuCl (1.0 mg, 2.5 mol %), KO t Bu (2.2 mg, 5 mol %), and (*S*)-DTBM-SEGPPOS (14.2 mg, 3 mol %). Compound **2d** was purified by flash column chromatography (5% ethyl acetate in hexane) and obtained as colorless liquid in 91% yield.

^1H NMR (500 MHz, CDCl_3) δ 7.31 (s, 2H), 4.44 – 4.30 (m, 2H), 1.88 – 1.57 (m, 7H), 1.41 – 1.05 (m, 7H), 1.21 (s, 12H), 0.91 – 0.74 (m, 2H).

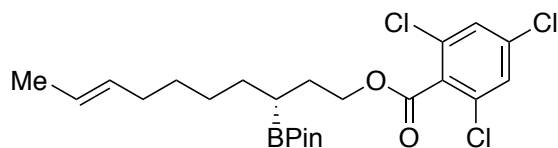
^{13}C NMR (151 MHz, CDCl_3) δ 164.03, 135.86, 132.60, 132.45, 127.87, 83.01, 66.24, 38.60, 36.76, 33.66, 33.15, 30.04, 26.60, 26.37, 26.33, 24.77, 24.60, 17.07.

^{11}B NMR (192 MHz, CDCl_3) δ 34.1.

HRMS (ESI+) Calculated for $\text{C}_{23}\text{H}_{32}\text{B}^{35}\text{Cl}_3\text{O}_4\text{Na}$ [$\text{M}+\text{Na}$] $^+$: 511.1347, Found: 511.1351.

$[\alpha]_{\text{D}}^{23} = -3.3$ ($c = 1.0$, DCM).

SFC analysis indicated 99% ee (compound **3d**) after oxidation.



Compound 2e was synthesized according to the **General Procedure Condition A** with **1e** (72.3 mg, 0.200 mmol), HBPIn (59 μ L, 0.4 mmol, 2 equiv), CuCl (2.0 mg, 10 mol %), KO t Bu (4.4 mg, 20 mol %), and (*S*)-DTBM-SEGPPOS (25.9 mg, 11 mol %). Compound **2e** was purified by flash column chromatography (5% ethyl acetate in hexane) and obtained as colorless liquid in 66% yield (contains <5% constitutional isomers).

^1H NMR (500 MHz, CDCl_3) δ 7.32 (s, 2H), 5.39 – 5.36 (m, 2H), 4.45 – 4.30 (m, 2H), 1.98 – 1.73 (m, 4H), 1.66 – 1.55 (m, 3H), 1.49 – 1.24 (m, 6H), 1.21 (s, 12H), 1.17 – 1.11 (m, 1H).

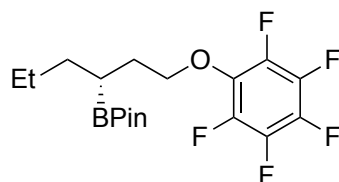
^{13}C NMR (151 MHz, CDCl_3) δ 164.04, 135.87, 132.61, 132.49, 131.46, 127.89, 124.58, 83.06, 66.27, 32.38, 30.78, 29.72, 29.65, 28.38, 24.76, 24.66, 19.93, 17.86.

^{11}B NMR (192 MHz, CDCl_3) δ 33.8.

HRMS (EI+) Calculated for $\text{C}_{22}\text{H}_{29}\text{B}^{35}\text{Cl}_3\text{O}_4$ [$\text{M}-\text{CH}_3$] $^+$: 473.1224, Found: 473.1222.

$[\alpha]_{\text{D}}^{23} = -2.5$ ($c = 1.0$, DCM).

SFC analysis indicated 97% ee (compound **3e**) after oxidation.



Compound 2f was synthesized according to the **General Procedure Condition A** with **1f** (106 mg, 0.398 mmol), HBPIn (71 μ L, 0.48 mmol, 1.2 equiv), CuCl (1.0 mg, 2.5 mol %), KO t Bu (2.2 mg, 5 mol %), and (*S*)-DTBM-SEGPPOS (14.2 mg, 3 mol %). **2f** was purified by flash column

chromatography (2.5% ethyl acetate in hexane) and obtained as colorless liquid in 77% yield (contains <5% constitutional isomer **2f'**).

$^1\text{H NMR}$ (500 MHz, CDCl_3) δ 4.21 – 4.06 (m, 2H), 1.91 – 1.73 (m, 2H), 1.49 – 1.39 (m, 1H), 1.38 – 1.27 (m, 3H), 1.20 (s, 12H), 1.20 – 1.11 (m, 1H), 0.87 (t, $J = 7.1$ Hz, 3H).

$^{13}\text{C NMR}$ (151 MHz, CDCl_3) δ 141.91 ($J_{\text{C-F}} = 246$ Hz), 137.95 ($J_{\text{C-F}} = 246$ Hz), 137.14 ($J_{\text{C-F}} = 246$ Hz), 133.80, 83.06, 75.49, 33.35, 31.12, 24.70, 24.62, 22.07, 19.53, 14.22.

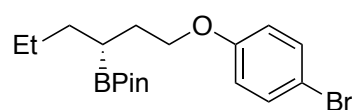
$^{11}\text{B NMR}$ (192 MHz, CDCl_3) δ 33.5.

$^{19}\text{F NMR}$ (376 MHz, CDCl_3) δ -156.0 (d, $J = 20.5$ Hz, 2F), -163.19 (t, $J = 22.8$ Hz, 2F), -163.52 (t, $J = 21.8$ Hz, 1F).

HRMS (EI+) Calculated for $\text{C}_{18}\text{H}_{25}\text{BF}_5\text{O}_3$ $[\text{M}+\text{H}]^+$: 395.1817, Found: 395.1821.

$[\alpha]_{\text{D}}^{23} = -6.8$ ($c = 1.0$, DCM).

HPLC analysis indicated 98% ee (compound **3f**) after oxidation.



Compound 2g was synthesized according to the **General Procedure Condition A** with **1g** (102 mg, 0.400 mmol), HBPin (71 μL , 0.48 mmol, 1.2 equiv), CuCl (1.0 mg, 2.5 mol %), $\text{KO}t\text{Bu}$ (2.2 mg, 5 mol %), and (*S*)-DTBM-SEGPHOS (14.2 mg, 3 mol %). Compound **2g** was purified by flash column chromatography (2.5% ethyl acetate in hexane) and obtained as white solid in 62% yield along with its constitutional isomer **2g'** in 16% yield (78% combined yield).

$^1\text{H NMR}$ (500 MHz, CDCl_3) δ 7.33 (d, $J = 8.9$ Hz, 2H), 6.77 (d, $J = 8.9$ Hz, 2H), 3.96 – 3.88 (m, 2H), 1.97 – 1.71 (m, 2H), 1.51 – 1.43 (m, 1H), 1.42 – 1.28 (m, 3H), 1.23 (s, 12H), 1.19 – 1.13 (m, 1H), 0.90 (t, $J = 6.9$ Hz, 3H).

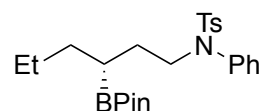
$^{13}\text{C NMR}$ (151 MHz, CDCl_3) δ 158.20, 132.02, 116.37, 112.39, 82.94, 67.93, 33.40, 30.35, 24.77, 24.71, 22.07, 19.91, 14.30.

$^{11}\text{B NMR}$ (192 MHz, CDCl_3) δ 33.8.

HRMS (EI+) Calculated for $\text{C}_{18}\text{H}_{28}\text{BBrO}_3$ $[\text{M}]^+$: 382.1315, Found: 382.1320.

$[\alpha]_{\text{D}}^{23} = -9.2$ ($c = 1.0$, DCM).

SFC analysis indicated 98% ee (compound **3g**) after oxidation.



Compound 2h was synthesized according to the **General Procedure Condition B** with **1h** (132 mg, 0.401 mmol), HBPin (71 μL , 0.48 mmol, 1.2 equiv), CuCl (2.0 mg, 5 mol %), $\text{KO}t\text{Bu}$ (4.4 mg, 5 mol %), and (*S*)-DTBM-SEGPHOS (25.9 mg, 5.5 mol %). Compound **2h** was purified by flash column chromatography (10% ethyl acetate in hexane) and obtained as colorless sticky oil in 84% yield.

$^1\text{H NMR}$ (500 MHz, CDCl_3) δ 7.45 (d, $J = 8.4$ Hz, 2H), 7.32 – 7.24 (m, 3H), 7.21 (d, $J = 8.0$ Hz, 2H), 7.03 (dd, $J = 7.9, 1.8$ Hz, 2H), 3.58 – 3.47 (m, 2H), 2.39 (s, 3H), 1.60 – 1.41 (m, 2H), 1.39 – 1.28 (m, 1H), 1.28 – 1.12 (m, 3H), 1.19 (s, 6H), 1.19 (s, 6H), 1.03 – 0.99 (m, 1H), 0.81 (t, $J = 7.0$ Hz, 3H).

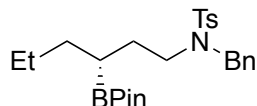
$^{13}\text{C NMR}$ (151 MHz, CDCl_3) δ 142.98, 139.17, 135.31, 129.11, 128.65, 128.62, 127.52, 127.48, 82.85, 50.02, 33.08, 29.60, 24.66, 24.54, 21.93, 21.35, 20.27, 14.15.

^{11}B NMR (192 MHz, CDCl_3) δ 33.5.

HRMS (ESI+) Calculated for $\text{C}_{25}\text{H}_{37}\text{BNO}_4\text{S}$ $[\text{M}+\text{H}]^+$: 458.2531, Found: 458.2531.

$[\alpha]_{\text{D}}^{23} = -10.1$ ($c = 1.0$, DCM).

SFC analysis indicated 96% ee (compound **3h**) after oxidation.



Compound 2i was synthesized according to the **General Procedure Condition B** with **1i** (137 mg, 0.399 mmol), HBPIn (71 μL , 0.48 mmol, 1.2 equiv), CuCl (2.0 mg, 5 mol %), KOtBu (4.4 mg, 5 mol %), and (*S*)-DTBM-SEGPPOS (25.9 mg, 5.5 mol %). Compound **2i** was purified by flash column chromatography (10% ethyl acetate in hexane) and obtained as colorless sticky oil in 81% yield.

^1H NMR (500 MHz, CDCl_3) 7.74 (d, $J = 8.3$ Hz, 2H), 7.32 – 7.21 (m, 7H), 4.37 (d, $J = 15.0$ Hz, 1H), 4.32 (d, $J = 15.0$ Hz, 1H), 3.11 (t, $J = 8.3$ Hz, 2H), 2.42 (s, 3H), 1.51 – 1.41 (m, 1H), 1.41 – 1.32 (m, 1H), 1.30 – 1.23 (m, 1H), 1.20 – 1.07 (m, 3H), 1.15 (s, 6H), 1.14 (s, 6H), 0.80 (t, $J = 7.0$ Hz, 3H), 0.80 – 0.74 (m, 1H).

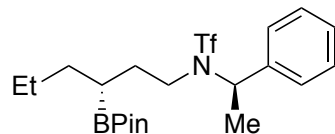
^{13}C NMR (151 MHz, CDCl_3) δ 142.82, 137.39, 136.47, 129.44, 128.28, 128.04, 127.40, 127.00, 82.80, 51.14, 47.04, 32.89, 28.65, 24.57, 24.51, 21.83, 21.32, 20.59, 14.11.

^{11}B NMR (192 MHz, CDCl_3) δ 33.5.

HRMS (ESI+) Calculated for $\text{C}_{26}\text{H}_{38}\text{BNO}_4\text{S}$ $[\text{M}+\text{H}]^+$: 472.2690, Found: 472.2690.

$[\alpha]_{\text{D}}^{23} = -1.7$ ($c = 1.0$, DCM).

SFC analysis indicated 99% ee (compound **3i**) after oxidation.



Compound 2j was synthesized according to the **General Procedure Condition C** with **1j** (67.1 mg, 0.200 mmol), HBPIn (59 μL , 0.4 mmol, 2 equiv), CuCl (2.0 mg, 10 mol %), KOtBu (4.4 mg, 20 mol %), and (*S*)-DTBM-SEGPPOS (25.9 mg, 11 mol %). Compound **2j** was purified by flash column chromatography (5% ethyl acetate in hexane) and obtained as colorless liquid in 86% yield.

^1H NMR (500 MHz, CDCl_3) δ 7.44 (d, $J = 7.6$ Hz, 2H), 7.37 (t, $J = 7.5$ Hz, 2H), 7.32 (t, $J = 7.2$ Hz, 1H), 5.23 (q, $J = 7.2$ Hz, 1H), 3.19 – 3.08 (m, 2H), 1.71 (d, $J = 7.1$ Hz, 3H), 1.63 – 1.50 (m, 1H), 1.34 – 1.23 (m, 2H), 1.21 – 1.12 (m, 3H), 1.17 (s, 12H), 0.81 (t, $J = 6.9$ Hz, 3H), 0.73 – 0.65 (m, 1H).

^{13}C NMR (151 MHz, CDCl_3) δ 138.67, 128.64, 128.29, 127.58, 119.99 (q, $J_{\text{C-F}} = 323.5$ Hz), 83.07, 57.62, 45.26, 33.11, 31.85, 24.70, 24.68, 21.85, 21.07, 17.03, 14.15.

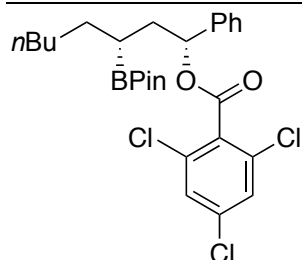
^{11}B NMR (192 MHz, CDCl_3) δ 33.5.

^{19}F NMR (376 MHz, CDCl_3) δ -75.2 (s).

HRMS (EI+) Calculated for $\text{C}_{20}\text{H}_{30}\text{BF}_3\text{NO}_4\text{S}$ $[\text{M}-\text{CH}_3]^+$: 448.1931, Found: 448.1935.

$[\alpha]_{\text{D}}^{23} = 14.4$ ($c = 1.0$, DCM).

^1H NMR analysis indicated >20:1 d.r..



Compound 2k was synthesized according to the **General Procedure Condition C** with **1k** (82.3 mg, 0.200 mmol), HBPIn (59 μ L, 0.4 mmol, 2 equiv), CuCl (2.0 mg, 10 mol %), KOtBu (4.4 mg, 20 mol %), and (*S*)-DTBM-SEGPHOS (25.9 mg, 11 mol %). Compound **2k** was purified by flash column chromatography (3% ethyl acetate in hexane) and obtained as colorless sticky oil in 77% yield.

^1H NMR (500 MHz, CDCl_3) δ 7.46 – 7.40 (m, 2H), 7.38 – 7.33 (m, 2H), 7.31 – 7.27 (m, 1H), 7.31 (s, 2H), 6.04 (dd, $J = 8.2, 6.5$ Hz, 1H), 2.20 (dt, $J = 13.7, 7.8$ Hz, 1H), 1.86 (ddd, $J = 14.2, 8.0, 6.5$ Hz, 1H), 1.51 – 1.43 (m, 2H), 1.33 – 1.21 (m, 6H), 1.24 (s, 12H), 1.11 (quintet, $J = 7.6$ Hz, 1H), 0.87 (t, $J = 6.9$ Hz, 3H).

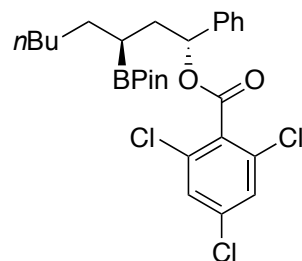
^{13}C NMR (151 MHz, CDCl_3) δ 163.30, 139.77, 135.82, 132.63, 132.44, 128.26, 128.06, 127.88, 127.05, 83.09, 77.67, 37.39, 32.08, 30.33, 28.46, 24.83, 24.71, 22.52, 19.35, 13.98.

^{11}B NMR (192 MHz, CDCl_3) δ 33.8.

HRMS (ESI+) Calculated for $\text{C}_{27}\text{H}_{34}\text{B}^{35}\text{Cl}_3\text{O}_4\text{Na}$ $[\text{M}+\text{Na}]^+$: 561.1508, Found: 561.1509.

$[\alpha]_{\text{D}}^{23} = 30.4$ ($c = 1.0$, DCM).

^1H NMR analysis indicated >20:1 d.r..



Compound 2l was synthesized according to the **General Procedure Condition C** with **1k** (82.3 mg, 0.200 mmol), HBPIn (59 μ L, 0.4 mmol, 2 equiv), CuCl (2.0 mg, 10 mol %), KOtBu (4.4 mg, 20 mol %), and (*R*)-DTBM-SEGPHOS (25.9 mg, 11 mol %). Compound **2l** was purified by flash column chromatography (3% ethyl acetate in hexane) and obtained as white solid in 76% yield.

^1H NMR (500 MHz, CDCl_3) δ 7.44 (d, $J = 7.5$ Hz, 2H), 7.35 (t, $J = 7.5$ Hz, 2H), 7.32 (s, 2H), 7.29 (t, $J = 7.3$ Hz, 1H), 6.11 (dd, $J = 9.6, 4.3$ Hz, 1H), 2.05 (ddd, $J = 14.6, 9.6, 5.3$ Hz, 1H), 1.97 (ddd, $J = 14.3, 10.3, 4.4$ Hz, 1H), 1.52 – 1.38 (m, 2H), 1.36 – 1.23 (m, 7H), 1.28 (s, 6H), 1.26 (s, 6H), 0.87 (t, $J = 6.8$ Hz, 3H).

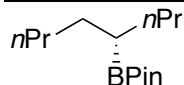
^{13}C NMR (151 MHz, CDCl_3) δ 163.46, 140.25, 135.78, 132.64, 132.50, 128.23, 127.94, 127.85, 126.70, 83.06, 79.04, 38.17, 32.06, 31.28, 28.37, 24.94, 24.69, 22.49, 20.23, 14.00.

^{11}B NMR (192 MHz, CDCl_3) δ 33.8.

HRMS (ESI+) Calculated for $\text{C}_{27}\text{H}_{34}\text{B}^{35}\text{Cl}_3\text{O}_4\text{Na}$ $[\text{M}+\text{Na}]^+$: 561.1508, Found: 561.1505.

$[\alpha]_{\text{D}}^{23} = 46.5$ ($c = 1.0$, DCM).

^1H NMR analysis indicated >20:1 d.r..



Compound 2m was synthesized according to the **General Procedure Condition D** with *trans*-4-octene (471 μ L, 3.00 mmol, 3 equiv), HBPIn (145 μ L, 1.00 mmol, 1 equiv), CuCl (10.0 mg, 10 mol %), KO t Bu (22.0 mg, 5 mol %), and (*S*)-DTBM-SEGPHOS (130 mg, 11 mol %). Compound **2m** was purified by flash column chromatography (2.5% ethyl acetate in hexane) and obtained as colorless liquid in 34% yield.

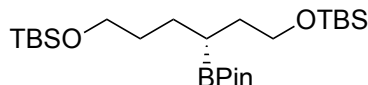
^1H NMR (500 MHz, CDCl_3) δ 1.43 – 1.20 (m, 10H), 1.24 (s, 12 H), 0.99 – 0.93 (m, 1H), 0.89 – 0.86 (m, 6H),

^{13}C NMR (151 MHz, CDCl_3) δ 82.66, 33.74, 31.53, 31.06, 24.73, 24.73, 23.73, 22.94, 22.37, 14.39, 14.04.

^{11}B NMR (192 MHz, CDCl_3) δ 33.9.

$[\alpha]_{\text{D}}^{23} = 2.2$ ($c = 1.0$, DCM).

^{19}F NMR analysis indicated 98% ee (compound **3m**) after oxidation.



Compound 2n was synthesized according to the **General Procedure Condition C** with **1n** (138 mg, 0.400 mmol), HBPIn (118 μ L, 0.8 mmol, 2 equiv), CuCl (4.0 mg, 10 mol %), KO t Bu (8.8 mg, 10 mol %), and (*S*)-DTBM-SEGPHOS (11 mol %, 51.9 mg). Compound **2n** was purified by flash column chromatography (2.5% ethyl acetate in hexane) and obtained as colorless liquid in 74% yield.

^1H NMR (500 MHz, CDCl_3) δ 3.62 – 3.51 (m, 4H), 1.63 (ddd, $J = 14.2, 9.1, 5.5$ Hz, 1H), 1.59 – 1.32 (m, 5H), 1.19 (s, 12H), 1.03 – 0.97 (m, 1H), 0.85 (s, 18H), 0.00 (s, 6H), 0.00 (s, 6H).

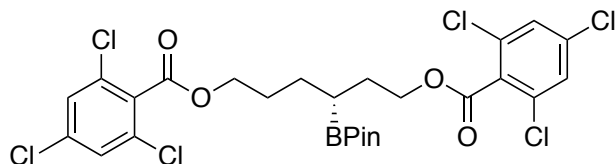
^{13}C NMR (151 MHz, CDCl_3) δ 82.78, 63.40, 62.86, 34.29, 32.37, 27.25, 25.98, 25.95, 24.78, 24.74, 19.40, 18.33, 18.30, -5.25, -5.28, -5.29, -5.29.

^{11}B NMR (192 MHz, CDCl_3) δ 33.8.

HRMS (EI+) Calculated for $\text{C}_{24}\text{H}_{54}\text{BO}_4\text{Si}_2$ $[\text{M}+\text{H}]^+$: 473.3654, Found: 473.3650.

$[\alpha]_{\text{D}}^{23} = -0.6$ ($c = 1.0$, DCM).

^{19}F NMR analysis indicated >98% ee (compound **3n**) after oxidation.



Compound 2o was synthesized according to the **General Procedure Condition C** with **1o** (106 mg, 0.200 mmol), HBPIn (59 μ L, 0.4 mmol, 2 equiv), CuCl (2.0 mg, 10 mol %), KO t Bu (4.4 mg, 20 mol %), and (*S*)-DTBM-SEGPHOS (25.9 mg, 11 mol %). Compound **2o** was purified by flash column chromatography (10% ethyl acetate in hexane) and obtained as white solid in 82% yield.

^1H NMR (500 MHz, CDCl_3) δ 7.33 (s, 2H), 7.32 (s, 2H), 4.46 – 4.31 (m, 4H), 1.96 – 1.71 (m, 4H), 1.63 – 1.46 (m, 2H), 1.23 – 1.16 (m, 1H), 1.21 (s, 12H).

^{13}C NMR (151 MHz, CDCl_3) δ 164.03, 164.02, 135.94, 135.93, 132.56, 132.55, 132.35, 132.32, 127.93, 127.90, 83.26, 66.62, 65.99, 29.60, 27.78, 27.14, 24.74, 24.66, 19.55.

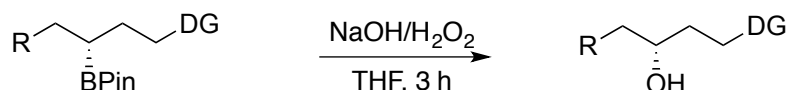
^{11}B NMR (192 MHz, CDCl_3) δ 33.8.

HRMS (ESI+) Calculated for $C_{26}H_{27}BCl_6O_6Na$ $[M+Na]^+$: 678.9924, Found: 678.9930.
 $[\alpha]_D^{23} = -0.7$ ($c = 1.0$, DCM).

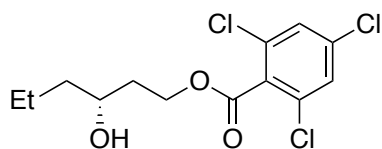
SFC analysis indicated 97% ee (compound **3o**) after oxidation.

2.4.4 Oxidation of Secondary Boronates

Representative procedure for oxidation of secondary boronates



In a 20-mL scintillation vial, the secondary boronate (20 – 100 mg) was dissolved in 2 mL THF. The vial was cooled in an ice bath and added a premixed solution of NaOH (2 M, aq.)/30% H_2O_2 (2:1, 3 mL). The reaction was warmed to rt and allowed to stir for 3 hours before the addition of water (5 mL) and ethyl acetate (5 mL). The phases were separated, and the aqueous layer was extracted twice with 5 mL ethyl acetate. The organic phases were combined, dried over Na_2SO_4 , and concentrated *in vacuo*. The pure product was obtained by flash column chromatography (CombiFlash).



Compound 3a was purified by flash column chromatography (16% ethyl acetate in hexane) and obtained as colorless liquid in 90% yield.

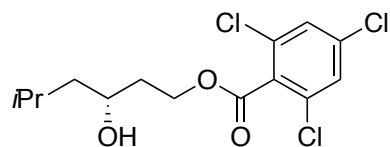
1H NMR (500 MHz, $CDCl_3$) δ 7.34 (s, 2H), 4.61 (ddd, $J = 11.0, 8.7, 5.2$ Hz, 1H), 4.49 (dt, $J = 11.1, 5.6$ Hz, 1H), 3.83 – 3.79 (m, 1H), 1.96 (dddd, $J = 14.6, 9.1, 6.1, 3.3$ Hz, 1H), 1.88 (brs, 1H), 1.78 (ddt, $J = 14.5, 9.2, 5.2$ Hz, 1H), 1.53 – 1.31 (m, 4H), 0.92 (t, $J = 6.8$ Hz, 3H).

^{13}C NMR (151 MHz, $CDCl_3$) δ 164.23, 136.14, 132.54, 132.14, 128.02, 68.14, 63.84, 39.70, 36.07, 18.71, 13.95.

HRMS (EI+) Calculated for $C_{13}H_{15}^{35}Cl_3O_3$ $[M]^+$: 324.0087, Found: 324.0086.

$[\alpha]_D^{23} = -9.4$ ($c = 1.0$, DCM).

SFC analysis (OZ-H, 10% IPA/ CO_2 , 2.5 mL/min, 220 nm) indicated 97% ee: t_R (major) = 3.4 min, t_R (minor) = 3.0 min.



Compound 3b was purified by flash column chromatography (16% ethyl acetate in hexane) and obtained as colorless liquid in 99% yield.

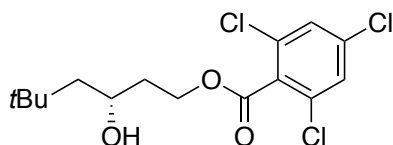
1H NMR (500 MHz, $CDCl_3$) δ 7.34 (s, 2H), 4.64 (ddd, $J = 11.0, 8.9, 5.1$ Hz, 1H), 4.47 (ddd, $J = 11.0, 6.0, 5.0$ Hz, 1H), 3.88 (tt, $J = 9.1, 3.7$ Hz, 1H), 1.97 – 1.91 (m, 1H), 1.91 (brs, 1H), 1.83 – 1.70 (m, 2H), 1.45 (ddd, $J = 14.1, 9.1, 5.3$ Hz, 1H), 1.23 (ddd, $J = 13.5, 8.9, 4.1$ Hz, 1H), 0.91 (d, $J = 6.6$ Hz, 3H), 0.89 (d, $J = 6.6$ Hz, 3H).

^{13}C NMR (151 MHz, CDCl_3) δ 164.27, 136.14, 132.54, 132.13, 128.02, 66.39, 63.76, 46.75, 36.66, 24.50, 23.37, 21.92.

HRMS (EI+) Calculated for $\text{C}_{14}\text{H}_{17}^{35}\text{Cl}_3\text{O}_3$ $[\text{M}]^+$: 338.0243, Found: 338.0244.

$[\alpha]_{\text{D}}^{23} = -6.3$ ($c = 1.0$, DCM).

SFC analysis (OZ-H, 20% IPA/ CO_2 , 1.5 mL/min, 220 nm) indicated 99% ee: t_{R} (major) = 2.2 min, t_{R} (minor) = 2.0 min.



Compound 3c was purified by flash column chromatography (16% ethyl acetate in hexane) and obtained as colorless liquid in 99% yield.

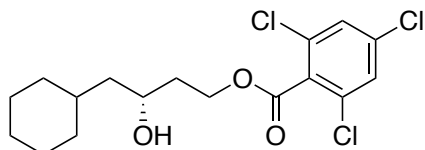
^1H NMR (500 MHz, CDCl_3) δ 7.35 (s, 2H), 4.65 (ddd, $J = 11.1, 9.0, 5.0$ Hz, 1H), 4.45 (dt, $J = 10.9, 5.6$ Hz, 1H), 3.99 – 3.93 (m, 1H), 1.94 – 1.87 (m, 1H), 1.83 – 1.76 (m, 2H), 1.45 (dd, $J = 14.6, 8.4$ Hz, 1H), 1.36 (dd, $J = 14.6, 2.5$ Hz, 1H), 0.96 (s, 9H).

^{13}C NMR (151 MHz, CDCl_3) δ 164.35, 136.17, 132.56, 132.13, 128.05, 66.04, 63.70, 51.25, 38.13, 30.30, 30.10.

HRMS (EI+) Calculated for $\text{C}_{15}\text{H}_{19}^{35}\text{Cl}_3\text{O}_3$ $[\text{M}]^+$: 352.0400, Found: 352.0392.

$[\alpha]_{\text{D}}^{23} = -6.5$ ($c = 1.0$, DCM).

SFC analysis (OD-H, 20% IPA/ CO_2 , 1.5 mL/min, 220 nm) indicated 99% ee: t_{R} (major) = 2.1 min, t_{R} (minor) = 1.7 min.



Compound 3d was purified by flash column chromatography (16% ethyl acetate in hexane) and obtained as colorless liquid in 92% yield.

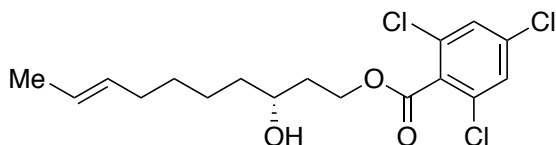
^1H NMR (500 MHz, CDCl_3) δ 7.35 (s, 2H), 4.63 (ddd, $J = 11.0, 8.9, 5.1$ Hz, 1H), 4.54 – 4.42 (m, 1H), 3.92 (tt, $J = 8.5, 3.5$ Hz, 1H), 1.94 (dddd, $J = 14.7, 9.1, 6.0, 3.3$ Hz, 1H), 1.84 (brs, 1H), 1.79 – 1.74 (m, 2H), 1.72 – 1.60 (m, 4H), 1.45 – 1.39 (m, 2H), 1.33 – 1.08 (m, 4H), 1.01 – 0.90 (m, 1H), 0.90 – 0.78 (m, 1H).

^{13}C NMR (151 MHz, CDCl_3) δ 164.28, 136.15, 132.56, 132.14, 128.04, 65.80, 63.79, 45.41, 36.73, 34.14, 33.99, 32.77, 26.51, 26.30, 26.13.

HRMS (EI+) Calculated for $\text{C}_{17}\text{H}_{21}^{35}\text{Cl}_2^{37}\text{ClO}_3$ $[\text{M}]^+$: 380.0527, Found: 380.0514.

$[\alpha]_{\text{D}}^{23} = -4.3$ ($c = 1.0$, DCM).

SFC analysis (OZ-H, 20% IPA/ CO_2 , 1.5 mL/min, 220 nm) indicated 99% ee: t_{R} (major) = 3.6 min, t_{R} (minor) = 3.0 min.



Compound 3e was purified by flash column chromatography (12% ethyl acetate in hexane) and obtained as colorless liquid in 95% yield.

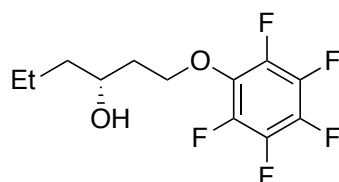
^1H NMR (500 MHz, CDCl_3) δ 7.37 (s, 2H), 5.46 – 5.37 (m, 2H), 4.66 – 4.61 (m, 1H), 4.53 – 4.49 (m, 1H), 3.86 – 3.78 (m, 1H), 2.02 – 1.95 (m, 3H), 1.85 – 1.77 (m, 2H), 1.71 – 1.59 (d, $J = 3.5$ Hz, 3H), 1.56 – 1.30 (m, 6H).

^{13}C NMR (151 MHz, CDCl_3) δ 164.23, 136.16, 132.56, 132.14, 131.17, 128.04, 124.91, 68.44, 63.83, 37.43, 36.06, 32.43, 29.43, 25.02, 17.88.

HRMS (ESI+) Calculated for $\text{C}_{17}\text{H}_{21}^{35}\text{Cl}_3\text{O}_3\text{Na}$ [$\text{M}+\text{Na}$] $^+$: 401.0448, Found: 401.0452.

$[\alpha]_{\text{D}}^{23} = -6.0$ ($c = 1.0$, DCM).

SFC analysis (AD-H, 10% MeOH/ CO_2 , 2.5 mL/min, 220 nm) indicated 97% ee: t_{R} (major) = 3.7 min, t_{R} (minor) = 5.0 min.



Compound 3f was purified by flash column chromatography (12% ethyl acetate in hexane) and obtained as colorless liquid in 64% yield.

^1H NMR (500 MHz, CDCl_3) δ 4.38 – 4.34 (m, 1H), 4.31 – 4.27 (m, 1H), 3.95 – 3.91 (m, 1H), 1.98 (dddd, $J = 14.0, 8.4, 5.7, 3.2$ Hz, 1H), 1.88 – 1.77 (m, 1H), 1.76 (brs, 1H), 1.54 – 1.45 (m, 3H), 1.43 – 1.37 (m, 1H), 0.95 (t, $J = 6.7$ Hz, 3H).

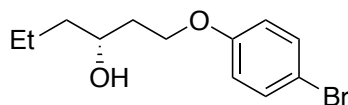
^{13}C NMR (151 MHz, CDCl_3) δ 141.80 ($J_{\text{C-F}} = 246$ Hz), 138.01 ($J_{\text{C-F}} = 251$ Hz), 137.41 ($J_{\text{C-F}} = 239$ Hz), 133.66, 73.40, 68.63, 39.91, 37.15, 18.73, 13.96.

^{19}F NMR (376 MHz, CDCl_3) δ -156.10 (d, $J = 18.8$ Hz, 2F), -162.10 – -163.03 (m, 3F).

HRMS (EI+) Calculated for $\text{C}_{12}\text{H}_{13}\text{F}_5\text{O}_2$ [M] $^+$: 284.0836, Found: 284.0835.

$[\alpha]_{\text{D}}^{23} = -10.2$ ($c = 1.0$, DCM).

HPLC analysis (AD-H, 3% IPA/Hex, 1.0 mL/min, 254 nm) indicated 98% ee: t_{R} (major) = 11.8 min, t_{R} (minor) = 10.6 min.



Compound 3g was purified by flash column chromatography (16% ethyl acetate in hexane) and obtained as colorless liquid in 90% yield.

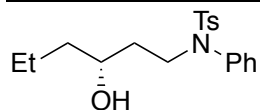
^1H NMR (500 MHz, CDCl_3) δ 7.36 (d, $J = 9.0$ Hz, 2H), 6.78 (d, $J = 9.0$ Hz, 2H), 4.13 (ddd, $J = 9.4, 7.3, 5.2$ Hz, 1H), 4.08 – 4.04 (m, 1H), 3.92 – 3.83 (m, 1H), 2.00 (brs, 1H), 1.98 – 1.90 (m, 1H), 1.90 – 1.77 (m, 1H), 1.54 – 1.44 (m, 3H), 1.44 – 1.32 (m, 1H), 0.94 (t, $J = 6.7$ Hz, 3H).

^{13}C NMR (151 MHz, CDCl_3) δ 157.85, 132.22, 116.27, 112.94, 69.39, 65.95, 39.83, 36.35, 18.74, 14.02.

HRMS (EI+) Calculated for $\text{C}_{12}\text{H}_{17}\text{BrO}_2$ [M] $^+$: 272.0412, Found: 272.0410.

$[\alpha]_{\text{D}}^{23} = -5.3$ ($c = 1.0$, DCM).

SFC analysis (AS-H, 15% IPA/ CO_2 , 2.5 mL/min, 220 nm) indicated 98% ee: t_{R} (major) = 4.7 min, t_{R} (minor) = 2.4 min.



Compound 3h was purified by flash column chromatography (25% ethyl acetate in hexane) and obtained as white solid in 97% yield.

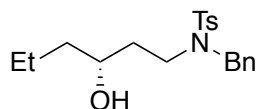
^1H NMR (500 MHz, CDCl_3) δ 7.48 (d, J = 8.3 Hz, 2H), 7.36 – 7.27 (m, 3H), 7.24 (d, J = 8.0 Hz, 2H), 7.09 – 7.00 (m, 2H), 3.97 – 3.80 (m, 2H), 3.45 (ddd, J = 13.6, 6.4, 4.1 Hz, 1H), 2.45 (brs, 1H), 2.41 (s, 3H), 1.57 – 1.50 (m, 1H), 1.49 – 1.26 (m, 5H), 0.89 (t, J = 7.0 Hz, 3H).

^{13}C NMR (151 MHz, CDCl_3) δ 143.41, 139.01, 135.20, 129.40, 129.03, 128.75, 127.92, 127.59, 67.83, 47.57, 39.35, 35.45, 21.47, 18.83, 13.97.

HRMS (ESI+) Calculated for $\text{C}_{19}\text{H}_{25}\text{NO}_3\text{SNa}$ $[\text{M}+\text{Na}]^+$: 370.1447, Found: 370.1443.

$[\alpha]_{\text{D}}^{23} = -48.2$ (c = 1.0, DCM).

SFC analysis (AS-H, 10% IPA/ CO_2 , 2.5 mL/min, 220 nm) indicated 96% ee: t_{R} (major) = 3.6 min, t_{R} (minor) = 3.0 min.



Compound 3i was purified by flash column chromatography (25% ethyl acetate in hexane) and obtained as white solid in 97% yield.

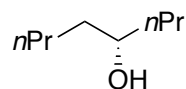
^1H NMR (500 MHz, CDCl_3) δ 7.72 (d, J = 8.3 Hz, 2H), 7.32 (d, J = 8.0 Hz, 2H), 7.30 – 7.25 (m, 5H), 4.51 (d, J = 14.6 Hz, 1H), 4.06 (d, J = 14.5 Hz, 1H), 3.63 – 3.40 (m, 2H), 2.97 (ddd, J = 14.5, 6.9, 3.7 Hz, 1H), 2.44 (s, 3H), 2.33 (brs, 1H), 1.39 – 1.06 (m, 6H), 0.83 (t, J = 7.1 Hz, 3H).

^{13}C NMR (151 MHz, CDCl_3) δ 143.38, 136.51, 136.37, 129.73, 128.53, 128.46, 127.84, 127.12, 67.68, 53.15, 45.71, 39.16, 35.78, 21.45, 18.67, 13.96.

HRMS (ESI+) Calculated for $\text{C}_{20}\text{H}_{27}\text{NO}_3\text{SNa}$ $[\text{M}+\text{Na}]^+$: 384.1604, Found: 384.1599.

$[\alpha]_{\text{D}}^{23} = -11.9$ (c = 1.0, DCM).

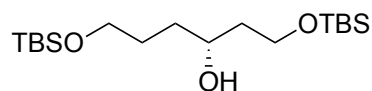
SFC analysis (OZ-H, 20% IPA/ CO_2 , 2.5 mL/min, 220 nm) indicated 99% ee: t_{R} (major) = 3.8 min, t_{R} (minor) = 2.9 min.



Compound 3m was purified by flash column chromatography (12% ethyl acetate in hexane) and obtained as colorless liquid in 80% yield.

$[\alpha]_{\text{D}}^{23} = -0.3$ (c = 1.0, DCM).

^{19}F NMR analysis with Mosher ester indicated 98% ee.



Compound 3n was purified by flash column chromatography (12% ethyl acetate in hexane) and obtained as colorless liquid in 91% yield.

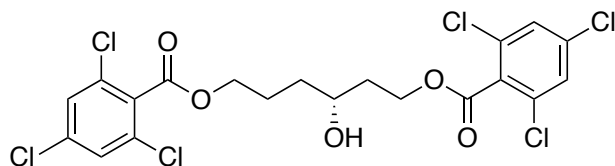
^1H NMR (500 MHz, CDCl_3) δ 3.90 – 3.86 (m, 1H), 3.84 – 3.77 (m, 2H), 3.67 – 3.60 (m, 3H), 1.70 – 1.45 (m, 6H), 0.89 (s, 9H), 0.88 (s, 9H), 0.07 (s, 6H), 0.04 (s, 6H)

^{13}C NMR (151 MHz, CDCl_3) δ 71.37, 63.35, 62.47, 38.60, 34.23, 29.00, 25.94, 25.86, 18.31, 18.14, -5.34, -5.34, -5.51, -5.54.

HRMS (ESI+) Calculated for $\text{C}_{18}\text{H}_{43}\text{O}_3\text{Si}_2$ $[\text{M}+\text{H}]^+$: 363.2745, Found: 363.2745.

$[\alpha]_{\text{D}}^{23} = 1.0$ ($c = 1.0$, DCM).

^{19}F NMR analysis with Mosher ester indicated >98% ee.



Compound 30 was purified by flash column chromatography (25% ethyl acetate in hexane) and obtained as white solid in 92% yield.

^1H NMR (500 MHz, CDCl_3) δ 7.35 (s, 2H), 7.34 (s, 2H), 4.64 (ddd, $J = 11.1, 8.9, 4.9$ Hz, 1H), 4.49 – 4.45 (m, 1H), 4.43 – 4.39 (m, 2H), 3.89 – 3.82 (m, 1H), 2.07 (brs, 1H), 2.02 – 1.90 (m, 2H), 1.89 – 1.78 (m, 2H), 1.69 – 1.56 (m, 2H).

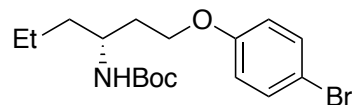
^{13}C NMR (151 MHz, CDCl_3) δ 164.26, 164.05, 136.24, 136.10, 132.53, 132.53, 132.19, 131.98, 128.06, 128.00, 67.86, 66.30, 63.60, 36.24, 33.67, 24.72.

HRMS (ESI+) Calculated for $\text{C}_{20}\text{H}_{16}^{35}\text{Cl}_6\text{O}_5\text{Na}$ $[\text{M}+\text{Na}]^+$: 568.9021, Found: 568.9021.

$[\alpha]_{\text{D}}^{23} = -3.4$ ($c = 0.5$, DCM).

SFC analysis (OD-H, 20% IPA/ CO_2 , 2.5 mL/min, 220 nm) indicated 97% ee: t_{R} (major) = 5.3 min, t_{R} (minor) = 6.2 min.

2.4.5 Derivatization of Secondary Boronates



Compound 4a was synthesized according to the following procedure.

In an argon-filled drybox, an oven-dried flask was charged with a freshly prepared solution of *O*-methylhydroxylamine (880 μL , 0.68 M in THF, 3 equiv). The solution was diluted with 1 mL of THF. The flask was capped, removed from the box, and cooled to -78 $^{\circ}\text{C}$. A solution of *n*BuLi (240 μL , 2.5 M in hexanes, 3 equiv) was added dropwise. The resulting mixture was allowed to stir for 30 min. A separate flask was charged with **2g** (77 mg, 0.20 mmol) and THF (1 mL) in the drybox. The solution of **2g** was then added dropwise to the solution of lithiated *O*-methylhydroxylamine. The reaction mixture was warmed to rt and then heated at 60 $^{\circ}\text{C}$. After 12 hours, the flask was cooled to rt and Boc anhydride (155 μL , 3.3 equiv) was added. After 1 h at rt, the reaction was quenched with water (10 mL). The mixture was extracted with ethyl acetate (15 mL) twice. The combined organic layers were combined, dried over Na_2SO_4 , and concentrated *in vacuo*. The crude material was purified by flash column chromatography (12% ethyl acetate in hexane). Compound **4a** was obtained as white solid in 72% yield.

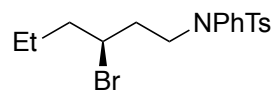
^1H NMR (500 MHz, CDCl_3) δ 7.34 (d, $J = 8.8$ Hz, 2H), 6.76 (d, $J = 8.9$ Hz, 2H), 4.48 (d, $J = 9.2$ Hz, 1H), 4.02 – 3.94 (m, 2H), 3.79 – 3.72 (m, 1H), 2.07 – 1.89 (m, 1H), 1.87 – 1.75 (m, 1H), 1.51 – 1.32 (m, 4H), 1.40 (s, 9H), 0.91 (t, $J = 7.1$ Hz, 3H).

^{13}C NMR (151 MHz, DCl_3) δ 157.93, 155.58, 132.14, 116.32, 112.76, 79.00, 65.63, 48.17, 37.68, 34.77, 28.33, 19.07, 13.89.

HRMS (ESI-) Calculated for $\text{C}_{17}\text{H}_{25}\text{BrNO}_3$ $[\text{M}-\text{H}]^-$: 370.1023, Found: 370.1021.

$[\alpha]_{\text{D}}^{23} = -7.5$ ($c = 1.0$, DCM).

SFC analysis (OJ-H, 5% IPA/ CO_2 , 2.5 mL/min, 220 nm) indicated 97% ee: t_{R} (major) = 3.4 min, t_{R} (minor) = 2.1 min.



Compound 4b was synthesized according to the following procedure.

In an argon-filled drybox, an oven-dried flask was charged with 3,5-bis(trifluoromethyl)-1-bromobenzene (69 μL , 2 equiv) and 1 mL THF. The flask was capped, removed from the box, and cooled to -78 $^\circ\text{C}$. A solution of $n\text{BuLi}$ (160 μL , 2.5 M in hexanes, 2 equiv) was added dropwise. The resulting mixture was allowed to stir for 1 h. A separate flask was charged with **2h** (91 mg, 0.20 mmol) and THF (1 mL) in the drybox. The solution of **2h** was then dropwise added to the solution of aryllithium. The reaction mixture was allowed to stir at -78 $^\circ\text{C}$ for 30 min and at rt for 30 min. The resulting solution was added a solution of NBS (71 mg, 2 equiv) in THF (1 mL) dropwise. After stirring at rt for 1 h, 20% $\text{Na}_2\text{S}_2\text{O}_3$ solution was added. The mixture was extracted with ethyl acetate (15 mL) twice. The combined organic layers were combined, dried over Na_2SO_4 , and concentrated *in vacuo*. The crude material was purified by flash column chromatography (10% ethyl acetate in hexane). Compound **4b** was obtained as light brown oil in 85% yield.

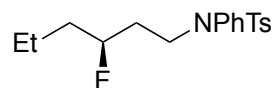
^1H NMR (500 MHz, CDCl_3) δ 7.48 (d, $J = 7.9$ Hz, 2H), 7.35 – 7.29 (m, 3H), 7.26 (d, $J = 7.9$ Hz, 2H), 7.06 (dd, $J = 7.4$ Hz, 2H), 4.08 (tt, $J = 8.8, 4.3$ Hz, 1H), 3.81 – 3.68 (m, 2H), 2.43 (s, 3H), 2.05 – 1.92 (m, 2H), 1.82 – 1.68 (m, 2H), 1.58 – 1.45 (m, 1H), 1.44 – 1.35 (m, 1H), 0.90 (t, $J = 7.4$ Hz, 3H).

^{13}C NMR (151 MHz, CDCl_3) δ 143.44, 139.20, 134.85, 129.35, 129.01, 128.53, 127.91, 127.67, 53.91, 49.09, 40.99, 37.92, 21.46, 20.53, 13.25.

HRMS (EI+) Calculated for $\text{C}_{19}\text{H}_{24}\text{BrNO}_2\text{S}$ $[\text{M}]^+$: 407.0711, Found: 407.0709.

$[\alpha]_{\text{D}}^{23} = 14.6$ ($c = 1.0$, DCM).

SFC analysis (AD-H, 10% MeOH/ CO_2 , 2.5 mL/min, 220 nm) indicated 97% ee: t_{R} (major) = 2.6 min, t_{R} (minor) = 2.8 min.



Compound 4c was synthesized according to the following procedure.

To a solution of **2h** (77 mg, 0.20 mmol) in THF (2 mL) at 0 $^\circ\text{C}$ was added PhLi (106 μL , 1.8 M in hexanes, 0.95 equiv) dropwise. The solution was allowed to stir for 30 min. Anhydrous MeCN (0.5 mL) was added, and the volatile materials were evaporated by high vacuum. MeCN (2.5 mL) was then added to the flask. A separate flask was charged with Selecfluor I (92 mg, 1.3 equiv) and 4 \AA molecular sieves (150 mg). To the latter flask was added MeCN (2.5 mL), and the flask was cooled to -20 $^\circ\text{C}$. Styrene (11 μL , 0.5 equiv) was added. The resulting mixture was stirred briefly, and the solution of ate complex was added dropwise at -20 $^\circ\text{C}$. The flask was allowed to stir at -20 $^\circ\text{C}$ for 20 h. A premixed solution of NaOH (2 M, aq.)/30% H_2O_2 (2:1, 3 mL) was added dropwise at 0 $^\circ\text{C}$. The resulting solution was warmed to rt and allowed to stir for 3 h before being

quenched with water (10 mL). The mixture was extracted with ethyl acetate (15 mL) twice. The organic layers were combined, dried over Na_2SO_4 , and concentrated *in vacuo*. The crude material was purified by flash column chromatography (8% ethyl acetate in hexane). Compound **4c** was obtained as white solid in 67% yield.

^1H NMR (500 MHz, CDCl_3) δ 7.46 (d, $J = 8.0$ Hz, 2H), 7.34 – 7.29 (m, 3H), 7.24 (d, $J = 8.0$ Hz, 2H), 7.04 (dd, $J = 7.6, 2.2$ Hz, 2H), 4.57 (dtt, $J = 49.5$ ($^1J_{\text{H-F}}$), 8.2, 4.0 Hz, 1H), 3.75 – 3.69 (m, 1H), 3.62 (ddd, $J = 13.5, 8.3, 5.4$ Hz, 1H), 2.42 (s, 3H), 1.84 – 1.64 (m, 2H), 1.58 – 1.28 (m, 4H), 0.89 (t, $J = 7.1$ Hz, 3H).

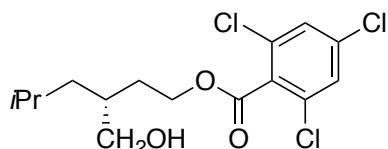
^{13}C NMR (151 MHz, CDCl_3) δ 143.41, 139.22, 135.01, 129.37, 129.04, 128.65, 127.91, 127.73, 91.47 (d, $J_{\text{C-F}} = 167.6$ Hz), 47.16 – 47.11 (d, $J_{\text{C-F}} = 45.3$ Hz), 37.08 (d, $J_{\text{C-F}} = 20.4$ Hz), 34.30 (d, $J_{\text{C-F}} = 21.0$ Hz), 21.51, 18.20 (d, $J_{\text{C-F}} = 4.8$ Hz), 13.79.

^{19}F NMR (376 MHz, CDCl_3) δ -181.9 – -182.2 (m).

HRMS (EI+) Calculated for $\text{C}_{27}\text{H}_{29}\text{O}_2\text{N}^{35}\text{Cl}_3$ $[\text{M}]^+$: 349.1512, Found: 349.1512.

$[\alpha]_{\text{D}}^{23} = 8.0$ ($c = 1.0$, DCM).

HPLC analysis (AS-H, 5% IPA/Hex, 0.6 mL/min, 254 nm) indicated 70% ee: t_{R} (major) = 24.9 min, t_{R} (minor) = 23.0 min.



Compound 4d was synthesized according to the following procedure.

In an argon-filled drybox, an oven-dried flask was charged with **1b** (90 mg, 0.20 mmol), dibromomethane (35 μL , 2.5 equiv) and THF (2 mL). The flask was capped, removed from the drybox, and cooled to -78 $^{\circ}\text{C}$. A solution of *n*BuLi (176 μL , 2.5 M in hexanes, 2.2 equiv) was added dropwise. The resulting mixture was allowed to stir for 10 min, warmed to rt and stirred for an additional 2 h. The reaction mixture was cooled to 0 $^{\circ}\text{C}$, and a premixed solution of NaOH (2 M, aq.)/30% H_2O_2 (2:1, 3 mL) was added dropwise. The resulting solution was warmed to rt and allowed to stir for 3 h before being quenched with water (10 mL). The mixture was extracted with ethyl acetate (15 mL) twice. The organic layers were combined, dried over Na_2SO_4 , and concentrated *in vacuo*. The crude material was purified by flash column chromatography (20% ethyl acetate in hexane). Compound **4d** was obtained as a colorless oil in 70% yield.

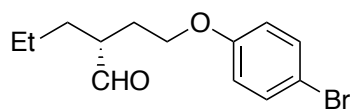
^1H NMR (500 MHz, CDCl_3) δ 7.35 (s, 2H), 4.52 – 4.45 (m, 2H), 3.65 (dd, $J = 10.8, 4.0$ Hz, 1H), 3.55 (dd, $J = 10.8, 5.4$ Hz, 1H), 1.92 – 1.83 (m, 1H), 1.82 – 1.72 (m, 3H), 1.71 – 1.62 (m, 1H), 1.30 – 1.24 (m, 1H), 1.17 – 1.12 (m, 1H), 0.89 (d, $J = 6.6$ Hz, 6H).

^{13}C NMR (151 MHz, CDCl_3) δ 164.13, 136.07, 132.54, 132.26, 128.01, 65.27, 64.96, 40.48, 35.09, 30.42, 25.30, 22.95, 22.65.

HRMS (EI+) Calculated for $\text{C}_{15}\text{H}_{19}\text{Cl}_3\text{O}_3$ $[\text{M}]^+$: 352.0400, Found: 352.0399.

$[\alpha]_{\text{D}}^{23} = 2.1$ ($c = 1.0$, DCM).

SFC analysis (OD-H, 10% IPA/ CO_2 , 10 MPa, 2.5 mL/min, 220 nm) indicated 99% ee: t_{R} (major) = 4.1 min, t_{R} (minor) = 3.3 min.



Compound 4e was synthesized according to the following procedure.

In an argon-filled drybox, an oven-dried flask was charged with DCM (78 μ L, 6 equiv) and THF (2 mL). The flask was capped, removed from the box, and cooled to -100 $^{\circ}$ C. A solution of *n*BuLi (320 μ L, 2.5 M in hexanes, 4 equiv) was added dropwise. The resulting mixture was allowed to stir for 10 min. A separate flask was charged with **2g** (77 mg, 0.20 mmol) and THF (1.5 mL) in the drybox. The solution of **2g** then was added dropwise to the solution of LiCHCl₂. The reaction mixture was allowed to warm to rt over 2 h. The reaction mixture was cooled to 0 $^{\circ}$ C, and a premixed solution of NaOH (2 M, aq.)/30% H₂O₂ (2:1, 3 mL) was added dropwise. The resulting solution was warmed to rt and allowed to stir for 3 h before being quenched with water (10 mL). The mixture was extracted with ethyl acetate (15 mL) twice. The organic layers were combined, dried over Na₂SO₄, and concentrated *in vacuo*. The crude material was purified by flash column chromatography (5% ethyl acetate in hexane). Compound **4e** was obtained as colorless oil in 65% yield.

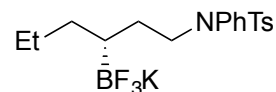
¹H NMR (500 MHz, CDCl₃) δ 9.66 (d, *J* = 2.4 Hz, 1H), 7.41 – 7.30 (m, 2H), 6.78 – 6.71 (m, 2H), 3.95 (t, *J* = 6.1 Hz, 2H), 2.59 – 2.47 (m, 1H), 2.15 (ddt, *J* = 14.6, 8.5, 6.1 Hz, 1H), 1.91 (dtd, *J* = 14.5, 6.3, 4.6 Hz, 1H), 1.77 – 1.65 (m, 1H), 1.54 – 1.45 (m, 1H), 1.41 – 1.33 (m, 2H), 0.94 (t, *J* = 7.3 Hz, 3H).

¹³C NMR (151 MHz, CDCl₃) δ 204.25, 157.70, 132.24, 116.26, 113.01, 65.76, 48.78, 30.94, 28.32, 20.11, 14.04.

HRMS (EI+) Calculated for C₁₃H₁₇BrO₂ [M]⁺: 284.0412, Found: 284.0410s.

$[\alpha]_D^{23}$ = 8.2 (c = 1.0, DCM).

SFC analysis (AS-H, 5% IPA/CO₂, 2.5 mL/min, 220 nm) indicated 93% ee: t_R (major) = 4.7 min, t_R (minor) = 2.8 min.



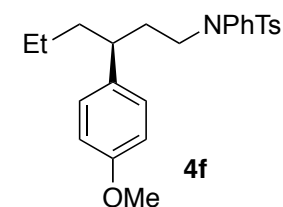
Compound 2h-BF₃K was synthesized according to a literature procedure and obtained as white solid in 80% yield.

¹H NMR (600 MHz, acetone-*d*₆) δ 7.48 (d, *J* = 8.3 Hz, 2H), 7.36 – 7.24 (m, 5H), 7.10 – 7.04 (m, 2H), 3.70 (ddd, *J* = 13.0, 11.1, 5.1 Hz, 1H), 3.59 (ddd, *J* = 13.0, 10.9, 5.5 Hz, 1H), 2.40 (s, 3H), 1.46 (dddd, *J* = 12.7, 10.9, 7.7, 5.1 Hz, 1H), 1.36 – 1.26 (m, 2H), 1.26 – 1.19 (m, 1H), 1.19 – 1.09 (m, 1H), 0.99 (dddd, *J* = 12.7, 10.1, 7.9, 5.0 Hz, 1H), 0.75 (t, *J* = 7.3 Hz, 3H), 0.27 – 0.18 (m, 1H).

¹³C NMR (151 MHz, acetone-*d*₆) δ 143.93, 141.01, 137.28, 130.19, 129.57, 129.43, 128.45, 128.02, 51.83, 34.69, 31.22, 26.31, 22.72, 21.47, 15.27.

¹¹B NMR (192 MHz, acetone-*d*₆) δ 4.9.

¹⁹F NMR (376 MHz, acetone-*d*₆) δ -142.8 (s).



Compound 4f was synthesized according to the following procedure.

In an argon-filled drybox, a one dram-vial was charged with **2h-BF₃K** (53 mg, 0.12 mmol), K₂CO₃ (50 mg, 3 equiv), Pd-*t*Bu₃P G3 catalyst (13.7 mg, 20 mol %), 4-chloroanisole (18 μL, 1.2 equiv) and toluene (0.5 mL). The vial was capped with a teflon-coated cap with septum and removed from the drybox. Degassed water (0.25 mL) was added to the vial. The cap was quickly replaced by a teflon-coated cap without septum. The vial was sealed with electric tape, and heated at 100 °C for 48 h. The reaction mixture was added water (10 mL). The mixture was extracted with ethyl acetate (15 mL) twice. The combined organic layers were combined, dried over Na₂SO₄, and concentrated *in vacuo*. The crude material was purified by flash column chromatography (10% ethyl acetate in hexane). Compound **4f** was obtained as white solid in 38% yield.

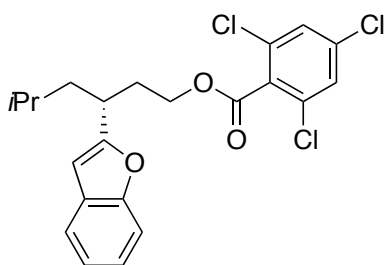
¹H NMR (600 MHz, CDCl₃) δ 7.37 (d, *J* = 8.2 Hz, 2H), 7.34 – 7.27 (m, 3H), 7.18 (d, *J* = 7.9 Hz, 2H), 7.02 – 6.97 (m, 2H), 6.97 – 6.92 (m, 2H), 6.84 – 6.74 (m, 2H), 3.78 (s, 3H), 3.45 – 3.41 (m, 1H), 3.29 – 3.25 (m, 1H), 2.53 (tt, *J* = 9.7, 4.8 Hz, 1H), 2.39 (s, 3H), 1.80 – 1.72 (m, 1H), 1.65 – 1.59 (m, 1H), 1.49 – 1.35 (m, 2H), 1.11 – 1.03 (m, 2H), 0.78 (t, *J* = 7.3 Hz, 3H).

¹³C NMR (151 MHz, CDCl₃) δ 157.85, 143.13, 139.36, 136.69, 135.25, 129.24, 128.85, 128.73, 128.40, 127.66, 127.66, 113.68, 55.17, 48.92, 41.80, 39.14, 35.53, 21.47, 20.42, 13.96.

HRMS (EI+) Calculated for C₂₆H₃₁NO₃S [M]⁺: 437.2025, Found: 437.2016.

[α]_D²³ = -6.3 (c = 1.0, DCM).

HPLC analysis (OD-H, 3% IPA/Hex, 1.0 mL/min, 254 nm) indicated 87% ee: t_R (major) = 7.1 min, t_R (minor) = 6.3 min.



Compound 4g was synthesized according to the following procedure.

In an argon-filled drybox, an oven-dried flask was charged with benzofuran (28 μL, 1.25 equiv). The solution was diluted with 1 mL THF. The flask was capped, removed from the box, and cooled to -78 °C. A solution of *n*BuLi (100 μL, 1.25 equiv) was added dropwise. The resulting mixture was warmed to rt and stirred for 1 h. A separate flask was charged with **1b** (90 mg, 0.20 mmol) and THF (1 mL) in the drybox. Then the solution of **1b** was added dropwise to the solution of lithiated benzofuran at -78 °C. After 1 h at -78 °C, the resulting solution was added dropwise to a solution of NBS (71 mg, 2 equiv) in THF (1 mL). After stirring at -78 °C for 1 h, a 20% aqueous solution of Na₂S₂O₃ was added. The mixture was warmed to rt and extracted with ethyl acetate (15 mL) twice. The combined organic layers were combined, dried over Na₂SO₄, and concentrated *in vacuo*. The crude material was purified by flash column chromatography (2.5% ethyl acetate in hexane). Compound **4g** was obtained as white solid in 71% yield.

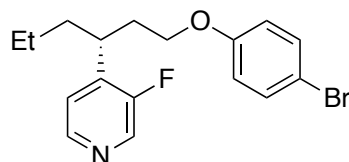
¹H NMR (500 MHz, CDCl₃) δ 7.54 – 7.47 (m, 1H), 7.46 – 7.38 (m, 1H), 7.35 (s, 2H), 7.25 – 7.16 (m, 2H), 6.46 (s, 1H), 4.41 – 4.37 (m, 1H), 4.31 – 4.27 (m, 1H), 3.17 – 3.11 (m, 1H), 2.20 – 2.09 (m, 2H), 1.86 – 1.79 (m, 1H), 1.52 – 1.41 (m, 2H), 0.91 (d, *J* = 6.2 Hz, 3H), 0.87 (d, *J* = 6.3 Hz, 3H).

¹³C NMR (151 MHz, CDCl₃) δ 163.95, 160.02, 154.65, 136.05, 132.51, 132.20, 128.51, 127.99, 123.27, 122.46, 120.34, 110.86, 103.19, 64.52, 43.03, 34.23, 33.19, 25.61, 23.25, 21.78.

HRMS (EI+) Calculated for $C_{22}H_{21}^{35}Cl_3O_3 [M]^+$: 438.0556, Found: 438.0558.

$[\alpha]_D^{23} = -40.6$ ($c = 1.0$, DCM).

SFC analysis (OJ-H, 5% IPA/CO₂, 2.5 mL/min, 220 nm) indicated 99% ee: t_R (major) = 3.8 min, t_R (minor) = 3.4 min.



Compound 4h was synthesized according to the following procedure.

In an argon-filled drybox, an oven-dried flask was charged with diisopropylamine (61 μ L, 2.2 equiv) and THF (0.5 mL). The flask was capped, removed from the drybox, and cooled to -78 $^{\circ}$ C. A solution of *n*BuLi (160 μ L, 2.5 M in hexanes, 2 equiv) was added dropwise. The resulting mixture was warmed to rt and allowed to stir for 15 min. A solution of 3-fluoropyridine (34 μ L, 2 equiv) in THF (1 mL) was added dropwise to the solution of LDA at -60 $^{\circ}$ C. A solution of **2g** (77 mg, 0.20 mmol) in THF (1 mL) was added after 30 min. The reaction mixture was allowed to stir for 2 h at the same temperature. TrocCl (61 μ L, 2.2 equiv) was added, and the mixture was allowed to warm to rt overnight. The mixture was quenched with water and extracted with ethyl acetate (15 mL) twice. The organic layers were combined, dried over Na₂SO₄, and concentrated *in vacuo*. The obtained material was dissolved in THF (2 mL), and the reaction mixture was cooled to 0 $^{\circ}$ C. A premixed solution of NaOH (2 M, aq.)/30% H₂O₂ (2:1, 3 mL) was added dropwise. The resulting solution was warmed to rt and allowed to stir for 3 h before being quenched with water (10 mL). The mixture was extracted with ethyl acetate (15 mL) twice. The organic layers were combined, dried over Na₂SO₄, and concentrated *in vacuo*. The crude material was purified by flash column chromatography (20% ethyl acetate in hexane). Compound **4h** was obtained as colorless oil in 83% yield.

¹H NMR (500 MHz, CDCl₃) δ 8.36 (s, 1H), 8.32 (d, $J = 4.9$ Hz, 1H), 7.31 (d, $J = 9.0$ Hz, 2H), 7.13 (t, $J = 5.6$ Hz, 1H), 6.64 (d, $J = 8.9$ Hz, 2H), 3.82 (dt, $J = 9.4, 5.9$ Hz, 1H), 3.73 – 3.69 (m, 1H), 3.21 (tt, $J = 9.9, 5.5$ Hz, 1H), 2.21 – 2.14 (m, 1H), 2.08 – 2.00 (m, 1H), 1.73 – 1.62 (m, 2H), 1.27 – 1.12 (m, 2H), 0.87 (t, $J = 7.3$ Hz, 3H).

¹³C NMR (151 MHz, CDCl₃) δ 158.43 ($J_{C-F} = 254$ Hz), 157.70, 145.71 ($J_{C-F} = 4.8$ Hz), 140.27 (d, $J_{C-F} = 12.2$ Hz), 138.09 (d, $J_{C-F} = 25.8$ Hz), 132.14, 123.32, 116.13, 112.84, 65.84, 37.11, 35.29, 34.25, 20.43, 13.82.

¹⁹F NMR (376 MHz, CDCl₃) δ -131.4 (s).

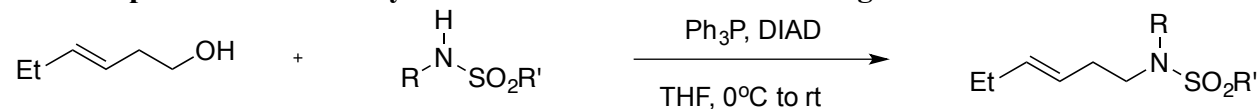
HRMS (EI+) Calculated for $C_{17}H_{19}BrFO_3 [M]^+$: 351.0634, Found: 351.0636.

$[\alpha]_D^{23} = -49.5$ ($c = 1.0$, DCM).

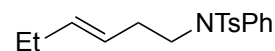
SFC analysis (OJ-H, 10% IPA/CO₂, 2.5 mL/min, 220 nm) indicated 97% ee: t_R (major) = 5.3 min, t_R (minor) = 4.2 min.

2.4.6 Synthesis of Substrates

General procedure for the synthesis of the sulfonamides through Mitsunobu reactions



A 100 mL oven-dried round-bottom flask was charged with *trans*-3-hexenol (1 equiv, 5 mmol), sulfonamide (1.2 equiv), Ph₃P (1.0 equiv) and THF (20 mL). The flask was cooled to 0 °C, and DIAD (1.2 equiv) was added dropwise. The mixture was allowed to warm to room temperature and was stirred for 24-48 h. After cooling to rt, saturated NH₄Cl(aq) was added to quench the reaction. The mixture was extracted with ethyl acetate (twice) and dried over anhydrous Na₂SO₄. The crude product obtained after filtration and concentration *in vacuo* was purified by flash column chromatography with hexanes and ethyl acetate as eluents to afford the pure product.

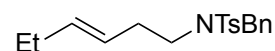


1h was obtained in 84% isolated yield as white solid.

¹H NMR (600 MHz, CDCl₃) δ 7.47 (d, *J* = 8.3 Hz, 2H), 7.33 – 7.27 (m, 3H), 7.23 (d, *J* = 8.0 Hz, 2H), 7.07 – 7.00 (m, 2H), 5.44 – 5.39 (m, 1H), 5.31 – 5.25 (m, 1H), 3.54 (t, *J* = 7.5 Hz, 2H), 2.41 (s, 3H), 2.11 (q, *J* = 7.1 Hz, 2H), 1.98 – 1.93 (m, 2H), 0.93 (t, *J* = 7.5 Hz, 3H).

¹³C NMR (151 MHz, CDCl₃) δ 143.19, 139.10, 135.42, 134.77, 129.28, 128.91, 128.86, 127.76, 127.64, 124.61, 50.49, 31.65, 25.52, 21.48, 13.62.

HRMS (EI⁺) Calculated for C₁₉H₂₃NO₂S [M]⁺: 329.1450, Found: 329.1446.

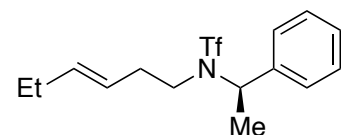


1i was obtained in 59% isolated yield as sticky oil.

¹H NMR (500 MHz, CDCl₃) δ 7.74 (d, *J* = 8.2 Hz, 2H), 7.37 – 7.25 (m, 7H), 5.34 – 5.29 (m, 1H), 5.13 – 5.07 (m, 1H), 4.34 (s, 2H), 3.16 – 3.09 (m, 2H), 2.43 (s, 3H), 2.05 – 1.99 (q, *J* = 7.9 Hz, 2H), 1.92 – 1.87 (m, 2H), 0.89 (t, *J* = 7.4 Hz, 3H).

¹³C NMR (151 MHz, CDCl₃) δ 143.04, 137.16, 136.38, 134.49, 129.56, 128.39, 128.15, 127.57, 127.03, 124.70, 51.75, 47.76, 31.37, 25.38, 21.37, 13.48.

HRMS (EI⁺) Calculated for C₂₀H₂₅NO₂S [M]⁺: 344.1606, Found: 344.1601.



1j was obtained in 64% isolated yield as colorless liquid.

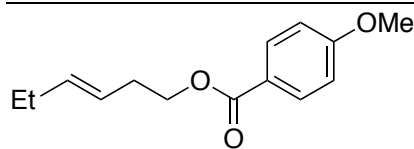
¹H NMR (600 MHz, CDCl₃) δ 7.62 – 7.29 (m, 5H), 5.35 – 5.26 (m, 2H), 5.11 – 5.06 (m, 1H), 3.18 (t, *J* = 8.4 Hz, 2H), 2.18 – 2.09 (m, 1H), 1.96 – 1.91 (m, 2H), 1.82 – 1.70 (m, 1H), 1.72 (d, *J* = 7.2 Hz, 3H), 0.93 (t, *J* = 7.5 Hz, 3H).

¹³C NMR (151 MHz, CDCl₃) δ 138.49, 135.26, 128.73, 128.48, 127.63, 123.85, 120.07 (q, *J*_{C-F} = 323.6 Hz), 57.41, 45.27, 33.63, 25.39, 16.39, 13.42.

¹⁹F NMR (376 MHz, CDCl₃) δ -131.4 (m).

HRMS (EI⁺) Calculated for C₁₅H₂₀F₃NO₂S [M]⁺: 335.1167, Found: 335.1164.

[α]_D²³ = 18.2 (c = 1.0, DCM).

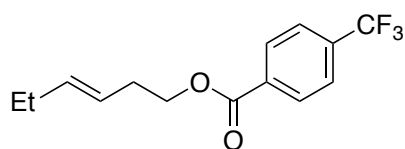


S1b was obtained in 66% isolated yield as colorless liquid.

$^1\text{H NMR}$ (500 MHz, CDCl_3) δ 8.33 (d, $J = 8.8$ Hz, 2H), 7.25 (d, $J = 8.7$ Hz, 2H), 5.98 – 5.91 (m, 1H), 5.82 – 5.75 (m, 1H), 4.63 (t, $J = 6.8$ Hz, 2H), 4.19 (s, 3H), 2.78 (q, $J = 6.9$ Hz, 2H), 2.41 – 2.31 (m, 2H), 1.31 (t, $J = 7.5$ Hz, 3H).

$^{13}\text{C NMR}$ (151 MHz, CDCl_3) δ 165.93, 163.02, 134.79, 131.25, 123.97, 122.63, 113.26, 55.01, 31.89, 25.42, 13.50.

EI-MS Calculated for $\text{C}_{14}\text{H}_{18}\text{O}_3$ $[\text{M}]^+$: 234.1, Found: 234.0.

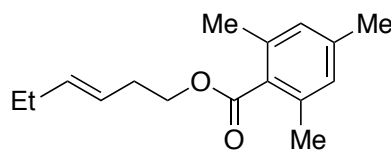


S1c was obtained in 41% isolated yield as colorless liquid.

$^1\text{H NMR}$ (500 MHz, CDCl_3) δ 8.23 – 8.10 (d, $J = 8.2$ Hz, 2H), 7.71 (d, $J = 8.4$ Hz, 2H), 5.65 – 5.58 (m, 1H), 5.47 – 5.40 (m, 1H), 4.37 (t, $J = 6.8$ Hz, 2H), 2.48 (q, $J = 6.7$ Hz, 2H), 2.09 – 1.96 (m, 2H), 0.98 (t, $J = 7.5$ Hz, 3H).

$^{13}\text{C NMR}$ (151 MHz, CDCl_3) δ 165.12, 135.32, 134.20 (q, $J_{\text{C-F}} = 32.6$ Hz), 133.61, 129.82, 125.19, 123.74, 123.59 (q, $J_{\text{C-F}} = 272.7$ Hz), 64.96, 31.89, 25.53, 13.51.

EI-MS Calculated for $\text{C}_{14}\text{H}_{15}\text{O}_2\text{F}_2$ $[\text{M-F}]^+$: 253.1, Found: 253.0.



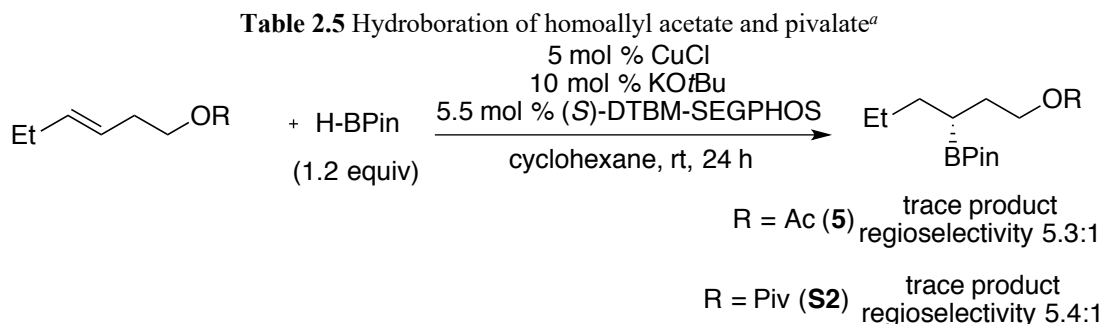
S1d was obtained in 99% isolated yield as colorless liquid (10% of an unidentified impurity is present).

$^1\text{H NMR}$ (600 MHz, CDCl_3) δ 6.87 (s, 2H), 5.66–5.61 (m, 1H), 5.49–5.44 (m, 1H), 4.36 (t, $J = 6.8$ Hz, 2H), 2.47 (q, $J = 6.7$ Hz, 2H), 2.33 (s, 6H), 2.30 (s, 3H), 2.11–2.00 (m, 2H), 1.01 (t, $J = 7.5$ Hz, 3H).

$^{13}\text{C NMR}$ (151 MHz, CDCl_3) δ 170.07, 139.10, 136.29, 135.06, 131.16, 128.35, 124.23, 64.55, 32.00, 25.60, 21.06, 19.77, 13.62.

HRMS (EI+) Calculated for $\text{C}_{16}\text{H}_{22}\text{O}_2$ $[\text{M}]^+$: 246.1620, Found: 246.1618.

2.4.7. Hydroboration of Homoallyl Benzoate Derivatives and Homoallyl Acetate (**5**) and Pivalate

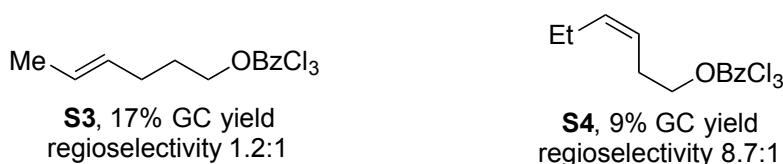


^aRegioselectivity was determined by GC analysis.

The hydroboration reactions of **S1a-S1d**, **1a**, **5**, and **S2** were conducted following the **General Procedure Condition B** with a slight alteration:

In an argon-filled dry box, a 1-dram vial was charged with CuCl (1.0 mg, 5 mol %), KOtBu (2.2 mg, 10 mol %), (S)-DTBM-SEGPHOS (13.0 mg, 5.5 mol %) and cyclohexane (200 μ L). The mixture was allowed to stir at ambient temperature for 3 minutes before the addition of pinacolborane (35 μ L, 0.24 mmol, 1.2 equiv). After brief stirring (30 – 60 seconds), the solution was added the alkene (0.2 mmol, 1 equiv), which was pre-weighed in another vial. The second vial was then washed twice with 100 μ L cyclohexane each time. The vial was then capped, sealed with electrical tape, and removed from the box. After 24 h of stirring at rt, The reaction vial was added 1,3,5-trimethoxybenzene (16.8 mg, 0.1 mmol) as an internal standard and diluted with 2 mL of ethyl acetate and the resulting solution was filtered through silica gel. An aliquot of 0.3 mL was taken for GC analysis. The rest of the crude material was concentrated *in vacuo* and analyzed by ¹H NMR spectroscopy.

2.4.8 Effect of Olefin Position and Geometry on the Hydroboration



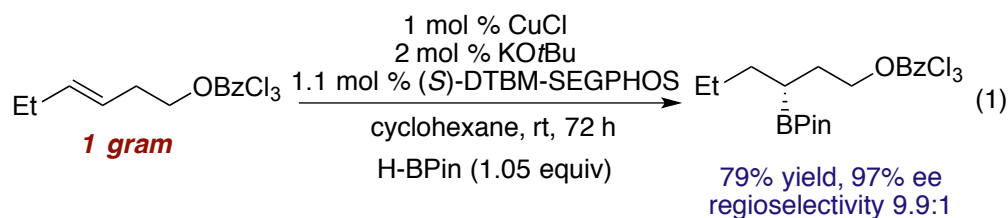
Both the reactivity and regioselectivity of the hydroboration are sensitive to the structure of the substrate. *cis*-Alkene **S4**, which is analogous to the *trans*-alkene **1a**, underwent hydroboration in low yield (9% by GC) and with regioselectivity that is slightly lower than that of its *trans*-counterpart. The homoallylic trichlorobenzoate **S3** underwent hydroboration with poor regioselectivity (1.2:1) and low yield (17% by GC).

Experimental procedure:

In an argon-filled dry box, a 1-dram vial was charged with CuCl (1.0 mg, 10 mol %), KOtBu (2.2 mg, 20 mol %), (S)-DTBM-SEGPHOS (13.0 mg, 11 mol %) and cyclohexane (100 μ L). The mixture was allowed to stir at ambient temperature for 3 minutes before the addition of

pinacolborane (29 μL , 0.2 mmol, 2.0 equiv). After brief stirring (30 – 60 seconds), the solution was added the alkene (0.1 mmol, 1 equiv), which was pre-weighed in another vial. The second vial was then washed twice with 50 μL cyclohexane each time. The vial was added 10 μL dodecane, then capped, sealed with electrical tape, and removed from the box. After 84 h of stirring at rt, the reaction mixture was filtered through celite. An aliquot was taken for GC analysis.

2.4.9 Hydroboration of **1a** on a Gram Scale

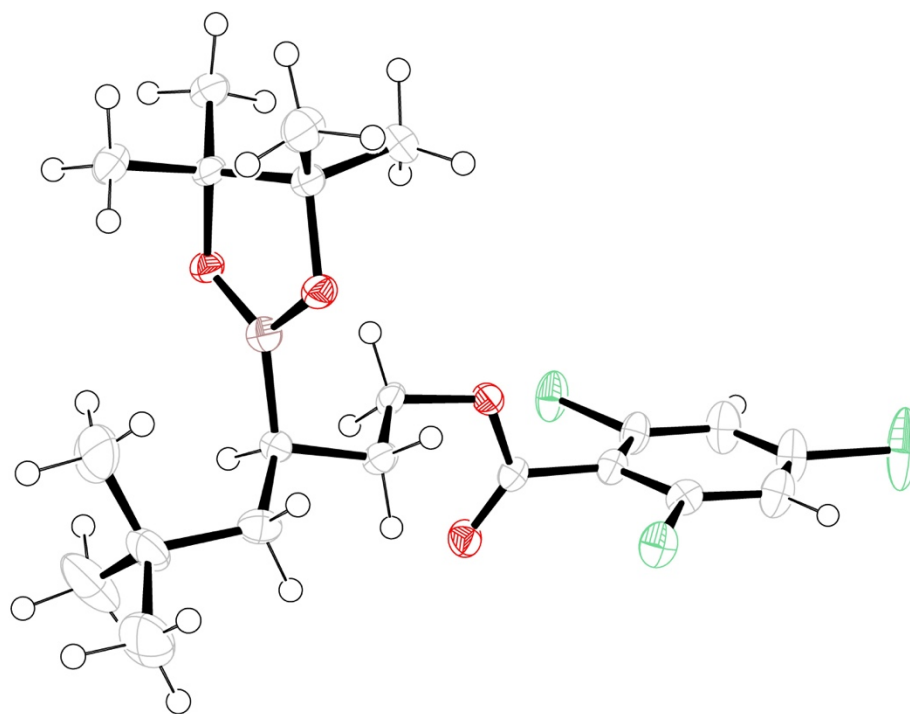


In an argon-filled dry box, a 20 mL vial was charged with CuCl (3.3 mg, 1 mol %), KOtBu (7.3 mg, 2 mol %), (S)-DTBM-SEGPHOS (42.2 mg, 1.1 mol %) and cyclohexane (2 mL). The mixture was allowed to stir at ambient temperature for 3 minutes before the addition of pinacolborane (500 μL , 3.45 mmol, 1.06 equiv). After brief stirring (30 – 60 seconds), the solution was added **1a** (1.00 g, 3.25 mmol, 1 equiv), which was pre-weighed in another vial. The second vial was then washed five times with 500 μL cyclohexane each time. The vial was then capped, sealed with electrical tape, and removed from the box. After 72 h of stirring at rt, an aliquot of 20 μL was removed and analyzed by GC. The reaction vial was diluted with 20 mL of ethyl acetate and the resulting solution was filtered through Celite. The crude material was concentrated *in vacuo* and purified by flash column chromatography (CombiFlash, 2.4% ethyl acetate in hexanes) to afford the pure product in colorless oil (1.124 g, 79% yield).

2.4.10 Assignment of Absolute Stereochemistry

The absolute configuration of **2c** was unambiguously determined to be *R* at the boron-bound stereocenters, as established by single-crystal x-ray crystallography. The absolute configurations of all other hydroboration products were assigned by analogy. The absolute configurations of all secondary alcohols were assigned by the established retention of configuration for oxidation of boronates. The absolute configurations of all products from derivatization were assigned by the established retention of configuration for the transformations,^{17,20,21a-b} except for compounds **4b**, **4c** and **4f**, which were assigned as by the established inversion of configuration.^{18,19,21c}

Figure 2.1 ORTEP drawing of compound 2c



2.4.11 Crystallographic Information of Compound 2c

A colorless block 0.150 x 0.120 x 0.100 mm in size was mounted on a cryoloop with Paratone oil. Data were collected in a nitrogen gas stream at 100(2) K. The crystal-to-detector distance was 50 mm, and the exposure time was 10 seconds per frame using a scan width of 2.0°. Data collection was 100.0% complete to 25.000° in θ . A total of 29929 reflections were collected covering the indices, $-11 \leq h \leq 11$, $-13 \leq k \leq 13$, $-14 \leq l \leq 14$. 8930 reflections were found to be symmetry independent, with an R_{int} of 0.0282. Indexing and unit cell refinement indicated a primitive, triclinic lattice. The space group was found to be P 1 (No. 1). The data were integrated using the Bruker SAINT software program and scaled using the SADABS software program. Solution by iterative methods (SHELXT-2014) produced a complete heavy-atom phasing model consistent with the proposed structure. All non-hydrogen atoms were refined anisotropically by full-matrix least squares (SHELXL-2014). All hydrogen atoms were placed using a riding model. Their positions were constrained, relative to their parent atom, using the appropriate HFIX command in SHELXL-2014. The absolute configuration was unambiguously determined to be *R* at all chiral centers.

Empirical formula	$\text{C}_{21}\text{H}_{30}\text{BCl}_3\text{O}_4$
Formula weight	463.61
Temperature	100(2) K

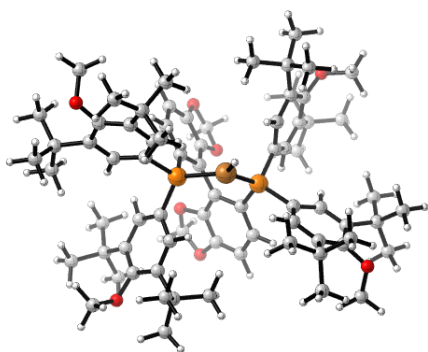
Wavelength	0.71073 Å	
Crystal system	Triclinic	
Space group	P 1	
Unit cell dimensions	a = 9.8418(5) Å	$\alpha = 101.9250(10)^\circ$.
	b = 11.2380(6) Å	$\beta = 109.9040(10)^\circ$.
	c = 12.2846(7) Å	$\gamma = 94.5190(10)^\circ$.
Volume	1233.43(12) Å ³	
Z	2	
Density (calculated)	1.248 Mg/m ³	
Absorption coefficient	0.394 mm ⁻¹	
F(000)	488	
Crystal size	0.150 x 0.120 x 0.100 mm ³	
Theta range for data collection	1.820 to 25.354°.	
Index ranges	-11<=h<=11, -13<=k<=13, -14<=l<=14	
Reflections collected	29929	
Independent reflections	8930 [R(int) = 0.0282]	
Completeness to theta = 25.000°	100.0 %	
Absorption correction	Semi-empirical from equivalents	
Max. and min. transmission	0.928 and 0.855	
Refinement method	Full-matrix least-squares on F ²	
Data / restraints / parameters	8930 / 3 / 537	
Goodness-of-fit on F ²	1.047	
Final R indices [I>2sigma(I)]	R1 = 0.0371, wR2 = 0.0920	
R indices (all data)	R1 = 0.0406, wR2 = 0.0952	
Absolute structure parameter	-0.026(15)	
Extinction coefficient	n/a	
Largest diff. peak and hole	0.380 and -0.330 e.Å ⁻³	

2.4.12 DFT Calculations

General

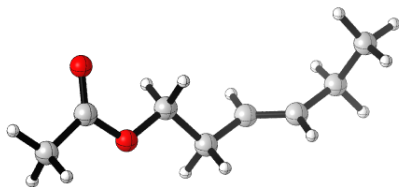
DFT calculations were conducted at the Molecular Graphics and Computation Facility at the University of California, Berkeley. The geometry optimizations of all structures were performed with the B3LYP functional with Gaussian 09 revision D01 package. SDD and 6-31G(d) basis sets were used for Cu and all other atoms, respectively. Single-point energies were calculated with the M06 functional. SDD and 6-311+G(d,p) basis sets were used for Cu and all other atoms, respectively. The SMD model for cyclohexane was used for the solvent corrections. Frequency calculations were also conducted with the optimized geometries to confirm that the stationary points were minima (zero imaginary frequencies) or transition states (one imaginary frequency).

(R)-DTBM-SEGPHOSCuH



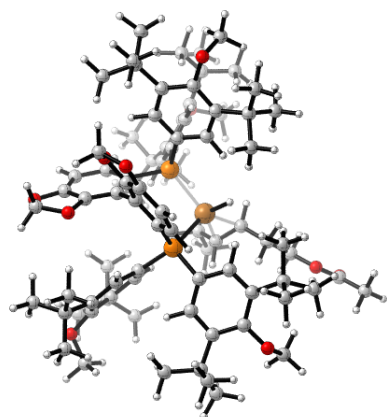
Thermal correction to Enthalpy= 1.699458
Thermal correction to Gibbs Free Energy= 1.472397
Sum of electronic and zero-point Energies= -4360.797109
Sum of electronic and thermal Enthalpies= -4360.703004
Sum of electronic and thermal Free Energies= -4360.930064
SMD E(M06)= -4360.921482

5

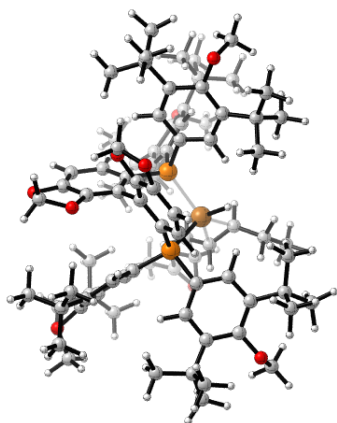


Thermal correction to Enthalpy= 0.222673
Thermal correction to Gibbs Free Energy= 0.168480
Sum of electronic and zero-point Energies= -463.521300
Sum of electronic and thermal Enthalpies= -463.507949
Sum of electronic and thermal Free Energies= -463.562142
SMD E(M06)= -463.543395

5a

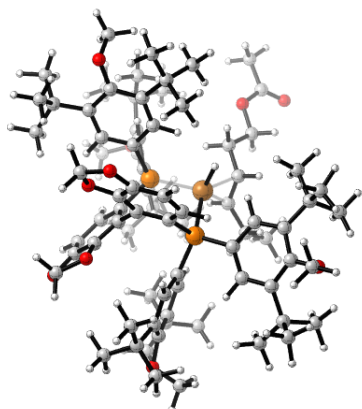


Thermal correction to Enthalpy= 1.924303
Thermal correction to Gibbs Free Energy= 1.666342
Sum of electronic and zero-point Energies= -4824.293878
Sum of electronic and thermal Enthalpies= -4824.186121
Sum of electronic and thermal Free Energies= -4824.444082
SMD E(M06)= -4824.474162

5b

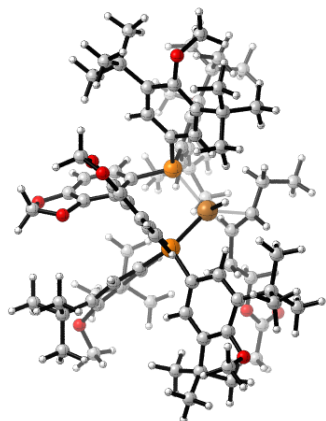
Thermal correction to Enthalpy= 1.924386
Thermal correction to Gibbs Free Energy= 1.666060
Sum of electronic and zero-point Energies= -4824.293753
Sum of electronic and thermal Enthalpies= -4824.185849
Sum of electronic and thermal Free Energies= -4824.444175
SMD E(M06)= -4824.474911

5c



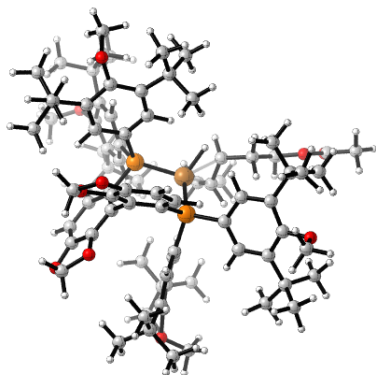
Thermal correction to Enthalpy= 1.924107
Thermal correction to Gibbs Free Energy= 1.663384
Sum of electronic and zero-point Energies= -4824.298627
Sum of electronic and thermal Enthalpies= -4824.190362
Sum of electronic and thermal Free Energies= -4824.451085
SMD E(M06)= -4824.480391

5d



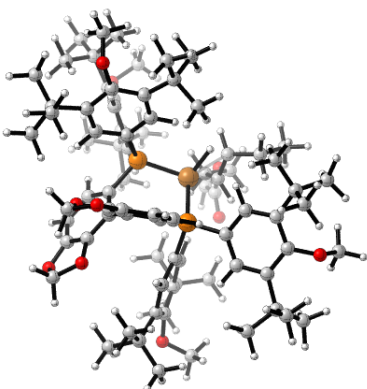
Thermal correction to Enthalpy= 1.924272
Thermal correction to Gibbs Free Energy= 1.664016
Sum of electronic and zero-point Energies= -4824.297963
Sum of electronic and thermal Enthalpies= -4824.189853
Sum of electronic and thermal Free Energies= -4824.450109
SMD E(M06)= -4824.480572

5a-TS



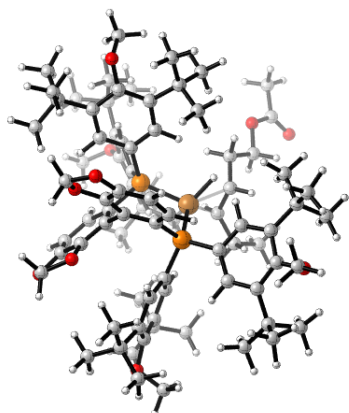
Thermal correction to Enthalpy= 1.922268
Thermal correction to Gibbs Free Energy= 1.665889
Sum of electronic and zero-point Energies= -4824.272558
Sum of electronic and thermal Enthalpies= -4824.165349
Sum of electronic and thermal Free Energies= -4824.421728
SMD E(M06)= -4824.455071
Imaginary frequency: -805.35

5b-TS



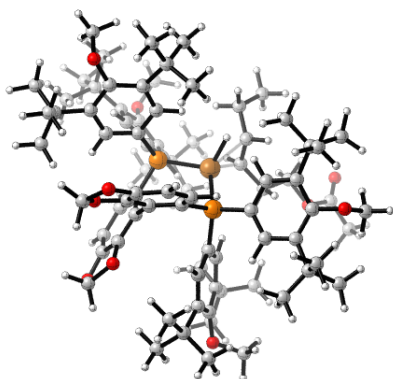
Thermal correction to Enthalpy= 1.923238
Thermal correction to Gibbs Free Energy= 1.672464
Sum of electronic and zero-point Energies= -4824.277137
Sum of electronic and thermal Enthalpies= -4824.170803
Sum of electronic and thermal Free Energies= -4824.421577
SMD E(M06)= -4824.461300
Imaginary frequency: -763.31

5c-TS



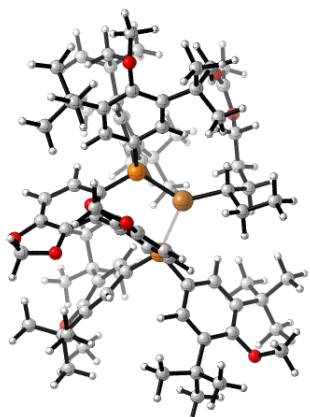
Thermal correction to Enthalpy= 1.922511
Thermal correction to Gibbs Free Energy= 1.665107
Sum of electronic and zero-point Energies= -4824.278911
Sum of electronic and thermal Enthalpies= -4824.171633
Sum of electronic and thermal Free Energies= -4824.429037
SMD E(M06)= -4824.460361
Imaginary frequency: -798.60

5d-TS

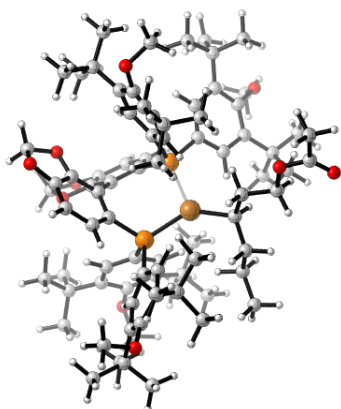


Thermal correction to Enthalpy= 1.922495
Thermal correction to Gibbs Free Energy= 1.665022
Sum of electronic and zero-point Energies= -4824.282307
Sum of electronic and thermal Enthalpies= -4824.175208
Sum of electronic and thermal Free Energies= -4824.432682
SMD E(M06)= -4824.463088
Imaginary frequency: -796.89

6a

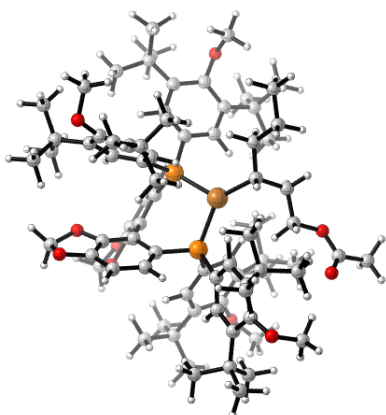


Thermal correction to Enthalpy=	1.928907
Thermal correction to Gibbs Free Energy=	1.675333
Sum of electronic and zero-point Energies=	-4824.319573
Sum of electronic and thermal Enthalpies=	-4824.212383
Sum of electronic and thermal Free Energies=	-4824.465957
SMD E(M06)=	-4824.505523

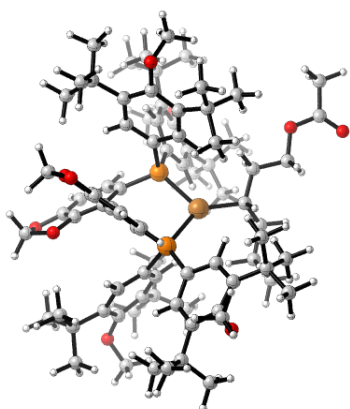
6b

Thermal correction to Enthalpy=	1.928317
Thermal correction to Gibbs Free Energy=	1.669714
Sum of electronic and zero-point Energies=	-4824.322985
Sum of electronic and thermal Enthalpies=	-4824.215344
Sum of electronic and thermal Free Energies=	-4824.473947
SMD E(M06)=	-4824.506018

6c



Thermal correction to Enthalpy=	1.928485
Thermal correction to Gibbs Free Energy=	1.671974
Sum of electronic and zero-point Energies=	-4824.326591
Sum of electronic and thermal Enthalpies=	-4824.219258
Sum of electronic and thermal Free Energies=	-4824.475768
SMD E(M06)=	-4824.505372

6d

Thermal correction to Enthalpy=	1.928497
Thermal correction to Gibbs Free Energy=	1.671691
Sum of electronic and zero-point Energies=	-4824.321275
Sum of electronic and thermal Enthalpies=	-4824.213884
Sum of electronic and thermal Free Energies=	-4824.470690
SMD E(M06)=	-4824.505544

2.5 References

Parts of this chapter were reprinted with permission from:
 “Diverse Asymmetric Hydrofunctionalization of Aliphatic Internal Alkenes through Catalytic Regioselective Hydroboration”
 Xi, Y.; Hartwig, J. F. *J. Am. Chem. Soc.* **2016**, *138*, 6703.

- [1] Wang, J. *Stereoselective Alkene Synthesis*; Springer-Verlag Berlin Heidelberg, 2012.
- [2] Coombs, J. R.; Morken, J. P. *Angew. Chem. Int. Ed.* **2016**, *55*, 2636.
- [3] Ananikov, V. P.; Tanaka, M. *Hydrofunctionalization*; Springer Berlin Heidelberg, 2013.
- [4] He, X.; Hartwig, J. F. *J. Am. Chem. Soc.* **1996**, *118*, 1696.
- [5] (a) Hartwig, J. F. *Chem. Soc. Rev.* **2011**, *40*, 1992; (b) Hartwig, J. F. *Acc. Chem. Res.* **2012**, *45*, 864.
- [6] (a) Murphy, J. M.; Liao, X.; Hartwig, J. F. *J. Am. Chem. Soc.* **2007**, *129*, 15434; (b) Liskey, C. W.; Liao, X.; Hartwig, J. F. *J. Am. Chem. Soc.* **2010**, *132*, 11389; (c) Robbins, D. W.; Hartwig, J. F. *Angew. Chem. Int. Ed.* **2013**, *52*, 933.
- [7] (a) Matteson, D. S. *Stereodirected Synthesis with Organoboranes*; Springer Berlin Heidelberg, 1995; (b) Crudden, Cathleen M.; Edwards, D. *Eur. J. Org. Chem.* **2003**, *2003*, 4695; (c) Scott, H. K.; Aggarwal, V. K. *Chem. Eur. J.* **2011**, *17*, 13124; (d) Leonori, D.; Aggarwal, V. K. *Angew. Chem. Int. Ed.* **2015**, *54*, 1082.
- [8] (a) Burgess, K.; Ohlmeyer, M. J. *Chem. Rev.* **1991**, *91*, 1179; (b) Beletskaya, I.; Pelter, A. *Tetrahedron* **1997**, *53*, 4957.
- [9] (a) Rubina, M.; Rubin, M.; Gevorgyan, V. *J. Am. Chem. Soc.* **2003**, *125*, 7198; (b) Carroll, A.-M.; O'Sullivan, T. P.; Guiry, P. J. *Adv. Synth. Catal.* **2005**, *347*, 609; (c) Lee, Y.; Hoveyda, A. H. *J. Am. Chem. Soc.* **2009**, *131*, 3160; (d) Noh, D.; Chea, H.; Ju, J.; Yun, J. *Angew. Chem. Int. Ed.* **2009**, *48*, 6062.
- [10] (a) Smith, S. M.; Thacker, N. C.; Takacs, J. M. *J. Am. Chem. Soc.* **2008**, *130*, 3734; (b) Smith, S. M.; Takacs, J. M. *J. Am. Chem. Soc.* **2010**, *132*, 1740; (c) Smith, S. M.; Hoang, G. L.; Pal, R.; Khaled, M. O. B.; Pelter, L. S. W.; Zeng, X. C.; Takacs, J. M. *Chem. Commun.* **2012**, *48*, 12180; (d) Hoang, G. L.; Yang, Z.-D.; Smith, S. M.; Pal, R.; Miska, J. L.; Pérez, D. E.; Pelter, L. S. W.; Zeng, X. C.; Takacs, J. M. *Org. Lett.* **2015**, *17*, 940; (e) Shoba, V. M.; Thacker, N. C.; Bochat, A. J.; Takacs, J. M. *Angew. Chem. Int. Ed.* **2016**, *55*, 1465.
- [11] Xi, Y.; Butcher, T. W.; Zhang, J.; Hartwig, J. F. *Angew. Chem. Int. Ed.* **2016**, *55*, 776.
- [12] Lipshutz, B. H.; Frieman, B. A. *Angew. Chem. Int. Ed.* **2005**, *44*, 6345.
- [13] Yang, Y.; Shi, S.-L.; Niu, D.; Liu, P.; Buchwald, S. L. *Science* **2015**, *349*, 62.
- [14] Won, J.; Noh, D.; Yun, J.; Lee, J. Y. *J. Phys. Chem. A* **2010**, *114*, 12112.
- [15] (a) Evans, D. A.; Fu, G. C. *J. Am. Chem. Soc.* **1991**, *113*, 4042; (b) Evans, D. A.; Fu, G. C.; Hoveyda, A. H. *J. Am. Chem. Soc.* **1992**, *114*, 6671.
- [16] (a) Noh, D.; Yoon, S. K.; Won, J.; Lee, J. Y.; Yun, J. *Chem. Asian J.* **2011**, *6*, 1967; (b) Feng, X.; Jeon, H.; Yun, J. *Angew. Chem. Int. Ed.* **2013**, *52*, 3989; (c) Lee, H.; Lee, B. Y.; Yun, J. *Org. Lett.* **2015**, *17*, 764; (d) Grigg, R. D.; Van Hoveln, R.; Schomaker, J. M. *J. Am. Chem. Soc.* **2012**, *134*, 16131.
- [17] Mlynarski, S. N.; Karns, A. S.; Morken, J. P. *J. Am. Chem. Soc.* **2012**, *134*, 16449.
- [18] Larouche-Gauthier, R.; Elford, T. G.; Aggarwal, V. K. *J. Am. Chem. Soc.* **2011**, *133*, 16794.
- [19] Sandford, C.; Rasappan, R.; Aggarwal, V. K. *J. Am. Chem. Soc.* **2015**, *137*, 10100.
- [20] (a) Matteson, D. S.; Majumdar, D. *J. Am. Chem. Soc.* **1980**, *102*, 7588; (b) Sonawane, R. P.; Jheengut, V.; Rabalakos, C.; Larouche-Gauthier, R.; Scott, H. K.; Aggarwal, V. K. *Angew. Chem. Int. Ed.* **2011**, *50*, 3760.
- [21] (a) Bonet, A.; Odachowski, M.; Leonori, D.; Essafi, S.; Aggarwal, V. K. *Nat. Chem.* **2014**, *6*, 584; (b) Llaveria, J.; Leonori, D.; Aggarwal, V. K. *J. Am. Chem. Soc.* **2015**, *137*, 10958; (c) Li, L.; Zhao, S.; Joshi-Pangu, A.; Diane, M.; Biscoe, M. R. *J. Am. Chem. Soc.* **2014**, *136*, 14027.

[22] The alkene insertion step will be enantio- and regiodetermining if it is irreversible, which is suggested by the experimental observations that neither alkene isomerization nor chain-walking products were observed.

[23] The formation of alkylboronate from alkylcopper intermediate and pinacolborane was proposed to proceed by retention of stereochemistry. See Ref. 14 and 16a.

[24] Xu, L.; Hilton, M. J.; Zhang, X.; Norrby, P.-O.; Wu, Y.-D.; Sigman, M. S.; Wiest, O. *J. Am. Chem. Soc.* **2014**, *136*, 1960.

CHAPTER 3

Mechanistic Study of the Copper-Catalyzed Asymmetric Hydroboration of Alkenes

3.1 Introduction

The hydroboration of alkenes is a classic and synthetically valuable organic transformation that converts alkenes to organoboron compounds. Because organoboron compounds are versatile synthetic intermediates for constructing carbon-carbon and carbon-heteroatom bonds,¹ hydroboration has been investigated extensively since its discovery.² Many boron reagents have been designed to modulate the chemo-, regio-, and stereoselectivity of the reaction,³ including those that create stereogenic centers at which the carbon-boron bond is formed.^{4, 5}

Catalytic hydroboration reactions^{6, 7} occur with selectivities⁸⁻¹⁰ that often complement those of non-catalyzed reactions. For example, Evans reported examples of hydroboration reactions, catalyzed by iridium and rhodium complexes, that were directed by the coordinating functional groups within the substrate, leading to high regio- and diastereoselectivity.^{11, 12} Catalysts for enantioselective hydroboration also have been developed.¹³ Following the initial reports by Burgess and Hayashi,^{9, 14} Takacs reported rhodium systems that catalyze directed hydroboration of disubstituted¹⁵ and trisubstituted alkenes^{16, 17} with high regio- and enantioselectivity.

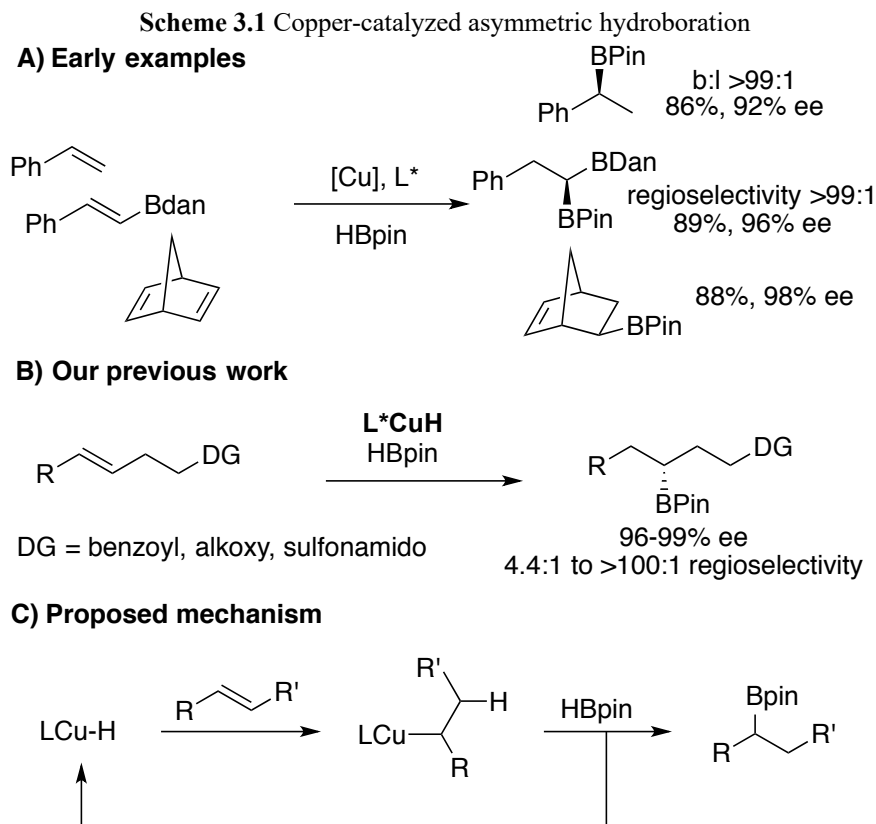
The first copper-catalyzed asymmetric hydroboration of alkenes was reported by Yun in 2009 (Scheme 3.1 A).^{18, 19} A combination of a copper(I) precatalyst, base, and chiral, non-racemic bisphosphine catalyzed hydroboration of vinylarenes with high regio- and enantioselectivity. Later, the reaction was extended to the hydroboration of vinyl boronates²⁰ and norbornadienes²¹ by the same group. In both cases, high enantioselectivity was achieved.

Last year, we reported a copper-catalyzed enantioselective hydroboration of non-conjugated internal alkenes²² with high regioselectivity that complements that of Takacs' rhodium system (Scheme 3.1 B).¹⁵⁻¹⁷ In contrast to many olefin functionalizations catalyzed by transition metals,^{10, 23-29} functionalizations of alkenes catalyzed by copper complexes occur without competing isomerization of the alkene or migration of an alkylmetal intermediate along the alkyl chain. Experimental observations and DFT calculations implied that the regioselectivity is controlled by the electronic effects of the polar functional groups proximal to the alkene moiety. Aliphatic secondary boronates prepared by this method were converted to a diverse set of functionalized compounds efficiently with complete or predominant conservation of the enantiomeric excess of the products from the hydroboration.³⁰

Yun and co-workers have investigated the mechanism of copper-catalyzed hydroboration by DFT calculations.^{31, 32} A copper(I) hydride³³⁻³⁶ was invoked as the key intermediate in these reactions. A simple mechanism is depicted in Scheme 3.1 C. A copper(I) hydride inserts an alkene to form an alkylcopper intermediate, which undergoes stereoretentive transmetalation with HBpin to afford the product and regenerate the copper hydride. DFT calculations provided a rationalization for the greater reactivity of catalysts containing bidentate, electron-rich phosphines than of catalysts containing monodentate phosphines.³¹

We have conducted experiments, in addition to computations, on the catalytic cycle to determine the effects of ligands and substrates on the identity of the catalyst, the relative rates of individual steps of the cycle, and the steps that influence regioselectivity and stereoselectivity. Our previous study²² showed that the reactions occurred in high yields only with alkenes that bear inductively electron-withdrawing groups proximal to the alkene moiety. Unactivated 1,2-disubstituted alkenes underwent hydroboration in lower yields under harsher conditions (higher catalyst loading, large excess of alkene) than did non-conjugated 1,2-disubstituted alkenes that are electronically activated. Understanding the mechanism may enable the development of catalysts that are capable of engaging substrates that are less reactive than vinylarenes and polarized 1,2-

disubstituted alkenes. Furthermore, understanding the origin of the absence of chain walking of the copper catalyst during the hydroboration³⁷ may help design new catalysts that possess this unusual property.



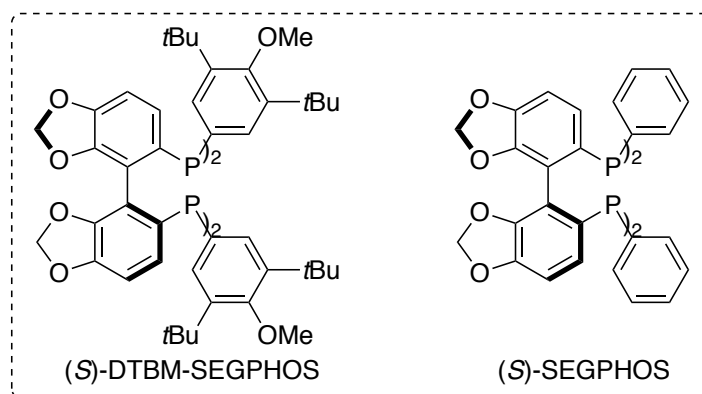
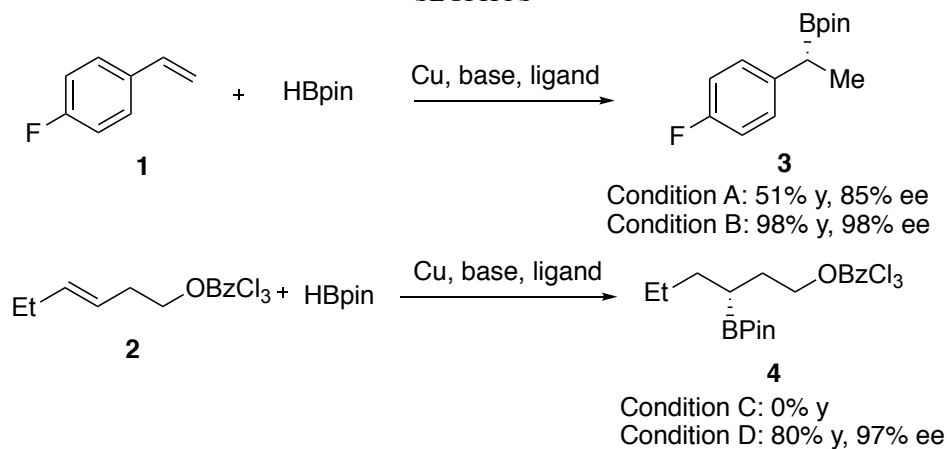
Herein, we report detailed mechanistic studies on the copper-catalyzed asymmetric hydroboration of vinylarenes and internal alkenes. A series of catalytically relevant copper(I) complexes have been synthesized and fully characterized. The reactivity and catalytic competency of these complexes have been evaluated, and kinetic studies show that the turnover-limiting and reversible steps of the reaction depend on the type of alkene. Additional experiments have been conducted to probe the origin of the stereochemical outcome of the reaction, and DFT calculations provide a view into the origin of regioselectivity and enantioselectivity. The hydrofunctionalization of alkenes, which adds a hydrogen atom and a functional group across an olefin concomitantly, is the most direct approach to introduce a functional group to an organic molecule. This reaction produces value-added products utilizing alkenes as the starting material, which are commercially available on the large scale and are readily accessible through chemical synthesis. Because hydrofunctionalization is an addition reaction, it proceeds with complete atom-economy, thereby forming no co-products which separation and disposal are required. In light of these advantages, extensive efforts have been devoted to developing efficient catalysts to promote these processes.

3.2 Results and Discussion

Effects of the Ligands on Catalyst Activity. During our initial discovery of copper-catalyzed hydroboration of non-conjugated internal alkenes,²² we found that the reactivity of the catalyst strongly depends on subtle changes to the structure of the ancillary ligand. The catalyst formed from (*S*)-DTBM-SEGPHOS was highly active for the hydroboration of vinylarenes and non-conjugated internal alkenes containing an electron-withdrawing group, such as *trans*-3-hexenyl 2,4,6-trichlorobenzoate. However, the catalyst derived from (*S*)-SEGPHOS did not catalyze the hydroboration of the internal alkene.

We hypothesized that the difference in reactivity between the catalysts derived from these two ligands resulted,^{38, 39} at least in part, from the difference of the form of the corresponding copper hydride complexes. Almost all copper hydride complexes that are relevant to homogenous catalysis and have been characterized previously are oligomers, with nuclearities ranging from dimers to hexamers.³⁴ Complexes in higher-order forms were also reported.³³ Copper hydride complexes ligated by biaryl bisphosphines have not been isolated,⁴⁰⁻⁴⁶ and full characterization of a monomeric copper hydride ligated by an extremely bulky N-heterocyclic carbene ligand was only recently reported by Bertrand.^{47,48} To understand how the ligand structure influences the reactivity of the active catalyst, we investigated complexes in hydroboration reactions containing copper complexes of DTBM-SEGPHOS and of SEGPHOS.

Scheme 3.2 Hydroboration of **1** and **2** catalyzed by copper catalysts ligated by (*S*)-SEGPHOS and (*S*)-DTBM-SEGPHOS^a



^aConditions: A) 5 mol % CuCl, 10 mol % KO^tBu, 5.5 mol % (*S*)-SEGPHOS, toluene, rt, 54 h; B) 2 mol % CuCl, 4 mol % KO^tBu, 2.2 mol % (*S*)-DTBM-SEGPHOS, cyclohexane, rt, 1 h; C) 5 mol % CuCl, 10 mol % KO^tBu, 5.5 mol % (*S*)-SEGPHOS, cyclohexane, rt, 48 h; A) 2.5 mol % CuCl, 5 mol % KO^tBu, 3 mol % (*S*)-DTBM-SEGPHOS, cyclohexane, rt, 36 h. GC yields.

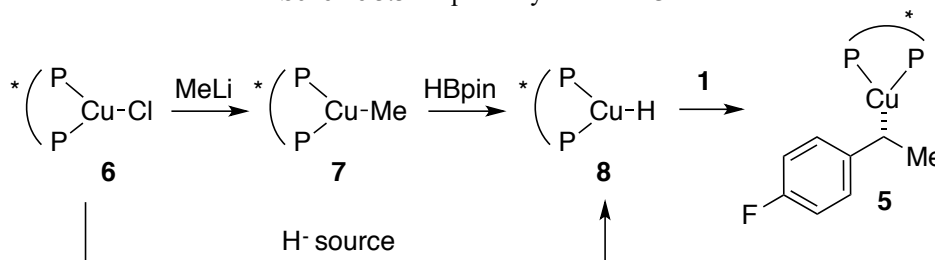
3.2.1 Mechanistic Studies on Hydroboration Catalyzed by DTBM-SEGPHOS-Ligated Copper(I)

Our mechanistic studies encompass reactions of two model substrates shown in Scheme 3.2, 4-fluorostyrene (**1**),⁴⁹ and the internal alkene *trans*-3-hexenyl 2,4,6-trichlorobenzoate (**2**). These reactions are discussed below, and the kinetic behavior and resting states of the catalysts are much different for the two catalytic reactions. The following sections describe the identity of the complexes in the reactions, the kinetic behavior of the systems, studies on the stoichiometric reactions of the complexes, experiments on the stereochemical outcome of the reactions, and theoretical investigations by DFT calculations.

Synthesis and Characterization of Complexes that are Competent Intermediates in the Hydroboration of Vinylarene **1 with HBpin.** Monitoring the hydroboration reaction of vinylarene **1** with 1.05 equivalent of HBpin at room temperature by ³¹P NMR spectroscopy revealed two major species. The reaction was conducted in a 1:1 mixture of cyclohexane and benzene; the reaction in cyclohexane alone was too fast to monitor at room temperature.

Two species were observed throughout the reaction. The major species, which was determined to account for about 70% of the phosphorus content, is free (*S*)-DTBM-SEGPHOS. This result shows that during the catalytic reaction, most of the ligand remains unbound, which is consistent with Buchwald's observation in a related hydroamination system.⁵⁰ A minor species was observed as a singlet at -7.2 ppm in the ³¹P NMR spectra; this chemical shift is consistent with a complex containing the ligand bound to copper. ¹⁹F NMR spectra of the reactions contained a small but distinct peak at -129.9 ppm, in addition to peaks corresponding to reagent **1** and product **3**. Because the complex corresponding to this resonance contains a fluorine atom, we hypothesized that the species corresponding to the small resonance at -129.9 ppm could be the phenethylcopper(I) complex (DTBM-SEGPHOS)Cu[1-(4-fluoro)phenethyl] (**5**). Although most of the phosphine ligand remains unbound during the hydroboration of **1**, our mechanistic study focused on the structure and reactions of the ligated copper species, rather than identifying the NMR-silent unligated copper species. The unligated species, such as CuH aggregates, are unlikely to lie on the catalytic cycle because the enantioselectivity of the catalytic process is high.

Scheme 3.3 Proposed synthesis of **5**^a



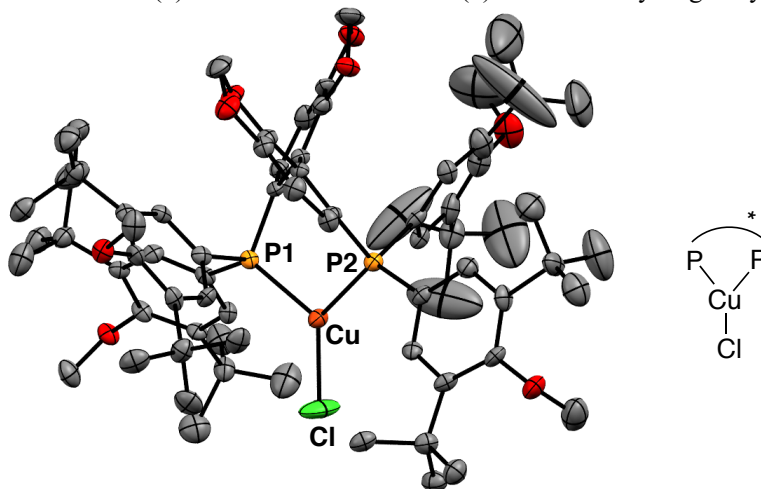
^aThe ancillary ligand on **5-8** is (*S*)-DTBM-SEGPHOS.

To gain further information on the identity of **5**, we synthesized this complex independently by insertion of vinylarene **1** into copper hydride **8**, as shown in Scheme 3.3. To do so, hydride **8** was prepared by borylation of methylcopper complex **7** with HBpin or addition of hydride sources to copper chloride **6**. Methylcopper complex **7** was prepared from chloride **6**.

(*S*)-DTBM-SEGPHOSCuCl (**6**) was isolated in 94% yield from CuCl and (*S*)-DTBM-SEGPHOS. Single-crystal X-ray diffraction of **6** revealed a monomeric structure, with a trigonal planar geometry at the copper (I) center (Figure 3.1). Unlike the dimeric structure^{51, 52} of copper complexes ligated by biaryl bisphosphines that are smaller than DTBM-SEGPHOS, the monomeric structure of **6** is likely to result from the severe steric congestion imposed by the bulky DTBM-SEGPHOS ligand.

Methyl copper⁵³⁻⁵⁸ complex **7** was isolated in 86% yield from the reaction of **6** with methyl-lithium at -35 °C. Although complex **7** is stable as a solid at room temperature for at least 24 h, it decomposed in benzene under argon in ambient light overnight, and a solution of **7** reacted with air instantaneously. The solid-state structure of **7** contained a slightly unsymmetrical Y-shaped copper(I) center like that in chloride **6** (Figure 3.2).

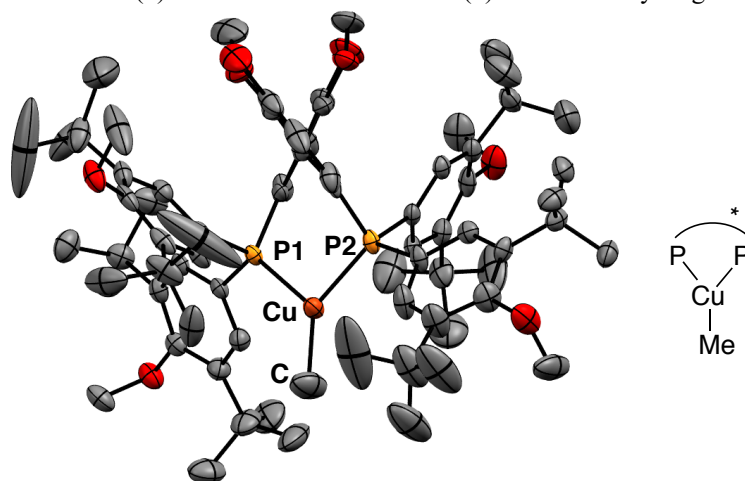
Figure 3.1 Solid-state structure of (*S*)-DTBM-SEGPHOSCuCl (**6**) determined by single crystal x-ray diffraction^a



^aThe thermal ellipsoids were set to 30% probability. All hydrogen atoms were omitted for clarity. Selected bond lengths (Å): Cu–Cl = 2.178(2). Selected bond angles (deg): P1–Cu–Cl = 126.15(9), P2–Cu–Cl = 131.68(9).

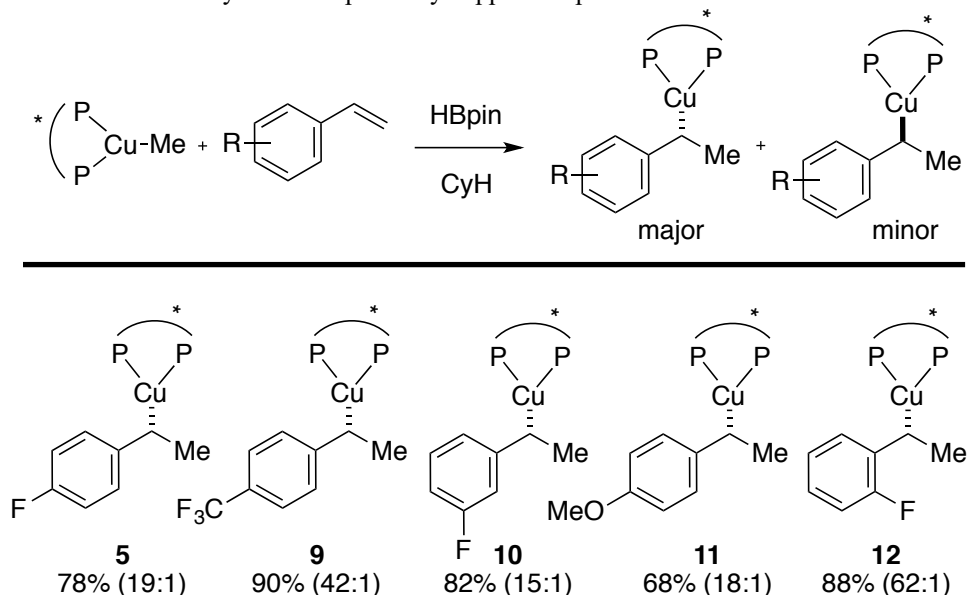
The reaction of equimolar amounts of methyl complex **7** and HBpin did not yield a ligated copper hydride **8**. Instead, only free ligand was observed, suggesting that such a hydride complex is not stable in solution. This instability we observed contrasts Lipshutz's proposal that the copper hydride ligated by DTBM-SEGPHOS is a stable monomer.⁴⁴ The reaction of chloride **6** with potassium triethylborohydride⁴¹ formed a copper triethylborohydride complex,⁵⁹ rather than terminal hydride **8**. Attempts to sequester the BEt₃ moiety of the copper triethylborohydride by adding various bases led to decomposition.

Thus, phenethylcopper complex **5** was prepared by generating a DTBM-SEGPHOS-ligated copper hydride in the presence of the vinylarene (Scheme 3.4). The reaction of **6**, NaHBet₃ and vinylarene **1** in cyclohexane afforded **5** in 66% yield. A higher yield (78% by ¹⁹F NMR spectroscopy) was obtained by treating a mixture of methylcopper complex **7** with vinylarene **1** and HBpin in cyclohexane.

Figure 3.2 Solid-state structure of (*S*)-DTBM-SEGPHOSCuCH₃ (**7**) determined by single crystal x-ray diffraction^a

^aThe thermal ellipsoids were set to 30% probability. All hydrogen atoms were omitted for clarity. Selected bond lengths (Å): Cu–C = 1.95(1). Selected bond angles (deg): P1–Cu–C = 128.4(3), P2–Cu–C = 133.5(3).

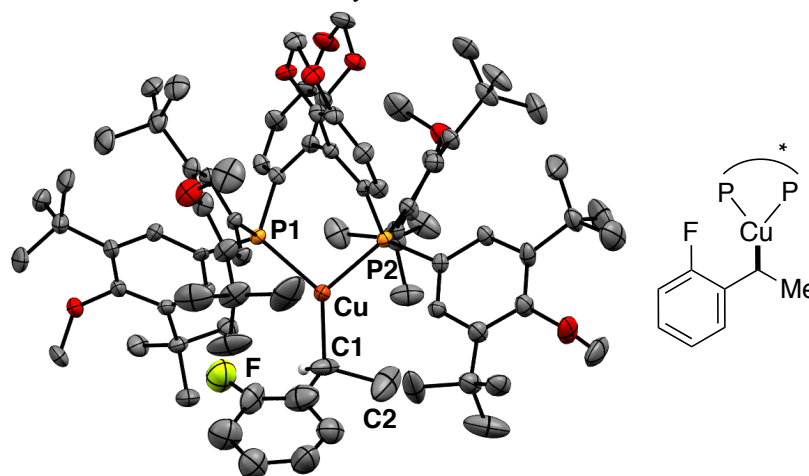
Complex **5** was stable in the solution for several hours before decomposition of **5** to generate free ligand began to be observed by NMR spectroscopy. A quartet at 2.85 ppm and a doublet at 1.73 ppm in the ¹H NMR spectrum of **5** with a mutual coupling constant of 7.2 Hz clearly indicated the presence of a phenethyl moiety. A correlation between the quartet and the doublet was confirmed by ¹H COSY experiments. By analogous methods, a series of phenethylcopper complexes (**9–12**) were synthesized from **7**, HBpin, and the corresponding vinylarenes (Scheme 3.4). Like complex **5**, complexes **9–12** were fully characterized in solution by multinuclear NMR spectroscopy.

Scheme 3.4 Synthesis of phenethylcopper complexes and their diastereomers^a

^aThe ancillary ligand on **5** and **9–12** is (*S*)-DTBM-SEGPHOS. Yields were determined by NMR spectroscopy using an internal standard. The ratio in parenthesis refers to the ratio of the two diastereomers.

We found that a minor product (**5'**, **9'-12'**) formed along with the major phenethylcopper complex in all the cases. Moreover, solutions containing an approximately 19:1 ratio of **5** to **5'** converted slowly over time to a lower ratio of the two complexes. After 1 h, a 13:1 ratio of isomers was observed, and after 13 h a 4:1 ratio was observed. The minor species consistently exhibited a ^{31}P NMR signal just 1 ppm downfield of that corresponding to the major species and a ^{19}F NMR signal just 0.3 ppm upfield of that corresponding to the major species.

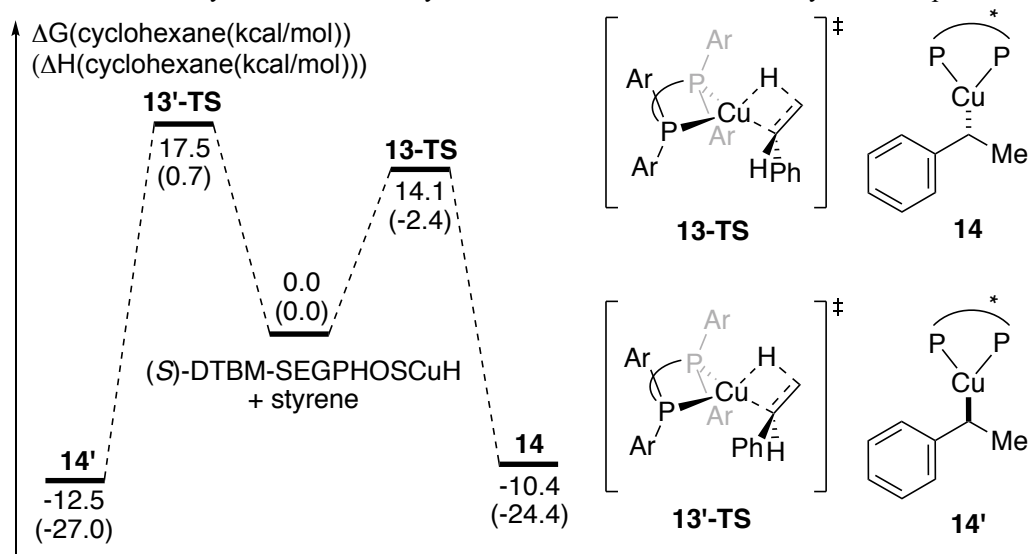
Figure 3.3 Solid-state structure of (*S*)-DTBM-SEGPHOSCu[(*S*)-CH(2-F-C₆H₄)Me] determined by single crystal x-ray diffraction^a



^aThe thermal ellipsoids were set to 30% probability. All hydrogen atoms except the benzylic hydrogen atom were omitted for clarity. Selected bond lengths (Å): Cu–C = 2.03(1). Selected bond angles (deg): P1–Cu–C = 130.0(4), P2–Cu–C = 130.8(4).

We proposed that the minor species (**5'**, **9'-12'**) are the diastereomers of **5** and **9-12**, with the configuration at the benzylic carbon opposite to those in complexes **5** and **9-12**. Concomitant decomposition of the complexes prevented full equilibration and determination of the equilibrium ratio of diastereomers.

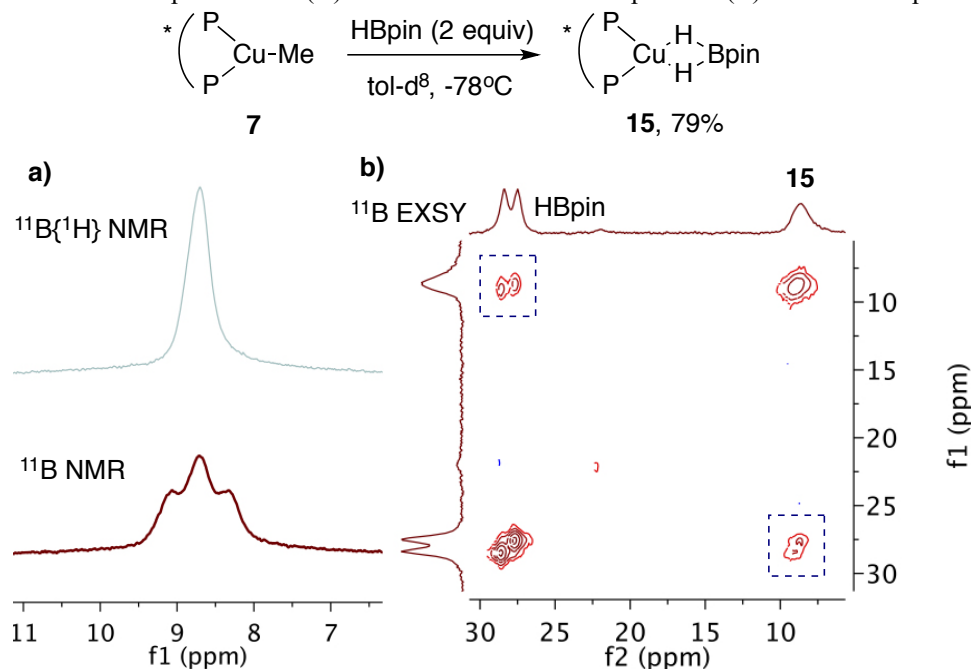
The connectivity of the phenethylcopper(I) complex was unambiguously established by x-ray diffraction analysis (Figure 3.3) of a DTBM-SEGPHOS-ligated 1-(2-fluoro)phenethylcopper complex. This complex is a trigonal planar d^{10} -Cu(I) complex, with a structure similar to that of methyl complex **7**, but with a slightly longer metal-carbon bond. The phenethyl group in this complex is bound in an η^1 -coordination mode, like that of the NHC-ligated benzylcopper complexes reported by Sadighi⁶⁰ and Schomaker.⁶¹ The fluorine atom on the aromatic ring is 3.47 Å from the copper center, indicating the absence of a potential interaction between these two atoms. Although the bulk sample of the crystals formed by recrystallization consisted of a mixture of the two diastereomers **12** and **12'**, the crystal solved by x-ray diffraction contained a single diastereomer with an (*S*) configuration at the benzylic carbon. Because the epimerization of the phenethylcopper complexes occurred during the work-up and recrystallization process, even at -40 °C, we were unable to obtain a sufficient quantity of homochiral crystals to characterize a bulk sample of a single diastereomer of the phenethylcopper complex in solution.

Scheme 3.5 Pathways for insertion of styrene into LCu-H bond calculated by DFT computations^a

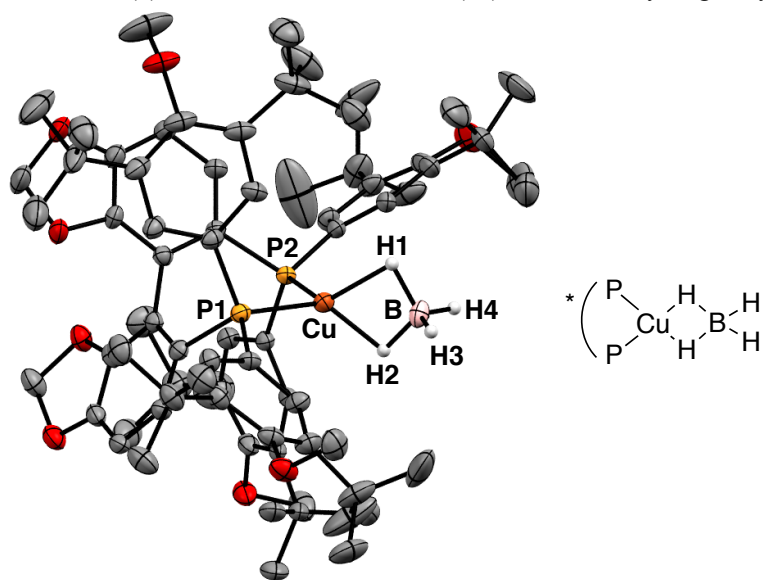
^aCalculations were carried out at the M06/6-311+g(d,p)/SDD//B3LYP/6-31g(d)/SDD level of theory.

However, information on the configuration of the benzylic carbon in the kinetic and thermodynamic isomers of the phenethylcopper complexes was gained by DFT. We calculated the relative energies of the two diastereomeric phenethylcopper complexes and the transition states leading to them (Scheme 3.5). The results show that the activation barrier leading to the parent phenethylcopper complex **14** is 3.4 kcal/mol lower than that leading to its diastereomer **14'**. However, **14** is higher in energy than **14'** by 2.1 kcal/mol. These DFT calculations are consistent with formation of one diastereomer that isomerizes to another over time and imply that the benzylic center in **5** and **9-12** has an (*R*) configuration and that in the more stable diastereomers **5'** and **9'-12'** have the same (*S*) configuration that was observed by X-ray diffraction. Further evidence for these assignments is given later in this paper.

Synthesis and Characterization of Complexes that are Catalytically Relevant to the Hydroboration of Internal Alkene 2. Monitoring a hydroboration reaction of internal alkene **2** with 1.2 equivalents of HBpin catalyzed by a combination of CuCl, KO^tBu, and (*S*)-DTBM-SEGPHOS at room temperature revealed the presence of two phosphorus-containing species. As observed for the reaction of vinylarene **1**, the major phosphorus-containing species, which corresponded to 90% of the total phosphine content, is free (*S*)-DTBM-SEGPHOS. A broad ³¹P NMR resonance corresponding to a minor species, dihydridoborate complex **15**, was observed at 8.0 ppm in cyclohexane. Dihydridoborate complex **15** was generated independently by treating methylcopper complex **7** with two equivalents of HBpin in toluene-*d*₈ at -78 °C. Complex **15** formed in 79% yield, as determined by ¹H NMR spectroscopy. The solution of **15** is stable at or below 0 °C. Above 0 °C, the clear pale-yellow solution turned bright orange-red, and the ³¹P NMR spectrum contained the resonances of decomposition, most likely forming a dimeric copper hydride complex, as evidenced by a pentet signal in the ¹H NMR spectrum (see section 3.4.2). Because this thermal instability of **15** prevented isolation in pure form, complex **15** was characterized by a series of solution NMR spectroscopic methods.

Figure 3.4 ^{11}B NMR spectra of **15** (A) and 2D- ^{11}B EXSY NMR spectrum (B) of **15** and HBpin at $-10\text{ }^\circ\text{C}$ ^a

^aThe ancillary ligand on **7** and **15** is (*S*)-DTBM-SEGPHOS.

Figure 3.5 Solid-state structure of (*S*)-DTBM-SEGPHOSCuBH₄ (**16**) determined by single crystal x-ray diffraction^a

^aThe thermal ellipsoids were set to 30% probability. All hydrogen atoms that are bound to carbon atoms were omitted for clarity.

^{11}B NMR experiments provided strong evidence that complex **15** is a dihydridoborate complex. The proton decoupled $^{11}\text{B}\{^1\text{H}\}$ NMR spectrum of **15** at $-60\text{ }^\circ\text{C}$ contained a sharp singlet at 8.8 ppm (Figure 3.4 A), whereas the proton coupled ^{11}B NMR spectrum at $-60\text{ }^\circ\text{C}$ consisted of a triplet with $^1J_{\text{H-B}} = 72\text{ Hz}$, implying that the boron atom is bound to two hydrides. The substantially

exergonic by only 0.8 kcal/mol in solution. This small energy for formation of the complex between **8** and HBpin is consistent with the rapid exchange of the HBpin in dihydridoborate **15** with free HBpin by dissociation of HBpin from **15** to form hydride **8**.

Evaluation of the Kinetic Competency of Observed Copper Complexes The kinetic relevance of phenethylcopper **5** and copper dihydridoborate **15** was investigated by monitoring the catalytic hydroboration of vinylarene **1** and internal alkene **2**, respectively. Complexes **5** and **15** were generated in situ from methyl complex **7** for these studies. As shown in Figure 3.14 and 3.15, the reactions catalyzed by **5** and **15** generated from **7** are much faster than those catalyzed by the combination of CuCl, KO*t*Bu, and (*S*)-DTBM-SEGPHOS. These data show that **5** and **15** are kinetically competent to be intermediates in the catalytic reactions of the two alkenes.

Determination of Empirical Rate Law. The empirical rate laws of the hydroboration of vinylarene **1** and internal alkene **2** with HBpin were determined by the method of initial rates with methylcopper **7** as the catalyst⁷⁰ (see section 3.4.5). Kinetic experiments on the reaction of **1** with HBpin indicate that the hydroboration of **1** is first-order in [HBpin] and [Cu], but zero-order in vinylarene [**1**] (Figure 3.12). These data, like our data on the resting state of the catalyst, are consistent with turnover-limiting borylation of a phenethylcopper intermediate, rather than insertion of the vinylarene into a copper hydride.

rate law for hydroboration of **1**

$$rate = k_1[Cu][HBpin] \quad (1)$$

rate law for hydroboration of **2**

$$rate = \frac{k_1 k_2 [Cu][alkene]}{k_{-1}[HBpin] + k_2[alkene]} \quad (2)$$

$$\frac{1}{k_{obs}} = \frac{1}{k_1} + \frac{k_{-1}}{k_1 k_2} \frac{[HBpin]}{[alkene]} \quad (3)$$

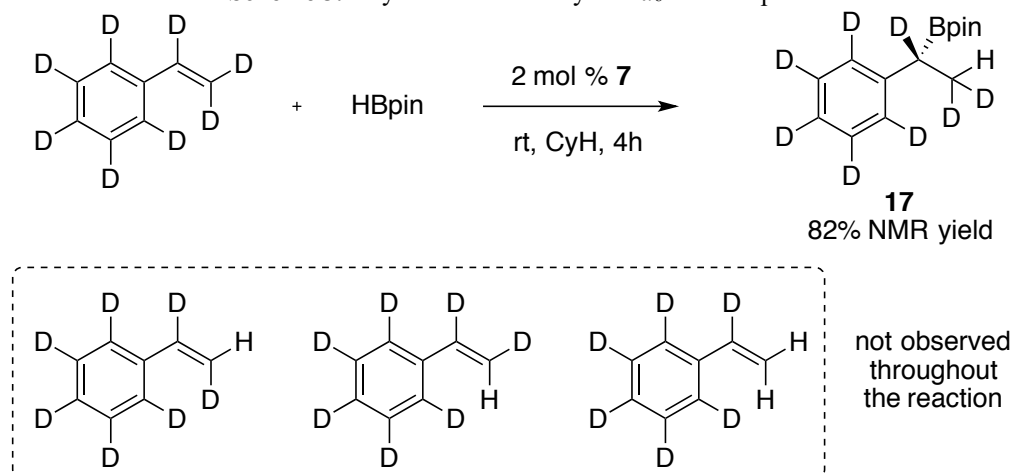
(double reciprocal form)

Kinetic experiments on the reaction of internal alkene **2** with HBpin showed that the orders in the reagents for this reaction are different from those for the reaction of **1** with HBpin. The reaction of **2** is inverse order in [HBpin], positive order in [**2**], and first-order in [Cu], as revealed by linear graphs of 1/rate vs [HBpin] and 1/rate vs 1/[**2**] (Figure 3.13). Equation 2 shows the rate law derived from the kinetic study, and equation 3 shows the double reciprocal form of the rate equation. These data, in combination with the observation of an adduct of a copper hydride and HBpin as the resting state, indicate that one molecule of HBpin dissociates from the resting state prior to the turnover-limiting step and that the turnover-limiting step is insertion of the alkene into a copper hydride.

Insertion of Alkenes into Hydride **8 Generated from Methyl Complex **7** and HBpin.** To investigate the elementary steps in the proposed catalytic cycle (Scheme 1C) and determine how these steps control the overall catalysis, we studied each step individually. As shown in Scheme 3.4, the reaction of vinylarene **1** with methyl complex **7** and HBpin forms phenethylcopper complex **5**. This reaction occurs within 1 minute at room temperature. In contrast, no alkylcopper

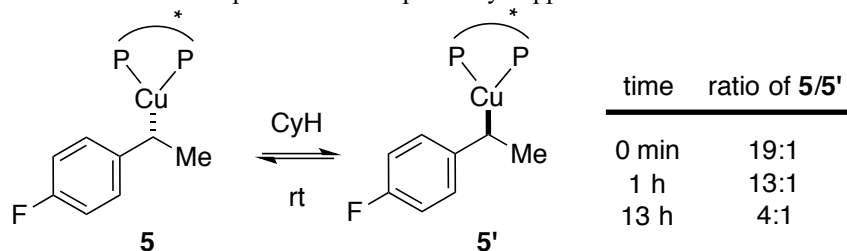
product was detected from the reaction of internal alkene **2** with **7** and HBpin. Our data on the exchange of the borane in complex **15** with free HBpin imply that the reaction of **7** with HBpin generates hydride **8**, which rapidly reacts with the vinylarene to form the final product phenethylcopper **5**. The lack of reaction of **2** with a 1:1 mixture of **7** and HBpin leads to decomposition of the copper hydride generated from methyl **7** and HBpin (vide supra).

Scheme 3.7 Hydroboration of styrene-*d*₈ with HBpin



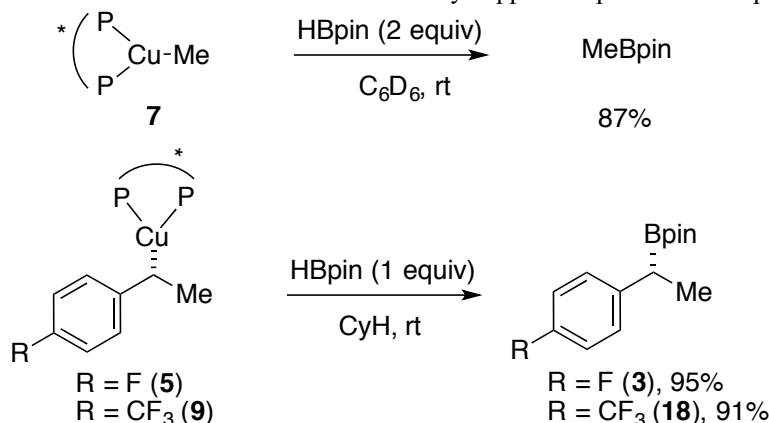
The potential reversibility of the insertion of alkenes into copper hydrides could affect the origin of enantioselectivity of the hydroboration process. To probe the reversibility of alkene insertion during the catalytic reactions, we performed an isotope-labeling experiment (Scheme 3.7). The reaction of styrene-*d*₈ with HBpin catalyzed by methylcopper **7** was monitored by both ¹H and ²H NMR spectroscopy. If the alkene insertion were reversible and fast, incorporation of hydrogen atoms into styrene-*d*₈ would be detected.⁵⁰ However, such incorporation of hydrogen was not observed; **17** was the only product of the reaction, implying that insertion of the alkene is irreversible in the catalytic hydroboration of vinylarenes.

Scheme 3.8 Epimerization of phenethylcopper **5** to **5'** in solution^a



^aThe ancillary ligand on **5** and **5'** is (*S*)-DTBM-SEGPHOS. The ratio was determined by ¹⁹F NMR spectroscopy.

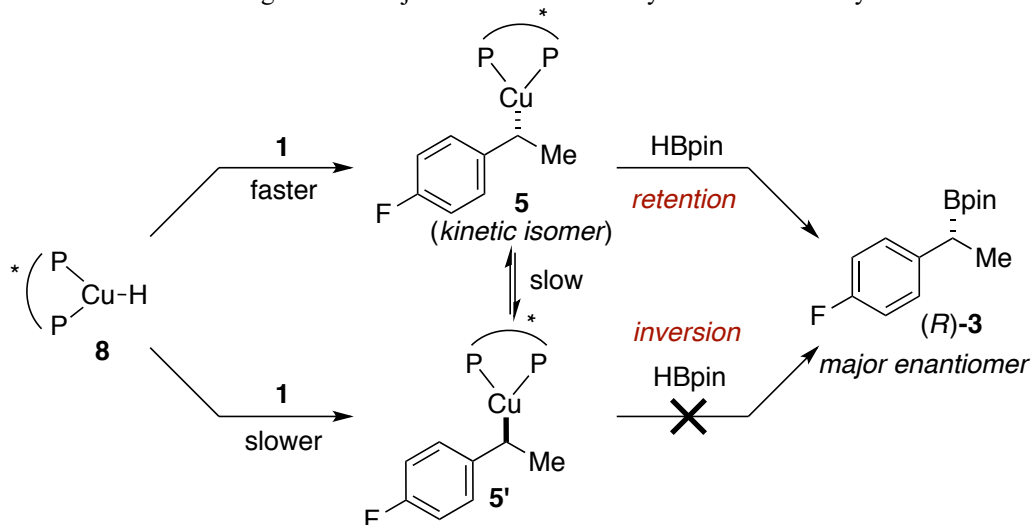
This irreversibility contrasts the observed epimerization⁷¹ of phenethylcopper compounds from the kinetic to thermodynamic diastereomers (vide supra). Thus, we compared the time scale of the epimerization to that of the borylation of an alkylcopper complex. The epimerization of phenethylcopper **5** to **5'**, as determined by ¹⁹F NMR spectroscopy in cyclohexane (Scheme 3.8) occurred over the time scale of hours, whereas the stoichiometric reaction between 4-fluorostyrene

Scheme 3.10 Stoichiometric reaction of alkylcopper complexes and HBpin^a

^aThe ancillary ligand on **5**, **7** and **9** is (*S*)-DTBM-SEGPHOS.

Although we cannot conduct the reaction of HBpin with the putative secondary alkyl complex generated from insertion of the internal alkene into a copper hydride (*vide supra*), we presume that the rate of reaction of this secondary alkyl complex lies between that of the methylcopper complex and that of the less electron-rich secondary phenethylcopper complexes.

Stereochemistry of the Individual Steps of the Mechanism for Hydroboration. High enantioselectivity is obtained from the catalytic hydroboration with a wide range of alkenes. To understand the origins of this high enantioselectivity, we investigated the stereochemical outcome of each step in the proposed catalytic cycle.

Scheme 3.11 Origin of the major enantiomer of the hydroboration of vinylarene **1**^a

^aThe ancillary ligand on **5**, **5'** and **8** is (*S*)-DTBM-SEGPHOS.

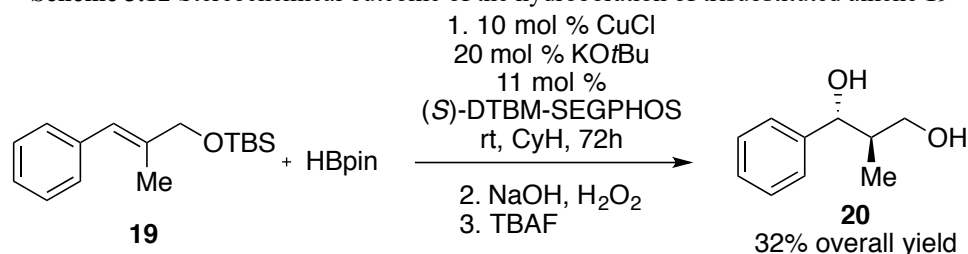
The alkene insertion is turnover-limiting during the reaction of internal alkene **2** and, therefore, determines the enantioselectivity and regioselectivity of the catalytic hydroboration. However, the insertion of vinylarene **1** occurs before the turnover-limiting reaction of HBpin with the phenethylcopper complex.

Several mechanistic scenarios could account for the observed enantioselectivity and the absolute configuration of the products (Scheme 3.11). The enantioselectivity could be controlled by an irreversible alkene insertion step or the relative energies of transition states for the borylation of the copper alkyl complex. In the latter case, the enantioselectivity would result from Curtin-Hammett control, and the alkene insertion must be reversible. Because our studies on the alkene insertion demonstrated that this step is irreversible during the catalytic process, the absolute configuration of the product of the catalytic process results from the stereoselectivity of the insertion step and the degree of retention or inversion of configuration during the borylation of the resulting alkylcopper complex.

The catalytic reaction could occur by stereoretentive borylation of phenethylcopper **5** or by stereoinvertive borylation of **5'**. Our data on reactions of vinylarenes are consistent with reaction of the kinetically formed diastereomer **5** with HBpin to form the (*R*) enantiomer of the product. Because our DFT calculation predicted that the thermodynamically more stable diastereomer has the (*S*) configuration and the kinetically formed diastereomer has the (*R*) configuration, the reaction of HBpin with the phenethylcopper complex and, by analogy, with the alkylcopper complex would occur with retention of configuration.

To avoid uncertainties in this argument, due to its basis on our DFT calculations, we distinguished more directly between reactions of HBpin with inversion or retention of configuration by determining the relative configuration of the product from the hydroboration of a trisubstituted alkene, such as **19**. Hydroboration of trisubstituted alkene **19**, followed by oxidative work-up and TBS deprotection, afforded diol **20** in 32% yield with exclusive diastereoselectivity (Scheme 3.12). The relative configuration of the stereogenic centers in **20** was confirmed to be *anti* by comparing its ¹H NMR spectrum to those previously reported. Because the oxidation of an enantioenriched boronate by NaOH/H₂O₂ has been well established to be stereoretentive, and alkene insertion into metal hydrides occurs by *syn*-addition,⁷² the borylation of the alkylcopper intermediate must be *stereoretentive*.⁷³ This result is consistent with the result of Yun on the hydroboration of a deuterium-labeled styrene derivative,³² and the stereoretentive borylation is consistent with the observation of only phenethylcopper **5**, not **5'**, throughout the hydroboration of vinylarene **1**.

Scheme 3.12 Stereochemical outcome of the hydroboration of trisubstituted alkene **19**

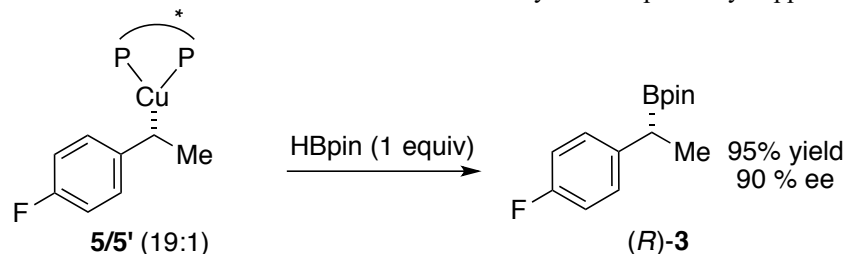


Second, we determined the stereochemical outcome of the stoichiometric borylation experimentally (Scheme 3.13). The 19:1 mixture of diastereomers (**5/5'**) formed from methylcopper complex **7**, HBpin, and 4-fluorostyrene was allowed to react with HBpin. The ee value (90%) of the boronate product **3** was assessed by HPLC after oxidative work-up. The starting 19:1 mixture of **5** and **5'** and the observed ee value for the product of the reaction of this mixture of diastereomers is consistent with a borylation reaction that is stereospecific.

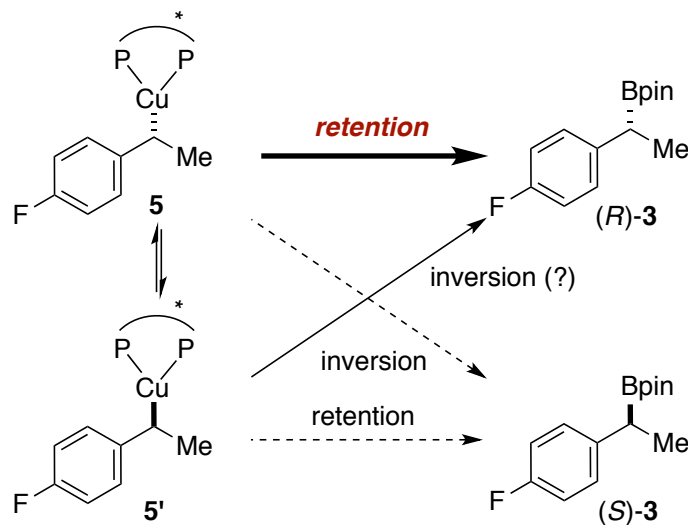
The absolute configuration of the product **3** from the reaction of phenethylcopper **5** and HBpin is (*R*), as shown in Scheme 3.13. Because the results from the hydroboration of alkene **19**

indicate that the borylation is stereoretentive, the benzylic configuration of **5** must be (*R*). This configuration determined experimentally is consistent with our predicted configuration for the kinetically formed diastereomer by DFT calculations (vide supra).

Scheme 3.13 Stereochemical outcome of the borylation of phenethylcopper **5**^a



Possible mechanisms:

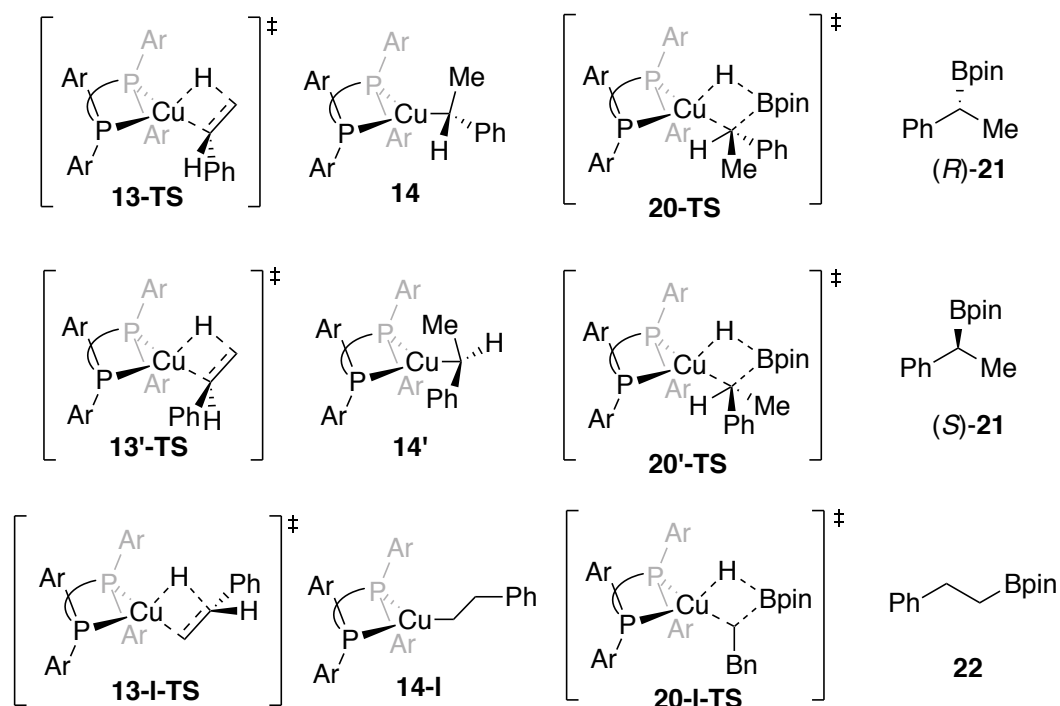
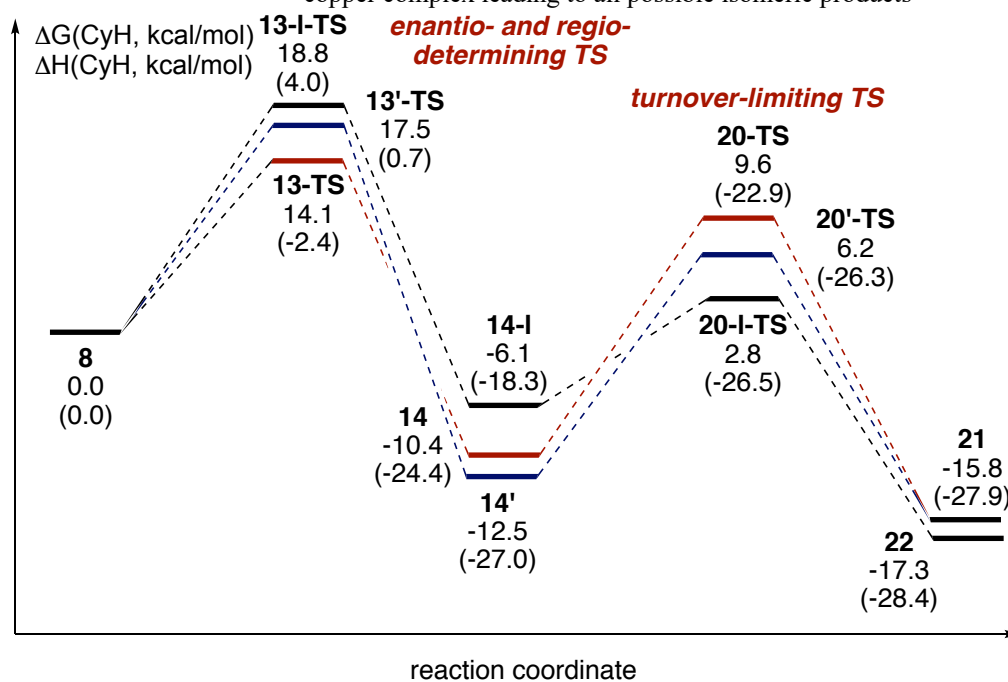


^aThe ancillary ligand on **5** and **5'** is (*S*)-DTBM-SEGPHOS.

DFT Computational Studies of the Full Catalytic Cycles to Form All Isomeric Products.

Earlier in this paper we presented DFT computations on the insertion of styrene into hydride **8** to gain information on the configuration of the benzylic carbon in the thermodynamic and kinetic stereoisomers of phenethylcopper complexes **14** and **14'** (Scheme 3.5). In this section, we provide the full free energy profiles for the hydroboration of styrene and *trans*-2-butene.⁷⁴ Previously, Yun and co-workers³¹ investigated the mechanism of the reaction and how the ligand controls the catalytic efficiency by DFT calculations.⁷⁵ Our computational results here demonstrate how the enantioselectivity and regioselectivity of the reactions are controlled and how the identity of the alkene influences each elementary step in the catalytic cycle.

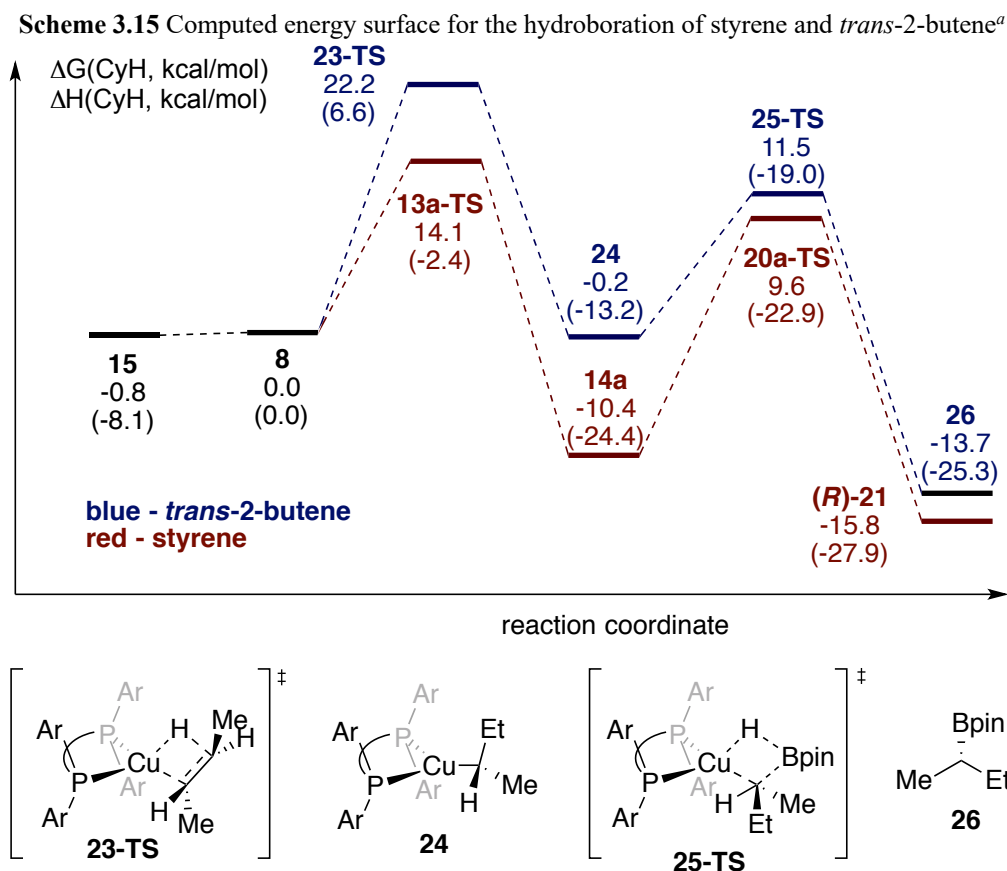
Scheme 3.14 Computed energy surface for the hydroboration of styrene catalyzed by a DTBM-SEGPHOS-ligated copper complex leading to all possible isomeric products^a



^aThe ancillary ligand is (*S*)-DTBM-SEGPHOS. See section 3.4.8 for computational details.

Scheme 3.14 illustrates the calculated reaction pathway for hydroboration of styrene catalyzed by DTBM-SEGPHOS-ligated copper complex, leading to all three possible isomeric

products (*R*)-**21**, (*S*)-**21** and linear **22**. The pathway labeled in red represents the reaction that leads to branched product (*R*)-**21**, the major enantiomer and constitutional isomer of the hydroboration of styrene. The path labeled in blue represents the reaction that leads to the minor enantiomer of the branched product (*S*)-**21**. The path labeled in black represents the reaction that leads to the linear product **22**.



^aThe ancillary ligand is (*S*)-DTBM-SEGPHOS. See section 3.4.8 for computational details.

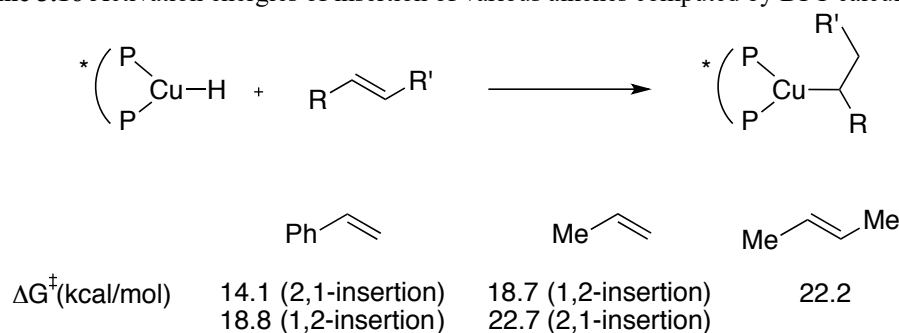
The computed energies shown in the reaction coordinate predict that the turnover-limiting step is the borylation of the phenethylcopper species; the activation barrier for this step is higher than that for the alkene insertion step. This computational result is consistent with our kinetic studies and observation of phenethylcopper complex **5** throughout the hydroboration of vinylarene **1**. In addition, the calculations predict that the alkene insertion is irreversible because the activation barrier for the forward reaction, borylation of a phenethylcopper intermediate (20.0 kcal/mol through **13-TS**), is smaller than the barrier for the reverse reaction, alkene deinsertion (24.5 kcal/mol). These calculated energies also imply that the alkene insertion is the enantioselectivity- and regioselectivity-determining step, as determined experimentally.

Scheme 3.15 shows the reaction coordinates for the hydroboration of styrene (shown in red) and *trans*-2-butene (shown in blue) together. Consistent with the results from our kinetic experiments, the calculations imply that alkene insertion is the turnover-limiting step of the hydroboration of the internal alkene. This change in turnover-limiting step results from differences in the

relative activation energies of the alkene insertion and the borylation of the resulting alkylcopper complex for reactions of the two types of alkenes. The activation barrier for insertion of *trans*-2-butene is higher than that for insertion of styrene, and the barrier for borylation of the copper-alkyl bond is lower than that for borylation of the copper-phenethyl bond.

To determine how electronic and steric effects control the alkene insertion, we calculated the activation barrier for insertion of propene (Scheme 3.16) and compared the factors controlling the barrier for this reaction to those for insertions of vinylarenes. Unlike the insertion of styrene for which 2,1-insertion is favored over 1,2-insertion, the insertion of propene favors 1,2-insertion over 2,1-insertion. The 1,2-insertion of propene is favored by 4.0 kcal/mol. The barrier to both 1,2- and 2,1-insertion of propene was computed to be significantly higher than that for 2,1-insertion of styrene, indicating that the electron-withdrawing phenyl group of the styrene causes the barrier for the insertion to be substantially lower than the barrier for insertion of propene. The barrier for 2,1-insertion of propene is close to that for insertion of *trans*-2-butene, indicating that the additional methyl group on the alkene does not significantly affect the barrier to insertion into the copper hydride.

Scheme 3.16 Activation energies of insertion of various alkenes computed by DFT calculations^a



^aThe ancillary ligand is (*S*)-DTBM-SEGPHOS.

Natural bond orbital (NBO) analysis provides a rationalization for why 2,1-insertion of styrene is favored over 1,2-insertion (Scheme 3.17). The preference for 2,1-insertion of styrene is not a result of potential π - π interaction between the ligand and the styrene or potential formation of an η^3 -phenethylcopper species. The transition states and products for the insertion lack interactions between the aryl groups of the ligand and styrene, and both structures contain η^1 -phenethyl ligands without copper-arene interactions.

Instead, the results summarized in Scheme 3.17 show that the charges of the C-H and CH₂ units, as determined by NBO analysis, account for the relative stabilities of the transition states and products. The computed charge on the methine and methylene units of the transition states at which the Cu-C bond is forming (C(2)H for **13-TS**; C(1)H₂ for **13-I-TS**) is lower in **13-TS** leading to the branched phenethylcopper **14** than it is in **13-I-TS** leading to the linear phenethylcopper **14-I**. The NBO charge of the phenyl ring of the styrene in **13-TS** shares the negative charge to a greater extent than it does in **13-I-TS**. The computed charges on the *ortho* (C(4)H, C(8)H) and *para* (C(6)H) C-H units in **13-TS**, were substantial, whereas that on the *meta* (C(5)H and C(7)H) C-H units were nearly zero. A similar distribution of charges was computed at these positions in the insertion products **14** and **14-I**, although the charges on the copper-bound carbon and the *ortho* and *para* carbons on the aryl ring are larger than those in the transition state. These results suggest that

delocalization of the negative charge from the benzylic carbon atom of **13-TS** to the adjacent phenyl ring⁷⁶ leads to the lower barrier for 2,1-insertion of the styrene and greater stability of the product of 2,1-insertion of the vinylarene.

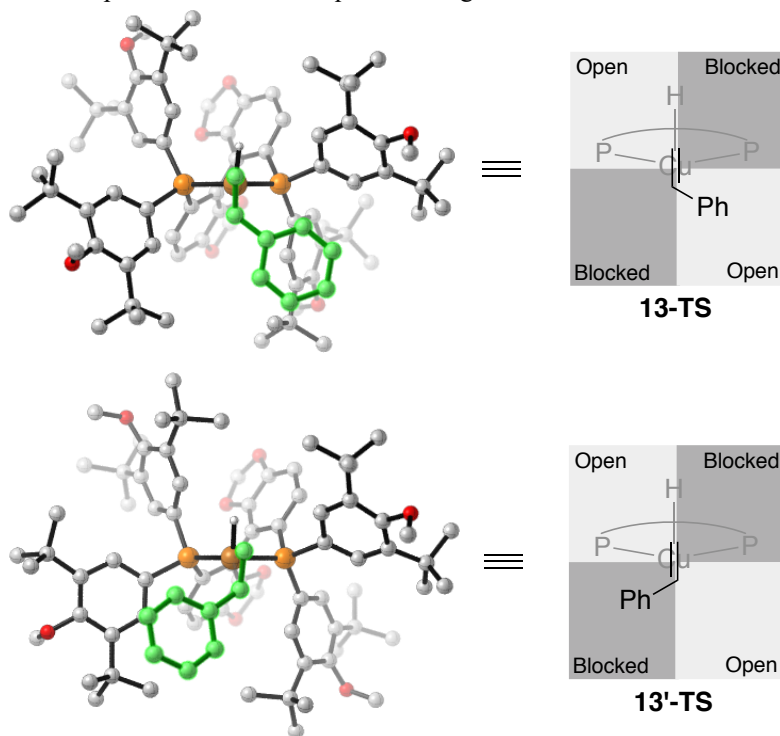
Scheme 3.17 NBO analysis of **13-TS**, **13-I-TS**, **14**, and **14-I**^a

	C1	C2	C3	C4	C5	C6	C7	C8
13-TS	-0.067	-0.236	-0.019	-0.039	0.005	-0.055	0.002	-0.039
13-I-TS	-0.269	-0.085	-0.035	-0.005	0.005	-0.018	0.007	-0.003
styrene	0.022	0.002	-0.077	0.018	0.008	0.003	0.006	0.018
14	-0.015	-0.471	-0.002	-0.043	-0.003	-0.060	-0.001	-0.044
14-I	-0.550	-0.022	-0.007	-0.005	0.000	-0.024	-0.007	-0.019

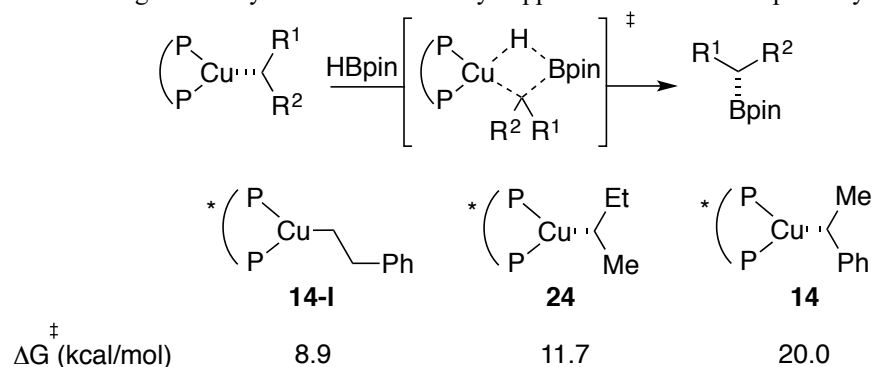
^aThe ancillary ligand is (*S*)-DTBM-SEGPHOS. NBO charges of hydrogen atoms were summed to those of the carbon atoms they are bound to.

This conclusion is consistent with the experimental observation that insertion of an electron-poor styrene is faster than the insertion of an electron-rich one. The transition state for the insertion should be stabilized more by an aryl ring containing an electron-withdrawing group in the former case than by an aryl ring containing an electron-donating group. Because the barrier for 1,2-insertion of styrene (18.8 kcal/mol) is computed to be very close to that for 1,2-insertion of propene (18.7 kcal/mol), our calculation provides a clear view of how electronic effects control the regioselectivity of the hydroboration of vinylarenes in the absence of metal-arene interactions.

The enantioselectivity⁷⁷ of the hydroboration is controlled by the relative energy (3.4 kcal/mol) of the two diastereomeric transition states **13-TS** and **13'-TS** for the insertion of styrene. The structures of **13-TS** and **13'-TS** can be visualized by quadrant diagrams (Scheme 3.18). For **13-TS**, the phenyl group of the styrene is located in the light gray regions, where axial aryl groups of the ligand are positioned. In contrast, for **13'-TS**, the phenyl group of the styrene is located in the dark gray regions, where equatorial aryl groups of the ligand are positioned. Because the equatorial aryl groups of the ligand are proximal to the coordinated styrene, a severe steric interaction between the equatorial aryl group and the phenyl group of the styrene was observed in **13'-TS**. This large difference in steric interactions within **13-TS** and **13'-TS** clearly leads to the observed enantioselectivity.

Scheme 3.18 DFT computed-structures and quadrant diagrams of transition states **13-TS** and **13'-TS**^a

^aAll hydrogen atoms that are bound to carbon atoms were omitted for clarity. Styrene moiety in the computed structures is highlighted in green.

Scheme 3.19 Activation energies of borylation of various alkylcopper intermediates computed by DFT calculations^a

^aThe ancillary ligand is (*S*)-DTBM-SEGPHOS.

The activation energies for the borylation⁷⁸ of a series of alkylcopper species were assessed by DFT calculations (Scheme 3.19).⁷⁹ Consistent with our experimental results, the barrier computed for reaction of HBpin with electron-rich, less bulky alkylcopper complexes is lower than that with electron-deficient, bulkier alkylcopper complexes. The rate for reaction of the methyl complex **7** with HBpin was too fast to measure, and the activation energy computed for the borylation of the primary phenethylcopper complex **14-I** is less than 10 kcal/mol. The computed barrier for borylation of the secondary alkylcopper species, *sec*-butyl complex **24**, is about 3 kcal/mol higher than that for borylation of the primary phenethylcopper species **14-I**. This borylation

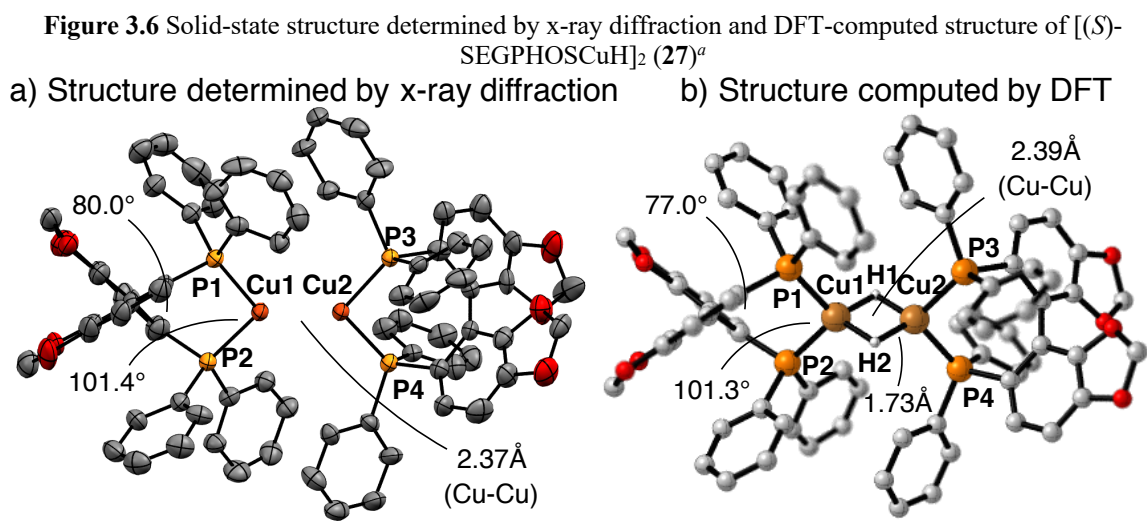
process is computed to have a higher barrier because the steric interactions between the alkyl group of **24** and HBpin in the transition state are more severe than that between HBpin and the linear phenethyl group of **14-I**. The free energy of activation for borylation of the secondary phenethylcopper complex **14** is computed to be much higher than that for borylation of the primary phenethylcopper complex **14-I** and for borylation of the *sec*-butyl complex **24**. In addition to steric effects, the lower charge on the copper-bound carbon atom of the phenethyl moiety than on the copper-bound carbon of the linear phenethylcopper complex is likely to be the origin of this large difference in activation energies.

3.2.2 Mechanistic Studies on Hydroboration Catalyzed by SEGPHOS-Ligated Copper(I)

The copper catalyst ligated by (*S*)-SEGPHOS was significantly less active than that ligated by (*S*)-DTBM-SEGPHOS. To understand this difference in reactivity and, thereby, reveal features of the catalyst that lead to high activity, we investigated the hydroboration of vinylarene **1** with the catalyst formed from (*S*)-SEGPHOS.

Synthesis and Characterization of Catalytically Relevant Complexes. Monitoring a hydroboration reaction of **1** with HBpin catalyzed by CuCl, KO*t*Bu, and (*S*)-SEGPHOS in toluene at room temperature by ³¹P NMR spectroscopy revealed multiple species at the early stage of the reaction. However, a broad signal at 1.9 ppm in the ³¹P NMR spectra became dominant as the reaction progressed to around 40% conversion.

The dimeric copper hydride complex, [(*S*)-SEGPHOSCuH]₂ (**27**), which corresponds to the ³¹P NMR chemical shift of 1.9 ppm, was independently synthesized by treating [(*S*)-SEGPHOSCuCl]₂⁵¹ with sodium triethylborohydride. The ¹H NMR spectrum of **27** in benzene-*d*₆ contained a characteristic broad singlet at 2.60 ppm, which was assigned to the hydride resonance. This chemical shift is similar to that of other phosphine-ligated copper hydride complexes reported previously.⁴⁴⁻⁴⁶ The corresponding copper deuteride analog was prepared, and its ²H NMR spectrum contained a broad singlet at 2.60 ppm. Complex **27** is stable in solid form at room temperature for at least 6 hours, but is unstable in solution. A concentrated THF or toluene solution of **27** at -40 °C decomposed overnight, and this decomposition prevented purification to afford a microanalytically pure sample.

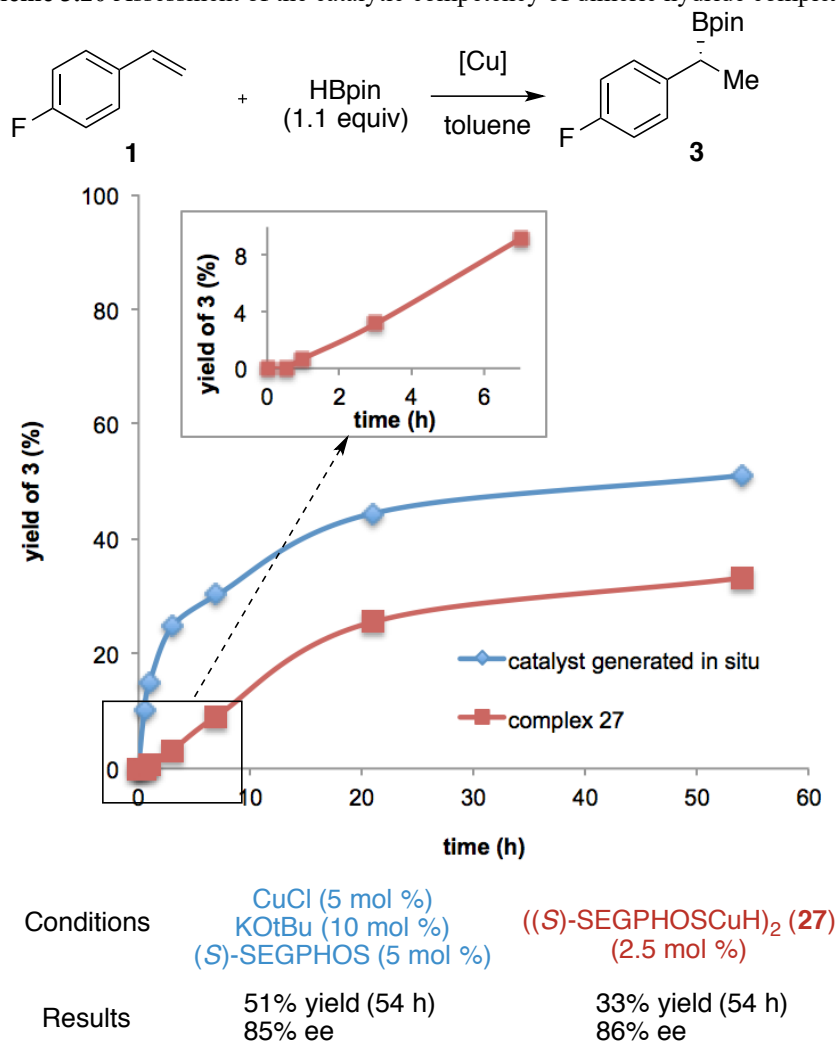


^aThe thermal ellipsoids were set to 30% probability. All hydrogen atoms were omitted for clarity. Electron density marking the positions of the hydrides was not clearly defined. Geometry optimizations were performed at the PBE/SDD/6-31G(d) level of theory. All hydrogen atoms that are bound to carbon atoms were omitted for clarity.

Despite its low stability, we obtained single crystals of complex **27** suitable for x-ray diffraction. The dimeric structure of [(*S*)-SEGPHOSCuH]₂ in the solid state was unambiguously confirmed (Figure 3.6 A). In the solid state, the two copper atoms and the four phosphorus atoms are almost in one plane (the dihedral angles of P1-Cu1-Cu2-P3, P2-Cu1-Cu2-P4 are 0.57° and 6.13°, respectively). The hydrides in the solid-state structure could not be located accurately.

Thus, the location of the hydrides, was investigated by DFT calculations on the most stable structure of **27**. Calculations with a series of different functionals showed that the copper center adopts a tetrahedral geometry with a Cu-H bond length of 1.73 Å (Figure 3.6 B; see section 3.4.8 for details). This result is consistent with geometries observed for other phosphine-ligated copper hydride complexes reported previously.

Scheme 3.20 Assessment of the catalytic competency of dimeric hydride complex **27**



Assessment of the Catalytic Relevance of Dimeric Copper Hydride 27 to the Hydroboration of Vinylarene 1. To assess whether dimeric hydride complex **27** is kinetically competent catalyst to be an intermediate in the hydroboration of vinylarene **1**, we monitored the reaction by GC. The profile for the reaction catalyzed by complex **27** clearly showed that the reaction occurs with an induction period of approximately 3 hours (Scheme 3.20).

The hydroboration of vinylarene **1** catalyzed by complex **27** is significantly slower than that catalyzed by a combination of CuCl, KO^tBu, and (*S*)-SEGPHOS. Although the ee of the products formed by the two catalytic systems were indistinguishable, the rate and the yield of the reaction catalyzed by the complex generated in situ is higher than those of the reaction initiated with complex **27** (Scheme 3.20). These results suggest that complex **27** is not catalytically competent to be an intermediate and, therefore, lies off the catalytic cycle. However, the similarity of the ee values obtained for the hydroboration catalyzed by complex **27** and by the system generated in situ suggests that the dimeric copper hydride **27** generates the active catalyst, which is presumably the monomeric complex (*S*)-SEGPHOSCuH (**28**).^{80, 81} The conversion of the mixture of copper complexes observed at early stages of the reaction to complex **27** likely results from a reduction in the rate of insertion of vinylarene **1** into hydride **28** because the vinylarene is consumed by the reaction.

3.2.3 Discussion

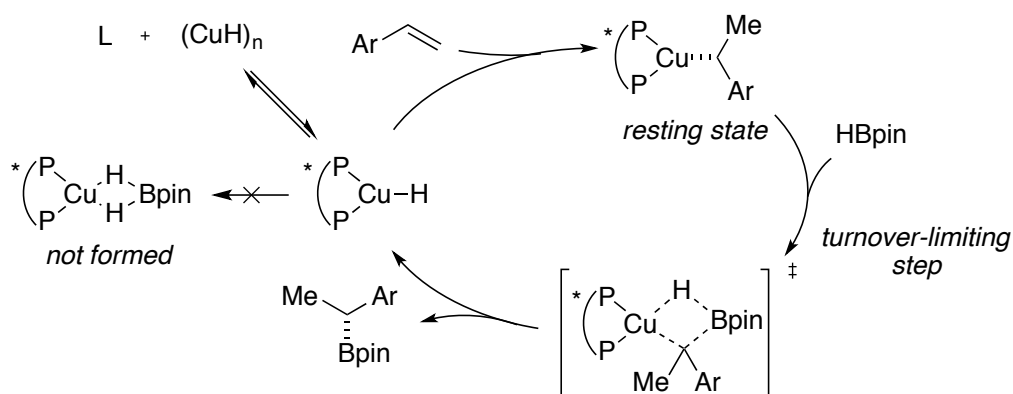
Proposed Mechanism for Hydroboration. Our experimental and computational studies provide unusually detailed information on the mechanism of an enantioselective, catalytic hydrofunctionalization of alkenes. The mechanism of the hydroboration of terminal vinylarenes and of the hydroboration of internal alkenes catalyzed by DTBM-SEGPHOS-ligated copper complexes that is consistent with all of our data is shown in Scheme 3.21. The catalytic cycle consists of two steps. The first step involves insertion of an alkene by a monomeric copper hydride to form an alkylcopper intermediate. The second step involves reaction of the alkylcopper with HBpin by a σ -bond metathesis mechanism to release the product and regenerate the copper hydride. This general mechanism occurs for all classes of alkenes, but the turnover-limiting step and catalyst resting state depend on the identity of the alkene.

Kinetic experiments revealed the turnover-limiting step in each proposed catalytic cycle. Phenethylcopper complex **5** was the only phosphine-ligated copper species observed during the hydroboration of vinylarene **1** with DTBM-SEGPHOS as the ligand, and the reaction of this complex with HBpin is the turnover-limiting step. In contrast, copper dihydridoborate **15** was the only phosphine-ligated copper species observed during the catalytic reaction of the internal alkene **2**, and the turnover-limiting step is the insertion of **2** into copper hydride **8**, which is formed by reversible dissociation of HBpin from **15**.

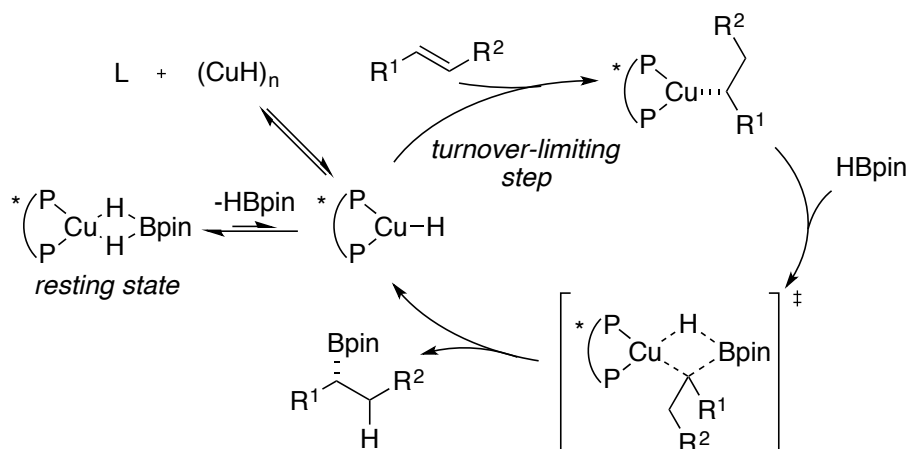
Experiments provided information about the origins of the configurations of the copper intermediates. For the hydroboration of vinylarene **1**, our experimental data showed that the alkene insertion is reversible in the absence of HBpin but is irreversible throughout the catalytic reaction because reaction of the phenethylcopper complex with HBpin is faster than epimerization of the phenethylcopper complex. Thus, the migratory insertion of the alkene sets the configuration of the product. For the hydroboration of internal alkene **2**, this step is also irreversible, and the configuration of the α -carbon of the alkylcopper intermediate is, again, set by the insertion.

Scheme 3.21 Proposed mechanism of copper-catalyzed hydroboration^a

A) Proposed mechanism for hydroboration of styrenes



B) Proposed mechanism for hydroboration of internal alkenes

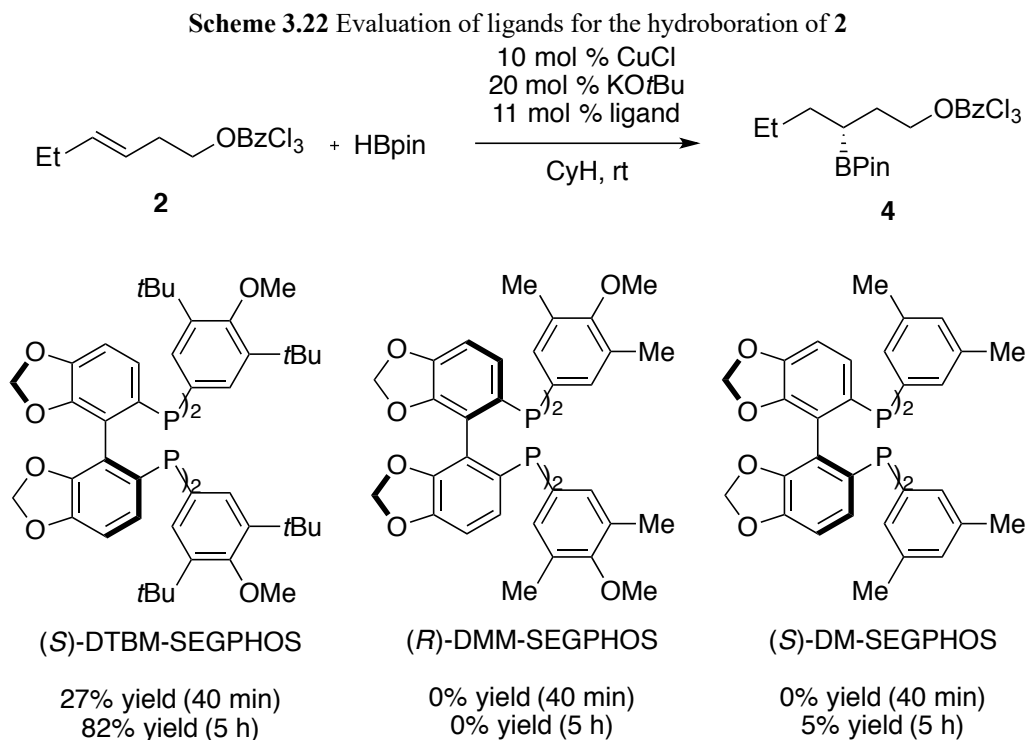


^aThe ancillary ligand is (*S*)-DTBM-SEGPHOS.

The irreversible insertion of internal alkene **2** explains the absence of isomerization of alkyl-copper intermediates through a chain-walking process in the hydroboration of **2**. The rapid conversion of the secondary alkylcopper complex to product prohibits migration of the copper along the alkyl chain by a series of deinsertion and insertion steps, even though deinsertion can occur. The computed barriers for reaction of the alkyl complexes with borane are 5-10 kcal/mol lower than the barrier for deinsertion of the alkyl complex to generate a copper hydride and the alkene. As noted in the beginning of this paper, a portion of the copper in the system is ligated by DTBM-SEGPHOS and a portion lacks the phosphine ligand, as determined by the observation of between 3:1 and 9:1 ratios of free DTBM-SEGPHOS to ligated DTBM-SEGPHOS in systems containing a 1.1:1 ratio of ligand to copper. However, the enantioselectivity of the catalytic process is high (>95%). For this reason, reactions through the unligated copper cannot account for a significant fraction of the product, and the intermediates we observe are also kinetically and chemically competent to lie on the catalytic cycle.

Effect of Ligand Steric Properties on the Catalytic Activity. The substitution pattern of the aryl rings in the ligand has a dramatic effect on the reactivity of the catalyst. Ligands containing

bulky groups, such as *tert*-butyl groups, at the 3,5-position of the aryl rings generate more active catalysts than those containing smaller groups at these positions. For example, DTBM-SEGPHOS formed a highly active catalyst, whereas DMM-SEGPHOS, with methyl groups at the 3- and 5-position of the aryl rings in place of *tert*-butyl groups, did not form an active catalyst (Scheme 3.22), although the electronic properties of DTBM-SEGPHOS are similar to those of DMM-SEGPHOS. Likewise, DM-SEGPHOS shown in Scheme 3.21 did not form an active catalyst for hydroboration of **2**. Our mechanistic studies on reactions catalyzed by complexes of DTBM-SEGPHOS and of SEGPHOS imply that this difference in catalyst activity results from the formation of catalytically incompetent, dimeric copper hydride complexes when the ligand is smaller than DTBM-SEGPHOS. Bulky ligands, such as DTBM-SEGPHOS, cause the copper complexes to remain mononuclear.



3.3 Conclusions

In summary, we report a detailed mechanistic study of the copper-catalyzed asymmetric hydroboration of alkenes. We studied the hydroboration of vinylarene **1** with both SEGPHOS and DTBM-SEGPHOS as the ligand and the hydroboration of internal alkene **2** with DTBM-SEGPHOS as the ligand. Several copper complexes have been isolated and fully characterized by x-ray diffraction and multinuclear NMR spectroscopy, and these complexes have been shown to be chemically and catalytically competent. Stoichiometric reactions provided insight into each elementary step in the catalytic cycle, and kinetic studies, along with the observation of catalytic intermediates, revealed the turnover-limiting step in the catalytic cycle. Through these experiments we have gained insight into the origin of the enantioselectivity and regioselectivity. DFT

calculations provided additional support and explanation for the experimental data. The following specific conclusions can be drawn from these data.

1. The catalyst speciation depended on the ligand and the alkene. With SEGPHOS as ligand, dinuclear copper species are dominant, but with the bulky ligand DTBM-SEGPHOS, all of the observed copper species were monomeric. For reactions of vinylarenes, the ligated catalyst resting state is a phenethylcopper(I) species, but for reactions of internal, unconjugated alkenes, the ligated catalyst resting state is a copper dihydridoborate complex.

2. Dimeric copper hydride complexes ligated by bidentate phosphines are not kinetically competent to be part of the catalytic system. Such complexes are formed by dimerization of the active monomeric copper hydride, and this process slows the rate of the catalysis. Catalysts in this system ligated by the bulky DTBM-SEGPHOS are highly active because they are mononuclear.

3. The hydroboration of vinylarene **1** is first-order in [HBpin] and [Cu] and zero-order in [1]; the hydroboration of internal alkene **2** is first-order in [Cu], inverse order in [HBpin], and positive order in [2]. Thus, the turnover-limiting step of the reactions of vinylarenes is the reaction of a phenethylcopper complex with HBpin, and the turnover-limiting step of the reactions of internal, unconjugated alkene is insertion of the alkene into a copper hydride generated by reversible dissociation of HBpin from DTBM-SEGPHOS-ligated dihydroborate complex **15**.

4. Stoichiometric reactions of the copper hydride and alkenes showed that an electron-poor vinylarene undergoes insertion much faster than an electron-rich vinylarene, which undergoes insertion faster than an unconjugated alkene, and these relative rates were explained by DFT calculations. NBO analysis provided a clear view on how the charge on the copper-bound carbon and delocalization of charge onto the aryl ring controls the rate of the alkene insertion, the regioselectivity of the reaction, and the rate of reaction with HBpin.

5. The alkene insertion is irreversible in the catalytic reactions. In the absence of HBpin, the epimerization of phenethylcopper intermediates to the corresponding diastereomers, by reversible deinsertion and insertion of the alkene, occurs in solution. However, the epimerization of the phenethylcopper complex, and therefore deinsertion and reinsertion, is slower than reaction of this complex with HBpin. Thus, epimerization and chain walking by deinsertion and reinsertion do not occur during the catalytic hydroboration.

6. Studies on the alkene insertion suggest that the enantioselectivity- and regioselectivity-determining step in the catalytic cycle is the alkene insertion step regardless of the alkene substrate and the ligand.

7. The rates of the borylation of discrete alkylcopper complexes with HBpin followed the trend: electron-rich > electron-poor copper complexes. The reaction occurs with retention of configuration to afford the corresponding boronates.

8. Evaluation of the effect of ligand properties on catalyst activity showed that the steric properties of the ligand dominate the reactivity of the copper catalyst. Sterically encumbered ligands form highly reactive catalysts. In particular, the steric bulk of the aryl rings of the ligand at the 3- and 5-positions affected the reactivity of the catalyst substantially by maintaining a monomeric form of the catalyst.

Overall, this study has revealed the fundamental principles that govern the efficiency of the copper catalysts for reactions with alkenes and selectivity of the alkene hydroboration. The interplay between the alkene insertion and borylation steps controls the overall catalyst speciation and reaction kinetics. More active catalytic systems are required for hydroboration of unactivated internal alkenes, and we hope an approach involving rational design of ligands through both

experiment and theory will increase the rate of this process. Such studies will be the subject of future work in our laboratory.

3.4 Experimental

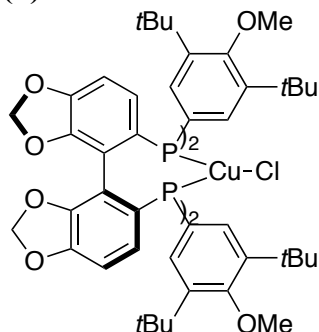
3.4.1 General Methods and Materials

All air-sensitive manipulations were performed in an argon-filled glovebox or using standard Schlenk techniques. Glassware was dried at 130 °C for at least 4 hours before use. Pentane, hexanes, THF, DCM, and toluene were collected from a solvent purification system containing a 0.33 m column of activated alumina under nitrogen. Anhydrous cyclohexane was purchased from Aldrich and used as received. CuCl, KO^tBu and pinacolborane (HBpin) were purchased from Aldrich. (*S*)-SEGPHOS was purchased from Strem Chemicals and (*S*)-DTBM-SEGPHOS was generously donated by Takasago. All other reagents purchased from commercial suppliers were stored in the glovebox and used as received. Deuterated solvents were purchased from Cambridge Isotope Laboratories and Aldrich and used as received.

¹H NMR spectra were recorded on Bruker AVQ-400, AV-500, AV-600, and AV-700 instruments with 400, 500, 600, and 700 MHz frequencies, and ¹³C NMR spectra were recorded on a Bruker AV-600 instrument with a ¹³C operating frequency of 150 MHz. ¹⁹F NMR spectra were recorded on a Bruker AV-600 spectrometer with a ¹⁹F operating frequency of 564 MHz. ¹¹B NMR spectra were recorded on a Bruker AV-600 spectrometer with a ¹¹B operating frequency of 192 MHz. Chemical shifts (δ) are reported in ppm relative to the residual solvent signal (CDCl₃ δ = 7.26 for ¹H NMR and δ = 77.0 for ¹³C NMR; benzene-*d*₆ = 7.16 ppm for ¹H NMR; toluene-*d*₈ = 2.09 ppm for ¹H NMR; cyclohexane-*d*₁₂ = 2.12 ppm for ¹H NMR). Quantitative analysis by GC was performed with dodecane as an internal standard. Chiral HPLC analysis was conducted on a Waters chromatography system. Elemental analyses were conducted at the Micro Analytical Facility operated by the College of Chemistry, University of California, Berkeley.

3.4.2 Synthesis and Characterization of Copper Complexes

(*S*)-DTBM-SEGPHOSCuCl (**6**)



Into a 20 mL vial was placed CuCl (30.0 mg, 0.303 mmol, 1.01 equiv) and (*S*)-DTBM-SEGPHOS (354.0 mg, 0.3000 mmol, 1 equiv) were added, followed by 6 mL of toluene and 2 mL of DCM. The vial was capped and allowed to stir at ambient temperature for 2 hours. The resulting solution was filtered through a pad of Celite and concentrated *in vacuo*. The resulting crude material was recrystallized with 15 drops of DCM and 6 mL of pentane at -40 °C. Crystals formed by the process

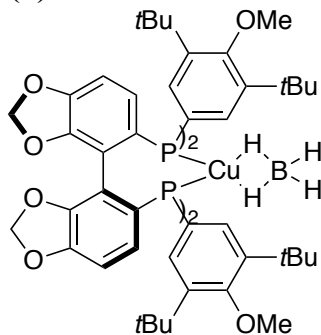
were suitable for x-ray crystallography. The crystals were washed with cold pentane and dried under vacuum to give complex **6** (359.8 mg, 94%) as an off-white solid.

^1H NMR (600 MHz, Toluene- d_8) δ 8.52 (br s, 4H), 7.80 (br s, 4H), 6.76 (dt, $J = 8.0, 4.8$ Hz, 2H), 6.18 (d, $J = 8.1$ Hz, 2H), 5.29 (d, $J = 1.4$ Hz, 2H), 5.13 (d, $J = 1.3$ Hz, 2H), 3.32 (s, 6H), 3.22 (s, 6H), 1.58 (s, 36H), 1.31 (s, 36H).

^{31}P NMR (243 MHz, Toluene- d_8) δ -4.8.

Anal. Calcd (%) for $\text{C}_{74}\text{H}_{100}\text{ClCuO}_8\text{P}_2$: C, 69.52; H, 7.88. Found: C, 69.73; H, 7.61.

(*S*)-DTBM-SEGP HOSCuBH_4 (**16**)



To a 20 mL vial containing (*S*)-DTBM-SEGP HOSCuCl (**6**, 76.7 mg, 0.600 mmol, 1 equiv), was added 2 mL of toluene. Sodium borohydride (56.7 mg, 1.50 mmol, 25 equiv) was then added in one portion. The vial was capped and allowed to stir at ambient temperature overnight. An aliquot was removed and analyzed by ^{31}P NMR spectroscopy to ensure full conversion. The aliquot was combined with the rest of the solution, and the combined material was filtered through a pad of Celite and concentrated *in vacuo*. The resulting solid was treated with 3 mL of pentane and dried under vacuum to give an analytically pure sample of **16** (60.4 mg, 80%) as a white solid. Crystals suitable for x-ray crystallography were obtained by recrystallizing the crude material in hexanes at rt.

^1H NMR (600 MHz, Toluene- d_8) δ 8.40 (br s, 4H), 7.85 (br s, 4H), 6.68 (dt, $J = 8.0, 4.9$ Hz, 2H), 6.15 (d, $J = 8.1$ Hz, 2H), 5.35 (s, 2H), 5.11 (s, 2H), 3.33 (s, 6H), 3.19 (s, 6H), 1.57 (s, 36H), 1.33 (s, 36H).

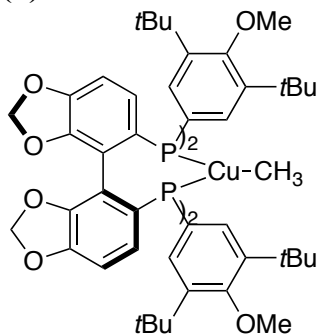
^{31}P NMR (243 MHz, Toluene- d_8) δ 0.5.

$^{11}\text{B}\{^1\text{H}\}$ NMR (192 MHz, Toluene- d_8) δ -28.0.

FT-IR (cm^{-1}): 2391 ($\nu(\text{B-H}_t)$), 2360 ($\nu(\text{B-H}_i)$), 1974 ($\nu(\text{B-H}_b)$), 1914 ($\nu(\text{B-H}_b)$).

Anal. Calcd (%) for $\text{C}_{74}\text{H}_{104}\text{BCuO}_8\text{P}_2$: C, 70.66; H, 8.33. Found: C, 70.55; H, 8.20.

(*S*)-DTBM-SEGP HOSCuCH_3 (**7**)



To a 20 mL vial containing a suspension of (*S*)-DTBM-SEGPHOSCuCl (**6**, 76.7 mg, 0.600 mmol, 1 equiv) in pentane pre-chilled to -35°C , was added a pre-chilled solution of MeLi (600 μL , 0.10 M in THF) dropwise. The vial was capped and allowed to warm to room temperature. After 45 minutes, the resulting yellow solution was passed through a syringe filter and concentrated *in vacuo*. The residue was re-dissolved in pentane and concentrated *in vacuo*. This material was re-crystallized by dissolving in a mixture of 20 drops of THF and 1 mL pentane and layering the resulting solution with 2 mL hexamethyldisiloxane at -40°C . The crystals were washed with cold hexamethyldisiloxane and dried under vacuum to give complex **7** (64.7 mg, 86%) as a bright yellow solid. Note: 8% (*S*)-DTBM-SEGPHOS is present as an impurity, which we were unable to remove by multiple recrystallization.

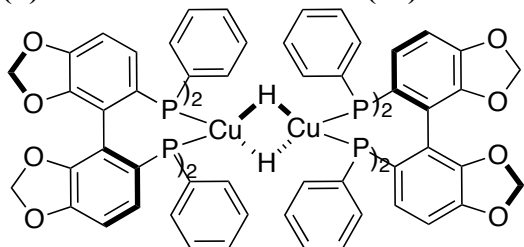
Crystals suitable for x-ray crystallography was obtained by layering a hexane solution of the crude material with hexamethyldisiloxane.

^1H NMR (600 MHz, Toluene- d_8) δ 8.44 (s, 4H), 7.82 (s, 4H), 6.71 (s, 2H), 6.19 (d, $J = 8.1$ Hz, 2H), 5.38 (s, 2H), 5.17 (d, $J = 1.4$ Hz, 2H), 3.36 (s, 6H), 3.25 (s, 6H), 1.57 (s, 36H), 1.36 (s, 36H), 0.62 (br s, 3H, Cu- CH_3).

^{31}P NMR (243 MHz, Toluene- d_8) δ -7.9.

Anal. Calcd (%) for $\text{C}_{75}\text{H}_{103}\text{CuO}_8\text{P}_2$: C, 71.60; H, 8.25. Found: C, 71.25; H, 7.96.

(*S*)-SEGPHOSCuH dimer (**27**)



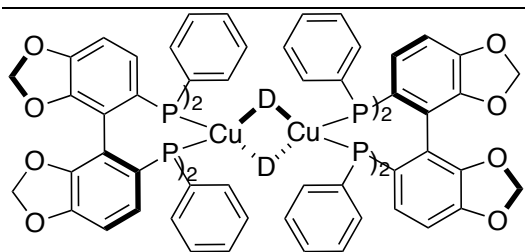
To a 20 mL vial containing a solution of [(*S*)-SEGPHOSCuCl] $_2$ (71.0 mg, 0.0500 mmol) in 1.5 mL of THF was added a solution of NaBHET_3 (100 μL , 1.0 M in THF) dropwise. The vial was capped and allowed to stir at room temperature for 10 minutes. The resulting solution was passed through a syringe filter. The filtrate was layered with pentane at -40°C . Yellow solids formed overnight were collected by filtration, washed by 4 mL of pentane and dried under vacuum to give complex **27** (42.0 mg, 62%) as a yellow solid. Yellow crystals suitable for x-ray crystallography were obtained by layering a dilute THF solution of **27** with hexanes.

^1H NMR (600 MHz, Benzene- d_6) δ 8.42 (br s, 8H), 8.32 (br s, 8H), 6.99 (t, $J = 7.4$ Hz, 4H), 6.91 (t, $J = 7.5$ Hz, 8H), 6.61 (t, $J = 7.6$ Hz, 8H), 6.54 (t, $J = 7.3$ Hz, 4H), 6.52 – 6.49 (m, 4H), 6.17 (d, $J = 8.1$ Hz, 4H), 5.41 (d, $J = 1.7$ Hz, 4H), 5.19 (d, $J = 1.8$ Hz, 4H), 2.60 (s, 2H).

^{31}P NMR (243 MHz, Benzene- d_6) δ 1.9.

We were unable to obtain a satisfactory elemental analysis.

(*S*)-SEGPHOSCuD dimer (**27-d**)

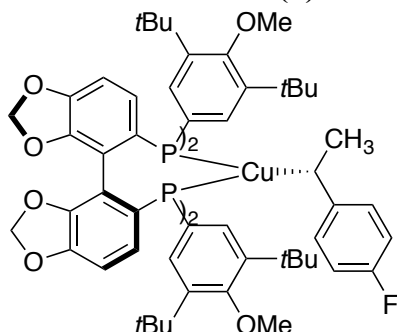


The deuteride dimer was synthesized by a procedure that is analogous to that used to prepare **27**, except LiDBEt_3 was used instead of NaHBEt_3 as the hydride source.

^2H NMR (600 MHz, Benzene) δ 2.60 (br s).

^{31}P NMR (243 MHz, Benzene) δ 1.9.

Characterization of (*S*)-DTBM-SEGPHOSCu[CH(4-F-C₆H₄)CH₃] (**5**) generated *in situ*



In a J-Young NMR tube, (*S*)-DTBM-SEGPHOSCuCH₃ (**7**) (25.2 mg, 0.0203 mmol) and 4-fluorostyrene (2.4 μL , 0.020 mmol) were dissolved in cyclohexane-*d*₁₂ (400 μL). A cyclohexane-*d*₁₂ solution of HBpin (50.0 μL , 0.0202 mmol, 0.401 M) was added in one portion. The tube was capped, shaken and inserted into an NMR instrument, and ^1H , ^{31}P , and ^{19}F NMR spectra were obtained.

The combined yield of complex **5** and its diastereomer **5'** (78%, 19:1) was determined by ^{19}F NMR spectroscopy on a sample generated in cyclohexane with 1,3-difluorobenzene as an internal standard, following the same procedure but with cyclohexane as the solvent.

^1H NMR (600 MHz, Cyclohexane-*d*₁₂) δ 7.50 (br s, 4H), 7.31 (t, $J = 5.4$ Hz, 4H), 6.63 (dt, $J = 8.1$, 4.1 Hz, 2H), 6.52 (dd, $J = 8.6$, 5.6 Hz, 2H), 6.35 (d, $J = 8.1$ Hz, 2H), 6.26 (t, $J = 8.8$ Hz, 2H), 5.50 (br s, 2H), 5.42 (d, $J = 1.7$ Hz, 2H), 3.77 (s, 6H), 3.65 (s, 6H), 2.85 (q, $J = 7.2$ Hz, 1H), 1.73 (d, $J = 7.2$ Hz, 3H), 1.49 (s, 36H), 1.37 (s, 36H).

^{31}P NMR (243 MHz, cyclohexane-*d*₁₂) δ -7.7.

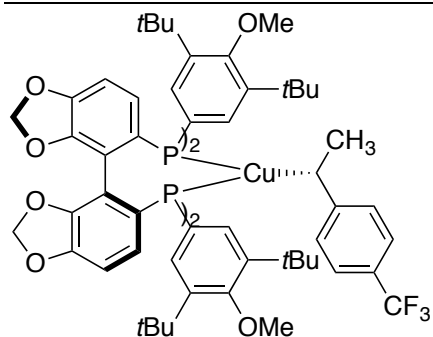
^{19}F NMR (564 MHz, cyclohexane-*d*₁₂) δ -130.0.

Minor diastereomer **5'**:

^{31}P NMR (192 MHz, cyclohexane-*d*₁₂) δ -6.2.

^{19}F NMR (564 MHz, cyclohexane-*d*₁₂) δ -130.4.

Characterization of (*S*)-DTBM-SEGPHOSCu[CH(4-CF₃-C₆H₄)CH₃] (**9**) *in situ*



In a J-Young NMR tube, (*S*)-DTBM-SEGPHOSCuCH₃ (**7**) (25.2 mg, 0.0203 mmol) and 4-trifluoromethylstyrene (3.0 μ L, 0.020 mmol) were dissolved in cyclohexane-*d*₁₂ (400 μ L). A cyclohexane-*d*₁₂ solution of HBpin (50.0 μ L, 0.0202 mmol, 0.401 M) was added in one portion. The tube was capped, shaken and inserted into an NMR instrument, and ¹H, ³¹P, and ¹⁹F NMR spectra were obtained.

The combined yield of complex **9** and its diastereomer **9'** (90%, 42:1) was determined by ¹⁹F NMR spectroscopy on a sample generated in cyclohexane with 4-bromobenzotrifluoride as an internal standard, following the same procedure but with cyclohexane as the solvent.

¹H NMR (600 MHz, Cyclohexane-*d*₁₂) δ 7.53 – 7.42 (m, 4H), 7.26 (t, *J* = 5.5 Hz, 4H), 6.78 (d, *J* = 8.2 Hz, 2H), 6.67 (dt, *J* = 8.2, 4.1 Hz, 2H), 6.51 (d, *J* = 8.2 Hz, 2H), 6.37 (d, *J* = 8.1 Hz, 2H), 5.48 (br s, 2H), 5.42 (d, *J* = 1.7 Hz, 2H), 3.79 (s, 6H), 3.64 (s, 6H), 3.06 (q, *J* = 6.8 Hz, 1H), 1.79 (d, *J* = 6.8 Hz, 3H), 1.50 (s, 36H), 1.36 (s, 36H).

³¹P NMR (243 MHz, cyclohexane-*d*₁₂) δ -6.6.

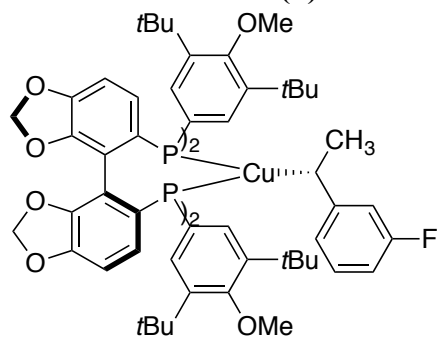
¹⁹F NMR (564 MHz, cyclohexane-*d*₁₂) δ -62.2.

Minor diastereomer **9'**:

³¹P NMR (192 MHz, cyclohexane-*d*₁₂) δ -5.6.

¹⁹F NMR (564 MHz, cyclohexane-*d*₁₂) δ -62.3.

Characterization of (*S*)-DTBM-SEGPHOSCu[CH(3-F-C₆H₄)CH₃] (**10**) *in situ*



In a J-Young NMR tube, (*S*)-DTBM-SEGPHOSCuCH₃ (**7**) (25.2 mg, 0.0203 mmol) and 3-fluorostyrene (2.4 μ L, 0.020 mmol) were dissolved in cyclohexane-*d*₁₂ (400 μ L). A cyclohexane-*d*₁₂ solution of HBpin (50.0 μ L, 0.0202 mmol, 0.401 M) was added in one portion. The tube was capped, shaken and inserted into an NMR instrument, and ¹H, ³¹P, and ¹⁹F NMR spectra were obtained.

The combined yield of complex **10** and its diastereomer **10'** (82%, 15:1) was determined by ^{19}F NMR spectroscopy on a sample generated in cyclohexane with 1,3-difluorobenzene as an internal standard, following the same procedure but with cyclohexane as the solvent.

^1H NMR (600 MHz, Cyclohexane- d_{12}) δ 7.48 (br s, 4H), 7.29 (t, $J = 5.4$ Hz, 4H), 6.67 (dt, $J = 8.2$, 4.1 Hz, 2H), 6.49 (dd, $J = 14.6$, 7.5 Hz, 1H), 6.43 (d, $J = 7.8$ Hz, 1H), 6.36 (d, $J = 8.1$ Hz, 2H), 6.13 (d, $J = 12.6$ Hz, 1H), 5.81 – 5.77 (t, $J = 8.2$ Hz, 1H), 5.48 (s, 2H), 5.42 (d, $J = 1.7$ Hz, 2H), 3.78 (s, 6H), 3.65 (s, 6H), 2.95 (q, $J = 7.0$ Hz, 1H), 1.72 (d, $J = 7.0$ Hz, 3H), 1.49 (s, 36H), 1.37 (s, 36H).

^{31}P NMR (243 MHz, cyclohexane- d_{12}) δ -7.2.

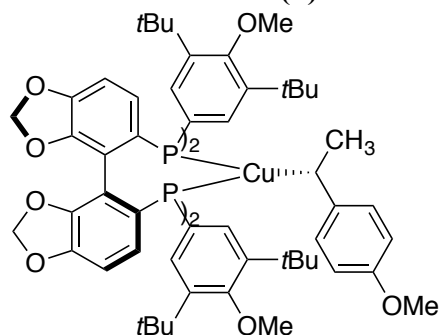
^{19}F NMR (564 MHz, cyclohexane- d_{12}) δ -116.9.

Minor diastereomer **10'**:

^{31}P NMR (192 MHz, cyclohexane- d_{12}) δ -5.9.

^{19}F NMR (564 MHz, cyclohexane- d_{12}) δ -117.2.

Characterization of (*S*)-DTBM-SEGPHOSCu[CH(4-OCH₃-C₆H₄)CH₃] (**11**) *in situ*



In a J-Young NMR tube, (*S*)-DTBM-SEGPHOSCuCH₃ (**7**) (25.2 mg, 0.0203 mmol) and 4-vinylanisole (2.7 μL , 0.020 mmol) were dissolved in cyclohexane- d_{12} (400 μL). A cyclohexane- d_{12} solution of HBpin (50.0 μL , 0.0202 mmol, 0.401 M) was added in one portion. The tube was capped, shaken and inserted into an NMR instrument, and ^1H and ^{31}P NMR spectra were obtained. The combined yield of complex **11** and its diastereomer **11'** (68%, 18:1) was determined by ^1H NMR spectroscopy on a sample generated with *p*-xylene as an internal standard.

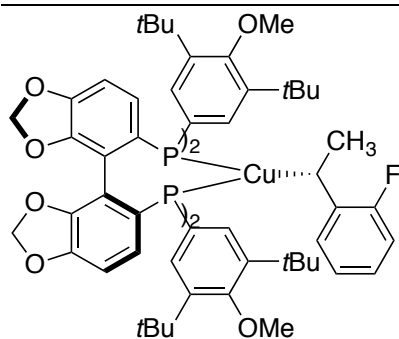
^1H NMR (600 MHz, Cyclohexane- d_{12}) δ 7.54 (br s, 4H), 7.32 (t, $J = 5.4$ Hz, 4H), 6.62 (td, $J = 8.0$, 4.0 Hz, 2H), 6.55 (d, $J = 8.4$ Hz, 2H), 6.33 (d, $J = 8.2$ Hz, 2H), 6.23 (d, $J = 8.4$ Hz, 2H), 5.51 (s, 2H), 5.42 (d, $J = 1.6$ Hz, 2H), 3.75 (s, 6H), 3.64 (s, 6H), 3.48 (s, 3H), 2.80 (q, $J = 7.5$ Hz, 1H), 1.74 (d, $J = 7.3$ Hz, 3H), 1.49 (s, 36H), 1.36 (s, 36H).

^{31}P NMR (243 MHz, cyclohexane- d_{12}) δ -7.9.

Minor diastereomer **11'**:

^{31}P NMR (192 MHz, cyclohexane- d_{12}) δ -6.3.

Characterization of (*S*)-DTBM-SEGPHOSCu[CH(2-F-C₆H₄)CH₃] (**12**) *in situ*



In a J-Young NMR tube, (*S*)-DTBM-SEGPHOSCuCH₃ (**7**) (25.2 mg, 0.0203 mmol) and 2-fluorostyrene (2.4 μL, 0.020 mmol) were dissolved in cyclohexane-*d*₁₂ (400 μL). A cyclohexane-*d*₁₂ solution of HBpin (50.0 μL, 0.0202 mmol, 0.401 M) was added in one portion. The tube was capped, shaken and inserted into an NMR instrument, and ¹H, ³¹P, and ¹⁹F NMR spectra were obtained.

The combined yield of complex **12** and its diastereomer **12'** (88%, 62:1) was determined by ¹H NMR spectroscopy on a sample generated with *p*-xylene as an internal standard.

¹H NMR (600 MHz, Cyclohexane-*d*₁₂) δ 7.44 (br s, 4H), 7.35 (br t, *J* = 5.3 Hz, 4H), 6.61 (dt, *J* = 8.1, 4.1 Hz, 2H), 6.42 – 6.25 (m, 5H), 6.03 (q, *J* = 6.7 Hz, 1H), 5.46 (s, 2H), 5.40 (s, 2H), 3.76 (s, 6H), 3.65 (s, 6H), 2.90 (q, *J* = 7.0 Hz, 1H), 1.74 (d, *J* = 7.0 Hz, 3H), 1.47 (s, 36H), 1.39 (s, 36H).

³¹P NMR (243 MHz, cyclohexane-*d*₁₂) δ -8.4.

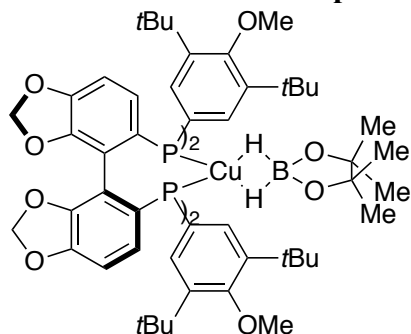
¹⁹F NMR (564 MHz, cyclohexane-*d*₁₂) δ -118.5.

Minor diastereomer **12'**:

³¹P NMR (192 MHz, cyclohexane-*d*₁₂) δ -6.6.

¹⁹F NMR (564 MHz, cyclohexane-*d*₁₂) δ -118.5.

Characterization of complex **15** generated *in situ*



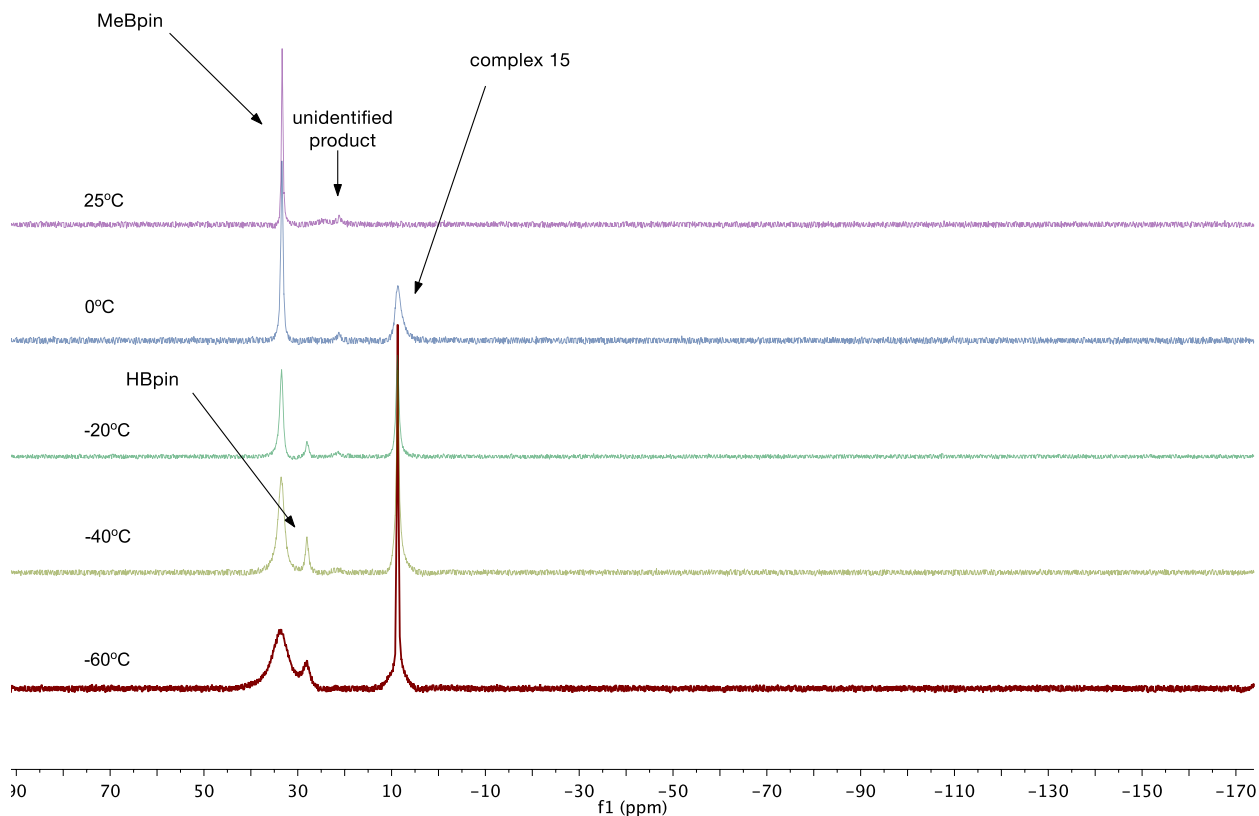
In a screw-capped NMR tube, (*S*)-DTBM-SEGPHOSCuCH₃ (**7**) (25.2 mg, 0.0203 mmol) was dissolved in toluene-*d*₈ (400 μL). The NMR tube was capped, removed from the glovebox and placed in a dry ice/acetone bath. A toluene-*d*₈ solution of HBpin (100 μL, 0.0400 mmol, 0.400 M) was added in one portion. The tube was shaken to ensure proper mixing and then inserted into an NMR instrument pre-cooled at the designated temperature. The yield of complex **15** (79%) was determined by ¹H NMR spectroscopy with *p*-xylene as an internal standard at 0 °C.

¹H NMR (600 MHz, Toluene-*d*₈, 0 °C) δ 9.20-7.40 (br m, 8H), 6.57 (dt, *J* = 9.6, 5.1 Hz, 2H), 6.11 (d, *J* = 8.1 Hz, 2H), 5.38 (s, 2H), 5.07 (s, 2H), 4.19 (br m, 2H), 3.36 (s, 6H), 3.20 (s, 6H), 1.93 – 1.20 (br m, 84H).

^{31}P NMR (243 MHz, Toluene- d_8 , 0 °C) δ 9.0.

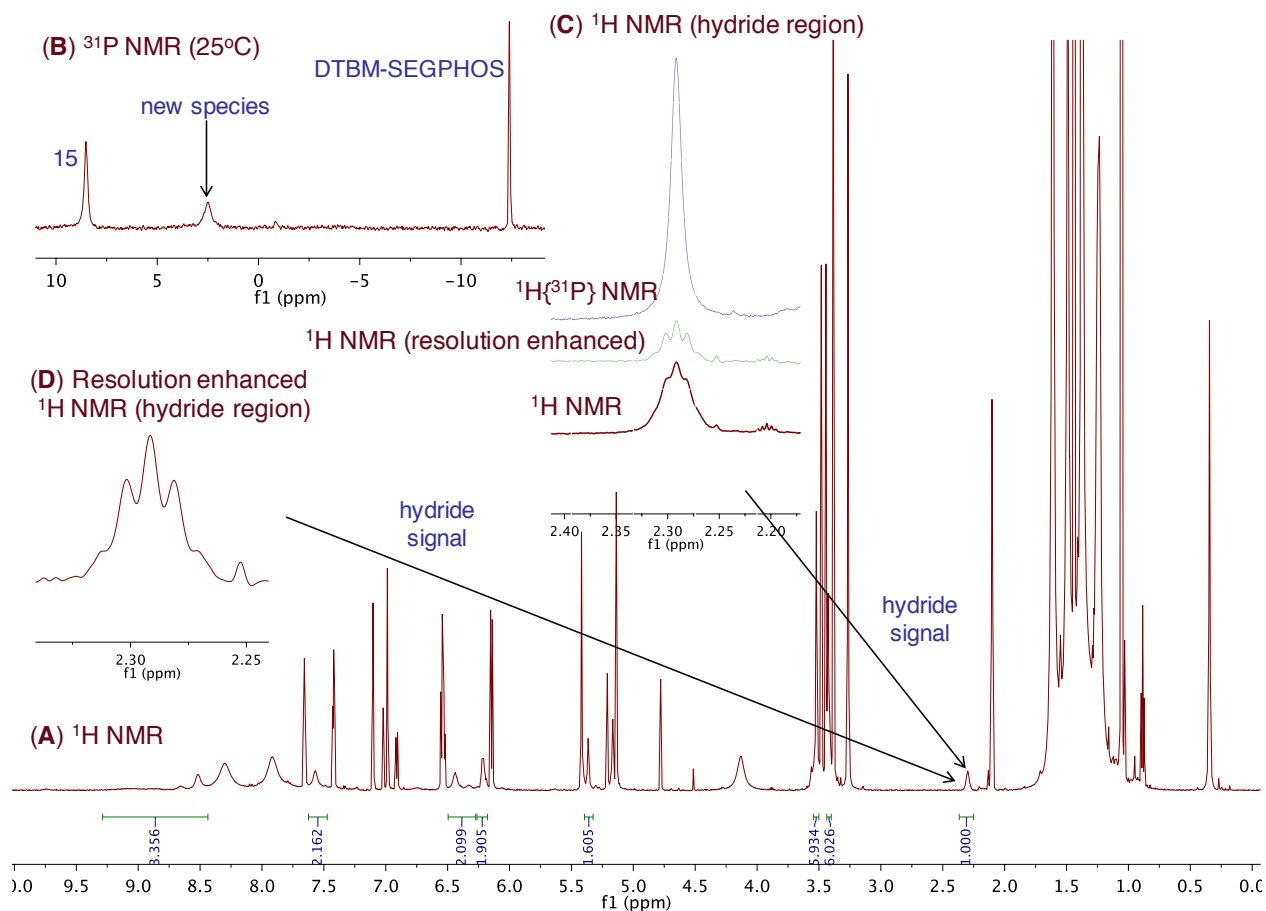
^{11}B NMR (192 MHz, Toluene- d_8 , -60 °C) δ 8.8 (t, $J = 72$ Hz).

Figure 3.7 VT $^{11}\text{B}\{^1\text{H}\}$ NMR spectra of **15**



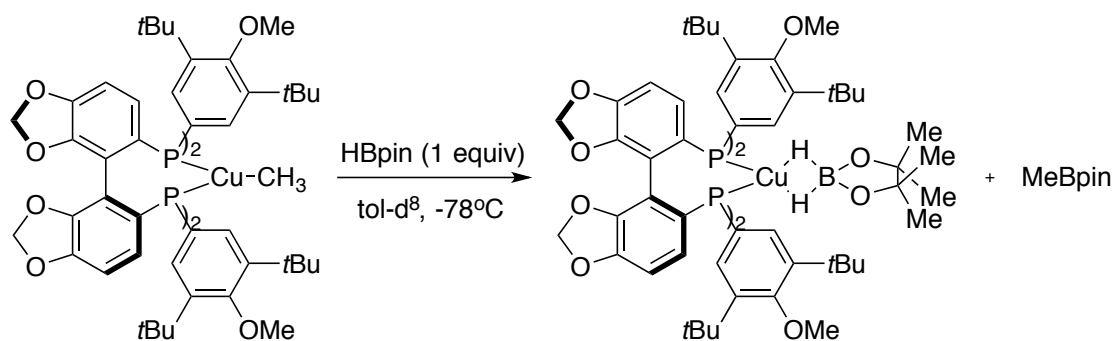
Note: Multiple baseline corrections were performed to remove the uneven baseline that results from boron in the borosilicate glass NMR tubes.

After warming the sample to 25 °C from -60 °C, decomposition products (2.4 ppm and -12.7 ppm) were observed by ^{31}P NMR spectroscopy. We observed a distinct resonance at 2.29 ppm in the ^1H NMR spectrum that appears as a quintet ($J_{\text{P-H}} = 5.1$ Hz) after resolution enhancement (Figure 3.8 D). This quintet was observed as a sharp singlet when the spectrum was acquired with ^{31}P decoupling, indicating that the proton is coupled to four equivalent phosphorus nuclei. These results imply that the decomposition product is likely a dimeric DTBM-SEGPHOS-ligated copper hydride.

Figure 3.8 ^1H , $^1\text{H}\{^{31}\text{P}\}$, $^{31}\text{P}\{^1\text{H}\}$ NMR spectra of **15** at 25°C

3.4.3 Stoichiometric Reactions

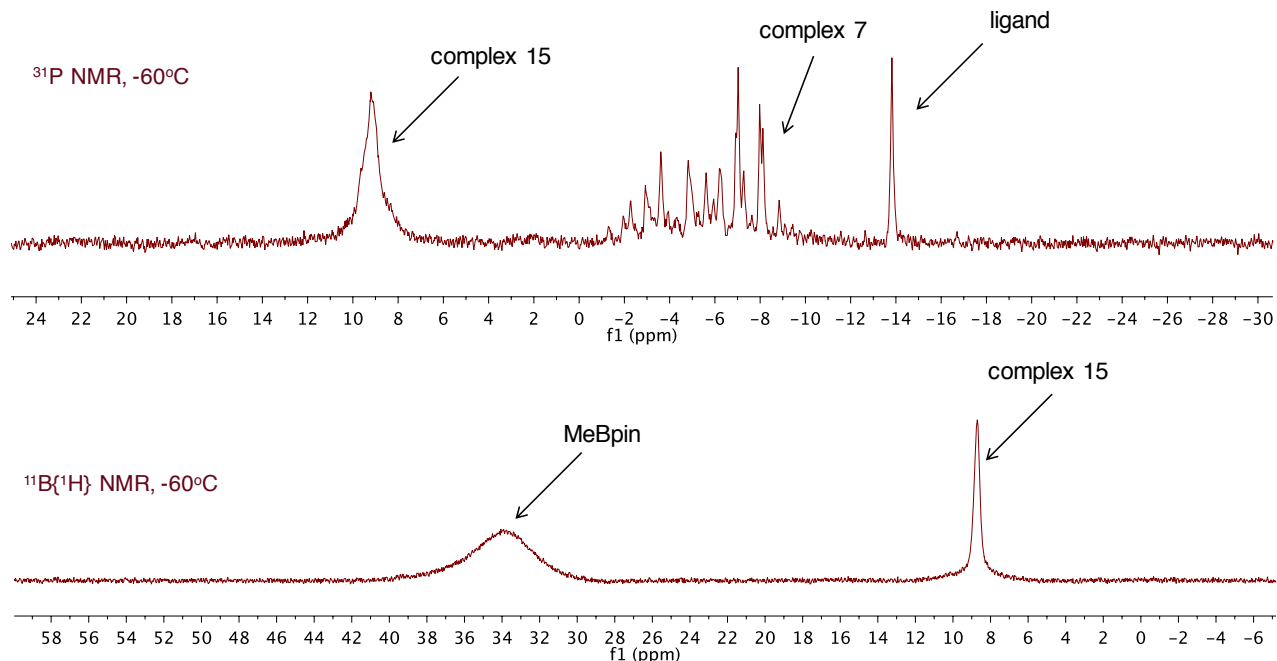
Reaction of (*S*)-DTBM-SEGPHOSCuCH₃ (**7**) and HBpin



In a screw-capped NMR tube, (*S*)-DTBM-SEGPHOSCuCH₃ (**7**) (25.2 mg, 0.0203 mmol) was dissolved in toluene-*d*₈ (400 μL). The solution was cooled to -78 $^{\circ}\text{C}$, and a toluene-*d*₈ solution of

HBpin (50.0 μL , 0.0200 mmol, 0.400 M) was added in one portion. The tube was shaken to ensure proper mixing and inserted into an NMR instrument pre-cooled at a designated temperature.

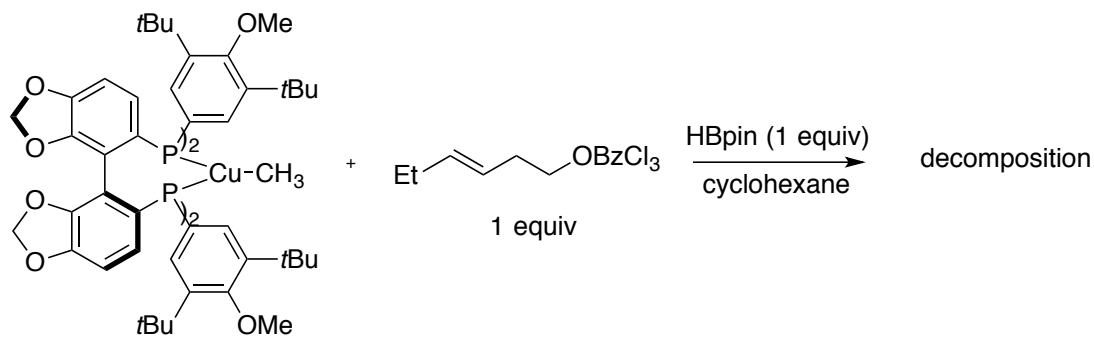
Figure 3.9 $^{31}\text{P}\{^1\text{H}\}$ and $^{11}\text{B}\{^1\text{H}\}$ NMR spectra of the reaction of **7** and HBpin at $-60\text{ }^\circ\text{C}$



Note: The ^{31}P NMR spectrum of **7** consists of multiple signals that correspond to each rotamer at low temperature, presumably due to restricted rotation of methoxy groups of DTBM-SEGPHOS. Such multiple peaks were not observed with an analogous complex DTB-SEGPHOSCuCl, which has otherwise an identical structure to complex **7**, except for the absence of the methoxy groups (DTB: 3,5-di-*tert*-butylphenyl).

The reaction of methyl complex **7** and 1 equivalent of HBpin at $-60\text{ }^\circ\text{C}$ afforded **15** as the only product. The ^{31}P NMR spectrum acquired at $-60\text{ }^\circ\text{C}$ indicated the presence of **15** and unreacted **7**. This result suggests that the reaction of **15** and **7** is slow at $-60\text{ }^\circ\text{C}$. After warming the sample to room temperature, complete decomposition to free ligand was observed.

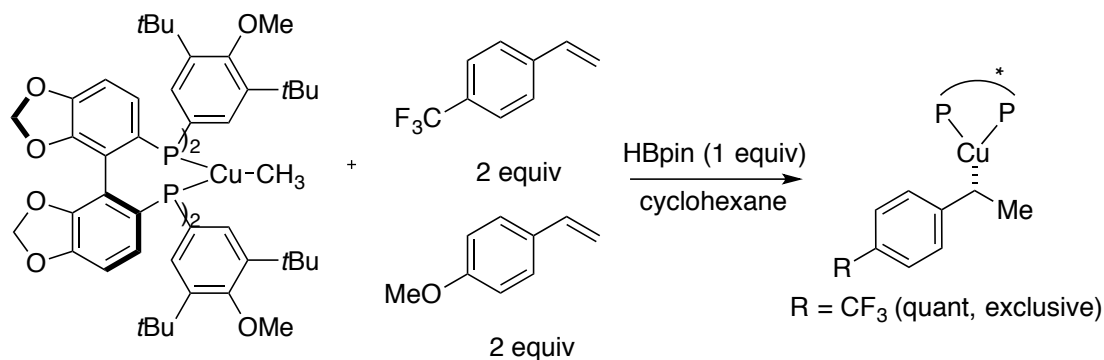
Reaction of (*S*)-DTBM-SEGPHOSCuCH₃ (**7**), **2** and HBpin



In a J-Young NMR tube, (*S*)-DTBM-SEGPHOSCuCH₃ (**7**) (12.6 mg, 0.0101 mmol) was dissolved in cyclohexane (350 μL). Solutions of **1** (25.0 μL , 0.400 M in cyclohexane) and HBpin (25.0 μL ,

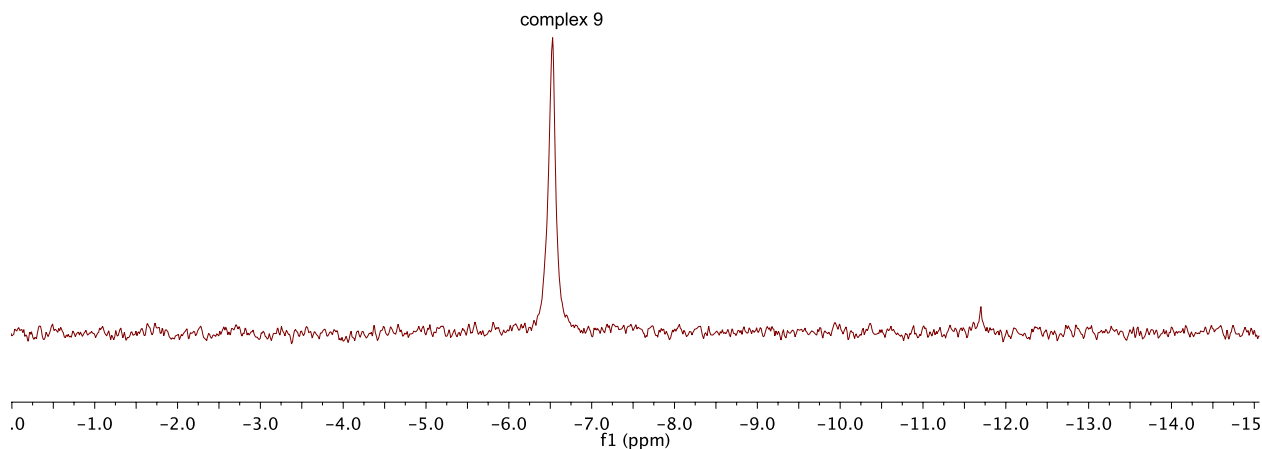
0.400 M in cyclohexane) were added. The NMR tube was capped and shaken. The sample was analyzed by ^{31}P NMR spectroscopy.

Competition experiment of 4-trifluoromethylstyrene and 4-vinylanisole for insertion



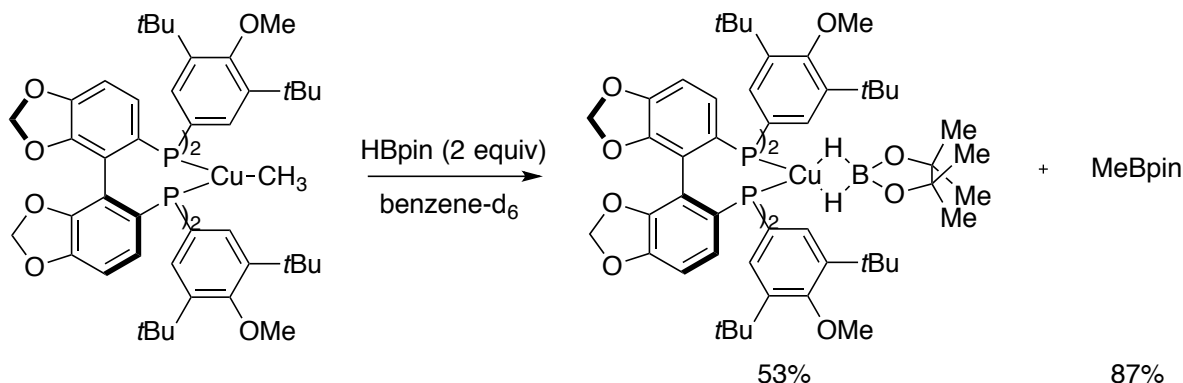
In a J-Young NMR tube, (*S*)-DTBM-SEGPHOSCuCH₃ (**7**) (12.6 mg, 0.0101 mmol) was dissolved in cyclohexane (225 μL). Solutions of 4-vinylanisole (50.0 μL , 0.400 M in cyclohexane), 4-trifluoromethylstyrene (50.0 μL , 0.400 M in cyclohexane), and 1,3-difluorobenzene (50 μL in cyclohexane) were added successively. A solution of HBpin in cyclohexane (25.0 μL , 0.400 M) was added. The NMR tube was capped and shaken. The sample was analyzed by ^{31}P and ^{19}F NMR spectroscopy.

Figure 3.10 $^{31}\text{P}\{^1\text{H}\}$ spectrum of the reaction mixture of methyl complex **7**, HBpin, 4-trifluoromethylstyrene, and 4-vinylanisole



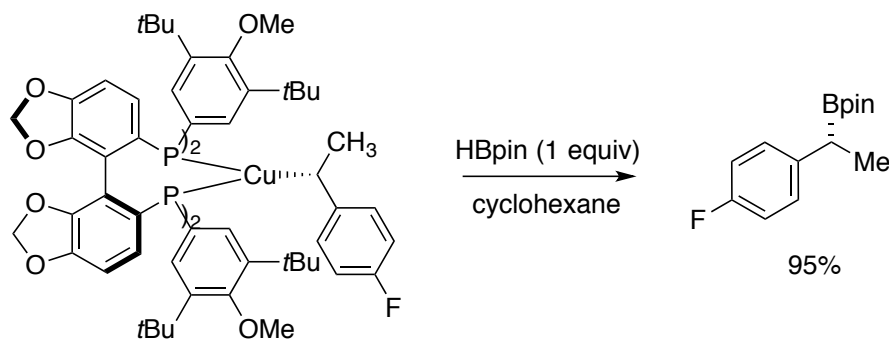
^{31}P NMR spectrum shows that complex **9** was formed exclusively.

Reaction of (*S*)-DTBM-SEGP₂HOSCuCH₃ with HBpin



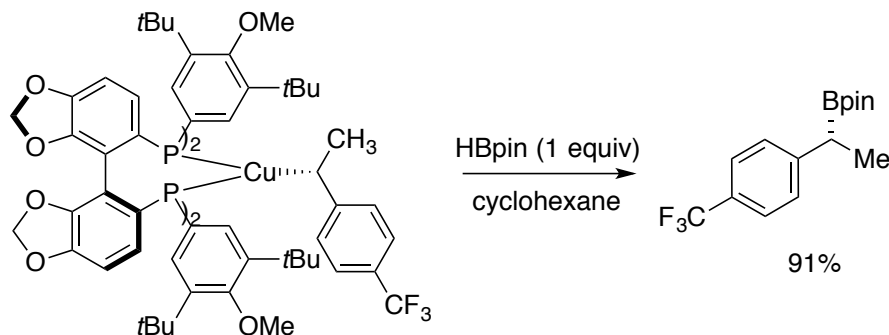
In a J-Young NMR tube, (*S*)-DTBM-SEGP₂HOSCuCH₃ (**7**) (12.6 mg, 0.0101 mmol) was dissolved in benzene-*d*₆ (300 μL). A benzene-*d*₆ solution of *p*-xylene (50.0 μL, 0.100 M) was added, followed by a benzene-*d*₆ solution of HBpin (20.0 μL, 0.0200 mmol, 1.00 M), each in one portion. The NMR tube was capped and shaken. The yields were determined by ¹H NMR spectroscopy.

Reaction of (*S*)-DTBM-SEGP₂HOSCuCHMe(4-F-C₆H₄) with HBpin



In a J-Young NMR tube, (*S*)-DTBM-SEGP₂HOSCuCH₃ (**7**) (25.2 mg, 0.0203 mmol) was dissolved in cyclohexane (200 μL). Solutions of 4-fluorostyrene (50.0 μL, 0.400 M in cyclohexane), 1,3-difluorobenzene (50.0 μL in cyclohexane), and HBpin (50.0 μL, 0.400 M in cyclohexane) were added subsequently. After the yield of **5** was determined by ¹⁹F NMR spectroscopy, a solution of HBpin (50.0 μL, 0.400 M in cyclohexane) was added. The sample was monitored by ³¹P and ¹⁹F NMR spectroscopy periodically.

After the reaction was complete, the solution was diluted with 2 mL of ethyl acetate and filtered through Celite. The volatile materials were removed by rotary evaporation, and the residue was dissolved in 1 mL THF. At 0 °C, a premixed solution of NaOH (2 M, aq)/30% H₂O₂ (2:1, 1.5 mL) was added. The reaction was warmed to room temperature and allowed to stir for 2.5 hours before adding water (2 mL) and ethyl acetate (5 mL). The phases were separated, and the organic phases were combined, dried over Na₂SO₄, and concentrated *in vacuo*. The crude sample was analyzed by HPLC with a chiral stationary phase.

Reaction of (*S*)-DTBM-SEGP₂HOSCuCHMe(4-CF₃-C₆H₄) with HBpin

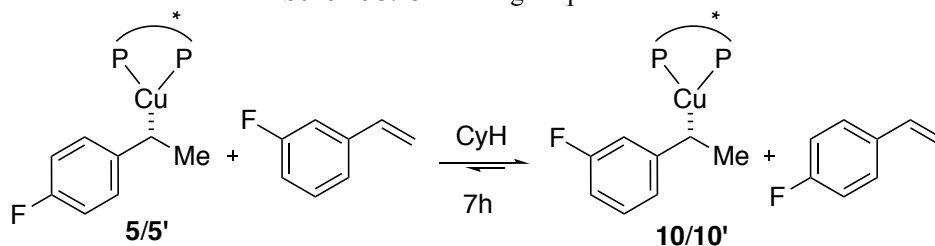
In a J-Young NMR tube, (*S*)-DTBM-SEGP₂HOSCuCH₃ (**7**) (25.2 mg, 0.0203 mmol) was dissolved in cyclohexane (200 μ L). Solutions of 4-trifluoromethylstyrene (50.0 μ L, 0.400 M in cyclohexane), 4-bromobenzotrifluoride (50 μ L in cyclohexane) as a ¹⁹F NMR internal standard, and HBpin (50.0 μ L, 0.400 M in cyclohexane) were added subsequently. After the yield was determined by ¹⁹F NMR spectroscopy, a solution of HBpin (50.0 μ L, 0.400 M in cyclohexane) was added. The sample was monitored by ³¹P and ¹⁹F NMR spectroscopy periodically.

Exchange experiments

The reaction of 4-fluorophenethylcopper complex **5** (formed in situ) and 1 equivalent of 3-fluorostyrene was monitored periodically by ¹⁹F and ³¹P NMR spectroscopy. After 10 minutes, 3-fluorophenethylcopper complex **10** was detected by ¹⁹F NMR spectroscopy. Complex **10** became the major copper species after 7 hours. The decrease in the concentration of **5** and 3-fluorostyrene corresponded to the increase in the concentration of **10** and 4-fluorostyrene. This result demonstrates that **5** reacts with 3-fluorostyrene to afford **10** and 4-fluorostyrene. The product (**10**) is likely formed from β -hydrogen elimination, dissociation of 4-fluorostyrene, coordination of 3-fluorostyrene, and migratory insertion. Analogous experiments were conducted with **10** (made in situ) and 4-fluorostyrene. Again, after 7 hours we observed both **5** and 3-fluorostyrene. However, **10** remained the major phenethylcopper species, suggesting that **10** is thermodynamically more stable than **5**. Because the decomposition of the phenethylcopper complexes occurs before the time required to reach the equilibrium, determination of the equilibrium constant was not possible.

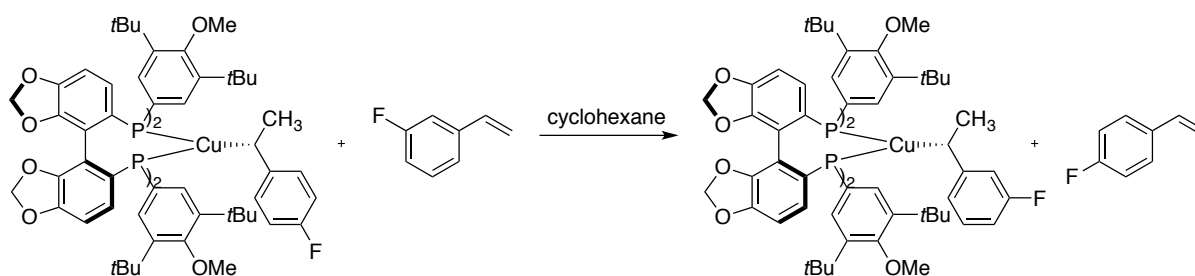
Similar observations were made about the reactions of 4-fluorophenethylcopper **5** and other styrenes, such as 2-fluorostyrene and 4-trifluoromethylstyrene. In all cases, the experiments indicated that phenethylcopper complex containing electron-deficient phenethyl groups are more thermodynamically stable than phenethylcopper complexes containing electron-rich phenethyl groups.

Scheme 3.23 Exchange experiments



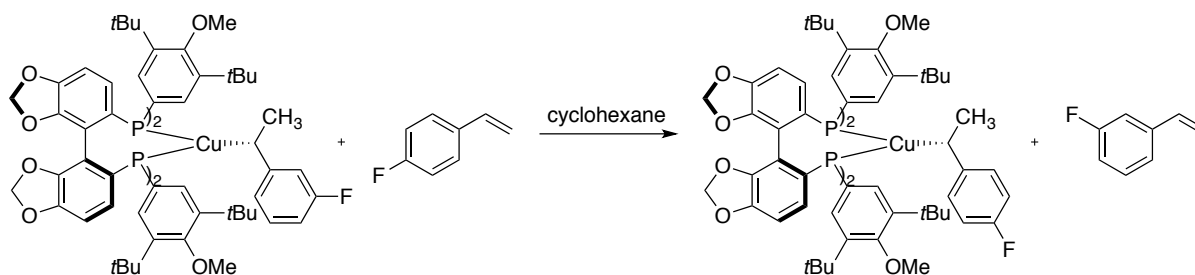
reaction direction	[5/5']	[4-F-styrene]	[10/10']	[3-F-styrene]
left to right	0.0040 M	0.0248 M	0.0204 M	0.0172 M
right to left	0.0036 M	0.0332 M	0.0244 M	0.0054 M

Procedures: reaction of (*S*)-DTBM-SEGP₂HOSCuCHMe(4-F-C₆H₄) with 3-fluorostyrene



In a J-Young NMR tube, (*S*)-DTBM-SEGP₂HOSCuCH₃ (**7**) (25.2 mg, 0.0203 mmol) was dissolved in cyclohexane (300 μL). Solutions of 4-fluorostyrene (50.0 μL, 0.400 M in cyclohexane), 1,3-difluorobenzene (50.0 μL in cyclohexane), and HBpin (50.0 μL, 0.400 M in cyclohexane) were added subsequently. After the yield of **5** was determined by ¹⁹F NMR spectroscopy, a solution of 3-fluorostyrene (50.0 μL, 0.400 M in cyclohexane) was added. The sample was monitored by ³¹P and ¹⁹F NMR spectroscopy periodically.

Procedures: reaction of (*S*)-DTBM-SEGP₂HOSCuCHMe(3-F-C₆H₄) with 4-fluorostyrene

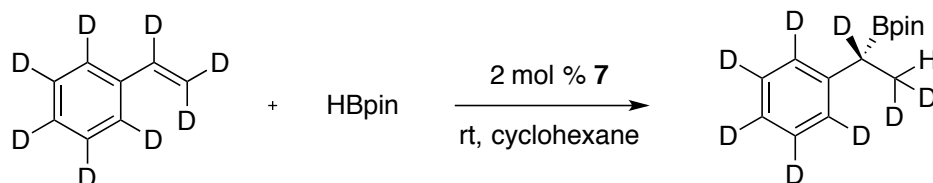


In a J-Young NMR tube, (*S*)-DTBM-SEGP₂HOSCuCH₃ (**7**) (25.2 mg, 0.0203 mmol) was dissolved in cyclohexane (300 μL). Solutions of 3-fluorostyrene (50.0 μL, 0.400 M in cyclohexane),

1,3-difluorobenzene (50 μL in cyclohexane), and HBpin (50.0 μL , 0.400 M in cyclohexane) were added subsequently. After the yield of **10** was determined by ^{19}F NMR spectroscopy, a solution of 4-fluorostyrene (50.0 μL , 0.400 M in cyclohexane) was added. The sample was monitored by ^{31}P and ^{19}F NMR spectroscopy periodically.

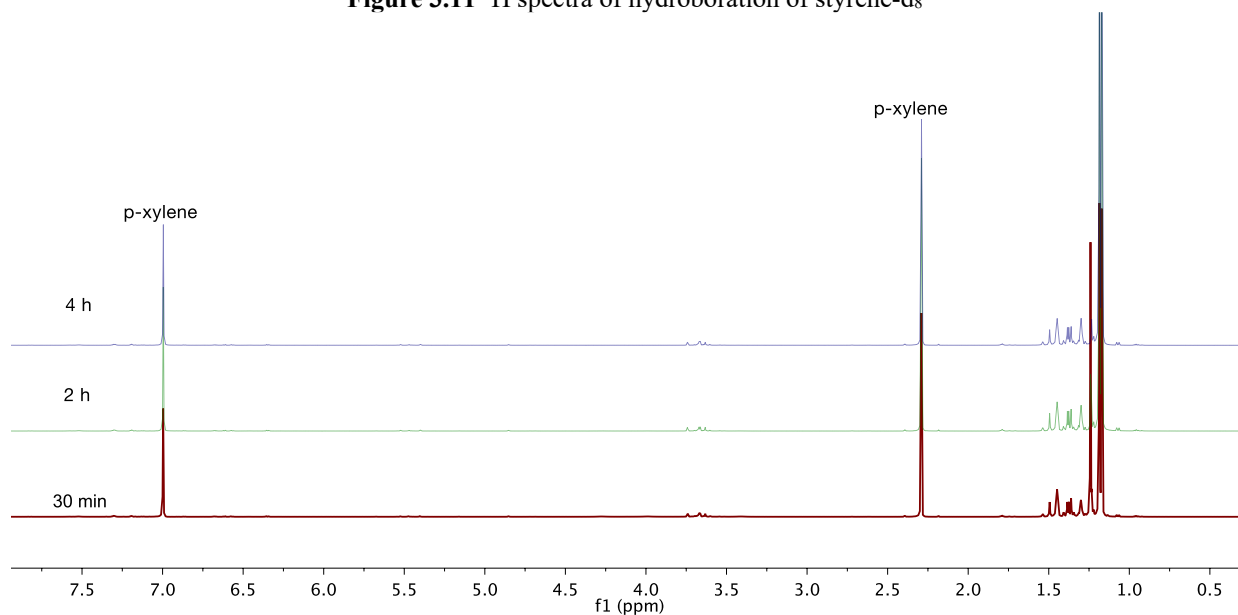
3.4.4 Stereochemistry of Hydroboration

Hydroboration of styrene- d_8 catalyzed by (*S*)-DTBM-SEGPLHOSCuCH₃ (**7**)

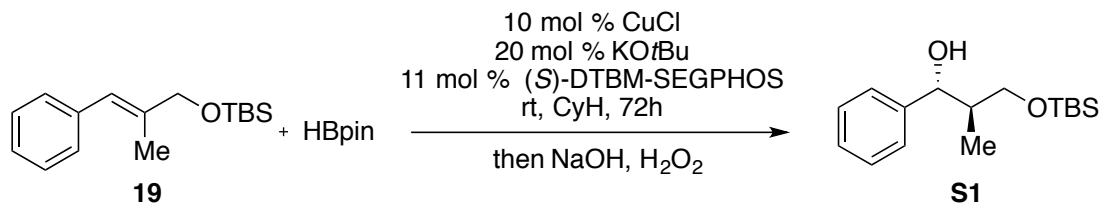


Into a J-Young NMR tube, were added (*S*)-DTBM-SEGPLHOSCuCH₃ (**7**) (2.5 mg, 0.0020 mmol, 2 mol %), styrene- d_8 (11.5 μL , 0.100 mmol), and *p*-xylene (5 μL), followed by cyclohexane- d_{12} (370 μL). HBpin (14.5 μL , 0.100 mmol) was then added, and the reaction was monitored by ^1H NMR spectroscopy periodically. Another reaction with cyclohexane as the solvent and THF- d_8 as an internal standard was monitored by ^1H and ^2H NMR spectroscopy periodically. The experiment was also repeated with 8 equivalent of styrene- d_8 .

Figure 3.11 ^1H spectra of hydroboration of styrene- d_8



The ^1H NMR spectra show that the incorporation of hydrogen atoms into styrene- d_8 did not occur.

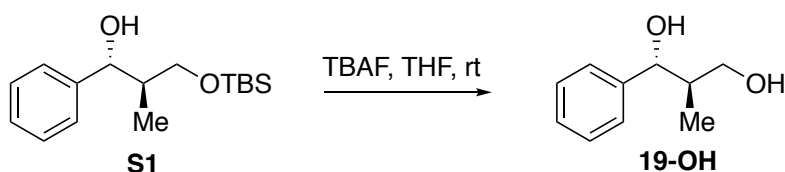
Hydroboration of trisubstituted alkene **19**

A 1-dram vial was charged with CuCl (4.0 mg, 10 mol %), KO t Bu (8.8 mg, 20 mol %), (S)-DTBM-SEGPHOS (52.8 mg, 11 mol %) and cyclohexane (400 μ L). The mixture was allowed to stir at ambient temperature for 3 minutes before the addition of pinacolborane (71 μ L, 0.48 mmol). To the solution was added **19** (105 mg, 0.400 mmol), which was pre-weighed in another vial. The second vial was then washed four times with 100 μ L cyclohexane each time. After 72 h of stirring at rt, the reaction vial was diluted with 2 mL of ethyl acetate, and the resulting solution was filtered through Celite. The crude material was concentrated *in vacuo* and purified by flash column chromatography (CombiFlash, 5% ethyl acetate in hexanes) to afford an inseparable mixture that consisted of **19** and the product.

In a 20-mL scintillation vial the above mixture was dissolved in 2 mL of THF. The vial was cooled in an ice bath and a premixed solution of NaOH (2 M, aq.)/30% H₂O₂ (2:1, 3 mL) was added. The reaction was warmed to rt and allowed to stir for 3 hours before the addition of water (5 mL) and ethyl acetate (5 mL). The phases were separated, and the aqueous layer was extracted twice with 5 mL of ethyl acetate. The organic phases were combined, dried over Na₂SO₄, and concentrated *in vacuo*. Alcohol **S1** was purified by preparative TLC (10% ethyl acetate in hexanes) and obtained as a colorless liquid in 45% yield (50.5 mg, 0.180 mmol).

¹H NMR (600 MHz, CDCl₃) δ 7.39 – 7.31 (m, 4H), 7.31 – 7.21 (m, 1H), 4.58 (d, J = 7.4 Hz, 1H), 4.45 (br s, 1H), 3.79 (dd, J = 10.0, 3.8 Hz, 1H), 3.63 (dd, J = 10.1, 7.3 Hz, 1H), 2.03 – 1.95 (m, 1H), 0.95 (s, 10H), 0.75 (d, J = 7.0 Hz, 3H), 0.12 (s, 6H).

¹³C NMR (151 MHz, CDCl₃) δ 143.62, 128.06, 127.21, 126.60, 79.89, 68.09, 41.30, 25.80, 18.10, 13.89, -5.60, -5.68.



A 1-dram vial was charged with **S1** (9.8 mg, 0.035 mmol) and THF (300 μ L). To the mixture was added TBAF (100 μ L, 1.0 M in THF), and the resulting solution was allowed to stir at ambient temperature for 4 hours. Water (5 mL) and ethyl acetate (5 mL) were added. The phases were separated, and the aqueous layer was extracted twice with 5 mL of ethyl acetate. The organic phases were combined, dried over Na₂SO₄, and concentrated *in vacuo*. The pure diol was purified by preparative TLC (50% ethyl acetate in hexanes) and obtained as a colorless liquid in 72% yield (4.2 mg, 0.025 mmol).

¹H NMR (500 MHz, CDCl₃) δ 7.40 – 7.35 (m, 4H), 7.34 – 7.30 (m, 1H), 4.56 (d, J = 8.4 Hz, 1H), 3.85 – 3.64 (m, 2H), 3.02 (br s, 1H), 2.99 (br s, 1H), 2.08 (dtd, J = 8.2, 7.0, 3.5 Hz, 1H), 0.72 (d, J = 7.0 Hz, 3H).

$[\alpha]_{\text{D}}^{23} = +49.5$ (c = 0.42, CHCl₃).

The relative configuration of the stereogenic centers was established by comparing the ^1H NMR spectra with NMR data in the literature.^{82,83} All chemical shifts matched those reported. The characteristic coupling constant (8.4 Hz) for the proton resonance at 4.56 ppm (the benzylic methine) indicates an *anti* configuration; the coupling constant for the ^1H NMR signal at 4.94 ppm for the benzylic methine of the *syn* isomer is 3.9 Hz.⁸⁴

The absolute configuration was confirmed by comparing the optical rotation to the value reported previously for (2*R*,3*R*)-2-Methyl-1-phenylpropane-1,3-diol.

$$[\alpha]_{\text{D}}^{24} = +35.17 \text{ (c = 0.34, CHCl}_3\text{)}^{82}$$

$$[\alpha]_{\text{D}}^{20} = +50 \text{ (c = 0.5, CHCl}_3\text{)}^{83}$$

3.4.5 Kinetic Studies

Procedure for kinetic studies of the hydroboration of vinylarene **1**

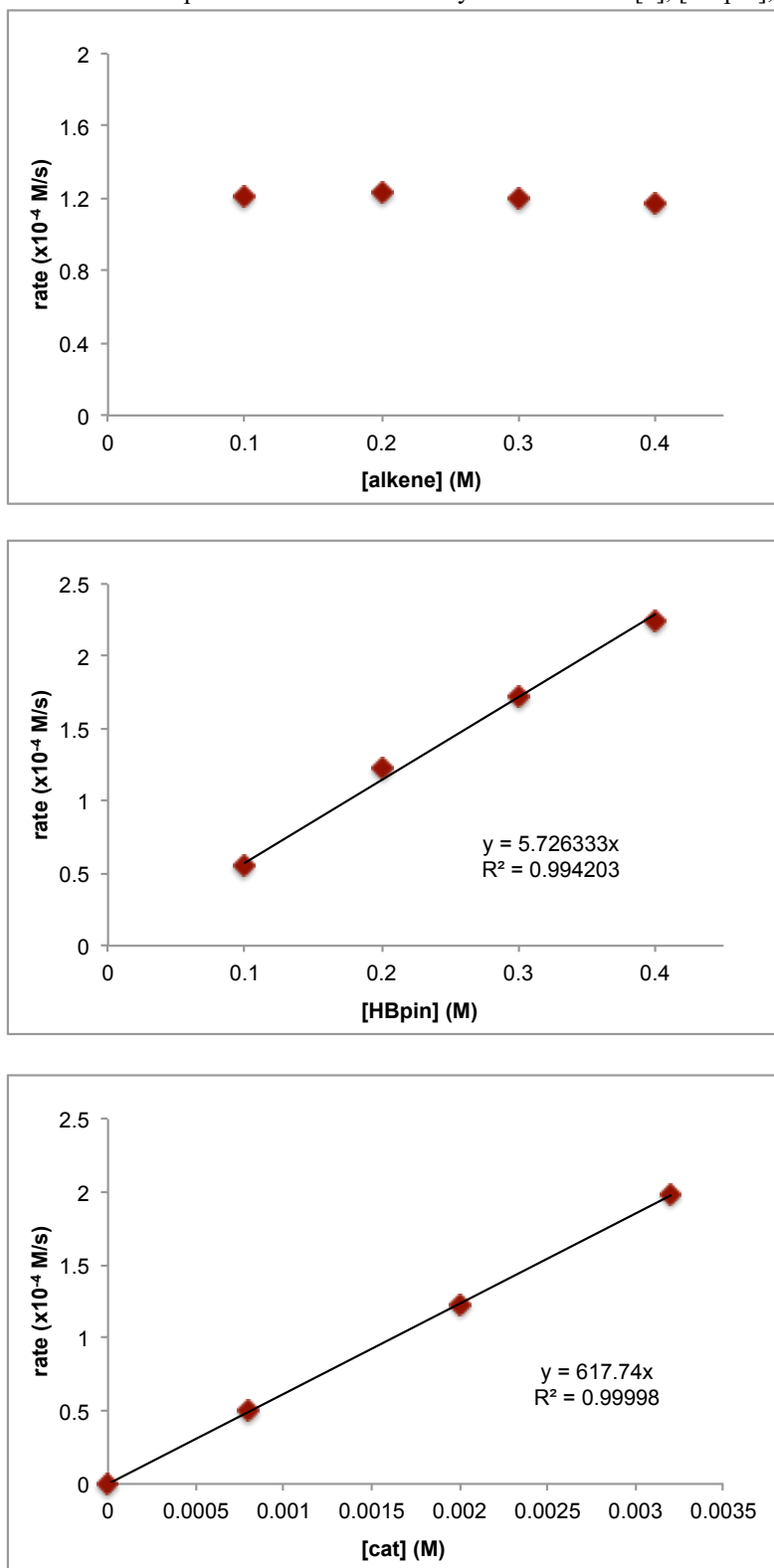
In an argon-filled glove box, a 4 mL vial was charged with alkene **1** (0.0500-0.200 mmol) as a solution in cyclohexane (2.00 M), dodecane (10.0 μL , 0.0440 mmol), complex **7** (0.400-1.60 μmol) as a solution in cyclohexane (0.0400 M), and cyclohexane (enough to bring total volume to 500 μL). HBpin (0.0500-0.300 mmol) as a solution in cyclohexane (2.00 M) was added to the vial to initiate the reaction. At various time points, aliquots were removed from the mixture and analyzed by gas chromatography.

From the chromatograms, the initial rate of the formation of **3** was calculated. The initial rates of formation of **3** for reactions conducted with various concentrations of **1**, complex **7**, and HBpin are tabulated in Table 3.1.

Table 3.1 Initial rates for hydroboration of **1**

entry	[1]/M	[HBpin]/M	[7]/M	initial rate (M/s)
1	0.200	0.200	0.00200	1.2×10^{-4}
2	0.100	0.200	0.00200	1.2×10^{-4}
3	0.300	0.200	0.00200	1.2×10^{-4}
4	0.400	0.200	0.00200	1.2×10^{-4}
5	0.200	0.100	0.00200	5.6×10^{-5}
6	0.200	0.300	0.00200	1.7×10^{-4}
7	0.200	0.400	0.00200	2.3×10^{-4}
8	0.200	0.200	0.00080	5.0×10^{-5}
9	0.200	0.200	0.00320	2.0×10^{-4}

The kinetic dependence of the initial rates on the concentrations of **1**, complex **7**, and HBpin are summarized in Figure 3.12.

Figure 3.12 Kinetic dependence of the rates of hydroboration on [1], [HBpin], and [7]

Procedure for kinetic studies on the hydroboration of internal alkene 2

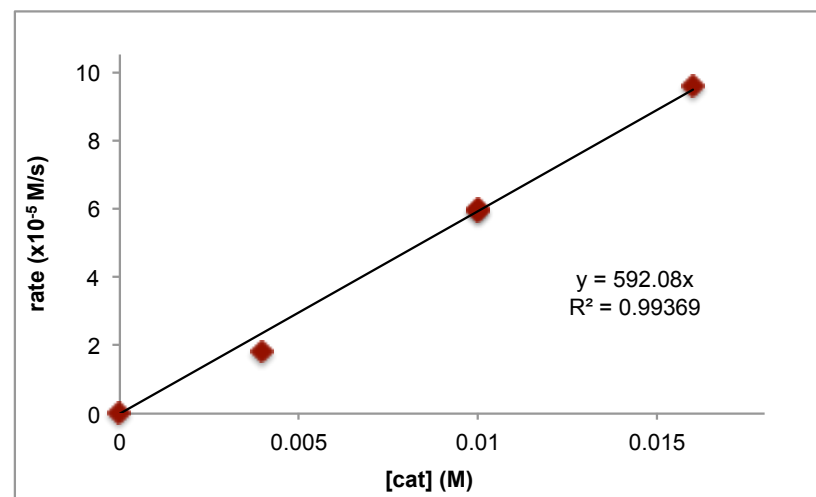
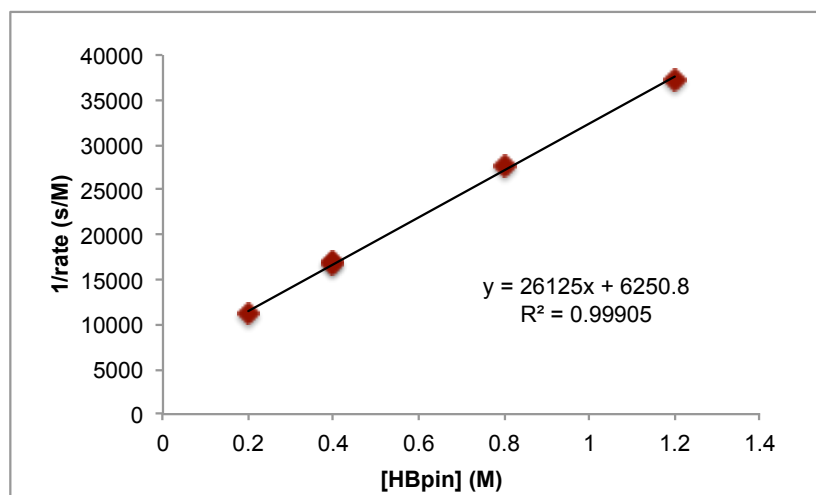
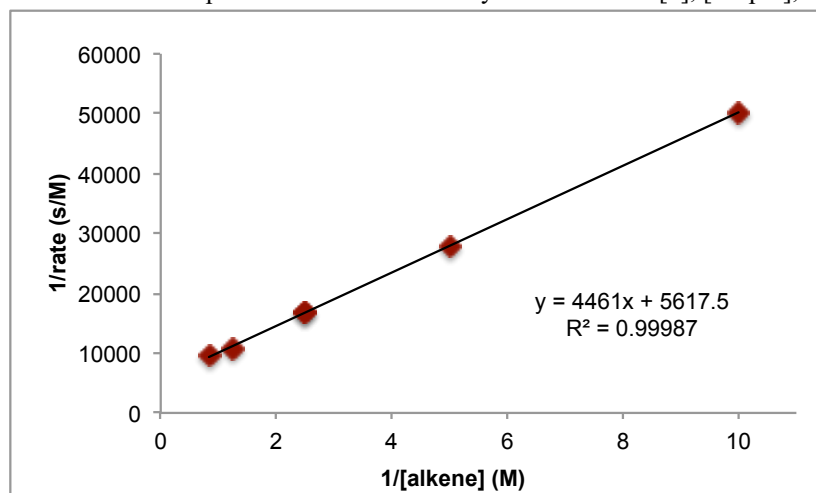
In an argon-filled glove box, a 4 mL vial was charged with alkene **2** (0.0250-0.300 mmol) as a solution in cyclohexane (2.00 M), dodecane (10.0 μL , 0.0440 mmol), complex **7** (0.050-0.200 mmol) as a solution in cyclohexane (0.100 M), and cyclohexane (enough to bring total volume to 250 μL). HBpin (0.0500-0.300 mmol) as a solution in cyclohexane (2.00 M) was added to the vial to initiate the reaction. At various time points, aliquots were removed from the mixture and analyzed by gas chromatography.

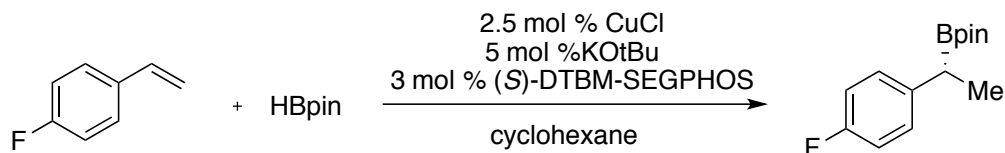
From the chromatograms, the initial rate of formation of **4** was calculated. The initial rates of formation of **4** for reactions conducted with various concentrations of **2**, complex **7**, and HBpin are tabulated in Table 3.2.

Table 3.2 Initial rates for hydroboration of **2**

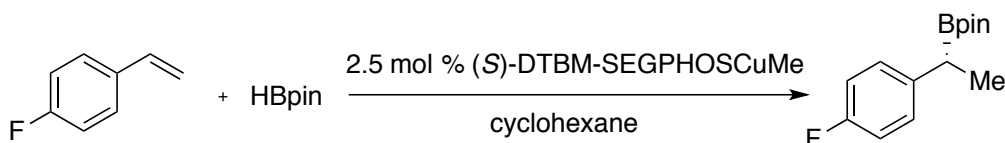
entry	[1]/M	[HBpin]/M	[7]/M	initial rate (M/s)
1	0.400	0.400	0.0100	6.0×10^{-5}
2	0.400	0.400	0.0100	5.9×10^{-5}
3	0.200	0.400	0.0100	3.6×10^{-5}
4	0.100	0.400	0.0100	2.0×10^{-5}
5	0.800	0.400	0.0100	9.2×10^{-5}
6	1.20	0.400	0.0100	1.1×10^{-4}
7	0.400	0.800	0.0100	3.6×10^{-5}
8	0.400	1.20	0.0100	2.7×10^{-5}
9	0.400	0.200	0.0100	9.0×10^{-5}
10	0.400	0.400	0.00400	1.8×10^{-5}
11	0.400	0.400	0.0160	9.6×10^{-5}

Kinetic dependence of the initial rates on the concentrations of **2**, complex **7**, and HBpin are summarized in Figure 3.13.

Figure 3.13 Kinetic dependence of the rates of hydroboration on [2], [HBpin], and [7]

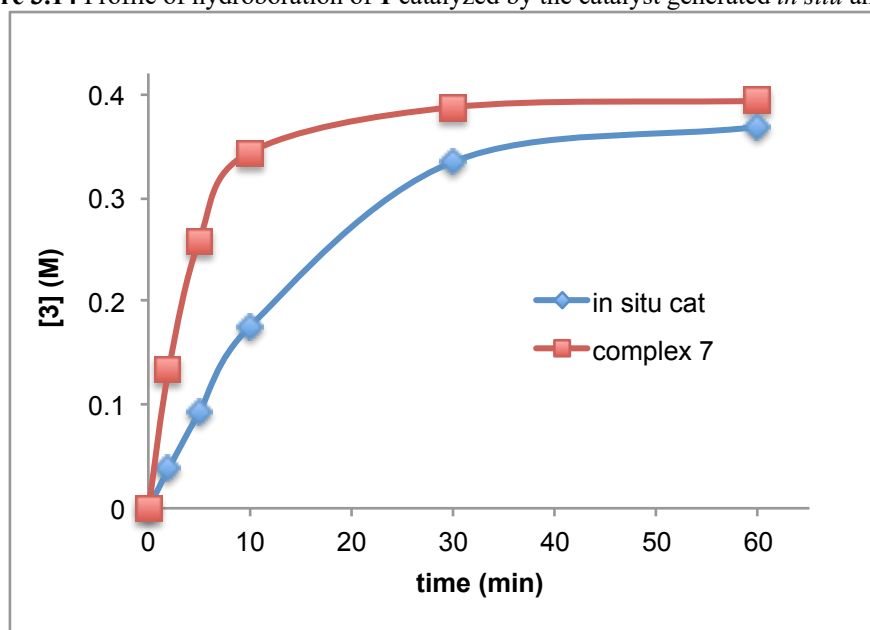
Monitoring hydroboration of **1** with HBpin catalyzed by Cu/(*S*)-DTBM-SEGPHOS

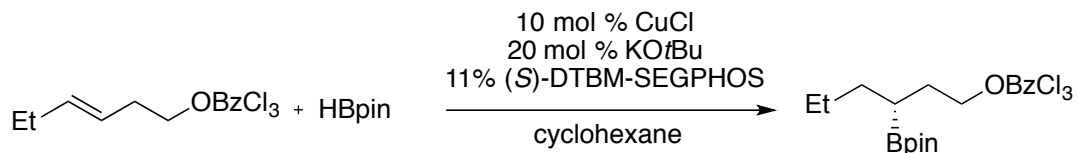
In an argon-filled glove box, a 4 mL vial was charged with CuCl (1.0 mg, 2.5 mol %), KOtBu (2.2 mg, 5 mol %), (*S*)-DTBM-SEGPHOS (14.2 mg, 3 mol %), dodecane (40.0 μ L, 0.176 mmol), and cyclohexane (400 μ L). The mixture was allowed to stir at rt for 3 minutes before the addition of HBpin (61.0 μ L, 0.420 mmol). Alkene **1** (48.0 μ L, 0.402 mmol) and cyclohexane (451 μ L) was added to the vial to initiate the reaction. At various time points, aliquots were removed from the mixture and analyzed by gas chromatography.



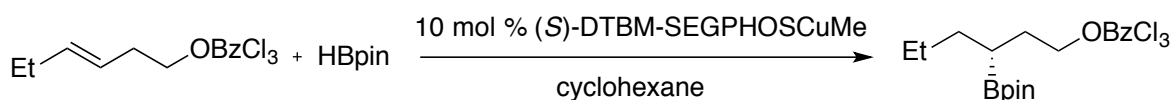
In an argon-filled glove box, a 4 mL vial was charged with complex **7** (12.6 mg, 10 mol %), dodecane (10.0 μ L, 0.0440 mmol), alkene **1** (48.0 μ L, 0.402 mmol) and cyclohexane (851 μ L). HBpin (61.0 μ L, 0.420 mmol) was added to the vial to initiate the reaction. At various time points, aliquots were removed from the mixture and analyzed by gas chromatography. The yield was 98%, and the ee was 98%.

Figure 3.14 Profile of hydroboration of **1** catalyzed by the catalyst generated *in situ* and by **7**



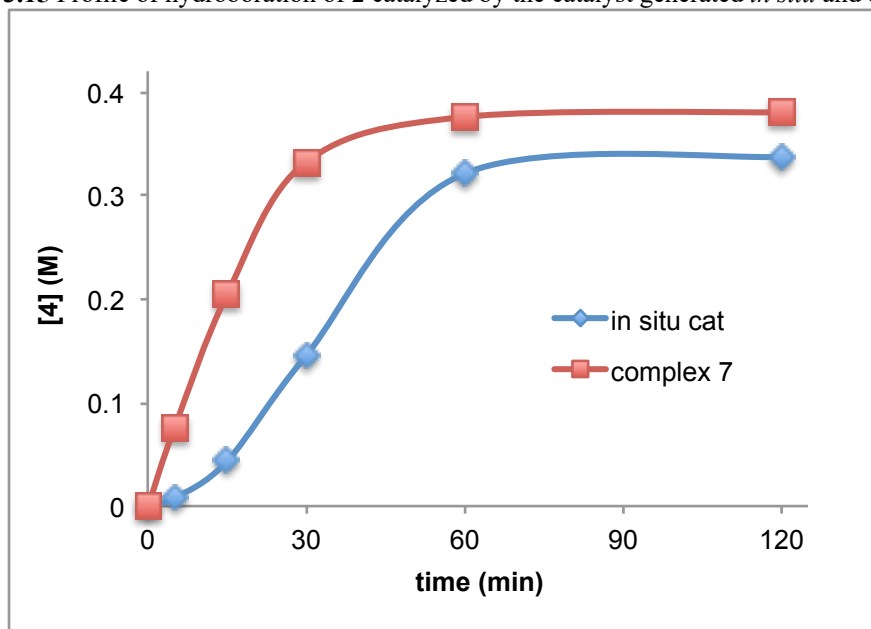
Monitoring hydroboration of **2** with HBpin catalyzed by Cu/(*S*)-DTBM-SEGPHOS

In an argon-filled glove box, a 4 mL vial was charged with CuCl (1.0 mg, 10 mol %), KO t Bu (2.2 mg, 20 mol %), (*S*)-DTBM-SEGPHOS (13.2 mg, 11 mol %), dodecane (10.0 μ L, 0.0440 mmol), and cyclohexane (130 μ L). The mixture was allowed to stir at rt for 3 minutes before addition of HBpin (60.0 μ L, 0.120 mmol) as a solution in cyclohexane (2.00 M). Alkene **2** (50.0 μ L, 0.100 mmol) as a solution in cyclohexane (2.00 M) and cyclohexane (130 μ L) were added to the vial to initiate the reaction. At various time points, aliquots were removed from the mixture and analyzed by gas chromatography.

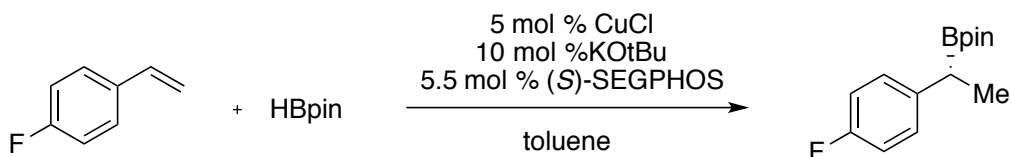


In an argon-filled glove box, a 4 mL vial was charged with complex **7** (12.6 mg, 10 mol %), dodecane (10.0 μ L, 0.0440 mmol), alkene **2** (50.0 μ L, 0.100 mmol) as a solution in cyclohexane (2.00 M) and cyclohexane (130 μ L). HBpin (60.0 μ L, 0.120 mmol) as a solution in cyclohexane (2.00 M) was added to the vial to initiate the reaction. At various time points, aliquots were removed from the mixture and analyzed by gas chromatography. The yield was 96%, and the ee was 95%.

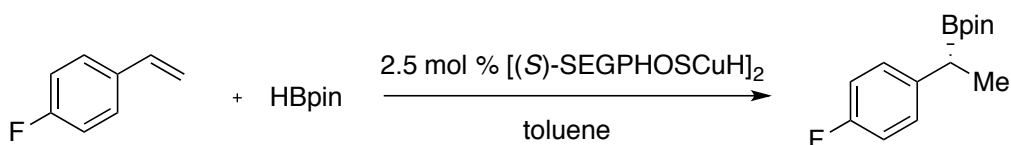
Figure 3.15 Profile of hydroboration of **2** catalyzed by the catalyst generated *in situ* and by pure **7**



Monitoring hydroboration of **1** with HBpin catalyzed by Cu/(*S*)-SEGPHOS



In an argon-filled glove box, a 4 mL vial was charged with CuCl (2.0 mg, 5 mol %), KOtBu (4.4 mg, 10 mol %), (*S*)-SEGPHOS (13.3 mg, 11 mol %), dodecane (10.0 μ L, 0.0440 mmol), and toluene (400 μ L). The mixture was allowed to stir for 5 min before the addition of HBpin (64.0 μ L, 0.441 mmol, 1.1 equiv) and alkene **1** (48 μ L, 0.40 mmol). At various time points, aliquots were removed from the mixture and analyzed by gas chromatography.

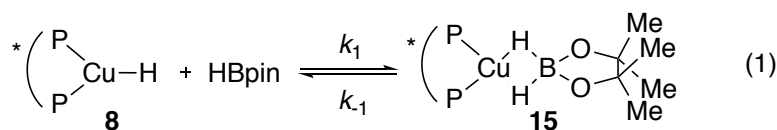


In an argon-filled glove box, a 4 mL vial was charged with SEGPHOS-ligated complex **27** (13.5 mg, 2.5 mol %, 5 mol % per Cu), dodecane (10.0 μ L, 0.0440 mmol), HBpin (64.0 μ L, 0.441 mmol, 1.1 equiv) and alkene **1** (48.0 μ L, 0.402 mmol) and toluene (400 μ L). At various time points, aliquots were removed from the mixture and analyzed by gas chromatography.

3.4.6 2D ^{11}B -EXSY Study of the Equilibrium of Dihydridoborate **15** and HBpin

2D ^{11}B -EXSY⁴ spectra were collected on a Bruker AV-600 spectrometer. The temperature was maintained at $-10\text{ }^\circ\text{C}$ throughout the experiment. To determine the exchanges rates, EXSY experiments were conducted with a mixing time of 3 ms. The reference spectra were obtained with a mixing time of 0 ms. The experiment was repeated at different [HBpin].

The areas of the peaks were determined by integration. From these numbers, the exchange rate matrices and the magnetization exchange rate constants (k_1' and k_{-1}') were calculated by EXSY CALC program.⁵ The magnetization exchange rate constants were converted to the chemical exchange rate constants (k_1 and k_{-1}) by the following equations.



$$k_1 = k_1' / [\text{HBpin}] \quad (2)$$

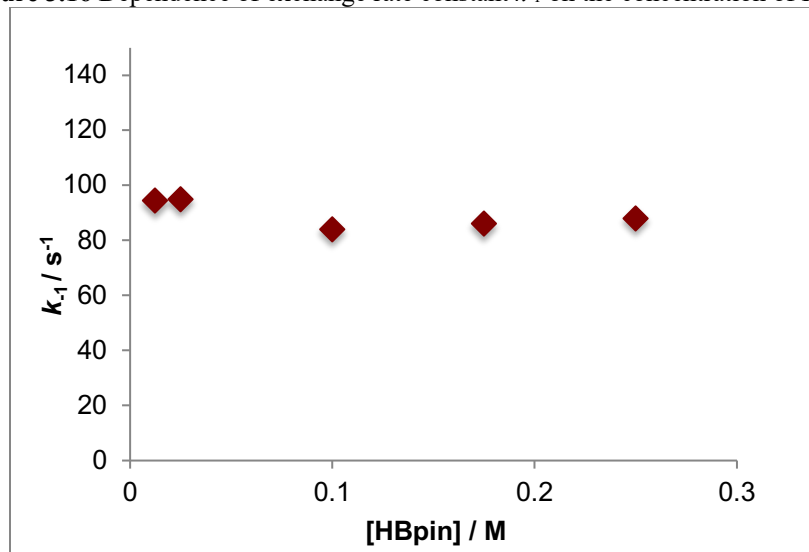
$$k_{-1} = k_{-1}' \quad (3)$$

The magnetization exchange rate constants are tabulated in Table S3.

Table 3.3 Magnetization exchange rate constants at different [HBpin] calculated by EXSY CALC

[HBpin]	k_1' (s ⁻¹)	k_{-1}' (s ⁻¹)
0.0125	61.6	94.4
0.0250	57.1	94.8
0.100	16.2	84.0
0.175	10.7	86.1
0.250	5.8	87.8

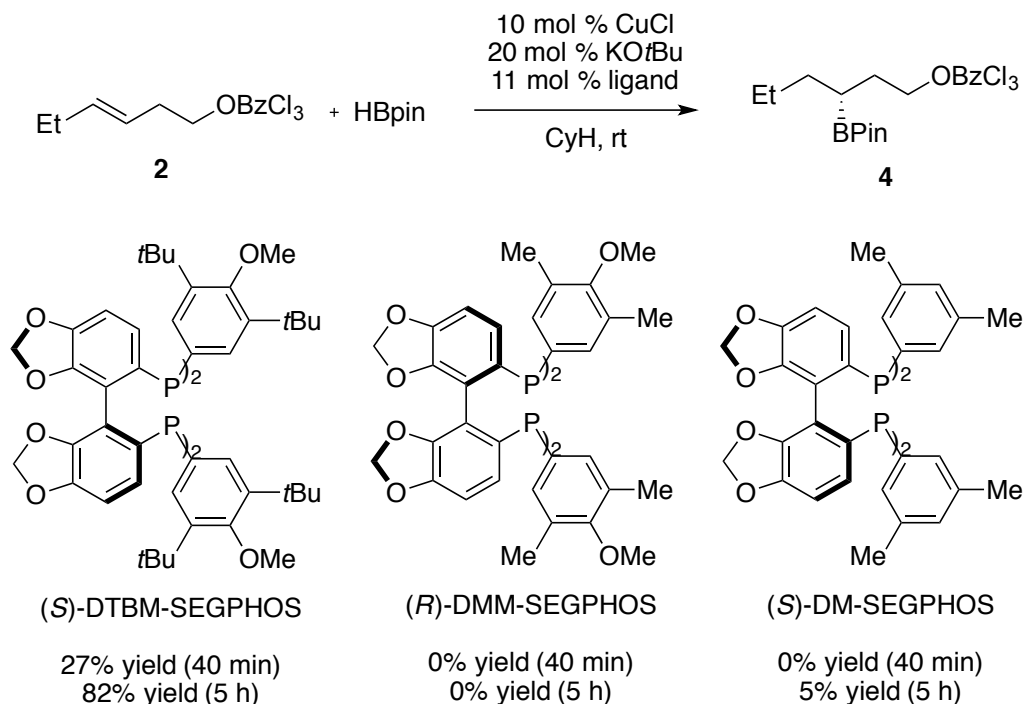
A zero-order dependence of the exchange rate constant (k_{-1}) on the concentrations of HBpin was established by plotting k_{-1} against [HBpin], as shown in Figure 3.16.

Figure 3.16 Dependence of exchange rate constant k_{-1} on the concentration of HBpin

Representative procedure for sample preparation:

In a screw-capped NMR tube, (*S*)-DTBM-SEGPHOSCuCH₃ (**7**) (12.6 mg, 0.0101 mmol) was dissolved in toluene-*d*₈ (enough to make a total volume of 400 μL). The NMR tube was capped, removed from the glovebox and placed in a dry ice/acetone bath. A toluene-*d*₈ solution of HBpin (100 μL, 0.0400 mmol, 0.400 M) was added in one portion. The tube was shaken to ensure proper mixing and then inserted into an NMR instrument pre-cooled at -10 °C.

3.4.7 Effect of Ligand Steric Properties on the Hydroboration of Internal Alkene 2

**Experimental procedure:**

In an argon-filled glove box, a 4 mL vial was charged with CuCl (2.0 mg, 10 mol %), KOtBu (4.4 mg, 10 mol %), ligand (11 mol %), dodecane (20.0 μ L, 0.0880 mmol), and cyclohexane (160 μ L). The mixture was allowed to stir at rt for 3 minutes before addition of HBpin (120 μ L, 0.240 mmol) as a solution in cyclohexane (2.00 M). Alkene **2** (100 μ L, 0.200 mmol) as a solution in cyclohexane (2.00 M) was added to the vial to initiate the reaction. At various time points, aliquots were removed from the mixture and analyzed by gas chromatography.

3.4.8 Computational Details**General Remarks**

DFT calculations were conducted at the Molecular Graphics and Computation Facility at the University of California, Berkeley. Unless otherwise noted, geometry optimizations were performed with the B3LYP functional with Gaussian 09 revision D01 package. SDD and 6-31G(d) basis sets were used for Cu and all other atoms, respectively. Single-point energies were calculated with the M06 functional. SDD and 6-311+G(d,p) basis sets were used for Cu and all other atoms, respectively. The SMD model was used for solvent corrections. Frequency calculations were also conducted with the optimized geometries to confirm that the stationary points were minima (zero imaginary frequencies) or transition states (one imaginary frequency). IRC calculations were conducted for important transition states to ensure that those are linked to proper starting materials and products. The structures were generated using CYLView.

Summary of electronic energies of all computed structures

Electronic energies of all computed structures are summarized in Table 3.4, which include zero-point energies, enthalpies, free energies, thermal corrections to enthalpies, and free energies, and single-point energies corrected with the SMD model. Imaginary frequencies are also included for all the transition states.

Table 3.4 Summary of electronic energies of calculated structures with DTBM-SEGPBOS as the ligand^a

	E	H	G	H _{corr}	G _{corr}	E(SMD)	imaginary frequency
8	- 4360.796451	- 4360.701812	- 4360.931044	1.698341	1.469109	- 4360.917267	-
13-TS	- 4670.281882	- 4670.180113	- 4670.422261	1.841272	1.599123	- 4670.399011	- 799.27
13'-TS	- 4670.278835	- 4670.177491	- 4670.419211	1.841579	1.599858	- 4670.394369	- 750.35
13-I-TS	- 4670.275714	- 4670.173983	- 4670.418862	1.840728	1.59585	- 4670.388258	- 818.52
14	- 4670.324731	- 4670.222436	- 4670.468488	1.846479	1.600427	- 4670.439344	-
14'	- 4670.326699	- 4670.224496	- 4670.469802	1.846591	1.601285	- 4670.443523	-
14-I	- 4670.321417	- 4670.219067	- 4670.467989	1.846312	1.59739	- 4670.429488	-
20-TS	- 5081.961915	- 5081.850075	- 5082.110248	2.049762	1.789589	-5082.15288	- 190.50
20'-TS	- 5081.960773	- 5081.848873	- 5082.109191	2.049765	1.789447	- 5082.158224	- 180.48
20-I-TS	- 5081.981417	-5081.86902	- 5082.134474	2.048864	1.783409	- 5082.157628	- 208.06
21	-721.231672	-721.213494	-721.277035	0.34824	0.2847	- 721.2403754	-
22	-721.232787	-721.214646	-721.279728	0.348148	0.283066	- 721.2410909	-
15	- 4772.479959	- 4772.375084	- 4772.623574	1.903874	1.655384	- 4772.661129	-
23-TS	- 4517.876509	- 4517.776304	- 4518.014518	1.814634	1.576419	- 4518.041636	- 831.92
24	- 4517.919045	- 4517.818422	- 4518.060841	1.819978	1.577559	- 4518.078461	-
25-TS	- 4929.570483	- 4929.459973	- 4929.717952	2.023146	1.765167	- 4929.803601	- 172.13
26	-568.831615	-568.815135	-568.874067	0.321916	0.262984	- 568.8934795	-
sty-rene	-309.514545	-309.50683	-309.546034	0.141426	0.102221	- 309.4764362	-
HBpin	-411.679090	-411.668611	-411.712239	0.201943	0.158315	- 411.7145532	-

<i>trans</i> -2-butene	-157.118418	-157.112008	-157.145812	0.114902	0.081098	- 157.1334841	-
23-TS-1-propene	- 4478.594876	- 4478.496221	- 4478.731915	1.784950	1.549256	- 4478.749606	- 813.05
23-TS-b-propene	- 4478.589200	- 4478.490448	- 4478.725601	1.784931	1.549778	- 4478.743765	- 875.81
propene	-117.827483	-117.822462	-117.852487	0.085096	0.055071	- 117.8370391	-

^aSingle-point energies were corrected with a SMD solvation model in cyclohexane. Unit for electronic energies is Hartree and unit for imaginary frequencies is cm⁻¹.

DFT Study on the Structure of Complex 27

Various DFT functionals were examined to reproduce the structure of complex **27** determined by single-crystal X-ray diffraction. The calculations were performed with Gaussian 09 revision D01 package. In all cases, SDD and 6-31G(d) basis sets were used for Cu and all other atoms, respectively. The results are summarized in Table 3.6. Calculations with PBE and BP86 as the functionals provided the most consistent results for the Cu-Cu bond length and averaged P-Cu-P bond angle, but the calculated dihedral angle of the ligand deviated from that determined by the x-ray study. A small difference was observed between the Cu-Cu bond length and P-Cu-P bond angles determined by x-ray and those calculated with B3LYP-D3 and M06 functionals, but good agreement between the dihedral angle of the ligand from X-ray and calculations with B3LYP-D3 and M06 functionals. Calculations with all the functionals showed that the copper center adopts a tetrahedral geometry with a Cu-H bond length of 1.73(1) Å.

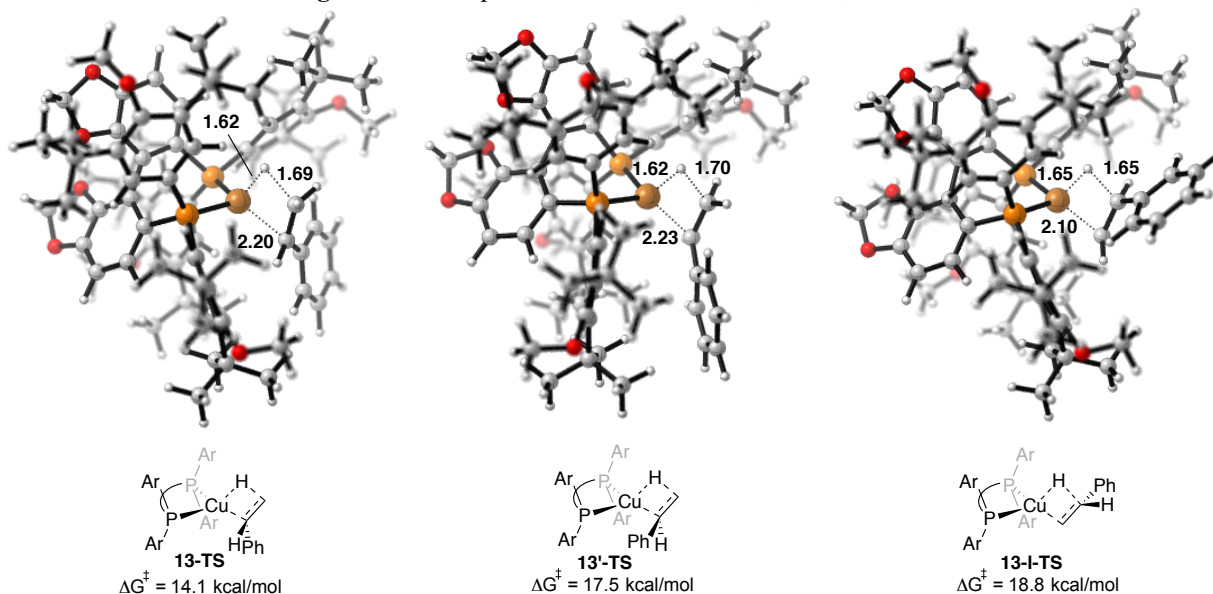
Table 3.6. DFT calculation results for complex **27**

DFT functional	Cu-Cu (Å)	averaged P-Cu-P (°)	P-averaged ligand dihedral angle (°)	Averaged Cu-H (Å)	Geometry at copper center
x-ray structure	2.374	101.4	80.0	-	-
B3LYP-D3	2.324	102.6	79.4	1.73	tetrahedral
M06	2.343	102.4	79.9	1.74	tetrahedral
PBE	2.387	101.3	77.0	1.73	tetrahedral
BP86	2.390	100.9	76.6	1.73	tetrahedral

Structures of key transition states and intermediates for the hydroboration with (*S*)-DTBM-SEGPHOS

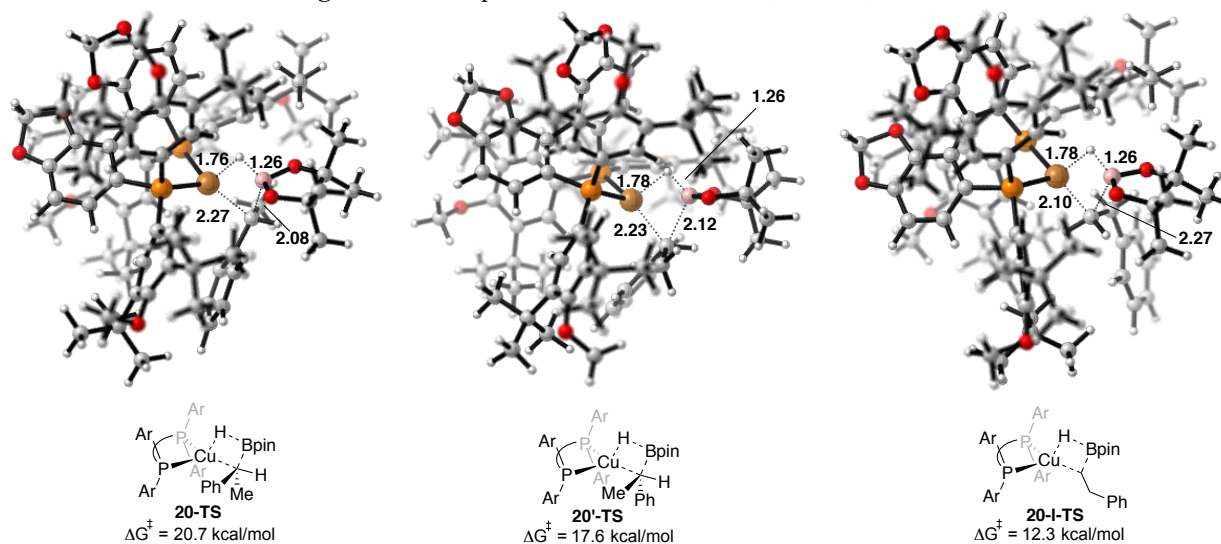
The structures of transition states **13-TS**, **13'-TS**, and **13-I-TS** for alkene insertion into the copper hydride **8** computed at the M06/6-311+g(d,p)/SDD//B3LYP/6-31g(d)/SDD level of theory are shown in Figure 3.17.

Figure 3.17 Computed structures of 13-TS, 13'-TS, 13-I-TS



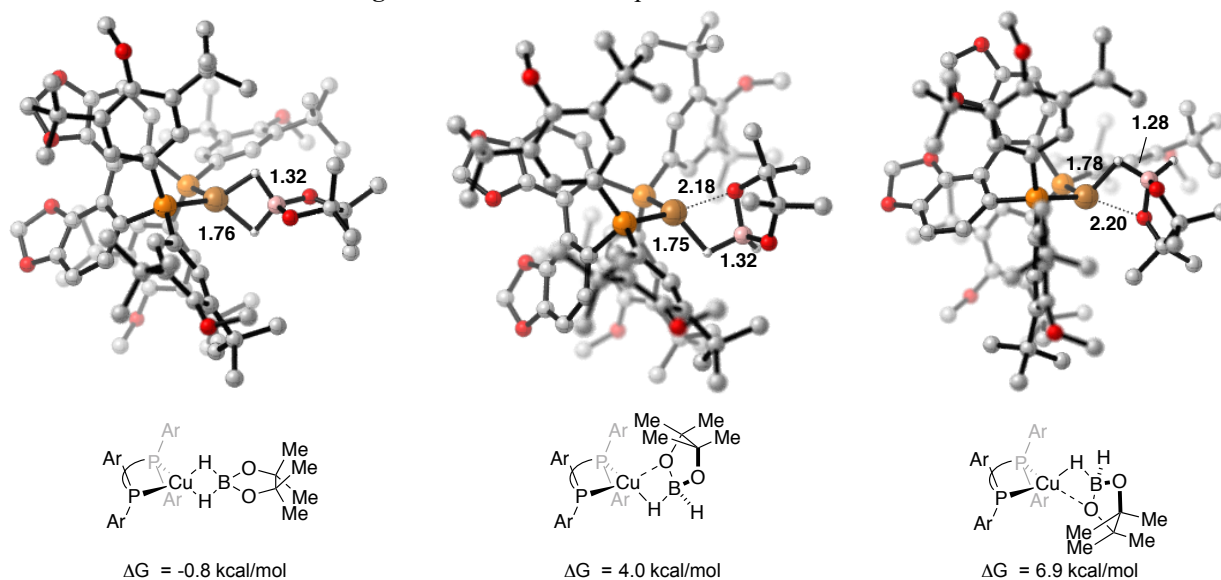
The structures of transition states for the borylation of **20-TS**, **20'-TS**, and **20-I-TS** computed at the M06/6-311+g(d,p)/SDD//B3LYP/6-31g(d)/SDD level of theory are shown in Figure 3.18.

Figure 3.18 Computed structures of 20a-TS, 20b-TS, 20c-TS



Evaluation of possible structures of 15

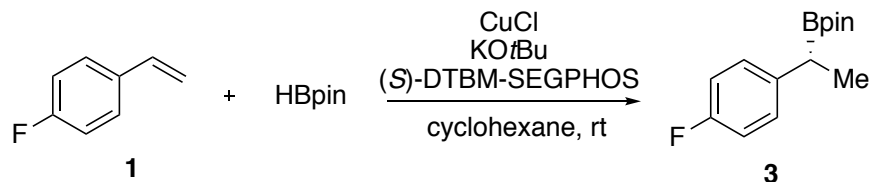
We computed several different structures of dihydridoborate **15**. The structures of a κ^2 -dihydridoborate with two bridging hydrides, and the structures of two κ^2 -dihydridoborates with only one bridging hydride were calculated. As illustrated in Figure 3.19, the structure with two bridging hydrides is clearly more stable than the structures with only one bridging hydride.

Figure 3.19 Evaluation of possible structures of 15^a

^aSingle-point energies were corrected with a SMD solvation model in cyclohexane and relative to sum of **8** and HBpin.

3.4.9 Hydroboration of Vinylarene **1**

Procedure for the hydroboration of **1** catalyzed by Cu/DTBM-SEGPHOS



In an argon-filled dry box, a 1-dram vial was charged with CuCl (2.0 mg, 2 mol %), KOtBu (4.4 mg, 4 mol %), (*S*)-DTBM-SEGPHOS (26.4 mg, 2.2 mol %) and cyclohexane (200 μ L). The mixture was allowed to stir at ambient temperature for 3 minutes before the addition of pinacolborane (152 μ L, 1.05 mmol, 1.05 equiv). After brief stirring (30 – 60 seconds), the solution was added the alkene (119 μ L, 1.00 mmol, 1 equiv) and cyclohexane (800 μ L). The vial was then capped, sealed with electrical tape, and removed from the box. After 4 h of stirring at rt, the reaction vial was diluted with 2 mL of ethyl acetate and the resulting solution was filtered through Celite. The crude material was concentrated *in vacuo* and purified by flash column chromatography (CombiFlash, 5% ethyl acetate in hexanes) to afford the product in 83% yield (208.0 mg, 0.832 mmol).

¹H NMR (600 MHz, CDCl₃) δ 7.21 – 7.11 (m, 2H), 7.01 – 6.86 (m, 2H), 2.41 (q, *J* = 7.5 Hz, 1H), 1.31 (d, *J* = 7.5 Hz, 3H), 1.21 (s, 6H), 1.20 (s, 6H).

¹³C NMR (151 MHz, CDCl₃) δ 160.82 (d, *J*_{C-F} = 242.6 Hz), 140.48 (d, *J*_{C-F} = 2.9 Hz) 128.96 (d, *J*_{C-F} = 7.6 Hz) 114.91 (d, *J*_{C-F} = 21.0 Hz), 83.30, 24.56, 24.52, 17.19 (the benzylic carbon was not detected because of the rapid relaxation of the bound boron atom).

¹⁹F NMR (192 MHz, CDCl₃) δ 33.5.

¹¹B NMR (564 MHz, CDCl₃) δ -120.0.

The compound was reported previously.¹⁴ Our data are a corrected version of the published data. Our values include ¹³C-¹⁹F coupling.

Procedures for the hydroboration of **1** reported in Scheme 3.2

The reactions were conducted following the above procedure, but with a slight alteration outlined by the following conditions.

Condition A in Scheme 3.2: **1** (48.0 μ L, 0.400 mmol), HBPIn (64.0 μ L, 0.440 mmol, 1.1 equiv), CuCl (2.0 mg, 5 mol %), KO t Bu (4.4 mg, 10 mol %), and (*S*)-DTBM-SEGPPOS (26.4 mg, 5.5 mol %), cyclohexane (400 μ L), 54 h.

Condition B in Scheme 3.2: **1** (60.0 μ L, 0.500 mmol), HBPIn (76.0 μ L, 0.525 mmol, 1.05 equiv), CuCl (1.0 mg, 2 mol %), KO t Bu (2.2 mg, 4 mol %), and (*S*)-DTBM-SEGPPOS (13.2 mg, 4.4 mol %), cyclohexane (500 μ L), 4 h.

Yields were determined by GC using dodecane as an internal standard.

Enantioselectivity was determined by HPLC analysis after oxidation of the boronate by H₂O₂/NaOH.

HPLC conditions: OB-H, 5% IPA/hexanes, 0.5 mL/min, 210 nm; t_R (major) = 18.8 min, t_R (minor) = 17.0 min.

3.4.10 Crystallographic Information

Complex **6**

A colorless prism 0.060 x 0.050 x 0.030 mm in size was mounted on a Cryoloop with Paratone oil. Data were collected in a nitrogen gas stream at 100(2) K. The crystal-to-detector distance was 40 mm, and the exposure time was 60 seconds per frame using a scan width of 1.0°. Data collection was 100.0% complete to 25.000° in θ . A total of 54649 reflections were collected, covering the indices, $-16 \leq h \leq 16$, $-27 \leq k \leq 27$, $-35 \leq l \leq 35$. 17071 reflections were found to be symmetry independent, with an R_{int} of 0.0630. Indexing and unit cell refinement indicated a primitive, orthorhombic lattice. The space group was found to be P2₁2₁2₁ (No. 19). The data were integrated using the Bruker SAINT software program and scaled using the SADABS software program. Solution by iterative methods (SHELXT-2014) produced a complete heavy-atom phasing model consistent with the proposed structure. All non-hydrogen atoms were refined anisotropically by full-matrix least-squares (SHELXL-2014). All hydrogen atoms were placed using a riding model. Their positions were constrained relative to their parent atom using the appropriate HFIX command in SHELXL-2014.

Table 3.7 Crystal data and structure refinement for **6**.

Empirical formula	C ₇₄ H ₁₀₀ ClCuO ₈ P ₂	
Formula weight	1278.46	
Temperature	100(2) K	
Wavelength	0.71073 Å	
Crystal system	Orthorhombic	
Space group	P2 ₁ 2 ₁ 2 ₁	
Unit cell dimensions	a = 13.8472(11) Å	$\alpha = 90^\circ$
	b = 23.0453(15) Å	$\beta = 90^\circ$
	c = 29.284(2) Å	$\gamma = 90^\circ$

Volume	9344.8(12) Å ³
Z	4
Density (calculated)	0.909 Mg/m ³
Absorption coefficient	0.336 mm ⁻¹
F(000)	2736
Crystal size	0.060 x 0.050 x 0.030 mm ³
Theta range for data collection	1.391 to 25.381°.
Index ranges	-16<=h<=16, -27<=k<=27, -35<=l<=35
Reflections collected	54649
Independent reflections	17071 [R(int) = 0.0630]
Completeness to theta = 25.000°	100.0 %
Absorption correction	Semi-empirical from equivalents
Max. and min. transmission	0.928 and 0.844
Refinement method	Full-matrix least-squares on F ²
Data / restraints / parameters	17071 / 0 / 803
Goodness-of-fit on F2	1.061
Final R indices [I>2sigma(I)]	R1 = 0.0718, wR2 = 0.1748
R indices (all data)	R1 = 0.0971, wR2 = 0.1850
Absolute structure parameter	0.048(7)
Extinction coefficient	n/a
Largest diff. peak and hole	0.537 and -0.387 e.Å ⁻³

Complex 7•C₆H₁₈OSi₂

A yellow prism 0.100 x 0.080 x 0.060 mm in size was mounted on a Cryoloop with Paratone oil. Data were collected in a nitrogen gas stream at 100(2) K. Crystal-to-detector distance was 40 mm and exposure time was 60 seconds per frame using a scan width of 1.0°. Data collection was 100.0% complete to 25.000° in θ . A total of 147781 reflections were collected covering the indices, $-23 \leq h \leq 23$, $-31 \leq k \leq 28$, $-41 \leq l \leq 42$. 33109 reflections were found to be symmetry independent, with an R_{int} of 0.0576. Indexing and unit cell refinement indicated a primitive, orthorhombic lattice. The space group was found to be $P2_12_12_1$ (No. 19). The data were integrated using the Bruker SAINT software program and scaled using the SADABS software program. Solution by iterative methods (SHELXT-2014) produced a complete heavy-atom phasing model consistent with the proposed structure. All non-hydrogen atoms were refined anisotropically by full-matrix least-squares (SHELXL-2014). All hydrogen atoms were placed using a riding model. Their positions were constrained relative to their parent atom using the appropriate HFIX command in SHELXL-2014.

Table 3.8 Crystal data and structure refinement for 7•C₆H₁₈OSi₂.

Empirical formula	C ₈₁ H ₁₂₁ CuO ₉ P ₂ Si ₂
Formula weight	1420.43
Temperature	100(2) K
Wavelength	0.71073 Å
Crystal system	Orthorhombic
Space group	$P2_12_12_1$
Unit cell dimensions	$a = 19.7038(15)$ Å $\alpha = 90^\circ$

	$b = 26.008(2) \text{ \AA}$	$\beta = 90^\circ$
	$c = 35.273(3) \text{ \AA}$	$\gamma = 90^\circ$
Volume	$18076(3) \text{ \AA}^3$	
Z	8	
Density (calculated)	1.044 Mg/m^3	
Absorption coefficient	0.350 mm^{-1}	
F(000)	6128	
Crystal size	$0.100 \times 0.080 \times 0.060 \text{ mm}^3$	
Theta range for data collection	$1.155 \text{ to } 25.364^\circ$	
Index ranges	$-23 \leq h \leq 23, -31 \leq k \leq 28, -41 \leq l \leq 42$	
Reflections collected	147781	
Independent reflections	33109 [R(int) = 0.0576]	
Completeness to theta = 25.000°	100.0 %	
Absorption correction	Semi-empirical from equivalents	
Max. and min. transmission	0.928 and 0.867	
Refinement method	Full-matrix least-squares on F^2	
Data / restraints / parameters	33109 / 0 / 1710	
Goodness-of-fit on F^2	1.023	
Final R indices [$I > 2\sigma(I)$]	$R1 = 0.0678, wR2 = 0.1711$	
R indices (all data)	$R1 = 0.0969, wR2 = 0.1908$	
Absolute structure parameter	0.005(3)	
Extinction coefficient	n/a	
Largest diff. peak and hole	1.005 and $-0.707 \text{ e.\AA}^{-3}$	

Complex $12' \cdot 2C_7H_8 \cdot C_6H_{18}OSi_2$

A yellow plate $0.160 \times 0.120 \times 0.040 \text{ mm}$ in size was mounted on a Cryoloop with Paratone oil. Data were collected in a nitrogen gas stream at $100(2) \text{ K}$. Crystal-to-detector distance was 60 mm and exposure time was 20 seconds per frame using a scan width of 2.0° . Data collection was 99.8% complete to 67.000° in θ . A total of 306878 reflections were collected covering the indices, $-16 \leq h \leq 16, -24 \leq k \leq 27, -34 \leq l \leq 34$. 17588 reflections were found to be symmetry independent, with an R_{int} of 0.0963. Indexing and unit cell refinement indicated a primitive, orthorhombic lattice. The space group was found to be $P2_12_12_1$ (No. 19). The data were integrated using the Bruker SAINT software program and scaled using the SADABS software program. Solution by iterative methods (SHELXT-2014) produced a complete heavy-atom phasing model consistent with the proposed structure. All non-hydrogen atoms were refined anisotropically by full-matrix least-squares (SHELXL-2016). All hydrogen atoms were placed using a riding model. Their positions were constrained relative to their parent atom using the appropriate HFIX command in SHELXL-2016. Absolute stereochemistry was unambiguously determined to be *S* at C1.

Table 3.9 Crystal data and structure refinement for $12' \cdot 2C_7H_8 \cdot C_6H_{18}OSi_2$.

Empirical formula	$C_{102}H_{142}CuFO_9P_2Si_2$
Formula weight	1712.81
Temperature	$100(2) \text{ K}$
Wavelength	1.54178 \AA
Crystal system	Orthorhombic

Space group	P2 ₁ 2 ₁ 2 ₁	
Unit cell dimensions	a = 14.0112(9) Å	$\alpha = 90^\circ$
	b = 23.8266(17) Å	$\beta = 90^\circ$
	c = 28.7899(19) Å	$\gamma = 90^\circ$
Volume	9611.2(11) Å ³	
Z	4	
Density (calculated)	1.184 Mg/m ³	
Absorption coefficient	1.318 mm ⁻¹	
F(000)	3688	
Crystal size	0.160 x 0.120 x 0.040 mm ³	
Theta range for data collection	2.407 to 68.497°.	
Index ranges	-16 ≤ h ≤ 16, -24 ≤ k ≤ 27, -34 ≤ l ≤ 34	
Reflections collected	306878	
Independent reflections	17588 [R(int) = 0.0963]	
Completeness to theta = 67.000°	99.8 %	
Absorption correction	Semi-empirical from equivalents	
Max. and min. transmission	0.749 and 0.607	
Refinement method	Full-matrix least-squares on F ²	
Data / restraints / parameters	17588 / 3 / 1006	
Goodness-of-fit on F ²	1.090	
Final R indices [I > 2σ(I)]	R1 = 0.1031, wR2 = 0.2649	
R indices (all data)	R1 = 0.1089, wR2 = 0.2704	
Absolute structure parameter	0.006(17)	
Extinction coefficient	n/a	
Largest diff. peak and hole	1.081 and -0.839 e.Å ⁻³	

Complex 16

A colorless prism 0.050 x 0.040 x 0.030 mm in size was mounted on a Cryoloop with Paratone oil. Data were collected in a nitrogen gas stream at 100(2) K. Crystal-to-detector distance was 60 mm and exposure time was 10 seconds per frame using a scan width of 2.0°. Data collection was 99.6% complete to 67.000° in θ . A total of 232804 reflections were collected covering the indices, $-23 \leq h \leq 18$, $-31 \leq k \leq 31$, $-42 \leq l \leq 42$. 32838 reflections were found to be symmetry independent, with an R_{int} of 0.0717. Indexing and unit cell refinement indicated a primitive, orthorhombic lattice. The space group was found to be P2₁2₁2₁ (No. 19). The data were integrated using the Bruker SAINT software program and scaled using the SADABS software program. Solution by iterative methods (SHELXT-2014) produced a complete heavy-atom phasing model consistent with the proposed structure. All non-hydrogen atoms were refined anisotropically by full-matrix least-squares (SHELXL-2014). All hydrogen atoms were placed using a riding model. Their positions were constrained relative to their parent atom using the appropriate HFIX command in SHELXL-2014.

Table 3.10 Crystal data and structure refinement for **16**.

Empirical formula	C ₇₄ H ₁₀₄ BCuO ₈ P ₂
Formula weight	1257.86
Temperature	100(2) K

Wavelength	1.54178 Å	
Crystal system	Orthorhombic	
Space group	P2 ₁ 2 ₁ 2 ₁	
Unit cell dimensions	a = 19.5026(11) Å	$\alpha = 90^\circ$
	b = 26.0918(16) Å	$\beta = 90^\circ$
	c = 35.420(2) Å	$\gamma = 90^\circ$
Volume	18023.9(19) Å ³	
Z	8	
Density (calculated)	0.927 Mg/m ³	
Absorption coefficient	0.995 mm ⁻¹	
F(000)	5408	
Crystal size	0.050 x 0.040 x 0.030 mm ³	
Theta range for data collection	2.103 to 68.488°.	
Index ranges	-23 ≤ h ≤ 18, -31 ≤ k ≤ 31, -42 ≤ l ≤ 42	
Reflections collected	232804	
Independent reflections	32838 [R(int) = 0.0717]	
Completeness to theta = 67.000°	99.6 %	
Absorption correction	Semi-empirical from equivalents	
Max. and min. transmission	0.929 and 0.737	
Refinement method	Full-matrix least-squares on F ²	
Data / restraints / parameters	32838 / 0 / 1605	
Goodness-of-fit on F ²	1.065	
Final R indices [I > 2σ(I)]	R1 = 0.0458, wR2 = 0.1175	
R indices (all data)	R1 = 0.0547, wR2 = 0.1229	
Absolute structure parameter	0.010(7)	
Extinction coefficient	n/a	
Largest diff. peak and hole	0.428 and -0.283 e.Å ⁻³	

Complex 27

A yellow prism 0.100 x 0.080 x 0.050 mm in size was mounted on a Cryoloop with Paratone oil. Data were collected in a nitrogen gas stream at 200(2) K. Crystal-to-detector distance was 60 mm and exposure time was 20 seconds per frame using a scan width of 2.0°. Data collection was 100.0% complete to 67.000° in θ . A total of 178733 reflections were collected covering the indices, $-26 \leq h \leq 26$, $-26 \leq k \leq 25$, $-21 \leq l \leq 21$. 15250 reflections were found to be symmetry independent, with an R_{int} of 0.0510. Indexing and unit cell refinement indicated a primitive, tetragonal lattice. The space group was found to be P4 (No. 75). The data were integrated using the Bruker SAINT software program and scaled using the SADABS software program. Solution by iterative methods (SHELXT-2014) produced a complete heavy-atom phasing model consistent with the proposed structure. All non-hydrogen atoms were refined anisotropically by full-matrix least-squares (SHELXL-2014). All hydrogen atoms were placed using a riding model. Their positions were constrained relative to their parent atom using the appropriate HFIX command in SHELXL-2014.

Table 3.11 Crystal data and structure refinement for **27**.

Empirical formula $\text{C}_{76}\text{H}_{58}\text{Cu}_2\text{O}_8\text{P}_4$

Formula weight	1350.18	
Temperature	200(2) K	
Wavelength	1.54178 Å	
Crystal system	Tetragonal	
Space group	P4	
Unit cell dimensions	a = 21.5938(4) Å	$\alpha = 90^\circ$
	b = 21.5938(4) Å	$\beta = 90^\circ$
	c = 17.8485(4) Å	$\gamma = 90^\circ$
Volume	8322.6(4) Å ³	
Z	4	
Density (calculated)	1.078 Mg/m ³	
Absorption coefficient	1.719 mm ⁻¹	
F(000)	2784	
Crystal size	0.100 x 0.080 x 0.050 mm ³	
Theta range for data collection	2.046 to 68.402°	
Index ranges	-26 ≤ h ≤ 26, -26 ≤ k ≤ 25, -21 ≤ l ≤ 21	
Reflections collected	178733	
Independent reflections	15250 [R(int) = 0.0510]	
Completeness to theta = 67.000°	100.0 %	
Absorption correction	Semi-empirical from equivalents	
Max. and min. transmission	0.929 and 0.817	
Refinement method	Full-matrix least-squares on F ²	
Data / restraints / parameters	15250 / 1 / 814	
Goodness-of-fit on F2	1.066	
Final R indices [I > 2σ(I)]	R1 = 0.0799, wR2 = 0.2013	
R indices (all data)	R1 = 0.0941, wR2 = 0.2204	
Absolute structure parameter	n/a	
Extinction coefficient	n/a	
Largest diff. peak and hole	1.858 and -0.534 e.Å ⁻³	

3.5. References

Parts of this chapter were reprinted with permission from:

“Mechanistic Studies of Copper-Catalyzed Asymmetric Hydroboration of Alkenes”

Xi, Y.; Hartwig, J. F. *J. Am. Chem. Soc.* **2017**, *139*, 12758.

- [1] Matteson, D. S., *Stereodirected Synthesis with Organoboranes*. Springer Berlin Heidelberg: 1995.
- [2] Brown, H. C.; Rao, B. C. S., *J. Am. Chem. Soc.* **1956**, *78*, 5694.
- [3] Zaidlewicz, M., *Hydroboration*. John Wiley & Sons, Inc.: 2000.
- [4] Brown, H. C.; Singaram, B., *Acc. Chem. Res.* **1988**, *21*, 287.
- [5] Thomas, S. P.; Aggarwal, V. K., *Angew. Chem. Int. Ed.* **2009**, *48*, 1896.
- [6] Burgess, K.; Ohlmeyer, M. J., *Chem. Rev.* **1991**, *91*, 1179.
- [7] Beletskaya, I.; Pelter, A., *Tetrahedron* **1997**, *53*, 4957.
- [8] Männig, D.; Nöth, H., *Angew. Chem. Int. Ed.* **1985**, *24*, 878.

- [9] Hayashi, T.; Matsumoto, Y.; Ito, Y., *J. Am. Chem. Soc.* **1989**, *111*, 3426.
- [10] Obligacion, J. V.; Chirik, P. J., *J. Am. Chem. Soc.* **2013**, *135*, 19107.
- [11] Evans, D. A.; Fu, G. C., *J. Am. Chem. Soc.* **1991**, *113*, 4042.
- [12] Evans, D. A.; Fu, G. C.; Hoveyda, A. H., *J. Am. Chem. Soc.* **1992**, *114*, 6671.
- [13] Crudden, Cathleen M.; Edwards, D., *Eur. J. Org. Chem.* **2003**, *2003*, 4695.
- [14] Burgess, K.; Ohlmeyer, M. J., *J. Org. Chem.* **1988**, *53*, 5178.
- [15] Smith, S. M.; Thacker, N. C.; Takacs, J. M., *J. Am. Chem. Soc.* **2008**, *130*, 3734.
- [16] Smith, S. M.; Takacs, J. M., *J. Am. Chem. Soc.* **2010**, *132*, 1740.
- [17] Shoba, V. M.; Thacker, N. C.; Bochat, A. J.; Takacs, J. M., *Angew. Chem. Int. Ed.* **2016**, *55*, 1465.
- [18] Noh, D.; Chea, H.; Ju, J.; Yun, J., *Angew. Chem. Int. Ed.* **2009**, *48*, 6062.
- [19] Copper-catalyzed formal hydroboration using B₂pin₂ and an alcohol, which operates by a mechanism that is distinct to the copper-catalyzed hydroboration with HBpin, also effectly affords enantioenriched boronates. See: (a) Lee, Y.; Hoveyda, A. H. *J. Am. Chem. Soc.* **2009**, *131*, 3160; (b) Corberán, R.; Mszar, N. W.; Hoveyda, A. H. *Angew. Chem. Int. Ed.* **2011**, *50*, 7079.
- [20] Feng, X.; Jeon, H.; Yun, J., *Angew. Chem. Int. Ed.* **2013**, *52*, 3989.
- [21] Lee, H.; Lee, B. Y.; Yun, J., *Org. Lett.* **2015**, *17*, 764.
- [22] Xi, Y.; Hartwig, J. F., *J. Am. Chem. Soc.* **2016**, *138*, 6703.
- [23] Johnson, L. K.; Killian, C. M.; Brookhart, M., *J. Am. Chem. Soc.* **1995**, *117*, 6414.
- [24] Kochi, T.; Hamasaki, T.; Aoyama, Y.; Kawasaki, J.; Kakiuchi, F., *J. Am. Chem. Soc.* **2012**, *134*, 16544.
- [25] Werner, E. W.; Mei, T.-S.; Burckle, A. J.; Sigman, M. S., *Science* **2012**, *338*, 1455.
- [26] Bair, J. S.; Schramm, Y.; Sergeev, A. G.; Clot, E.; Eisenstein, O.; Hartwig, J. F., *J. Am. Chem. Soc.* **2014**, *136*, 13098.
- [27] Larionov, E.; Lin, L.; Guénée, L.; Mazet, C., *J. Am. Chem. Soc.* **2014**, *136*, 16882.
- [28] Vasseur, A.; Bruffaerts, J.; Marek, I., *Nat. Chem.* **2016**, *8*, 209.
- [29] Lata, C. J.; Crudden, C. M., *J. Am. Chem. Soc.* **2010**, *132*, 131.
- [30] Leonori, D.; Aggarwal, V. K., *Angew. Chem. Int. Ed.* **2015**, *54*, 1082.
- [31] Won, J.; Noh, D.; Yun, J.; Lee, J. Y., *J. Phys. Chem. A* **2010**, *114*, 12112.
- [32] Noh, D.; Yoon, S. K.; Won, J.; Lee, J. Y.; Yun, J., *Chem. Asian J.* **2011**, *6*, 1967.
- [33] Dhayal, R. S.; van Zyl, W. E.; Liu, C. W., *Acc. Chem. Res.* **2016**, *49*, 86.
- [34] Jordan, A. J.; Lalic, G.; Sadighi, J. P., *Chem. Rev.* **2016**, *116*, 8318.
- [35] Pirnot, M. T.; Wang, Y.-M.; Buchwald, S. L., *Angew. Chem. Int. Ed.* **2016**, *55*, 48.
- [36] Deutsch, C.; Krause, N.; Lipshutz, B. H., *Chem. Rev.* **2008**, *108*, 2916.
- [37] In our previous study (see ref. 21), we did not observe products that resulted from chain-walking of the copper catalyst.
- [38] Lipshutz, B. H., *Synlett* **2009**, *2009*, 509.
- [39] Lipshutz, B. H.; Noson, K.; Chrisman, W.; Lower, A., *J. Am. Chem. Soc.* **2003**, *125*, 8779.
- [40] Bezman, S. A.; Churchill, M. R.; Osborn, J. A.; Wormald, J., *J. Am. Chem. Soc.* **1971**, *93*, 2063.
- [41] Goeden, G. V.; Caulton, K. G., *J. Am. Chem. Soc.* **1981**, *103*, 7354.
- [42] Lemmen, T. H.; Folting, K.; Huffman, J. C.; Caulton, K. G., *J. Am. Chem. Soc.* **1985**, *107*, 7774.
- [43] Goeden, G. V.; Huffman, J. C.; Caulton, K. G., *Inorg. Chem.* **1986**, *25*, 2484.
- [44] Lipshutz, B. H.; Frieman, B. A., *Angew. Chem. Int. Ed.* **2005**, *44*, 6345.

- [45] Eberhart, M. S.; Norton, J. R.; Zuzek, A.; Sattler, W.; Ruccolo, S., *J. Am. Chem. Soc.* **2013**, *135*, 17262.
- [46] Zall, C. M.; Linehan, J. C.; Appel, A. M., *J. Am. Chem. Soc.* **2016**, *138*, 9968.
- [47] A DTBM-SEGPHOS-ligated copper hydride was characterized *in situ* by ^1H NMR spectroscopy by Lipshutz, which was proposed to be a monomer.
- [48] Romero, E. A.; Olsen, P. M.; Jazzar, R.; Soleilhavoup, M.; Gembicky, M.; Bertrand, G., *Angew. Chem. Int. Ed.* **2017**, *56*, 4024.
- [49] Yun reported the hydroboration of **1** catalyzed by a combination of CuCl, NaOtBu, and (*S,S,R,R*)-tangphos with high enantioselectivity. See ref. 18.
- [50] Bandar, J. S.; Pirnot, M. T.; Buchwald, S. L., *J. Am. Chem. Soc.* **2015**, *137*, 14812.
- [51] Lipshutz, B. H.; Frieman, B.; Birkedal, H., *Org. Lett.* **2004**, *6*, 2305.
- [52] Hattori, G.; Sakata, K.; Matsuzawa, H.; Tanabe, Y.; Miyake, Y.; Nishibayashi, Y., *J. Am. Chem. Soc.* **2010**, *132*, 10592.
- [53] Yamamoto, A.; Miyashita, A.; Yamamoto, T.; Ikeda, S., *Bull. Chem. Soc. Jpn.* **1972**, *45*, 1583.
- [54] Mankad, N. P.; Gray, T. G.; Laitar, D. S.; Sadighi, J. P., *Organometallics* **2004**, *23*, 1191.
- [55] Schaper, F.; Foley, S. R.; Jordan, R. F., *J. Am. Chem. Soc.* **2004**, *126*, 2114.
- [56] Goj, L. A.; Blue, E. D.; Delp, S. A.; Gunnoe, T. B.; Cundari, T. R.; Pierpont, A. W.; Petersen, J. L.; Boyle, P. D., *Inorg. Chem.* **2006**, *45*, 9032.
- [57] Pérez, M.; Fañanás-Mastral, M.; Bos, P. H.; Rudolph, A.; Harutyunyan, S. R.; Feringa, B. L., *Nat. Chem.* **2011**, *3*, 377.
- [58] Coan, P. S.; Folting, K.; Huffman, J. C.; Caulton, K. G., *Organometallics* **1989**, *8*, 2724.
- [59] Collins, L. R.; Rajabi, N. A.; Macgregor, S. A.; Mahon, M. F.; Whittlesey, M. K., *Angew. Chem. Int. Ed.* **2016**, *55*, 15539.
- [60] Laitar, D. S.; Tsui, E. Y.; Sadighi, J. P., *Organometallics* **2006**, *25*, 2405.
- [61] Schmid, S. C.; Van Hoveln, R.; Rigoli, J. W.; Schomaker, J. M., *Organometallics* **2015**, *34*, 4164.
- [62] Chakraborty, S.; Zhang, J.; Patel, Y. J.; Krause, J. A.; Guan, H., *Inorg. Chem.* **2013**, *52*, 37.
- [63] Harder, S.; Spielmann, J., *J. Organomet. Chem.* **2012**, *698*, 7.
- [64] Mukherjee, D.; Ellern, A.; Sadow, A. D., *Chem. Sci.* **2014**, *5*, 959.
- [65] Bontemps, S.; Vendier, L.; Sabo-Etienne, S., *Angew. Chem. Int. Ed.* **2012**, *51*, 1671.
- [66] Hatanaka, T.; Ohki, Y.; Tatsumi, K., *Chem. Asian J.* **2010**, *5*, 1657.
- [67] Hebden, T. J.; Denney, M. C.; Pons, V.; Piccoli, P. M. B.; Koetzle, T. F.; Schultz, A. J.; Kaminsky, W.; Goldberg, K. I.; Heinekey, D. M., *J. Am. Chem. Soc.* **2008**, *130*, 10812.
- [68] Lachaize, S.; Essalah, K.; Montiel-Palma, V.; Vendier, L.; Chaudret, B.; Barthelat, J.-C.; Sabo-Etienne, S., *Organometallics* **2005**, *24*, 2935.
- [69] Schlecht, S.; Hartwig, J. F., *J. Am. Chem. Soc.* **2000**, *122*, 9435.
- [70] We selected methylcopper **7** as the catalyst for kinetic studies to avoid the induction period and lack of homogeneity of the hydroboration of internal alkene **2** catalyzed by the combination of CuCl, KOtBu, and (*S*)-DTBM-SEGPHOS.
- [71] Sadighi reported the isomerization of an NHC-ligated β -borylalkylcopper complex to the corresponding α -borylalkylcopper complex through β -hydrogen elimination and reinsertion. See ref. 58.
- [72] Hartwig, J. F., In *Organotransition Metal Chemistry: From Bonding to Catalysis*, University Science Books: Sausalito, CA, 2010; p 349.

[73] The benzylic configuration in **20** was determined to be *R* by comparing the optical rotation value to the literature value. The benzylic configuration in **20** is the same as that of (*R*)-1-(4-fluorophenyl)ethanol obtained from the hydroboration of **1** and oxidation of its product (*R*)-**3**, suggesting that the origin of asymmetric induction for reaction of the simple styrene **1** is similar to that of the trisubstituted alkene **19**.

[74] Computations were conducted at the M06/6-311+g(d,p)/SDD//B3LYP/6-31g(d)/SDD level of theory, which has been applied to many copper hydride-catalyzed hydrofunctionalization reactions.

[75] Many of the results of our calculations that include solvation correction with the SMD continuum model are different from those reported by Yun and co-workers, who reported calculations in the gas phase. For example, we did not find that the lowest energy pathways involve dechelation of the DTBM-SEGPHOS ligand for the borylation of phenethylcopper intermediates.

[76] From the NBO analysis, the bond order (1.127) of the C2-C3 bond in transition state **13-TS** supports a partial delocalization of the negative charge from the C2 atom to the phenyl ring. We did not obtain an order (1.0357) for the C2-C3 bond that supports the presence of such delocalization in transition state 13-I-TS.

[77] Yang, Y.; Shi, S.-L.; Niu, D.; Liu, P.; Buchwald, S. L., *Science* **2015**, 349, 62.

[78] DFT computational studies on the borylation of phenethylcopper intermediates of the Cu-SEGPHOS system showed that this reaction occurs by a σ -bond metathesis mechanism, not a pathway involving oxidative addition of the B-H bond of HBpin, followed by reductive elimination to form the C-B bond. See Supporting Information for details.

[79] Our DFT calculations showed that both phosphorus atoms are bound to the copper in the transition state structure of the borylation. This result contrasts those of Yun and co-workers (see ref. 31), who conclude that one of the phosphorus atoms is dissociated from the copper in the transition state structure for the borylation step.

[80] Issenhuth, J.-T.; Notter, F.-P.; Dagonne, S.; Dedieu, A.; Bellemin-Laponnaz, S., *Eur. J. Inorg. Chem.* **2010**, 2010, 529.

[81] Vergote, T.; Nahra, F.; Merschaert, A.; Riant, O.; Peeters, D.; Leysens, T., *Organometallics* **2014**, 33, 1953.

[82] Denmark, S. E.; Beutner, G. L. *J. Am. Chem. Soc.* **2003**, 125, 7800.

[83] Pietruszka, J.; Schöne, N. *Eur. J. Org. Chem.* **2004**, 5011.

[84] Liu, Z.; Takeuchi, T.; Pluta, R.; Arteaga, F. A.; Kumagai, N.; Shibasaki, M. *Org. Lett.* **2017**, 19, 710.

CHAPTER 4

Development of Ligands Containing Trimethylgermyl Groups for Asymmetric Hydroboration of 1,1-Disubstituted Alkenes and Hydroboration of Unactivated 1,2-Disubstituted Alkenes

4.1 Introduction

Organoboron compounds are important and versatile synthetic intermediates in organic chemistry.¹ Because they participate in many reactions that form carbon-carbon and carbon-heteroatom bonds,² they are widely used as building blocks in the synthesis of pharmaceuticals, materials, and agrochemicals. More important, many synthetic transformations that organoboron compounds undergo are stereospecific.³ Therefore, use of enantioenriched organoboron compounds provides access to an array of enantioenriched compounds containing a diverse range of functional groups.

Catalytic asymmetric hydroboration^{4, 5} is an attractive method to access enantioenriched organoboron compounds because it utilizes alkenes, which are abundant feedstocks, as the starting materials. Compared to non-catalyzed asymmetric hydroboration,^{6, 7} the catalytic variant does not require stoichiometric amounts of chiral borane reagents and also has the potential to achieve chemo-, regio-, and stereoselectivity that are different than those of the non-catalyzed ones.^{5, 8-11} Many transition-metal complexes catalyze hydroboration enantioselectively.^{9, 12-18} However, the majority of the olefins that undergo hydroboration with high levels of enantioselectivity have been limited to conjugated alkenes,^{9, 11, 12, 19-21} strained alkenes,^{22, 23} and alkenes bearing adjacent directing groups.^{13, 15, 20, 21} For example, hydroboration of 1,1-aryl,alkyl-disubstituted alkenes occurred with high levels of enantiocontrol (>95:5 er),^{16, 17, 24} but, the hydroboration of 1,1-alkyl,alkyl-disubstituted alkenes occurred with enantioselectivity that is generally low.^{7, 16, 17, 24} Yun and co-workers reported a copper catalytic system that afforded high enantioselectivity for hydroboration of 1,1-disubstituted alkenes that contain one primary alkyl group and one alkyl group with branching at the α carbon,²⁵ but the hydroboration of 1,1-disubstituted alkenes that contain two different primary alkyl groups occurred with only modest enantioselectivity (below 85:15 er). In fact, examples of any type of hydrofunctionalizations of 1,1-disubstituted alkenes that bear two different primary alkyl groups with high enantioselectivity²⁶ are rare (Scheme 4.1 A).²⁷⁻³⁰

Ancillary ligands modulate the reactivity and selectivity of metal catalysts. For asymmetric catalysis, achieving high levels of enantioselectivity largely relies on the ability of the catalyst to differentiate between substituents within a substrate. This differentiation is usually achieved by a bonding interaction or a through-space interaction between substrates and catalysts.³¹⁻³⁵ For example, binding of one of the two prochiral faces of a 1,1-disubstituted alkene can result from the ability of the catalyst to differentiate between two substituents of the alkene.

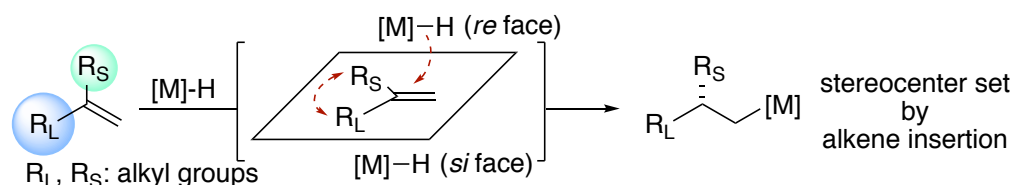
Recently, our group reported a comprehensive mechanistic study on the copper-catalyzed asymmetric hydroboration.³⁶ We found that large substituents on the 3- and 5-positions of the phenyl group on the phosphorus of the ancillary ligands enhance the activity of the catalysts and the enantioselectivity of the reaction. Later, Liu and Buchwald deduced from DFT calculations that these large substituents on the ligands stabilize the transition states of olefin insertion by attractive dispersion interactions.^{37, 38} Thus, we envisioned that a ligand with proper substituents at 3- and 5-positions could create a catalyst that would differentiate between the two prochiral faces of a 1,1-disubstituted alkene by the size of the two primary alkyl substituents appended to the olefin (Scheme 4.1 B).

Herein, we report the preparation of two new bisphosphine ligands, (*R*)-TMG-SYNPHOS (**L11**) and DTMGM-SEGPHOS (**L13**), both bearing trimethylgermyl groups at the 3- and 5-positions of the phenyl group on the phosphorus of the ligand, and their application in the copper-catalyzed hydroboration (Scheme 4.1 C). Catalysts formed from (*R*)-TMG-SYNPHOS significantly improve the enantioselectivity of the hydroboration of 1,1-disubstituted alkenes that bear

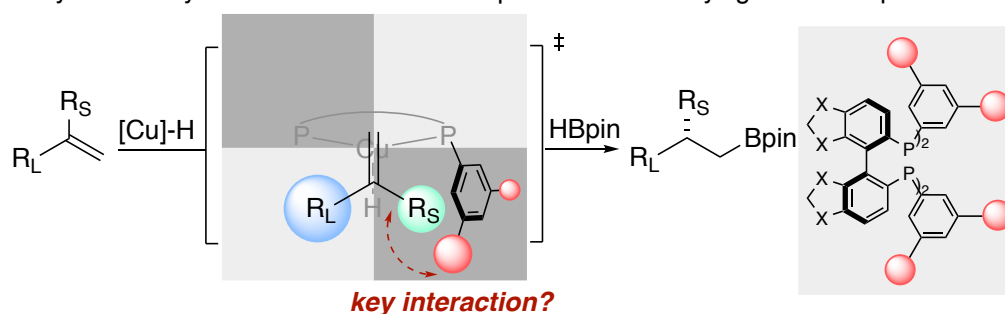
two different primary alkyl groups. These catalysts are also much more active than those formed from (*S*)-DTBM-SEGPHOS. Guided by this result, we discovered that the activity of the copper catalyst ligated by DTMGM-SEGPHOS towards hydroboration of unactivated internal alkenes was much higher than that of catalysts formed from (*S*)-DTBM-SEGPHOS.

Scheme 4.1 Copper-catalyzed asymmetric hydroboration of 1,1-disubstituted alkenes

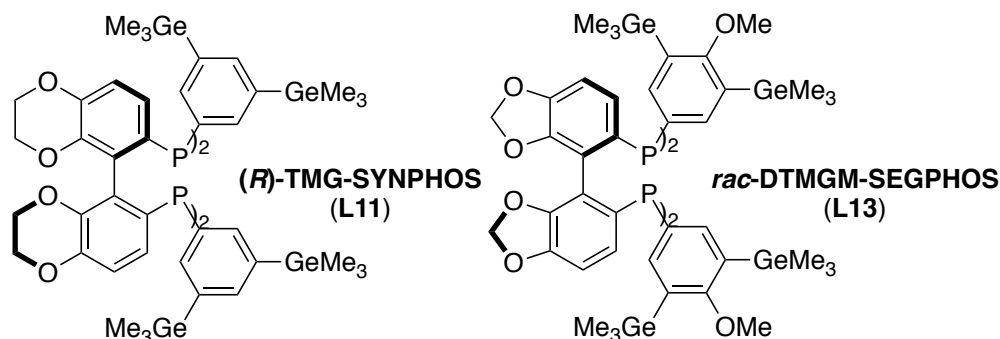
A Challenge in asymmetric catalysis - differentiation of alkyl groups



B Asymmetric synthesis of boronates with β -stereocenters by ligand development



C Structures of the new ligands reported in this study



4.2 Results and Discussion

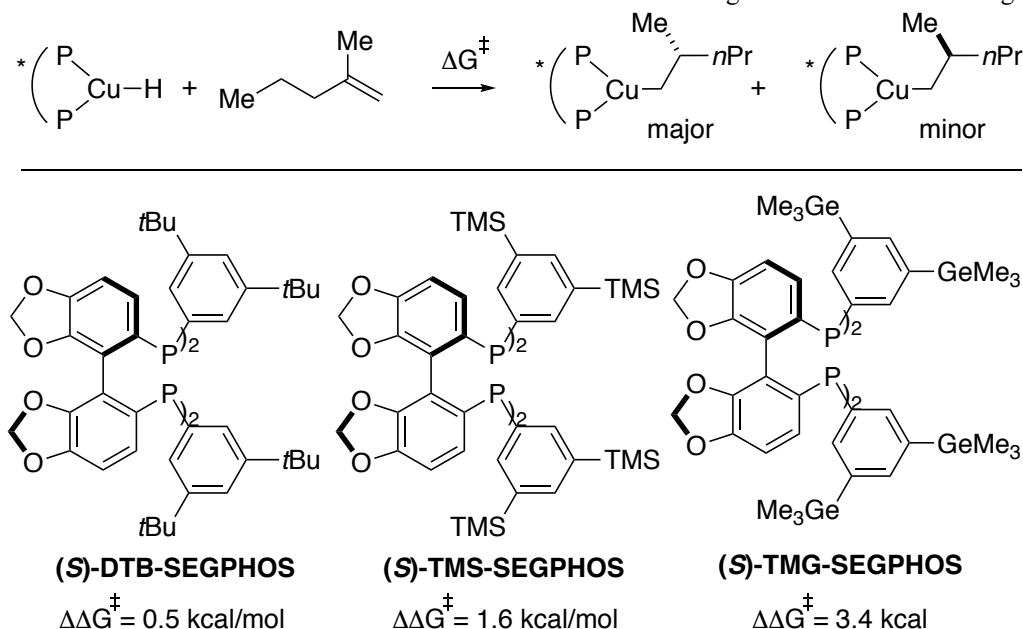
4.2.1 Development of Asymmetric Hydroboration of 1,1-Disubstituted Alkenes Bearing Two Primary Alkyl Groups

To develop a metal-ligand system that catalyzes the hydroboration of 1,1-disubstituted alkenes bearing two primary alkyl groups with high levels of enantioselectivity, we sought to modify the aryl substituents on the phosphorus of (*S*)-DTBM-SEGPHOS. For many reactions catalyzed by complexes with axially chiral biaryl bisphosphines, larger substituents on the P-aryl groups lead to higher enantioselectivity. Previous studies on copper-catalyzed enantioselective hydroboration

have shown that the large substituents on the phosphorus-bound aryl rings improved the enantioselectivity³⁶ and the use of (*S*)-TMS-SEGPHOS as the ligand improved the enantioselectivity of prior rhodium-catalyzed silylations of C-H bonds.^{39, 40} We postulated that trimethylgermyl groups, which are larger than trimethylsilyl and *tert*-butyl groups because carbon-germanium bonds are longer than carbon-carbon and carbon-silicon bonds, would lead to a system that has the potential to catalyze the hydroboration of 1,1-disubstituted alkenes with high enantioselectivity.

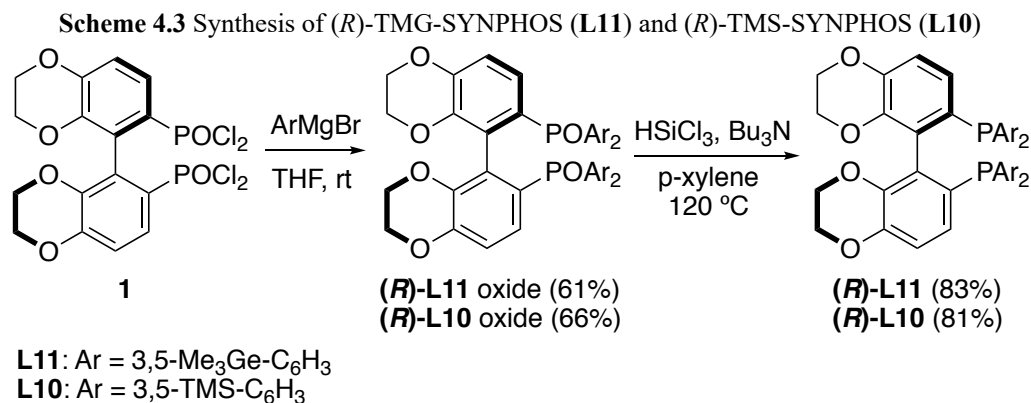
To test this potential, we conducted DFT calculations of the transition state for olefin insertion into copper hydride complexes containing a series of SEGPHOS ligands varying the at the 3- and 5-positions of the phosphorus-bound phenyl group (Scheme 4.2). The results showed that the difference in computed activation energies between transition states leading to the major and minor products increased with increased size of the substituents at the 3- and 5-positions from *tert*-butyl to trimethylsilyl to trimethylgermyl. We also found that the computed barrier for olefin insertion decreased with increased size of the 3,5-substituents.

Scheme 4.2 DFT calculation of transition states of olefin insertion using a series of SEGPHOS ligands



Synthesis of (*R*)-TMG-SYNPHOS and (*R*)-TMS-SYNPHOS. The trend of enantioselectivity predicted by DFT calculations prompted us to devise a synthetic route to prepare ligands that contain 3,5-trimethylgermyl groups. We choose to prepare SYNPHOS derivatives first, instead of SEGPHOS derivatives, because it is convenient to access enantioenriched SYNPHOS ligands by laboratory resolution. Ligands that contain 3,5-trimethylstannyl groups would have the potential to create catalysts that are more active and enantioselective than ligands that contain 3,5-trimethylgermyl groups. However, the high toxicity of tin compounds and potential ligand

modification by reactions of the C-Sn bonds of the ligand led us to pursue the synthesis of germyl-substituted ligands instead of stannyl-substituted ligands.



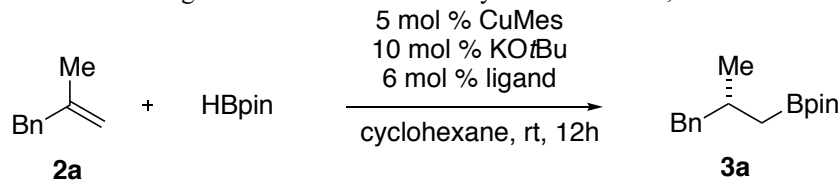
As depicted in Scheme 4.3, (*R*)-TMG-SYNPHOS was prepared in just two steps starting from known intermediates.^{41, 42} The Grignard reaction between (*R*)-(2,2',3,3'-tetrahydro-[5,5'-bibenzo[*b*][1,4]dioxine]-6,6'-diyl)bisphosphonic dichloride (**1**), which was synthesized in three steps,⁴¹ and the corresponding aryl magnesium bromide, which was generated from 3,5-bis(trimethylgermyl)phenyl bromide⁴³ formed (*R*)-TMG-SYNPHOS oxide in 61% yield. (*R*)-TMS-SYNPHOS oxide was prepared in 66% yield by an analogous route. Reduction of the phosphine oxide in the presence of trichlorosilane and tributylamine afforded the corresponding phosphines in 81-83% yield. The overall yields from the two-step syntheses were close to 50%. Based on this procedure, a total of one gram of each ligand was prepared.

Effects of the ligands on enantioselectivity. Initial studies to evaluate the effect of a series of axially chiral biaryl bisphosphines on the enantioselectivity of the copper-catalyzed hydroboration are shown in Table 4.1. These reactions were conducted with 2-methyl-1-phenylpropene (**2a**), which contains a benzyl and a methyl group on the olefin. Yun reported that the enantioselectivity of the reaction of **2a** under conditions they developed with (*S*)-DTBM-SEGPHOS as ligand was only (82:18 er).²⁵ This prior result implies that the catalyst formed from (*S*)-DTBM-SEGPHOS inadequately differentiates a benzyl from a methyl group to achieve high enantioselectivity. Our reactions were conducted with 5 mol % mesitylcopper, 10 mol % potassium *tert*-butoxide, and 5.5 mol % ligand in cyclohexane. Consistent with Yun's results, the reaction of **2a** with (*S*)-DTBM-SEGPHOS as the ligand occurred in 83:17 er (entry 1).

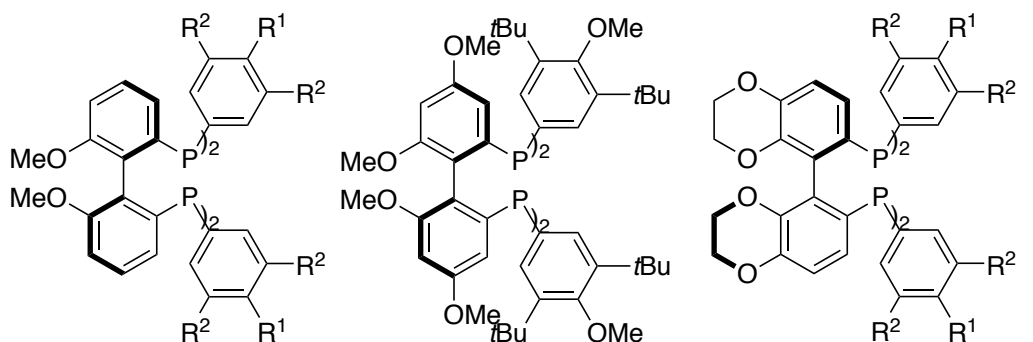
To evaluate the effect of the aryl substituents of the phosphorus on the enantioselectivity, we surveyed a series of MeO-BIPHEP ligands that are commercially available (entries 2-6). We found that catalysts formed from ligands that lack methoxy groups at the 4-position of the phenyl group on the phosphorus of the ligand (**L3**) led to higher enantioselectivity than those formed from ligands that have methoxy groups at the 4-position (**L2**). Varying the size of the substituents at the 3- and 5-positions of the phenyl group on the phosphorus of the ligand indicated that the enantioselectivity is higher for reactions conducted with ligands containing trimethylsilyl groups at these positions (**L6**) than for those conducted with ligands containing *tert*-butyl groups at these positions (**L2**, **L3**). This result is consistent with our DFT computations that predict that larger substituents at the 3- and 5-positions of the phenyl group on the phosphorus of the ligand will lead to higher

enantioselectivity. The reaction conducted with ligand **L5**, which contains 3,5-diisopropyl-4-dimethylaminophenyl groups, proceeded with modest enantioselectivity.

Table 4.1 Evaluation of ligands for enantioselective hydroboration of 1,1-disubstituted alkene **2a**^a



selected ligand structures



(*R*)-**L2**: R¹=OMe, R²=*t*Bu

(*R*)-**L3**: R¹=H, R²=*t*Bu

(*R*)-**L4**: R¹=H, R²=*t*Bu

(*R*)-**L5**: R¹=H, R²=Me

(*R*)-**L6**: R¹=H, R²=TMS

(*R*)-**L7**

(*R*)-**L9**: R¹=OMe, R²=*t*Bu

(*R*)-**L10**: R¹=H, R²=TMS

(*R*)-**L11**: R¹=H, R²=GeMe₃

entry	ligand	T	yield ^b (%)	er
1	(<i>S</i>)-DTBM-SEGPHOS (L1)	rt	93	17:83
2	(<i>R</i>)-DTBM-MeOBIPHEP (L2)	rt	81	80:20
3	(<i>S</i>)-DTB-MeOBIPHEP (L3)	rt	95	18:82
4	(<i>R</i>)-DM-MeOBIPHEP (L4)	rt	<5	-
5	(<i>R</i>)-DIPDMA-MeOBIPHEP (L5)	rt	82	77:23
6	(<i>R</i>)-TMS-MeOBIPHEP (L6)	rt	83	86:14
7	(<i>R</i>)-DTBM-garphos (L7)	rt	81	78:22
8	(<i>R</i>)-DTBM-BINAP (L8)	rt	91	79:21
9	(<i>R</i>)-DTBM-SYNPHOS (L9)	rt	93	85:15
10	(<i>R</i>)-TMS-SYNPHOS (L10)	rt	87	88:12
11 ^c	(<i>R</i>)-TMS-SYNPHOS (L10)	-15°C	48	92:8
12 ^c	(<i>R</i>)-TMG-SYNPHOS (L11)	-15°C	93	94:6
13 ^c	(<i>S</i>)-DTBM-SEGPHOS (L1)	-15°C	<5	-

^aReaction conditions: **2a** (0.1 mmol), HBpin (0.25 mmol, 2.5 equiv), CuMes (10 mol %), KOtBu (20 mol %) and ligand (11 mol %) in cyclohexane (0.15 mL), rt, 24 h; ^bDetermined by GC using dodecane as an internal standard; ^c**2a**

(0.2 mmol), HBpin (0.24 mmol, 1.2 equiv), CuMes (5 mol %), KO t Bu (10 mol %) and ligand (5 mol %) in decalin (0.14 mL), 72 h.

The effect of the ligand backbone on enantioselectivity is shown by entries 1, 2, and 7-9. These reactions were conducted with several classes of ligands containing the same 3,5-di-*tert*-butyl-4-methoxyphenyl (DTBM) groups. The ligand (**L9**) that contains a 2,2',3,3'-tetrahydro-[5,5'-bibenzo[*b*][1,4]dioxine backbone (SYNPHOS) led to the highest enantioselectivity among a SEGPHOS ligand, a BIPHEP ligand, a SYNPHOS ligand, a garphos ligand, and a BINAP ligand.

Having found that the backbone of SYNPHOS ligands lead to the highest enantioselectivity, we examined reactions catalyzed by copper complexes of (*R*)-TMS-SYNPHOS in more detail. The enantioselectivity of the reaction conducted at room temperature with (*R*)-TMS-SYNPHOS (88:12 er, entry 10) was higher than that with (*R*)-DTBM-SYNPHOS (85:15 er). Reducing the reaction temperature from room temperature to -15 °C increased the enantioselectivity of the reaction with (*R*)-TMS-SYNPHOS further to 92:8 er (entry 11). The reaction conducted with (*R*)-TMG-SYNPHOS that contains 3,5-bis(trimethylgermyl)phenyl groups proceeded with a higher enantioselectivity than that conducted with TMS-SYNPHOS and was a high 94:6 er at -15 °C (entry 12). This new ligand, (*R*)-TMG-SYNPHOS, formed a catalyst that was particularly active for the reactions of 1,1-disubstituted alkenes, in addition to one that reacts with high enantioselectivity. For comparison, the catalyst formed from (*S*)-DTBM-SEGPHOS was inactive for hydroboration of alkene **2a** at -15 °C (entry 13) whereas the catalyst formed from (*R*)-TMG-SYNPHOS gave the hydroboration product in high yield, as well as high er, at this temperature.

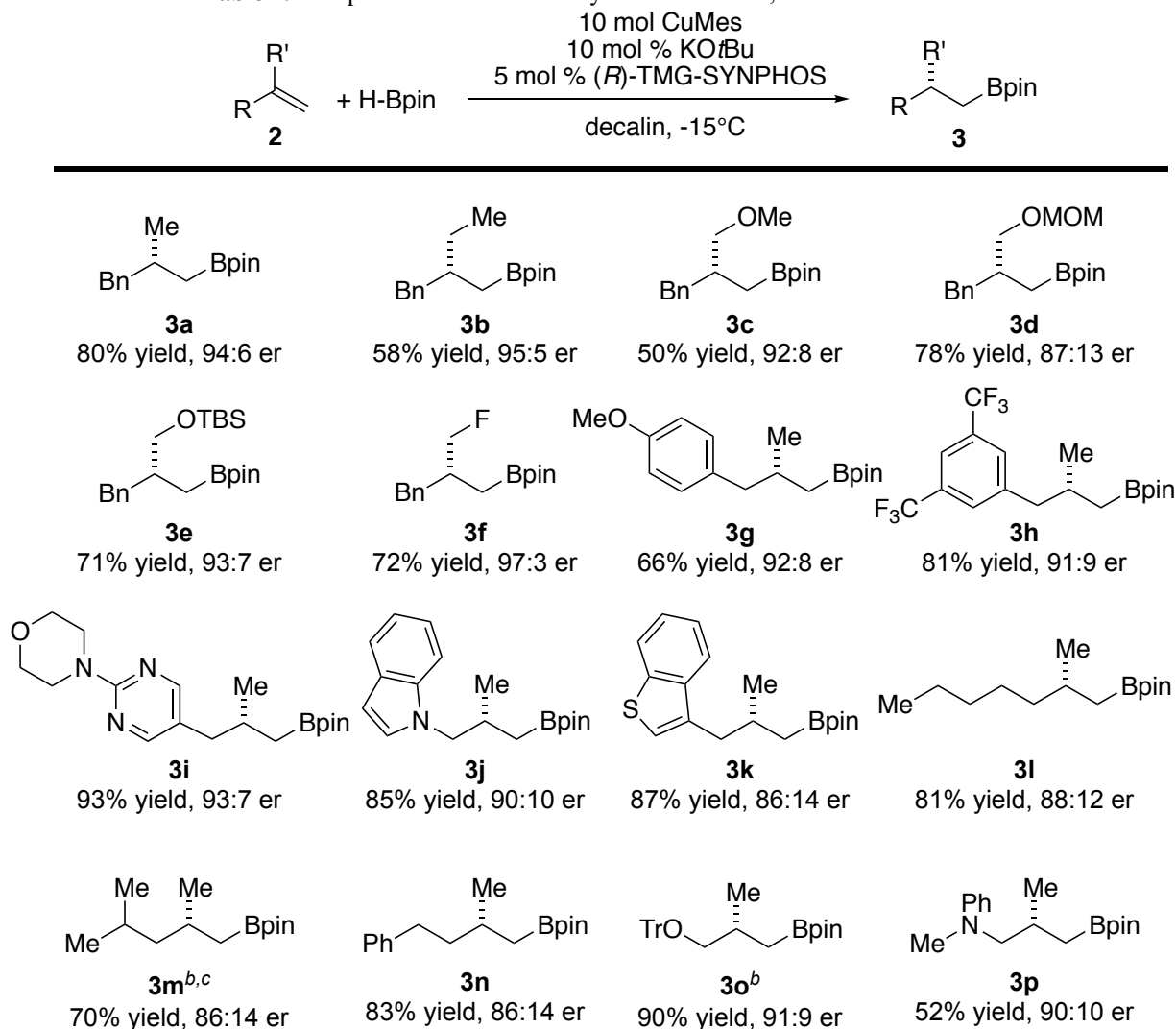
A few factors were essential to achieve the improved enantioselectivity. First, the catalyst formed from (*R*)-TMG-SYNPHOS that contains large 3,5-bis(trimethylgermyl)phenyl substituents most effectively differentiates the two prochiral faces of **1a** among the complexes formed from all the ligands examined. Second, the large 3,5-bis(trimethylgermyl)phenyl substituents on the ligand caused the catalyst to be highly active, and this activity allowed the reaction to be conducted at low temperatures.

Scope of the asymmetric hydroboration of 1,1-disubstituted alkenes. Having established conditions for the asymmetric hydroboration, we examined the scope of the asymmetric hydroboration of 1,1-disubstituted alkenes that contain two different primary alkyl groups. First, the reactions proceeded with consistently high enantioselectivity with 1,1-alkenes that contain a benzyl group and a primary alkyl group, such as a methyl group (**2a**), an ethyl group (**2b**), a methoxy group (**2c**), a 2-methoxyethoxy group (**2d**), a silyloxy group (**2e**), and a fluorine atom (**2f**). Enantioselectivity equal to or higher than 95:5 er was obtained for the reactions of **3b** and **2f**. Second, the reactions of 1,1-alkenes that contain a methyl group and a (hetero)arylmethyl group proceeded with high enantioselectivity when the aryl group was either electron-rich or electron-poor or was a heteroaryl ring, such as pyrimidine (**2i**), indole (**2j**), or benzothiophene (**2k**). The reactions of alkenes containing 6,5-fused electron-rich heterocycles were less enantioselective than those containing electron-poor heterocycles.

Reactions of alkenes containing a methyl group and a primary alkyl group that is not benzyl also were investigated. In general, the enantioselectivities of these reactions were lower (<90:10 er) than those of the reactions of alkenes **2a**, **2g**, and **2h** just discussed that contain arylmethyl groups, but the enantioselectivities were still substantial. Alkenes containing an sp³-hybridized carbon containing a substituent at the position β to the alkene (**2m**) were much less reactive towards the hydroboration than those lacking a group at this position (**2l**) or those containing an sp²-hybridized carbon β to the alkene (**2a**). This lower reactivity is likely due to weaker binding of the

alkene containing substituents at this position. Thus, the reaction was conducted at -5°C instead of -15°C to obtain the corresponding product in a reasonable yield. Finally, the reaction of alkenes containing a trityl ether moiety (**2o**) and a tertiary amine moiety (**2p**) proceeded with good enantioselectivity.

Table 4.2 Scope of enantioselective hydroboration of 1,1-disubstituted alkenes^a



^aReaction conditions: **2** (0.2 mmol), HBpin (0.24 mmol, 1.2 equiv), CuMes (10 mol %), KOtBu (10 mol %) and **L11** (5 mol %) in decalin, 72 h, -15°C ; ^breactions conducted at -5°C ; ^c3 equivalent of alkene instead of 1.2 equiv used.

Development of hydroboration of unactivated 1,2-disubstituted alkenes. Having observed a significant increase in the activity and selectivity of the copper catalyst for the hydroboration of 1,1-disubstituted alkenes, we tested whether ligands that contain trimethylgermyl

groups would also enhance the rate and selectivity of the hydroboration of other types of alkenes that have been challenging to achieve.

Many catalysts promote the hydroboration of nonconjugated internal alkenes, but catalysts that directly add B-H bonds across the alkene double bond without chain-walking isomerization^{10, 44-51} are rare.^{13, 18} The rarity of such catalysts is due to faster β -hydrogen elimination from the secondary alkylmetal species formed by insertion of the internal alkene than from the corresponding primary alkylmetal species.⁵² Previously, we showed that the reactions of internal alkenes bearing electron-withdrawing groups β to the alkene moiety occurred in high yield and without the formation of side products resulting from chain-walking processes.¹⁸ However, the reactions of unactivated 1,2-disubstituted alkenes required a large excess of alkenes and proceeded in lower yields than did reactions of nonconjugated 1,2-disubstituted alkenes that are electronically activated. Our previous mechanistic study showed that the reactions of 1,2-disubstituted alkenes is inverse-order in [HBpin] and positive-order in [alkene] and that the olefin insertion is the rate-limiting step.³⁶ Thus, if a ligand that increases the rate of alkene insertion could be identified, then the reaction of unactivated 1,2-disubstituted alkenes might proceed in high yields and the need for excess of such alkenes could be eliminated.

Synthesis of DTMSM-SEGPHOS and DTMGM-SEGPHOS. To test the effect of silyl and germanyl substituents on the rate of reactions of 1,2-disubstituted alkenes, we prepared two new ligands, DTMSM-SEGPHOS (**L12**) and DTMGM-SEGPHOS (**L13**), which contain 3,5-bis(trimethylsilyl)-4-methoxyphenyl groups and 3,5-bis(trimethylgermanyl)-4-methoxyphenyl groups, respectively. Previously in this chapter we showed that the catalysts formed from ligands that contain trimethylsilyl or trimethylgermanyl groups at the 3- and 5-positions of the phenyl group on the phosphorus are more active for copper-catalyzed hydroboration than those formed from ligands that have trimethylsilyl or *tert*-butyl groups at the 3- and 5-positions.

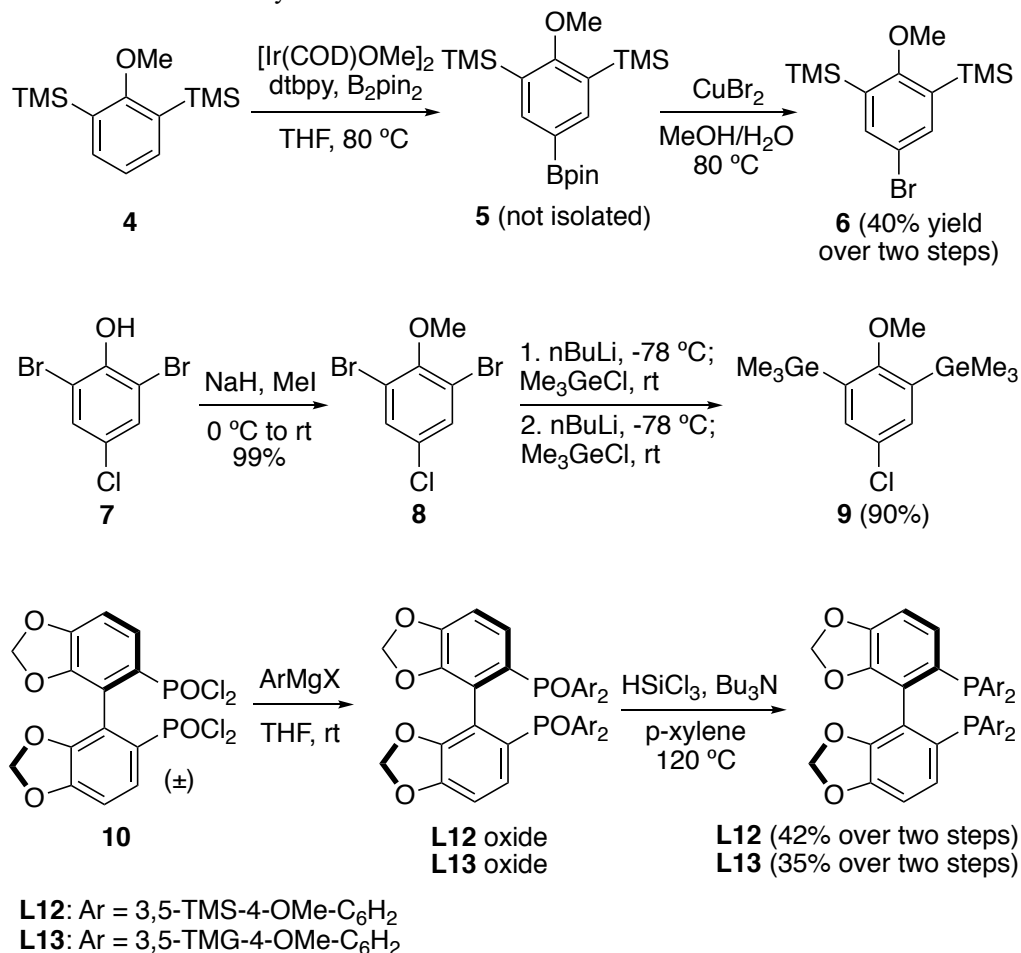
The synthetic route to DTMSM-SEGPHOS and DTMGM-SEGPHOS is depicted in Scheme 4.4. Analogous to the synthesis shown in Scheme 4.3, these two ligands were assembled by the reaction between the bisphosphonic dichloride (**10**) and the Grignard reagent derived from the corresponding aryl bromide. However, the corresponding aryl bromides for the 3,5-substituted methoxyaryl ligands could not be synthesized by sequential lithium-halogen exchange reactions of 2,4,6-tribromoanisole, which was used for the synthesis of 3,5-bis(trimethylgermanyl)phenyl bromide and 3,5-bis(trimethylsilyl)phenyl bromide,⁴² because the exchange reaction on the tribromoanisole was not sufficiently selective for the positions ortho to the methoxy group.

Instead, 3,5-bis(trimethylsilyl)-4-methoxyphenyl bromide (**4**) was prepared by a sequence consisting of C-H borylation and bromination, which was developed by our group.⁵³ Starting with 2,6-bis(trimethylsilyl)anisole (**5**), the iridium-catalyzed C-H borylation occurred with complete *para*-selectivity to afford 2,6-bis(trimethylsilyl)-4-(pinacolato)boryl anisole (**6**), which was used as a crude material in the subsequent copper-mediated bromination to afford the aryl bromide in 40% overall yield.

However, when we used the same procedure for the synthesis of 3,5-bis(trimethylgermanyl)-4-methoxyphenyl bromide, we observed the formation of degermylation products that were inseparable from the desired bromination product. Therefore, we prepared 3,5-bis(trimethylgermanyl)-4-methoxyphenyl chloride (**9**) from 2,6-dibromo-4-chlorophenol (**7**). Methylation of **7** proceeded in quantitative yield to afford 2,6-dibromo-4-chloroanisole (**8**). The carbon-bromine bonds in **8** were converted to C-GeMe₃ bonds by a sequence of lithium-halogen exchange reactions and

germylation, while the carbon-chlorine bond remained intact. Overall, chloride **9** was obtained in 90% yield over two steps from 2,6-dibromo-4-chlorophenol (**7**).

Scheme 4.4 Synthesis of DTMSM-SEGPHOS and DTMGM-SEGPHOS

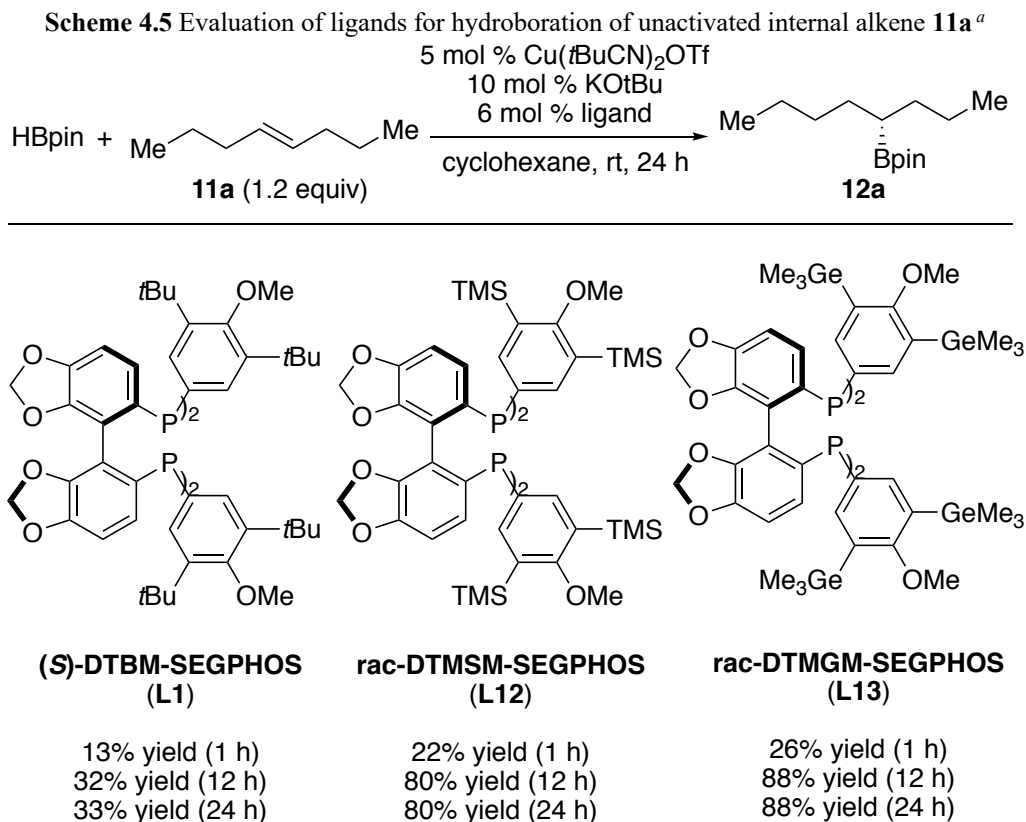


With bromide **6** and chloride **9** prepared in multigram scale, DTMSM-SEGPHOS and DTMGM-SEGPHOS were synthesized in two steps in 35–42% yield, respectively. The racemic forms of these ligands were used to evaluate the effect of substituents on reaction rate and conversion.

Effects of the ligands on catalyst activity. To determine the effect of the substituents on the reactivity of catalyst for hydroboration of alkenes besides the 1,1-disubstituted alkenes, we conducted the hydroboration reactions of the internal alkene, *trans*-4-octene with the catalysts formed from the ligand used in previous studies,¹⁸ DTBM-SEGPHOS (**L1**), and the two ligands introduced this work, DTMSM-SEGPHOS (**L12**), and DTMGM-SEGPHOS (**L13**). The reactions were conducted with Cu(*t*BuCN)₂OTf, a copper salt reported by our group,⁵⁴ as the copper source. The catalyst formed from Cu(*t*BuCN)₂OTf was more active than that formed from CuCl, which was

used previously.^{14, 18} This change allowed the reaction to be evaluated with only 1.2 equivalents of alkene instead of the 3 equivalents of alkene used in earlier studies.

We found that reactions conducted with catalysts derived from DTMSM-SEGPHOS, and DTMGM-SEGPHOS reacted faster and in higher yield (>80% yield) than did that with DTBM-SEGPHOS (33% yield). The reactions with the catalyst containing DTBM-SEGPHOS ligand stopped after 12 hours, presumably due to catalyst decomposition. These results show that the catalysts ligated by DTMSM-SEGPHOS, and DTMGM-SEGPHOS are much more reactive towards insertion of unactivated internal alkenes than that ligated by DTBM-SEGPHOS.



^aReaction conditions: **11a** (0.24 mmol, 1.2 equiv), HBpin (0.2 mmol, 1 equiv), Cu(*t*BuCN)₂OTf (5 mol %), KOtBu (10 mol %), and ligand (5.5 mol %) in cyclohexane (0.14 mL), rt, 24 h.

4.3 Conclusions

In summary, we have developed two new ligands that contain trimethylgermyl groups at the 3- and 5-positions of the phosphine-bound aryl ring and applied these ligands to the copper-catalyzed hydroboration of alkenes. The enantioselectivity of the reactions of 1,1-disubstituted alkenes that contain two primary alkyl groups catalyzed by the copper complex derived from (*R*)-TMG-SYNPHOS are significantly higher than those of these reactions with prior catalysts. This higher enantioselectivity is because the catalyst ligated by bisphosphines that contain bulky groups at the 3- and 5-positions of the phenyl ring of the phosphorus effectively differentiate the two primary alkyl groups on the alkene. The modification of existing ligands containing these bulky germanium-containing groups also substantially enhances the activity of the copper catalyst

toward the hydroboration. The catalyst ligated by DTMGM-SEGPHOS is particularly active toward the hydroboration of unactivated internal alkenes. The high activity of the catalyst allowed the reaction to be conducted with 1.2 equivalent of alkene, which is sufficiently lower than 3 equivalents required by previous methods. We anticipate that the unique steric property and the facile synthesis of these two ligands containing trimethylgermyl groups would lead to applications in other transition-metal-catalyzed reactions.

4.4 Experimental

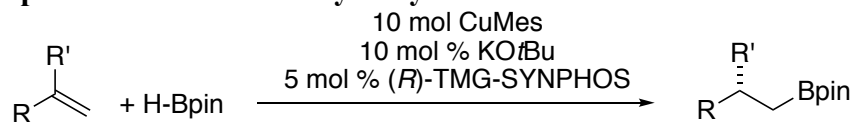
4.4.1 General Methods and Materials

All reagents were purchased from commercial suppliers, stored in the glove box and used as received. Glassware was dried at 130 °C for at least 4 hours before use. Decalin was dried over CaH₂, degassed, and stored in a dry box. (*S*)-DTBM-SEGPHOS was used as received from Takasago. Pinacolborane (HBPin) was purchased from Aldrich and stored in a dry box. All catalytic reactions were set up in an argon-filled dry box with oven-dried glassware and were stirred with Teflon-coated magnetic stirring bars. Flash column chromatography was carried out with a Teledyne Isco CombiFlash® R_f system using RediSep R_f Gold™ columns.

¹H NMR spectra were recorded on Bruker AV-600 instruments with 600 MHz frequencies, and ¹³C were recorded on a Bruker AV-600 instrument with a ¹³C operating frequency of 150 MHz. ¹⁹F NMR spectra were recorded on a Bruker AV-600 spectrometer with a ¹⁹F operating frequency of 564 MHz. Chemical shifts (δ) are reported in ppm relative to the residual solvent signal (CDCl₃ δ = 7.26 for ¹H NMR and δ = 77.0 for ¹³C NMR = 7.26 ppm). Quantitative analysis by GC was performed with dodecane as an internal standard. GC analysis was performed on an Agilent 7890 GC equipped with an HP-5 column (25 m x 0.20 mm x 0.33 μm film) and an FID detector. Chiral SFC analysis was conducted on a JASCO SFC system. Chiral HPLC analysis was conducted on Waters chromatography system. Racemic samples were obtained using racemic DTBM-SEGPHOS as the ligand, which was prepared by mixing equal amounts of (*S*)-DTBM-SEGPHOS and (*R*)-DTBM-SEGPHOS.

4.4.2 General Procedure for Catalytic Hydroboration

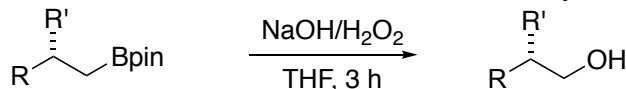
Representative procedure for the catalytic hydroboration on a 0.2 mmol scale



In an argon-filled dry box, a 1-dram vial was charged with CuMes (3.6 mg, 10 mol %), KO*t*Bu (2.2 mg, 10 mol %), (*R*)-TMG-SYNPHOS (15.7 mg, 5 mol %) and decalin (140 μL). The mixture was allowed to stir at ambient temperature for 5 minutes before being placed in a freezer at -40°C. After 15 minutes, pinacolborane (35.0 μL, 0.241 mmol, 1.2 equiv) was quickly added while keeping the vial cold, followed by the addition of the alkene in neat (0.2 mmol, 1 equiv). The vial was then capped, sealed with electrical tape, removed from the box, and placed in an isopropanol bath at -15°C. After 72 h of stirring at this temperature, the reaction was diluted with 2 mL of ethyl

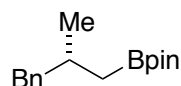
acetate and the resulting solution was filtered through Celite. The crude material was concentrated *in vacuo* and purified by flash column chromatography (CombiFlash) to afford the pure product.

Representative procedure for determination of enantioselectivity



In a 20-mL scintillation vial, the secondary boronate (5 – 20 mg) was dissolved in 1 mL THF. The vial was cooled in an ice bath and added a premixed solution of NaOH (2 M, aq.)/30% H₂O₂ (2:1, 1.5 mL). The reaction was warmed to rt and allowed to stir for 2.5 hours before the addition of water (3 mL) and ethyl acetate (3 mL). The phases were separated, and the aqueous layer was extracted with 3 mL ethyl acetate. The organic phases were combined, dried over Na₂SO₄, and concentrated *in vacuo*. This material was used for determination of enantioselectivity directly without further purification.

4.4.3 Compound Characterization



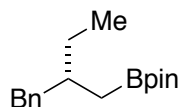
Compound 3a was synthesized according to the **General Procedure** with **2a** (30.0 μ L, 0.204 mmol). Compound **3a** was purified by flash column chromatography (2% ethyl acetate in hexanes) and obtained as a colorless oil in 80% yield.

¹H NMR (600 MHz, CDCl₃) δ 7.28 – 7.26 (m, 2H), 7.23 – 7.09 (m, 3H), 2.63 (dd, J = 13.2, 6.3 Hz, 1H), 2.45 (dd, J = 13.2, 7.8 Hz, 1H), 2.10 – 1.95 (m, 1H), 1.26 (s, 12H), 0.93 (d, J = 6.5 Hz, 3H), 0.90 (dd, J = 15.4, 5.8 Hz, 4H), 0.71 (dd, J = 15.4, 8.5 Hz, 1H).

¹³C NMR (151 MHz, CDCl₃) δ 141.61, 129.26, 127.98, 125.54, 82.85, 46.00, 31.69, 24.88, 24.77, 21.97, 19.45.

¹¹B NMR (192 MHz, CDCl₃) δ 33.4.

SFC analysis of the corresponding alcohol after oxidation (OD-H, 10% IPA/CO₂, 10 MPa, 2.5 mL/min, 220 nm) indicated 94:6 er: t_R (major) = 1.9 min, t_R (minor) = 2.2 min.



Compound 3b was synthesized with an alternation to the **General Procedure** using **2b** (43.9 mg, 1.5 equiv) and pinacolborane (29.0 μ L, 0.200 mmol). Compound **3b** was purified by flash column chromatography (2% ethyl acetate in hexanes) and obtained as a colorless oil in 58% yield.

¹H NMR (600 MHz, CDCl₃) δ 7.28 – 7.24 (m, 2H), 7.19 – 7.4 (m, 3H), 2.60 – 2.50 (m, 2H), 1.89 – 1.82 (m, 1H), 1.39 – 1.32 (m, 1H), 1.24 (s, 12H), 1.27 – 1.19 (m, 1H), 0.88 (t, J = 7.4 Hz, 3H), 0.82 – 0.72 (m, 2H).

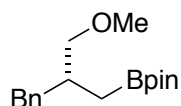
¹³C NMR (151 MHz, CDCl₃) δ 141.70, 129.35, 127.97, 125.47, 82.82, 42.70, 37.88, 28.31, 24.84, 24.83, 16.09, 11.14.

¹¹B NMR (192 MHz, CDCl₃) δ 34.0.

HRMS (EI⁺) Calculated for C₁₇H₂₇BO₂ [M]⁺: 274.2104, Found: 274.2103.

$[\alpha]_D^{23} = -7.0$ ($c = 0.5$, DCM).

SFC analysis of the corresponding alcohol after oxidation (OD-H, 3% IPA/CO₂, 10 MPa, 2.5 mL/min, 220 nm) indicated 95:5 er: t_R (major) = 3.1 min, t_R (minor) = 2.9 min.



Compound 3c was synthesized according to the **General Procedure** with **2c** (32.4 mg, 0.200 mmol). Compound **3c** was purified by flash column chromatography (2% ethyl acetate in hexanes) and obtained as a colorless oil in 50% yield.

¹H NMR (600 MHz, CDCl₃) δ 7.26 (t, $J = 7.5$ Hz, 2H), 7.20 – 7.14 (m, 3H), 3.30 (s, 3H), 3.26 (dd, $J = 9.1, 5.7$ Hz, 1H), 3.14 (dd, $J = 9.1, 6.9$ Hz, 1H), 2.67 (dd, $J = 13.4, 7.0$ Hz, 1H), 2.55 (dd, $J = 13.4, 7.1$ Hz, 1H), 2.25 – 2.15 (m, 1H), 1.23 (s, 12H), 0.81 (dd, $J = 15.5, 5.8$ Hz, 1H), 0.74 (dd, $J = 15.5, 8.4$ Hz, 1H).

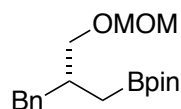
¹³C NMR (151 MHz, CDCl₃) δ 140.63, 129.39, 128.05, 125.67, 82.81, 77.06, 58.58, 40.25, 36.86, 24.84, 24.79, 14.39.

¹¹B NMR (192 MHz, CDCl₃) δ 33.7.

HRMS (EI+) Calculated for C₁₆H₂₄BO₃ [M–CH₃]⁺: 275.1819, Found: 275.1813.

$[\alpha]_D^{23} = 4.4$ ($c = 0.57$, DCM).

SFC analysis of the corresponding alcohol after oxidation (AD-H, 2% MeOH/CO₂, 10 MPa, 4.0 mL/min, 220 nm) indicated 92:8 er: t_R (major) = 5.5 min, t_R (minor) = 6.3 min.



Compound 3d was synthesized according to the **General Procedure** with **2d** (38.4 mg, 0.200 mmol). Compound **3d** was purified by flash column chromatography (2% ethyl acetate in hexanes) and obtained as a colorless oil in 78% yield.

¹H NMR (600 MHz, CDCl₃) δ 7.26 (t, $J = 7.5$ Hz, 2H), 7.23 – 7.16 (m, 3H), 4.60 (s, 2H), 3.41 (dd, $J = 9.3, 5.5$ Hz, 1H), 3.35 (s, 3H), 3.34 (dd, $J = 9.3, 6.2$ Hz, 1H), 2.71 (dd, $J = 13.4, 7.1$ Hz, 1H), 2.58 (dd, $J = 13.4, 7.1$ Hz, 1H), 2.21 (hept, $J = 6.9$ Hz, 1H), 0.88 – 0.78 (m, 2H).

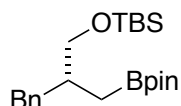
¹³C NMR (151 MHz, CDCl₃) δ 140.64, 129.34, 128.09, 125.72, 96.44, 82.85, 71.86, 55.10, 40.25, 36.98, 24.88, 24.77, 14.29.

¹¹B NMR (192 MHz, CDCl₃) δ 33.7.

HRMS (EI+) Calculated for C₁₇H₂₆BO₄ [M–CH₃]⁺: 305.1924, Found: 305.1922.

$[\alpha]_D^{23} = 2.8$ ($c = 0.948$, DCM).

SFC analysis of the corresponding alcohol after oxidation (AD-H, 5% MeOH/CO₂, 10 MPa, 2.5 mL/min, 220 nm) indicated 87:13 er: t_R (major) = 4.4 min, t_R (minor) = 4.7 min.



Compound 3e was synthesized according to the **General Procedure** with **2e** (52.5 mg, 0.200 mmol). Compound **3e** was purified by flash column chromatography (2% ethyl acetate in hexanes) and obtained as a colorless oil in 71% yield.

^1H NMR (600 MHz, CDCl_3) δ 7.26 (d, $J = 7.5$ Hz, 2H), 7.22 – 7.15 (m, 3H), 3.50 (dd, $J = 9.7, 4.7$ Hz, 1H), 3.40 (dd, $J = 9.8, 6.1$ Hz, 1H), 2.80 (dd, $J = 13.2, 6.9$ Hz, 1H), 2.51 (dd, $J = 13.2, 7.0$ Hz, 1H), 2.08 – 1.99 (m, 1H), 1.24 (s, 12H), 0.93 (s, 9H), 0.80 (d, $J = 7.2$ Hz, 2H), 0.05 (s, 3H), 0.04 (s, 3H).

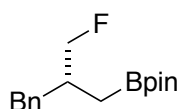
^{13}C NMR (151 MHz, CDCl_3) δ 141.21, 129.49, 127.96, 125.51, 82.84, 66.29, 39.41, 39.10, 25.96, 24.87, 24.82, 18.31, 13.18, -5.34, -5.39.

^{11}B NMR (192 MHz, CDCl_3) δ 34.0.

HRMS (ESI+) Calculated for $\text{C}_{20}\text{H}_{40}\text{BO}_3\text{Si}$ $[\text{M}+\text{H}]^+$: 391.2834, Found: 391.2823.

$[\alpha]_{\text{D}}^{23} = 5.0$ ($c = 1.0$, DCM).

SFC analysis of the corresponding alcohol after oxidation (AD-H, 5% IPA/ CO_2 , 10 MPa, 2.5 mL/min, 220 nm) indicated 93:7 er: t_{R} (major) = 1.8 min, t_{R} (minor) = 2.1 min.



Compound 3f was synthesized according to the **General Procedure** with **2f** (30.0 mg, 0.200 mmol). Compound **3f** was purified by flash column chromatography (2% ethyl acetate in hexane) and obtained as a colorless oil in 72% yield.

^1H NMR (600 MHz, CDCl_3) δ 7.28 (t, $J = 7.4$ Hz, 2H), 7.24 – 7.16 (m, 3H), 4.28 (dd, $J = 47.7, 5.5$ Hz, 2H), 2.72 (dd, $J = 13.5, 7.4$ Hz, 1H), 2.61 (dd, $J = 13.5, 6.9$ Hz, 1H), 2.31 – 2.19 (m, 1H), 1.24 (s, 12H), 0.91 – 0.79 (m, 1H).

^{13}C NMR (151 MHz, CDCl_3) δ 139.88, 129.35, 128.21, 125.95, 86.93 (d, $J = 168.4$ Hz), 83.10, 38.96, 37.48 (d, $J = 18.2$ Hz), 24.81, 24.77, 13.11.

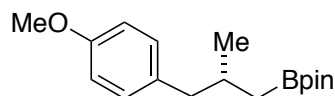
^{11}B NMR (192 MHz, CDCl_3) δ 33.7.

^{19}F NMR (564 MHz, CDCl_3) δ -224.61 (td, $J = 47.7, 21.0$ Hz).

HRMS (EI+) Calculated for $\text{C}_{16}\text{H}_{23}\text{BO}_2$ $[\text{M}-\text{HF}]^+$: 258.1791, Found: 258.1788.

$[\alpha]_{\text{D}}^{23} = 10.7$ ($c = 0.656$, DCM).

SFC analysis of the corresponding alcohol after oxidation (IC-H, 3% IPA/ CO_2 , 10 MPa, 2.5 mL/min, 220 nm) indicated 97:3 er: t_{R} (major) = 4.0 min, t_{R} (minor) = 3.7 min.



Compound 3g was synthesized according to the **General Procedure** with **2g** (32.4 mg, 0.200 mmol). Compound **3g** was purified by flash column chromatography (5% ethyl acetate in hexanes) and obtained as a colorless oil in 66% yield.

^1H NMR (600 MHz, CDCl_3) δ 7.07 (d, $J = 8.5$ Hz, 2H), 6.81 (d, $J = 8.5$ Hz, 1H), 3.78 (s, 3H), 2.54 (dd, $J = 13.4, 6.4$ Hz, 1H), 2.38 (dd, $J = 13.4, 7.8$ Hz, 1H), 2.00 – 1.91 (m, 1H), 1.24 (d, $J = 1.8$ Hz, 12H), 0.89 (d, $J = 6.7$ Hz, 3H), 0.87 (dd, $J = 15.2, 5.8$ Hz, 1H), 0.67 (dd, $J = 15.5, 8.6$ Hz, 1H).

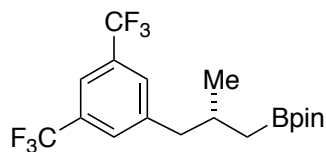
^{13}C NMR (151 MHz, CDCl_3) δ 157.59, 133.72, 130.11, 113.39, 82.84, 55.17, 45.08, 31.82, 24.88, 24.76, 21.92, 19.48.

^{11}B NMR (192 MHz, CDCl_3) δ 33.5.

HRMS (EI+) Calculated for $\text{C}_{17}\text{H}_{27}\text{BO}_3$ $[\text{M}]^+$: 290.2053, Found: 290.2056.

$[\alpha]_{\text{D}}^{23} = 5.7$ ($c = 0.51$, DCM).

SFC analysis of the corresponding alcohol after oxidation (OJ-H, 5% IPA/ CO_2 , 10 MPa, 2.5 mL/min, 220 nm) indicated 92:8 er: t_{R} (major) = 3.5 min, t_{R} (minor) = 3.2 min.



Compound 3h was synthesized according to the **General Procedure** with **2h** (53.6 mg, 0.200 mmol). Compound **3h** was purified by flash column chromatography (2% ethyl acetate in hexanes) and obtained as a colorless oil in 81% yield.

$^1\text{H NMR}$ (600 MHz, CDCl_3) δ 7.69 (s, 1H), 7.61 (s, 2H), 2.74 (dd, $J = 13.4, 6.5$ Hz, 1H), 2.57 (dd, $J = 13.4, 7.7$ Hz, 1H), 2.09 – 1.98 (m, 1H), 1.25 (s, 12H), 0.93 (d, $J = 6.6$ Hz, 3H), 0.86 (dd, $J = 15.6, 5.7$ Hz, 1H), 0.71 (dd, $J = 15.6, 8.2$ Hz, 1H).

$^{13}\text{C NMR}$ (151 MHz, CDCl_3) δ 143.98, 131.18 (q, $J = 33.1$ Hz), 129.28, 123.45 (q, $J = 272.6$ Hz), 120.14 – 119.52 (m).

83.06, 45.21, 31.53, 24.80, 24.68, 21.77, 19.04.

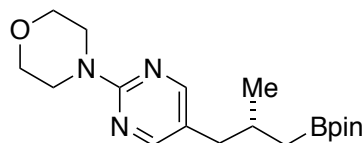
$^{11}\text{B NMR}$ (192 MHz, CDCl_3) δ 32.8.

$^{19}\text{F NMR}$ (564 MHz, CDCl_3) δ -64.5 (m).

HRMS (EI+) Calculated for $\text{C}_{18}\text{H}_{23}\text{BF}_6\text{O}_2$ $[\text{M}]^+$: 396.1695, Found: 396.1702.

$[\alpha]_{\text{D}}^{23} = 7.5$ ($c = 0.924$, DCM).

^1H and ^{19}F NMR analysis of the Mosher ester of the corresponding alcohol after oxidation indicated 91:9 er.



Compound 3i was synthesized according to the **General Procedure** with **2i** (43.9 mg, 0.200 mmol). Compound **3i** was purified by flash column chromatography (10% ethyl acetate in hexanes) and obtained as a white solid in 93% yield.

$^1\text{H NMR}$ (600 MHz, CDCl_3) δ 8.11 (s, 2H), 3.75 – 3.68 (m, 8H), 2.36 (dd, $J = 13.8, 6.6$ Hz, 1H), 2.25 (dd, $J = 13.8, 7.4$ Hz, 1H), 1.90 – 1.80 (m, 1H), 1.20 (s, 12H), 0.88 (d, $J = 6.6$ Hz, 3H), 0.80 (dd, $J = 15.5, 5.8$ Hz, 1H), 0.62 (dd, $J = 15.5, 8.3$ Hz, 1H).

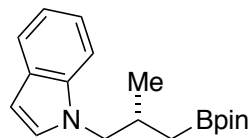
$^{13}\text{C NMR}$ (151 MHz, CDCl_3) δ 160.79, 158.05, 122.43, 82.91, 66.76, 44.33, 39.09, 31.42, 24.84, 24.72, 21.74, 18.69.

$^{11}\text{B NMR}$ (192 MHz, CDCl_3) δ 33.7.

HRMS (ESI+) Calculated for $\text{C}_{18}\text{H}_{31}\text{BN}_3\text{O}_3$ $[\text{M}+\text{H}]^+$: 348.2453, Found: 348.2469.

$[\alpha]_{\text{D}}^{23} = 3.4$ ($c = 0.943$, DCM).

SFC analysis of the corresponding alcohol after oxidation (AD-H, 20% IPA/ CO_2 , 10 MPa, 2.5 mL/min, 220 nm) indicated 93:7 er: t_{R} (major) = 2.2 min, t_{R} (minor) = 2.0 min.



Compound 3j was synthesized according to the **General Procedure** with **2j** (34.2 mg, 0.200 mmol). Compound **3j** was purified by flash column chromatography (5% ethyl acetate in hexanes) and obtained as a colorless oil in 85% yield.

$^1\text{H NMR}$ (600 MHz, CDCl_3) δ 7.67 (d, $J = 7.9$ Hz, 1H), 7.47 (d, $J = 8.2$ Hz, 1H), 7.24 (t, $J = 7.5$ Hz, 1H), 7.21 – 7.10 (m, 2H), 6.52 (d, $J = 2.9$ Hz, 1H), 4.11 (dd, $J = 14.1, 6.5$ Hz, 1H), 3.89 (dd, $J = 14.1, 8.2$ Hz, 1H), 2.45 – 2.29 (m, 1H), 1.30 (s, 12H), 0.97 (d, $J = 6.6$ Hz, 3H), 0.91 (dd, $J = 15.8, 6.1$ Hz, 1H), 0.79 (dd, $J = 15.8, 8.0$ Hz, 1H).

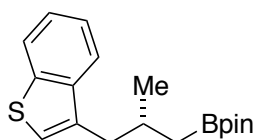
$^{13}\text{C NMR}$ (151 MHz, CDCl_3) δ 136.33, 128.58, 128.51, 121.17, 120.78, 119.06, 109.87, 100.63, 83.17, 54.42, 30.87, 24.95, 24.84, 20.29, 17.20.

$^{11}\text{B NMR}$ (192 MHz, CDCl_3) δ 33.8.

HRMS (ESI+) Calculated for $\text{C}_{19}\text{H}_{26}\text{B}^{35}\text{Cl}_3\text{O}_4$ $[\text{M}+\text{H}]^+$: 300.2129, Found: 300.2138.

$[\alpha]_{\text{D}}^{23} = 17.4$ ($c = 0.5$, DCM).

SFC analysis of the corresponding alcohol after oxidation (OD-H, 15% IPA/ CO_2 , 10 MPa, 2.5 mL/min, 220 nm) indicated 90:10 er: t_{R} (major) = 3.3 min, t_{R} (minor) = 3.0 min.



Compound 3k was synthesized according to the **General Procedure** with **2k** (37.6 mg, 0.200 mmol). Compound **3k** was purified by flash column chromatography (4% ethyl acetate in hexanes) and obtained as a colorless oil in 87% yield.

$^1\text{H NMR}$ (600 MHz, CDCl_3) δ 7.87 (t, $J = 8.7$ Hz, 2H), 7.48 – 7.32 (m, 2H), 7.09 (s, 1H), 2.89 (dd, $J = 14.0, 6.1$ Hz, 1H), 2.68 (dd, $J = 14.0, 8.1$ Hz, 1H), 2.25 – 2.18 (m, 1H), 1.27 (s, 12H), 0.99 (d, $J = 6.4$ Hz, 3H), 0.99 – 0.94 (m, 1H), 0.81 (dd, $J = 15.6, 7.8$ Hz, 1H).

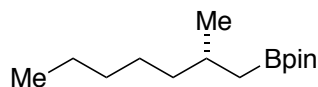
$^{13}\text{C NMR}$ (151 MHz, CDCl_3) δ 140.42, 139.45, 136.15, 123.87, 123.59, 122.72, 122.22, 122.05, 82.96, 38.53, 29.90, 24.94, 24.81, 22.55, 19.84.

$^{11}\text{B NMR}$ (192 MHz, CDCl_3) δ 33.9.

HRMS (EI+) Calculated for $\text{C}_{18}\text{H}_{25}\text{BO}_2\text{S}$ $[\text{M}]^+$: 316.1668, Found: 316.1671.

$[\alpha]_{\text{D}}^{23} = 9.0$ ($c = 1.0$, DCM).

SFC analysis of the corresponding alcohol after oxidation (AD-H, 10% IPA/ CO_2 , 10 MPa, 2.5 mL/min, 220 nm) indicated 86:14 er: t_{R} (major) = 4.7 min, t_{R} (minor) = 5.1 min.



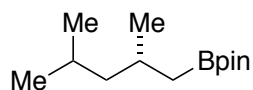
Compound 3l was synthesized according to the **General Procedure** with **2l** (31.5 μL , 0.200 mmol). Compound **3l** was purified by flash column chromatography (2% ethyl acetate in hexanes) and obtained as a colorless oil in 81% yield.

$^1\text{H NMR}$ (600 MHz, CDCl_3) δ 1.69 – 1.62 (m, 1H), 1.23 (s, 12H), 1.32 – 1.10 (m, 8H), 0.89 (d, $J = 6.7$ Hz, 3H), 0.86 (t, $J = 7.1$ Hz, 3H), 0.81 (dd, $J = 15.3, 5.9$ Hz, 1H), 0.62 (dd, $J = 15.3, 8.3$ Hz, 1H).

$^{13}\text{C NMR}$ (151 MHz, CDCl_3) δ 82.70, 39.55, 32.08, 29.44, 26.93, 24.80, 24.72, 22.62, 22.34, 19.68, 14.04.

$^{11}\text{B NMR}$ (192 MHz, CDCl_3) δ 33.0.

^1H NMR analysis of the Mosher ester of the corresponding alcohol after oxidation indicated 88:12 er.



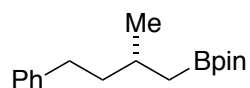
Compound 3m was synthesized according to the **General Procedure** with an alteration. The reaction was carried out with alkene **2m** (84.6 μL , 3 equiv) and HBpin (29.0 μL , 0.200 mmol) at -5°C for 72 h. Compound **3m** was purified by flash column chromatography (2% ethyl acetate in hexanes) and obtained as a colorless oil in 80% yield.

^1H NMR (600 MHz, CDCl_3) δ 1.77 – 1.70 (m, 1H), 1.62 – 1.54 (m, 1H), 1.22 (s, 12H), 1.09 – 0.99 (m, 2H), 0.86 (d, $J = 6.6$ Hz, 3H), 0.82 (d, $J = 6.6$ Hz, 3H), 0.81 (d, $J = 6.6$ Hz, 3H), 0.77 (dd, $J = 15.2, 5.8$ Hz, 1H), 0.59 (dd, $J = 15.2, 8.2$ Hz, 1H).

^{13}C NMR (151 MHz, CDCl_3) δ 82.68, 49.31, 26.98, 25.39, 24.78, 24.73, 23.21, 22.39, 20.07.

^{11}B NMR (192 MHz, CDCl_3) δ 33.7.

^1H NMR analysis of the Mosher ester of the corresponding alcohol after oxidation indicated 86:14 er.



Compound 3n was synthesized according to the **General Procedure** with **2n** (29.2 mg, 0.200 mmol). Compound **3n** was purified by flash column chromatography (2% ethyl acetate in hexanes) and obtained as a colorless oil in 83% yield.

^1H NMR (600 MHz, CDCl_3) δ 7.28 (t, $J = 7.5$ Hz, 2H), 7.21 – 7.16 (m, 3H), 2.68 – 2.58 (m, 2H), 1.83 – 1.78 (m, 1H), 1.68 – 1.59 (m, 1H), 1.56 – 1.48 (m, 1H), 1.27 (s, 12H), 1.01 (d, $J = 6.7$ Hz, 3H), 0.92 (dd, $J = 15.4, 5.8$ Hz, 1H), 0.74 (dd, $J = 15.3, 8.3$ Hz, 1H).

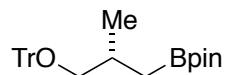
^{13}C NMR (151 MHz, CDCl_3) δ 143.16, 128.32, 128.19, 125.44, 82.85, 41.52, 33.77, 29.38, 24.87, 24.80, 22.26, 19.56.

^{11}B NMR (192 MHz, CDCl_3) δ 33.7.

HRMS (EI+) Calculated for $\text{C}_{17}\text{H}_{27}\text{BO}_2$ $[\text{M}]^+$: 274.2104, Found: 274.2100.

$[\alpha]_{\text{D}}^{23} = -4.4$ ($c = 0.858$, DCM).

SFC analysis of the corresponding alcohol after oxidation (AD-H, 2% MeOH/ CO_2 , 10 MPa, 4.0 mL/min, 220 nm) indicated 86:14 er: t_{R} (major) = 5.3 min, t_{R} (minor) = 5.6 min.



Compound 3o was synthesized according to the **General Procedure** with an alteration. The reaction was carried out with alkene **2o** (62.9 mg, 0.200 mmol) and HBpin (35.0 μL , 1.2 equiv) in decalin (600 μL) at -5°C for 72 h. Compound **3o** was purified by flash column chromatography (5% ethyl acetate in hexanes) and obtained as a colorless oil in 90% yield.

^1H NMR (600 MHz, CDCl_3) δ 7.52 – 7.43 (m, 6H), 7.30 (t, $J = 7.6$ Hz, 6H), 7.26 – 7.19 (m, 3H), 2.97 (dd, $J = 8.5, 5.6$ Hz, 1H), 2.84 (dd, $J = 8.5, 7.1$ Hz, 1H), 1.22 (s, 6H), 1.21 (s, 6H), 1.05 (d, $J = 6.7$ Hz, 3H), 0.97 (dd, $J = 15.6, 5.8$ Hz, 1H), 0.69 (dd, $J = 15.6, 8.8$ Hz, 1H).

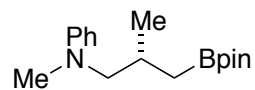
^{13}C NMR (151 MHz, CDCl_3) δ 144.57, 128.81, 127.59, 126.68, 85.96, 82.85, 69.94, 30.45, 24.84, 24.73, 19.91, 16.45.

^{11}B NMR (192 MHz, CDCl_3) δ 33.9.

HRMS (EI+) Calculated for $\text{C}_{29}\text{H}_{35}\text{BO}_3$ $[\text{M}]^+$: 442.2679, Found: 442.2682.

$[\alpha]_{\text{D}}^{23} = -8.1$ ($c = 0.942$, DCM).

SFC analysis of the corresponding alcohol after oxidation (AD-H, 10% IPA/ CO_2 , 10 MPa, 2.5 mL/min, 220 nm) indicated 91:9 er: t_{R} (major) = 4.3 min, t_{R} (minor) = 3.7 min.



Compound 3p was synthesized according to the **General Procedure** with **2p** (32.2 mg, 0.200 mmol). Compound **3p** was purified by flash column chromatography (10% ethyl acetate in hexanes) and obtained as a yellow oil in 52% yield.

^1H NMR (600 MHz, CDCl_3) δ 7.22 (t, $J = 7.1$ Hz, 2H), 6.74 (d, $J = 8.2$ Hz, 2H), 6.67 (t, $J = 7.2$ Hz, 1H), 3.23 (dd, $J = 14.5, 6.7$ Hz, 1H), 3.01 (dd, $J = 14.5, 8.2$ Hz, 1H), 2.96 (s, 3H), 2.27 – 2.15 (m, 1H), 1.26 (s, 6H), 1.25 (s, 6H), 0.97 (d, $J = 6.6$ Hz, 3H), 0.88 (dd, $J = 15.6, 6.5$ Hz, 1H), 0.71 (dd, $J = 15.6, 7.8$ Hz, 1H).

^{13}C NMR (151 MHz, CDCl_3) δ 149.79, 128.93, 115.55, 111.92, 82.97, 61.59, 39.44, 28.93, 24.92, 24.79, 20.48, 17.20.

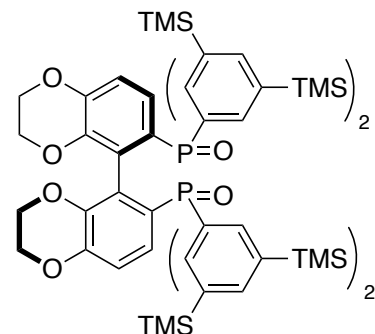
^{11}B NMR (192 MHz, CDCl_3) δ 33.2.

HRMS (ESI+) Calculated for $\text{C}_{17}\text{H}_{29}\text{BNO}_2$ $[\text{M}+\text{H}]^+$: 290.2286, Found: 290.2294.

$[\alpha]_{\text{D}}^{23} = 5.2$ ($c = 0.5$, DCM).

SFC analysis of the corresponding alcohol after oxidation (OD-H, 3% IPA/ CO_2 , 10 MPa, 2.5 mL/min, 220 nm) indicated 90:10 er: t_{R} (major) = 3.1 min, t_{R} (minor) = 2.7 min.

4.4.4 Ligand Synthesis



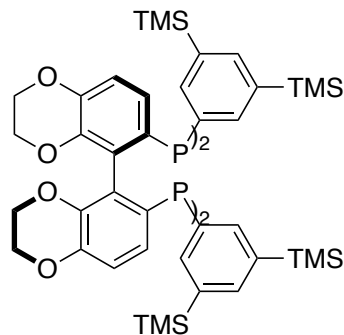
(*R*)-TMS-SYNPHOS oxide

A 20 mL vial was charged with magnesium turnings (144 mg, 12 equiv) and THF (2 mL). 3,5-Bis(trimethylsilyl)bromobenzene (1.66 g, 11 equiv) was added in one portion. The vial was allowed to stir at ambient temperature for 1 h and placed in a heating block set to 65 °C. After 2 h at this temperature, the vial was cooled to rt, and the solution was taken up into a syringe. In a 25 mL round-bottom flask, (*R*)-(2,2',3,3'-tetrahydro-[5,5'-bibenzo[*b*][1,4]dioxine]-6,6'-diyl)bisphosphonic dichloride (252 mg, 0.500 mmol), synthesized by a known procedure,⁴¹ was dissolved in 1 mL THF. The flask was cooled to 0 °C and the Grignard solution was added dropwise over the course of 20 minutes. The resulting brown solution was allowed to warm to rt and stir overnight. The reaction was quenched with water, and the organic material was extracted with EtOAc. The

organic phase was combined and dried over Na_2SO_4 . The crude material was purified by flash chromatography with 65% EtOAc in hexanes as eluent. The title compound was isolated as a pale solid (411 mg, 66% yield).

^1H NMR (600 MHz, CDCl_3) δ 7.82 (d, $J = 11.5$, 4H), 7.77 (d, $J = 11.2$, 4H), 7.71 (s, 2H), 7.67 (s, 2H), 6.74 (dd, $J = 8.1$, 2.6 Hz, 2H), 6.67 (dd, $J = 12.9$, 8.4 Hz, 2H), 3.98 (ddd, $J = 10.0$, 7.1, 2.4 Hz, 2H), 3.72 (ddd, $J = 11.5$, 5.2, 2.3 Hz, 2H), 3.50 (ddd, $J = 11.7$, 5.3, 2.5 Hz, 2H), 3.10 (ddd, $J = 11.9$, 7.0, 2.3 Hz, 2H), 0.22 (s, 36H), 0.13 (s, 36H).

^{31}P NMR (243 MHz, CDCl_3) δ 29.3.



(*R*)-TMS-SYNPHOS

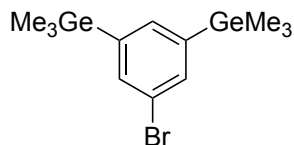
A 20 mL screw-capped vial was charged with (*R*)-TMS-SYNPHOS oxide (382 mg, 0.306 mmol). Mesitylene (2 mL) and Bu_3N (1.09 mL, 15 equiv) were added to the vial. Trichlorosilane (371 μL , 12 equiv) in mesitylene (1 mL) was then added dropwise to the solution. Once the evolution of gas ceased, the vial was sealed with a Teflon-lined cap and placed in a 120 °C heating block. After 22 h, the vial was removed from the heating block and placed in an ice bath. Under a stream of nitrogen and vigorous stirring, an aqueous solution of NaOH (25%, 2 mL) was added to the vial dropwise. The vial was sealed and placed in an 80 °C heating block. After 1 hour, a biphasic mixture had formed. The organic material was extracted with EtOAc. The organic solution was washed with a 2 M solution of HCl and dried over Na_2SO_4 . The crude material was purified by flash chromatography with 10% EtOAc in hexanes as eluent to yield the title compound as a white solid, which was stored under nitrogen (303 mg, 81% yield).

^1H NMR (600 MHz, CDCl_3) δ 7.54 (s, 2H), 7.46 (s, 6H), 7.36 (s, 4H), 6.78 (d, $J = 8.4$ Hz, 2H), 6.66 (d, $J = 8.3$ Hz, 2H), 4.03 (ddd, $J = 11.4$, 6.7, 2.3 Hz, 2H), 3.77 – 3.70 (m, 2H), 3.66 (ddd, $J = 11.6$, 5.3, 2.2 Hz, 2H), 3.20 – 3.02 (m, 2H), 0.19 (s, 36H), 0.08 (s, 36H).

^{31}P NMR (243 MHz, CDCl_3) δ -15.2.

HRMS (ESI+) Calculated for $\text{C}_{64}\text{H}_{97}\text{O}_4\text{P}_2\text{Si}_8$ $[\text{M}+\text{H}]^+$: 1215.5011, Found: 1215.5005.

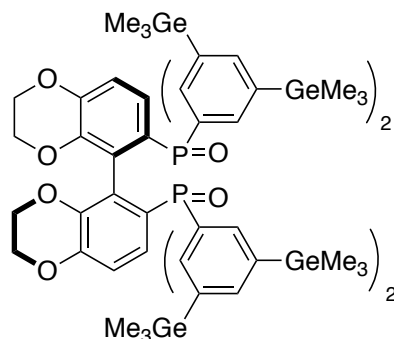
$[\alpha]_{\text{D}}^{23} = 22.7$ ($c = 0.295$, DCM).



A 250 mL round-bottom flask was charged with 1,3,5-tribromobenzene (3.15 g, 10.0 mmol) and diethyl ether (50 mL), and a magnetic stirbar. The flask was cooled to -78 °C. *n*BuLi (2.5 M in hexanes, 4.2 mL, 1.06 equiv) was added to the suspensions dropwise, and the mixture was stirred for an additional 30 minutes. The reaction mixture was re-cooled to -78 °C, and Me_3GeCl (1.4 mL,

1.14 equiv) was added. The reaction was warmed to rt and stirred for an additional 1 hour. The reaction mixture was again cooled to $-78\text{ }^{\circ}\text{C}$, and $n\text{BuLi}$ (2.5 M in hexanes, 4.8 mL, 1.2 equiv) was added dropwise. The resulting mixture was warmed to $0\text{ }^{\circ}\text{C}$ and stirred for 1 hour. The reaction mixture was re-cooled to $-78\text{ }^{\circ}\text{C}$, and Me_3GeCl (1.7 mL, 1.4 equiv) was added. After being stirred overnight at rt, the reaction was quenched by addition of 50 mL of water. The organic material was extracted with diethyl ether. The resulting solution was dried over Na_2SO_4 , and filtered through celite. The solvent was removed *in vacuo*. The crude materials were purified by flash chromatography with hexanes as eluent to afford a clear liquid, which was a mixture of the title compound and tris(trimethylgermyl)benzene in a 3.5:1 molar ratio (2.2 g, ca. 55% yield).

$^1\text{H NMR}$ (600 MHz, CDCl_3) δ 7.58 (s, 2H), 7.49 (s, 1H), 0.45 (s, 18H).



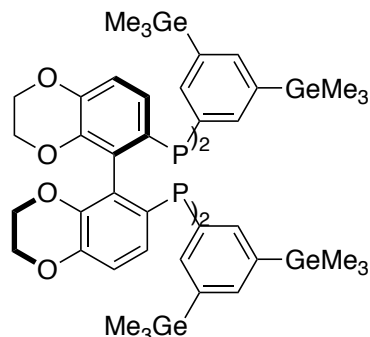
(*R*)-TMG-SYNPHOS oxide

A 20 mL vial was charged with magnesium turnings (180 mg, 15 equiv) and THF (2 mL). 3,5-Bis(trimethylsilyl)bromobenzene (2.34 g, 12 equiv) was added in one portion. The vial was allowed to stir at ambient temperature for 1 h and placed in a heating block set to $65\text{ }^{\circ}\text{C}$. After 2 h at this temperature, the vial was cooled to rt, and the solution was taken up into a syringe. In a 25 mL round-bottom flask, (*R*)-(2,2',3,3'-tetrahydro-[5,5'-bibenzo[*b*][1,4]dioxine]-6,6'-diyl)bisphosphonic dichloride (252 mg, 0.500 mmol), synthesized by a known procedure,⁴¹ was dissolved in 1 mL THF. The flask was cooled to $0\text{ }^{\circ}\text{C}$ and the Grignard solution was added dropwise over the course of 20 minutes. The resulting brown solution was allowed to warm to rt and stir overnight. The reaction was quenched with water, and the organic material was extracted with EtOAc. The organic phase was combined and dried over Na_2SO_4 . The crude material was purified by flash chromatography with 65% EtOAc in hexanes as eluent. The title compound was isolated as a pale solid (489 mg, 61% yield).

$^1\text{H NMR}$ (600 MHz, CDCl_3) δ 7.75 (dd, $J = 11.5, 1.2\text{ Hz}$, 4H), 7.70 (dd, $J = 11.1, 1.2\text{ Hz}$, 4H), 7.61 (s, 2H), 7.56 (s, 2H), 6.73 (dd, $J = 8.4, 3.1\text{ Hz}$, 2H), 6.69 (dd, $J = 12.8, 8.4\text{ Hz}$, 2H), 3.98 (ddd,

$J = 11.3, 6.9, 2.4$ Hz, 2H), 3.73 (ddd, $J = 11.3, 5.0, 2.3$ Hz, 2H), 3.51 (ddd, $J = 11.5, 4.9, 2.4$ Hz, 2H), 3.12 (ddd, $J = 11.5, 6.9, 2.3$ Hz, 2H), 0.34 (s, 36H), 0.25 (s, 36H).

^{31}P NMR (243 MHz, CDCl_3) δ 29.1.



(*R*)-TMG-SYNPHOS

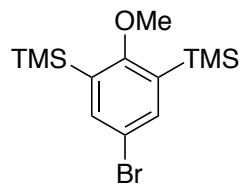
A 20 mL screw-capped vial was charged with (*R*)-TMG-SYNPHOS oxide (489 mg, 0.292 mmol). Mesitylene (2 mL) and Bu_3N (1.04 mL, 15 equiv) were added to the vial. Trichlorosilane (354 μL , 12 equiv) in mesitylene (4 mL) was then added dropwise to the solution. Once the evolution of gas ceased, the vial was sealed with a Teflon-lined cap and placed in a 120 °C heating block. After 22 h, the vial was removed from the heating block and placed in an ice bath. Under a stream of nitrogen and vigorous stirring, an aqueous solution of NaOH (25%, 2 mL) was added to the vial dropwise. The vial was sealed and placed in an 80 °C heating block. After 1 hour, a biphasic mixture had formed. The organic material was extracted with EtOAc. The organic solution was washed with a 2 M solution of HCl and dried over Na_2SO_4 . The crude material was purified by flash chromatography with 10% EtOAc in hexanes as eluent to yield the title compound as a white solid, which was stored under nitrogen (303 mg, 83% yield).

^1H NMR (600 MHz, CDCl_3) δ 7.43 (s, 2H), 7.40 – 7.36 (m, 4H), 7.35 (d, $J = 1.5$ Hz, 2H), 7.29 (dd, $J = 4.2, 1.9$ Hz, 4H), 6.79 (d, $J = 8.4$ Hz, 2H), 6.68 (dt, $J = 8.4, 1.6$ Hz, 2H), 4.03 (ddd, $J = 11.5, 6.8, 2.3$ Hz, 2H), 3.74 (ddd, $J = 11.3, 5.2, 2.2$ Hz, 2H), 3.67 (ddd, $J = 11.5, 5.2, 2.4$ Hz, 2H), 3.13 (ddd, $J = 11.6, 6.8, 2.2$ Hz, 2H), 0.31 (s, 32H), 0.20 (s, 32H).

^{31}P NMR (243 MHz, CDCl_3) δ -15.0.

HRMS (ESI+) Calculated for $\text{C}_{64}\text{H}_{97}\text{O}_4\text{P}_2\text{Ge}_8$ $[\text{M}+\text{H}]^+$: 1572.0631, Found: 1572.0647.

$[\alpha]_{\text{D}}^{23} = 18.3$ ($c = 0.525$, DCM).

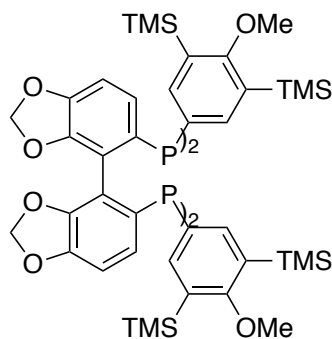


A 20 mL vial was charged with $[\text{Ir}(\text{COD})_2\text{OMe}]_2$ (10.0 mg, 0.5 mol %), dtbpy (8.0 mg, 1.0 mol %), B_2pin_2 (533 mg, 0.7 equiv), 2,6-bis(trimethylsilyl)anisole **4** (758 mg, 3.00 mmol), and 3 mL of THF. The vial was capped, sealed with electrical tape, and placed in a heating block set to 80 °C. This procedure was repeated twice. After being stirred at 80 °C for 20 h, the contents of the three reaction vials were combined and concentrated *in vacuo*. In a 500 mL round-bottom flask, the resulting crude material was dissolved in 10 mL of THF and added 25 mL of methanol and 25 mL of water. The reaction mixture was heated to 80 °C. Aliquots of the reaction were taken

periodically and analyzed by GC. After 3 days of reaction, the flask was cooled to rt. The organic materials were extracted with diethyl ether (50 mL) three times. The organic layers were combined and dried over Na₂SO₄. The crude material was purified by flash chromatography with 5% EtOAc in hexanes as eluent to yield compound **6** as a colorless liquid (1.18 mg, 40% yield).

¹H NMR (600 MHz, CDCl₃) δ 7.55 (s, 2H), 3.73 (s, 3H), 0.36 (s, 18H).

¹³C NMR (151 MHz, CDCl₃) δ 170.12, 139.49, 135.32, 117.76, 63.64, 0.01.



DTMSM-SEGPBOS

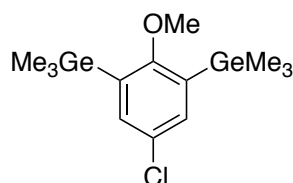
A 20 mL vial was charged with magnesium turnings (90 mg, 15 equiv) and THF (2 mL). 2,6-Bis(trimethylsilyl)-4-bromoanisole **6** (750 mg, 12 equiv) was added in one portion. The vial was allowed to stir at ambient temperature for 1 h and placed in a heating block set to 65 °C. After 2 h at this temperature, the vial was cooled to rt, and the solution was taken up into a syringe. In a 25 mL round-bottom flask, (2,2',3,3'-tetrahydro-[4,4'-bibenzo-1,3-dioxole]-6,6'-diyl)bisphosphonic dichloride (119 mg, 0.250 mmol), synthesized by a known procedure,⁴² was dissolved in 1 mL THF. The flask was cooled to 0 °C and the Grignard solution was added dropwise over the course of 20 minutes. The resulting brown solution was allowed to warm to rt and stir overnight. The reaction was quenched with water, and the organic material was extracted with EtOAc. The organic phase was combined and dried over Na₂SO₄. The crude material was purified by flash chromatography with 65% EtOAc in hexanes as eluent. The phosphine oxide was isolated along with a small fraction of impurities. This material was used directed in the next step.

A 20 mL screw-capped vial was charged with the crude phosphine oxide. Mesitylene (1 mL) and Bu₃N (357 μL, 15 equiv) were added to the vial. Trichlorosilane (121 μL, 12 equiv) in mesitylene (0.5 mL) was then added dropwise to the solution. Once the evolution of gas ceased, the vial was sealed with a Teflon-lined cap and placed in a 120 °C heating block. After 22 h, the vial was removed from the heating block and placed in an ice bath. Under a stream of nitrogen and vigorous stirring, an aqueous solution of NaOH (25%, 2 mL) was added to the vial dropwise. The vial was sealed and placed in an 80 °C heating block. After 1 hour, a biphasic mixture had formed. The organic material was extracted with EtOAc. The organic solution was washed with a 2 M solution of HCl and dried over Na₂SO₄. The crude material was purified by flash chromatography with 10%

EtOAc in hexanes as eluent to yield the title compound as a white solid, which was stored under nitrogen (137 mg, 42% yield).

^1H NMR (600 MHz, CDCl_3) δ 7.49 – 7.46 (m, 4H), 7.34 – 7.31 (m, 4H), 6.74 (d, $J = 8.0$, 2H), 6.58 (dt, $J = 8.0$, 1.8 Hz, 2H), 5.67 (d, $J = 1.8$ Hz, 2H), 4.83 (d, $J = 1.9$ Hz, 2H), 3.74 (s, 6H), 3.70 (s, 6H), 0.23 (s, 36H), 0.22 (s, 36H).

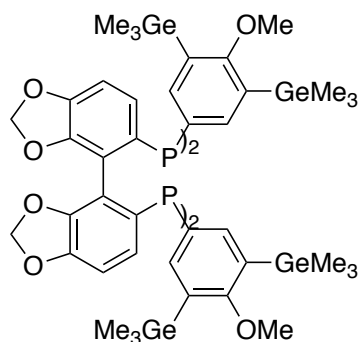
^{31}P NMR (243 MHz, CDCl_3) δ -15.2.



A 250 mL round-bottom flask was charged with 2,6-dibromo-4-chloroanisole (900 mg, 3.00 mmol) and diethyl ether (6 ml), and a magnetic stirbar. The flask was cooled to $-78\text{ }^\circ\text{C}$. $n\text{BuLi}$ (2.5 M in hexanes, 4.2 mL, 1.0 equiv) was added to the suspensions dropwise, and the mixture was stirred for an additional 30 minutes. The reaction mixture was re-cooled to $-78\text{ }^\circ\text{C}$, and Me_3GeCl (1.4 ml, 1.1 equiv) was added. The reaction was warmed to rt and stirred for an additional 1 hour. The reaction mixture was again cooled to $-78\text{ }^\circ\text{C}$, and $n\text{BuLi}$ (2.5 M in hexanes, 4.8 mL, 1.2 equiv) was added dropwise. The resulting mixture was warmed to $0\text{ }^\circ\text{C}$ and stirred for 1 hour. The reaction mixture was re-cooled to $-78\text{ }^\circ\text{C}$, and Me_3GeCl (1.7 ml, 1.3 equiv) was added. After being stirred overnight at rt, the reaction was quenched by addition of 50 mL of water. The organic material was extracted with diethyl ether. The resulting solution was dried over Na_2SO_4 , and filtered through celite. The solvent was removed *in vacuo*. The crude materials were purified by flash chromatography with hexanes as eluent to afford compound **9** as a clear liquid (90% yield).

^1H NMR (600 MHz, CDCl_3) δ 7.32 (s, 2H), 3.70 (s, 3H), 0.48 (d, $J = 1.6$ Hz, 18H).

^{13}C NMR (151 MHz, CDCl_3) δ 167.82, 136.43, 135.09, 129.51, 63.30, -0.32.



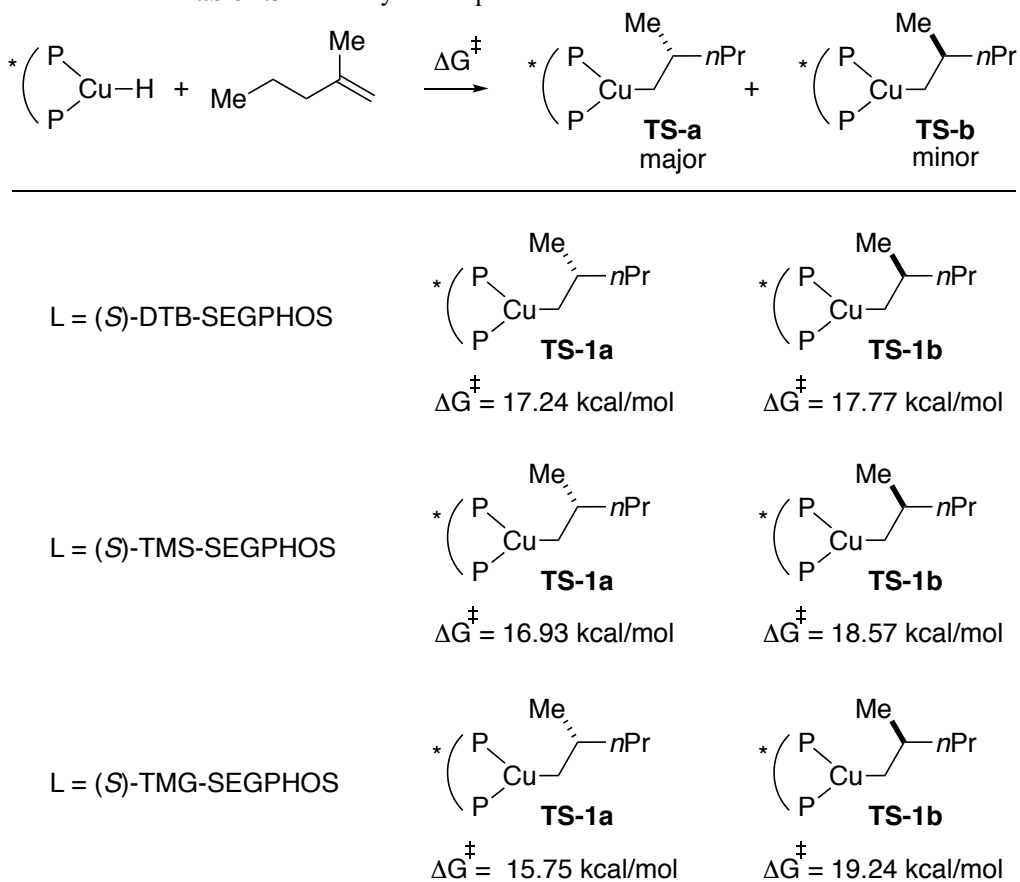
A 20 mL vial was charged with magnesium turnings (216 mg, 21 equiv) and THF (2 ml). 2,6-Bis(trimethylgermyl)-4-chloroanisole **9** (2.26 g, 14 equiv) was added in one portion. The vial was allowed to stir at ambient temperature for 1 h and placed in a heating block set to $65\text{ }^\circ\text{C}$. After 2 h at this temperature, the vial was cooled to rt, and the solution was taken up into a syringe. In a 25 mL round-bottom flask, (2,2',3,3'-tetrahydro-[4,4'-bibenzo-1,3-dioxole]-6,6'-diyl)bisphosphonic dichloride (200 mg, 0.420 mmol), synthesized by a known procedure,⁴² was dissolved in 1 mL THF. The flask was cooled to $0\text{ }^\circ\text{C}$ and the Grignard solution was added dropwise over the course of 20 minutes. The resulting brown solution was allowed to warm to rt and stir overnight. The reaction was quenched with water, and the organic material was extracted with EtOAc. The

with the M06 functional. SDD and 6-311+G(d,p) basis sets were used for Cu and all other atoms, respectively. The SMD model was used for solvent corrections. Frequency calculations were also conducted with the optimized geometries to confirm that the stationary points were minima (zero imaginary frequencies) or transition states (one imaginary frequency). The structures were generated using CYLView.

Summary of computed barriers for alkene insertion

Activation barrier for individual transition states was summarized in Table 4.3.

Table 4.3 Summary of computed barriers for alkene insertion^a



Summary of energies of all computed structures

Electronic energies, enthalpies, free energies, and imaginary frequencies of all computed structures are tabulated in Table 4.4.

Table 4.4 Summary of computational data of all calculated structures^a

	E(SCF)	H	G	H _{corr}	G _{corr}	E(SMD)	imaginary frequency
(DTB-SEGPHOS) CuH	-3904.410198	-3902.853677	-3903.063643	-3903.023227	-3901.466706	-3901.676672	-
TS-1a	-4140.231944	-4138.500006	-4138.72712	-4138.736438	-4137.0045	-4137.231614	-788.74
TS-1b	-4140.231859	-4138.49992	-4138.726929	-4138.735699	-4137.003759	-4137.230769	-791.00
(TMS-SEGPHOS) CuH	-5915.770875	-5914.283518	-5914.543578	-5914.462822	-5912.975465	-5913.235525	-
TS-2a	-6151.592582	-6149.929783	-6150.207924	-6150.175622	-6148.512822	-6148.790964	-805.70
TS-2b	-6151.592403	-6149.929612	-6150.206974	-6150.173781	-6148.51099	-6148.788352	-803.57
(TMG-SEGPHOS) CuH	-20197.64335	-20196.1597	-20196.43834	-20213.72581	-20212.24215	-20212.52079	-
TS-3a	-20433.46527	-20431.8062	-20432.10074	-20449.44265	-20447.78357	-20448.07811	-811.45
TS-3b	-20433.4651	-20431.80602	-20432.10072	-20449.43694	-20447.77786	-20448.07255	-801.67
alkene	-235.853286	-235.678478	-235.718884	-235.7168236	-235.5420156	-235.5824216	-

^aSingle-point energies were corrected with a SMD solvation model in cyclohexane. Unit for electronic energies is Hartree and unit for imaginary frequencies is cm⁻¹.

4.5 References

- [1] Hall, D. G., *Boronic Acids: Preparation and Applications in Organic Synthesis and Medicine*. Wiley-VCH: Weinheim, 2005.
- [2] Matteson, D. S., *Stereodirected Synthesis with Organoboranes*. Springer: Berlin, Heidelberg, 1995.
- [3] Leonori, D.; Aggarwal, V. K., *Angew. Chem. Int. Ed.* **2015**, *54*, 1082.
- [4] Crudden, Cathleen M.; Edwards, D., *Eur. J. Org. Chem.* **2003**, *2003*, 4695.
- [5] Burgess, K.; Ohlmeyer, M. J., *Chem. Rev.* **1991**, *91*, 1179.
- [6] Brown, H. C.; Singaram, B., *Acc. Chem. Res.* **1988**, *21*, 287.
- [7] Thomas, S. P.; Aggarwal, V. K., *Angew. Chem. Int. Ed.* **2009**, *48*, 1896.
- [8] Männig, D.; Nöth, H., *Angew. Chem. Int. Ed.* **1985**, *24*, 878.
- [9] Hayashi, T.; Matsumoto, Y.; Ito, Y., *J. Am. Chem. Soc.* **1989**, *111*, 3426.
- [10] Obligacion, J. V.; Chirik, P. J., *J. Am. Chem. Soc.* **2013**, *135*, 19107.
- [11] Crudden, C. M.; Hleba, Y. B.; Chen, A. C., *J. Am. Chem. Soc.* **2004**, *126*, 9200.
- [12] Burgess, K.; Ohlmeyer, M. J., *J. Org. Chem.* **1988**, *53*, 5178.
- [13] Smith, S. M.; Thacker, N. C.; Takacs, J. M., *J. Am. Chem. Soc.* **2008**, *130*, 3734.
- [14] Noh, D.; Chea, H.; Ju, J.; Yun, J., *Angew. Chem. Int. Ed.* **2009**, *48*, 6062.
- [15] Smith, S. M.; Takacs, J. M., *J. Am. Chem. Soc.* **2010**, *132*, 1740.
- [16] Chen, J.; Xi, T.; Lu, Z., *Org. Lett.* **2014**, *16*, 6452.
- [17] Zhang, L.; Zuo, Z.; Wan, X.; Huang, Z., *J. Am. Chem. Soc.* **2014**, *136*, 15501.
- [18] Xi, Y.; Hartwig, J. F., *J. Am. Chem. Soc.* **2016**, *138*, 6703.

- [19] Feng, X.; Jeon, H.; Yun, J., *Angew. Chem. Int. Ed.* **2013**, *52*, 3989.
- [20] Shoba, V. M.; Thacker, N. C.; Bochat, A. J.; Takacs, J. M., *Angew. Chem. Int. Ed.* **2016**, *55*, 1465.
- [21] Chakrabarty, S.; Takacs, J. M., *J. Am. Chem. Soc.* **2017**, *139*, 6066.
- [22] Rubina, M.; Rubin, M.; Gevorgyan, V., *J. Am. Chem. Soc.* **2003**, *125*, 7198.
- [23] Lee, H.; Lee, B. Y.; Yun, J., *Org. Lett.* **2015**, *17*, 764.
- [24] Chen, J.; Xi, T.; Ren, X.; Cheng, B.; Guo, J.; Lu, Z., *Org. Chem. Front* **2014**, *1*, 1306.
- [25] Jang, W. J.; Song, S. M.; Moon, J. H.; Lee, J. Y.; Yun, J., *J. Am. Chem. Soc.* **2017**, *139*, 13660.
- [26] Teo, W. J.; Ge, S., *Angew. Chem. Int. Ed.* **2018**, *57*, 12935.
- [27] Chen, J.; Lu, Z., *Org. Chem. Front* **2018**, *5*, 260.
- [28] Zhu, S.; Buchwald, S. L., *J. Am. Chem. Soc.* **2014**, *136*, 15913.
- [29] Chen, J.; Cheng, B.; Cao, M.; Lu, Z., *Angew. Chem. Int. Ed.* **2015**, *54*, 4661.
- [30] Deng, Y.; Wang, H.; Sun, Y.; Wang, X., *ACS Catal.* **2015**, *5*, 6828.
- [31] Tolman, C. A., *Chem. Rev.* **1977**, *77*, 313.
- [32] Clarke, M. L.; Frew, J. J. R., Ligand electronic effects in homogeneous catalysis using transition metal complexes of phosphine ligands. In *Organometallic Chemistry: Volume 35*, The Royal Society of Chemistry: 2009; Vol. 35, pp 19.
- [33] Raynal, M.; Ballester, P.; Vidal-Ferran, A.; van Leeuwen, P. W. N. M., *Chem. Soc. Rev.* **2014**, *43*, 1660.
- [34] Straker, R. N.; Peng, Q.; Mekareeya, A.; Paton, R. S.; Anderson, E. A., *Nat. Comm.* **2016**, *7*, 10109.
- [35] Neel, A. J.; Hilton, M. J.; Sigman, M. S.; Toste, F. D., *Nature* **2017**, *543*, 637.
- [36] Xi, Y.; Hartwig, J. F., *J. Am. Chem. Soc.* **2017**, *139*, 12758.
- [37] Lu, G.; Liu, R. Y.; Yang, Y.; Fang, C.; Lambrecht, D. S.; Buchwald, S. L.; Liu, P., *J. Am. Chem. Soc.* **2017**, *139*, 16548.
- [38] Thomas, A. A.; Speck, K.; Kevlishvili, I.; Lu, Z.; Liu, P.; Buchwald, S. L., *J. Am. Chem. Soc.* **2018**, *140*, 13976.
- [39] Zhang, Q.-W.; An, K.; Liu, L.-C.; Yue, Y.; He, W., *Angew. Chem. Int. Ed.* **2015**, *54*, 6918.
- [40] Zhang, Q.-W.; An, K.; Liu, L.-C.; Zhang, Q.; Guo, H.; He, W., *Angew. Chem. Int. Ed.* **2017**, *56*, 1125.
- [41] Berhal, F.; Esseiva, O.; Martin, C.-H.; Tone, H.; Genet, J.-P.; Ayad, T.; Ratovelomanana-Vidal, V., *Org. Lett.* **2011**, *13*, 2806.
- [42] Sevov, C. S.; Hartwig, J. F., *J. Am. Chem. Soc.* **2014**, *136*, 10625.
- [43] See section 4.4 for details.
- [44] Lata, C. J.; Crudden, C. M., *J. Am. Chem. Soc.* **2010**, *132*, 131.
- [45] Pereira, S.; Srebnik, M., *J. Am. Chem. Soc.* **1996**, *118*, 909.
- [46] Pereira, S.; Srebnik, M., *Tetrahedron Lett.* **1996**, *37*, 3283.
- [47] Chen, X.; Cheng, Z.; Guo, J.; Lu, Z., *Nat. Commun.* **2018**, *9*, 3939.
- [48] Obligacion, J. V.; Chirik, P. J., *Org. Lett.* **2013**, *15*, 2680.
- [49] Ruddy, A. J.; Sydora, O. L.; Small, B. L.; Stradiotto, M.; Turculet, L., *Chem. Eur. J.* **2014**, *20*, 13918.
- [50] Palmer, W. N.; Diao, T.; Pappas, I.; Chirik, P. J., *ACS Catal.* **2015**, *5*, 622.
- [51] Scheuermann, M. L.; Johnson, E. J.; Chirik, P. J., *Org. Lett.* **2015**, *17*, 2716.
- [52] Hartwig, J. F., *Organotransition Metal Chemistry, from Bonding to Catalysis*. University Science Books: New York, 2010.

- [53] Murphy, J. M.; Liao, X.; Hartwig, J. F., *J. Am. Chem. Soc.* **2007**, *129*, 15434.
- [54] Fier, P. S.; Hartwig, J. F., *J. Am. Chem. Soc.* **2012**, *134*, 10795.
- [55] Bandar, J. S.; Pirnot, M. T.; Buchwald, S. L. *J. Am. Chem. Soc.* **2015**, *137*, 14812.
- [56] McGhee, A.M.; Kizirian, J.-C.; Procter, D. J. *Org. Biomol. Chem.* **2007**, *5*, 1021.
- [57] Myers, A. G.; Yang, B. H.; Chen, H.; McKinstry, L.; Kopecky, D. J.; Gleason, J. L. *J. Am. Chem. Soc.* **1997**, *119*, 6496.
- [58] Brenna, E.; Gatti, F. G.; Monti, D.; Parmeggiani, F.; Sacchetti, A. *ChemCatChem* **2012**, *4*, 653.
- [59] Murakata, M.; Tsutsui, H.; Hoshino, H. *Heterocycles* **1997**, *46*, 517.
- [60] Gaunt, M. J.; Jessiman, A.S.; Orsini, P.; Tanner, H. R.; Hook, D. F.; Ley, S. V. *Org. Lett.* **2003**, *5*, 4819.
- [61] Skaanderup, P. R.; Jensen, T. *Org. Lett.* **2008**, *10*, 2821.

CHAPTER 5

Copper-Catalyzed Formal Hydroamination of Unsymmetrical Internal Alkenes

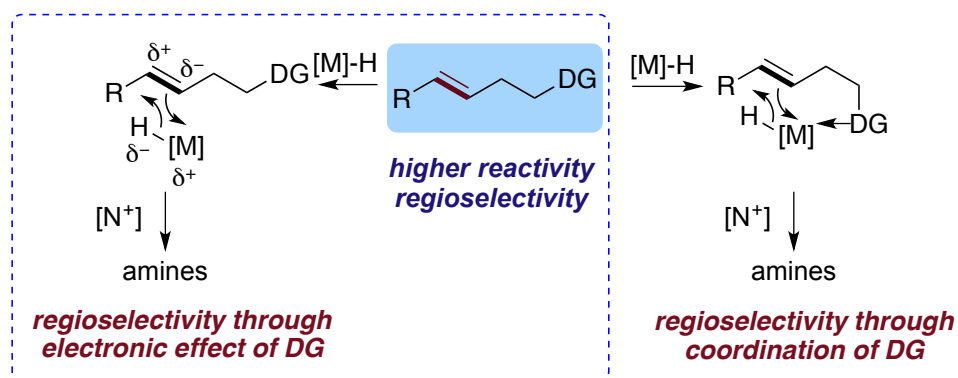
5.1 Introduction

Additions to alkenes are a fundamental class of reaction,¹ but the hydrofunctionalization of internal alkenes is challenging due to the low reactivity of internal alkenes and the difficulty in controlling the regioselectivity and stereoselectivity of addition of the H-X bond. Directed^{2,3} hydrogenations⁴ have been developed in which binding of the catalyst to the functional group controls the face of the alkene to which the addition occurs, and this concept has been extended to directed hydrofunctionalizations, such as hydrosilylation,^{5,6} hydroboration,⁷⁻¹⁰ and hydroacylation,¹¹⁻¹³ in which a polar substituent controls the carbon to which the functional group is bound. Although basic functional groups bind to the catalyst in some classes of directed addition reactions, the electronic properties of the polar group could control the regioselectivity of olefin functionalization in other cases, particularly the palladium-catalyzed oxidative functionalization of alkenes.¹⁴⁻¹⁶

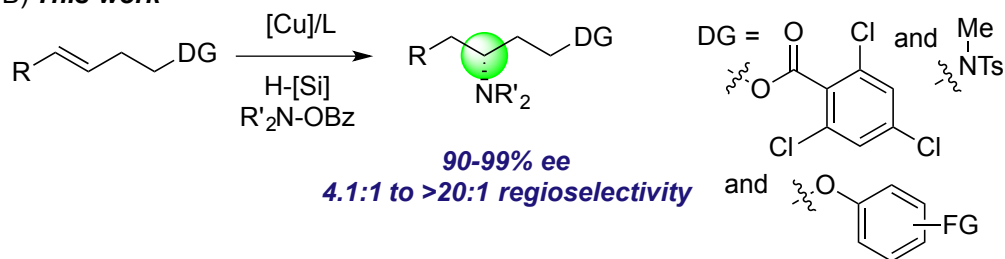
Although the hydroamination of alkenes has been widely studied,¹⁷⁻¹⁹ hydroaminations with alkenes containing directing groups are limited.²⁰ Our group has reported the hydroamination of internal α,β -unsaturated esters and nitriles²¹ and β -substituted vinylarenes,²² but the reactivity and regioselectivity of the reactions of these substrates is dominated by conjugation of the alkene to the carbonyl or arene substituents. The transition-metal catalyzed hydroamination of unconjugated alkenes directed by a functional group is limited to a single set of reactions of *N*-allyl imines.^{20,23,24}

Scheme 5.1 Regioselective hydroamination of unactivated internal alkenes with high regioselectivity.

A) Directing strategy for regioselective hydroamination



B) *This work*



The hydroamination of alkenes has been investigated with many classes of catalyst and reagents. The intramolecular addition of the N-H bonds of amines to alkenes has been reported with

complexes of many transition metals, and reactions catalyzed by those of the late transition metals occur with high compatibility for functional groups.²⁵⁻²⁹ Recently, Miura³⁰ and Buchwald³¹ showed independently that the intermolecular reaction of a hydride from a silane and an electrophilic amino ($^+NR_2$) group from a hydroxylamine derivative, rather than the N-H bond of an amine, gives rise to the products from formal hydroamination³²⁻³⁴ of vinylarenes and later 1,1-disubstituted alkenes.³⁵ During the course of our study on directed hydroamination of internal alkenes, Buchwald also reported reactions of symmetrical internal alkenes, as well as two unsymmetrical alkenes bearing unfunctionalized alkyl groups.³⁶ However, three equivalents of internal olefins were required to achieve high yields, making the utility of this method for reactions of valuable alkenes limited.

Here, we disclose our results showing that the formal hydroamination of internal alkenes containing an oxygen or nitrogen substituent in the homoallylic position occurs with high regioselectivity and enantioselectivity, and without the need for excess olefin. The observed regioselectivity results from the electronic effect of the substituent on the alkene, rather than direct coordination of the functionality to the metal. These results suggest that the inductive effects of remote electronegative groups on regioselectivity can be large enough to cause regioselectivity at an alkene to be high.¹⁴⁻¹⁶ This directed chemistry provides a simple route to highly enantioenriched 1,3-aminoalcohol derivatives, which are prevalent in natural products and pharmaceuticals^{37, 38} and are useful synthetic building blocks.³⁹

5.2 Results and Discussion

To probe the effect of functional groups on the regioselectivity for the formal hydroamination of internal alkenes, we first investigated the reaction of *trans*-3-hexenyl benzyl ether (**1a**) with diethoxymethylsilane (DEMS) and *N,N*-dibenzyl-*O*-benzoyl hydroxylamine (Table 5.1, entry 1). The reaction of these reagents in the presence of 10 mol % Cu(PPh₃)H and 11 mol % (*S*)-DTBM-SEGPHOS⁴⁰ in THF at room temperature for 84 hours gave the hydroamination products in moderate yield and regioselectivity (50 % yield, 3.3:1 regioselectivity). Modification of the electronic properties of the aryl group on the benzyl ether from electron-rich *p*-methoxy benzyl ether **1b** to electron-poor *p*-trifluoromethyl benzyl ether **1c** did not alter the yield and regioselectivity significantly. However, the regioselectivity was slightly higher for the reaction of the more electron-poor **1c** (entry 3).

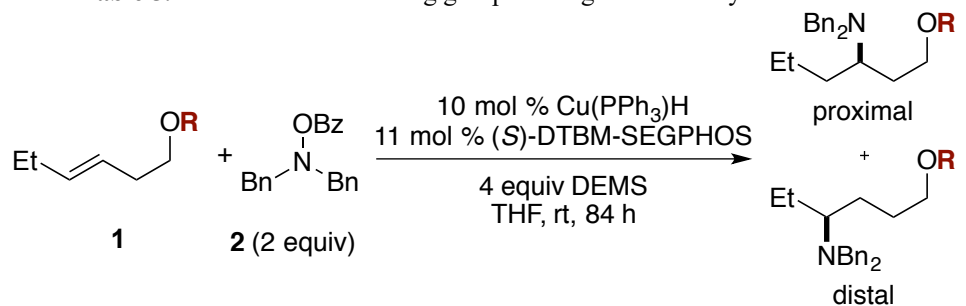
Thus, this formal hydroamination was conducted on an internal alkene bearing a more electron-withdrawing benzoyl group (**1d**). The regioselectivity of the reaction of the homoallylic benzoate was clearly higher than that for reaction of the homoallylic ethers (**1a-1c**). However the yield for reaction of the benzoate was lower, due to competing reduction of the ester in both the starting material (**1d**) and the corresponding hydroamination products.

To suppress the competing reduction, we studied reactions of benzoates bearing substituents at the *ortho* positions. Indeed, the reaction of an internal olefin bearing a 2,4,6-trichlorobenzoyl group (**1e**) afforded the hydroamination products in high yield, with high regioselectivity and without formation of the competing reduction product. Moreover, this reaction occurred with excellent enantioselectivity.

Reactions of alkenes containing other electron-deficient groups, such as phenyl ethers (**1f**, **1g**) and a tosylate (**1h**) were also studied. The reactions of the olefins bearing phenyl ether groups formed the addition product in higher yield and regioselectivity than those of reactions of olefins bearing alkyl ether groups. The yield and regioselectivity of reactions of alkenes bearing more

electron-deficient phenyl ethers were higher than those of reactions of alkenes bearing less electron-deficient phenyl ethers (**1f** vs **1g**). However, the removal of the phenyl ether group requires harsh conditions, rendering it impractical for directing the hydroamination. The alkene bearing a tosylate group reacted to less than 5% conversion (**1h**).

Table 5.1 Evaluation of directing groups for regioselective hydroamination^a

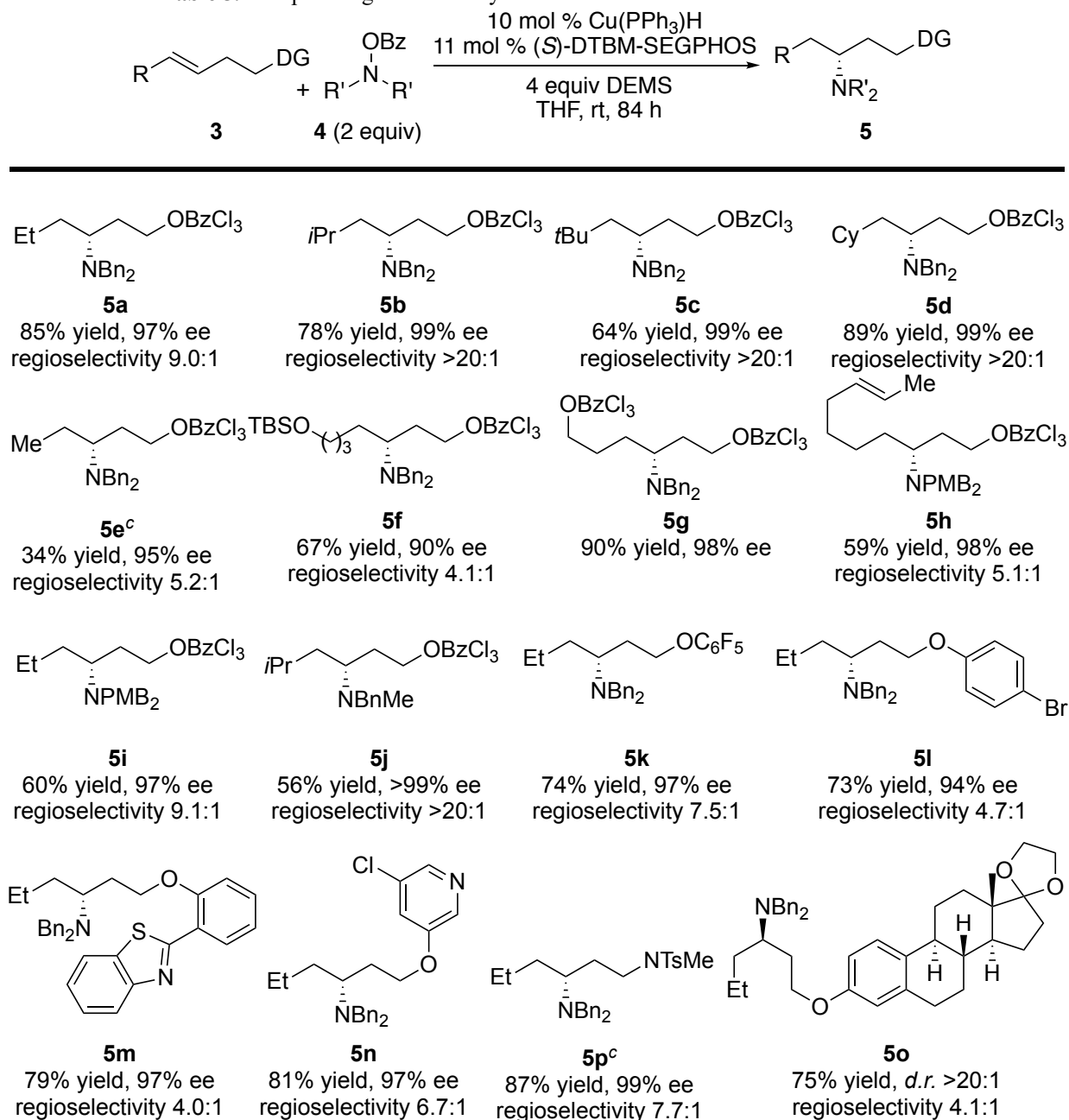


entry	R group	conversion ^b (%)	yield ^b (%)	p:d ^c	ee ^d (%)
1	Bn (1a)	55	50	3.3:1 ^e	-
2	PMB (1b)	48	46	3.2:1 ^e	-
3	4-CF ₃ -C ₆ H ₄ CH ₂ (1c)	56	52	3.6:1 ^e	-
4	Bz (1d)	>95	39	7.1:1	99
5	BzCl ₃ ^f (1e)	90	84	9.0:1	97
6	C ₆ F ₅ (1f)	90	81	7.6:1	97
7	4-Br-C ₆ H ₄ (1g)	84	83	4.6:1	94
8	Ts (1h)	<5	0	-	-

^aReaction conditions: **1** (0.05 mmol), **2** (0.10 mmol, 2 equiv), Cu(PPh₃)H (10 mol %) and (S)-DTBM-SEGPHOS (11 mol %) in THF (0.14 mL), rt, 84 h; ^bDetermined by ¹H NMR spectroscopy using 1,3,5-trimethoxybenzene as internal standard; ^cProximal:distal ratio was determined by analysis of the ¹H NMR spectra of the crude reaction mixture; ^dDetermined by SFC for the major isomer; ^eDetermined by GC; ^fBzCl₃ = 2,4,6-trichlorobenzoyl.

The scope of the reactions of alkenes containing the 2,4,6-trichlorobenzoyl group is summarized in the top section of Table 5.2. Alkenes containing ethyl-, isopropyl-, *tert*-butyl-, and cyclohexyl substituents (**3a-3d**) underwent hydroamination in good isolated yields with consistently high regioselectivity and excellent enantioselectivity. The alkenes with branching α to the alkene formed a single constitutional isomer, but the most hindered alkene bearing a *tert*-butyl group reacted in slightly lower yield than those with secondary alkyl substituents at this position. Methyl-substituted alkene (**3e**) underwent the reaction in low yield, but the lower yield was due to the lack of conversion, rather than formation of side products.

A series of functional groups are tolerated. Reactions of alkenes in substrates containing a silyl ether (**3f**) occur at the alkene, although lower regioselectivity (4.1:1) was observed, perhaps because the functional groups counterbalance the electronic influence of the homoallylic ester. Site-selective hydroamination of a non-conjugated diene occurred at the alkene proximal to the ester over the alkene distal to the ester (**3h**). Internal alkenes containing a phenyl ether unit **3k-3o** (evaluated due to their facile synthesis) reacted in the presence of halogens on the arene of the ether, as well as ketals and heteroarenes.

Table 5.2 Scope of regioselective hydroamination of unactivated internal alkenes^a

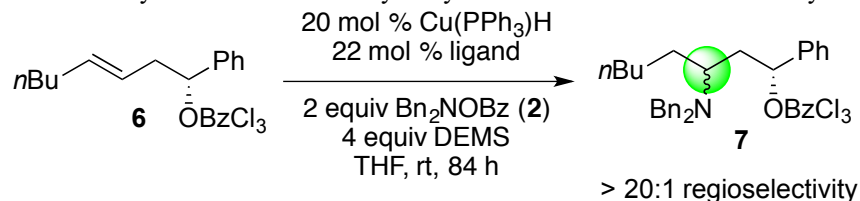
^aReaction conditions: **3** (0.2 mmol), **4** (0.4 mmol), Cu(PPh₃)H (10 mol %) and (S)-DTBM-SEGPHOS (11 mol %) in THF (0.2 mL), rt, 84 h; ^bRegioselectivity and diastereoselectivity were determined by analysis of the ¹H NMR spectrum of the crude reaction mixture; ^cCu(PPh₃)H (15 mol %) and (S)-DTBM-SEGPHOS (17 mol %) used; ^dCu(PPh₃)H (20 mol %) and (S)-DTBM-SEGPHOS (22 mol %) used.

This reaction was found to be very sensitive to the substituents at nitrogen of the *O*-benzoylhydroxylamine. *N,N*-dibenzyl- and *N*-benzyl-*N*-alkyl-*O*-benzoylhydroxylamines underwent

hydroamination in good yields (**5j**, **5k**) and high regioselectivity, but the reaction of an *N,N*-dialkyl-*O*-benzoylhydroxylamine provided the product in low yield.⁴¹

Furthermore, to expand the scope of functionalized alkenes that undergo this formal hydroamination, we found that substrates (**3p**) that contain functionality connected at the homoallylic position by heteroatoms other than oxygen, also underwent hydroamination in high yield with good regioselectivity and excellent enantioselectivity. This method provides access to enantioenriched 1,3-diamine derivatives.

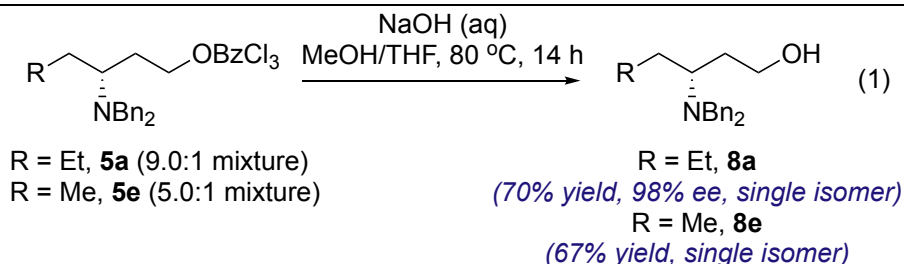
Table 5.3 Study of diastereoselectivity of hydroamination of a chiral homoallylic ester



entry	ligand	products	yield ^a	<i>d.r.</i> ^b
1	(<i>S</i>)-DTBM-SEGPHOS	 (7a)	55%	>20:1
2	(<i>R</i>)-DTBM-SEGPHOS	 (7b)	20%	11:1
3	<i>rac</i> -DTBM-SEGPHOS	 (7a)	(35%)	4:1

^aIsolated yields. Yield in parenthesis refers to NMR yields using 1,3,5-trimethoxybenzene as internal standard. ^bDetermined by analysis of ¹H NMR spectroscopy.

To assess whether the chiral catalyst could control the diastereoselectivity for the hydroamination of chiral alkenes, we conducted the reaction of enantiopure internal alkene **6** bearing a stereogenic center at the site of the homoallylic benzoate. The copper complex ligated by either (*S*)-DTBM-SEGPHOS or (*R*)-DTBM-SEGPHOS formed the addition products with excellent diastereoselectivity (>20:1 and 11:1, respectively) and regioselectivity (>20:1). The configuration at the carbon bearing the amino group was controlled by the configuration of the catalyst. When the reaction was conducted with *rac*-DTBM-SEGPHOS as the ligand, a *d.r.* of 4:1 in favor of the 1,3-*syn*-aminoester was observed. This result indicates that reaction of the (*R*)-substrate catalyzed by the (*S*)-DTBM-SEGPHOS complex is faster than the reaction of this substrate catalyzed by the (*R*)-DTBM-SEGPHOS complex. We have not identified an achiral phosphine that catalyzes the reaction to determine the inherent substrate bias on the diastereoselectivity.



The 2,4,6-trichlorobenzoate groups of the hydroamination products (**5a** and **5e**) can be readily removed under saponification conditions. The corresponding 1,3-aminoalcohols (**8a** and **8e**) were obtained as single isomers in high yield with high enantiomeric excess (eq 1).

Table 5.4 Effect of olefin position and geometry on the hydroamination^a

entry	substrate	product	NMR yield (convn), ee regioselectivity
1	 (9f)	 (5a)	84% (90%), 97% ee regioselectivity 9.0:1
2	 (9a)	 (10a)	15% (16%), 67% ee regioselectivity 9.0:1
3	 (9b)	 (10b)	24% (28%) regioselectivity 1.2:1
4	 (9c)	 (10c)	97% (100%)

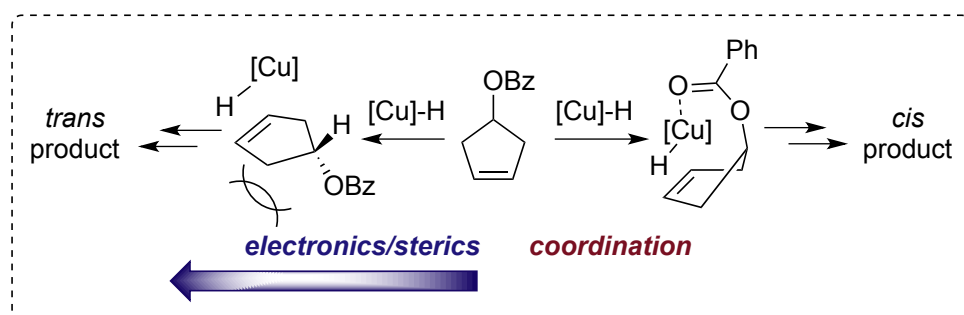
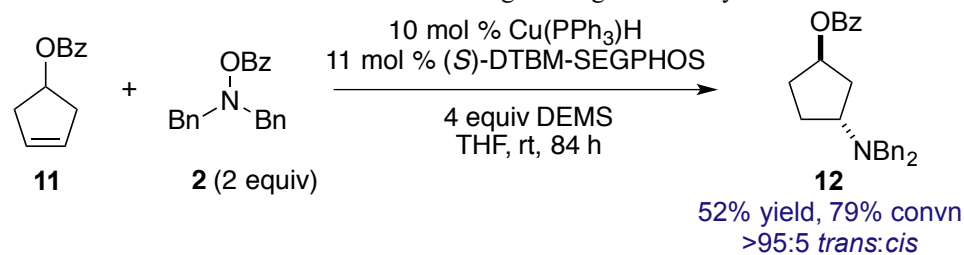
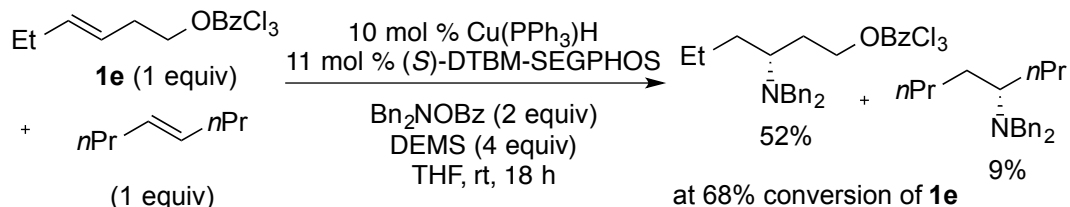
^aYield and conversion were determined by ¹H NMR spectroscopy using 1,3,5-trimethoxybenzene as internal standard.

To gain insight into the effects of the structure of the substrate on the observed regioselectivity, we conducted reactions of a series of substrates that vary in the geometry and position of the alkene (Table 5.4). The *cis*-alkene (**9a**) underwent hydroamination in low yield and with low enantioselectivity, but did react with high regioselectivity. The substrate **9b** in which the alkene is positioned one carbon further away from the directing group underwent hydroamination with poor regioselectivity (1.2:1) and low yield (24%). Allylic benzoate **9c** underwent S_N2' addition of hydride and subsequent hydroamination to afford the terminal amine (**10c**) in nearly quantitative yield.

While the higher regioselectivity with substrates containing more electron-withdrawing and less basic substituents than with less electron-withdrawing and more basic substituents suggest that the regioselectivity of hydroamination arises from the electronic effects of the directing group, we sought less equivocal data on the origin of the regioselectivity. To distinguish between

regioselectivity derived from the electronic effects of the proximal polar group and regioselectivity derived from direct coordination to the catalyst, we conducted the hydroamination of cyclopentene **11** (Scheme 5.2). If the regioselectivity occurs by coordination of the benzoate to the copper catalyst, insertion of the alkene would occur predominantly on the same face of the alkene as the directing group. This selectivity, followed by stereoretentive^{31, 42, 43} electrophilic amination, would provide the *cis*-aminoester. If the regioselectivity occurs by an influence of the electronic properties of the polar group without direct coordination of the ester to the catalyst, the copper hydride would preferentially approach the alkene on the face opposite the ester unit, to avoid steric repulsions between the group and the catalyst. In this scenario, subsequent stereoretentive electrophilic amination would provide the *trans*-aminoester.

Scheme 5.2 Probe of origin of regioselectivity.

Scheme 5.3 Relative reactivity of homoallylic benzoate **1e** and *trans*-4-octene

The hydroamination of **11** afforded the *trans* product exclusively (52% yield). Thus, coordination of the directing group to the copper hydride intermediate during the alkene insertion step is unlikely and the stereoselectivity for reaction of this substrate is consistent with a model for regioselectivity of the acyclic substrates due to inductive effects.

Finally, to test whether the 2,4,6-trichlorobenzoate simply leads to selectivity or increases the reactivity of the substrate, we conducted the reaction with a combination of *trans*-4-octene and **1e**. The reaction was conducted under the standard conditions at partial conversion (68 % of **1e**, 18 h)

to gauge the relative reactivity (Scheme 5.3). This experiment showed that alkene **1e** reacts significantly faster than *trans*-4-octene.

5.3 Conclusions

In summary, we report the regioselective hydroamination of unsymmetrical internal alkenes with excellent enantioselectivity and regioselectivity controlled by synthetically valuable substituents that impart an electronic effect on the alkene. The 2,4,6-trichlorobenzoate group controls the regioselectivity and activates the alkene towards hydroamination, and it can be removed easily to afford synthetically useful enantioenriched 1,3-aminoalcohols. Studies on the cyclic substrate **11** support our hypothesis that the regioselectivity originates from the electronic and steric effects on the alkene. Evaluation of suitable directing groups for hydroamination reactions by the addition of the N-H bonds of the amines to alkenes are currently underway in our laboratory.

5.4 Experimental

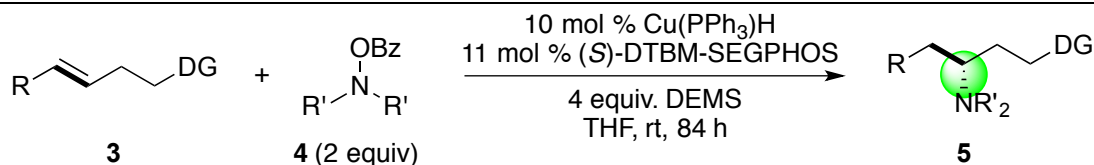
5.4.1 General Methods and Materials

All reagents were purchased from commercial suppliers, stored in the glove box and used as received. Glassware was dried at 130 °C for at least 4 hours before use. THF was collected from a solvent purification system containing a 0.33 m column of activated alumina under nitrogen and stored in a dry box over molecular sieves. [Cu(PPh₃)H]₆ was purchased from Aldrich. (*S*)-DTBM-SEGPHOS was used received as from Takasago. (*R*)-DTBM-SEGPHOS was purchased from Strem. Diethoxymethylsilane (DEMS) was purchased from Alfa Aesar and stored in a freezer in a drybox. All catalytic reactions were set up in an argon-filled dry box with oven-dried glassware and were stirred with Teflon-coated magnetic stirring bars.

¹H NMR spectra were recorded on Bruker AVB-400, AVQ-400, AV-500 and AV-600 instruments with 400, 400, 500, and 600 MHz frequencies, and ¹³C were recorded on a Bruker AV-600 instrument with a ¹³C operating frequency of 150 MHz. ¹⁹F NMR spectra were recorded on a Bruker AVQ-400 spectrometer with a ¹⁹F operating frequency of 376 MHz. Chemical shifts (δ) are reported in ppm relative to the residual solvent signal (δ = 7.26 for ¹H NMR and δ = 77.0 for ¹³C NMR). Crude reaction mixtures were analyzed by ¹H NMR spectroscopy recorded on the Bruker AV-500. Quantitative analysis by ¹H NMR spectroscopy was performed with 1,3,5-trimethoxybenzene as an internal standard. High-resolution mass spectral data were obtained with a Thermo Finnigan LTQ FT Instrument in the QB3/Chemistry Mass Spectrometry Facility, University of California, Berkeley. GC analysis was performed on an Agilent 7890 GC equipped with an HP-5 column (25 m x 0.20 mm x 0.33 μm film) and an FID detector. Chiral SFC analysis was conducted on a JASCO SFC system. Chiral HPLC analysis was conducted on Waters chromatography system. Racemic samples were obtained using racemic DTBM-SEGPHOS as the ligand. Analtech preparative TLC plates were purchased from Aldrich (catalog no Z265829) and used as received.

5.4.2. General Procedure for Catalytic Hydroamination

General procedure for the catalytic hydroamination on a 0.2 mmol scale (General Procedure)



In a argon-filled dry box, a 1-dram vial was charged with $[\text{Cu}(\text{PPh}_3)\text{H}]_6$ (6.4 mg, 10 mol % of Cu-H units), (*S*)-DTBM-SEGPHOS (26.0 mg, 11 mol %) and THF (140 μL). The mixture was allowed to stir vigorously at ambient temperature for 5 minutes before the addition of diethoxymethylsilane (128 μL , 0.8 mmol, 4 equiv). After brief stirring (10 – 30 seconds), the solution was transferred to another 1-dram vial that contained the alkene (0.2 mmol, 1 equiv) and the *O*-benzoyl-hydroxylamine derivative (0.4 mmol, 2 equiv). The former vial was washed with THF (60 μL), and the wash solution was transferred to the latter vial. The vial was then capped, sealed with electrical tape, and removed from the box. After 84 h of stirring at rt, the reaction was diluted with ethyl acetate (3 mL). A 1 mL aliquot was taken and filtered through a short pad of silica gel. The resulting solution was concentrated *in vacuo* and then analyzed by ^1H NMR spectroscopy. Once the regioselectivity was determined, this solution was recombined with the reaction solution, concentrated, and directly purified by flash column chromatography to afford the crude product. To remove the residual silanol as a byproduct, the crude product was purified by preparative TLC.

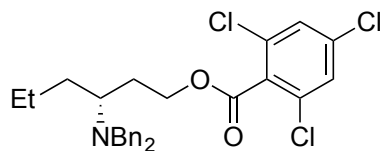
Purification of **5k** and **5l** by an acid-base extraction procedure:

After determination of the regioselectivity by ^1H NMR spectroscopy, the reaction solution was concentrated *in vacuo*. The crude material was dissolved in 20 mL ether and extracted with 10 mL of a 1M HCl solution five times. The aqueous layers were combined, basified by 15 mL of a 6M KOH solution (pH 14 by pH test paper), and extracted with 10 mL of DCM five times. The DCM extracts were combined and concentrated *in vacuo*. Finally, preparative TLC was used to obtain the pure product.

General procedure for the catalytic hydroamination on a 0.05 mmol scale for reaction development

In an argon-filled dry box, a dram vial was charged with the alkene (0.05 mmol, 1 equiv), *N,N*-dibenzyl-*O*-benzoyl-hydroxylamine (32.0 mg, 0.1 mmol, 2 equiv) and THF (65 μL). A separate stock solution (110 μL) containing $[\text{Cu}(\text{PPh}_3)\text{H}]_6$ (1.6 mg, 10 mol % of Cu-H units), (*S*)-DTBM-SEGPHOS (6.5 mg, 11 mol %) and diethoxymethylsilane (32 μL , 0.2 mmol, 4 equiv) in THF was added to the vial. The vial was then capped and removed from the box. After 84 h of stirring at rt, the reaction was diluted with ethyl acetate (2 mL) and 1,3,5-trimethoxybenzene was added as an internal standard. The regioselectivity and yield were determined by ^1H NMR spectroscopy.

5.4.3 Compound Characterization

**5a**

Compound 5a was synthesized according to the **General Procedure** with **3a** (61.4 mg, 0.2 mmol), $\text{Bn}_2\text{N-OBz}$ (128 mg, 0.4 mmol, 2 equiv), DEMS (128 μL , 0.8 mmol, 4 equiv), $\text{Cu}(\text{PPh}_3)\text{H}$ (10 mol %, 6.4 mg), and (*S*)-DTBM-SEGPHOS (11 mol %, 26 mg). **5a** was purified by flash column chromatography (hexanes:ether = 60:1) and then preparative TLC (hexanes:ether = 8:1) and obtained as pale yellow oil in 85% yield along with the inseparable isomer **5a'** (ratio after purification: 9.0:1; before purification: 9.0:1).

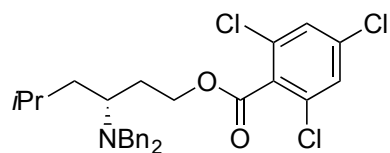
^1H NMR (500 MHz, CDCl_3) δ 7.43 – 7.32 (m, 6H), 7.30 (t, $J = 7.5$ Hz, 4H), 7.22 (m, 2H), 4.67 – 4.54 (m, 1H), 4.40 (dt, $J = 10.7, 7.1$ Hz, 1H), 3.69 (d, $J = 13.6$ Hz, 2H), 3.56 (d, $J = 13.6$ Hz, 2H), 2.74 (quint, $J = 6.7$ Hz, 1H), 2.04 (m, 1H), 1.87 – 1.73 (m, 2H), 1.42 – 1.24 (m, 3H), 0.91 (t, $J = 7.3$ Hz, 3H).

^{13}C NMR (151 MHz, CDCl_3) δ 163.97, 140.09, 135.89, 132.61, 132.36, 128.84, 128.14, 127.92, 126.78, 65.03, 54.29, 53.44, 31.28, 29.12, 20.29, 14.26.

HRMS (ESI+) Calculated for $\text{C}_{27}\text{H}_{29}\text{O}_2\text{N}^{35}\text{Cl}_3$ $[\text{M}+\text{H}]^+$: 504.1258, Found: 504.1250.

$[\alpha]_{\text{D}}^{23} = -10.6$ ($c = 1.0$, DCM).

SFC analysis (OD-H, 10% IPA/ CO_2 , 10 MPa, 2.5 mL/min, 220 nm) indicated 97% ee: t_{R} (major) = 5.6 min, t_{R} (minor) = 6.3 min.

**5b**

Compound 5b was synthesized according to the **General Procedure** with **3b** (64.3 mg, 0.2 mmol), $\text{Bn}_2\text{N-OBz}$ (128 mg, 0.4 mmol, 2 equiv), DEMS (128 μL , 0.8 mmol, 4 equiv), $\text{Cu}(\text{PPh}_3)\text{H}$ (10 mol %, 6.4 mg), and (*S*)-DTBM-SEGPHOS (11 mol %, 26 mg). **5b** was purified by flash column chromatography (hexanes:ether = 60:1) and then preparative TLC (hexanes:ether = 8:1) and obtained as pale yellow oil in 78% yield.

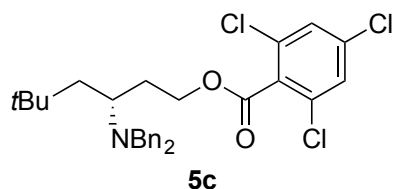
^1H NMR (500 MHz, CDCl_3) δ 7.38 – 7.36 (m, 6H), 7.30 (t, $J = 7.5$ Hz, 4H), 7.22 (t, $J = 7.5$ Hz, 2H), 4.59 (dt, $J = 10.6, 6.8$ Hz, 1H), 4.41 (dt, $J = 10.6, 7.0$ Hz, 1H), 3.66 (d, $J = 13.6$ Hz, 2H), 3.55 (d, $J = 13.6$ Hz, 2H), 2.78 (quint, $J = 6.5$ Hz, 1H), 2.07 (m, 1H), 1.81 – 1.68 (m, 2H), 1.65 – 1.59 (m, 1H), 1.17 (m, 1H), 0.86 (d, $J = 6.5$ Hz, 3H), 0.80 (d, $J = 6.5$ Hz, 3H).

^{13}C NMR (151 MHz, CDCl_3) δ 163.95, 140.05, 135.86, 132.57, 132.29, 128.86, 128.08, 127.87, 126.76, 64.99, 53.32, 52.35, 38.44, 29.13, 24.93, 23.08, 22.65.

HRMS (ESI+) Calculated for $\text{C}_{28}\text{H}_{31}\text{O}_2\text{N}^{35}\text{Cl}_3$ $[\text{M}+\text{H}]^+$: 518.1415, Found: 518.1418.

$[\alpha]_{\text{D}}^{23} = -1.2$ ($c = 1.0$, DCM).

SFC analysis (OD-H, 10% IPA/ CO_2 , 10 MPa, 2.5 mL/min, 220 nm) indicated 99% ee: t_{R} (major) = 4.9 min, t_{R} (minor) = 5.5 min.



Compound 5c was synthesized according to the **General Procedure** with **3c** (67.1 mg, 0.2 mmol), $\text{Bn}_2\text{N-OBz}$ (128 mg, 0.4 mmol, 2 equiv), DEMS (128 μL , 0.8 mmol, 4 equiv), $\text{Cu}(\text{PPh}_3)\text{H}$ (10 mol %, 6.4 mg), and (*S*)-DTBM-SEGPHOS (11 mol %, 26 mg). **5c** was purified by flash column chromatography (hexanes:ether = 60:1) and then preparative TLC (hexanes:ether = 8:1) and obtained as pale yellow oil in 64% yield.

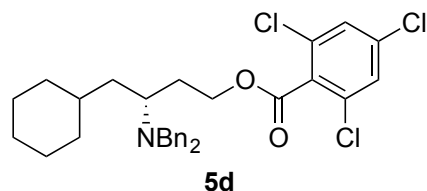
$^1\text{H NMR}$ (500 MHz, CDCl_3) δ 7.38 – 7.31 (m, 6H), 7.28 – 7.26 (m, 4H), 7.18 (t, $J = 7.3$ Hz, 2H), 4.61 (ddd, $J = 10.7, 7.4, 5.5$ Hz, 1H), 4.43 (dt, $J = 10.7, 7.1$ Hz, 1H), 3.69 (d, $J = 13.8$ Hz, 2H), 3.40 (d, $J = 13.8$ Hz, 2H), 2.73 (dddd, $J = 9.7, 7.2, 4.2, 2.2$ Hz, 1H), 2.12 – 2.00 (m, 1H), 1.82 (dtd, $J = 14.4, 7.2, 4.2$ Hz, 1H), 1.74 (dd, $J = 14.0, 2.3$ Hz, 1H), 1.09 (dd, $J = 14.0, 7.7$ Hz, 1H), 0.85 (s, 9H).

$^{13}\text{C NMR}$ (151 MHz, CDCl_3) δ 164.02, 140.02, 135.92, 132.66, 132.34, 128.89, 128.15, 127.95, 126.84, 65.17, 53.44, 51.90, 42.36, 32.21, 30.38, 30.20.

HRMS (ESI+) Calculated for $\text{C}_{29}\text{H}_{33}\text{O}_2\text{N}^{35}\text{Cl}_3$ $[\text{M}+\text{H}]^+$: 532.1571, Found: 532.1569.

$[\alpha]_{\text{D}}^{23} = -1.7$ ($c = 1.0$, DCM).

SFC analysis (OD-H, 10% IPA/ CO_2 , 10 MPa, 2.5 mL/min, 220 nm) indicated 99% ee: t_{R} (major) = 4.7 min, t_{R} (minor) = 5.2 min.



Compound 5d was synthesized according to the **General Procedure** with **3d** (72.3 mg, 0.2 mmol), $\text{Bn}_2\text{N-OBz}$ (128 mg, 0.4 mmol, 2 equiv), DEMS (128 μL , 0.8 mmol, 4 equiv), $\text{Cu}(\text{PPh}_3)\text{H}$ (10 mol %, 6.4 mg), and (*S*)-DTBM-SEGPHOS (11 mol %, 26 mg). **5d** was purified by flash column chromatography (hexanes:ether = 60:1) and then preparative TLC (hexanes:ether = 8:1) and obtained as pale yellow oil in 89% yield.

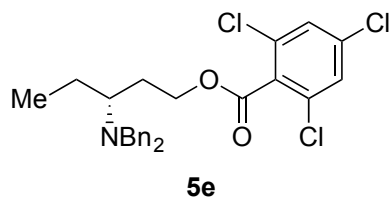
$^1\text{H NMR}$ (500 MHz, CDCl_3) δ 7.37 – 7.35 (m, 6H), 7.28 (t, $J = 7.4$ Hz, 4H), 7.21 (t, $J = 7.2$ Hz, 2H), 4.58 (dt, $J = 10.6, 6.7$ Hz, 1H), 4.39 (dt, $J = 10.6, 6.9$ Hz, 1H), 3.64 (d, $J = 13.6$ Hz, 2H), 3.53 (d, $J = 13.6$ Hz, 2H), 2.80 (quint, $J = 6.7$ Hz, 1H), 2.08 – 2.01 (m, 1H), 1.80 – 1.73 (m, 1H), 1.73 – 1.59 (m, 5H), 1.45 – 1.28 (m, 2H), 1.24 – 1.10 (m, 3H), 0.94 – 0.78 (m, 3H).

$^{13}\text{C NMR}$ (151 MHz, CDCl_3) δ 163.93, 140.10, 135.84, 132.56, 132.29, 128.84, 128.04, 127.85, 126.72, 64.96, 53.29, 51.57, 36.91, 34.42, 33.83, 33.42, 29.23, 26.56, 26.33, 26.25.

HRMS (ESI+) Calculated for $\text{C}_{31}\text{H}_{35}\text{O}_2\text{N}^{35}\text{Cl}_3$ $[\text{M}+\text{H}]^+$: 558.1728, Found: 558.1732.

$[\alpha]_{\text{D}}^{23} = -9.7$ ($c = 1.0$, DCM).

SFC analysis (OD-H, 10% IPA/ CO_2 , 10 MPa, 2.5 mL/min, 220 nm) indicated 99% ee: t_{R} (major) = 5.3 min, t_{R} (minor) = 6.0 min.



Compound 5e was synthesized according to the **General Procedure** with **3e** (58.7 mg, 0.2 mmol), $\text{Bn}_2\text{N-OBz}$ (128 mg, 0.4 mmol, 2 equiv), DEMS (128 μL , 0.8 mmol, 4 equiv), $\text{Cu}(\text{PPh}_3)\text{H}$ (15 mol %, 9.6 mg), and (*S*)-DTBM-SEGPHOS (17 mol %, 39 mg). **5e** was purified by flash column chromatography (hexanes:ether = 60:1) and then preparative TLC (hexanes:ether = 8:1) and obtained as colorless oil in 34% yield along with the inseparable isomer **5e'** (ratio after purification: 5.0:1; before purification: 5.2:1).

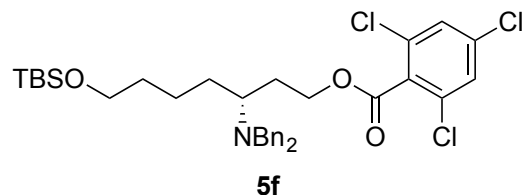
$^1\text{H NMR}$ (500 MHz, CDCl_3) δ 7.35 – 7.33 (m, 6H), 7.26 (t, $J = 7.3\text{ Hz}$, 4H), 7.18 (t, $J = 7.4\text{ Hz}$, 2H), 4.57 (ddd, $J = 10.7, 7.5, 6.0\text{ Hz}$, 1H), 4.37 (dt, $J = 10.7, 7.1\text{ Hz}$, 1H), 3.66 (d, $J = 13.6\text{ Hz}$, 2H), 3.53 (d, $J = 13.6\text{ Hz}$, 2H), 2.61 (tt, $J = 8.1, 5.7$, 1H), 2.03 – 1.94 (m, 1H), 1.84 – 1.74 (m, 2H), 1.35 – 1.26 (m, 1H), 0.91 (t, $J = 7.4\text{ Hz}$, 3H).

$^{13}\text{C NMR}$ (151 MHz, CDCl_3) δ 163.98, 140.06, 135.88, 132.60, 132.35, 128.81, 128.13, 127.92, 126.76, 65.02, 56.37, 53.45, 28.71, 21.73, 11.87.

HRMS (ESI+) Calculated for $\text{C}_{26}\text{H}_{27}\text{O}_2\text{N}^{35}\text{Cl}_3$ $[\text{M}+\text{H}]^+$: 490.1102, Found: 490.1104.

$[\alpha]_{\text{D}}^{23} = +0.8$ ($c = 0.5$, DCM).

SFC analysis (OD-H, 10% IPA/ CO_2 , 10 MPa, 2.5 mL/min, 220 nm) indicated 95% ee: t_{R} (major) = 4.9 min, t_{R} (minor) = 5.4 min.



Compound 5f was synthesized according to the **General Procedure** with **3f** (90.4 mg, 0.2 mmol), $\text{Bn}_2\text{N-OBz}$ (128 mg, 0.4 mmol, 2 equiv), DEMS (128 μL , 0.8 mmol, 4 equiv), $\text{Cu}(\text{PPh}_3)\text{H}$ (10 mol %, 6.4 mg), and (*S*)-DTBM-SEGPHOS (11 mol %, 26 mg). **5f** was purified by flash column chromatography (hexanes:ether = 40:1) and then preparative TLC (hexanes:ether = 6:1) and obtained as pale yellow oil in 67% yield along with the inseparable isomer **5f'** (ratio after purification: 4.3:1; before purification: 4.1:1).

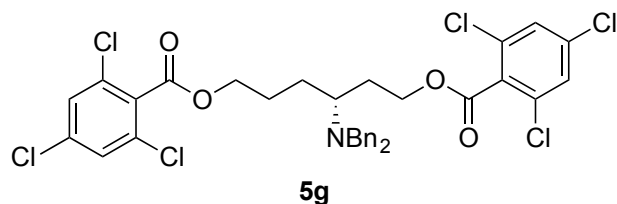
$^1\text{H NMR}$ (500 MHz, CDCl_3) δ 7.38 – 7.33 (m, 6H), 7.27 (t, $J = 7.5\text{ Hz}$, 4H), 7.20 (t, $J = 7.4\text{ Hz}$, 2H), 4.56 (dt, $J = 10.7, 6.6\text{ Hz}$, 1H), 4.37 (dt, $J = 10.7, 7.1\text{ Hz}$, 1H), 3.66 (d, $J = 13.6\text{ Hz}$, 2H), 3.61 (t, $J = 6.3\text{ Hz}$, 2H), 3.55 (d, $J = 13.5\text{ Hz}$, 2H), 2.76 – 2.66 (m, 1H), 2.06 – 1.99 (m, 1H), 1.82 – 1.72 (m, 2H), 1.54 – 1.29 (m, 5H), 0.93 (s, 9H), 0.08 (s, 6H).

$^{13}\text{C NMR}$ (151 MHz, CDCl_3) δ 163.98, 140.03, 135.90, 132.62, 132.34, 128.83, 128.14, 127.92, 126.78, 65.00, 63.02, 54.65, 53.45, 32.97, 29.08, 28.99, 25.98, 23.51, 18.34, -5.25.

HRMS (ESI+) Calculated for $\text{C}_{34}\text{H}_{45}\text{O}_3\text{N}^{35}\text{Cl}_3\text{Si}$ $[\text{M}+\text{H}]^+$: 648.2229, Found: 648.2236.

$[\alpha]_{\text{D}}^{23} = -7.6$ ($c = 1.0$, DCM).

SFC analysis (OD-H, 20% IPA/ CO_2 , 10 MPa, 1.5 mL/min, 220 nm) indicated 90% ee: t_{R} (major) = 3.9 min, t_{R} (minor) = 4.3 min.



Compound 5g was synthesized according to the **General Procedure** with **3g** (106.2 mg, 0.2 mmol), $\text{Bn}_2\text{N-OBz}$ (128 mg, 0.4 mmol, 2 equiv), DEMS (128 μL , 0.8 mmol, 4 equiv), $\text{Cu}(\text{PPh}_3)\text{H}$ (10 mol %, 6.4 mg), and (*S*)-DTBM-SEGPHOS (11 mol %, 26 mg). **5g** was purified by flash column chromatography (hexanes:ethyl acetate = 50:1) and then preparative TLC (hexanes:ethyl acetate = 5:1) and obtained as an off-white foam in 90% yield.

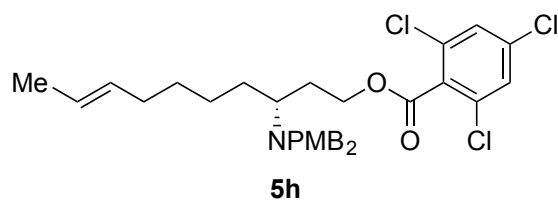
^1H NMR (500 MHz, CDCl_3) δ 7.40 – 7.32 (m, 8H), 7.28 (t, $J = 7.1$ Hz, 4H), 7.21 (t, 7.3 Hz, 2H), 4.53 (dt, $J = 10.8, 6.7$ Hz, 1H), 4.41 (dt, $J = 10.8, 6.7$ Hz, 1H), 4.38 – 4.30 (m, 2H), 3.61 (s, 4H), 2.76 (quint, $J = 6.7$ Hz, 1H), 2.17 – 2.10 (m, 1H), 1.95 – 1.67 (m, 4H), 1.53 – 1.43 (m, 1H).

^{13}C NMR (151 MHz, CDCl_3) δ 163.95, 163.87, 139.63, 136.02, 135.94, 132.52, 132.49, 132.23, 132.14, 128.76, 128.16, 127.98, 127.90, 126.87, 66.34, 64.66, 54.09, 53.34, 28.42, 26.07, 25.89.

HRMS (ESI+) Calculated for $\text{C}_{34}\text{H}_{30}\text{O}_4\text{N}^{35}\text{Cl}_6$ $[\text{M}+\text{H}]^+$: 726.0301, Found: 726.0297.

$[\alpha]_{\text{D}}^{23} = -7.6$ ($c = 1.0$, DCM).

SFC analysis (AD-H, 20% IPA/ CO_2 , 10 MPa, 2.5 mL/min, 220 nm) indicated 98% ee: t_{R} (minor) = 5.1 min, t_{R} (major) = 5.7 min.



Compound 5h was synthesized according to the **General Procedure** with **3h** (72.3 mg, 0.2 mmol), $\text{PMB}_2\text{N-OBz}$ (151 mg, 0.4 mmol, 2 equiv), DEMS (128 μL , 0.8 mmol, 4 equiv), $\text{Cu}(\text{PPh}_3)\text{H}$ (10 mol %, 6.4 mg), and (*S*)-DTBM-SEGPHOS (11 mol %, 26 mg). **5h** was purified by preparative TLC (hexanes:ether = 5:1) and obtained as pale yellow oil in 59% yield along with the inseparable isomer **5h'** (ratio after purification: 5.9:1; before purification: 5.1:1).

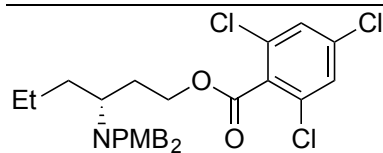
^1H NMR (500 MHz, CDCl_3) δ 7.33 (s, 2H), 7.25 – 7.21 (m, 4H), 6.82 – 6.76 (m, 4H), 5.52 – 5.35 (m, 2H), 4.55 (ddd, $J = 10.6, 7.4, 5.9$ Hz, 2H), 4.33 (dt, $J = 10.6, 7.1$ Hz, 2H), 3.78 (s, 6H), 3.56 (d, $J = 13.3$ Hz, 2H), 3.42 (d, $J = 13.4$ Hz, 2H), 2.66 (tt, $J = 8.0, 5.5$ Hz, 1H), 2.03 – 1.87 (m, 3H), 1.83 – 1.59 (m, 5H), 1.36 – 1.17 (m, 5H).

^{13}C NMR (151 MHz, CDCl_3) δ 163.99, 158.48, 135.89, 132.57, 132.36, 132.18, 131.33, 129.85, 127.91, 124.75, 113.51, 65.04, 55.17, 54.07, 52.56, 32.45, 29.53, 29.09, 28.64, 26.55, 17.92.

HRMS (ESI+) Calculated for $\text{C}_{33}\text{H}_{39}\text{O}_4\text{N}^{35}\text{Cl}_3$ $[\text{M}+\text{H}]^+$: 618.1939, Found: 618.1945.

$[\alpha]_{\text{D}}^{23} = -6.7$ ($c = 1.0$, DCM).

SFC analysis (OZ-H, 20% IPA/ CO_2 , 10 MPa, 1.5 mL/min, 220 nm) indicated 98% ee: t_{R} (major) = 4.1 min, t_{R} (minor) = 5.9 min.

**5i**

Compound 5i was synthesized according to the **General Procedure** with **3a** (61.4 mg, 0.2 mmol), $\text{PMB}_2\text{N-OBz}$ (151 mg, 0.4 mmol, 2 equiv), DEMS (128 μL , 0.8 mmol, 4 equiv), $\text{Cu}(\text{PPh}_3)\text{H}$ (10 mol %, 6.4 mg), and (*S*)-DTBM-SEGPHOS (11 mol %, 26 mg). **5i** was purified by flash column chromatography (hexanes:ethyl acetate = 50:1) and obtained as pale yellow oil in 60% yield.

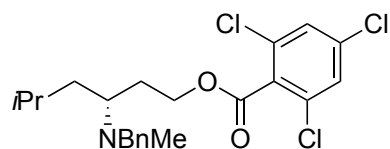
$^1\text{H NMR}$ (500 MHz, CDCl_3) δ 7.33 (s, 2H), 7.24 (d, $J = 8.4$ Hz, 4H), 6.80 (d, $J = 8.4$ Hz, 4H), 4.56 (dt, $J = 10.5, 6.8$ Hz, 1H), 4.34 (dt, $J = 10.6, 7.1$ Hz, 1H), 3.78 (s, 6H), 3.57 (d, $J = 13.4$ Hz, 2H), 3.43 (d, $J = 13.4$ Hz, 2H), 2.72 – 2.65 (m, 1H), 2.01 – 1.92 (m, 1H), 1.81 – 1.64 (m, 2H), 1.37 – 1.18 (m, 3H), 0.87 (t, $J = 7.2$ Hz, 3H).

$^{13}\text{C NMR}$ (151 MHz, CDCl_3) δ 163.97, 158.40, 135.84, 132.50, 132.30, 132.14, 129.81, 127.86, 113.45, 65.02, 55.13, 53.79, 52.48, 31.04, 29.04, 20.26, 14.24.

HRMS (ESI+) Calculated for $\text{C}_{29}\text{H}_{33}\text{O}_4\text{N}^{35}\text{Cl}_3$ $[\text{M}+\text{H}]^+$: 564.1470, Found: 564.1473.

$[\alpha]_{\text{D}}^{23} = -2.1$ ($c = 1.0$, DCM).

SFC analysis (AD-H, 20% IPA/ CO_2 , 10 MPa, 2.5 mL/min, 220 nm) indicated 97% ee: t_{R} (minor) = 2.8 min, t_{R} (major) = 5.6 min.

**5j**

Compound 5j was synthesized according to the **General Procedure** with **3b** (64.3 mg, 0.2 mmol), BnMeN-OBz (97 mg, 0.4 mmol, 2 equiv), DEMS (128 μL , 0.8 mmol, 4 equiv), $\text{Cu}(\text{PPh}_3)\text{H}$ (10 mol %, 6.4 mg), and (*S*)-DTBM-SEGPHOS (11 mol %, 26 mg). **5j** was purified by acid-base extraction and then preparative TLC (hexanes:ether = 8:1) and obtained as a colorless oil in 56% yield.

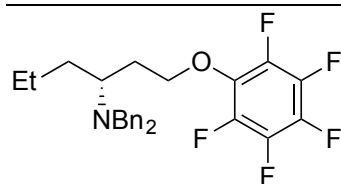
$^1\text{H NMR}$ (500 MHz, CDCl_3) δ 7.35 (s, 2H), 7.32 – 7.26 (m, 4H), 7.21 (t, $J = 7.1$ Hz, 1H), 4.59 – 4.49 (m, 2H), 3.61 (d, $J = 13.4$ Hz, 1H), 3.54 (d, $J = 13.4$ Hz, 1H), 2.82 (tt, $J = 8.0, 5.9$ Hz, 1H), 2.14 (s, 3H), 1.98 – 1.89 (m, 1H), 1.82 – 1.74 (m, 1H), 1.74 – 1.66 (m, 1H), 1.53 – 1.46 (m, 1H), 1.18 – 1.10 (m, 1H), 0.91 (d, $J = 6.6$ Hz, 3H), 0.89 (d, $J = 6.6$ Hz, 3H).

$^{13}\text{C NMR}$ (151 MHz, CDCl_3) δ 164.12, 140.15, 135.96, 132.59, 132.44, 128.55, 128.12, 127.98, 126.71, 65.06, 58.06, 57.11, 38.39, 35.82, 29.42, 25.04, 23.10, 22.63.

HRMS (ESI+) Calculated for $\text{C}_{22}\text{H}_{27}\text{O}_2\text{N}^{35}\text{Cl}_3$ $[\text{M}+\text{H}]^+$: 442.1102, Found: 442.1101.

$[\alpha]_{\text{D}}^{23} = -13.8$ ($c = 0.5$, DCM).

$^1\text{H NMR}$ analysis of the amine (enantioenriched and racemic samples) with (*S*)-*O*-acetylmandelic acid indicated >99% ee.¹

**5k**

Compound 5k was synthesized according to the **General Procedure** with **3k** (53.2 mg, 0.2 mmol), $\text{Bn}_2\text{N-OBz}$ (128 mg, 0.4 mmol, 2 equiv), DEMS (128 μL , 0.8 mmol, 4 equiv), $\text{Cu}(\text{PPh}_3)\text{H}$ (10 mol %, 6.4 mg), and (*S*)-DTBM-SEGPHOS (11 mol %, 26 mg). **5k** was purified by flash column chromatography (100% hexanes) and then preparative TLC (100% hexanes) and obtained as pale yellow oil in 74% yield along with the inseparable isomer **5k'** (ratio after purification: 9.0:1; before purification: 7.7:1).

^1H NMR (500 MHz, CDCl_3) δ 7.39 – 7.30 (m, 4H), 7.28 (t, $J = 7.3$ Hz, 4H), 7.21 (t, $J = 7.1$ Hz, 2H), 4.36 (dt, $J = 8.5, 6.7$ Hz, 1H), 4.13 (dt, $J = 8.8, 7.2$ Hz, 1H), 3.67 (d, $J = 13.6$ Hz, 2H), 3.51 (d, $J = 13.6$ Hz, 2H), 2.72 (tt, $J = 8.5, 5.0$ Hz, 1H), 2.04 – 1.93 (m, 1H), 1.83 – 1.70 (m, 2H), 1.41 – 1.33 (m, 2H), 1.31 – 1.21 (m, 1H), 0.92 (t, $J = 7.3$ Hz, 3H).

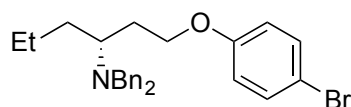
^{13}C NMR (151 MHz, CDCl_3) δ 141.36 ($J_{\text{C-F}} = 242$ Hz), 140.16, 137.90 ($J_{\text{C-F}} = 249$ Hz), 136.78 ($J_{\text{C-F}} = 249$ Hz), 133.77, 128.80, 128.07, 126.75, 73.89, 54.09, 53.45, 31.00, 30.88, 20.25, 14.11.

^{19}F NMR (376 MHz, CDCl_3) δ -156.37 ($J = 23$ Hz, 2F), -163.06 ($J = 19$ Hz, 2F), -164.16 ($J = 21$ Hz, 1F).

HRMS (ESI+) Calculated for $\text{C}_{26}\text{H}_{27}\text{ONF}_5$ $[\text{M}+\text{H}]^+$: 464.2007, Found: 464.2013.

$[\alpha]_{\text{D}}^{23} = -10.1$ ($c = 1.0$, DCM).

SFC analysis (OD-H, 6% IPA/ CO_2 , 10 MPa, 1.0 mL/min, 220 nm) indicated 97% ee: t_{R} (major) = 6.8 min, t_{R} (minor) = 7.3 min.

**5l**

Compound 5l was synthesized according to the **General Procedure** with **3l** (51.0 mg, 0.2 mmol), $\text{Bn}_2\text{N-OBz}$ (128 mg, 0.4 mmol, 2 equiv), DEMS (128 μL , 0.8 mmol, 4 equiv), $\text{Cu}(\text{PPh}_3)\text{H}$ (10 mol %, 6.4 mg), and (*S*)-DTBM-SEGPHOS (11 mol %, 26 mg). **5l** was purified by flash column chromatography (100% hexanes) and then preparative TLC (hexanes:ether = 20:1) and obtained as a colorless oil in 73% yield along with the inseparable isomer **5l'** (ratio after purification: 4.8:1; before purification: 4.7:1).

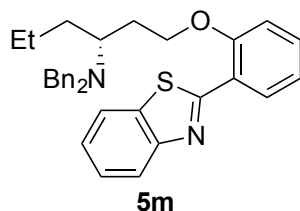
^1H NMR (500 MHz, CDCl_3) δ 7.39 – 4.33 (m, 6H), 7.28 (t, $J = 7.2$ Hz, 4H), 7.22 (t, $J = 7.4$ Hz, 2H), 6.69 (d, 8.9 Hz, 2H), 4.01 – 3.92 (m, 2H), 3.67 (d, $J = 13.7$ Hz, 2H), 3.55 (d, $J = 13.7$ Hz, 2H), 2.76 (tt, $J = 7.8, 5.9$ Hz, 1H), 2.06 – 1.98 (m, 1H), 1.81 – 1.69 (m, 2H), 1.43 – 1.33 (m, 2H), 1.32 – 1.24 (m, 1H), 0.90 (t, $J = 7.3$ Hz, 3H).

^{13}C NMR (151 MHz, CDCl_3) δ 158.08, 140.28, 132.06, 128.79, 128.10, 126.75, 116.23, 112.41, 66.18, 54.00, 53.40, 31.39, 29.78, 20.29, 14.22.

HRMS (ESI+) Calculated for $\text{C}_{26}\text{H}_{31}\text{ON}^{79}\text{Br}$ $[\text{M}+\text{H}]^+$: 452.1584, Found: 452.1586.

$[\alpha]_{\text{D}}^{23} = +15.0$ ($c = 1.0$, DCM).

SFC analysis (OD-H, 8% IPA/CO₂, 10 MPa, 4.0 mL/min, 220 nm) indicated 94% ee: t_R (major) = 3.3 min, t_R (minor) = 3.6 min.



Compound 5m was synthesized according to the **General Procedure** with **3m** (61.9 mg, 0.2 mmol), Bn₂N-OBz (128 mg, 0.4 mmol, 2 equiv), DEMS (128 μL, 0.8 mmol, 4 equiv), Cu(PPh₃)H (10 mol %, 6.4 mg), and (*S*)-DTBM-SEGPHOS (11 mol %, 26 mg). **5m** was purified by preparative TLC (hexanes:ether = 20:1) and obtained as a colorless oil in 79% yield along with the inseparable isomer **5m'** (ratio after purification: 3.8:1; before purification: 4.0:1).

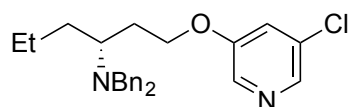
¹H NMR (500 MHz, CDCl₃) δ 8.63 (dd, *J* = 7.7, 1.5 Hz, 1H), 8.17 (d, *J* = 8.0 Hz, 1H), 7.89 (d, *J* = 8.0 Hz, 1H), 7.56 – 7.47 (m, 3H), 7.42 – 7.28 (m, 5H), 7.20 – 7.15 (m, 4H), 7.09 (t, *J* = 7.3 Hz, 2H), 7.05 (d, *J* = 8.5 Hz, 1H), 4.40 – 4.36 (m, 1H), 4.29 – 4.25 (m, 1H), 3.81 (d, *J* = 13.5 Hz, 2H), 3.52 (d, *J* = 13.5 Hz, 2H), 3.08 (tt, *J* = 9.0, 4.2 Hz, 1H), 2.20 – 1.81 (m, 3H), 1.70 – 1.30 (m, 3H), 1.07 (t, *J* = 7.3 Hz, 3H).

¹³C NMR (151 MHz, CDCl₃) δ 163.15, 156.59, 151.94, 140.08, 136.12, 131.55, 129.32, 128.65, 127.98, 126.65, 125.65, 124.24, 122.57, 122.03, 120.94, 120.57, 111.90, 66.70, 53.84, 53.44, 30.85, 30.29, 20.54, 14.50.

HRMS (ESI+) Calculated for C₃₃H₃₅ON₂S [M+H]⁺: 507.2465, Found: 507.2468.

[α]_D²³ = -41.2 (c = 1.0, DCM).

SFC analysis (AD-H, 20% IPA/CO₂, 10 MPa, 2.5 mL/min, 220 nm) indicated 97% ee: t_R (major) = 3.5 min, t_R (minor) = 4.2 min.



Compound 5n was synthesized according to the **General Procedure** with **3n** (42.3 mg, 0.2 mmol), Bn₂N-OBz (128 mg, 0.4 mmol, 2 equiv), DEMS (128 μL, 0.8 mmol, 4 equiv), Cu(PPh₃)H (10 mol %, 6.4 mg), and (*S*)-DTBM-SEGPHOS (11 mol %, 26 mg). **5n** was purified by preparative TLC (hexanes:ether = 20:1) and obtained as a colorless oil in 81% yield along with the inseparable isomer **5n'** (ratio after purification: 7.1:1; before purification: 6.7:1).

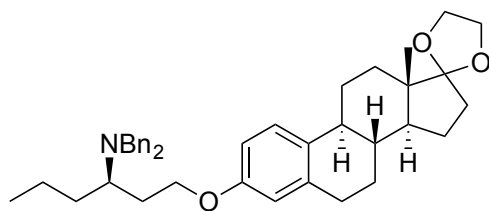
¹H NMR (500 MHz, CDCl₃) δ 8.18 (d, *J* = 1.5 Hz, 1H), 8.04 (d, *J* = 2.5 Hz, 1H), 7.34 – 7.18 (m, 10H), 7.02 (s, 1H), 3.99 (t, *J* = 6.0 Hz, 2H), 3.69 (d, *J* = 13.5 Hz, 2H), 3.50 (d, *J* = 13.5 Hz, 2H), 2.77 (tt, *J* = 9.0, 4.8 Hz, 1H), 1.96 – 1.91 (m, 1H), 1.82 – 1.75 (m, 2H), 1.44 – 1.34 (m, 2H), 1.32 – 1.25 (m, 1H), 0.94 (t, *J* = 7.3 Hz, 3H).

¹³C NMR (151 MHz, CDCl₃) δ 155.30, 140.23, 140.10, 135.87, 131.68, 128.78, 128.07, 126.77, 120.97, 66.32, 53.49, 53.33, 30.81, 29.86, 20.35, 14.19.

HRMS (ESI+) Calculated for C₂₅H₃₀ON₂³⁵Cl [M+H]⁺: 409.2041, Found: 49.2046.

[α]_D²³ = -4.7 (c = 1.0, DCM).

HPLC analysis (OD-H, 5% IPA/hexanes, 0.5 mL/min, 220 nm) indicated 97% ee: t_R (major) = 15.0 min, t_R (minor) = 16.6 min.

**5o**

Compound 5o was synthesized according to the **General Procedure** with **3o** (79.3 mg, 0.2 mmol), $\text{Bn}_2\text{N-OBz}$ (128 mg, 0.4 mmol, 2 equiv), DEMS (128 μL , 0.8 mmol, 4 equiv), $\text{Cu}(\text{PPh}_3)\text{H}$ (10 mol %, 6.4 mg), and (*S*)-DTBM-SEGPHOS (11 mol %, 26 mg). **5o** was purified by flash column chromatography (hexanes:ether = 20:1) and then preparative TLC (hexanes:ether = 6:1) and obtained as pale foam in 75% yield along with the inseparable isomer **5o'** (ratio after purification: 4.2:1; before purification: 4.1:1).

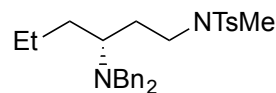
^1H NMR (500 MHz, CDCl_3) δ 7.41 (d, $J = 7.2$ Hz, 4H), 7.34 (t, $J = 7.5$ Hz, 4H), 7.26 (m, 3H), 6.70 (dd, $J = 8.5, 2.5$ Hz, 1H), 6.61 (d, $J = 2.5$ Hz, 1H), 4.09 – 3.91 (m, 6H), 3.68 (d, $J = 13.5$ Hz, 2H), 3.62 (d, $J = 13.5$ Hz, 2H), 2.93 – 2.86 (m, 2H), 2.78 (quint, $J = 6.5$ Hz, 1H), 2.41 – 2.37 (m, 1H), 2.33 – 2.28 (m, 1H), 2.17 – 2.08 (m, 2H), 1.98 – 1.68 (m, 6H), 1.62 – 1.29 (m, 9H), 0.96 (s, 1H), 0.91 (t, $J = 7.0$ Hz, 3H).

^{13}C NMR (151 MHz, CDCl_3) δ 156.79, 140.36, 137.77, 132.41, 128.84, 128.05, 126.66, 126.13, 119.39, 114.47, 111.88, 66.16, 65.19, 64.53, 54.29, 53.38, 49.34, 46.14, 43.62, 39.08, 34.21, 31.89, 30.72, 29.77, 29.71, 27.02, 26.15, 22.35, 20.21, 14.32, 14.19.

HRMS (ESI+) Calculated for $\text{C}_{40}\text{H}_{52}\text{O}_3\text{N}$ $[\text{M}+\text{H}]^+$: 594.3942, Found: 594.3950.

$[\alpha]_{\text{D}}^{23} = +27.5$ ($c = 1.0$, DCM).

^1H NMR analysis indicated a diastereochemistry of >20:1.

**5p**

Compound 5p was synthesized according to the **General Procedure** with **3p** (53.5 mg, 0.2 mmol), $\text{Bn}_2\text{N-OBz}$ (128 mg, 0.4 mmol, 2 equiv), DEMS (128 μL , 0.8 mmol, 4 equiv), $\text{Cu}(\text{PPh}_3)\text{H}$ (15 mol %, 9.6 mg), and (*S*)-DTBM-SEGPHOS (17 mol %, 39 mg). **5p** was purified by preparative TLC (hexanes:ether = 10:1) and obtained as a colorless oil in 87% yield along with the inseparable isomer **5p'** (ratio after purification: 8.4:1; before purification: 7.7:1).

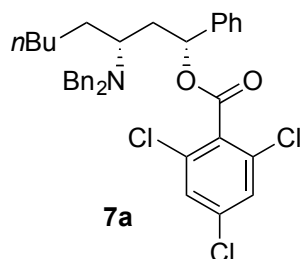
^1H NMR (500 MHz, CDCl_3) δ 7.69 (d, $J = 8.5$ Hz, 2H), 7.38 – 7.32 (m, 10H), 7.28 – 7.25 (m, 2H), 3.66 (d, $J = 13.5$ Hz, 2H), 3.50 (d, $J = 13.5$ Hz, 2H), 3.36 (ddd, $J = 13.2, 10.5, 5.4$ Hz, 1H), 2.70 – 2.65 (m, 1H), 2.67 (s, 3H), 2.50 – 2.46 (m, 1H), 2.48 (s, 3H), 1.83 – 1.76 (m, 1H), 1.74 – 1.67 (m, 1H), 1.56 – 1.51 (m, 1H), 1.36 – 1.29 (m, 2H), 1.25 – 1.20 (m, 1H), 0.90 (t, $J = 7.5$ Hz, 3H).

^{13}C NMR (151 MHz, CDCl_3) δ 143.02, 140.19, 134.54, 129.47, 128.89, 128.09, 127.40, 126.73, 55.29, 53.33, 48.77, 34.92, 31.00, 28.71, 21.43, 20.31, 14.20.

HRMS (ESI+) Calculated for $\text{C}_{28}\text{H}_{37}\text{O}_2\text{N}_2\text{S}$ $[\text{M}+\text{H}]^+$: 465.2570, Found: 465.2569.

$[\alpha]_{\text{D}}^{23} = -4.8$ ($c = 1.0$, DCM).

HPLC analysis (AD-H, 5% IPA/CO₂, 1.0 mL/min, 220 nm) indicated 99% ee: t_R (major) = 9.5 min, t_R (minor) = 10.5 min.



Compound 7a was synthesized according to the **General Procedure** with **6** (82.3 mg, 0.2 mmol), Bn₂N-OBz (128 mg, 0.4 mmol, 2 equiv), DEMS (128 μ L, 0.8 mmol, 4 equiv), Cu(PPh₃)H (20 mol %, 12.8 mg), and (*S*)-DTBM-SEGPHOS (22 mol %, 52 mg). **7a** was purified by preparative TLC (hexanes:ether = 20:1) and obtained as a colorless oil in 55% yield.

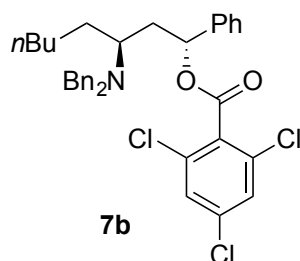
¹H NMR (500 MHz, CDCl₃) δ 7.38 (d, J = 7.0 Hz, 4H), 7.32 – 7.26 (m, 11H), 7.13 – 7.11 (m, 2H), 6.04 (t, J = 7.0 Hz, 1H), 3.63 (d, J = 13.0 Hz, 2H), 3.57 (d, J = 13.5 Hz, 2H), 2.65 (quint, J = 6.5 Hz, 1H), 2.47 – 2.41 (m, 1H), 1.85 – 1.80 (m, 1H), 1.72 – 1.65 (m, 1H), 1.41 – 1.34 (m, 1H), 1.31 – 1.20 (m, 4H), 1.14 – 1.06 (m, 2H), 0.87 (t, J = 7.3 Hz, 3H).

¹³C NMR (151 MHz, CDCl₃) δ 163.17, 140.19, 139.43, 135.75, 132.60, 132.26, 129.12, 128.19, 128.12, 128.01, 127.87, 127.04, 126.76, 77.09, 53.51, 53.47, 36.71, 31.63, 28.97, 26.28, 22.59, 13.98.

HRMS (ESI+) Calculated for C₃₅H₃₇O₂N³⁵Cl₃ [M+H]⁺: 608.1884, Found: 608.1891.

$[\alpha]_D^{23}$ = +28.5 (c = 1.0, DCM).

¹H NMR analysis indicated a diastereoselectivity of >20:1.



Compound 7b was synthesized according to the **General Procedure** with **6** (82.3 mg, 0.2 mmol), Bn₂N-OBz (128 mg, 0.4 mmol, 2 equiv), DEMS (128 μ L, 0.8 mmol, 4 equiv), Cu(PPh₃)H (20 mol %, 12.8 mg), and (*R*)-DTBM-SEGPHOS (22 mol %, 52 mg). **7b** was purified by preparative TLC (hexanes:ether = 20:1) and obtained as a colorless oil in 20% yield.

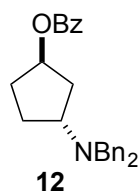
¹H NMR (500 MHz, CDCl₃) δ 7.43 – 7.2 (m, 17H), 6.16 (t, J = 6.7 Hz, 1H), 3.66 (d, J = 13.5 Hz, 2H), 3.52 (d, J = 13.5 Hz, 2H), 2.67 (quint, J = 6.3 Hz, 1H), 2.24 – 2.19 (m, 1H), 2.11 – 2.05 (m, 1H), 1.79 – 1.73 (m, 1H), 1.43 – 1.38 (m, 2H), 1.33 – 1.27 (m, 3H), 1.22 – 1.11 (m, 2H), 0.91 (t, J = 7.5 Hz, 3H).

¹³C NMR (151 MHz, CDCl₃) δ 163.08, 140.07, 139.67, 135.88, 132.71, 132.19, 128.83, 128.45, 128.24, 128.12, 127.91, 127.07, 126.74, 77.59, 54.94, 53.69, 36.93, 31.69, 29.87, 26.39, 22.63, 14.02.

HRMS (ESI+) Calculated for C₃₅H₃₇O₂N³⁵Cl₃ [M+H]⁺: 608.1884, Found: 608.1891.

$[\alpha]_D^{23}$ = +6.8 (c = 0.5, DCM)

^1H NMR analysis indicated a diastereoselectivity of 11:1.



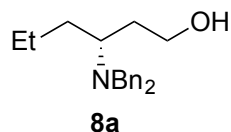
Compound 12 was synthesized according to the **General Procedure** with **11** (37.6 mg, 0.2 mmol), $\text{Bn}_2\text{N-OBz}$ (128 mg, 0.4 mmol, 2 equiv), DEMS (128 μL , 0.8 mmol, 4 equiv), $\text{Cu}(\text{PPh}_3)\text{H}$ (10 mol %, 6.4 mg), and (*S*)-DTBM-SEGPHOS (11 mol %, 26 mg). **12** was purified by preparative TLC (hexanes:ethyl acetate = 8:1) and obtained as pale yellow oil along in 52% yield.

^1H NMR (500 MHz, CDCl_3) δ 7.99 – 7.94 (m, 2H), 7.58 – 7.52 (m, 1H), 7.42 (t, J = 7.8 Hz, 2H), 7.38 (d, J = 7.5 Hz, 4H), 7.31 (t, J = 7.4 Hz, 4H), 7.23 (t, J = 7.4 Hz, 2H), 5.42 (tt, J = 6.3, 3.7 Hz, 1H), 3.66 (d, J = 14.1 Hz, 2H), 3.62 (d, J = 14.0 Hz, 2H), 3.56 (quint, J = 8.1 Hz, 1H), 2.23 – 2.11 (m, 1H), 2.08 – 1.93 (m, 3H), 1.82 – 1.75 (m, 1H), 1.72 – 1.65 (m, 1H).

^{13}C NMR (151 MHz, CDCl_3) δ 166.20, 140.10, 132.73, 130.64, 129.48, 128.60, 128.24, 128.14, 126.73, 76.11, 60.24, 55.28, 35.07, 31.20, 26.63.

HRMS (ESI+) Calculated for $\text{C}_{26}\text{H}_{28}\text{O}_2\text{N} [\text{M}+\text{H}]^+$: 386.2115, Found: 386.2112.

The absolute stereochemistry has not been determined.



Compound 8a was synthesized according to the following procedure.

To a 20-mL vial that contained compound **5a** (121 mg, 0.24 mmol) was added 0.5 mL THF, 0.5 mL MeOH and 0.5 mL 2M NaOH solution. The vial was then capped and placed in an 80 $^\circ\text{C}$ heating block. After stirring overnight (14 h), the solution was diluted with ethyl acetate (10 mL) and water (10 mL). Phase was separated and the aqueous solution was extracted with another 10 mL ethyl acetate. The organic layers were combined, dried over Na_2SO_4 , and concentrated. The crude mixture was then purified by preparative TLC (hexanes:ethyl acetate = 3:1) to afford **8a** (50 mg, 70% yield) as colorless oil.

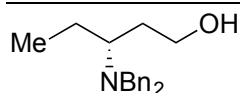
^1H NMR (500 MHz, CDCl_3) δ 7.33 (d, J = 4.0 Hz, 8H), 7.27 – 7.24 (m, 2H), 4.78 (brs, 1H), 3.88 (d, J = 13.0 Hz, 2H), 3.77 (dt, J = 10.6, 4.4 Hz, 1H), 3.52 (td, J = 10.1, 3.0 Hz, 1H), 3.34 (d, J = 13.0 Hz, 2H), 2.79 (tt, J = 10.1, 3.2 Hz, 1H), 1.89 (dtd, J = 14.5, 10.2, 4.0 Hz, 1H), 1.84 – 1.72 (m, 1H), 1.51 (dq, J = 14.6, 3.7 Hz, 1H), 1.45 – 1.32 (m, 1H), 1.23 (tt, J = 14.5, 8.5 Hz, 2H), 0.95 (t, J = 7.0 Hz, 3H).

^{13}C NMR (151 MHz, CDCl_3) δ 139.06, 129.21, 128.42, 127.15, 63.18, 58.14, 53.27, 31.53, 29.52, 20.59, 14.31.

HRMS (ESI+) Calculated for $\text{C}_{20}\text{H}_{28}\text{ON} [\text{M}+\text{H}]^+$: 298.2165, Found: 298.2163.

$[\alpha]_{\text{D}}^{23} = -53.2$ (c = 1.0, DCM).

SFC analysis (OD-H, 10% IPA/ CO_2 , 10 MPa, 2.5 mL/min, 220 nm) indicated 98% ee: t_{R} (major) = 2.9 min, t_{R} (minor) = 4.4 min.

**8e**

Compound 8e was synthesized according to the following procedure.

To a 20-mL vial that contained compound **5e** (28 mg, 0.057 mmol) was added 0.3 mL THF, 0.3 mL MeOH and 0.3 mL 2M NaOH solution. The vial was then capped and placed in an 80 °C heating block. After stirring overnight (14 h), the solution was diluted with ethyl acetate (10 mL) and water (10 mL). Phase was separated and the aqueous solution was extracted with another 10 mL ethyl acetate. The organic layers were combined, dried over Na₂SO₄, and concentrated. The crude mixture was then purified by preparative TLC (hexanes:ethyl acetate = 3:1) to afford **8e** (10.8 mg, 67% yield) as a colorless oil.

¹H NMR (500 MHz, CDCl₃) δ 7.33 (d, *J* = 4.4 Hz, 8H), 7.33 – 7.22 (m, 2H), 4.72 (brs, 1H), 3.88 (d, *J* = 13.1 Hz, 2H), 3.76 (dt, *J* = 10.8, 4.4 Hz, 1H), 3.50 (ddd, *J* = 10.7, 9.5, 3.2 Hz, 1H), 3.34 (d, *J* = 13.1 Hz, 2H), 2.67 (tt, *J* = 10.3, 3.2 Hz, 1H), 1.92 – 1.79 (m, 2H), 1.52 (m, 1H), 1.25 – 1.18 (m, 1H), 0.89 (t, *J* = 7.4 Hz, 3H).

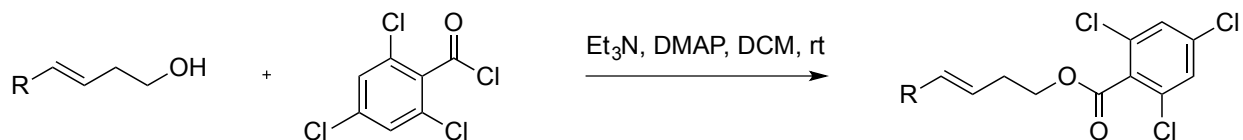
¹³C NMR (151 MHz, CDCl₃) δ 139.05, 129.23, 128.45, 127.17, 63.22, 60.25, 53.34, 30.91, 20.02, 12.07.

HRMS (ESI+) Calculated for C₁₉H₂₆ON [M+H]⁺: 284.2009, Found: 284.2003.

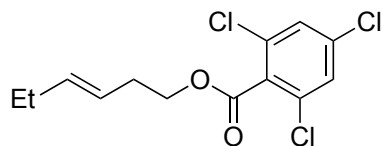
[α]_D²³ = -45.5 (c = 1.0, CHCl₃).

5.4.4 Substrate Synthesis

General procedure for the synthesis of the 2,4,6-trichlorobenzoates through acylation (Procedure A)



A 20 mL dram vial was charged with the homoallylic alcohol (1 equiv, 5 mmol) and DCM (10 mL), followed by Et₃N (2 equiv) and DMAP (100 mg). The vial was cooled to 0 °C, and 2,4,6-trichlorobenzoyl chloride (1.2 equiv) was added dropwise. The mixture was allowed to warm to room temperature and to stir overnight. Saturated NH₄Cl was added to quench the reaction. The mixture was extracted with ethyl acetate (twice) and dried over anhydrous Na₂SO₄. The crude product obtained after filtration and concentration *in vacuo* was purified by flash column chromatography with hexanes and ethyl acetate (V:V=20:1) as eluents to afford the pure product.

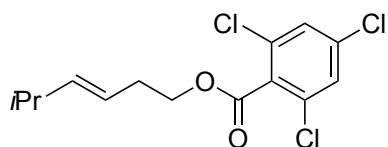
**3a**

3a (1e) was obtained by **Procedure A** in 98% isolated yield as a colorless liquid.

^1H NMR (500 MHz, CDCl_3) δ 7.34 (s, 2H), 5.61 (dtt, $J = 15.4, 6.3, 1.3$ Hz, 1H), 5.41 (dtt, $J = 15.4, 6.8, 1.5$ Hz, 1H), 4.39 (t, $J = 6.9$ Hz, 2H), 2.46 (qd, $J = 6.9, 1.2$ Hz, 2H), 2.02 (quint, $J = 7.5$ Hz, 2H), 0.97 (t, $J = 7.5$ Hz, 3H).

^{13}C NMR (151 MHz, CDCl_3) δ 163.94, 135.94, 135.39, 132.55, 132.26, 127.90, 123.44, 66.14, 31.60, 25.54, 13.54.

HRMS Calculated for $\text{C}_{13}\text{H}_{14}\text{O}_2^{35}\text{Cl}_2^{37}\text{Cl}$ $[\text{M}]^+$: 309.0030, Found: 309.0027.

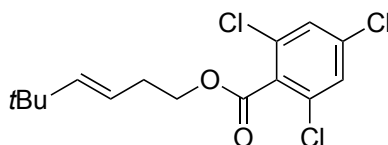
**3b**

3b was obtained by **Procedure A** in 60% isolated yield as a colorless liquid.

^1H NMR (400 MHz, CDCl_3) δ 7.34 (s, 2H), 5.54 (dd, $J = 15.4, 6.6$ Hz, 1H), 5.37 (dt, $J = 15.4, 6.6$ Hz, 1H), 4.38 (t, $J = 6.9$ Hz, 2H), 2.45 (q, $J = 6.8$ Hz, 2H), 2.25 (octet, $J = 6.6$ Hz, 1H), 0.96 (d, $J = 6.8$ Hz, 6H).

^{13}C NMR (101 MHz, CDCl_3) δ 164.08, 140.96, 136.01, 132.61, 132.31, 127.98, 121.47, 66.32, 31.60, 31.04, 22.38.

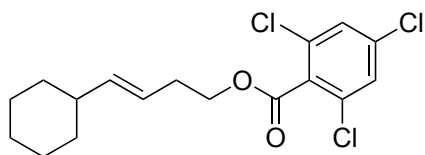
HRMS (EI+) Calculated for $\text{C}_{14}\text{H}_{15}\text{O}_2^{35}\text{Cl}_3$ $[\text{M}]^+$: 320.0138, Found: 320.0131.

**3c**

3c was obtained by **Procedure A** in 71% isolated yield as a colorless liquid.

^1H NMR (400 MHz, CDCl_3) δ 7.35 (s, 2H), 5.60 (dt, $J = 15.4, 1.2$ Hz, 1H), 5.34 (dt, $J = 15.4, 6.7$ Hz, 1H), 4.38 (t, $J = 6.9$ Hz, 2H), 2.46 (qd, $J = 6.8, 1.2$ Hz, 2H), 0.99 (s, 9H).

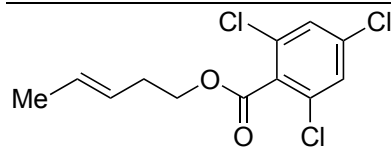
^{13}C NMR (101 MHz, CDCl_3) δ 164.11, 144.85, 136.02, 132.61, 132.33, 127.99, 119.20, 66.46, 33.01, 31.68, 29.57.

**3d**

3d was obtained by **Procedure A** in 95% isolated yield as a colorless liquid.

^1H NMR (600 MHz, CDCl_3) δ 7.33 (s, 2H), 5.51 (dd, $J = 15.5, 6.6$ Hz, 1H), 5.37 (dtd, $J = 15.5, 6.7, 0.8$ Hz, 1H), 4.38 (t, $J = 6.8$ Hz, 2H), 2.45 (q, $J = 6.8$ Hz, 2H), 1.95 – 1.86 (m, 1H), 1.72 – 1.60 (m, 5H), 1.28–1.20 (m, 2H), 1.17 – 1.09 (m, 1H), 1.07 – 1.00 (m, 2H).

^{13}C NMR (151 MHz, CDCl_3) δ 163.99, 139.79, 135.95, 132.57, 132.28, 127.92, 121.87, 66.29, 40.63, 32.90, 31.69, 26.12, 25.99.

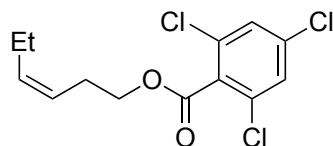
**3e**

3e was obtained by **Procedure A** in 75% isolated yield as a colorless liquid.

$^1\text{H NMR}$ (400 MHz, CDCl_3) δ 7.34 (s, 2H), 5.57 (dq, $J = 15.2, 6.4, 1.2$ Hz, 1H), 5.44 (dq, $J = 15.2, 6.6, 1.5$ Hz, 1H), 4.38 (t, $J = 6.8$ Hz, 2H), 2.45 (q, $J = 6.8$ Hz, 2H), 1.67 (dd, $J = 6.3, 1.3$ Hz, 3H).

$^{13}\text{C NMR}$ (101 MHz, CDCl_3) δ 164.05, 136.01, 132.60, 132.30, 128.42, 127.98, 125.73, 66.11, 31.70, 18.00.

HRMS (EI+) Calculated for $\text{C}_{12}\text{H}_{11}\text{O}_2^{35}\text{Cl}_3$ $[\text{M}]^+$: 291.9825, Found: 291.9827.

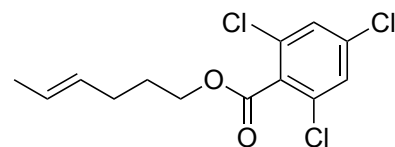
**9a**

9a was obtained by **Procedure A** in 99% isolated yield as a colorless liquid.

$^1\text{H NMR}$ (500 MHz, CDCl_3) δ 7.35 (s, 2H), 5.68 – 5.47 (m, 1H), 5.44 – 5.28 (m, 1H), 4.37 (t, $J = 7.0$ Hz, 2H), 2.98 – 2.36 (q, $J = 7.0$ Hz, 2H), 2.07 (quint, $J = 7.5$ Hz, 2H), 0.96 (t, $J = 7.5$ Hz, 3H).

$^{13}\text{C NMR}$ (151 MHz, CDCl_3) δ 163.90, 135.94, 134.84, 132.54, 132.20, 127.89, 123.05, 65.90, 26.45, 20.59, 14.06.

HRMS Calculated for $\text{C}_{13}\text{H}_{14}\text{O}_2^{35}\text{Cl}_3$ $[\text{M}+\text{H}]^+$: 307.0059, Found: 307.0042.

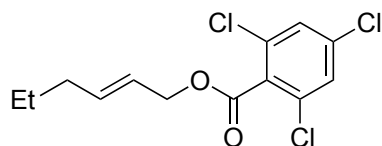
**9b**

9b was obtained by **Procedure A** in 80% isolated yield as a colorless liquid.

$^1\text{H NMR}$ (500 MHz, CDCl_3) δ 7.35 (s, 2H), 5.53 – 5.36 (m, 2H), 4.38 (t, $J = 6.6$ Hz, 2H), 2.12 (q, $J = 7.0$ Hz, 2H), 1.82 (quint, $J = 7.0$ Hz, 2H), 1.65 (dd, $J = 6.0, 1.3$ Hz, 1H).

$^{13}\text{C NMR}$ (151 MHz, CDCl_3) δ 163.93, 135.89, 132.48, 132.32, 129.49, 127.87, 126.09, 65.87, 28.65, 28.16, 17.80.

HRMS (ESI+) Calculated for $\text{C}_{13}\text{H}_{14}\text{O}_2^{35}\text{Cl}_3$ $[\text{M}+\text{H}]^+$: 307.0054, Found: 307.0052.

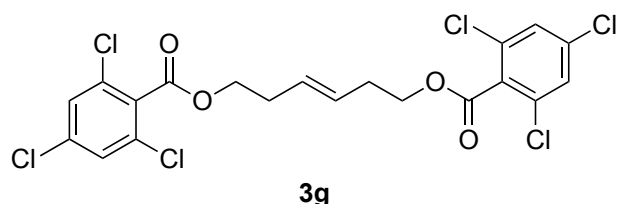
**9c**

9c was obtained by **Procedure A** in 97% isolated yield as a colorless liquid.

^1H NMR (500 MHz, CDCl_3) δ 7.34 (s, 2H), 5.89 (dt, $J = 14.8, 6.7, 1.2$ Hz, 1H), 5.67 (dt, $J = 15.0, 6.7, 1.5$ Hz, 1H), 4.82 (dd, $J = 6.7, 1.0$ Hz, 2H), 2.06 (q, $J = 7.0$ Hz, 2H), 1.42 (h, $J = 7.3$ Hz, 2H), 0.91 (t, $J = 7.4$ Hz, 3H).

^{13}C NMR (151 MHz, CDCl_3) δ 163.74, 137.86, 135.95, 132.59, 132.16, 127.90, 122.82, 67.14, 34.22, 21.89, 13.53.

HRMS (EI+) Calculated for $\text{C}_{13}\text{H}_{13}\text{O}_2^{35}\text{Cl}_3$ $[\text{M}]^+$: 305.9981, Found: 305.9982.

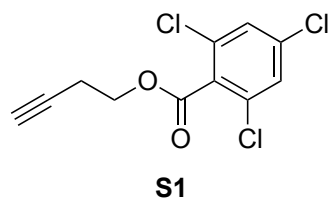


3g was obtained by **Procedure A** in 30% isolated yield as a white solid.

^1H NMR (500 MHz, CDCl_3) δ 7.34 (s, 4H), 5.56 (t, $J = 3.7$ Hz, 2H), 4.40 (t, $J = 6.7$ Hz, 4H), 2.52 – 2.46 (m, 4H).

^{13}C NMR (151 MHz, CDCl_3) δ 163.98, 136.08, 132.57, 132.16, 128.23, 128.00, 65.74, 31.70.

HRMS (ESI+) Calculated for $\text{C}_{20}\text{H}_{14}\text{O}_4^{35}\text{Cl}_6\text{Na}$ $[\text{M}+\text{Na}]^+$: 550.8915, Found: 550.8922.



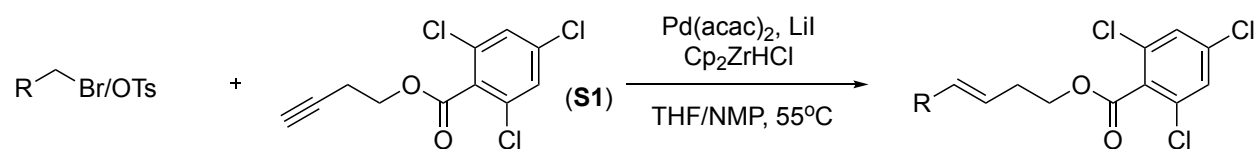
S1 was obtained by **Procedure A** in 99% isolated yield as a colorless liquid, which turned into a white solid upon standing.

^1H NMR (500 MHz, CDCl_3) δ 7.35 (s, 2H), 4.49 (t, $J = 6.9$ Hz, 2H), 2.68 (td, $J = 6.9, 2.7$ Hz, 2H), 2.03 (t, $J = 2.7$ Hz, 1H).

^{13}C NMR (151 MHz, CDCl_3) δ 163.61, 136.17, 132.58, 131.71, 127.93, 79.33, 70.33, 63.90, 18.73.

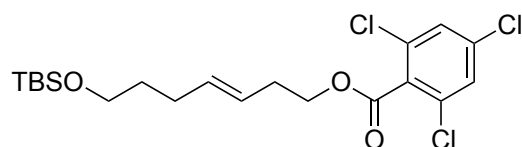
HRMS (EI+) Calculated for $\text{C}_{11}\text{H}_7\text{O}_2^{35}\text{Cl}_3$ $[\text{M}]^+$: 275.9512, Found: 275.9514.

General procedure for the synthesis of the 2,4,6-trichlorobenzoates through hydrozirconation/Negishi coupling (Procedure B)



The functionalized homopropargylic esters were prepared by a modified procedure, originally reported by Fu and co-workers.² In a drybox, a 20-mL vial was charged with homopropargylic ester **S1** (2 mmol, 2 equiv). THF (2 mL) and Schwartz's reagent were then added in one portion. The resulting mixture was stirred at rt for 1 h to afford a clear yellow solution, indicating complete consumption of the Schwartz's reagent. In a separate 20-mL vial, $\text{Pd}(\text{acac})_2$ (5 mol %) and LiI (2 equiv) were added in NMP (2 mL). The solution of the alkenyl zirconium solution in THF was

then added. Finally, the corresponding bromide or tosylate was added neat. The vial was then capped and taped with electrical tape, removed from the box and placed in a 55°C heating block. After 24-48 h, the reaction mixture was concentrated and filtered through a short column of silica gel with ether. The crude mixture obtained after evaporation of ether was purified by flash column chromatography and preparative TLC, if necessary, to yield the pure product for the hydroamination.

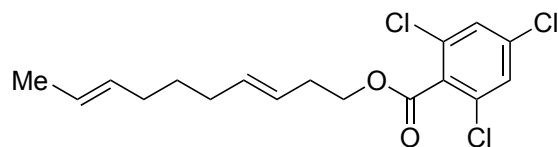
**3f**

3f was obtained by **Procedure B** in 53% isolated yield as colorless liquid.

$^1\text{H NMR}$ (600 MHz, CDCl_3) δ 7.34 (s, 2H), 5.57 (dt, $J = 15.3, 7.8$ Hz, 1H), 5.44 (dt, $J = 15.3, 6.7$ Hz, 1H), 4.38 (t, $J = 6.8$ Hz, 2H), 3.59 (t, $J = 6.4$ Hz, 2H), 2.46 (q, $J = 6.7$ Hz, 2H), 2.06 (q, $J = 7.2$ Hz, 2H), 1.57 (quint, $J = 7.2$ Hz, 2H), 0.89 (s, 9H), 0.03 (s, 6H).

$^{13}\text{C NMR}$ (151 MHz, CDCl_3) δ 164.03, 136.01, 133.41, 132.60, 132.29, 127.98, 124.81, 66.14, 62.47, 32.36, 31.68, 28.85, 25.93, 18.31, -5.30.

HRMS (ESI+) Calculated for $\text{C}_{20}\text{H}_{30}\text{O}_3^{35}\text{Cl}_3\text{Si}$ $[\text{M}+\text{H}]^+$: 451.1024, Found: 451.1020.

**3h**

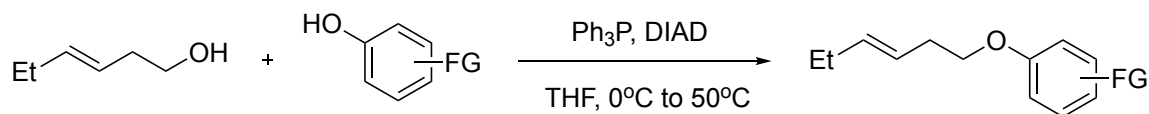
3h was obtained by **Procedure B** in 44% isolated yield as colorless liquid.

$^1\text{H NMR}$ (600 MHz, CDCl_3) δ 7.34 (s, 2H), 5.65 – 5.50 (m, 1H), 5.48 – 5.33 (m, 3H), 4.38 (t, $J = 6.8$ Hz, 2H), 2.51 – 2.40 (m, 2H), 2.07 – 1.89 (m, 4H), 1.65 (d, $J = 0.6$ Hz, 2H), 1.39 (quint, $J = 7.5$ Hz, 2H).

$^{13}\text{C NMR}$ (151 MHz, CDCl_3) δ 164.03, 136.02, 133.75, 132.63, 132.33, 131.13, 127.99, 124.95, 124.70, 66.19, 32.01, 31.94, 31.71, 29.12, 17.90.

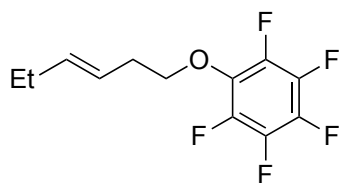
HRMS (EI+) Calculated for $\text{C}_{17}\text{H}_{19}\text{O}_2^{35}\text{Cl}_3$ $[\text{M}]^+$: 360.0451, Found: 360.0447.

General procedure for the synthesis of the phenyl ethers through a Mitsunobu reaction (Procedure C)



A 100 mL oven-dried round-bottom flask was charged with *trans*-3-hexenol (1 equiv, 10 mmol), phenol (1.2 equiv), Ph_3P (1.0 equiv) and THF (20 mL). The flask was cooled to 0 °C, and DIAD (1.2 equiv) was added dropwise. The mixture was allowed to warm to room temperature and was stirred for 24-48 h. If the reaction did not reach completion, the flask was then heated at

50 °C for 12 h. After cooling to rt, saturated $\text{NH}_4\text{Cl}(\text{aq})$ was added to quench the reaction. The mixture was extracted with ethyl acetate (twice) and dried over anhydrous Na_2SO_4 . The crude product obtained after filtration and concentration *in vacuo* was purified by flash column chromatography with hexanes and ethyl acetate as eluents to afford the pure product.

**3k**

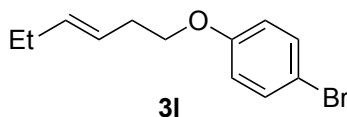
3k (1f) was obtained by **Procedure C** in 83% isolated yield as a colorless liquid.

^1H NMR (500 MHz, CDCl_3) δ 5.61 (dt, $J = 15.3, 6.3$ Hz, 1H), 5.42 (dt, $J = 15.3, 6.8$ Hz, 1H), 4.16 (t, $J = 6.8$ Hz, 2H), 2.46 (q, $J = 6.7$ Hz, 2H), 2.02 (quint, $J = 7.4$ Hz, 2H), 0.97 (t, $J = 7.5$ Hz, 3H).

^{13}C NMR (151 MHz, CDCl_3) δ 141.86 ($J_{\text{C-F}} = 248$ Hz), 138.02 ($J_{\text{C-F}} = 252$ Hz), 137.26 ($J_{\text{C-F}} = 243$ Hz), 135.66, 133.72, 123.32, 75.31, 33.13, 25.63, 13.50.

^{19}F NMR (376 MHz, CDCl_3) δ -156.19 (d, $J = 20.8$ Hz, 2F), -163.26 (t, $J = 20.7$ Hz, 2F), -163.53 (t, $J = 21.4$ Hz, 1F).

HRMS (EI+) Calculated for $\text{C}_{12}\text{H}_{11}\text{OF}_5$ $[\text{M}]^+$: 266.0730, Found: 266.0726.

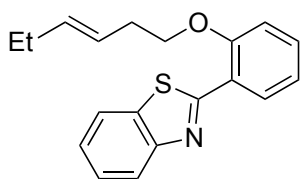
**3l**

3l (1g) was obtained by **Procedure C** in 95% isolated yield as a colorless liquid.

^1H NMR (500 MHz, CDCl_3) δ 8.24 – 8.13 (m, 2H), 7.19 (t, $J = 2.3$ Hz, 1H), 5.62 (dt, $J = 15.3, 6.3$ Hz, 1H), 5.44 (dtt, $J = 15.3, 6.8, 1.4$ Hz, 1H), 3.99 (t, $J = 6.8$ Hz, 2H), 2.48 (q, $J = 6.8$ Hz, 2H), 2.03 (quint, $J = 7.4$ Hz, 2H), 0.98 (t, $J = 7.45$ Hz, 3H).

^{13}C NMR (151 MHz, CDCl_3) δ 155.22, 140.38, 135.99, 135.32, 131.71, 123.45, 120.94, 68.38, 32.08, 25.46, 13.48.

HRMS (EI+) Calculated for $\text{C}_{12}\text{H}_{15}\text{O}^{79}\text{Br}$ $[\text{M}]^+$: 254.0306, Found: 254.0308.

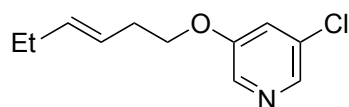
**3m**

3m was obtained by **Procedure C** in 57% isolated yield as colorless liquid.

^1H NMR (500 MHz, CDCl_3) δ 8.56 (d, $J = 7.6$ Hz, 1H), 8.10 (d, $J = 8.0$ Hz, 1H), 7.94 (d, $J = 7.7$ Hz, 1H), 7.49 (t, $J = 7.9$ Hz, 1H), 7.44 (t, $J = 8.2$ Hz, 1H), 7.37 (t, $J = 7.6$ Hz, 1H), 7.12 (t, $J = 7.4$ Hz, 1H), 7.05 (d, $J = 8.2$ Hz, 1H), 5.71 (dt, $J = 15.3, 6.2$ Hz, 1H), 5.62 (dt, $J = 15.3, 6.6$ Hz, 1H), 4.23 (t, $J = 6.8$ Hz, 2H), 2.73 (q, $J = 6.8$ Hz, 2H), 2.06 (quint, $J = 7.4$ Hz, 2H), 0.99 (t, $J = 7.5$ Hz, 3H).

^{13}C NMR (151 MHz, CDCl_3) δ 163.16, 156.56, 151.99, 136.14, 135.31, 131.64, 129.50, 125.78, 124.44, 124.36, 122.66, 122.19, 121.13, 120.93, 112.22, 69.20, 32.54, 25.66, 13.68.

HRMS (EI+) Calculated for C₁₂H₁₉NOS [M]⁺: 309.1187, Found: 309.1186.

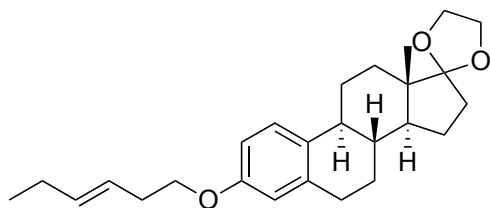
**3n**

3n was obtained by **Procedure C** in 40 % isolated yield as a dark brown liquid.

¹H NMR (500 MHz, CDCl₃) δ 8.18 (d, *J* = 10.7 Hz, 2H), 7.19 (t, *J* = 2.3 Hz, 1H), 5.68 – 5.56 (m, 1H), 5.49 – 5.40 (m, 1H), 3.99 (t, *J* = 6.8 Hz, 2H), 2.48 (qd, *J* = 6.8, 1.3 Hz, 2H), 2.06 – 1.99 (m, 2H), 0.98 (t, *J* = 7.5 Hz, 3H).

¹³C NMR (151 MHz, CDCl₃) δ 155.22, 140.38, 135.99, 135.32, 131.71, 123.45, 120.94, 68.38, 32.08, 25.46, 13.48.

HRMS (EI+) Calculated for C₁₁H₁₄ON³⁵Cl [M]⁺: 211.0764, Found: 211.0766.

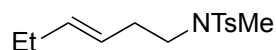
**3o**

3o was obtained by **Procedure C** in 57% isolated yield as a sticky oil.

¹H NMR (500 MHz, CDCl₃) δ 7.19 (d, *J* = 8.5 Hz, 1H), 6.70 (dd, *J* = 8.6, 2.8 Hz, 1H), 6.63 (d, *J* = 2.7 Hz, 1H), 5.65 – 5.56 (m, 1H), 5.50 – 5.44 (m, 1H), 4.01 – 3.87 (m, 6H), 2.88 – 2.79 (m, 2H), 2.45 (qd, *J* = 6.9, 1.3 Hz, 2H), 2.36 – 2.28 (m, 1H), 2.23 (td, *J* = 12.9, 11.9, 4.1 Hz, 1H), 2.07 – 1.99 (m, 3H), 1.92 – 1.73 (m, 4H), 1.63 (ddd, *J* = 12.1, 10.6, 7.0 Hz, 1H), 1.50 – 1.30 (m, 4H), 0.98 (t, *J* = 7.5 Hz, 3H), 0.88 (s, 3H).

¹³C NMR (151 MHz, CDCl₃) δ 156.73, 137.81, 134.54, 132.51, 126.17, 124.50, 119.33, 114.43, 111.98, 67.68, 65.15, 64.49, 49.26, 46.07, 43.55, 39.00, 34.16, 32.51, 30.65, 29.73, 26.95, 26.08, 25.59, 22.29, 14.26, 13.68.

HRMS (EI+) Calculated for C₂₆H₃₆O₃ [M]⁺: 396.2664, Found: 396.2668.

**3p**

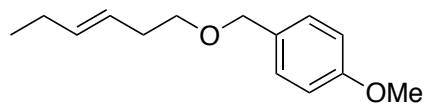
3p was obtained by **Procedure C** with N-methyltosylamide instead of phenol in 44% isolated yield as a sticky oil.

¹H NMR (500 MHz, CDCl₃) δ 7.68 (d, *J* = 8.2 Hz, 2H), 7.33 (d, *J* = 7.9 Hz, 2H), 7.28 (s, 2H), 5.54 (dt, *J* = 15.3, 6.5 Hz, 1H), 5.39 – 5.29 (m, 1H), 3.03 (t, *J* = 7.5 Hz, 2H), 2.74 (s, 3H), 2.44 (s, 3H), 2.24 (q, *J* = 7.3 Hz, 2H), 2.08 – 1.97 (m, 2H), 0.97 (t, *J* = 7.5 Hz, 3H).

¹³C NMR (151 MHz, CDCl₃) δ 143.07, 134.71, 129.50, 127.24, 127.24, 124.61, 50.03, 34.64, 31.06, 25.46, 21.36, 13.56.

HRMS (ESI+) Calculated for C₁₄H₂₂O₂NS [M+H]⁺: 268.1366, Found: 268.1364.

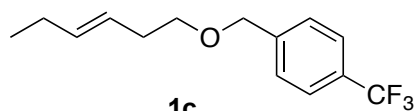
Characterization of other compounds

**1b**

$^1\text{H NMR}$ (400 MHz, CDCl_3) δ 7.36-7.23 (m, 2H), 6.95-6.85 (m, 2H), 5.62-5.50 (m, 1H), 5.46-5.38 (m, 1H), 4.46 (s, 2H), 3.81 (s, 3H), 3.46 (t, $J = 7.0$ Hz, 2H), 2.39-2.26 (m, 2H), 2.06-1.98 (m, 2H), 0.98 (t, $J = 7.5$ Hz, 3H).

$^{13}\text{C NMR}$ (151 MHz, CDCl_3) δ 159.15, 133.97, 130.68, 129.14, 125.36, 113.70, 72.44, 69.96, 55.04, 33.11, 25.66, 13.79.

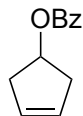
HRMS (EI+) Calculated for $\text{C}_{14}\text{H}_{20}\text{O}_2$ $[\text{M}]^+$: 220.1463, Found: 220.1467.

**1c**

$^1\text{H NMR}$ (400 MHz, CDCl_3) δ 7.61 (d, $J = 8.1$ Hz, 2H), 7.46 (d, $J = 8.0$ Hz, 2H), 5.61-5.54 (m, 1H), 5.47-5.39 (m, 1H), 4.58 (s, 2H), 3.51 (t, $J = 6.8$ Hz, 2H), 2.39-2.29 (m, 2H), 2.09-1.97 (m, 2H), 0.98 (t, $J = 7.5$ Hz, 3H).

$^{13}\text{C NMR}$ (151 MHz, CDCl_3) δ 142.88, 134.28, 129.60 (q, $J_{\text{C-F}} = 31.2$ Hz), 127.37, 125.15, 125.02, 123.34, 71.87, 70.63, 32.99, 25.59, 13.63.

HRMS (EI+) Calculated for $\text{C}_{14}\text{H}_{17}\text{OF}_3$ $[\text{M}]^+$: 258.1232, Found: 258.1228.

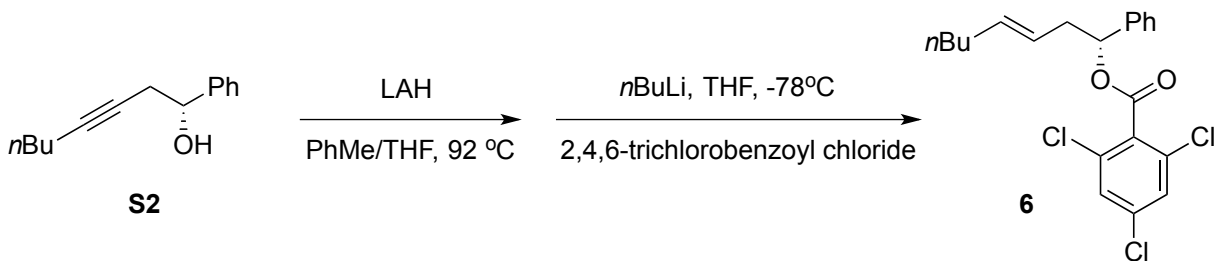
**13**

$^1\text{H NMR}$ (500 MHz, CDCl_3) δ 8.18 – 7.91 (m, 2H), 7.60 – 7.48 (m, 1H), 7.42 (t, $J = 7.7$ Hz, 2H), 5.77 (s, 2H), 5.62 (tt, $J = 7.0, 2.5$ Hz, 1H), 2.86 (dd, $J = 16.8, 7.0$ Hz, 2H), 2.65 – 2.51 (m, 2H).

$^{13}\text{C NMR}$ (151 MHz, CDCl_3) δ 166.46, 133.40, 132.74, 130.55, 129.50, 128.21, 74.74, 39.76.

HRMS (EI+) Calculated for $\text{C}_{12}\text{H}_{13}\text{O}$ $[\text{M}]^+$: 189.0916, Found: 189.0915.

Synthesis of compound 6



To a dry, 100 mL round-bottom flask was added lithium aluminum hydride (569 mg, 15 mmol). The flask was equipped with a reflux condenser and to the flask was added 6 mL toluene.

A solution of **S2** (1.01 g, 5 mmol) in 6 mL THF was added to the flask dropwise. After the addition, the flask was capped, degassed with nitrogen three times and heated at 92 °C. After 36 h, the flask was cooled to rt, diluted with 20 mL ether, and carefully quenched by a solution of potassium sodium tartrate at 0 °C. After vigorous stirring overnight, the layers were separated. The aqueous layer was extracted with 20 mL ether twice. The combined organic extracts were concentrated and passed through a short pad of silica gel. This mixture was used directly in the following reaction.

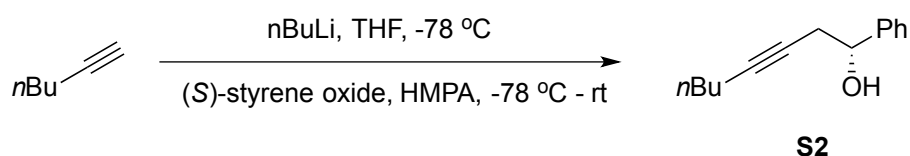
To a solution of **S2** in THF (10 mL) was added *n*BuLi (2 mL, 2.5 M in hexane) at -78 °C under nitrogen. After 30 minutes, 2,4,6-chlorobenzoyl chloride (7.5 mmol) was added dropwise in neat. The reaction was warmed to rt and allowed to stir overnight. Water (10 mL) was added to quench the reaction and the layers were separated. Aqueous layer was extracted with 20 mL ethyl acetate twice. The combined organic extracts were concentrated and the crude material was purified by flash column chromatography to afford **6** (1.40 g, 67%) as a colorless liquid.

¹H NMR (500 MHz, CDCl₃) δ 7.42 – 7.29 (m, 7H), 6.03 (t, *J* = 6.7 Hz, 1H), 5.57 – 5.43 (m, 1H), 5.38 – 5.32 (m, 1H), 2.76 (dt, *J* = 14.4, 7.3 Hz, 1H), 2.60 (dt, *J* = 14.2, 6.5 Hz, 1H), 1.96 (q, *J* = 7.0 Hz, 2H), 1.35 – 1.19 (m, 4H), 0.86 – 0.82 (t, *J* = 7.0 Hz, 3H).

¹³C NMR (151 MHz, CDCl₃) δ 163.26, 138.85, 135.91, 134.70, 132.58, 132.23, 128.24, 128.14, 127.90, 126.94, 123.89, 78.56, 39.17, 32.17, 31.30, 22.04, 13.87.

HRMS (EI+) Calculated for C₂₁H₂₁O₂³⁵Cl₃ [M]⁺: 410.0607, Found: 410.0601.

[α]_D²³ = +37 (c = 1.0, DCM).



*n*BuLi (8 mL, 2.5 M in hexane) was added to a solution of 1-hexyne (2.3 mL, 20 mmol) in THF (40 mL) at -78 °C under nitrogen. After stirring for 1 h, HMPA (4 mL) and (*S*)-styrene oxide (2.28 mL, 20 mmol) were rapidly added, and the reaction was allowed to reach rt and stir for 24 h. A solution of NH₄Cl (20 mL) was added to quench the reaction, and the layers were separated. The aqueous layer was extracted with ethyl acetate (15 mL) twice. The combined organic extracts were concentrated, and the crude material was purified by flash column chromatography to afford **S2** (1.36 g, 34%) as a colorless liquid.

¹H NMR (600 MHz, CDCl₃) δ 7.40 – 7.33 (m, 4H), 7.31 – 7.27 (m, 1H), 4.79 (t, *J* = 0.6 Hz, 3H), 2.74 – 2.65 (m, 1H), 2.65 – 2.54 (m, 2H), 2.17 (tt, *J* = 7.1, 2.4 Hz, 2H), 1.53 – 1.44 (m, 2H), 1.41 – 1.35 (m, 2H), 0.91 (t, *J* = 7.3 Hz, 3H).

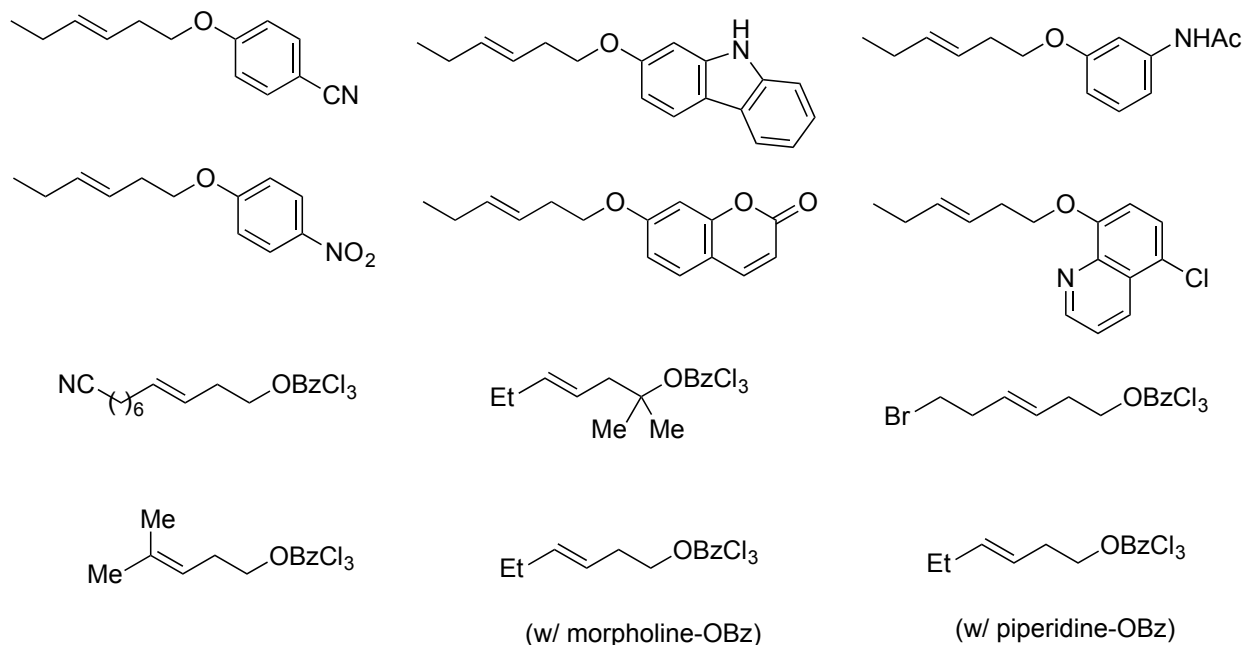
¹³C NMR (151 MHz, CDCl₃) δ 142.76, 128.19, 127.57, 125.67, 83.34, 75.91, 72.50, 30.86, 29.89, 21.81, 18.31, 13.50.

HRMS (EI+) Calculated for C₁₄H₁₈O [M]⁺: 202.1358, Found: 202.1354.

[α]_D²³ = +38 (c = 1.0, DCM).

5.4.5 Substrate Limitations

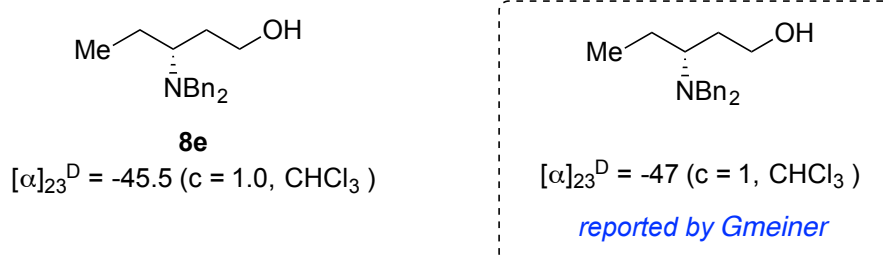
Table 5.5 Internal alkenes that did not react or reacted in low yield



5.4.6 Assignment of Absolute Stereochemistry

Compound **8e** has been synthesized previously by Gmeiner and co-workers.⁴⁴ We compared the optical rotation of **8e** synthesized by hydroamination and saponification to the value that was reported. The absolute configurations of all other amines were assigned by analogy.

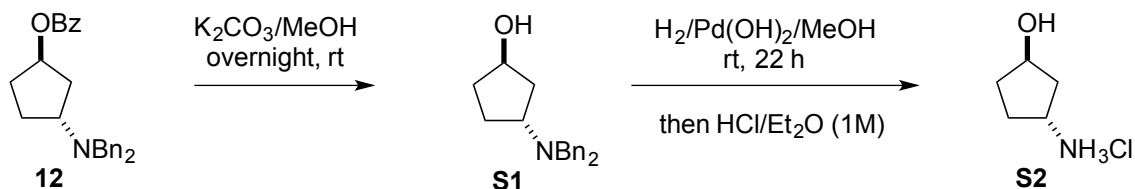
Figure 5.1 Comparison of optical rotation
Synthesized from hydroamination/saponification



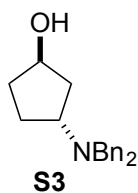
5.4.7. Determination of the diastereoselectivity for hydroamination of cyclopent-3-en-1-yl benzoate

The stereochemical outcome for the hydroamination of **11** was determined by the following derivatization. The benzoate group and benzyl groups of **12** were removed by saponification and hydrogenation, respectively. The corresponding aminoalcohol was converted to its HCl salt. The

NMR spectrum of this salt was compared to the authentic samples purchased from Combi-Blocks Inc. (San Diego, USA).



from hydroamination of **11**



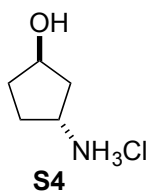
Compound **S3** was obtained by the following procedure:

To a methanol solution (5 mL) of compound **12** (106 mg, 0.27 mmol) was added K_2CO_3 (500 mg). The solution was purged with nitrogen, sealed and stirred overnight. Ethyl acetate (10 mL) and water (10 mL) were added to quench the reaction. The two phases were separated, and the aqueous solution was extracted with 10 mL of ethyl acetate 5 times. The organic layers were combined, dried over Na_2SO_4 , and concentrated. The crude mixture was then purified by preparative TLC (hexanes:ethyl acetate 3:1) to afford **S3** (59 mg, 77%) as an off-white solid.

^1H NMR (500 MHz, CDCl_3) δ 7.37 (d, $J = 7.1$ Hz, 4H), 7.30 (t, $J = 7.5$ Hz, 4H), 7.25 – 7.19 (m, 2H), 4.35 (tt, $J = 5.7, 3.4$ Hz, 1H), 3.59 (s, 4H), 3.54 (quint, $J = 8.1$ Hz, 1H), 2.00 – 1.92 (m, 2H), 1.86 – 1.74 (m, 2H), 1.66 – 1.58 (m, 1H), 1.56 – 1.49 (m, 1H).

^{13}C NMR (151 MHz, CDCl_3) δ 140.26, 128.56, 128.10, 126.67, 72.80, 59.97, 55.24, 37.96, 34.33, 26.36.

HRMS (ESI+) Calculated for $\text{C}_{19}\text{H}_{24}\text{ON}$ $[\text{M}+\text{H}]^+$: 282.1852, Found: 282.1846.

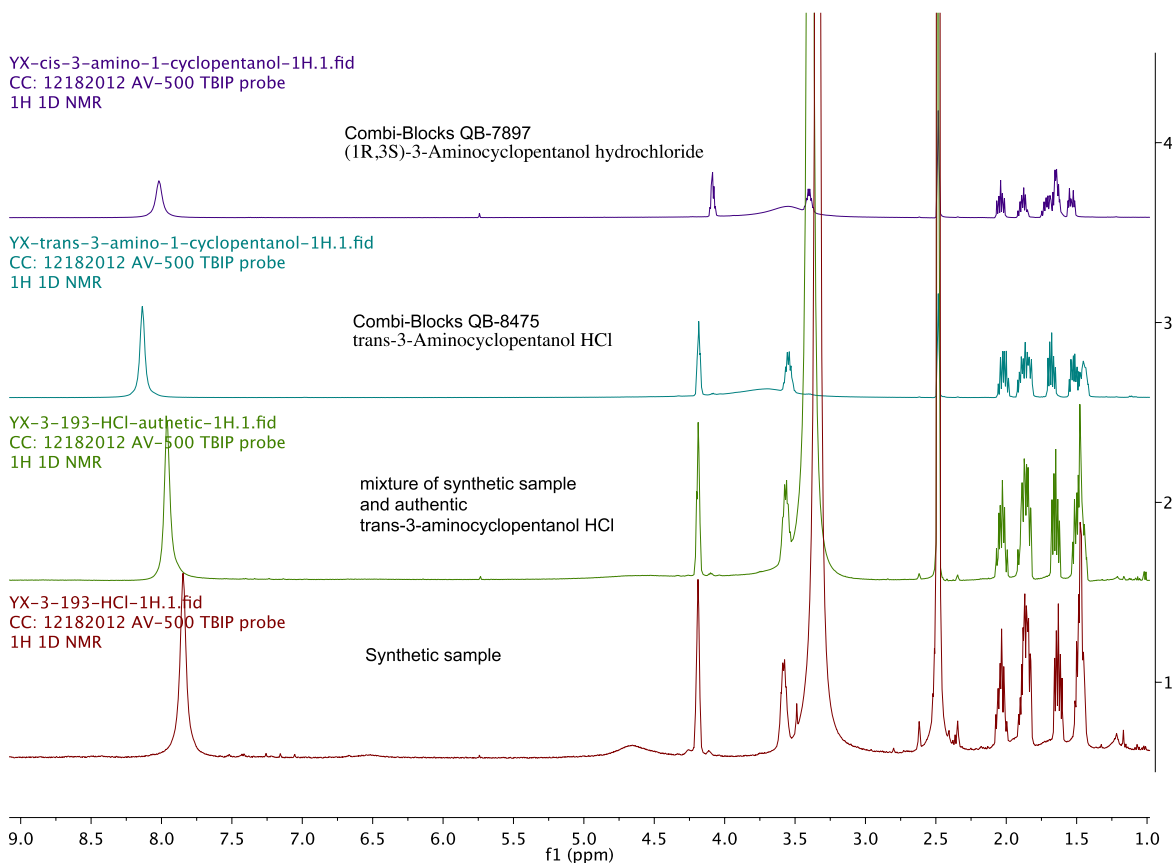


Compound **S4** was obtained by the following procedure:

To an oven-dry flask was added **S3** (14 mg), methanol (1.5 mL) and $\text{Pd}(\text{OH})_2$ (3 mg). The flask was then evacuated and refilled with hydrogen gas three times. The reaction was allowed to stir at rt for 22 h before filtering through a short pad of Celite. The resulting solution was concentrated, and the crude material was purified by preparative TLC (100 % methanol) to afford the aminoalcohol. To the aminoalcohol in 1 mL DCM was added 1M HCl solution in ether (5 equiv). The solution was allowed to stir at rt for 2 h. The organic solution was then removed by pipette, and the vial was washed with 1 mL ether three times to afford the pure aminoalcohol HCl salt (2 mg) as a sticky oil after drying under high vacuum for overnight.

^1H NMR (500 MHz, $\text{DMSO-}d_6$) δ 7.85 (brs, 3H), 4.65 (brs, 1H), 4.19 (tt, $J = 5.6, 2.9$ Hz, 1H), 3.61 – 3.55 (m, 1H), 2.11 – 1.97 (m, 1H), 1.92 – 1.83 (m, 2H), 1.66 – 1.60 (m, 1H), 1.51 – 1.44 (m, 2H).

Figure 5.2 Comparison of ^1H NMR spectra of synthetic **S4**, authentic *trans*-3-aminocyclopentanol HCl, authentic *cis*-3-aminocyclopentanol HCl and the mixture of synthetic **S4** and authentic *trans*-3-aminocyclopentanol HCl (full spectra)



The chemical shifts of all peaks for synthetic **S4** and authentic *trans*-3-aminocyclopentanol HCl match. Particularly, the chemical shift and splitting of α -H of the ammonium moiety in the synthetic and commercial samples of *trans*-3-aminocyclopentanol HCl match each other (δ 4.18 (tt, $J = 5.7, 3.0$ Hz, 1H) for synthetic **S4** vs δ 4.19 (tt, $J = 5.6, 2.9$ Hz, 1H) for commercial **S4**), while those for *cis*-3-aminocyclopentanol HCl do not match (δ 4.09 (quint, $J = 4.8$ Hz, 1H)).

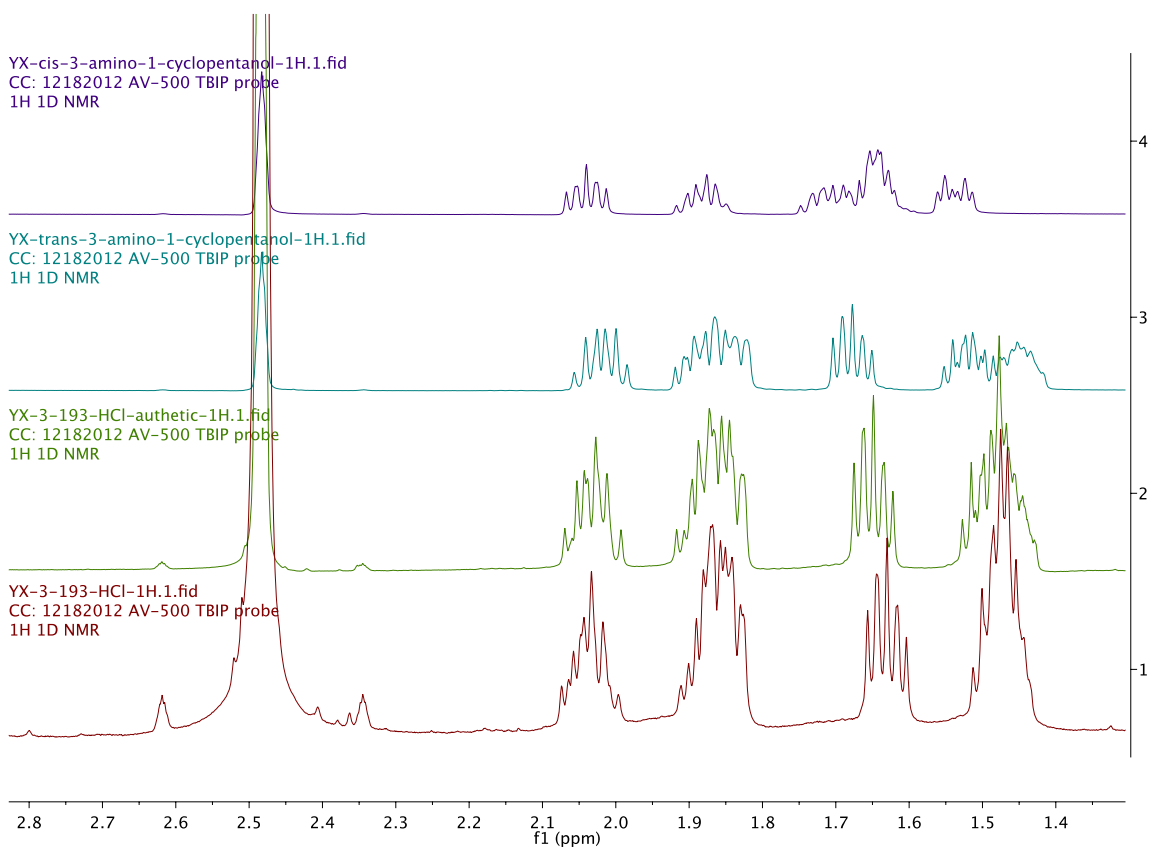
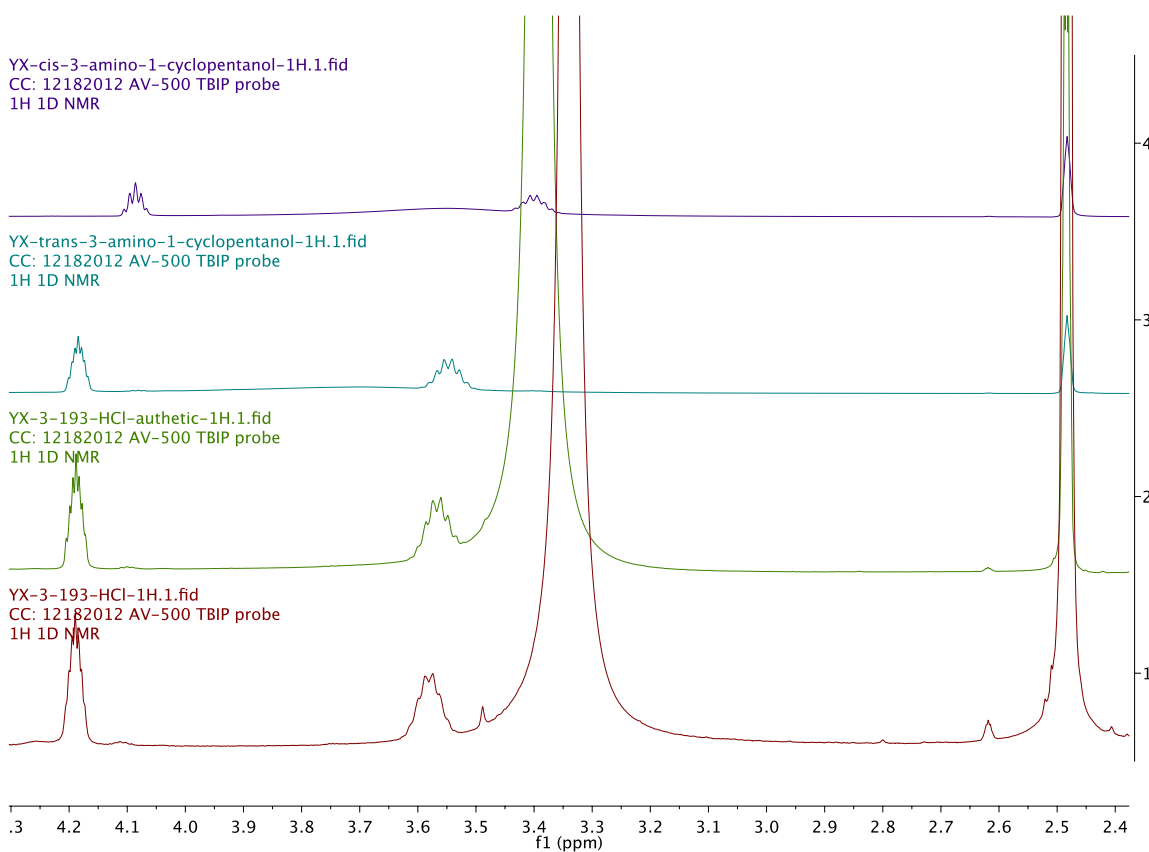
Figure 5.3 Comparison of ^1H NMR spectra (2.8-1.3 ppm region)

Figure 5.4 Comparison of ^1H NMR spectra (4.3-2.4 ppm region)

5.4.8 Competition Experiment between **1e** and *trans*-4-Octene

In a argon-filled dry box, a 1-dram vial was charged with $[\text{Cu}(\text{PPh}_3)\text{H}]_6$ (6.4 mg, 10 mol % of Cu-H units), (*S*)-DTBM-SEGPHOS (26.0 mg, 11 mol %) and THF (140 μL). The mixture was allowed to stir vigorously at ambient temperature for 5 minutes before the addition of diethoxymethylsilane (128 μL , 0.8 mmol, 4 equiv). After brief stirring (10 – 30 seconds), the solution was transferred to another 1-dram vial that contained the alkene **1e** (61.4 mg, 0.2 mmol, 1 equiv), *trans*-4-octene (31 μL , 0.2 mmol, 1 equiv), and $\text{Bn}_2\text{N-OBz}$ (128 mg, 0.4 mmol, 2 equiv). The former vial was washed with THF (60 μL), and the wash solution was transferred to the latter vial. Dodecane (10 μL) was added to the vial, and the vial was capped, sealed with electrical tape, and removed from the box. After 18 h of stirring at rt, the reaction was diluted with ethyl acetate (3 mL). A 0.5 mL aliquot was taken and analyzed by GC. The ratio was determined based on the average of two runs.

5.5 References

Parts of this chapter were reprinted with permission from:
 “Regioselective, Asymmetric Formal Hydroamination of Unactivated Internal Alkenes”
 Xi, Y.; Butcher, T. W.; Zhang, J.; Hartwig, J. F. *Angew. Chem. Int. Ed.* **2016**, *55*, 776.

- [1] V. P. Ananikov, T. T., *Hydrofunctionalization*. Springer: Berlin Heidelberg: 2013.
- [2] Hoveyda, A. H.; Evans, D. A.; Fu, G. C., *Chem. Rev.* **1993**, *93*, 1307.
- [3] Rousseau, G.; Breit, B., *Angew. Chem. Int. Ed.* **2011**, *50*, 2450.
- [4] Crabtree, R. H.; Davis, M. W., *J. Org. Chem.* **1986**, *51*, 2655.
- [5] Perales, J. B.; Van Vranken, D. L., *J. Org. Chem.* **2001**, *66*, 7270.
- [6] Kawasaki, Y.; Ishikawa, Y.; Igawa, K.; Tomooka, K., *J. Am. Chem. Soc.* **2011**, *133*, 20712.
- [7] Evans, D. A.; Fu, G. C., *J. Am. Chem. Soc.* **1991**, *113*, 4042.
- [8] Garrett, C. E.; Fu, G. C., *J. Org. Chem.* **1998**, *63*, 1370.
- [9] Rubina, M.; Rubin, M.; Gevorgyan, V., *J. Am. Chem. Soc.* **2003**, *125*, 7198.
- [10] Smith, S. M.; Takacs, J. M., *J. Am. Chem. Soc.* **2010**, *132*, 1740.
- [11] Coulter, M. M.; Dornan, P. K.; Dong, V. M., *J. Am. Chem. Soc.* **2009**, *131*, 6932.
- [12] Coulter, M. M.; Kou, K. G. M.; Galligan, B.; Dong, V. M., *J. Am. Chem. Soc.* **2010**, *132*, 16330.
- [13] Murphy, S. K.; Bruch, A.; Dong, V. M., *Angew. Chem. Int. Ed.* **2014**, *53*, 2455.
- [14] Mei, T.-S.; Werner, E. W.; Burckle, A. J.; Sigman, M. S., *J. Am. Chem. Soc.* **2013**, *135*, 6830.
- [15] Morandi, B.; Wickens, Z. K.; Grubbs, R. H., *Angew. Chem. Int. Ed.* **2013**, *52*, 9751.
- [16] Xu, L.; Hilton, M. J.; Zhang, X.; Norrby, P.-O.; Wu, Y.-D.; Sigman, M. S.; Wiest, O., *J. Am. Chem. Soc.* **2014**, *136*, 1960.
- [17] Müller, T. E.; Hultsch, K. C.; Yus, M.; Foubelo, F.; Tada, M., *Chem. Rev.* **2008**, *108*, 3795.
- [18] Huang, L.; Arndt, M.; Gooßen, K.; Heydt, H.; Gooßen, L. J., *Chem. Rev.* **2015**, *115*, 2596.
- [19] Hannedouche, J.; Schulz, E., *Chemistry – A European Journal* **2013**, *19*, 4972.
- [20] Ickes, A. R.; Ensign, S. C.; Gupta, A. K.; Hull, K. L., *J. Am. Chem. Soc.* **2014**, *136*, 11256.
- [21] Kawatsura, M.; Hartwig, J. F., *Organometallics* **2001**, *20*, 1960.
- [22] Johns, A. M.; Sakai, N.; Ridder, A.; Hartwig, J. F., *J. Am. Chem. Soc.* **2006**, *128*, 9306.
- [23] MacDonald, M. J.; Schipper, D. J.; Ng, P. J.; Moran, J.; Beauchemin, A. M., *J. Am. Chem. Soc.* **2011**, *133*, 20100.
- [24] Zhao, S.-B.; Bilodeau, E.; Lemieux, V.; Beauchemin, A. M., *Org. Lett.* **2012**, *14*, 5082.
- [25] Bender, C. F.; Widenhofer, R. A., *Chem. Commun.* **2006**, 4143.
- [26] Johns, A. M.; Utsunomiya, M.; Incarvito, C. D.; Hartwig, J. F., *J. Am. Chem. Soc.* **2006**, *128*, 1828.
- [27] Liu, Z.; Hartwig, J. F., *J. Am. Chem. Soc.* **2008**, *130*, 1570.
- [28] Hesp, K. D.; Tobisch, S.; Stradiotto, M., *J. Am. Chem. Soc.* **2010**, *132*, 413.
- [29] Julian, L. D.; Hartwig, J. F., *J. Am. Chem. Soc.* **2010**, *132*, 13813.
- [30] Miki, Y.; Hirano, K.; Satoh, T.; Miura, M., *Angew. Chem. Int. Ed.* **2013**, *52*, 10830.
- [31] Zhu, S.; Niljianskul, N.; Buchwald, S. L., *J. Am. Chem. Soc.* **2013**, *135*, 15746.
- [32] Rucker, R. P.; Whittaker, A. M.; Dang, H.; Lalic, G., *J. Am. Chem. Soc.* **2012**, *134*, 6571.
- [33] Strom, A. E.; Hartwig, J. F., *J. Org. Chem.* **2013**, *78*, 8909.
- [34] Gui, J.; Pan, C.-M.; Jin, Y.; Qin, T.; Lo, J. C.; Lee, B. J.; Spergel, S. H.; Mertzman, M. E.; Pitts, W. J.; La Cruz, T. E.; Schmidt, M. A.; Darvatkar, N.; Natarajan, S. R.; Baran, P. S., *Science* **2015**, *348*, 886.
- [35] Zhu, S.; Buchwald, S. L., *J. Am. Chem. Soc.* **2014**, *136*, 15913.
- [36] Yang, Y.; Shi, S.-L.; Niu, D.; Liu, P.; Buchwald, S. L., *Science* **2015**, *349*, 62.
- [37] Kondo, S.; Shibahara, S.; Takahashi, S.; Maeda, K.; Umezawa, H.; Ohno, M., *J. Am. Chem. Soc.* **1971**, *93*, 6305.

- [38] Lebrun, B.; Braekman, J.-C.; Daloze, D.; Kalushkov, P.; Pasteels, J. M., *Tetrahedron Letters* **2001**, *42*, 4621.
- [39] Lait, S. M.; Rankic, D. A.; Keay, B. A., *Chem. Rev.* **2007**, *107*, 767.
- [40] Lipshutz, B. H.; Frieman, B. A., *Angew. Chem. Int. Ed.* **2005**, *44*, 6345.
- [41] The reactions conducted with morpholine- and piperidine-derived O-benzoylhydroxylamines gave low conversions and yields (<20%). Attempts to optimize this reaction by using modified aminating reagents with substituents on O-benzoyl group were unsuccessful.
- [42] Campbell, M. J.; Johnson, J. S., *Org. Lett.* **2007**, *9*, 1521.
- [43] Niljianskul, N.; Zhu, S.; Buchwald, S. L., *Angew. Chem. Int. Ed.* **2015**, *54*, 1638.
- [44] Gmeiner, P.; Junge, D; Kaertner, A. *J. Org. Chem.* **1994**, *59*, 6766.

CHAPTER 6

Iridium-Catalyzed Asymmetric Hydroamination of Unactivated Internal Alkenes

6.1 Introduction

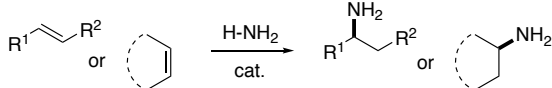
Hydroamination of olefins, the addition of the N-H bond of an amine across an alkene, is a fundamental, yet challenging organic transformation that creates an alkylamine from two abundant chemical feedstocks, olefins and amines, with full atom economy.¹⁻³ The reaction is particularly important because amines, especially chiral amines, are prevalent substructures in a wide range of natural products and drugs. Although extensive efforts have been dedicated to developing efficient catalysts for hydroamination, the vast majority of the alkenes that undergo thermal intermolecular hydroamination have been limited to conjugated, strained, or terminal alkenes;²⁻⁴ only a few examples occur with internal alkenes.⁵⁻⁷ Recently, photoredox catalysis has created an alternative approach for the hydroamination of unactivated internal alkenes based on nitrogen-centered radical intermediates.^{8,9} However, simple thermal hydroaminations of internal alkenes and either thermal or photoredox methods for enantioselective hydroamination of such alkenes are lacking. In fact, current examples of direct, enantioselective hydroamination of any type of unactivated alkene form products with only moderate enantioselectivity.¹⁰⁻¹² Herein, we report a cationic iridium system that catalyzes intermolecular hydroamination of a range of unactivated acyclic and cyclic internal olefins to afford chiral amines with high levels of enantioselectivity ($\geq 90\%$ enantiomeric excess (ee)). The reaction design employs 2-amino-6-methylpyridine as the amine to enhance the rates of multiple steps within the catalytic cycle, while serving as an ammonia surrogate. This approach should create the potential to achieve hydroamination of a wide range of unactivated, multisubstituted olefins.

6.2 Results and Discussion

Chiral amines are essential structural motifs in a majority of active pharmaceutical ingredients and in many agrochemicals, and materials. They also serve as chiral catalysts, resolving reagents, and chiral auxiliaries.¹³ Thus, efficient methods to prepare chiral amines have been long sought. Traditional approaches include reductive amination,¹⁴ hydrogenation,¹⁵ nucleophilic addition of imines,¹⁶ and enzymatic reactions.¹⁷ However, these methods are not general and often require prefunctionalized starting materials. The recent development of the CuH-catalyzed “formal” hydroamination provided a solution to this problem.¹⁸ However, the use of silanes and electrophilic aminating reagents instead of amines undermines the atom-economy of the hydroamination reaction. To date, direct N-H additions of unactivated internal olefins that occur with high enantioselectivity are unknown.

Significant challenges confront the development of catalytic hydroaminations of unactivated olefins that bear more than one substituent (Figure 6.1 A). It is shown by both experiments and theoretical studies that the thermodynamic driving force is weak, and the kinetic barrier of combining two nucleophiles is high.^{1, 19} Moreover, catalysts for hydroamination often catalyze undesirable, competing olefin isomerizations,²⁰ and many olefin amination catalysts form oxidation amination products by β -hydrogen elimination of β -aminoalkyl intermediates.^{21, 22} Finally, because hydroamination is usually close to ergoneutral, isomerization and racemization of the products during the reaction can erode regioselectivity and enantioselectivity.²³

A. Catalytic hydroamination of unactivated internal alkenes



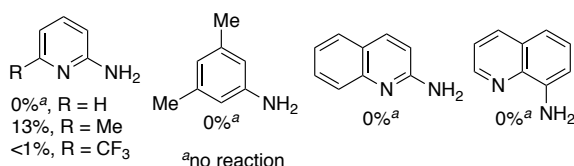
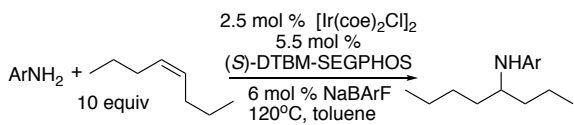
Challenges:

- lack of thermodynamic driving force
- low reactivity of internal alkenes
- mixture of side products
- control of enantioselectivity

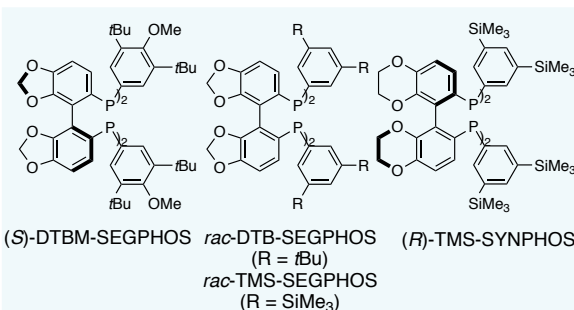
Previous strategy:

- photocatalytic system
- directed hydroamination
- formal hydroamination (w/ H^+ and NR_2^+ sources)

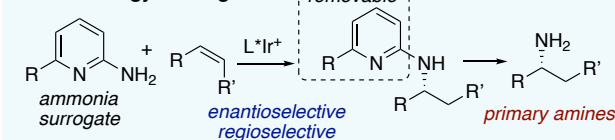
C. Identification of Ammonia Surrogates



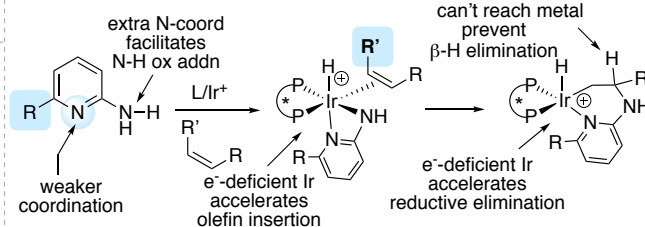
E. Ligand Structures



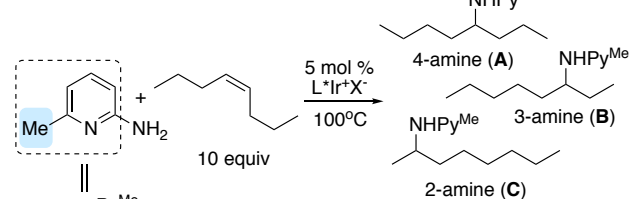
B. Our Strategy & Design



Hypothesis: cationic iridium
 bidentate amine



D. Identification of Reaction Conditions



L*	X	4-selectivity ^a	yield (A+B+C)
(S)-DTBM-SEGPHOS	BARF	48%	16%
(S)-DTBM-SEGPHOS	Cl	n/a	0%
rac-DTB-SEGPHOS	BARF	50%	42%
rac-TMS-SEGPHOS	BARF	83%	34%
(S)-DTBM-SEGPHOS	NTf ₂ ^b	63%	60% (-95% ee)
(R)-TMS-SYNPHOS	NTf ₂ ^b	89%	78% (97% ee)

^adefined as percentage of A/(A+B+C); ^bconducted at 120°C

Figure 6.1 Catalytic asymmetric hydroamination of unactivated internal olefins.

To address these challenges, we modified a prior neutral iridium complex containing a biphosphine ligand, which had catalyzed the formation of hydroamination and oxidative amination products from terminal alkenes and amides and indoles.²⁴⁻²⁶ We had shown that the reaction occurred by a mechanism comprising oxidative addition of N-H bonds, migratory insertion of olefins, and reductive elimination of C-H bonds.²¹ We envisioned that switching the iridium catalyst from neutral to cationic would lead to the formation of cationic iridium intermediates that would undergo migratory insertion of the olefin more rapidly,²⁷ a step that was shown to be rate-limiting in the reaction of terminal alkenes with the neutral catalyst.²¹ (Figure 6.1 B) If binding and insertion of the alkene were sufficiently enhanced, then the reaction scope might include internal alkenes. Cationic iridium complexes are known to enhance the rates for hydrogenation of internal alkenes, but have not been applied to hydroaminations of internal alkenes and have led to modest yields and low enantioselectivities for reactions of unactivated terminal alkenes.¹² In addition, adjacent coordinating groups on the amine (e.g. 2-aminopyridine derivatives) could facilitate the initial N-H oxidative addition, because the rate of oxidative addition of electron-deficient metal complexes is generally slower than that of electron-rich ones.²⁸ If properly placed, the coordinating groups of the amine also could form a rigid 6-membered iridacycle upon insertion of the alkene;

this geometry could suppress β -hydrogen elimination to form enamines. Such amines have been studied in the context of their relevance to medicinally active compounds but not as a means to enhance activity. Furthermore, a substituent nearby the binding group could modulate the strength of the coordination of the pyridine. Finally, if this reagent were based on a 2-aminopyridine scaffold, the pyridyl group of the product could be cleaved by known methods to reveal the corresponding primary amine.²⁹ Ultimately, the substituent on the amine, the development of a new phosphine ligand, and use of an uncommon counterion on the cationic iridium all contributed to the identification of a system for the enantioselective direct addition of an amine N-H bond to internal, unactivated alkenes.

Figure 6.1 D summarizes selected experiments showing the role of these components of the system on reaction yield and enantioselectivity. These experiments showed that 2-amino-6-methylpyridine underwent the hydroamination of *cis*-4-octene catalyzed by a combination of $[\text{Ir}(\text{coe})_2\text{Cl}]_2$, (*S*)-DTBM-SEGPHOS [(*S*)-(+)-5,5'-Bis[di(3,5-di-*tert*-butyl-4-methoxyphenyl)phosphino]-4,4'-bi-1,3-benzodioxole], and NaBARF [Sodium tetrakis[3,5-bis(trifluoromethyl)phenyl]borate]. Other amines underwent hydroamination in lower yield or no yield. The reaction catalyzed by a neutral iridium complex without addition of NaBARF under otherwise identical conditions (Figure 6.1D, entry 2) resulted in exclusive formation of oxidative amination products. With (*S*)-DTBM-SEGPHOS as the ligand and BARF as the anion, a mixture of 4-, 3- and 2-octylamines (**A**, **B**, and **C**) was obtained, due to competing olefin isomerization. Only 48% of amine **A** from direct addition was observed. Further studies indicated that ligands that are less electron-rich and more sterically encumbered than (*S*)-DTBM-SEGPHOS form catalysts with higher reactivity and selectivity towards **A** (Figure 6.1 D, entries 3, 4). In addition, reactions with triflimide as the counterion of the catalyst, instead of BARF, occurred to even higher conversions and selectivity (Figure 6.1 D, entry 5). Eventually, a highly active catalyst, [(*R*)-TMS-SYNPHOSIr(COD)]NTf₂ was identified (Figure 6.1 D, entry 6); this system catalyzed the model hydroamination reaction with both high enantioselectivity and good yield.

With this catalyst and reagent, we examined the scope of olefins that underwent hydroamination. Both symmetrical internal olefins and unsymmetrical internal olefins underwent hydroamination with 2-amino-6-methylpyridine. The reactions all proceeded with greater than 90% ee; reactions of unsymmetrical internal olefins occurred with synthetically useful regioselectivity (2.5:1 to 10:1). Functional groups with which the hydroamination was shown to be compatible include silyloxy groups (**3**, **7**), alkoxy groups (**5**), alkoxy carbonyl groups (**6**), and sulfonamido groups (**9**). Under a modified condition, the hydroamination of cyclic alkenes also occurred in high enantioselectivity. The reactions are compatible with cyclic alkenes of varying ring size (5-8 membered rings), although isomeric amines were significant side products from reactions of the larger-ring alkenes, due to competing olefin isomerization. Because of this isomerization, enantioselective reactions of cyclopentene derivatives were surveyed. These reactions occurred to give the product with 90-92% ee. High diastereoselectivity was observed for the *trans* product from a 4-methoxycarbonyl-substituted cyclopentene.

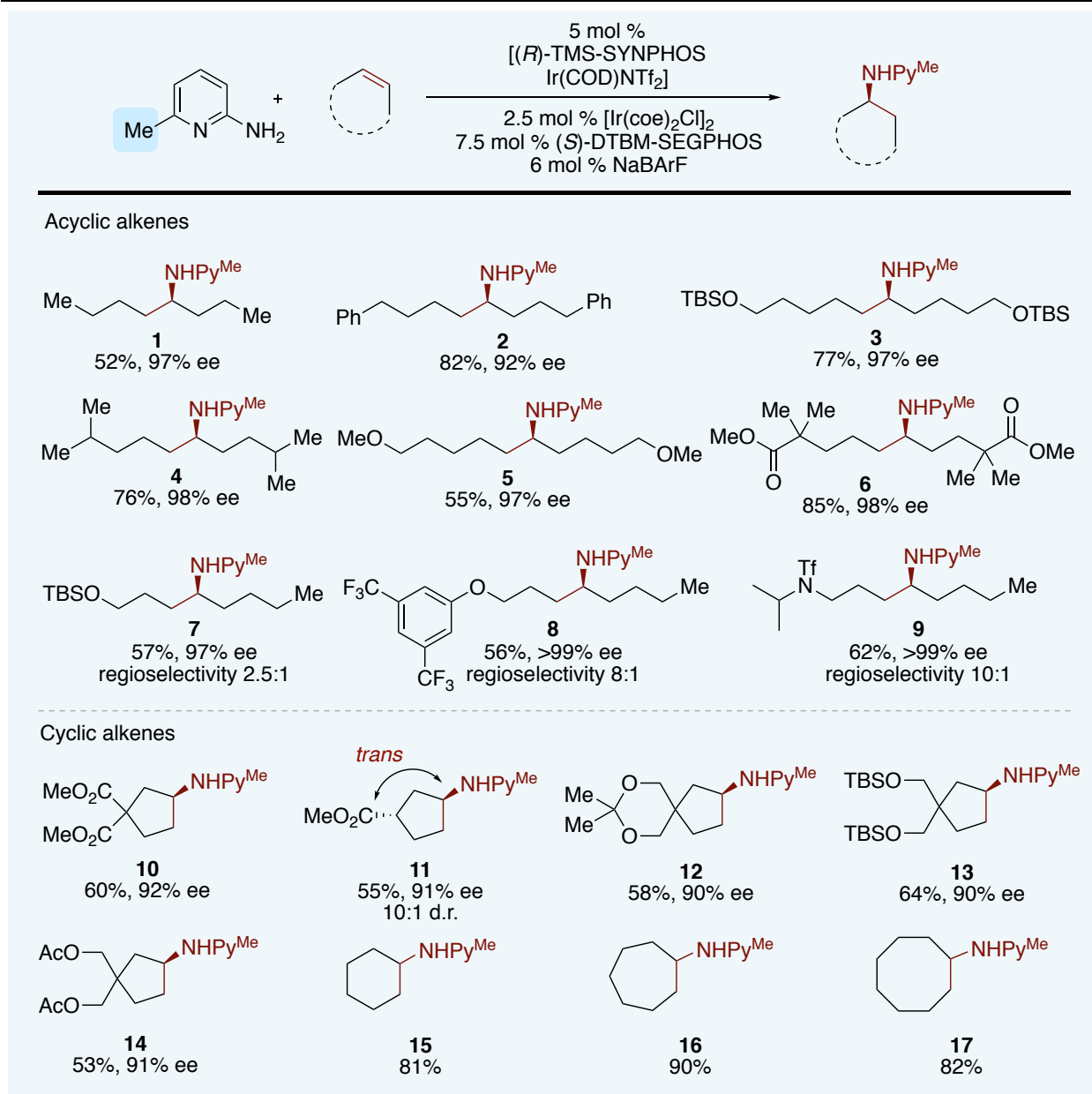


Figure 6.2 Scope of the olefins that undergo asymmetric hydroamination.

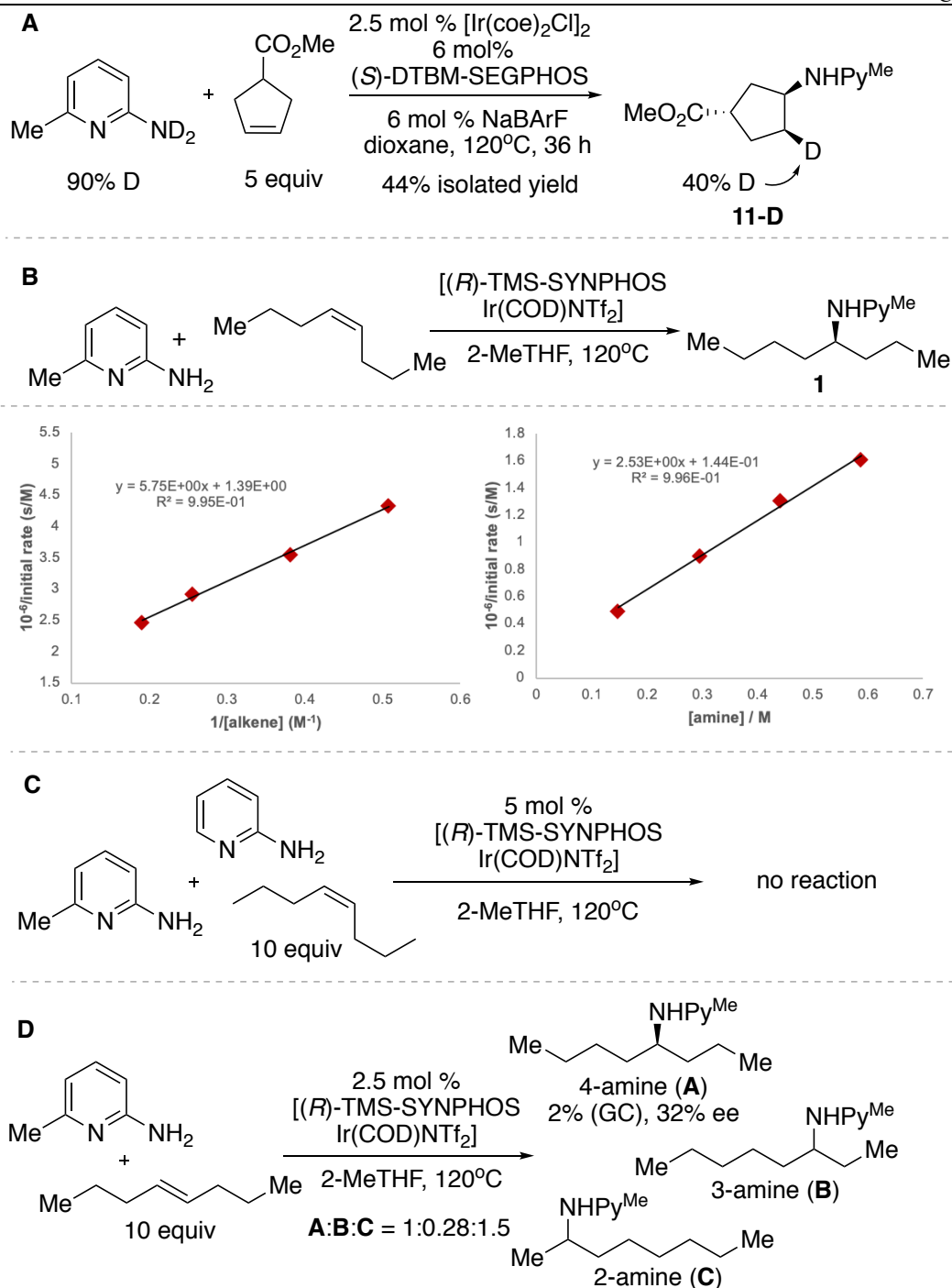
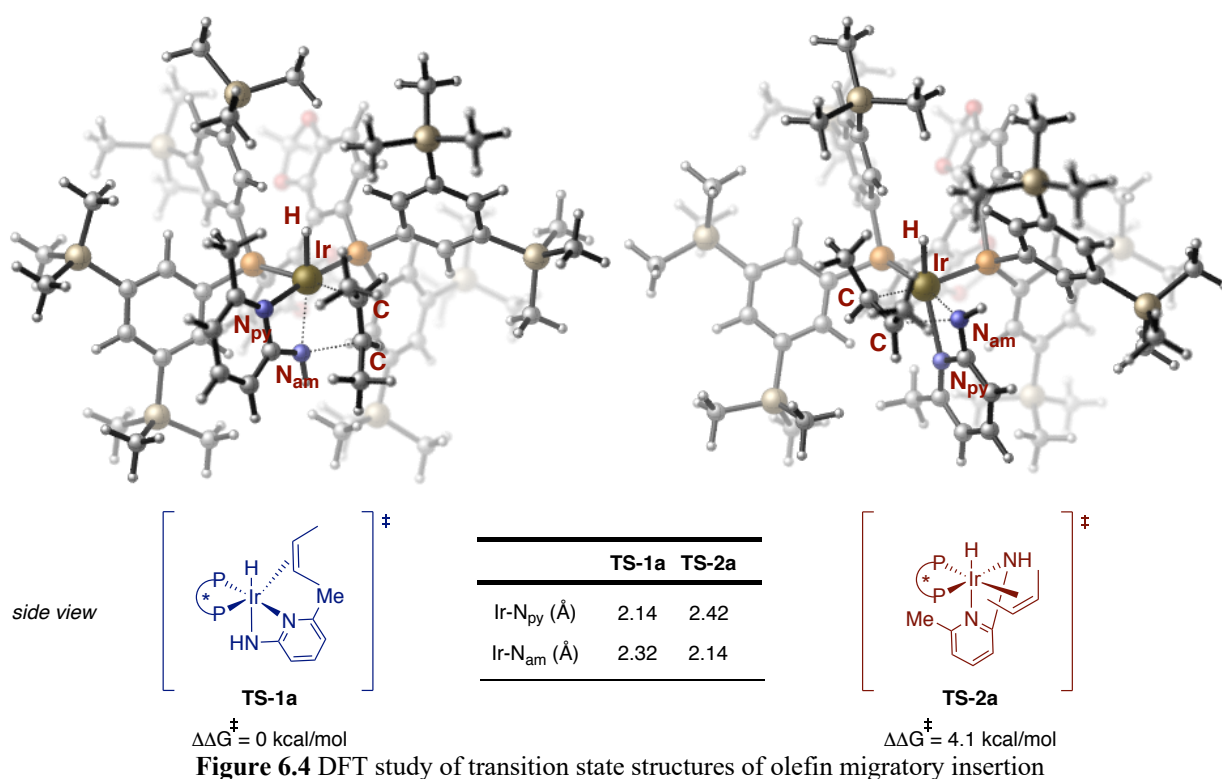


Figure 6.3 Mechanistic study of the hydroamination

To understand how the combination of a cationic iridium catalyst and 2-amino-6-methylpyridine enabled the hydroamination of unactivated internal alkenes, we conducted studies to investigate the reaction mechanism. The reaction of a substituted cyclopentene with *N,N*-dideuterio-2-amino-6-methylpyridine showed that the addition occurred in a *syn* fashion. This stereochemistry

is consistent with a mechanism that involves migratory insertion of an olefin, rather than nucleophilic attack on a metal-bound olefin complex (Figure 6.3 A). Kinetic experiments showed that the reaction is first order in [catalyst], positive order in [*cis*-4-octene], and inverse order in [2-amino-6-methylpyridine] (Figure 6.3 B). These data suggest that a molecule of 2-amino-6-methylpyridine dissociates reversibly from iridium in the catalyst resting state prior to rate-limiting insertion of the alkene, presumably into the metal-amido bond.²⁷ To elucidate why the methyl group of 2-amino-6-methylpyridine is essential in this reaction, we conducted the hydroamination of *cis*-4-octene with equimolar amounts of 2-amino-6-methylpyridine and 2-aminopyridine. While the reaction 2-amino-6-methylpyridine alone afforded the hydroamination product in high yield, the reaction that contained both 2-amino-6-methylpyridine and 2-aminopyridine provided neither hydroamination product (Figure 6.3 C). This result implies that stronger binding of the 2-aminopyridine than of 2-amino-6-methylpyridine inhibits the catalyst. It also implies that the methyl group of 2-amino-6-methylpyridine weakens the binding to the iridium center, therefore allowing for olefin binding and insertion. The olefin geometry influences the rate of the reaction; addition of 2-amino-6-methylpyridine to *trans*-4-octene occurred in much lower yield and enantioselectivity than addition to the *cis* isomer (Figure 6.3 D).



To understand the origin of the high levels of enantioselectivity in the hydroamination, we conducted density functional theory (DFT) calculations on the olefin migratory insertion. Based on the kinetic experiments, this step is likely the rate-limiting and enantio-determining step of the catalytic cycle. We calculated 12 possible isomeric transition states of migratory insertion that would lead to either enantiomer of the products with *cis*-2-butene as the model alkene. The structures of the lowest-energy transition states that lead to the major and minor products are illustrated

in Figure 6.4. The two transition states of many metal-catalyzed enantioselective hydrofunctionalization reactions of alkenes to form two enantiomers differ principally by the face of the olefin to which the metal is bound. In the current system, the orientation of ancillary ligands around the metal, in addition to the face of the olefin, differs greatly in the two transition states. The geometry of **TS-1a**, the transition state leading to the major product, contains meridionally oriented hydride pyridine and amido ligands with the hydride trans to the pyridine. In contrast, these three ligands in **TS-2a**, which is the lowest-energy transition state leading to the minor product, are arranged with the hydride trans to the pyridine donor. The geometry analogous to **1a** that would form the opposite enantiomer by orienting the methyl groups away from the pyridine ligand is higher in energy than **TS-2a**. **TS-1a** is likely the lowest energy transition state for several reasons. First, the Ir-N_{am} bond to the amido group, which is *trans* to a hydride in **TS-1a**, is elongated (2.32 Å), thereby leading to higher reactivity toward insertion. Second, the olefin is almost co-planar with the P-Ir-P plane in **TS-1a**, the olefin is perpendicular to the P-Ir-P plane whereas in **TS-2a**. These orientations place the substituents on the olefin in **TS-1a** further from the phosphine ligand than those on the olefin in **TS-2a**, thereby reducing steric hindrance. This analysis suggests that electronic and steric effects together impart high enantioselectivity in the hydroamination.

6.3 Conclusion

In summary, we have developed a direct, asymmetric N-H addition of amines to unactivated internal alkenes. A range of unactivated acyclic and cyclic internal olefins underwent the hydroamination to afford chiral amines with high levels of enantioselectivity. The use of cationic iridium and 2-amino-6-methylpyridine as the amine led to enhancements of the rates of multiple steps within the catalytic cycle and suppression of side reactions, thereby enabling the hydroamination of unactivated internal olefins. These design principles should provide a starting point to address the long-standing challenge of applying hydroamination of unactivated internal olefins to the synthesis of chiral amines and inspire advances in other asymmetric hydrofunctionalizations of internal olefins.

6.4 Experimental

6.4.1 General Methods and Materials

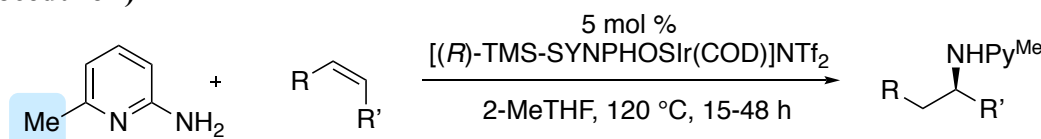
All reagents were purchased from commercial suppliers, stored in the glove box and used as received. Glassware was dried at 170 °C for at least 4 hours before use. Anhydrous 1,4-dioxane and 2-methyltetrahydrofuran were purchased from Acros, stored in a dry box, and used as received without further purification. [Ir(coe)₂Cl]₂ was prepared following a published procedure. (*S*)-DTBM-SEGPHOS was used as received from Takasago. 2-Amino-6-methylpyridine was purchased from Aldrich, recrystallized from a mixture of dichloromethane and hexanes, and stored in a dry box. All catalytic reactions were set up in a nitrogen-filled dry box with oven-dried glassware and were stirred with Teflon-coated magnetic stirring bars.

¹H NMR spectra were recorded on Bruker AV-600, and AV-700 instruments with 600 and 700 MHz frequencies, and ¹³C were recorded on Bruker AV-600 instrument with a ¹³C operating frequency of 150 MHz. Chemical shifts (δ) are reported in ppm relative to the residual solvent signal (CDCl₃ δ = 7.26 for ¹H NMR and δ = 77.0 for ¹³C NMR = 7.26 ppm). Quantitative analysis by GC was performed with dodecane as an internal standard. High-resolution mass spectral data

were obtained with a Thermo Finnigan LTQ FT Instrument in the QB3/Chemistry Mass Spectrometry Facility, University of California, Berkeley. GC analysis was performed on an Agilent 7890 GC and an FID detector. Chiral SFC analysis was conducted on a JASCO SFC system. Chiral HPLC analysis was conducted on Waters chromatography system and Agilent chromatography system.

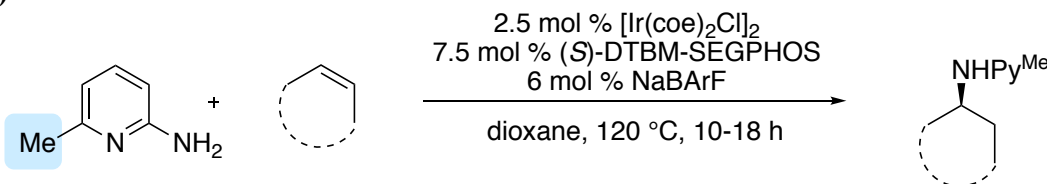
6.4.2 General Procedure for Catalytic Hydroamination

Representative procedure for the catalytic hydroamination of acyclic internal olefins (General Procedure I)



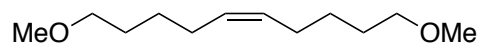
In a nitrogen-filled dry box, a 1-dram vial was charged with [(*R*)-TMS-SYNPHOSIr(COD)]NTf₂ (9.0 mg, 5.0 mol %), 2-amino-6-methylpyridine (10.8 mg, 0.100 mmol, 1 equiv), the corresponding olefin (10 equiv), and 2-methyltetrahydrofuran (50 μ L). 10.0 μ L of dodecane was added, and the vial was capped, sealed with electrical tape, and removed from the box. The reaction was heated to 120 $^{\circ}$ C in an aluminum heating block, and monitored by GC periodically. The reaction vial was diluted with 1 mL of ethyl acetate after the reaction reached around 90% conversion (Note: prolonged reaction time will result in racemization of products). The crude material was concentrated *in vacuo* and purified by preparative TLC to afford the pure product.

Representative procedure for the catalytic hydroamination of cyclic olefins (General Procedure II)



In a nitrogen-filled dry box, a 1-dram vial was charged with [Ir(coe)₂Cl]₂ (2.3 mg, 2.5 mol %), (*S*)-DTBM-SEGPHOS (8.8 mg, 7.5 mol %), sodium tetrakis[3,5-bis(trifluoromethyl)phenyl]borate (5.3 mg, 6.0 mol %), 2-amino-6-methylpyridine (10.8 mg, 0.100 mmol, 1 equiv), the corresponding olefin (5 equiv), and dioxane (100 μ L, if the olefin is a liquid; 150 μ L, if the olefin is a solid). 10.0 μ L of dodecane was added, and the vial was capped, sealed with electrical tape, and removed from the box. The reaction was heated to 120 $^{\circ}$ C in an aluminum heating block, and monitored by GC periodically. The reaction vial was diluted with 1 mL of ethyl acetate after the reaction reached around 80% conversion (Note: prolonged reaction time will result in racemization of products). The crude material was concentrated *in vacuo* and purified by preparative TLC to afford the pure product.

6.4.3 Synthesis of Substrates



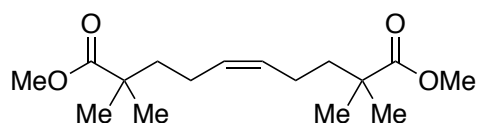
Compound S5 was synthesized according to the following procedure.

An oven-dried flask was charged with (*Z*)-dec-5-ene-1,10-diol (1.22 g, 7.00 mmol, 1 equiv) and 10 mL of DMF. The solution was cooled to 0 °C, and added sodium hydride (60% in mineral oil, 700 mg, 2.5 equiv) in portions. The resulting mixture was allowed to stir for 30 min. Methyl iodide was added (1.74 mL, 4 equiv) in one portion. The resulting mixture was warmed to rt. After stirring overnight, the reaction was quenched with water (10 mL). The mixture was extracted with ether (10 mL) twice. The organic layers were combined, washed with water three times, dried over Na₂SO₄, and concentrated *in vacuo*. The crude material was purified by flash column chromatography (hexanes). Compound **S5** was obtained as a colorless oil in 79% yield.

¹H NMR (600 MHz, CDCl₃) δ 5.40 – 5.35 (m, 2H), 3.39 (t, *J* = 6.6 Hz, 4H), 3.35 (s, 6H), 2.09 – 2.04 (m, 4H), 1.63 – 1.56 (m, 4H), 1.45 – 1.39 (m, 4H).

¹³C NMR (151 MHz, CDCl₃) δ 129.78, 72.77, 58.53, 29.25, 27.00, 26.22.

HRMS (EI+) Calculated for C₁₁H₂₁O₂ [M-CH₃]⁺: 185.1542, Found: 185.1539.



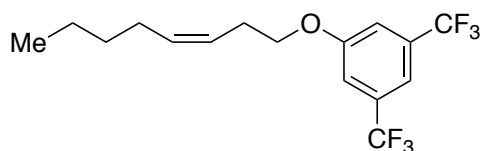
Compound S6 was synthesized according to the following procedure.

An oven-dried flask was charged with diisopropylamine (2.52 mL, 2.4 equiv) and 15 mL of THF. The flask was cooled to -78 °C, *n*-BuLi (6.6 mL, 2.5 M in hexanes, 2.2 equiv) was added, and then warmed to 0 °C. After 15 minutes, the reaction was cooled back to -78 °C and methyl isobutyrate (1.72 mL, 2 equiv) was added dropwise. The resulting enolate solution was allowed to stir for 30 minutes at the same temperature before (*Z*)-1,6-diiodohex-3-ene (7.5 mmol, 2.52 g, 1 equiv) was added. The solution was then warmed to rt. After stirring overnight at rt, the reaction was quenched with water (25 mL). The mixture was extracted with ethyl acetate (20 mL) twice. The organic layers were combined, dried over Na₂SO₄, and concentrated *in vacuo*. The crude material was purified by flash column chromatography (hexanes:ethyl acetate = 6:1). Compound **S6** was obtained as a colorless oil in 50% yield.

¹H NMR (600 MHz, CDCl₃) δ 5.40 – 5.35 (m, 2H), 3.64 (s, 6H), 1.96 – 1.86 (m, 4H), 1.58 – 1.49 (m, 4H), 1.16 (s, 12H).

¹³C NMR (151 MHz, CDCl₃) δ 178.16, 129.39, 51.57, 42.14, 40.59, 25.08, 22.81.

HRMS (EI+) Calculated for C₁₆H₂₈O₄ [M]⁺: 284.1988, Found: 284.1986.



Compound S8 was synthesized according to the following procedure.

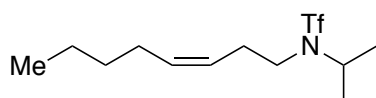
An oven-dried flask was charged with (*Z*)-3-octen-1-ol (1.81 mL, 12.0 mmol, 1 equiv), triphenylphosphine (3.14 g, 1 equiv), 3,5-bis(trifluoromethyl)phenol (2.01 mL, 1.1 equiv), and 12 mL of THF. The solution was cooled to 0 °C, and diisopropyl azodicarboxylate (2.83 mL, 1.2 equiv) was added dropwise. The resulting mixture was warmed to rt. After stirring overnight, the

reaction was quenched with water (10 mL). The mixture was extracted with ethyl acetate (15 mL) twice. The organic layers were combined, dried over Na_2SO_4 , and concentrated *in vacuo*. The crude material was purified by flash column chromatography (hexanes:ethyl acetate = 30:1). Compound **S8** was obtained as a colorless oil in 26% yield.

^1H NMR (600 MHz, CDCl_3) δ 7.47 (s, 1H), 7.32 (s, 2H), 5.64 – 5.56 (m, 1H), 5.50 – 5.45 (m, 1H), 4.07 (t, $J = 6.8$ Hz, 2H), 2.61 (q, $J = 6.9$ Hz, 2H), 2.12 (q, $J = 7.2$ Hz, 2H), 1.44 – 1.33 (m, 4H), 0.94 (t, $J = 7.0$ Hz, 3H).

^{13}C NMR (151 MHz, CDCl_3) δ 159.55, 133.41, 132.78 (q, $J_{\text{C-F}} = 33.3$ Hz), 123.79, 123.21 (q, $J_{\text{C-F}} = 273.3$ Hz), 114.80 (q, $J_{\text{C-F}} = 3.2$ Hz), 114.10 (hept, $J_{\text{C-F}} = 3.9$ Hz), 68.36, 31.74, 27.10, 27.10, 22.32, 13.87.

HRMS (EI+) Calculated for $\text{C}_{16}\text{H}_{18}\text{OF}_6$ $[\text{M}]^+$: 340.1262, Found: 340.1263.



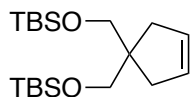
Compound S9 was synthesized according to the following procedure.

In an oven-dried flask was charged with (*Z*)-3-octen-1-ol (1.52 mL, 10.0 mmol, 1 equiv), triphenylphosphine (2.62 g, 1 equiv), *N*-isopropyltrifluoromethanesulfonamide (2.1 g, 1.1 equiv), and 12 mL of THF. The solution was cooled to 0 °C, and added diisopropyl azodicarboxylate (2.36 mL, 1.2 equiv) dropwise. The resulting mixture was warmed to 50 °C. After stirring for 5 days, the reaction was quenched with water (10 mL). The mixture was extracted with ethyl acetate (15 mL) twice. The organic layers were combined, dried over Na_2SO_4 , and concentrated *in vacuo*. The crude material was purified by flash column chromatography (hexanes:ethyl acetate = 10:1). Compound **S9** was obtained as a colorless oil in 60% yield.

^1H NMR (600 MHz, CDCl_3) δ 5.62 – 5.45 (m, 1H), 5.30 (dtt, $J = 10.8, 7.4, 1.7$ Hz, 1H), 4.19 (hept, $J = 6.8$ Hz, 1H), 3.34 – 3.11 (m, 2H), 2.45 (q, $J = 7.3$ Hz, 2H), 2.07 (q, $J = 7.2$ Hz, 2H), 1.35 (qdt, $J = 5.7, 3.5, 2.1$ Hz, 3H), 1.31 (d, $J = 6.8$ Hz, 6H), 0.92 (t, $J = 7.1$ Hz, 2H).

^{13}C NMR (151 MHz, CDCl_3) δ 133.47, 123.87, 120.03 (q, $J_{\text{C-F}} = 323.7$ Hz), 52.04, 43.78, 31.73, 29.64, 27.05, 22.26, 20.59, 13.86.

HRMS (EI+) Calculated for $\text{C}_{12}\text{H}_{22}\text{NO}_2\text{F}_3\text{S}$ $[\text{M}]^+$: 301.1323, Found: 301.1323.



Compound S13 was synthesized according to the following procedure.

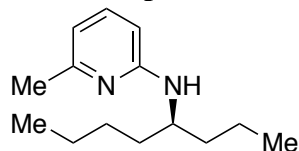
A 20 mL vial was charged with cyclopent-3-ene-1,1-diyldimethanol (560 mg, 4.37 mmol, 1 equiv), imidazole (892 mg, 3 equiv), and 10 mL DMF. The vial was cooled to 0 °C, and TBSCl (1.49 g, 2.2 equiv) was added in portions. The resulting mixture was warmed to rt. After stirring overnight, the reaction was quenched with water (10 mL). The mixture was extracted with ether (10 mL) twice. The organic layers were combined, washed with water three times, dried over Na_2SO_4 , and concentrated *in vacuo*. The crude material was purified by flash column chromatography (hexanes). Compound **S13** was obtained as a colorless oil in 98% yield.

^1H NMR (600 MHz, CDCl_3) δ 5.61 (s, 2H), 3.52 (s, 4H), 2.13 (s, 4H), 0.93 (s, 18H), 0.07 (s, 12H).

^{13}C NMR (151 MHz, CDCl_3) δ 129.00, 65.61, 48.92, 38.34, 25.92, 18.29, -5.47.

HRMS (EI+) Calculated for $\text{C}_{19}\text{H}_{40}\text{O}_2\text{Si}_2$ $[\text{M}]^+$: 356.2567, Found: 356.2545.

6.4.4 Compound Characterization



Compound 1 was synthesized according to the **General Procedure Condition I** with **S1** (157 μ L, 1.00 mmol), 2-amino-6-methylpyridine (10.8 mg, 0.100 mmol, 1 equiv), and [(*R*)-TMS-SYNPHOSIr(COD)]NTf₂ (4.5 mg, 2.5 mol %). The reaction time was 48 h. Compound **1** was purified by preparative TLC (hexanes:ethyl acetate = 5:1) and obtained as a yellow oil in 52% yield.

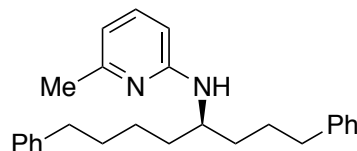
¹H NMR (600 MHz, CDCl₃) δ 7.32 (t, J = 8.3, 7.2 Hz, 1H), 6.40 (d, J = 7.2 Hz, 1H), 6.17 (d, J = 8.3 Hz, 1H), 4.39 (d, J = 9.1 Hz, 1H), 3.52 – 3.46 (m, 1H), 2.36 (s, 3H), 1.60 – 1.51 (m, 2H), 1.48 – 1.29 (m, 8H), 0.92 (t, J = 7.2 Hz, 3H), 0.90 (t, J = 7.2 Hz, 3H).

¹³C NMR (151 MHz, CDCl₃) δ 158.45, 157.00, 137.89, 111.49, 102.04, 51.50, 37.49, 34.91, 28.05, 24.27, 22.81, 19.09, 14.17, 14.04.

HRMS (EI+) Calculated for C₁₄H₂₄N₂ [M]⁺: 220.1939, Found: 220.1940.

$[\alpha]_D^{23}$ = -0.5 (c = 1.3, DCM).

GC analysis (CP-Chirasil-Dex CB column, 120 °C isothermal) indicated 97% ee: t_R (major) = 37.2 min, t_R (minor) = 38.2 min.



Compound 2 was synthesized according to the **General Procedure Condition I** with **S2** (264 mg, 1.00 mmol), 2-amino-6-methylpyridine (10.8 mg, 0.100 mmol, 1 equiv), and [(*R*)-TMS-SYNPHOSIr(COD)]NTf₂ (4.5 mg, 2.5 mol %). The reaction time was 30 h. Compound **2** was purified by preparative TLC (hexanes:ethyl acetate = 3:1) and obtained as a yellow oil in 82% yield. Note: A minor isomer of 6% was present.

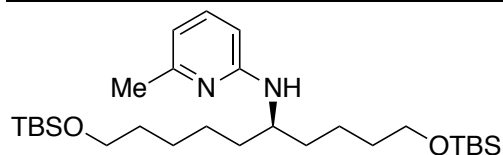
¹H NMR (600 MHz, CDCl₃) δ 7.36 – 7.28 (m, 5H), 7.26 – 7.12 (m, 6H), 6.44 (d, J = 7.3 Hz, 1H), 6.16 (d, J = 8.3 Hz, 1H), 4.39 (d, J = 9.2 Hz, 1H), 3.62 – 3.55 (m, 1H), 2.70 – 2.59 (m, 4H), 2.40 (s, 3H), 1.86 – 1.36 (m, 10H).

¹³C NMR (151 MHz, CDCl₃) δ 158.34, 157.01, 142.59, 142.33, 137.96, 128.43, 128.40, 128.31, 128.29, 125.76, 125.67, 111.68, 102.33, 51.49, 35.94, 35.88, 35.15, 34.83, 31.56, 27.71, 25.55, 24.31.

HRMS (EI+) Calculated for C₂₆H₃₂N₂ [M]⁺: 372.2565, Found: 372.2560.

$[\alpha]_D^{23}$ = 2.5 (c = 3.0, DCM).

HPLC analysis (OD-H, 97:3:0.1 hexanes/IPA/DEA, 1.0 mL/min, 254 nm) indicated 92% ee: t_R (major) = 11.8 min, t_R (minor) = 15.4 min.



Compound 3 was synthesized according to the **General Procedure Condition I** with **S3** (401 mg, 1.00 mmol), 2-amino-6-methylpyridine (10.8 mg, 0.100 mmol, 1 equiv), and [(*R*)-TMS-SYNPHOSIr(COD)]NTf₂ (9.0 mg, 5.0 mol %). The reaction time was 15 h. Compound **3** was purified by preparative TLC (hexanes:ethyl acetate = 6:1) and obtained as a yellow oil in 77% yield.

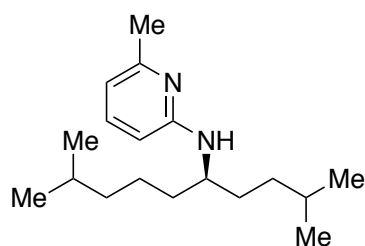
¹H NMR (600 MHz, CDCl₃) δ 7.29 (dd, *J* = 8.3, 7.2 Hz, 1H), 6.37 (d, *J* = 7.2 Hz, 1H), 6.13 (d, *J* = 8.3 Hz, 1H), 4.38 (d, *J* = 8.9 Hz, 1H), 3.65 – 3.53 (m, 4H), 3.53 – 3.42 (m, 1H), 2.33 (s, 3H), 1.60 – 1.28 (m, 14H), 0.88 (s, 9H), 0.87 (s, 9H), 0.10 – -0.02 (m, 12H).

¹³C NMR (151 MHz, CDCl₃) δ 158.32, 156.91, 137.88, 111.52, 102.11, 63.14, 63.03, 51.61, 35.16, 35.00, 32.86, 32.76, 25.94, 25.93, 25.92, 25.65, 24.20, 22.13, 18.32, 18.31, -5.31, -5.32.

HRMS (ESI+) Calculated for C₂₈H₅₇N₂O₂Si₂ [M]⁺: 509.3953, Found: 509.3945.

[α]_D²³ = 0.4 (c = 3.1, DCM).

HPLC analysis (2 AD-H columns, 99.1:0.1:0.3 hexanes/EtOH/*n*-butylamine, 0.3 mL/min, 254 nm) indicated 97% ee: t_R (major) = 34.9 min, t_R (minor) = 36.6 min.



Compound 4 was synthesized according to the **General Procedure Condition I** with **S4** (168 mg, 1.00 mmol), 2-amino-6-methylpyridine (10.8 mg, 0.100 mmol, 1 equiv), and [(*R*)-TMS-SYNPHOSIr(COD)]NTf₂ (9.0 mg, 5.0 mol %). The reaction time was 24 h. Compound **4** was purified by preparative TLC (hexanes:ethyl acetate = 5:1) and obtained as a yellow oil in 76% yield.

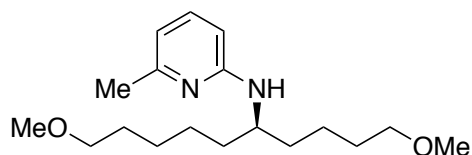
¹H NMR (600 MHz, CDCl₃) δ 7.31 (dd, *J* = 8.3, 7.2 Hz, 1H), 6.38 (d, *J* = 7.2 Hz, 1H), 6.14 (d, *J* = 8.3 Hz, 1H), 4.37 (d, *J* = 9.0 Hz, 1H), 3.47 – 3.35 (m, 1H), 2.34 (s, 3H), 1.61 – 1.12 (m, 12H), 0.87 – 0.83 (m, 12H).

¹³C NMR (151 MHz, CDCl₃) δ 158.37, 156.98, 137.86, 111.48, 102.04, 52.03, 39.02, 35.32, 34.95, 32.80, 28.15, 27.87, 24.25, 23.61, 22.64, 22.58, 22.55, 22.51.

HRMS (EI+) Calculated for C₁₈H₃₂N₂ [M]⁺: 276.2565, Found: 276.2563.

[α]_D²³ = 2.4 (c = 2.2, DCM).

HPLC analysis (OJ-H, 99.9:0.1:0.2 hexanes/EtOH/DEA, 0.5 mL/min, 300 nm) indicated 98% ee: t_R (major) = 7.9 min, t_R (minor) = 9.3 min.



Compound 5 was synthesized according to the **General Procedure Condition I** with **S5** (200 mg, 1.00 mmol), 2-amino-6-methylpyridine (10.8 mg, 0.100 mmol, 1 equiv), and [(*R*)-TMS-SYNPHOSIr(COD)]NTf₂ (13.5 mg, 7.5 mol %). The reaction time was 15 h. Compound **4** was purified by preparative TLC (hexanes:ethyl acetate = 3:1) and obtained as a yellow oil in 55% yield.

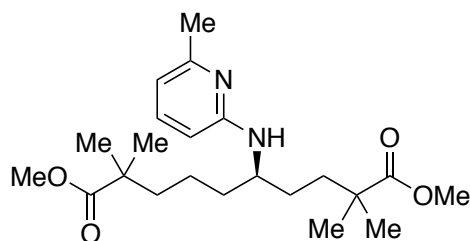
¹H NMR (500 MHz, CDCl₃) δ 7.35 (t, *J* = 7.8 Hz, 1H), 6.42 (d, *J* = 7.2 Hz, 1H), 6.19 (d, *J* = 8.3 Hz, 1H), 4.69 (br s, 1H), 3.55 – 3.47 (m, 1H), 3.40 – 3.36 (m, 4H), 3.35 (s, 3H), 3.35 (s, 3H), 2.38 (s, 3H), 1.65 – 1.35 (m, 14H).

¹³C NMR (151 MHz, CDCl₃) δ 158.22, 156.79, 137.99, 111.53, 102.23, 72.74, 72.67, 58.51, 58.48, 51.61, 35.03, 34.94, 29.67, 29.52, 26.20, 25.68, 24.09, 22.49.

HRMS (EI+) Calculated for C₁₈H₃₂N₂O₂ [M]⁺: 308.2464, Found: 308.2462.

[α]_D²³ = 0.9 (c = 1.4, DCM).

HPLC analysis (AS-H, 98:2:0.1 hexanes/IPA/DEA, 1.0 mL/min, 254 nm) indicated 97% ee: t_R (major) = 5.8 min, t_R (minor) = 8.2 min.



Compound 6 was synthesized according to the **General Procedure Condition I** with **S6** (284 mg, 1.00 mmol), 2-amino-6-methylpyridine (10.8 mg, 0.100 mmol, 1 equiv), and [(*R*)-TMS-SYNPHOSIr(COD)]NTf₂ (9.0 mg, 5.0 mol %). The reaction time was 36 h. Compound **4** was purified by preparative TLC (hexanes:ethyl acetate = 2:1) and obtained as a yellow oil in 85% yield.

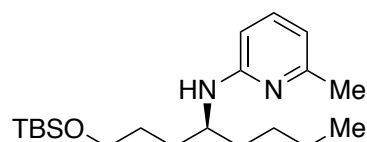
¹H NMR (600 MHz, CDCl₃) δ 7.30 (dd, *J* = 8.3, 7.3 Hz, 1H), 6.39 (d, *J* = 7.2 Hz, 1H), 6.12 (d, *J* = 8.3 Hz, 1H), 4.34 (d, *J* = 8.6 Hz, 1H), 3.60 (s, 3H), 3.60 (s, 3H), 3.49 – 3.43 (m, 1H), 2.33 (s, 3H), 1.67 – 1.19 (m, 10H), 1.13 (s, 3H), 1.13 (s, 3H), 1.12 (s, 3H), 1.12 (s, 3H).

¹³C NMR (151 MHz, CDCl₃) δ 178.36, 178.20, 158.08, 156.92, 137.86, 111.71, 102.41, 51.66, 51.62, 51.60, 42.20, 42.09, 40.62, 36.52, 35.34, 29.99, 25.19, 25.10, 25.09, 25.08, 24.19, 21.28.

HRMS (EI+) Calculated for C₂₂H₃₆N₂O₄ [M]⁺: 392.2675, Found: 392.2680.

[α]_D²³ = 6.4 (c = 3.1, DCM).

HPLC analysis (OD-H, 97:3:0.1 hexanes/EtOH/DEA, 1.0 mL/min, 254 nm) indicated 98% ee: t_R (major) = 10.7 min, t_R (minor) = 9.2 min.



Compound 7 was synthesized according to the **General Procedure Condition I** with **S7** (242 mg, 1.00 mmol), 2-amino-6-methylpyridine (10.8 mg, 0.100 mmol, 1 equiv), and [(*R*)-TMS-SYNPHOSIr(COD)]NTf₂ (9.0 mg, 5.0 mol %). The reaction time was 24 h. The regioselectivity was determined by GC to be 2.5:1. Compound **7** was purified by preparative TLC (hexanes:ethyl acetate = 5:1) and obtained as a yellow oil in 37% yield. The minor isomer **7'** was isolated as a

yellow oil in 20% yield, which contains 22% of a third isomer, which was likely resulted from hydroamination of the terminal alkene formed by isomerization.

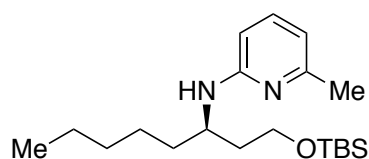
^1H NMR (500 MHz, CDCl_3) δ 7.35 (t, $J = 7.8$ Hz, 1H), 6.43 (d, $J = 7.3$ Hz, 1H), 6.21 (d, $J = 8.3$ Hz, 1H), 4.63 (br s, 1H), 3.65 (t, $J = 5.8$ Hz, 2H), 3.58 – 3.50 (m, 1H), 2.39 (s, 3H), 1.69 – 1.33 (m, 10H), 0.93 (s, 9H), 0.08 (s, 3H), 0.08 (s, 3H).

^{13}C NMR (151 MHz, CDCl_3) δ 158.31, 156.94, 137.84, 111.51, 102.19, 63.03, 51.42, 34.84, 31.26, 29.02, 28.00, 25.91, 24.23, 22.75, 18.28, 14.00, -5.34.

HRMS (EI+) Calculated for $\text{C}_{20}\text{H}_{38}\text{N}_2\text{OSi}$ $[\text{M}]^+$: 350.2753, Found: 350.2750.

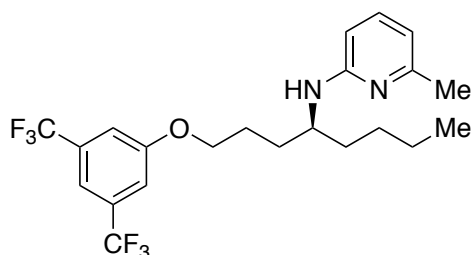
$[\alpha]_{\text{D}}^{23} = -0.5$ ($c = 1.3$, DCM).

HPLC analysis (AS-H, 100:0.1 hexanes/DEA, 0.3 mL/min, 254 nm) indicated 97% ee: t_{R} (major) = 16.7 min, t_{R} (minor) = 16.0 min.



Minor isomer **7'**

^1H NMR (600 MHz, CDCl_3) δ 7.30 (t, $J = 7.8$ Hz, 1H), 6.38 (d, $J = 7.2$ Hz, 1H), 6.25 (d, $J = 8.3$ Hz, 1H), 4.61 (br s, 1H), 3.75 – 3.63 (m, 3H), 2.34 (s, 3H), 1.78 – 1.70 (m, 1H), 1.68 – 1.61 (m, 1H), 1.59 – 1.53 (m, 1H), 1.50 – 1.44 (m, 1H), 1.43 – 1.38 (m, 1H), 1.35 – 1.23 (m, 5H), 0.89 (s, 9H), 0.02 (s, 3H), 0.01 (s, 3H).



Compound 8 was synthesized according to the **General Procedure Condition I** with **S8** (340 mg, 1.00 mmol), 2-amino-6-methylpyridine (10.8 mg, 0.100 mmol, 1 equiv), and $[(R)\text{-TMS-SYNPHOSIr}(\text{COD})]\text{NTf}_2$ (9.0 mg, 5.0 mol %). The reaction time was 18 h. The regioselectivity was determined by GC to be 8:1. **Compound 8** was purified by preparative TLC (hexanes:ethyl acetate = 5:1) and obtained as a yellow oil in 56% yield.

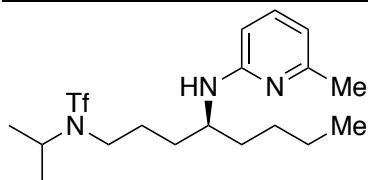
^1H NMR (600 MHz, CDCl_3) δ 7.43 (s, 1H), 7.32 (t, $J = 7.8$ Hz, 1H), 7.26 (s, 2H), 6.40 (d, $J = 7.3$ Hz, 1H), 6.18 (d, $J = 8.4$ Hz, 1H), 4.58 (br s, 1H), 4.07 – 4.01 (m, 2H), 3.66 – 3.60 (m, 1H), 2.34 (s, 3H), 1.98 – 1.76 (m, 3H), 1.66 – 1.46 (m, 3H), 1.44 – 1.27 (m, 4H), 0.88 (t, $J = 7.1$ Hz, 3H).

^{13}C NMR (151 MHz, CDCl_3) δ 159.54, 158.02, 156.69, 138.14, 132.70 (q, $J = 33.3$ Hz), 123.15 (q, $J = 272.8$ Hz), 114.72 (q, $J = 3.2$ Hz), 114.05 (hept, $J = 3.9$ Hz), 111.74, 102.59, 68.69, 51.19, 35.10, 31.47, 28.06, 25.39, 23.94, 22.70, 13.96.

HRMS (EI+) Calculated for $\text{C}_{22}\text{H}_{26}\text{N}_2\text{OF}_6$ $[\text{M}]^+$: 448.1949, Found: 448.1945.

$[\alpha]_{\text{D}}^{23} = 3.3$ ($c = 2.2$, DCM).

HPLC analysis (OD-H, 97:3 hexanes/IPA, 1.0 mL/min, 254 nm) indicated >99% ee: t_{R} (major) = 7.8 min, t_{R} (minor) = 9.2 min.



Compound 9 was synthesized according to the **General Procedure Condition I** with **S9** (301 mg, 1.00 mmol), 2-amino-6-methylpyridine (10.8 mg, 0.100 mmol, 1 equiv), and [(*R*)-TMS-SYNPHOSIr(COD)]NTf₂ (9.0 mg, 5.0 mol %). The reaction time was 36 h. The regioselectivity was determined by GC to be 10:1. Compound **9** was purified by preparative TLC (hexanes:ethyl acetate = 3:1) and obtained as a yellow oil in 62% yield.

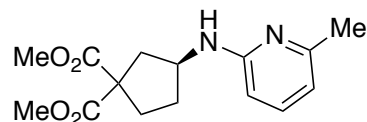
¹H NMR (600 MHz, CDCl₃) δ 7.32 (t, *J* = 7.8 Hz, 1H), 6.41 (d, *J* = 7.2 Hz, 1H), 6.17 (d, *J* = 8.4 Hz, 1H), 4.43 – 4.30 (m, 1H), 4.12 (hept, *J* = 6.8 Hz, 1H), 3.71 – 3.59 (m, 1H), 3.27 (t, *J* = 8.2 Hz, 2H), 2.35 (s, 3H), 1.84 – 1.71 (m, 2H), 1.64 – 1.52 (m, 2H), 1.49 – 1.41 (m, 2H), 1.40 – 1.28 (m, 4H), 1.23 (d, *J* = 6.8 Hz, 6H), 0.89 (t, *J* = 6.8 Hz, 3H).

¹³C NMR (151 MHz, CDCl₃) δ 158.13, 156.82, 138.00, 120.02 (q, *J* = 323.9 Hz), 111.81, 102.81, 52.03, 50.88, 44.42, 35.22, 32.35, 28.07, 27.90, 24.16, 22.81 (br), 22.70, 20.48 (br), 13.98.

HRMS (EI⁺) Calculated for C₁₈H₃₀F₃N₃O₂S [M]⁺: 409.2011, Found: 409.2013.

[α]_D²³ = 1.8 (c = 2.6, DCM).

HPLC analysis (OD-H, 97:3 hexanes/IPA, 1.0 mL/min, 254 nm) indicated >99% ee: t_R (major) = 8.1 min, t_R (minor) = 9.4 min.



Compound 10 was synthesized according to the **General Procedure Condition II** with **S10** (92.1 mg, 0.500 mmol), 2-amino-6-methylpyridine (10.8 mg, 0.100 mmol, 1 equiv), [Ir(coe)₂Cl]₂ (2.3 mg, 2.5 mol %), (*S*)-DTBM-SEGPHOS (8.8 mg, 7.5 mol %), and sodium tetrakis[3,5-bis(trifluoromethyl)phenyl]borate (5.3 mg, 6.0 mol %). The reaction time was 12 h. Compound **10** was purified by preparative TLC (hexanes:ethyl acetate = 2:1) and obtained as a yellow oil in 60% yield.

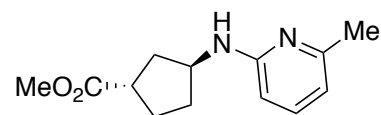
¹H NMR (600 MHz, CDCl₃) δ 7.36 (t, *J* = 7.8 Hz, 1H), 6.46 (d, *J* = 7.3 Hz, 1H), 6.23 (d, *J* = 8.3 Hz, 1H), 4.85 (s, 1H), 4.14 (sextet, *J* = 6.6 Hz, 1H), 3.77 (s, 3H), 3.75 (s, 3H), 2.73 (dd, *J* = 14.0, 7.1 Hz, 1H), 2.45 (ddd, *J* = 14.1, 8.1, 6.2 Hz, 1H), 2.38 (s, 3H), 2.28 (dt, *J* = 13.8, 7.6 Hz, 1H), 2.22 – 2.12 (m, 2H), 1.76 – 1.66 (m, 1H).

¹³C NMR (151 MHz, CDCl₃) δ 172.80, 172.64, 157.58, 156.72, 138.13, 112.30, 103.22, 58.98, 52.92, 52.85, 52.84, 40.99, 32.72, 32.37, 24.10.

HRMS (EI⁺) Calculated for C₁₅H₂₀N₂O₄ [M]⁺: 292.1423, Found: 292.1419.

[α]_D²³ = 4.9 (c = 0.70, DCM).

HPLC analysis (OD-H, 97:3 hexanes/IPA, 1.0 mL/min, 254 nm) indicated 92% ee: t_R (major) = 20.3 min, t_R (minor) = 23.4 min.



Compound 11 was synthesized according to the **General Procedure Condition II** with **S11** (63.1 mg, 0.500 mmol), 2-amino-6-methylpyridine (10.8 mg, 0.100 mmol, 1 equiv), $[\text{Ir}(\text{coe})_2\text{Cl}]_2$ (2.3 mg, 2.5 mol %), (*S*)-DTBM-SEGPHOS (8.8 mg, 7.5 mol %), and sodium tetrakis[3,5-bis(trifluoromethyl)phenyl]borate (5.3 mg, 6.0 mol %). The reaction time was 12 h. The diastereoselectivity was determined by GC to be 10:1. Compound **11** was purified by preparative TLC (hexanes:ethyl acetate = 2:1) and obtained as a yellow oil in 55% yield.

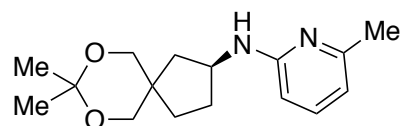
^1H NMR (600 MHz, CDCl_3) δ 7.34 (t, $J = 7.8$ Hz, 1H), 6.44 (d, $J = 7.3$ Hz, 1H), 6.20 (d, $J = 8.3$ Hz, 1H), 4.57 (br d, $J = 6.0$ Hz, 1H), 4.02 (sext, $J = 5.9$ Hz, 1H), 3.67 (s, 3H), 2.97 (quint, $J = 8.1$ Hz, 1H), 2.34 (s, 3H), 2.25 (dt, $J = 14.0, 7.2$ Hz, 1H), 2.22 – 2.14 (m, 1H), 2.09 (dtd, $J = 13.7, 8.3, 5.5$ Hz, 1H), 1.93 – 1.78 (m, 2H), 1.55 (dtd, $J = 13.2, 7.8, 5.6$ Hz, 1H).

^{13}C NMR (151 MHz, CDCl_3) δ 176.53, 157.85, 157.03, 138.04, 112.33, 102.49, 53.13, 51.77, 41.78, 36.75, 33.13, 27.95, 24.19.

HRMS (EI+) Calculated for $\text{C}_{13}\text{H}_{18}\text{N}_2\text{O}_2$ $[\text{M}]^+$: 234.1368, Found: 238.1368.

$[\alpha]_{\text{D}}^{23} = 7.6$ ($c = 0.66$, DCM).

HPLC analysis (OD-H, 97:3 hexanes/IPA, 1.0 mL/min, 254 nm) indicated 91% ee: t_{R} (major) = 19.0 min, t_{R} (minor) = 22.8 min.



Compound 12 was synthesized according to the **General Procedure Condition II** with **S12** (84.1 mg, 0.500 mmol), 2-amino-6-methylpyridine (10.8 mg, 0.100 mmol, 1 equiv), $[\text{Ir}(\text{coe})_2\text{Cl}]_2$ (2.3 mg, 2.5 mol %), (*S*)-DTBM-SEGPHOS (8.8 mg, 7.5 mol %), and sodium tetrakis[3,5-bis(trifluoromethyl)phenyl]borate (5.3 mg, 6.0 mol %). The reaction time was 12 h. Compound **12** was purified by preparative TLC (hexanes:ethyl acetate = 2:1) and obtained as a yellow oil in 58% yield.

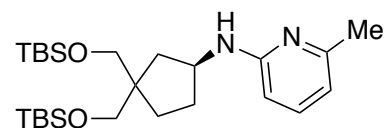
^1H NMR (500 MHz, CDCl_3) δ 7.33 (t, $J = 7.8$ Hz, 1H), 6.43 (d, $J = 7.3$ Hz, 1H), 6.18 (d, $J = 8.3$ Hz, 1H), 4.65 (br d, $J = 5.1$ Hz, 1H), 3.91 (sext, $J = 6.7$ Hz, 1H), 3.65 (s, 2H), 3.63 (d, $J = 11.4$ Hz, 1H), 3.59 (d, $J = 11.3$ Hz, 1H), 2.34 (s, 3H), 2.14 – 2.08 (m, 2H), 1.79 – 1.73 (m, 1H), 1.61 – 1.48 (m, 2H), 1.41 (s, 3H), 1.40 (s, 3H), 1.34 (dd, $J = 13.8, 6.9$ Hz, 1H).

^{13}C NMR (151 MHz, CDCl_3) δ 157.95, 156.94, 137.99, 112.22, 102.70, 97.74, 69.82, 69.38, 52.68, 40.75, 40.73, 32.23, 31.26, 24.18, 24.04, 23.52.

HRMS (EI+) Calculated for $\text{C}_{16}\text{H}_{24}\text{N}_2\text{O}_2$ $[\text{M}]^+$: 276.1838, Found: 276.1841.

$[\alpha]_{\text{D}}^{23} = -4.5$ ($c = 0.6$, DCM).

SFC analysis (OD-H, 20% IPA/ CO_2 , 10 MPa, 2.5 mL/min, 245 nm) indicated 90% ee: t_{R} (major) = 1.7 min, t_{R} (minor) = 2.4 min.



Compound 13 was synthesized according to the **General Procedure Condition II** with **S13** (178 mg, 0.500 mmol), 2-amino-6-methylpyridine (10.8 mg, 0.100 mmol, 1 equiv), $[\text{Ir}(\text{coe})_2\text{Cl}]_2$ (2.3 mg, 2.5 mol %), (*S*)-DTBM-SEGPHOS (8.8 mg, 7.5 mol %), and sodium tetrakis[3,5-bis(trifluoromethyl)phenyl]borate (5.3 mg, 6.0 mol %). The reaction time was 10 h. Compound **13**

was purified by preparative TLC (hexanes:ethyl acetate = 5:1) and obtained as a yellow oil in 64% yield.

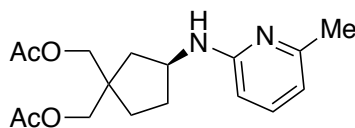
^1H NMR (700 MHz, CDCl_3) δ 7.34 (t, $J = 7.8$ Hz, 1H), 6.43 (d, $J = 7.3$ Hz, 1H), 6.21 (d, $J = 8.3$ Hz, 1H), 4.80 (d, $J = 7.2$ Hz, 1H), 3.93 (sext, $J = 7.0$ Hz, 1H), 3.49 (d, $J = 9.3$ Hz, 1H), 3.46 (d, $J = 9.3$ Hz, 1H), 3.45 (d, $J = 9.4$ Hz, 1H), 3.42 (d, $J = 9.3$ Hz, 1H), 2.37 (s, 3H), 2.08 – 2.02 (m, 1H), 2.01 – 1.97 (m, 1H), 1.65 (ddd, $J = 13.2, 7.7, 5.5$ Hz, 1H), 1.54 (dq, $J = 11.9, 7.5$ Hz, 1H), 1.48 (dt, $J = 12.9, 7.6$ Hz, 1H), 1.33 (dd, $J = 13.5, 7.0$ Hz, 1H), 0.93 (s, 9H), 0.92 (s, 9H), 0.07 (s, 6H), 0.07 (s, 3H), 0.07 (s, 3H).

^{13}C NMR (151 MHz, CDCl_3) δ 158.19, 156.88, 137.81, 111.70, 102.58, 67.23, 66.93, 53.34, 48.47, 38.78, 32.89, 29.06, 25.92, 25.87, 24.20, 18.31, 18.23, -5.49, -5.51, -5.51, -5.54.

HRMS (EI+) Calculated for $\text{C}_{25}\text{H}_{48}\text{N}_2\text{O}_2\text{Si}_2$ $[\text{M}]^+$: 464.3254, Found: 464.3256.

$[\alpha]_{\text{D}}^{23} = 3.2$ ($c = 2.6$, DCM).

HPLC analysis (OD-H, 99.9:0.1:0.1 hexanes/IPA/DEA, 1.0 mL/min, 254 nm) indicated 90% ee: t_{R} (major) = 9.0 min, t_{R} (minor) = 13.2 min.



Compound 14 was synthesized according to the **General Procedure Condition II** with **S14** (106 mg, 0.500 mmol), 2-amino-6-methylpyridine (10.8 mg, 0.100 mmol, 1 equiv), $[\text{Ir}(\text{coe})_2\text{Cl}]_2$ (2.3 mg, 2.5 mol %), (*S*)-DTBM-SEGPHOS (8.8 mg, 7.5 mol %), and sodium tetrakis[3,5-bis(trifluoromethyl)phenyl]borate (5.3 mg, 6.0 mol %). The reaction time was 12 h. **Compound 14** was purified by preparative TLC (hexanes:ethyl acetate = 2:1) and obtained as a yellow oil in 53% yield.

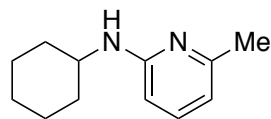
^1H NMR (600 MHz, CDCl_3) δ 7.35 (t, $J = 7.8$ Hz, 1H), 6.46 (d, $J = 7.3$ Hz, 1H), 6.19 (d, $J = 8.3$ Hz, 1H), 4.81 (br d, $J = 6.8$ Hz, 1H), 4.07 – 3.98 (m, 5H), 2.36 (s, 3H), 2.18 – 2.13 (m, 1H), 2.12 – 2.07 (m, 1H), 2.09 (s, 3H), 2.09 (s, 3H), 1.79 – 1.72 (m, 1H), 1.66 – 1.56 (m, 2H), 1.43 (dd, $J = 13.9, 7.0$ Hz, 1H).

^{13}C NMR (151 MHz, CDCl_3) δ 171.13, 171.07, 157.82, 156.91, 138.10, 112.28, 102.88, 67.97, 67.57, 52.92, 44.52, 39.48, 32.47, 30.12, 24.12, 20.89, 20.89.

HRMS (EI+) Calculated for $\text{C}_{17}\text{H}_{24}\text{N}_2\text{O}_4$ $[\text{M}]^+$: 320.1736, Found: 320.1739.

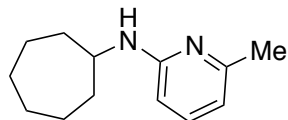
$[\alpha]_{\text{D}}^{23} = -0.7$ ($c = 1.0$, DCM).

HPLC analysis (OD-H, 85:15 hexanes/IPA, 1.0 mL/min, 254 nm) indicated 91% ee: t_{R} (major) = 23.9 min, t_{R} (minor) = 11.9 min.



Compound 15 was synthesized according to the **General Procedure Condition II** with **S15** (51 μL , 0.50 mmol), 2-amino-6-methylpyridine (10.8 mg, 0.100 mmol, 1 equiv), $[\text{Ir}(\text{coe})_2\text{Cl}]_2$ (2.3 mg, 2.5 mol %), (*S*)-DTBM-SEGPHOS (8.8 mg, 7.5 mol %), and sodium tetrakis[3,5-bis(trifluoromethyl)phenyl]borate (5.3 mg, 6.0 mol %). The reaction time was 24 h. **Compound 15** was purified by preparative TLC (hexanes:ethyl acetate = 6:1) and obtained as a yellow oil in 81% yield.

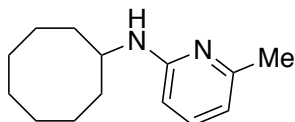
^1H NMR (600 MHz, CDCl_3) δ 7.33 (dd, $J = 8.3, 7.3$ Hz, 1H), 6.41 (d, $J = 7.2$ Hz, 1H), 6.20 (d, $J = 8.3$ Hz, 1H), 4.64 (br s, 1H), 3.44 – 3.35 (m, 1H), 2.36 (s, 3H), 2.07 – 2.00 (m, 2H), 1.80 – 1.74 (m, 2H), 1.65 (dt, $J = 13.0, 4.1$ Hz, 1H), 1.45 – 1.33 (m, 2H), 1.32 – 1.17 (m, 3H).
 ^{13}C NMR (151 MHz, CDCl_3) δ 157.69, 156.91, 138.00, 111.71, 102.54, 50.47, 33.24, 25.78, 24.84, 24.17.



Compound 16 was synthesized according to the **General Procedure Condition II** with **S16** (58 μL , 0.50 mmol), 2-amino-6-methylpyridine (10.8 mg, 0.100 mmol, 1 equiv), $[\text{Ir}(\text{coe})_2\text{Cl}]_2$ (2.3 mg, 2.5 mol %), (*S*)-DTBM-SEGPHOS (8.8 mg, 7.5 mol %), and sodium tetrakis[3,5-bis(trifluoromethyl)phenyl]borate (5.3 mg, 6.0 mol %). The reaction time was 12 h. Compound **16** was purified by preparative TLC (hexanes:ethyl acetate = 6:1) and obtained as a yellow oil in 91% yield.

^1H NMR (600 MHz, CDCl_3) δ 7.35 (t, $J = 7.8$ Hz, 1H), 6.42 (d, $J = 7.3$ Hz, 1H), 6.15 (d, $J = 8.3$ Hz, 1H), 4.76 (s, 1H), 3.62 – 3.55 (m, 1H), 2.37 (s, 3H), 2.04 – 1.97 (m, 2H), 1.75 – 1.46 (m, 10H).
 ^{13}C NMR (151 MHz, CDCl_3) δ 157.51, 156.82, 138.12, 111.68, 102.64, 52.62, 34.89, 28.30, 24.21, 24.10.

HRMS (EI+) Calculated for $\text{C}_{13}\text{H}_{20}\text{N}_4$ $[\text{M}]^+$: 204.1626, Found: 204.1628.



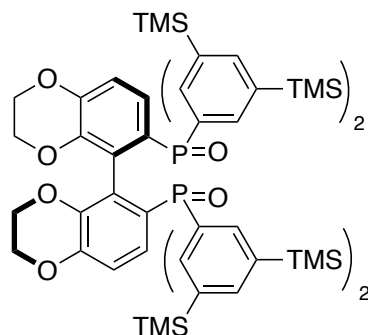
Compound 17 was synthesized according to the **General Procedure Condition II** with **S17** (65 μL , 0.50 mmol), 2-amino-6-methylpyridine (10.8 mg, 0.100 mmol, 1 equiv), $[\text{Ir}(\text{coe})_2\text{Cl}]_2$ (2.3 mg, 2.5 mol %), (*S*)-DTBM-SEGPHOS (8.8 mg, 7.5 mol %), and sodium tetrakis[3,5-bis(trifluoromethyl)phenyl]borate (5.3 mg, 6.0 mol %). The reaction time was 24 h. Compound **17** was purified by preparative TLC (hexanes:ethyl acetate = 6:1) and obtained as a yellow oil in 82% yield.

^1H NMR (600 MHz, CDCl_3) δ 7.34 (t, $J = 7.8$ Hz, 1H), 6.41 (d, $J = 7.3$ Hz, 1H), 6.15 (d, $J = 8.3$ Hz, 1H), 4.69 (s, 1H), 3.66 – 3.59 (m, 1H), 2.36 (s, 3H), 1.94 – 1.88 (m, 2H), 1.78 – 1.71 (m, 2H), 1.68 – 1.60 (m, 5H), 1.59 – 1.52 (m, 5H).

^{13}C NMR (151 MHz, CDCl_3) δ 157.56, 156.96, 138.01, 111.64, 102.59, 51.51, 32.34, 27.23, 25.77, 24.18, 23.86.

HRMS (EI+) Calculated for $\text{C}_{14}\text{H}_{22}\text{N}_2$ $[\text{M}]^+$: 218.1783, Found: 218.1786.

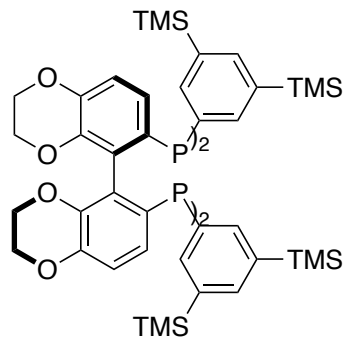
6.4.5 Synthesis of Ligands and Catalysts

**(R)-TMS-SYNPHOS oxide**

A 20 mL vial was charged with magnesium turnings (144 mg, 12 equiv) and THF (2 mL). 3,5-Bis(trimethylsilyl)bromobenzene (1.66 g, 11 equiv) was added in one portion. The vial was allowed to stir at ambient temperature for 1 h and placed in a heating block set to 65 °C. After 2 h at this temperature, the vial was cooled to rt, and the solution was taken up into a syringe. In a 25 mL round-bottom flask, (*R*)-(2,2',3,3'-tetrahydro-[5,5'-bibenzo[*b*][1,4]dioxine]-6,6'-diyl)bisphosphonic dichloride (252 mg, 0.500 mmol), synthesized by a known procedure, was dissolved in 1 mL THF. The flask was cooled to 0 °C and the Grignard solution was added dropwise over the course of 20 minutes. The resulting brown solution was allowed to warm to rt and stir overnight. The reaction was quenched with water, and the organic material was extracted with EtOAc. The organic phase was combined and dried over Na₂SO₄. The crude material was purified by flash chromatography with 65% EtOAc in hexanes as eluent. The title compound was isolated as a pale solid (411 mg, 66% yield).

¹H NMR (600 MHz, CDCl₃) δ 7.82 (d, *J* = 11.5, 4H), 7.77 (d, *J* = 11.2, 4H), 7.71 (s, 2H), 7.67 (s, 2H), 6.74 (dd, *J* = 8.1, 2.6 Hz, 2H), 6.67 (dd, *J* = 12.9, 8.4 Hz, 2H), 3.98 (ddd, *J* = 10.0, 7.1, 2.4 Hz, 2H), 3.72 (ddd, *J* = 11.5, 5.2, 2.3 Hz, 2H), 3.50 (ddd, *J* = 11.7, 5.3, 2.5 Hz, 2H), 3.10 (ddd, *J* = 11.9, 7.0, 2.3 Hz, 2H), 0.22 (s, 36H), 0.13 (s, 36H).

³¹P NMR (243 MHz, CDCl₃) δ 29.3.

**(R)-TMS-SYNPHOS**

A 20 mL screw-capped vial was charged with (*R*)-TMS-SYNPHOS oxide (382 mg, 0.306 mmol). Mesitylene (2 mL) and Bu₃N (1.09 mL, 15 equiv) were added to the vial. Trichlorosilane (371 μL, 12 equiv) in mesitylene (1 mL) was then added dropwise to the solution. Once the evolution of gas ceased, the vial was sealed with a Teflon-lined cap and placed in a 120 °C heating block. After 22 h, the vial was removed from the heating block and placed in an ice bath. Under a

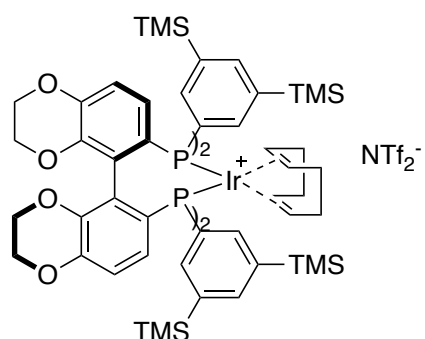
stream of nitrogen and vigorous stirring, an aqueous solution of NaOH (25%, 2 ml) was added to the vial dropwise. The vial was sealed and placed in an 80 °C heating block. After 1 hour, a biphasic mixture had formed. The organic material was extracted with EtOAc. The organic solution was washed with a 2 M solution of HCl and dried over Na₂SO₄. The crude material was purified by flash chromatography with 10% EtOAc in hexanes as eluent to yield the title compound as a white solid, which was stored under nitrogen (303 mg, 81% yield).

¹H NMR (600 MHz, CDCl₃) δ 7.54 (s, 2H), 7.46 (s, 6H), 7.36 (s, 4H), 6.78 (d, *J* = 8.4 Hz, 2H), 6.66 (d, *J* = 8.3 Hz, 2H), 4.03 (ddd, *J* = 11.4, 6.7, 2.3 Hz, 2H), 3.77 – 3.70 (m, 2H), 3.66 (ddd, *J* = 11.6, 5.3, 2.2 Hz, 2H), 3.20 – 3.02 (m, 2H), 0.19 (s, 36H), 0.08 (s, 36H).

³¹P NMR (243 MHz, CDCl₃) δ -15.2.

HRMS (ESI+) Calculated for C₆₄H₉₇O₄P₂Si₈ [M+H]⁺: 1215.5011, Found: 1215.5005.

[α]_D²³ = 22.7 (c = 0.295, DCM).



[(*R*)-TMS-SYNPHOSIr(COD)]NTf₂

A 20 mL screw-capped vial was charged with [Ir(COD)Cl]₂ (33.6 mg, 0.0500 mmol), silver triflimide (38.8 mg, 0.100 mmol), and 2 mL of dichloromethane. The reaction was allowed to stir for 30 minutes. A solution of (*R*)-TMS-SYNPHOS (122 mg, 0.100 mmol) in 2 mL of acetone was then added. The reaction was allowed to stir for an additional 30 minutes before being filtered through Celite. The filtrate was concentrated *in vacuo*, and the resulting solids were washed with pentane three times to yield the title compound as a green solid (165 mg, 92% yield).

¹H NMR (600 MHz, Toluene-*d*₈) δ 8.46 – 8.09 (br m, 2H), 7.91 (d, *J* = 6.3 Hz, 4H), 7.78 – 7.42 (br m, 2H), 7.62 (br s, 4H), 7.53 (t, *J* = 9.4 Hz, 2H), 6.57 (d, *J* = 8.8 Hz, 2H), 4.53 (t, *J* = 6.7 Hz, 2H), 4.06 – 3.99 (m, 4H), 3.92 (t, *J* = 10.2 Hz, 2H), 3.76 – 3.70 (m, 2H), 3.61 (q, *J* = 8.0 Hz, 2H), 2.41 (dtd, *J* = 15.7, 9.9, 5.5 Hz, 2H), 2.28 – 2.18 (m, 2H), 1.56 (dt, *J* = 13.9, 9.1 Hz, 2H), 1.32 – 1.24 (m, 2H), 0.46 – 0.19 (m, 36H), 0.27 (s, 36H).

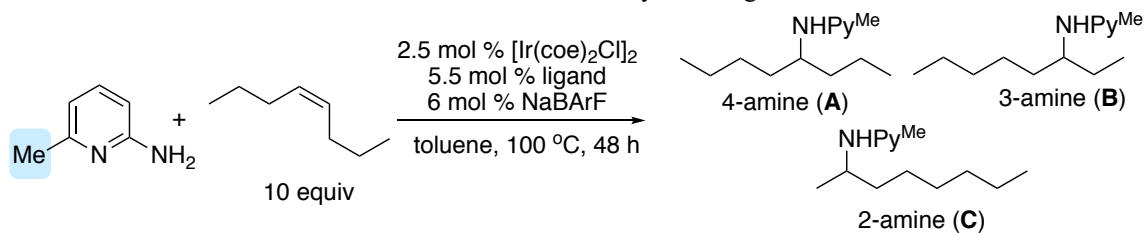
³¹P NMR (243 MHz, Toluene-*d*₈) δ 14.6.

¹⁹F NMR (576 MHz, Toluene-*d*₈) δ -78.6.

6.4.6. Summary of the Effect of Reaction Parameters

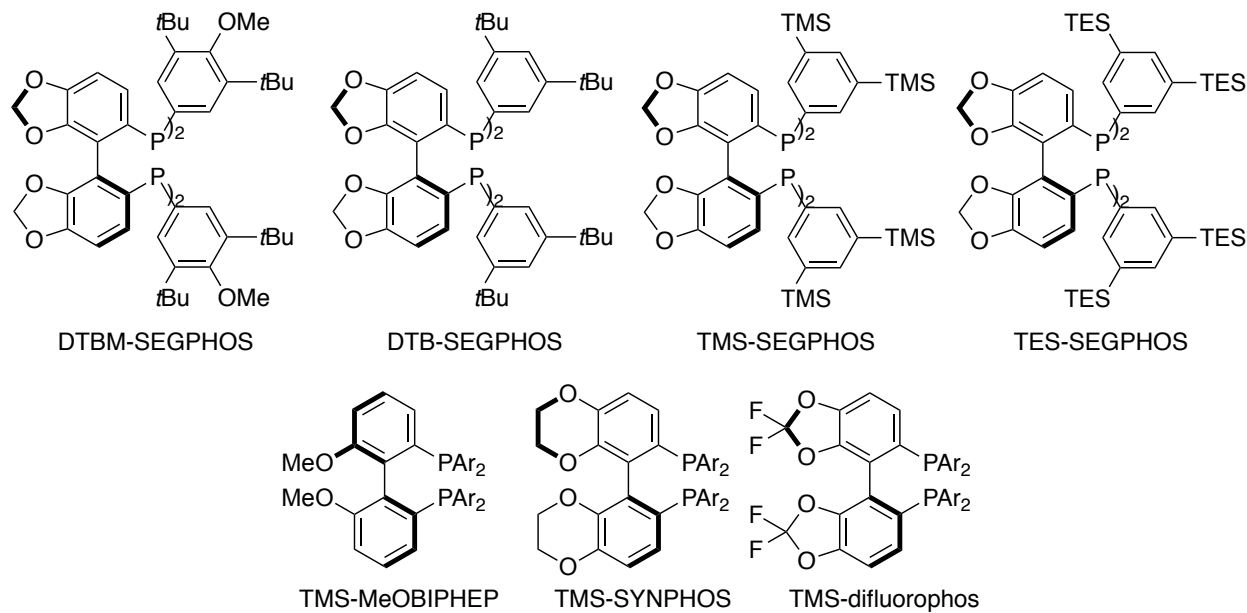
To improve the yield and the selectivity towards formation of 4-amine (**A**), we performed two rounds of studies. We examined a series of SEGPHOS ligands containing a range of different substituents on the P-aryl rings of the ligand. We found that catalysts formed from ligands lacking methoxy groups are more active than that formed from DTBM-SEGPHOS (Table 6.1, entries 1 and 2). The catalyst formed from TMS-SEGPHOS which has trimethylsilyl groups at the 3,5-position of the P-aryl rings of the ligand led to much higher 4-selectivity than the one formed from

Table 6.1 Effect of the identity of the ligands



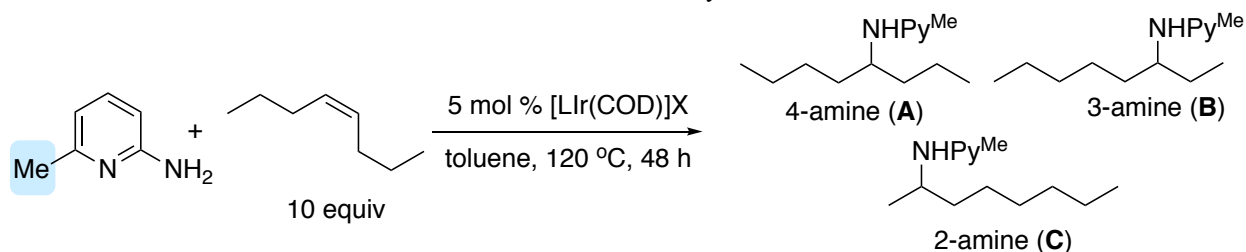
entry	ligand	4-selectivity ^a	yield (A+B+C)
1	(<i>S</i>)-DTBM-SEGPHOS	48%	16%
2	DTB-SEGPHOS	50%	42%
3	TMS-SEGPHOS	83%	34%
4	TES-SEGPHOS	n/a	2%
5	TMS-MeOBIPHEP	83%	22%
6	(<i>R</i>)-TMS-SYNPHOS	83%	26%
7	TMS-DIFLUOROPHOS	94%	13%

^adefined as percentage of **A**/(**A**+**B**+**C**)



Ar = 3,5-TMS-C₆H₃

Table 6.2 Effect of the identity of the anions



entry	ligand	anion	4-selectivity ^a	yield (A+B+C)
1	(S)-DTBM-SEGPHOS	OTf	83%	9%
2	(S)-DTBM-SEGPHOS	NTf ₂	63%	60%
3	(S)-DTBM-SEGPHOS	BF ₄	67%	9%
4	TMS-SEGPHOS	NTf ₂	88%	81%
5 ^b	TMS-SEGPHOS	NTf ₂	89%	85%
6 ^{b,c}	TMS-SEGPHOS	NTf ₂	73%	95%
7 ^{b,c,d}	TMS-SEGPHOS	NTf ₂	81%	74%
8 ^{c,d,e}	TMS-SEGPHOS	NTf ₂	71%	92%
9 ^b	(R)-TMS-SYNPHOS	NTf ₂	89%	78% (97% ee)

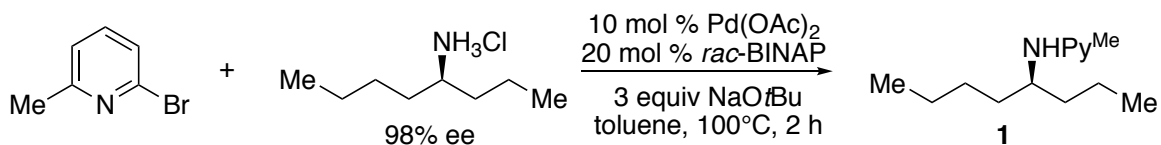
^adefined as percentage of A/(A+B+C); ^bsolvent was 2-MeTHF; ^c5 equiv olefin; ^d110 °C; ^esolvent was 1,4-dioxane.

DTB-SEGPHOS (entries 2 and 3). However, TES-SEGPHOS, which has bulky triethylsilyl groups at the same 3,5-position formed an inactive catalyst (entry 4). We surveyed a series of ligands containing 3,5-bis(trimethylsilyl)phenyl groups, and found that the catalyst formed from TMS-SEGPHOS is the most active among all examined.

We then studied the effect of anions on the yield and the selectivity towards formation of 4-amine (A) (Table 6.2). With anions other than BARF, COD complexes of iridium were used as the source of iridium. We found that the triflimide complexes (entries 2, 4) are particularly active towards the hydroamination and also lead to high selectivity towards formation of 4-amine (A). The yield and the selectivity were both slightly higher for reactions conducted in 2-MeTHF than in toluene (entry 5). Reducing the olefin amount from 10 equivalents to 5 equivalents led to a decrease in the selectivity (entry 6). A lower yield and lower 4-selectivity were observed when reducing the reaction temperature (entry 7). Switching the solvent from 2-MeTHF to dioxane led to an increase in yield but a decrease in 4-selectivity (entry 8). Finally, the reaction catalyzed by [(R)-TMS-SYNPHOSIr(COD)]NTf₂ in 2-MeTHF at 120 °C afforded the hydroamination products in 78% yield and 89% 4-selectivity. The ee of the major enantiomer was determined to be 97% ee.

6.4.7 Assignment of Absolute Stereochemistry

The absolute configuration of compound **1** was unambiguously determined to be *S* at the nitrogen-bound stereocenter by comparison of the chiral GC traces of the standard sample (*S*)-**1** prepared by the following procedure. The absolute configurations of all other hydroamination products were assigned by analogy.

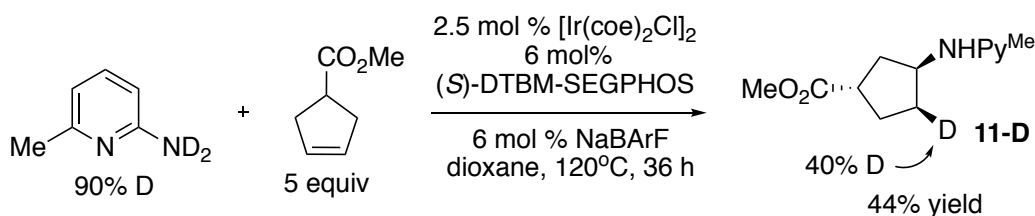


Experimental procedure for the palladium-catalyzed amination of 2-bromopyridine

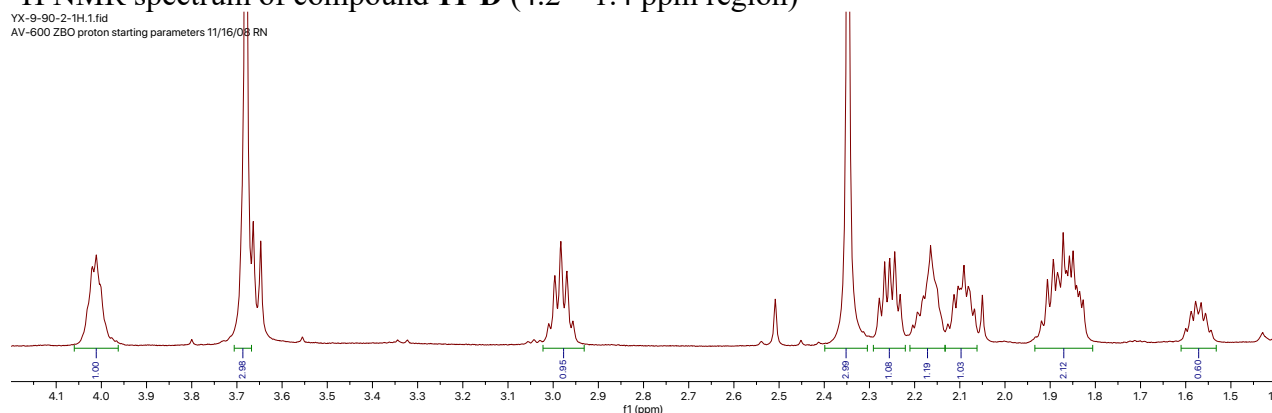
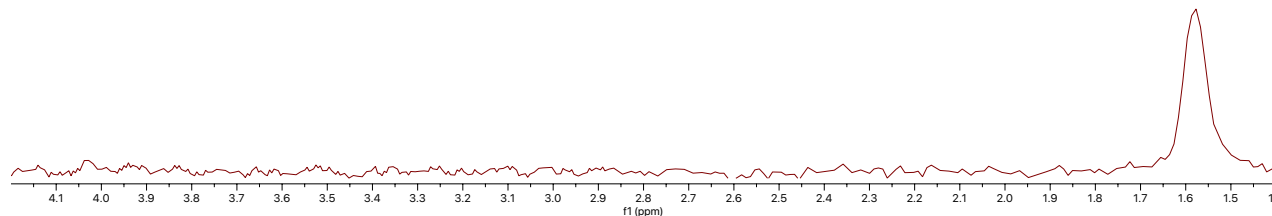
In a nitrogen-filled dry box, a 1-dram vial was charged with Pd(OAc)₂ (22.5 mg, 10 mol %), *rac*-BINAP (124.5 mg, 20 mol %), NaOtBu (288 mg, 3 equiv), (*S*)-4-amino-octane hydrochloride (166 mg, 1 equiv, 1.00 mmol), and 3 mL of toluene. 2-Bromo-6-methylpyridine (114 μL, 1 equiv, 1.00 mmol) was added, and the vial was capped, taped, and removed from the dry box. The reaction was allowed to stir at 100 °C for 2 hours, before being diluted with ethyl acetate. The material was filtered with celite and concentrated *in vacuo*. The crude material was purified by preparative TLC (hexanes:ethyl acetate = 5:1). Compound (*S*)-**1** was obtained as a yellow oil in 77% yield. The ee was 96%.

6.4.8 Preliminary Mechanistic Study

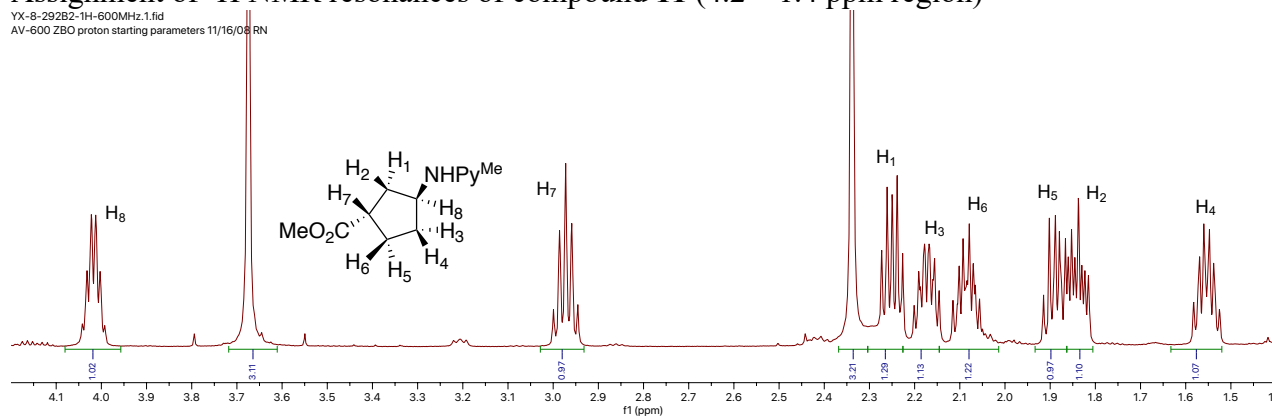
Deuterium-Labeling Experiment

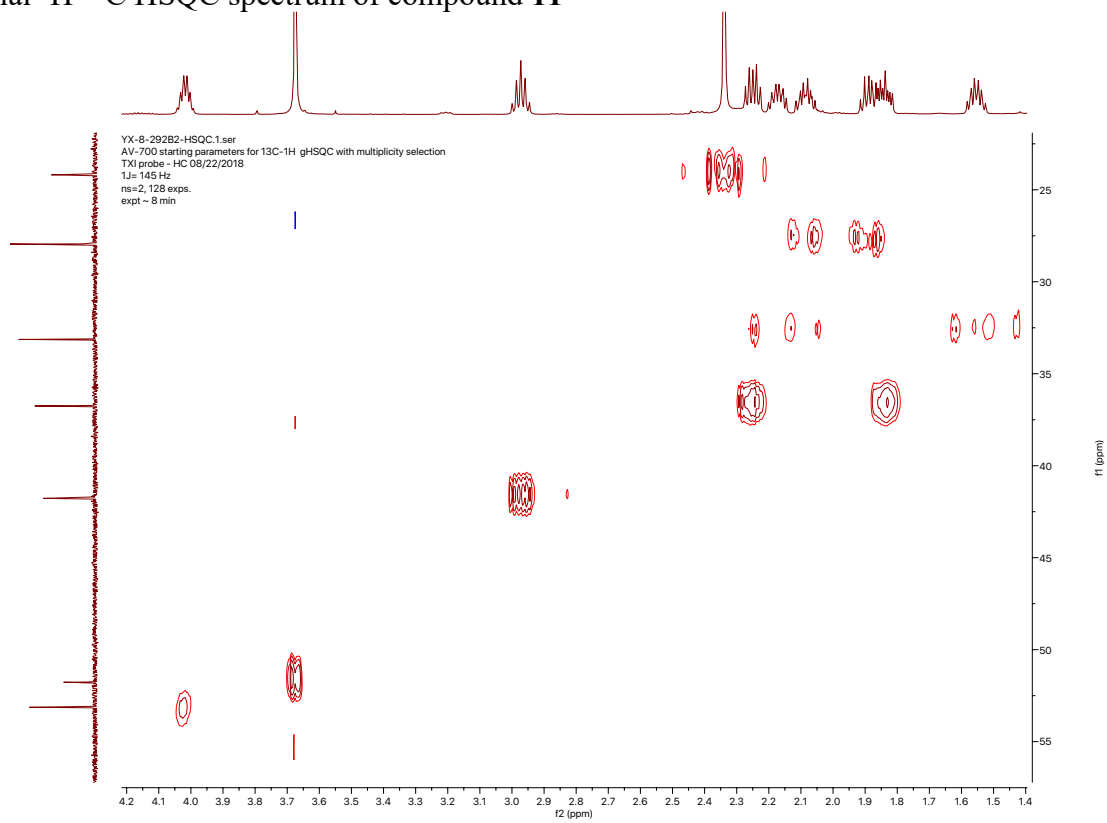


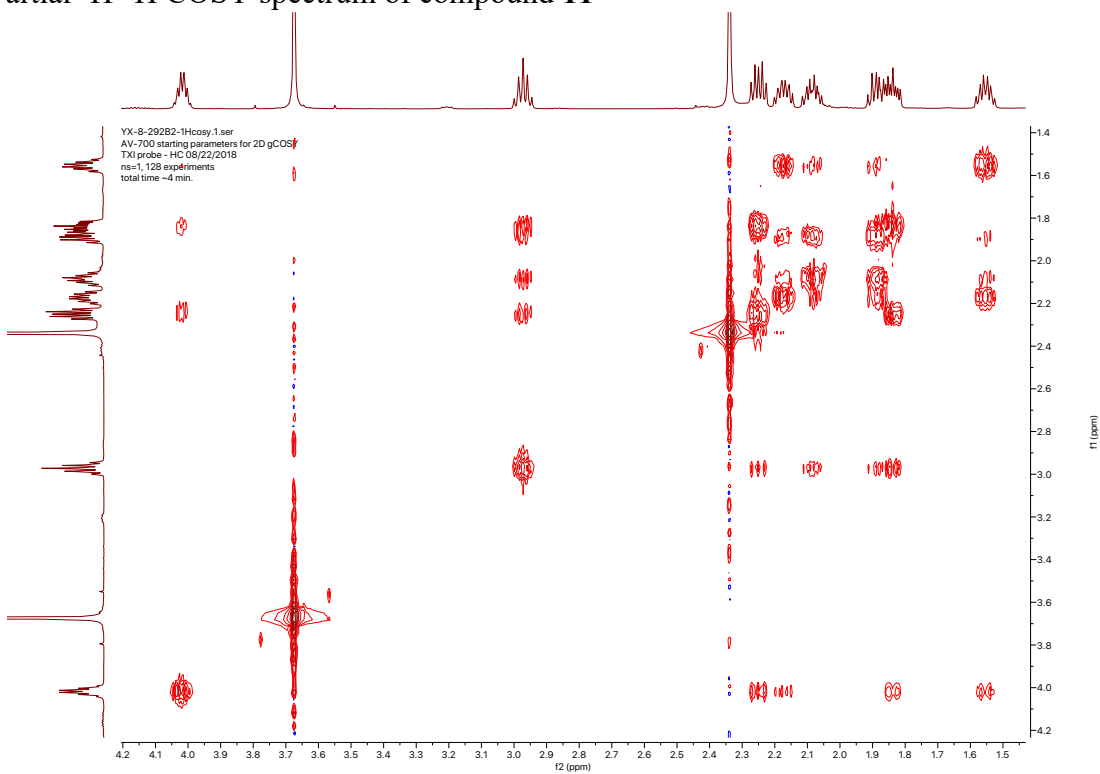
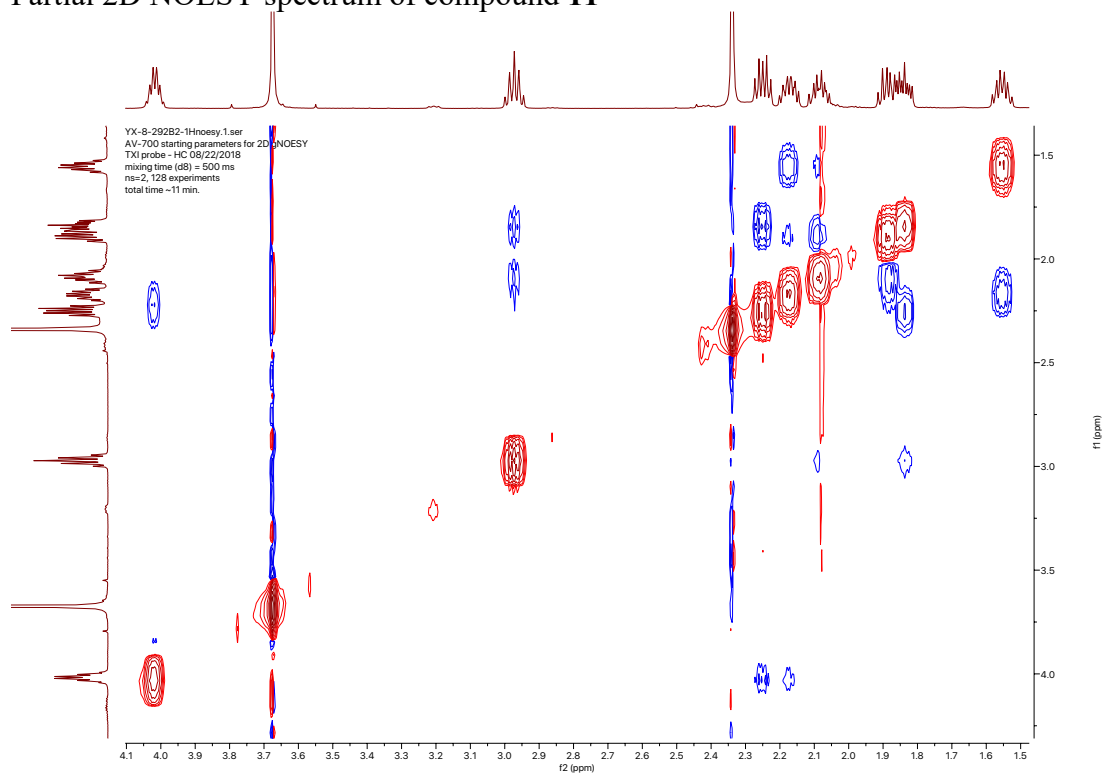
In a nitrogen-filled dry box, a 1-dram vial was charged with [Ir(coe)₂Cl]₂ (2.3 mg, 2.5 mol %), (*S*)-DTBM-SEGPHOS (8.8 mg, 7.5 mol %), sodium tetrakis[3,5-bis(trifluoromethyl)phenyl]borate (5.3 mg, 6.0 mol %), 2-amino-6-methylpyridine-d₂ (11.0 mg, 0.100 mmol, 1 equiv), **S11** (63.1 mg, 0.500 mmol), and dioxane (100 μL). 10.0 μL of dodecane was added, and the vial was capped, sealed with electrical tape, and removed from the box. The reaction was heated to 120 °C in an aluminum heating block. After 36 h, the reaction vial was diluted with 1 mL of ethyl acetate after the reaction reached around 90% conversion (Note: prolonged reaction time will result in racemization of products). The crude material was concentrated *in vacuo* and purified by preparative TLC. Compound **11-D** was purified by preparative TLC (hexanes:ethyl acetate = 2:1) and obtained as a yellow oil in 44% yield. ¹H NMR analysis showed a deuteration level of 40%. Assignment of ¹H NMR resonances of **11** is shown in the following section.

^1H NMR spectrum of compound **11-D (4.2 – 1.4 ppm region)**YX-9-90-2-1H.1.fid
AV-600 ZBO proton starting parameters 11/16/08 RN **^2H NMR spectrum of compound **11-D** (4.2 – 1.4 ppm region)**YX-9-90-2-2H.1.fid
AV-600 ZBO 2H, using lock coil, starting parameters 11/31/08 RN
No ^1H decoupling.**Proton NMR Assignment of Compound **11****

All proton NMR resonances of compound **11** were unambiguously assigned based on the COSY, HSQC, and NOESY spectra.

Assignment of ^1H NMR resonances of compound **11 (4.2 – 1.4 ppm region)**YX-8-292B2-1H-600MHz.1.fid
AV-600 ZBO proton starting parameters 11/16/08 RN

Partial ^1H - ^{13}C HSQC spectrum of compound **11**

Partial ^1H - ^1H COSY spectrum of compound **11**Partial 2D NOESY spectrum of compound **11**

6.4.9 Kinetic Experiments

Representative procedure for kinetic studies on the hydroamination of internal alkene S1

In a nitrogen-filled glove box, a 4 mL vial was charged with [(*R*)-TMS-SYNPHOSIr(COD)]NTf₂ (18.0 mg, 0.0100 mmol), 2-amino-6-methylpyridine (27.0 mg, 0.250 mmol), and 125 μ L of 2-MeTHF. The vial was capped, taken out of the glovebox, and heated at 120 °C for 15 minutes before being cooled to rt and brought back into the glovebox. In a separate 4 mL vial, S1 (230 μ L, 1.48 mmol), 25.0 μ L of the above stock solution, 2-amino-6-methylpyridine (25.0 μ L, 0.0500 mmol, 2.00 M in 2-MeTHF), and dodecane (10.0 μ L, 0.0440 mmol) were added. The vial was capped, sealed with electrical tape, and heated at 120 °C. At various time points, aliquots were removed from the mixture and analyzed by gas chromatography. Reaction rates were determined by measuring product formation at low conversion because the GC peak for the product was more accurate than that for the amine reactant due to tailing. The initial rates of formation of **1** for reactions conducted with various concentrations of S1, 2-amino-6-methylpyridine, and [(*R*)-TMS-SYNPHOSIr(COD)]NTf₂ are tabulated in Table 6.3.

Table 6.3 Initial rates for hydroamination of S1

entry	[amine]/M	[S1]/M	[Ir]/M	initial rate (M/s)
1	0.278	4.10	0.00278	3.21x10 ⁻⁷
2	0.278	4.10	0.00556	9.62x10 ⁻⁷
3	0.278	4.10	0.00833	1.72x10 ⁻⁶
4	0.278	4.10	0.0111	2.49x10 ⁻⁶
5	0.294	4.34	0.00588	1.11x10 ⁻⁶
6	0.147	4.34	0.00588	2.02x10 ⁻⁶
7	0.441	4.34	0.00588	7.69x10 ⁻⁷
8	0.588	4.34	0.00588	6.24x10 ⁻⁷
9	0.262	2.62	0.00314	2.83x10 ⁻⁷
10	0.262	1.97	0.00314	2.31x10 ⁻⁷
11	0.262	3.93	0.00314	3.42x10 ⁻⁷
12	0.262	5.24	0.00314	4.07x10 ⁻⁷

6.4.10 DFT Calculations

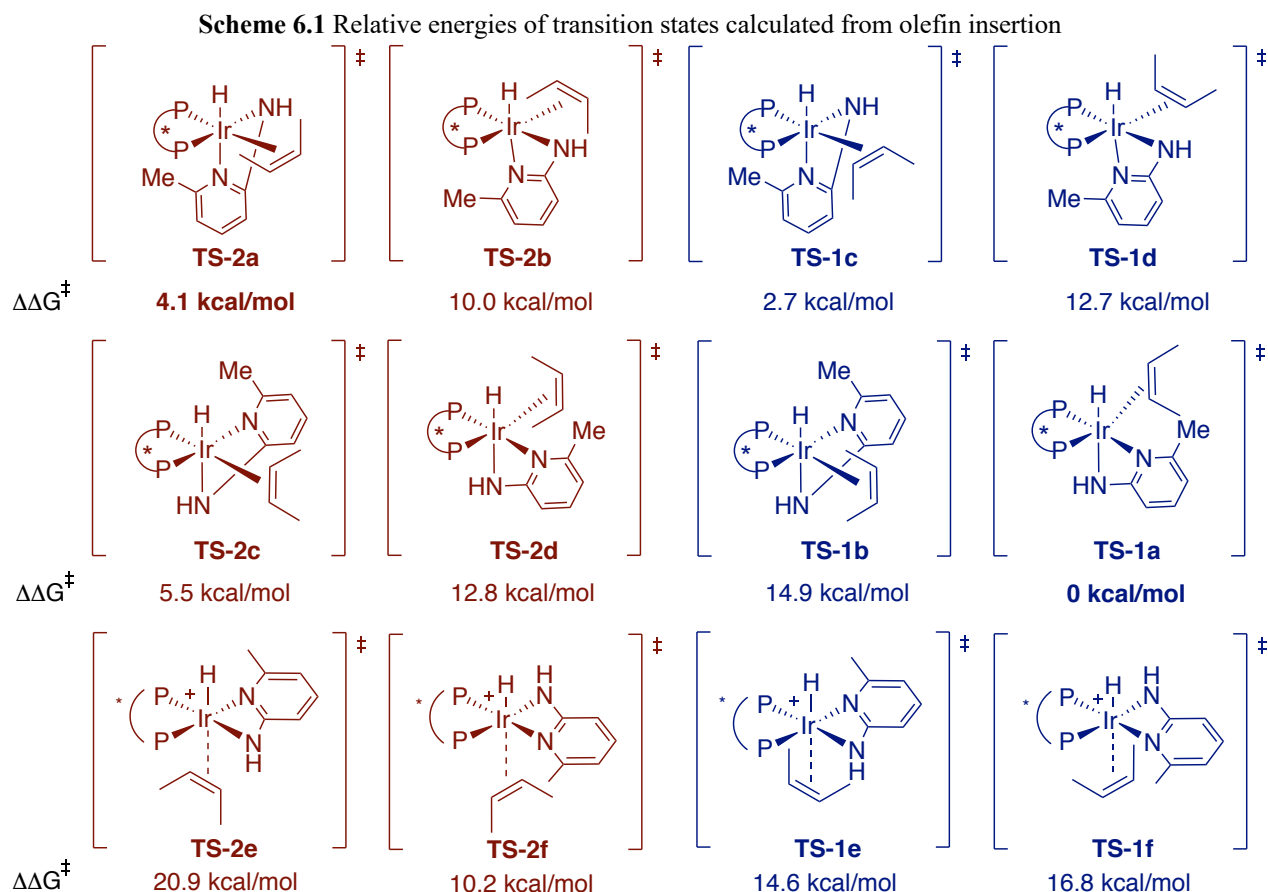
General remarks

Geometry optimizations and single-point energy calculations were conducted using Gaussian 09 revision D01 package. Geometries of all intermediates and transition states were optimized with the B3LYP functional with a mixed basis set of SDD for Ir and 6-31G(d) for all other atoms in the gas phase. Vibrational frequency calculations were performed for all the stationary points to confirm if the optimized structures are a local minimum or a transition state. A thermal correction to enthalpies and Gibbs free energies was applied at 393 K with the freqchk utility in Gaussian 09.

Solvation energy corrections were calculated in 1,4-dioxane with the SMD continuum solvation model. Solvation single-point energies were calculated with the M06 functional with a mixed basis set of SDD for Ir and 6-311+G(d,p) for other atoms. The structures were generated using CYL-View v1.0.

Evaluation of transition states of olefin insertion

We calculated 12 possible transition states for the olefin insertion step. (*S*)-TMS-SEGPHOS was used as the ligand and *cis*-2-butene was used as the model alkene. We calculated only the structures of the corresponding amidohydroiridium transition states as a naked cation, and did not take consideration of the effect of the anion.

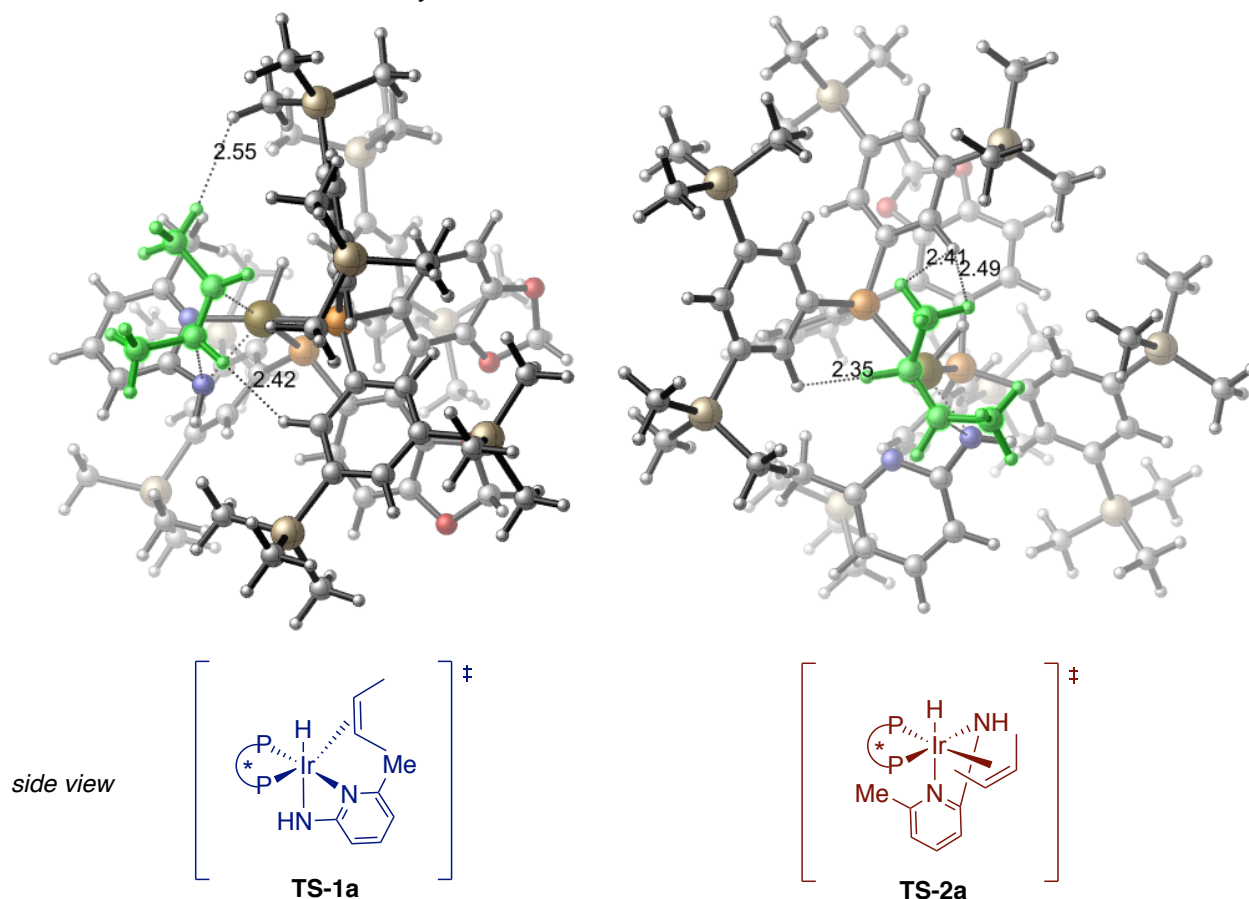


Transition states labeled in blue would lead to the formation of (*R*)-product after stereoretentive C-H reductive elimination and transition states labeled in red would lead to the formation of (*S*)-product. These energies are consistent with the outcome if (*S*)-TMS-SEGPHOS were used as the ligand in the reaction. The lowest-energy transition state would lead to the (*R*) product, and the catalytic reaction with (*R*)-TMS-SYNPHOS as ligand led to the formation of (*S*)-**1** experimentally.

There are three major types of structures in Scheme 6.1. The first four structures contain a pyridine ligand trans to the hydride, the second four contain an amido ligand trans to the hydride, and the last four contain an alkene ligand trans to the hydride. The isomers containing an alkene ligand trans to the hydride are in general higher in energy than the other two types of structures.

These relative energies are likely obtained because the axial position *trans* to the hydride is sterically the most crowded. Selected structures of transition states that contain a 5-coordinate iridium center without coordination of the pyridine instead of the 6-coordinate ones in Scheme 6.1 were also examined and are significantly higher in energy than those having a 6-coordinate iridium center.

Scheme 6.2 Analysis of steric effects of transition states **TS-1a** and **TS-2a**



As discussed in the main text, the different orientation of the ancillary ligands in **TS-1a** and **TS-1c** leads to a different olefin binding geometry. As depicted in Scheme 6.2, the olefin fragment in **TS-1c** is closer to the ligand than that in **TS-1a** is. The methyl group attached to the inner carbon of the olefin in **TS-1c** is directed towards one of the ligand sidearms. This steric interaction would be much more severe using olefins that have long alkyl chains, such as **S1**, than that is in **TS-1c**.

Evaluation of computational methods

The relative energies of the transition states of olefin insertion were evaluated using a few different levels of theory. We examined the optimized structure of **TS-1a** and **TS-2a** with three different levels of theory. Single point energy calculations using the M06, ω B97XD, PBE0, and PBE0D3BJ functionals were performed. The energy difference between **TS-1a** and **TS-2a** was calculated to be 3-4 kcal/mol with each of the functionals.

Table 6.4 Evaluation of computational methods

entry	method	$\Delta G(\text{TS2a}-\text{TS1a})$
1	M06/6-311+G(d,p)-SDD/SMD// B3LYP/6-31G(d)-SDD	4.1 kcal/mol
2	PBE0/6-311+G(d,p)-SDD/SMD// B3LYP/6-31G(d)-SDD	4.2 kcal/mol
3	ω B97XD/6-311+G(d,p)-SDD/SMD// B3LYP/6-31G(d)-SDD	3.8 kcal/mol
4	M06/6-311+G(d,p)-SDD/SMD// B3LYP-D3/6-31G(d)-LANL2DZ	3.6 kcal/mol
5	PBE0-D3BJ/6-311+G(d,p)- LANL2DZ /SMD// PBE0-D3BJ/6-31G(d)-LANL2DZ	3.2 kcal/mol

Summary of electronic energies of all computed structures

Electronic energies, enthalpies, free energies, and imaginary frequencies of all computed structures are tabulated in Table 6.5.

Table 6.5 Summary of computational data of all calculated structures^a

	B3LYP SCF energy	B3LYP enthalpy	B3LYP free energy	M06 SCF energy	M06 enthalpy	M06 free energy	imaginary frequency
TS-1a	-6322.267003	-6320.514002	-6320.9812	-6320.6875	-6318.9344	-6319.4016	-311.52
TS-1b	-6322.245769	-6320.492292	-6320.9557	-6320.6679	-6318.9145	-6319.3779	-362.16
TS-1c	-6322.261667	-6320.508402	-6320.9784	-6320.6806	-6318.9273	-6319.3973	-298.39
TS-1d	-6322.251365	-6320.497694	-6320.9593	-6320.6735	-6318.9198	-6319.3814	-334.13
TS-1e	-6322.249355	-6320.496064	-6320.9615	-6320.6662	-6318.9129	-6319.3783	-407.41
TS-1f	-6322.245042	-6320.491116	-6320.9576	-6320.6623	-6318.9084	-6319.3748	-396.86
TS-2a	-6322.264653	-6320.511023	-6320.9757	-6320.684	-6318.9304	-6319.3951	-303.43
TS-2b	-6322.258853	-6320.505499	-6320.9679	-6320.6767	-6318.9234	-6319.3857	-292.35
TS-2c	-6322.261231	-6320.507812	-6320.9724	-6320.6817	-6318.9283	-6319.3928	-321.28
TS-2d	-6322.246984	-6320.493394	-6320.9569	-6320.6713	-6318.9177	-6319.3812	-352.25
TS-2e	-6322.241346	-6320.487976	-6320.9513	-6320.6584	-6318.905	-6319.3684	-417.76
TS-2f	-6322.254104	-6320.501122	-6320.9723	-6320.6672	-6318.9142	-6319.3854	-437.62

^aUnit for electronic energies is Hartree and unit for imaginary frequencies is cm^{-1} . All enthalpies and free energies were corrected at 393K.

6.5 References

- [1] Müller, T. E.; Beller, M., *Chem. Rev.* **1998**, *98*, 675.
 [2] Müller, T. E.; Hultsch, K. C.; Yus, M.; Foubelo, F.; Tada, M., *Chem. Rev.* **2008**, *108*, 3795.

- [3] Huang, L.; Arndt, M.; Gooßen, K.; Heydt, H.; Gooßen, L. J., *Chem. Rev.* **2015**, *115*, 2596.
- [4] Reznichenko, A. L.; Hultsch, K. C., In *Hydroamination of Alkenes. In Organic Reactions*, 2015; pp 1.
- [5] Gurak, J. A.; Yang, K. S.; Liu, Z.; Engle, K. M., *J. Am. Chem. Soc.* **2016**, *138*, 5805.
- [6] Karshtedt, D.; Bell, A. T.; Tilley, T. D., *J. Am. Chem. Soc.* **2005**, *127*, 12640.
- [7] Zhang, J.; Yang, C.-G.; He, C., *J. Am. Chem. Soc.* **2006**, *128*, 1798.
- [8] Musacchio, A. J.; Lainhart, B. C.; Zhang, X.; Naguib, S. G.; Sherwood, T. C.; Knowles, R. R., *Science* **2017**, *355*, 727.
- [9] Nguyen, T. M.; Manohar, N.; Nicewicz, D. A., *Angew. Chem. Int. Ed.* **2014**, *53*, 6198.
- [10] Zhang, Z.; Lee, S. D.; Widenhofer, R. A., *J. Am. Chem. Soc.* **2009**, *131*, 5372.
- [11] Reznichenko, A. L.; Nguyen, H. N.; Hultsch, K. C., *Angew. Chem. Int. Ed.* **2010**, *49*, 8984.
- [12] Pan, S.; Endo, K.; Shibata, T., *Org. Lett.* **2012**, *14*, 780.
- [13] Nugent, T. C., *Chiral Amine Synthesis: Methods, Developments and Applications*. Wiley VCH: Weinheim, Germany, 2010.
- [14] Wang, C.; Xiao, J., Asymmetric Reductive Amination. In *Stereoselective Formation of Amines*, Li, W.; Zhang, X., Eds. Springer Berlin Heidelberg: Berlin, Heidelberg, 2014; pp 261.
- [15] Xie, J.-H.; Zhu, S.-F.; Zhou, Q.-L., *Chem. Rev.* **2011**, *111*, 1713.
- [16] Ellman, J. A.; Owens, T. D.; Tang, T. P., *Acc. Chem. Res.* **2002**, *35*, 984.
- [17] Patil, M. D.; Grogan, G.; Bommarius, A.; Yun, H., *ACS Catal.* **2018**, *8*, 10985.
- [18] Yang, Y.; Shi, S.-L.; Niu, D.; Liu, P.; Buchwald, S. L., *Science* **2015**, *349*, 62.
- [19] Johns, A. M.; Sakai, N.; Ridder, A.; Hartwig, J. F., *J. Am. Chem. Soc.* **2006**, *128*, 9306.
- [20] Liu, Z.; Hartwig, J. F., *J. Am. Chem. Soc.* **2008**, *130*, 1570.
- [21] Sevov, C. S.; Zhou, J.; Hartwig, J. F., *J. Am. Chem. Soc.* **2012**, *134*, 11960.
- [22] Utsunomiya, M.; Kuwano, R.; Kawatsura, M.; Hartwig, J. F., *J. Am. Chem. Soc.* **2003**, *125*, 5608.
- [23] Pawlas, J.; Nakao, Y.; Kawatsura, M.; Hartwig, J. F., *J. Am. Chem. Soc.* **2002**, *124*, 3669.
- [24] Casalnuovo, A. L.; Calabrese, J. C.; Milstein, D., *J. Am. Chem. Soc.* **1988**, *110*, 6738.
- [25] Dorta, R.; Egli, P.; Zürcher, F.; Togni, A., *J. Am. Chem. Soc.* **1997**, *119*, 10857.
- [26] Zhou, J.; Hartwig, J. F., *J. Am. Chem. Soc.* **2008**, *130*, 12220.
- [27] Hanley, P. S.; Hartwig, J. F., *Angew. Chem. Int. Ed.* **2013**, *52*, 8510.
- [28] Thompson, W. H.; Sears, C. T., *Inorg. Chem.* **1977**, *16*, 769.
- [29] Smout, V.; Peschiulli, A.; Verbeeck, S.; Mitchell, E. A.; Herrebout, W.; Bultinck, P.; Vande Velde, C. M. L.; Berthelot, D.; Meerpoel, L.; Maes, B. U. W., *J. Org. Chem.* **2013**, *78*, 9803.